

Quantum Theory Needs No 'Interpretation'

Christopher A. Fuchs and Asher Peres

Recently there has been a spate of articles, reviews, and letters in *PHYSICS TODAY* promoting various "interpretations" of quantum theory (see March 1998, page 42; April 1998, page 38; February 1999, page 11; July 1999, page 51; and August 1999, page 26). Their running theme is that from the time of quantum theory's emergence until the discovery of a particular interpretation, the theory was in a crisis because its foundations were unsatisfactory or even inconsistent. We are seriously concerned that the airing of these opinions may lead some readers to a distorted view of the validity of standard quantum mechanics. If quantum theory had been in a crisis, experimenters would have informed us long ago!

Our purpose here is to explain the internal consistency of an "interpretation without interpretation" for quantum mechanics. Nothing more is needed for using the theory and understanding its nature. To begin, let us examine the role of experiment in science. An experiment is an active intervention into the course of Nature: We set up this or that experiment to see how Nature reacts. We have learned something new when we can distill from the accumulated data a compact description of all that has been and an indication of which further experiments will corroborate that description. This is what science is about. If, from such a description, we can further distill a model of a free-standing "reality" independent of our interventions, then so much the better. Classical physics is the ultimate example of such a model. However, there is no logical necessity for a realistic worldview to always be obtainable. If the world is such that we can never identify a reality independent

of our experimental activity, then we must be prepared for that, too.

The thread common to all the non-standard "interpretations" is the desire to create a new theory with features that correspond to some reality independent of our potential experiments. But, trying to fulfill a classical worldview by encumbering quantum mechanics with hidden variables, multiple worlds, consistency rules, or spontaneous collapse, without any improvement in its predictive power, only gives the illusion of a better understanding. Contrary to those desires, quantum theory does not describe physical reality. What it does is provide an algorithm for computing probabilities for the macroscopic events ("detector clicks") that are the consequences of our experimental interventions. This strict definition of the scope of quantum theory is the only interpretation ever needed, whether by experimenters or theorists.

Quantum probabilities, like all probabilities, are computed by using any available information. This can include, but is not limited to information about a system's preparation. The mathematical instrument for turning the information into statistical predictions is the probability rule postulated by Max Born.¹ The conclusiveness of Born's rule is known today to follow from a theorem due to Andrew Gleason.² It is enough to assume that yes-no tests on a physical system are represented by projection operators P , and that probabilities are additive over orthogonal projectors. Then there exists a density matrix ρ describing the system such that the probability of a "yes" answer is $\text{tr}(\rho P)$. The compendium of probabilities represented by the "quantum state" ρ captures everything that can meaningfully be said about a physical system.

Here, it is essential to understand that the validity of the statistical nature of quantum theory is not restricted to situations where there are a large number of similar systems. Statistical predictions do apply to single events. When we are told that the probability of precipitation tomorrow is 35%, there is only one tomorrow. This tells us that it is advisable to

carry an umbrella. Probability theory is simply the quantitative formulation of how to make rational decisions in the face of uncertainty.

We do not deny the possible existence of an objective reality independent of what observers perceive. In particular, there is an "effective" reality in the limiting case of macroscopic phenomena like detector clicks or planetary motion: Any observer who happens to be present would acknowledge the objective occurrence of these events. However, such a macroscopic description ignores most degrees of freedom of the system and is necessarily incomplete. Can there also be a "microscopic reality" where every detail is completely described? No description of that kind can be given by quantum theory, nor by any other reasonable theory. John Bell formally showed³ that any objective theory giving experimental predictions identical to those of quantum theory would necessarily be nonlocal. It would eventually have to encompass everything in the universe, including ourselves, and lead to bizarre self-referential logical paradoxes. The latter are not in the realm of physics; experimental physicists never need bother with them.

We have experimental evidence that quantum theory is successful in the range from 10^{-10} to 10^{25} atomic radii; we have no evidence that it is universally valid. Yet, it is legitimate to attempt to extrapolate the theory beyond its present range, for instance, when we probe particle interactions at superhigh energies, or in astrophysical systems, including the entire universe. Indeed, a common question is whether the universe has a wavefunction. There are two ways to understand this. If this "wavefunction of the universe" has to give a complete description of everything, including ourselves, we again get the same meaningless paradoxes. On the other hand, if we consider just a few collective degrees of freedom, such as the radius of the universe, its mean density, total baryon number, and so on, we can apply quantum theory only to these degrees of freedom, which do not include ourselves and other insignificant details. This is not essentially

CHRIS FUCHS, previously the Lee DuBridge Prize Postdoctoral Fellow at Caltech, is now a Director-Funded Fellow at Los Alamos National Laboratory. His daytime research focuses on quantum information theory and quantum computation. ASHER PERES is the Gerard Swope Distinguished Professor of Physics at Technion-Israel Institute of Technology, in Haifa, Israel. He is the author of *Quantum Theory: Concepts and Methods* (Kluwer, Dordrecht, 1995).



different from quantizing the magnetic flux and the electric current in a SQUID while ignoring the atomic details. For sure, we can manipulate a SQUID more easily than we can manipulate the radius of the universe, but there is no difference in principle.

Does quantum mechanics apply to the observer? Why would it not? To be quantum mechanical is simply to be amenable to a quantum description. Nothing in principle prevents us from quantizing a colleague, say. Let us examine a concrete example: The observer is Cathy (an experimental physicist) who enters her laboratory and sends a photon through a beam splitter. If one of her detectors is activated, it opens a box containing a piece of cake; the other detector opens a box with a piece of fruit. Cathy's friend Erwin (a theorist) stays outside the laboratory and computes Cathy's wavefunction. According to him, she is in a 50/50 superposition of states with some cake or some fruit in her stomach. There is nothing wrong with that; this only represents his knowledge of Cathy. She knows better. As soon as one detector was activated, her wavefunction collapsed. Of course, nothing dramatic happened to her. She just acquired the knowledge of the kind of food she could eat. Some time later, Erwin peeks into the laboratory. Thereby he acquires new knowledge, and the wavefunction he uses to describe Cathy changes. From this example, it is clear that a wavefunction is only a mathematical expression for evaluating probabilities and depends on the knowledge of whoever is doing the computing.

Cathy's story inevitably raises the issue of reversibility; after all, quantum dynamics is time-symmetric. Can Erwin undo the process if he has not yet observed Cathy? In principle he can, because the only information Erwin possesses is about the consequences of his potential experiments, not about what is "really there." If Erwin has performed no observation, then there is no reason he cannot reverse Cathy's digestion and memories. Of course, for that he would need complete control of all the microscopic degrees of freedom of Cathy and her laboratory, but that is a practical problem, not a fundamental one.

The peculiar nature of a quantum state as representing information is strikingly illustrated by the quantum

teleportation process.⁴ In order to teleport a quantum state from one photon to another, the sender (Alice) and the receiver (Bob) need to divide between them a pair of photons in a standard entangled state. The experiment begins when Alice receives another photon whose polarization state is unknown to her but known to a third-party preparer. She performs a measurement on her two photons—one from the original, entangled pair and the other in a state unknown to her—and then sends Bob a classical



"What do you mean, 'a quantum fluctuation'? Didn't we discuss cause and effect?"

message of only two bits, instructing him how to reproduce that unknown state on his photon. This economy of transmission appears remarkable, because to completely specify the state of a photon, namely one point in the Poincaré sphere, we need an infinity of bits. However, this complete specification is not what is transferred. The two bits of classical information serve only to convert the preparer's information, from a description of the original photon to a description of the one in Bob's possession. The communication resource used up for doing that is the correlated pair that was shared by Alice and Bob.

It is curious that some well-intentioned theorists are willing to abandon the objective nature of physical "observables," and yet wish to retain the abstract quantum state as a surrogate reality. There is a temptation to believe that every quantum system has a wavefunction, even if the wavefunction is not explicitly known. Apparently, the root of this temptation is that in classical mechanics phase space points correspond to objective data, whereas in quantum mechanics Hilbert space points corre-

lated to quantum states. This analogy is misleading: Attributing reality to quantum states leads to a host of "quantum paradoxes." These are due solely to an incorrect interpretation of quantum theory. When correctly used, quantum theory never yields two contradictory answers to a well-posed question. In particular, no wavefunction exists either before or after we conduct an experiment. Just as classical cosmologists got used to the idea that there is no "time" before the big bang or after the big crunch, so too must we be careful about using "before" and "after" in the quantum context.

Quantum theory has been accused of incompleteness because it cannot answer some questions that appear reasonable from the classical point of view. For example, there is no way to ascertain whether a single system is in a pure state or is part of an entangled composite system. Furthermore, there is no dynamical description for the "collapse" of the wavefunction. In both cases the theory gives no answer because the wavefunction is not an objective entity. Collapse is something that happens in our description of the system, not to the system itself. Likewise, the time dependence of the wavefunction does not represent the evolution of a physical system. It only gives the evolution of our probabilities for the outcomes of potential experiments on that system. This is the only meaning of the wavefunction.

All this said, we would be the last to claim that the foundations of quantum theory are not worth further scrutiny. For instance, it is interesting to search for minimal sets of physical assumptions that give rise to the theory. Also, it is not yet understood how to combine quantum mechanics with gravitation, and there may well be important insight to be gleaned there. However, to make quantum mechanics a useful guide to the phenomena around us, we need nothing more than the fully consistent theory we already have. Quantum theory needs no "interpretation."

References

1. M. Born, *Zeits. Phys.* 37, 863 (1926); 38, 803 (1926).
2. A. M. Gleason, *J. Math. Mech.* 6, 885 (1957).
3. J. S. Bell, *Physics* 1, 195 (1964).
4. C. H. Bennett, G. Brassard, C. Crépeau, R. Jozsa, A. Peres, and W. K. Wootters, *Phys. Rev. Letters* 70, 1895 (1993).



ATOMS AND MOLECULES

**An Introduction for Students
of Physical Chemistry**

MARTIN KARPLUS
Harvard University

RICHARD N. PORTER
State University of New York
at Stony Brook



The Benjamin/Cummings Publishing Company
Menlo Park, California • Reading, Massachusetts
London • Amsterdam • Don Mills, Ontario • Sydney



**ATOMS AND MOLECULES An Introduction for
Students of Physical Chemistry**

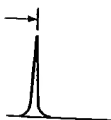
Copyright © 1970 by W. A. Benjamin, Inc. Philippines copyright 1970 by W. A. Benjamin, Inc.

All rights reserved. No part of this publication may be reproduced, stored in a retrieval system, or transmitted, in any form or by any means, electronic, mechanical, photocopying, recording, or otherwise, without the prior written permission of the publisher. Printed in the United States of America. Published simultaneously in Canada. Library of Congress Catalog Card No. 72-105272.

ISBN 0-8053-5218-8
OPORT-AL-8987

T
R. I. K., C. M. P.,
and thei





showing hyperfine interaction.

$$m, m_I \quad (7.197)$$

and has units of Hz. Equations (7.197) and (7.198) show that the hyperfine splitting increases linearly with the field. Thus, in weak fields, since the quantization of electron and nuclear spin is independent of the external field, the effect of the external field on the hyperfine splitting is negligible. For the frequencies of the external field, $\Delta m_s = \pm 1$, $\Delta m_I = 0$ are

$$\nu = \nu_0 \pm \frac{1}{2} \Delta \nu \quad (7.198a)$$

$$\nu = \nu_0 \pm \frac{1}{2} \Delta \nu \quad (7.198b)$$

the hyperfine constant a . The hyperfine splitting can be observed by varying the

$$\nu = \nu_0 \pm \frac{1}{2} \Delta \nu \quad (7.199)$$

that lead to resonance.

$$\frac{a h}{2 g \mu_B} = \frac{a h}{g \mu_B} \quad (7.200)$$

for other atoms. If $\Delta \nu$ is

$$9 \Delta \nu \quad (7.201)$$

these are quoted in both tables. The hyperfine splitting depends only on the hyperfine interaction and the external magnetic field. The hyperfine splitting depends only on the hyperfine interaction and the external magnetic field.

NMR chemical-shift measurements of systems with unpaired electrons) for determining the sign of a in appropriate cases.

For the hydrogen atom, the experimental value of a is 1420.4057 MHz or 506.84 G. Its source, already mentioned above, is the coupling between the nucleus and the electron magnetic moments. The quantitative expression for the hyperfine constant of a hydrogen atom expressed in Hz is

$$a = \frac{8\pi}{3h} g \mu_B g_N \mu_N |\psi(0)|^2 \quad (7.202)$$

where g_H and μ_N are the proton g factor and the nuclear magneton, respectively, and $|\psi(0)|^2$ represents the absolute value squared of the electron density at the nucleus. The coupling corresponding to Eq. 7.202 is often called the contact interaction, or *Fermi contact interaction*, after Enrico Fermi who showed (1930) that such an interaction should exist long before the ESR technique was introduced (1945-47). In addition to the Fermi contact term, there is another interaction between the electron and nuclear spins, which contributes for electrons in non- S states. This is the direct dipole-dipole term, which averages to zero in solution because of the rapid tumbling, but can be observed in solids when the molecules have fixed orientations.

From the form of the ground-state hydrogen-atom wave function (Section 3.2)

$$\psi_{1s} = (\pi a_0^3)^{-1/2} \exp\left(-\frac{r}{a_0}\right)$$

the electron density at the nucleus is

$$|\psi_{1s}(0)|^2 = \frac{1}{\pi a_0^3}$$

Substituting this result into Eq. 7.202 with the values for the various constants, we obtain 1422.75 MHz or 507.68 G, in reasonable agreement with experiment (see Problem 7.43). Correction for the finite mass of the proton [i.e., multiplication by $(1836.13/1837.13)^3$] gives the more accurate theoretical value 1420.43 MHz.

We consider now the extension of the hydrogen-atom results to more complex systems, in particular the organic radicals that are being intensively studied by ESR techniques. Such molecules contain many electrons, each of which has a spin and an associated magnetic moment. However, we can frequently neglect all of the inner-shell electrons, which form closed shells with paired spins, and restrict the discussion to the outermost electron with an unpaired spin that can interact with the external magnetic field. For the naphthalene negative ion (see Section 6.4.2), the ground-state



CONCEPTS OF MODERN PHYSICS

FOURTH EDITION

Arthur Beiser

McGRAW-HILL BOOK COMPANY

New York St. Louis San Francisco Auckland Bogotá Hamburg
London Madrid Mexico Milan Montreal New Delhi
Panama Paris São Paulo Singapore Sydney Tokyo Toronto



CONCEPTS OF MODERN PHYSICS

Copyright © 1987, 1981, 1973, 1967, 1963 by McGraw-Hill, Inc. All rights reserved. Printed in the United States of America. Except as permitted under the United States Copyright Act of 1976, no part of this publication may be reproduced or distributed in any form or by any means, or stored in a data base or retrieval system, without the prior written permission of the publisher.

2 3 4 5 6 7 8 9 0 DOCDOC 8 9 4 3 2 1 0 9 8 7

ISBN 0-07-004473-2

This book was set in Times Roman by Automated Composition Service.
The editor was Karen S. Misler;
the cover was designed by John Hite.
the production supervisors were Leroy Young and Friederich Schulte.
New drawings were done by Fine Line Illustrations, Inc.
Project supervision was done by The Total Book.
R. R. Donnelley & Sons Company was printer and binder.
See Acknowledgments on page 601. Copyrights included on this page by reference.

Library of Congress Cataloging-in-Publication Data

Beiser, Arthur.
Concepts of modern physics.

Includes bibliographical references and index.

1. Physics. I. Title.

QC21.2.B448 1987 530 86-20165
ISBN 0-07-004473-2



behavior of nuclei. Nevertheless, the nucleus turns out to be of paramount importance in the grand scheme of things. To begin with, the very existence of the various elements is due to the ability of nuclei to possess multiple electric charges. Furthermore, the energy involved in almost all natural processes can be traced to nuclear reactions and transformations. On a more parochial level, the liberation of nuclear energy in reactors and weapons has affected all our lives in one way or another.

11.1 DO NUCLEI CONTAIN ELECTRONS?

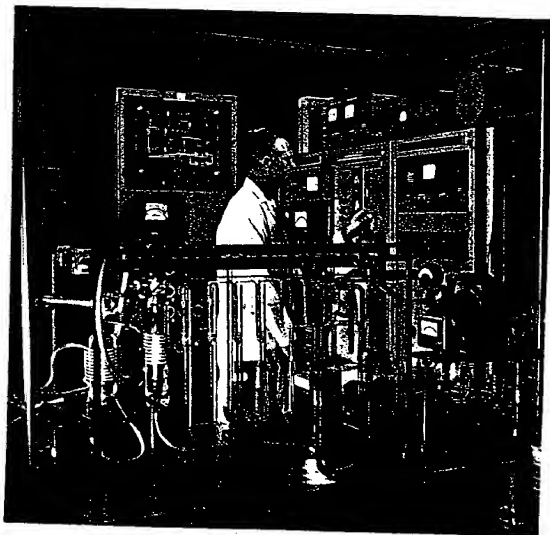
No

Nuclear forces are very strong

The electron structure of the atom was understood before even the composition of its nucleus was known. The reason is that the forces that hold the nucleus together are vastly stronger than the electric forces that hold the electrons to the nucleus, and it is correspondingly harder to break apart a nucleus to find out what is inside. Changes in the electron structure of an atom, such as those that occur when a photon is emitted or absorbed or when a chemical bond is formed or broken, involve energies of only a few electronvolts. Changes in nuclear structure, on the other hand, involve energies in the MeV range, a million times greater.

Let us begin our study of the nucleus with the most obvious question: Of what is it composed?

Mass spectrometer used to study the composition of meteorites.





Biographies of BlackLight Power, Corporation Employees

XUEMIN CHEN, PH.D.

Dr. Chen, graduated from Brigham Young University, Provo, Utah with a Ph.D. in Chemistry. Dr. Chen has extensive knowledge and hands-on experience in various calorimetric and thermal analysis techniques, and has designed and constructed calorimeters. At BLP, Dr. Chen is responsible for designing a water bath calorimeter, performs calorimetry research, and studies the heat generated by the BlackLight Process. Dr. Chen is a member of the American Chemical Society and Sigma Xi, The Scientific Research Society. Dr. Chen has twenty-four (24) publications and has presented at twenty-one (21) conferences.

ETHIRAJULU DAYALAN, PH.D.

Dr. Dayalan, Staff Electrochemist, graduated with a Ph.D. in Electrochemistry from the Indian Institute of Technology, Madras, India, and brings to BlackLight Power, Inc. (BLP) over 20 years of research and development experience in batteries, industrial electrochemical processes, electrode kinetics, electrocatalysis, corrosion, materials synthesis and surfactant systems. At BLP, Dr. Dayalan is responsible for the development of a battery using the Company's novel hydride technology. In so doing, he studies electrochemical properties of proprietary inorganic hydrides, including formulating and characterizing compounds, and studying compounds in test cells. Dr. Dayalan is a member of the Electrochemical Society, the Society for Advancement of Electrochemical Science and Technology, and the American Chemical Society. He has over thirty-five (35) publications and has presented in over thirty-five (35) conferences.

BALA DHANDAPANI, PH.D.

Dr. Dhandapani, Director, Chemical Synthesis and Analysis, graduated with a Ph.D. in Chemical Engineering from Clarkson University, Potsdam, NY, and brings to BlackLight Power, Inc. (BLP) expertise in the areas of synthesis, characterization and testing of novel materials. Dr. Dhandapani is responsible for coordinating the research efforts at BLP and serves as liaison between Program Managers and BLP's President. In addition, Dr. Dhandapani is responsible for characterization of novel materials and optimization of the BlackLight Process. Dr. Dhandapani is a member of the American Chemical Society and the Catalysis Society of New York. He has twenty (20) publications and has presented at ten (10) conferences.

JINQUAN DONG, PH.D.

Dr. Dong, Research Scientist, graduated with a Ph.D. in Chemistry from the City University of New York, and brings to BlackLight Power, Inc. (BLP) extensive knowledge of chemistry, spectroscopy and materials analysis. At BLP, Dr. Dong is responsible for studying the heat generated by the BlackLight Process using various calorimetric techniques. Dr. Dong is a member of the American Chemical Society and the Materials Research Society. He has published ten (10) research papers and has presented at eight (8) national and international meetings.



JILIANG HE, PH.D.

Dr. He, Manager, TOF-SIMS and XPS Program, graduated with a Ph.D. in Analytical Inorganic Chemistry from McGill University, Montreal, Canada, and brings to BlackLight Power, Inc. (BLP) extensive knowledge in synthesis, structural analysis and property characterization. At BLP, Dr. He is responsible for various analytical tests, data interpretation, synthesis of novel silicon compounds, and supports the spectroscopy studies of the BLP photoemission process. Dr. He is a member of the American Chemical Society. He has published twenty-seven (27) research papers in scientific journals and has presented at more than twenty (20) national and international scientific conferences.

ROBERT MAYO, PH.D.

Dr. Mayo, Director, Plasma-to-Electric Conversion Program, graduated from Purdue University with a Ph.D. in Nuclear Engineering. Dr. Mayo served most recently on the faculty in the Department of Nuclear Engineering at North Carolina State University, where, among other responsibilities, he served as Director of Graduate Programs. His most recent research and professional activities include: Pulsed Laser Evaporated (PLE) plasmas for advanced materials production; imaging, spectroscopic and particle plasma diagnostics for thin film heterostructures using Pulsed Laser Deposition; magnetized PLE plasma for plume control and controlled deposition. At BLP, Dr. Mayo provides expertise in the detailed characterization of chemically-driven plasma, as well as leadership in the analysis, design, and development of a plasma-to-electric conversion prototype. Dr. Mayo is a member of the American Physical Society-Division of Plasma Physics, the Fusion Power Associates, the American Nuclear Society, and the American Association for the Advancement of Science. He has published a book Introduction to Nuclear Concepts for Engineers, has published 37 journal articles, has made 72 conference presentations, and has completed 32 invited research presentations.

MARK NANSTEEL, PH.D.

Dr. Nansteel, Director, Plasma Cell Engineering, graduated with a Ph.D. in Mechanical Engineering from the University of California, Berkeley, and brings to BlackLight Power, Inc. (BLP) extensive expertise in heat and mass transfer/fluid dynamics. At BLP, Dr. Nansteel is primarily responsible for the characterization, optimization and development of the BlackLight Process. Dr. Nansteel is a member of the American Society of Mechanical Engineers and the Society for Industrial and Applied Mathematics. He has published seventeen (17) journal articles and has presented at three (3) conferences.



Biographies of BlackLight Power, Corporation Employees

PARESH RAY, PH.D.

Dr. Ray, Research Scientist, achieved his Ph.D. in Physical Chemistry from the Indian Institute of Science, Bangalore, India, where he studied nonlinear optical properties of polymeric, organic and organometallic materials. His post-doctoral work at the University of Chicago included photodissociation dynamics by molecular beam emission spectroscopy. At Columbia University, his post-doctoral work included reaction dynamics using molecular beam TOF/REMPI/Doppler spectroscopy. At BLP, Dr. Ray has been working on plasma dynamics of hydrogen-catalyzed plasma by EUV, VUV, UV-Visible and Doppler broadening spectroscopy. He is a member of the American Chemical Society. Dr. Ray has published twenty-eight (28) journal articles and has presented papers at eight (8) international symposia.

JAYASREE SANKAR, PH.D.

Dr. Sankar, Research Scientist, attained her Ph.D. in Metallorganic/Materials Chemistry from the University of Western Ontario, Canada. Her doctoral research at Western was "Chemical Vapor Deposition of Transition Metal and Metal Oxide Thin Films". Dr. Sankar brings to BlackLight Power, Inc. (BLP) a thorough understanding of chemical analytical techniques. At BLP, Dr. Sankar performs research and development work related to thick and thin films of hydride compounds on surfaces whereby she is preparing, characterizing and developing commercial applications of useful hydride films. Dr. Sankar is a member of the American Chemical Society and the Chemical Institute of Canada. She has published in over ten (10) refereed journals, and has made more than eight (8) presentations at international conferences.

ANDREAS VOIGT, PH.D.

Dr. Voigt, Senior Research Scientist, graduated summa cum laude in Chemistry from Georg-August University of Göttingen, Germany, on his doctoral thesis "Synthesis, Structure and Catalytic Reactivity of Metallasiloxanes-Model Compounds for Metal Doped Zeolites." Dr. Voigt brings expertise in synthetic and analytical chemistry to BlackLight Power, Inc. (BLP) where he conducts synthesis, isolation, purification and identification of novel inorganic chemicals in bench scale experiments. Dr. Voigt investigates chemical processes and reactions in high-temperature materials. Dr. Voigt is a member of the American Chemical Society. He has published one (1) book, one (1) book chapter, over twenty-nine (29) journal articles and has presented at six (6) international conferences.



RON WYDEN
OREGON

516 Hart Senate Building
Washington, DC
20510-3703
(202) 224-5244

e-mail:

senator@wyden.senate.gov

web site:

www.senate.gov/~wyden/

United States Senate

WASHINGTON, DC 20510-3703

April 5, 2000

The Honorable Q. Todd Dickinson
Commissioner of Patents and Trademarks
U.S. Department of Commerce
Washington, D.C. 20231

Committees:

Budget
Commerce, Science
& Transportation
Energy & Natural Resources
Environment & Public Works
Special Committee on Aging

Re: Blacklight Power, Inc.'s Patent Application Ser. No.
09/009,294

Oregon State Offices:

700 NE Multnomah St
Suite 450
Portland, OR 97232
(503) 326-7525

151 West 7th Ave
Suite 435
Eugene, OR 97401
(541) 431-0229

Sec Annex Building
105 Fir St
Suite 210
La Grande, OR 97850
(541) 962-7691

U.S. Courthouse
310 West 6th St
Room 118
Medford, OR 97501
(541) 858-5122

The Jamison Building
131 NW Hawthorne Ave
Suite 107
Bend, OR 97701
(541) 330-9142

707 13th St, SE
Suite 285
Salem, OR 97301
(503) 589-4555

Dear Commissioner Dickinson:

I am writing this letter on behalf of one of my constituents who is a member of the Board of Directors of Blacklight Power, Inc. It has come to my attention that the U.S. Patent & Trademark Office has withdrawn a Blacklight patent application, Ser. No. 09/009,294 ("294 application"), which was due to issue as U.S. Patent No. 6,030,601 on February 29, 2000. A copy of the February 17, 2000 Notice of withdrawal that was sent to Blacklight's counsel is attached. It is alleged by my constituent that the patent due to issue to Blacklight was withdrawn through an unusual process.

Please also find enclosed a copy of an abstract for a speech from an Official at the U.S. Department of State, Dr. Peter Zimmerman, who plans to present a paper to the American Physics Society in April. The abstract states that Dr. Zimmerman's "own Department and the Patent Office have fought back with success" against inventors of "hydrinos." According to Blacklight Power, the term "hydrinos" was coined and is used exclusively by the company.

My questions concerning this matter relate to: (1) any involvement you may have had in pulling the '294 application from issuance; (2) any *ex parte* communications that may have occurred between third parties and the Patent Office relating to Blacklight or its technology; and (3) how the State Department and the Patent Office may have "fought back with success" against Blacklight.



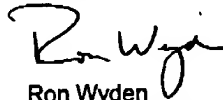
f
7

To address these concerns, I am requesting that you provide me with the following information:

- (a) A written description of your role and any relevant communications between you and other Patent Office personnel in withdrawing the '294 application from issue.
- (b) Copies of any written communications between third parties and the Patent Office relating to Blacklight or its technology, including any correspondence between you or other Patent Office personnel and the State Department, including Dr. Zimmerman; and any written communications between the Patent Office and any other Federal agencies relating to Blacklight or its technology.
- (c) The extent of any cooperation between Dr. Zimmerman, the U.S. State Department, and the Patent Office relating to Blacklight, its technology or the '294 application.

I look forward to your prompt response to this request. If you have any questions concerning this request, please contact Joshua Sheinkman of my staff at (202) 224-5244.

Sincerely,



Ron Wyden
United States Senator

Attachments: February 17, 2000 Notice of withdrawal
Peter D. Zimmerman, "Touching the Third Rail: Encounters with
Pseudoscience and Pseudoscientists," U.S. Department of State

CC: Kevin Baer, Esq., Attorney-Advisor, U.S. Patent Office
Janie Cooksey, U.S. Department of Commerce
Mr. C. Norman Winningstad



7
1



UNITED STATES DEPARTMENT OF COMMERCE
Patent and Trademark Office
ASSISTANT SECRETARY AND COMMISSIONER OF
PATENTS AND TRADEMARKS
Washington, D.C. 20231

PMW.2

Paper No.

FARKAS & MANELLI, PLLC
2000 M STREET NW
7TH FLOOR
WASHINGTON, DC 20036-3307

COPY MAILED

FEB 17 2000

**SPECIAL PROGRAMS OFFICE
DAC FOR PATENTS**

NOTICE

In re Application of
Randell L. Mills
Application No. 09/009,294
Filed: January 20, 1998
Attorney Docket No. 911319

The purpose of this communication is to inform you that the instant application, which has received Patent No. 6,030,601 and an issue date of February 29, 2000, is being withdrawn from issue pursuant to 37 CFR 1.313.

The application is being withdrawn to permit reopening of prosecution. This withdrawal was requested by the Director, Special Program Law Office.

The issue fee is refundable upon written request. However, if the application is again found allowable, the issue fee can be applied toward payment of the issue fee in the amount identified on the new Notice of Allowance and Issue Fee Due upon written request. This request and any balance due must be received on or before the due date noted in the new Notice of Allowance in order to prevent abandonment of the application.

This application, upon receipt in the Office of Petitions, will be forwarded to Technology Center AD 1745 for reopening of prosecution.

Telephone inquiries concerning this matter may be directed to the undersigned at (703) 305-8680.

Frances Hicks
Frances Hicks

Petitions Examiner
Office of Petitions
Office of the Deputy Assistant Commissioner
for Patent Policy and Projects



1
2



[Previous abstract](#) | [Graphical version](#) | [Text version](#) | [Next abstract](#)

Session J12 - FPS Awards Session-Business Meeting.

MIXED session, Sunday afternoon, April 30

101B, Long Beach Convention Center

[J12.001] Touching the Third Rail: Encounters with Pseudoscience and Pseudoscientists

Peter D. Zimmerman (United States Department of State, Washington, DC 20520)

Pseudoscience, and particularly "pseudophysics" is alive and thriving as we approach the turn of the millennium. Not only have many "inventors" of cold fusion spin-offs been making money from investors, but they and "inventors" of various kinds of "zero point energy" devices, perpetual motion machines, and other wonders such as "hydrinos" have found friends in the United States Senate. At least one Nobel Laureate in physics has come to their aid. The Web has been a powerful organizing force as well.

Some organizations, including my own Department and the Patent Office have fought back with success, but always at great cost in time and energy. Pseudophysicists and their friends have money, influence, and sometimes clout. They have not hesitated to use threats, personal attacks, and the full machinery by which government is made accountable to the public to strike at those who expose technical fraud. Encounters with pseudophysicists are like grabbing a hot wire: after the first contact it is hard to get free, and it can inflict serious injury. But you, and I, and all our colleagues in the APS must do what we can to ensure that U.S. policy is not manipulated by pseudoscience, to make certain that taxpayer money is not wasted on nonsense, and to restore public confidence in real science. This will take efforts at public education, work, and as I have learned in the last year not a little bit of courage. APS and FPS should be in the thick of the battle. This talk is an account of a year in the fray.

■ Part J of program listing



1

7/24/01 TUE 14:03 FAX 202 228-3224

SENATOR TORRICELLI

ROBERT G. TORRICELLI
NEW JERSEY

COMMITTEES:

GOVERNMENTAL AFFAIRS

JULS AND ADMINISTRATION

FOREIGN RELATIONS

FINANCE

United States Senate

113 DIRKSEN SENATE OFFICE BUILDING
WASHINGTON, DC 20510-3003
(202) 224-3224

ONE RIVERFRONT PLAZA
3RD FLOOR
NEWARK, NEW JERSEY 07102
(973) 824-5555

420 BENIGNO BLVD.
KORMAN INTERSTATE BUSINESS PARK
SUITE A-1
DELMAR, NEW JERSEY 08031
(856) 933-1245

<http://nonlocal.senate.gov>
Senator Torricelli@Torricelli.Senate.Gov

July 20, 2001

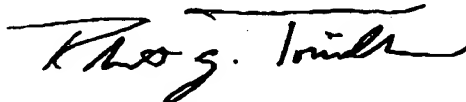
Nicholas P. Godici
Acting Undersecretary of Commerce for Intellectual Property
and Acting Director of the Patent and Trademark Office
U.S. Patent and Trademark Office
Washington, D.C. 20231

Dear Acting Director Godici:

I am writing you on behalf of Blacklight Power, Inc., one of my constituent companies. Recently, I received the attached letter from Blacklight detailing what seem to be very unusual circumstances that have arisen in the course of their attempts to obtain a patent for their new and intriguing technology. In my opinion, if the allegations set forth in this letter are indeed true, they raise troubling questions about the conduct of some representatives of the Patent Office.

I ask that you look into this matter and I look forward to receiving your response to the issues raised in the attached correspondence. Thank you for your consideration and your attention to this matter.

Sincerely,



Robert G. Torricelli
UNITED STATES SENATOR



**BLACKLIGHTTM**
P O W E R inc.493 Old Trenton Road
Cranbury, NJ 08512
Telephone (609) 490-1090
Fax (609) 490-1066

May 10, 2001

The Honorable Robert G. Torricelli, U.S. Senator
113 Dirksen Senate Office Building
Washington, DC 20510

Re: Investigation of Improper Actions by U.S. Patent Office

Dear Senator Torricelli:

We kindly request your assistance in investigating and addressing the highly improper actions taken by the U.S. Patent and Trademark Office (PTO) against a constituent of yours, BlackLight Power, Inc. (BlackLight). These actions not only threaten the livelihood of a thriving New Jersey company, but threaten to undermine the integrity of the U.S. patent system, as well as diminish our ability to effectively cope with the looming energy crisis in this country.

BlackLight is a small start-up company located in Cranbury, New Jersey. It employs 35 individuals, most of whom are research scientists, engineers, and technicians. For the past three years since BlackLight located its operations in New Jersey, BlackLight has worked tirelessly and has spent millions of dollars developing a new, commercially feasible, clean process for producing electricity from hydrogen. BlackLight's technology represents a significant advance in the field of energy production and the company has built a substantial business and scientific team to commercialize products. This technology is based on Dr. Randell L. Mills' theory and experimentally verified process of utilizing catalysts to relax the electron in hydrogen atoms to lower energy levels to thereby release clean energy and produce novel chemical products. Rest assured that our technology is not based on "cold fusion" or other speculative technologies.

BlackLight's new energy production process and novel chemical products are easily reproducible and have been independently verified by prestigious universities, government agencies and laboratories. Early generation power cells were confirmed by MIT Lincoln Labs, INEL, Westinghouse Corporation, NASA Lewis, Chalk River National Laboratory, Thermacore Corporation, and Pennsylvania State University. The chemical products were predicted and analyzed by 20 different types of tests performed at over 20 independent laboratories. BlackLight recently submitted 22 journal articles to journals, 16 of which are presently in press or published, which broadly disclose the test results for general peer review. The articles overwhelmingly verify BlackLight's novel hydrogen chemistry by reporting data from extreme ultraviolet (EUV) spectroscopy, plasma formation, power generation, and analysis of chemical products. BlackLight has also made 22 presentations of its results at scientific meetings over the past two years. The most recent presentation at the National Hydrogen Association, 12th Annual U.S. Hydrogen Meeting and Exposition, resulted in an invitation to submit an article to the published meeting proceedings.



The Honorable Robert G. Torricelli
May 10, 2001
Page 2 of 5

Because the theory involved is revolutionary and questions the validity of basic assumptions that underlie established Quantum Mechanics, Dr. Mills' work is highly controversial. And, as always is the case in "paradigm shifting" events, both Dr. Mills and his theory have been the subjects of criticism—and even derision—by a number of established and respected sources that have acknowledged their failure to even study BlackLights' published experimental results.

The promise inherent in the ultimate commercial application of BlackLight's theory to this nation and, indeed, to all mankind is truly staggering. It represents the potential capability for mankind to harness an unlimited source of energy with vastly lower environmental impacts from harmful waste product emissions or, as with nuclear energy systems, radioactive material disposition. With the advent of this nation's ever-increasing dependency on energy from politically unstable sources overseas, rapidly escalating fuel prices, and now the prospect of rolling blackouts, such as those already occurring in California, the need for alternative low-cost, abundant sources of energy in this country has never been greater.

As an initial step in bringing its energy technology to market, BlackLight sought to protect its intellectual property rights in that technology by filing numerous patent applications in the PTO. Unfortunately, the PTO has mishandled these applications and, in so doing, has failed to carry out its Constitutional mandate to advance the progress of science.

Specifically, evidence has been uncovered regarding the PTO's improper use of outside contacts, including officials from the State Department and the American Physical Society (APS) in what appears to be a concerted effort to subvert BlackLight's technology. For instance, there is strong evidence showing that PTO officials received unidentified *ex parte* communications from competitors of BlackLight that resulted in the PTO Commissioner withdrawing from issue several BlackLight applications that had been previously allowed. [Attachment 5, February 28, 2000 and Attachment 6, January 19, 2001 letters to Director Esther Kepplinger of the PTO] Indeed, Dr. Peter Zimmerman, former Chief Scientist at the State Department, has admitted that Dr. Robert Park—spokesperson for the APS, a BlackLight competitor—uses a contact in the PTO that Dr. Park refers to as "Deep Throat" to obtain confidential information, including information relating to BlackLight's previously allowed patent applications. Following withdrawal of BlackLight's patent applications from issue, an abstract written by Dr. Zimmerman appeared on the APS' website boasting that the PTO and State Department had "fought back with success" against BlackLight. [See copy of Abstract in Attachment 6, Tab C of January 19, 2001 letter to Director Kepplinger]

Although the APS' "Deep Throat" contact has been brought to the PTO's attention on several occasions, so far, PTO officials have refused to cooperate in providing any information relating to this subject. Inasmuch as U.S. patent applications are to be held in strict confidence, obviously, any breach of that confidentiality would be deeply troubling, but particularly so if



The Honorable Robert G. Torricelli
May 10, 2001
Page 3 of 5

information was being disseminated to one of BlackLight's competitors. [See copy of July 10, 2000 Letter to State Department in Attachment 6, Tab C of January 19, 2001 letter to Director Kepplinger]

The PTO has also taken extreme positions, perhaps in concert with outside competitive forces, to thwart the granting of BlackLight's patents. These actions include muzzling and essentially replacing the Examiners who had previously allowed BlackLight's patent applications with a "Secret Committee" of PTO officials assigned the task of rejecting those applications behind "closed doors." To this day, Examiner Langel, who has 28 years of experience in prosecuting patent applications, believes BlackLight's energy patent applications represent significant technological advances and therefore are allowable. Recent discussions with Examiner Langel confirm that, while he believes the experimental evidence supporting allowance of the applications submitted by BlackLight is overwhelming, he is being instructed by the Secret Committee to reject the applications despite the lack of adequate basis to do so.

Attempts by BlackLight to learn the full composition of the PTO's "Secret Committee," including the identity of outside consultants and/or competitors who may have served illegally as committee members in further breach of PTO confidentiality, have been met with only antagonism and outright aggression. Such hostility toward patent applicants is, to our knowledge, unprecedented and in clear violation of fundamental principles of due process that can only erode the trust and confidence that the public places in the PTO.

Although BlackLight has satisfied, indeed exceeded, the statutory requirements of patentability for its novel energy technology, BlackLight's counsel and company executives met with PTO officials at an interview conducted at the PTO on February 21, 2001 in an attempt to resolve this matter. Specifically, BlackLight attempted to discern through this interview the newly-minted patent standards that were being used to thwart BlackLight's applications, as well as the composition of the Secret Committee and outside consultants that were assembled to lead the PTO's attack against BlackLight.

PTO officials attending the interview flatly refused to even discuss BlackLight's request seeking the complete identity of the PTO's Secret Committee members. Indeed, Secret Committee Examiner Jagannathan, who led the interview on behalf of the PTO, became quite indignant in his response to BlackLight's inquiry, claiming that this information was not germane to the prosecution and, in a harsh tone, threatened to shut down the interview if BlackLight further inquired into the matter. Ironically, without an initial investigation conducted by BlackLight's counsel, the identity of Secret Committee Examiner Jagannathan and his own involvement in subverting BlackLight's patent applications would never have become known and he would not have been forced to attend the interview. Unfortunately, his appearance at the interview was used as yet another opportunity to "stonewall" BlackLight's attempt to obtain answers to legitimate questions. [Attachment 1, PTO mailing dated February 12, 2001 identifying certain members of Secret Committee]



The Honorable Robert G. Torricelli
May 10, 2001
Page 4 of 5

The PTO also made clear during the interview that it did not feel constrained to follow established statutory standards of patentability—standards that BlackLight had already met in obtaining allowance upon the first complete examination—and that it was free to create new, more onerous standards of patentability that apply only to BlackLight. The PTO absolutely refused to provide any guidance as to the level of experimental evidence that would be required to once again convince the PTO to allow BlackLight's patent applications and even went so far as to require that BlackLight's experimental evidence be published and evaluated by its competitors before it could be considered. Surely, when enacting the patent statutes, Congress never intended that applicants' competitors oversee the granting of U.S. patents.

Unfortunately, prior attempts to investigate this matter by Senator Max Cleland have been similarly thwarted. Twice now, Senator Cleland has requested relevant information from the PTO and, in both instances, the PTO has refused to honor his request. [Attachment 2]

The first excuse the PTO gave for its refusal was that the matter was the subject of litigation between the PTO and BlackLight over the withdrawal of the allowed patent applications from issuance, presently pending before the Court of Appeals for the Federal Circuit. That excuse, however, is simply untrue since the parties stipulated in the litigation that any unidentified *ex parte* communications the PTO may have received from third parties resulting in the withdrawal of BlackLight's patent applications are not germane to whether the withdrawal itself was legal. Incredibly, the PTO has further argued that the present prosecution of BlackLight's patent applications is a proceeding separate and distinct from the litigation over the legality of withdrawing those applications from issue. And yet, when pressed a second time to provide information relating to the persons involved in the present prosecution of the subject applications, the PTO had the audacity to claim that such information was still not germane. [Attachment 3, Interview Summary] Please be assured that the limited information BlackLight seeks regarding the PTO's improper actions is not the subject of any litigation and, thus, the PTO's refusal to provide that information will not be resolved by any pending court proceeding.

Other attempts to extract this information from the PTO through official government channels have also failed. For instance, BlackLight sought to have Secretary of Commerce Donald Evans conduct an inquiry into this matter since his Department has direct jurisdiction over the administration of the PTO. Secretary Evans' office, however, declined to intervene believing that there were "no compelling reasons" to do so and merely referred the matter back to the PTO. [Attachment 4, February 14, 2001 letter from Nicholas P. Godici, Acting Under Secretary of Commerce for Intellectual Property]

The PTO's continued avoidance in dealing with this inquiry is simply unacceptable and so we are now turning to you for help. The commercial deployment of BlackLight's technology in the U.S. stands to significantly impact our country's energy policies in a very positive way and, in the process, bring notoriety to the State of New Jersey. The fair administration of the



The Honorable Robert G. Torricelli

May 10, 2001

Page 5 of 5

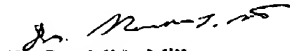
patent examination process, which hopefully will once again lead to the granting of patents on that technology, is an important step in that direction. Critical not just to BlackLight, but to all patent applicants, is knowing that the PTO is conducting itself with the utmost integrity and candor in the examination process. One way to assure ourselves of maintaining this worthy objective would be, with your help, to initiate an investigation into the PTO's improper actions by the General Accounting Office.

Any suggestions as to other actions we might take or other assistance you can provide in resolving this unfortunate situation would be greatly appreciated. Should you require any additional information regarding this matter, please feel free to contact my counsel, Jeffrey S. Melcher (202.261.1045) or Jeffrey A. Simenauer (202.261.1001), with any questions you may have.

In addition, in view of the potential importance of BlackLight's research to the United States and its close proximity to your New Jersey offices, we would be honored if you and certain of your staff would visit the company's facility in Cranbury for a personal briefing and tour of the laboratories, and witness for yourself the performance of our demonstration devices.

Thank you for your consideration of this important matter.

Sincerely yours,



Dr. Randell L. Mills
President, BlackLight Power, Inc.

Attachments



UNITED STATES
PATENT AND
TRADEMARK OFFICE

Administrator for External Affairs
Washington, DC 20231
www.uspto.gov

The Honorable Robert G. Torricelli
United States Senate
Washington, D.C. 20510-3003

AUG 14 2001

Dear Senator Torricelli:

Thank you for your letter on behalf of Dr. Randell L. Mills, President, Blacklight Power, Inc., regarding patent application serial number 09/009,294, and the circumstances concerning its withdrawal from issuance by the United States Patent and Trademark Office (USPTO).

Dr. Mills expresses concerns of "improper" acts by the USPTO, including the possibility of inappropriate communications with outside parties, with particular regard to the withdrawal of that application from allowance. In doing so, he offers a number of allegations to support his concerns.

However, the withdrawal from issue of patent application serial number 09/009,294 is the subject of litigation in the case of *Blacklight Power, Inc. v. Dickinson*, Civ. No. 00-0422 (D.D.C.). The case is currently on appeal to the Court of Appeals of the Federal Circuit from final judgment entered in favor of the USPTO on August 15, 2000, in the district court. Although Dr. Mills states that he does not consider the information requested regarding outside contacts, among other items, to be the subject of the litigation, it is our view that these issues were raised in the ongoing litigation. It would be inappropriate, therefore, to comment on this matter in detail. Furthermore, the application is still pending and the applicant possesses all procedural remedies, including, but not limited to, the opportunity to seek judicial relief.

In light of the pending status of the relevant litigation, any additional comment by the USPTO would be inappropriate.

We trust the foregoing will be useful in responding to your constituent. For your information, a similar letter of response about this matter is also being sent to Senator Jon S. Corzine.

Sincerely,

Robert L. Stoll
Administrator for External Affairs



ON S. CORZINE
NEW JERSEY

COMMITTEES:
LINKING, HOUSING, AND
URBAN AFFAIRS
ENVIRONMENT AND
PUBLIC WORKS
JOINT ECONOMIC

United States Senate

WASHINGTON, DC 20510-3004

502 SENATE HART OFFICE BUILDING
WASHINGTON, DC 20510
(202) 224-4744
ONE GATEWAY CENTER
11TH FLOOR
NEWARK, NJ 07102
(973) 645-3030
208 WHITE HORSE PIKE
SUITE 18-19
BARRINGTON, NJ 08007
(856) 757-5353

August 2, 2001

The Honorable Q. Todd Dickinson
United States Department of Commerce
Patent and Trademark Office
Washington, D.C. 20231

Re: Blacklight Power, Inc.'s Patent Application
Serial# 09/009,294

Dear Commisioner:

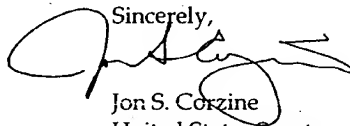
Enclosed is correspondence I received in reference to a matter involving your agency. This is a matter of particular interest to me and I would appreciate your fair and appropriate consideration.

In your reply, please reference Blacklight Power, Inc.

If you need further information, please contact Debbie Curto, Director of Constituent Services , at (973) 645 3502.

Again, thank you for your assistance.

Sincerely,



Jon S. Corzine
United States Senator

JSC:dpc

Enclosure



May 10, 2001

The Honorable Robert G. Torricelli, U.S. Senator
115 Dirksen Senate Building
Washington, DC. 20510

Re: Investigation of Improper Actions by U.S. Patent Office

Dear Senator Torricelli:

We kindly request your assistance in investigating and addressing the highly improper actions taken by the U.S. Patent and Trademark Office (PTO) against a constituent of yours, BlackLight Power, Inc. (BlackLight). These actions not only threaten the livelihood of a thriving New Jersey company, but threaten to undermine the integrity of the U.S. patent system, as well as diminish our ability to effectively cope with the looming energy crisis in this country.

BlackLight is a small start-up company located in Cranbury, New Jersey. It employs 35 individuals, most of whom are research scientists, engineers, and technicians. For the past three years since BlackLight located its operations in New Jersey, BlackLight has worked tirelessly and has spent millions of dollars developing a new, commercially feasible, clean process for producing electricity from hydrogen. BlackLight's technology represents a significant advance in the field of energy production and the company has built a substantial business and scientific team to commercialize products. This technology is based on Dr. Randell L. Mills' theory and experimentally verified process of utilizing catalysts to relax the electron in hydrogen atoms to lower energy levels to thereby release clean energy and produce novel chemical products. Rest assured that our technology is not based on "cold fusion" or other speculative technologies.

Blacklight's new energy production process and novel chemical products are easily reproducible and have been independently verified by prestigious universities, government agencies and laboratories. Early generation power cells were confirmed by MIT Lincoln Labs, INEL, Westinghouse Corporation, NASA Lewis, Chalk River National Laboratory, Thermacore Corporation, and Pennsylvania State University. The chemical products were predicted and analyzed by 20 different types of tests performed at over 20 independent laboratories. BlackLight recently submitted 22 journal articles to journals, 16 of which are presently in press or published, which broadly disclose the test results for general peer review. The articles overwhelmingly verify BlackLight's novel hydrogen chemistry by reporting data from extreme ultraviolet (EUV) spectroscopy, plasma formation, power generation, and analysis of chemical products. BlackLight has also made 22 presentations of its results at scientific meetings over the past two years.



1

The Honorable Robert G. Torricelli
May 10, 2001
Page 2 of 5

The most recent presentation at the National Hydrogen Association, 12th Annual U.S. Hydrogen Meeting and Exposition, resulted in an invitation to submit an article to the published meeting proceedings.

Because the theory involved is revolutionary and questions the validity of basic assumptions that underlie established Quantum Mechanics, Dr. Mills' work is highly controversial. And, as always is the case in "paradigm shifting" events, both Dr. Mills and his theory have been the subjects of criticism—and even derision—by a number of established and respected sources that have acknowledged their failure to even study BlackLight's published experimental results.

The promise inherent in the ultimate commercial application of BlackLight's theory to this nation and, indeed, to all mankind is truly staggering. It represents the potential capability for mankind to harness an unlimited source of energy with vastly lower environmental impacts from harmful waste product emissions or, as with nuclear energy systems, radioactive material disposition. With the advent of this nation's ever-increasing dependency on energy from politically unstable sources overseas, rapidly escalating fuel prices, and now the prospect of rolling blackouts, such as those already occurring in California, the need for alternative low-cost, abundant sources of energy in this country has never been greater.

As an initial step in bringing its energy technology to market, BlackLight sought to protect its intellectual property rights in that technology by filing numerous patent applications in the PTO. Unfortunately, the PTO has mishandled these applications and, in so doing, has failed to carry out its Constitutional mandate to advance the progress of science.

Specifically, evidence has been uncovered regarding the PTO's improper use of outside contacts, including officials from the State Department and the American Physical Society (APS) in what appears to be a concerted effort to subvert BlackLight's technology. For instance, there is strong evidence showing that PTO officials received unidentified *ex parte* communications from competitors of BlackLight that resulted in the PTO Commissioner withdrawing from issue several BlackLight applications that had been previously allowed. [Attachment 5, February 28, 2000 and Attachment 6, January 19, 2001 letters to Director Esther Keplinger of the PTO] Indeed, Dr. Peter Zimmerman, former Chief Scientist at the State Department, has admitted that Dr. Robert Park—spokesperson for the APS, a BlackLight competitor—uses a contact in the PTO that Dr. Park refers to as "Deep Throat" to obtain confidential information, including information relating to BlackLight's previously allowed patent applications. Following withdrawal of BlackLight's patent applications from issue, an abstract written by Dr. Zimmerman appeared on the APS' website boasting that the PTO and State Department had "fought back with success" against BlackLight. [See copy of Abstract



The Honorable Robert G. Torricelli
May 10, 2001
Page 3 of 5

in Attachment 6, Tab C of January 19, 2001 letter to Director Kepplinger]

Although the APS' "Deep Throat" contact has been brought to the PTO's attention on several occasions, so far, PTO officials have refused to cooperate in providing any information relating to this subject. Inasmuch as U.S. patent applications are to be held in strict confidence, obviously, any breach of that confidentiality would be deeply troubling, but particularly so if information was being disseminated to one of BlackLight's competitors. [See copy of July 10, 2000 Letter to State Department in Attachment 6, Tab C of January 19, 2001 letter to Director Kepplinger]

The PTO has also taken extreme positions, perhaps in concert with outside competitive forces, to thwart the granting of BlackLight's patents. These actions include muzzling and essentially replacing the Examiners who had previously allowed BlackLight's patent applications with a "Secret Committee" of PTO officials assigned the task of rejecting those applications behind "closed doors." To this day, Examiner Langel, who has 28 years of experience in prosecuting patent applications, believes BlackLight's energy patent applications represent significant technological advances and therefore are allowable. Recent discussions with Examiner Langel confirm that, while he believes the experimental evidence supporting allowance of the applications submitted by BlackLight is overwhelming, he is being instructed by the Secret Committee to reject the applications despite the lack of adequate basis to do so.

Attempts by BlackLight to learn the full composition of the PTO's "Secret Committee," including the identity of outside consultants and/or competitors who may have served illegally as committee members in further breach of PTO confidentiality, have been met with only antagonism and outright aggression. Such hostility toward patent applicants is, to our knowledge, unprecedented and in clear violation of fundamental principles of due process that can only erode the trust and confidence that the public places in the PTO.

Although BlackLight has satisfied, indeed exceeded, the statutory requirements of patentability for its novel energy technology, BlackLight's counsel and company executives met with PTO officials at an interview conducted at the PTO on February 21, 2001 in an attempt to resolve this matter. Specifically, BlackLight attempted to discern through this interview the newly-minted patent standards that were being used to thwart BlackLight's applications, as well as the composition of the Secret Committee and outside consultants that were assembled to lead the PTO's attack against BlackLight.

PTO officials attending the interview flatly refused to even discuss BlackLight's request seeking the complete identity of the PTO's Secret Committee members. Indeed, Secret Committee Examiner Jagannathan, who led the interview on behalf of the PTO, became quite indignant in his response to BlackLight's inquiry, claiming that



The Honorable Robert G. Torricelli
May 10, 2001
Page 4 of 5

this information was not germane to the prosecution and, in a harsh tone, threatened to shut down the interview if BlackLight further inquired into the matter. Ironically, without an initial investigation conducted by BlackLight's counsel, the identity of Secret Committee Examiner Jagannathan and his own involvement in subverting BlackLight's patent applications would never have become known and he would not have been forced to attend the interview. Unfortunately, his appearance at the interview was used as yet another opportunity to "stonewall" BlackLight's attempt to obtain answers to legitimate questions. [Attachment 1, PTO mailing dated February 12, 2001 identifying certain members of Secret Committee]

The PTO also made clear during the interview that it did not feel constrained to follow established statutory standards of patentability—standards that BlackLight had already met in obtaining allowance upon the first complete examination—and that it was free to create new, more onerous standards of patentability that apply only to BlackLight. The PTO absolutely refused to provide any guidance as to the level of experimental evidence that would be required to once again convince the PTO to allow BlackLight's patent applications and even went so far as to require that BlackLight's experimental evidence be published and evaluated by its competitors before it could be considered. Surely, when enacting the patent statutes, Congress never intended that applicants' competitors oversee the granting of U.S. patents.

Unfortunately, prior attempts to investigate this matter by Senator Max Cleland have been similarly thwarted. Twice now, Senator Cleland has requested relevant information from the PTO and, in both instances, the PTO has refused to honor his request. [Attachment 2]

The first excuse the PTO gave for its refusal was that the matter was the subject of litigation between the PTO and BlackLight over the withdrawal of the allowed patent applications from issuance, presently pending before the Court of Appeals for the Federal Circuit. That excuse, however, is simply untrue since the parties stipulated in the litigation that any unidentified *ex parte* communications the PTO may have received from third parties resulting in the withdrawal of BlackLight's patent applications are not germane to whether the withdrawal itself was legal. Incredibly, the PTO has further argued that the present prosecution of BlackLight's patent applications is a proceeding separate and distinct from the litigation over the legality of withdrawing those applications from issue. And yet, when pressed a second time to provide information relating to the persons involved in the present prosecution of the subject applications, the PTO had the audacity to claim that such information was still not germane. [Attachment 3, Interview Summary] Please be assured that the limited information BlackLight seeks regarding the PTO's improper actions is not the subject of any litigation and, thus, the PTO's refusal to provide that information will not be resolved by any pending court proceeding.



The Honorable Robert G. Torricelli
May 10, 2001
Page 5 of 5

Other attempts to extract this information from the PTO through official government channels have also failed. For instance, BlackLight sought to have Secretary of Commerce Donald Evans conduct an inquiry into this matter since his Department has direct jurisdiction over the administration of the PTO. Secretary Evans' office, however, declined to intervene believing that there were "no compelling reasons" to do so and merely referred the matter back to the PTO. [Attachment 4, February 14, 2001 letter from Nicholas P. Godici, Acting Under Secretary of Commerce for Intellectual Property]

The PTO's continued avoidance in dealing with this inquiry is simply unacceptable and so we are now turning to you for help. The commercial deployment of BlackLight's technology in the U.S. stands to significantly impact our country's energy policies in a very positive way and, in the process, bring notoriety to the State of New Jersey. The fair administration of the patent examination process, which hopefully will once again lead to the granting of patents on that technology, is an important step in that direction. Critical not just to BlackLight, but to all patent applicants, is knowing that the PTO is conducting itself with the utmost integrity and candor in the examination process. One way to assure ourselves of maintaining this worthy objective would be, with your help, to initiate an investigation into the PTO's improper actions by the General Accounting Office.

Any suggestions as to other actions we might take or other assistance you can provide in resolving this unfortunate situation would be greatly appreciated. Should you require any additional information regarding this matter, please feel free to contact my counsel, Jeffrey S. Melcher (202.261.1045) or Jeffrey A. Simenauer (202.261.1001), with any questions you may have.

In addition, in view of the potential importance of BlackLight's research to the United States and its close proximity to your New Jersey offices, we would be honored if you and certain of your staff would visit the company's facility in Cranbury for a personal briefing and tour of the laboratories, and witness for yourself the performance of our demonstration devices.

Thank you for your consideration of this important matter.

Sincerely yours,

Dr. Randell L. Mills
President, BlackLight Power, Inc.

Attachments





UNITED STATES
PATENT AND
TRADEMARK OFFICE

Administrator for External Affairs
Washington, DC 20231
www.uspto.gov

The Honorable Jon S. Corzine
United States Senate
One Gateway Center, 11th Floor
Newark, NJ 07102

AUG 14 2001

Attention: Debbie Curto

Dear Senator Corzine:

Thank you for your letter on behalf of Jeffrey S. Melcher, and his client, Dr. Randell L. Mills, President, Blacklight Power, Inc., regarding patent application serial number 09/009,294, and the circumstances concerning its withdrawal from issuance by the United States Patent and Trademark Office (USPTO).

Dr. Mills expresses concerns of "improper" acts by the USPTO, including the possibility of inappropriate communications with outside parties, with particular regard to the withdrawal of that application from allowance. In doing so, he offers a number of allegations to support his concerns.

However, the withdrawal from issue of patent application serial number 09/009,294 is the subject of litigation in the case of *Blacklight Power, Inc. v. Dickinson*, Civ. No. 00-0422 (D.D.C.). The case is currently on appeal to the Court of Appeals of the Federal Circuit from final judgment entered in favor of the USPTO on August 15, 2000, in the district court. Although Dr. Mills states that he does not consider the information requested regarding outside contacts, among other items, to be the subject of the litigation, it is our view that these issues were raised in the ongoing litigation. It would be inappropriate, therefore, to comment on this matter in detail. Furthermore, the application is still pending and the applicant possesses all procedural remedies, including, but not limited to, the opportunity to seek judicial relief.

In light of the pending status of the relevant litigation, any additional comment by the USPTO would be inappropriate.

We trust the foregoing will be useful in responding to your constituent. For your information, a similar letter of response about this matter is also being sent to Senator Robert G. Torricelli.

Sincerely,

Robert L. Stoll
Administrator for External Affairs



MAX CLELAND
GEORGIA

Telephone: (202) 224-3521
TDD/TTY: (202) 224-3203
www.senate.gov/~cleland

COMMITTEES:
ARMED SERVICES
COMMERCE
GOVERNMENTAL AFFAIRS
SMALL BUSINESS

United States Senate

WASHINGTON, DC 20510-1005

March 24, 2000

Ms. Janie Cooksey
Congressional Liaison
U.S. Department of Commerce
Patent and Trademark Office
Washington, DC 20231

Dear Ms. Cooksey:

The information enclosed is of the utmost importance to my constituent, Mr. Eric Jansson. The information provided raises significant questions about the procedures followed by the Patent and Trademark Office in the decision to withhold issuance of several patents.

I understand, from speaking to the representative of my constituent, that the decision to withhold issuance of these patents was made in a most unconventional fashion. I would very deeply appreciate a thorough review of this situation and a complete report on the basis for the decision which was made in this case.

As you will note, my constituent has a firm belief that the technology involved in this application has a very great commercial as well as social value. I would be grateful for all that you can do to assure that this matter is promptly addressed.

Thank you for your consideration.

Most respectfully,


Max Cleland
United States Senator

MC:jhs

SUITE 1700
75 SPRING STREET, S.W.
ATLANTA, GA 30303-3309
(404) 331-4811

SUITE 101
235 ROOSEVELT AVENUE
ALBANY, GA 31701-2372
(912) 430-7798

611 TELFAIR STREET
AUGUSTA, GA 30901-2324
(706) 722-4040

SUITE 101
120 12TH STREET
COLUMBUS, GA 31902-2461
(706) 649-7705

203 MARTIN LUTHER KING JR. BLVD.
DALTON, GA 30721-3004
(706) 275-8905

SUITE 203
401 CHERRY STREET
MACON, GA 31201-3384
(912) 755-1779

SUITE A
440 MALL BOULEVARD
SAVANNAH, GA 31406-4823
(912) 352-8283





UNITED STATES DEPARTMENT OF COMMERCE
Patent and Trademark Office
ASSISTANT SECRETARY AND COMMISSIONER
OF PATENTS AND TRADEMARKS
Washington, D.C. 20231

APR 21 2000

The Honorable Max Cleland
United States Senate
Washington, D.C. 20510-1005

Dear Senator Cleland:

Thank you for your recent letter concerning your constituent Eric Jansson.

The matter to which Mr. Jansson refers is currently in litigation in the case of *Blacklight Power, Inc. v. Dickinson*, Civ. No. 00-0422 (D.D.C.). It would be inappropriate, therefore, to comment in detail. Moreover, the application is still pending and the applicant possesses all procedural remedies, including, but not limited to, the opportunity to seek judicial relief.

The United States Patent and Trademark Office (USPTO) has moved for summary judgment in that litigation. Attached is a copy of the USPTO's Opposition to Plaintiff's Motion for Summary Judgment, including affidavits, recently filed in the litigation that addresses and denies the applicant's allegations concerning improper handling of the application.

I appreciate your letter and believe that the federal district court will fairly adjudicate the pending matter.

Sincerely,

Robert L. Stoll
Administrator for External Affairs

Enclosure



9.



UNITED STATES DEPARTMENT OF COMMERCE
Patent and Trademark Office
ASSISTANT SECRETARY AND COMMISSIONER
OF PATENTS AND TRADEMARKS
Washington, D.C. 20231

MAY 15 2000

The Honorable Max Cleland
United States Senate
Washington, D.C. 20510-1005

Dear Senator Cleland:

Thank you for your most recent letter on behalf of a constituent, Eric Jansson, regarding on-going litigation between the United States Patent and Trademark Office (USPTO) and Blacklight Power, Inc.

Your letter indicates that your constituent is an investor in Blacklight Power. In the litigation, Blacklight Power is represented by counsel. Thus, it would be inappropriate for the USPTO to communicate directly, or indirectly through your office, with a person represented by counsel. Moreover, any discovery in this matter should be conducted by counsel under the district court's supervision and procedures. Last, Blacklight Power is also represented by counsel before the USPTO in regards to its patent application. When counsel has appeared to represent the patent applicant, the USPTO does not conduct the patent application process with multiple parties nor with persons having some fractional interest in the patent application.

We appreciate your understanding of the nature of your request and your intention not to urge disclosure that would be inappropriate. The district court has scheduled a hearing on May 16, 2000, to hear arguments on the cross-motions for summary judgment. Given the pending litigation, issues concerning this application are best left for resolution by the parties counsel and the district court.

Sincerely,

A handwritten signature in cursive script that reads "Robert L. Stoll".

Robert L. Stoll
Administrator for External Affairs



United States Senate

WASHINGTON, DC 20510

December 20, 2001

Chairman Patrick Leahy
Senate Committee on the Judiciary
226 Dirksen Senate Office Building
Washington, D.C. 20510

Dear Chairman Leahy:

We are writing to you to bring to your attention actions taken by the United States Patent and Trademark Office (Patent Office) against BlackLight Power, Inc. In our opinion, if the allegations that are set forth in the accompanying documents are true, they raise questions about the conduct of some representatives of the Patent Office.

This issue was first brought to our attention over the last year and a half when BlackLight Power, Inc. contacted each of us regarding the Patent Office's withdrawal from issue of five BlackLight patent applications is apparently based on a revolutionary hydrogen chemistry that had been previously allowed after thorough examination. BlackLight's energy production technology is based on a novel catalytic process that releases large quantities of heat energy from hydrogen. This technology, which was invented by BlackLight's President and CEO, Dr. Randall L. Mills, and has been the subject of scientific studies conducted by over twenty independent laboratories and universities, may reduce U.S. dependence on foreign oil and eliminate environmental concerns.

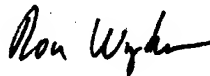
We have each written to the Patent Office for information about the facts or circumstances surrounding its consideration of the issuance of an earlier application as a patent to BlackLight (the '935 patent) that led to the subsequent withdrawal of BlackLight's patent application. However, the Patent Office has denied our requests for information because of its ongoing litigation with BlackLight.

It is important that the Patent Office not only maintain the confidentiality of patent applications but also conduct itself with the utmost integrity and candor during the entire application process. Consistent with established rules and regulations it is requested that the United States Senate Committee on the Judiciary review this matter. We are enclosing background materials and other supporting documentation to assist you. Thank you for your assistance with this matter.

Sincerely,



Max Cleland
United States Senator



Ron Wyden
United States Senator

Enclosures



United States Senate

WASHINGTON, DC 20510

December 20, 2001

The Honorable Donald L. Evans
Secretary of the U.S. Department of Commerce
14th Street and Constitution Avenue, N.W.
Suite 5854
Washington, D.C. 20230

Dear Secretary Evans,

We are writing to you to bring to your attention actions taken by the United States Patent and Trademark Office (Patent Office) against BlackLight Power, Inc. In our opinions, if the allegations that are set forth in the accompanying documents are true, they raise questions about the conduct of some representatives of the Patent Office.


This issue was first brought to our attention over the last year and a half when BlackLight Power, Inc. contacted each of us regarding the Patent Office's withdrawal from issue of five BlackLight patent applications which are apparently based on a revolutionary hydrogen chemistry that had been previously allowed after thorough examination. BlackLight's energy production technology is apparently based on a novel catalytic process that releases large quantities of heat energy from hydrogen. This pioneering technology, which was invented by BlackLight's President and CEO, Dr. Randall L. Mills, and has been the subject of scientific studies conducted by over twenty independent laboratories and universities, may reduce U.S. dependence on foreign oil and eliminate environmental concerns.

We have each written to the Patent Office for information about the facts or circumstances surrounding its consideration of the issuance of an earlier application as a patent to BlackLight (the '935 patent) that led to the subsequent withdrawal of BlackLight's patent application. However, the Patent Office has denied our requests for information because of its ongoing litigation with BlackLight. We also urge that the Patent Office establish communications with BlackLight in order to expedite the resolution of this matter.

It is critically important that the Patent Office not only maintain the confidentiality of patent applications but also conduct itself with the utmost integrity and candor during the entire patent application process. It is requested that the U.S. Department of Commerce review this matter, consistent with established rules and regulations, and we are enclosing background materials and other supporting documentation to assist you. Thank you for your assistance with this matter.

Sincerely,


Max Cleland
United States Senator


Ron Wyden
United States Senator

Enclosures



United States Senate

WASHINGTON, DC 20510

December 21, 2001

The Honorable Donald L. Evans
Secretary
Department of Commerce
14th Street and Constitution Avenue, N.W.
Suite 5854
Washington, D.C. 20230

Dear Secretary Evans:

We have been contacted regarding an ongoing dispute between BlackLight Power, Inc. and the U.S. Patent and Trademark Office. We ask for your assistance in reviewing this matter.

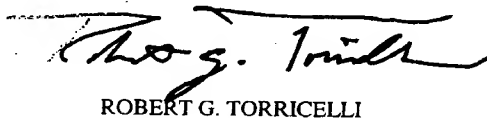
BlackLight Power is concerned about the rejection of five patent applications it submitted to the Patent and Trademark Office. According to the company, the applications were rejected despite the fact that BlackLight followed all applicable rules and procedures and the applications were initially approved by Patent Office examiners. BlackLight believes that the rejection of its applications was groundless and that the decision-making process was not fair and impartial.

We ask that your office review this matter to ensure that BlackLight's applications were reviewed in a fair manner consistent with the review of all patent applications.

Sincerely,



VON S. CORZINE



ROBERT G. TORRICELLI



Shelby T. Brewer

2121 Jamieson Avenue, Suite 1406
Alexandria, Virginia 22314

Tel: (703) 567-1284
Fax: (703) 566-7526
stbrewer@earthlink.net

December 21, 2001

VIA HAND DELIVERY

The Honorable James E. Rogan
Director, U.S. Patent and Trademark Office
Washington, D.C. 20231

Re: Patent Applications of BlackLight Power, Inc.

Dear Director Rogan:

I am writing to draw your attention to a matter involving the U.S. Patent and Trademark Office (PTO) that calls into question the professionalism, competence, and integrity of the PTO. As a former appointee (Reagan Administration, Assistant Secretary of Energy), technologist (nuclear engineering), and businessman (CEO and Chairman of several major US corporations over the past 15 years), I am heartened that you have finally taken up leadership of the PTO in the G.W. Bush Administration, and are in a position to reverse the sloth and abuses under the previous Administration. I have followed your public service career over the years, particularly your last term in the House, and am convinced that the President's choice to reform this critical agency could not have been more astute.

The matter that I invite your attention to involves the prosecution of a number of U.S. patent applications submitted by BlackLight Power, Inc., on whose Board of Directors I serve. My reasons for appealing to you in this matter are motivated not only by my fiduciary duty to protect BlackLight's best interests, but also by a sincere desire to assist you in avoiding unnecessary embarrassment this situation is sure to cause the Patent Office if left unresolved. We would be most pleased to personally meet with you and principles for the parties to see if together we can bring some closure to this matter in a way that is mutually acceptable to both sides.

Through your initial PTO briefing on important pending matters, you may be aware by now that five allowed applications relating to novel chemical compounds invented by BlackLight President and CEO, Dr. Randell L. Mills, were withdrawn from issue under extremely suspicious circumstances. That withdrawal led to a lawsuit that we filed in the D.C. District Court against Director Dickinson, which case was fully briefed and argued to the U.S. Court of Appeals for the Federal Circuit before a packed courtroom. The purpose of my letter is not to debate the legal issues in that case, as we are quite confident in our position based on the record presented to the Federal Circuit during oral argument. Rather, my aim is simply to make you aware of matters that PTO officials might have omitted from your initial briefing, including the prior administration's violation of well-established patent laws, rules, and procedures in prosecuting these and other BlackLight patent applications.



Director James E. Rogan
December 21, 2001
Page 2 of 5

To be sure, BlackLight fully expected that, like any pioneering technology, its novel hydrogen chemistry would be carefully scrutinized by the Patent Office during the application process. Indeed, the two highly-qualified Examiners originally assigned to review BlackLight's applications, Wayne Langel and Stephen Kalafut, conducted a thorough examination, initially questioning the operability of the disclosed technology on several grounds. Upon critical review of BlackLight's supporting scientific evidence, however, the Examiners issued U.S. Patent No. 6,024,935 ("the '935 patent") drawn to an energy cell and allowed the five other chemical compound applications that were subsequently withdrawn from issue.

Examiners Langel and Kalafut displayed the utmost professionalism and courtesy in prosecuting BlackLight's applications and we certainly commend them for their actions. Unfortunately, the same cannot be said for others whose actions in withdrawing and subsequently prosecuting these and other cases have undermined the U.S. patent system to the detriment of all patent applicants. I offer the following examples for your consideration as possible topics for future discussion:

(1) Undercutting the statutory presumption of validity under 35 U.S.C. § 282

Underlying this 50-year-old statute is the premise of administrative regularity, which presumes that well-trained examiners with expertise in their respective fields will properly carry out their examination duties by issuing only valid patents. This presumption was, in fact, confirmed by the capable work Examiners Langel and Kalafut performed in examining and issuing BlackLight's '935 patent. Nonetheless, PTO Associate Solicitor Kevin Baer, for some explained reason, attacked BlackLight by denigrating the entire patent system, including its examining corps, by stating in open court:

"[P]atent examiners do review [patent applications]. Unfortunately, patent examiners are swamped and sometimes things slip through."

"[E]xaminers are under tremendous pressure to produce work, and if they're going to approve [an application], they just approve it and kind of let it out the door."

Solicitor Baer's statements on behalf of the PTO should be alarming to just about everyone—with the possible exception of accused patent infringers—and most certainly do not reflect well on the agency. Part of our purpose in seeking a meeting is to make you aware of these and other outlandish statements and to give the PTO the opportunity to issue an appropriate public retraction.

(2) Disparagement of U.S. patents in violation of MPEP § 1701

According to this well-established PTO procedural guideline, "[p]ublic policy demands that every employee of the [Patent Office] refuse to express to any person any opinion as to the validity or invalidity of . . . any U.S. patent . . ." With the exception of exclusions that do not



Director James E. Rogan
December 21, 2001
Page 3 of 5

apply, "[t]he question of validity or invalidity is otherwise exclusively a matter to be determined by a court. Members of the patent examining corps are cautioned to be especially wary of any inquiry from any person outside the [Patent Office], including an employee of another Government agency, the answer to which might indicate that a particular patent should not have issued." The PTO clearly violated this admonition when it publicly disparaged the '935 patent on the record.

In yet another blatant violation of these PTO rules, Solicitor John Whealan responded to a reporter's inquiry by stating unequivocally for a soon-to-be published article that "the PTO issued BlackLight's '935 patent by mistake."

Once again, we wish to meet with you to discuss the PTO's retraction of these statements. More importantly, however, we seek an honest explanation why the PTO has singled out BlackLight for such disparate treatment and what can be done to put an end to it.

(3) PTO involvement with competitors of applicants in denying patent rights

Naturally concerned over who and what precipitated withdrawal of BlackLight's allowed applications from issue, we became suspicious that it might have been caused by competitors interfering with our valuable patent rights. Our suspicions heightened when we learned that Dr. Peter Zimmerman, former Chief Scientist for the State Department, had published an Abstract of an upcoming speech to the American Physical Society (APS), a BlackLight competitor, boasting that his Department and the Patent Office "have fought back with success" against BlackLight. In conversations with BlackLight's counsel, Dr. Zimmerman admitted that he received information concerning BlackLight's applications through e-mails from Dr. Robert Park, spokesman for the APS, who told him of a contact in the PTO referred to by Dr. Park as "Deep Throat."

If true, these actions would clearly violate the PTO's duty to maintain confidentiality of U.S. patent applications under 35 U.S.C. § 122, 18 U.S.C. § 2071, 37 C.F.R. § 1.14, and M.P.E.P. § 101, as well as raise other obvious concerns. We brought this information to the PTO's attention more than a year ago, but have yet to receive a response.

We would like to meet with you to discuss PTO investigations into this matter and the extent to which any breach of confidentiality may have occurred.

(4) Improperly creating new opposition procedures against the issuance of patents

Following withdrawal of BlackLight's applications from issue, counsel immediately began investigating the facts and circumstances surrounding that incident by questioning various PTO personnel. During that investigation, Director Esther Kepplinger admitted to counsel that she withdrew the applications in reaction to perceived heat—a "firestorm" as she put it—the Patent Office had received from an undisclosed outside source. Director Kepplinger further indicated that the withdrawal occurred only after the '935 patent had been brought to the



Director James E. Rogan
December 21, 2001
Page 4 of 5

attention of Director Dickinson by Gregory Arahorian, another PTO outsider well known for his public attacks on issued U.S. patents.

These events, which, in effect, created an entirely new, non-regulatory procedure for opposing the issuance of patents, are disturbing to say the least. In light of these circumstances, we firmly believe that we are entitled to a full accounting of how, out of the thousands of patents the PTO issues on a weekly basis, our '935 patent happened to come to its attention, thus leading to the withdrawal of other allowed applications.

Unfortunately, the PTO has been less than forthcoming in dealing with this matter as succinctly expressed by Solicitor Baer to District Court Judge Emmet G. Sullivan in the following comments: "I would even say, Your Honor, you could imagine in our head any scenario of how we learned about it. A blimp flying over us. It doesn't matter, because what matters, Your Honor, is the decision [to withdraw] itself." Apparently Judge Sullivan was unimpressed by those comments, noting in footnote 10 of his opinion his being "troubled by several steps in the PTO's process" and advising the PTO to "examine its patent issuance process so that their normal operations are not compromised by such seemingly suspicious procedures."

That worthwhile goal can only be fully achieved by a complete accounting of the events in question, which we hope will be among the topics discussed at an upcoming meeting.

(5) Withholding vital information concerning the examination process

Following Judge Sullivan's decision upholding the PTO's withdrawal procedure, now on appeal, the PTO replaced the original Examiners Langel and Kalafut with a "Secret Committee" to reject all BlackLight applications. To adequately respond, BlackLight's counsel has sought to discover the identity of all Committee members, as well as any outside consultants or competitors, involved in the examination process and the nature of their involvement. To our amazement, the PTO has thwarted those efforts at every turn, as well as similar inquiries into this matter by five U.S. Senators.

Through our own discovery efforts, one of the Secret Committee members contributing to the prosecution was identified as Vasudevan Jagannathan. Despite Examiner Jagannathan's role in examining our applications, he initially refused to admit his involvement. Examiner Jagannathan later refused to even attend an interview scheduled with Dr. Mills, counsel, and myself to discuss the pending rejections in an attempt to reach an agreement over the patentability of the claimed inventions. Examiner Jagannathan ultimately appeared at the interview, but only after being ordered to do so by his immediate supervisor, to whom we complained. The interview, however, almost ended as soon as it began when counsel requested full identification of those persons responsible for examining our pending applications. In response, Examiner Jagannathan became quite hostile, threatening to adjourn the interview if we further pressed that line of inquiry, unjustifiably asserting that it was "not germane" to the prosecution.



Director James E. Rogan
December 21, 2001
Page 5 of 5

We believe that such secret examination proceedings are not the way to conduct PTO business, especially in light of the suspicious circumstances surrounding withdrawal of BlackLight's applications. These proceedings do little to instill confidence in the examination process. Like any applicant, BlackLight is entitled to a fair hearing, which includes the right to directly confront those persons responsible for refusing us our patent grant. We hope that this issue will also be on the table for discussion should you be kind enough to grant us a meeting.

These are but a few of the more egregious examples of how the PTO has mishandled the examination process leading up to and following the withdrawal of BlackLight's applications from issue. Equally distressing is the substance of the Secret Committee's refusal to grant BlackLight's patents based on challenges to the operation of our disclosed hydrogen technology.

BlackLight has submitted an unprecedented amount of scientific evidence—costing tens of millions of dollars to produce—proving beyond question the operability of our technology. As former Assistant Secretary of Energy in the Reagan administration with a Ph.D. in Nuclear Engineering from M.I.T., I can personally attest to this fact. Anyone, however, with even a basic understanding of chemistry and, more importantly, an open mind willing to look seriously at our data, can confirm for themselves that Dr. Mills' novel hydrogen chemistry is producing truly astonishing results.

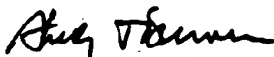
Incredibly, the Secret Committee has basically dismissed our scientific evidence or ignored it altogether on the basis that it supposedly violates "ideas" of modern science. For example, the scientific evidence we submitted includes spectroscopic data that is extraordinarily reliable in analyzing chemical compositions. Such data amounts to a "chemical fingerprint" that cannot be seriously disputed. Yet, Examiner Jagannathan dismissed that conclusive evidence out of hand as nothing more than "a bunch of squiggly lines."

Words can hardly express the extreme frustration—and forgive me for saying, deep resentment—we feel in having our pioneering technology treated in such a cavalier way. I could go on and on citing other examples of similar indignities suffered at the hands of the Secret Committee and, hopefully, we will be allowed to convey those details to you in person. Suffice it to say for now that the positions espoused by the Committee hardly satisfy the Constitutional directive that the patent system "promote the progress of science and the useful arts."

Please let me know at your earliest convenience if you share our desire for a meeting to discuss this matter. If you do, please further consider holding this meeting at our facilities in Cranbury, New Jersey so that you can witness first hand our working prototypes of Dr. Mills' energy cell and his assortment of novel hydride compounds exhibiting unusual properties.

I look forward to receiving your response and wish you well in your new undertaking.

Most sincerely,



Shelby T. Brewer



Testing the Current

By Charles Platt

Sunday, June 25, 2000; X05

VOODOO SCIENCE

The Road From Foolishness to Fraud

By Robert L. Park

Oxford Univ. 230 pp. \$25

For almost two decades, former physicist Robert Park has conducted a one-man search-and-destroy mission against inventors, scientists and pseudoscientists who make claims that he describes as "totally, indisputably, extravagantly wrong." As a Washington lobbyist and PR flack for the American Physical Society, Park is widely quoted whenever journalists need a rebuttal source who will scoff pithily at concepts such as magnetic healing or antigravity. He helped to establish a prestigious study panel that debunked Ronald Reagan's Star Wars Strategic Defense Initiative, and campaigned to discredit New Yorker journalist Paul Brodeur, who warned of possible health hazards caused by electromagnetic radiation from power lines. These and other battles are retold in Park's new book, *Voodoo Science*, which denounces the culprits he has most loved to hate over the years.

This book could have served a useful purpose. If public funds or private-investment capital really are being squandered by researchers who are self-deluded or even fraudulent, we need a thorough investigation. Alas, thoroughness is not Park's strong suit.

His primary source of information, quoted repeatedly in many of his rants, is the nightly TV news. Nothing seems to enrage him more than the sight of some upstart inventor getting air time for results that don't make sense; and Park's anger permeates his rebuttals, which border on character assassination. He contemptuously dismisses scientist James Patterson, for example, as a "caricature of an inventor" purely because of his physical appearance. There's no mention of his claim to fame as codeveloper of the fundamental laboratory technique of gas chromatography or his past consultancy work for Dow Chemical, Fairchild Semiconductor, Lockheed and the Atomic Energy Commission. Nor does Park allow Patterson any chance to explain or defend his work. In fact, none of the targets in *Voodoo Science* is allowed to speak for himself, apparently because Park chose not to talk to any of them.

This armchair journalism leads to some blunders. For instance, he mocks credentialed NASA scientists for investigating a gravity-shielding effect that he feels would violate a basic law of thermodynamics. If he had spoken to the researchers, they might have told him (as they told other journalists) why their theories entail no conflict with thermodynamics at all. Also, Park might have learned that the Russian emigre who prompted this work is not an obscure physicist (as he states) but a materials scientist claiming authorship of 30 papers and 10 patents.

Park's failure to gather first-hand data is unfortunate, but his selective omissions are far more serious. In at least one case, he violates basic principles of journalism and science itself by apparently suppressing information that conflicts with his foregone conclusion. He dismisses the phenomenon of nuclear fusion at low temperatures as "no closer to being proven than it was the day it was announced," despite hundreds of papers, including many from scientists affiliated with respected



universities, going far beyond the controversial claims that were made for "cold fusion" in 1989. Electrochemist Michael McKubre, at SRI International, confirms that he has submitted his papers to Park, who also attended a conference last year including presentations on this topic. Park chooses to mention none of this.

Such tactics are reminiscent of the behavior of a zealous DA who is so convinced that a suspect is guilty that he feels entitled to withhold some information from the jury. Since Park also "convicts" his suspects almost entirely by paraphrasing them in his own words, Voodoo Science is not the fair trial we might have hoped for.

This is unfortunate, because many of Park's targets have indeed made implausible claims, and may be guilty as charged. To be sure of this, however, we need a fairly argued refutation, not a perfunctory dismissal. The dividing line between valid data and artifacts is not always clear; the phenomenon of superconductivity, for instance, remained inexplicable for 42 years, as Park himself admits.

Despite Park's absolute faith in his own judgment, any rush to judgment entails a risk of convicting innocent people, while search-and-destroy missions may tend to cause collateral damage. This is a serious matter, since even poorly documented vitriol can jeopardize a scientist's reputation and future funding if it is disseminated with the complicity of a respected organization such as the American Physical Society.

Of course, so long as Park makes no mistakes, he may argue that his targets deserve their punishment. Still, his widely published attacks create a chilling effect that can discourage even legitimate scientists from discussing controversial work. This hardly seems consistent with the spirit of genuinely free inquiry that should energize science. Likewise, Park's reliance on second-hand data, his presentation of selective evidence and his refusal to quote his opponents are habits that seem unworthy of a scientist.

Charles Platt is a senior writer for Wired magazine.

© 2000 The Washington Post Company



IN THE UNITED STATES PATENT AND TRADEMARK OFFICE

In re PATENT Application of Mills

Group Art Unit: 1745

Application No. 09/009,294

Examiner: Kalafut

Filed: January 20, 1998

For: HYDRIDE COMPOUNDS

* * * * *

Filed Via Facsimile

November 19, 2001

**REQUEST FOR RECONSIDERATION
OF DECISION ON PETITION**

Director Jacqueline M. Stone
Technology Center 1700
United States Patent and Trademark Office
Washington, D.C. 20231

Director Stone:

Applicant kindly requests reconsideration of the Decision on Petition (Paper No. 37) denying Applicant's request to withdraw the finality of the Office Action mailed July 3, 2001.

I. Introduction

The PTO, through its Decision, effectively punishes Applicant for merely having requested a full and fair consideration of experimental data and other technical evidence that had been of record for almost 4 years in this case. The "Secret Committee," which is now prosecuting the subject application, for the first time took a position on that evidence in a Final Rejection, contrary to PTO rules, in what appears to be yet another attempt to subvert Applicant's technology.¹

The Decision, however, completely ignores these and other relevant facts, thus

¹ Applicant's March 1, 2001 response in this case provides background as to the genesis of the "Secret Committee" and some of the other unfair procedures that have been invoked against Applicant in prosecuting this and other BlackLight applications.



2

3

4

failing to even respond to the grounds on which Applicant's Petition was based. Instead, it merely maintains that the Final Rejection is based on the same statutory grounds and the same reasoning as the first Office Action, and responds to other evidence and arguments submitted by Applicant that have no bearing on whether the finality of that rejection was premature. As such, the Decision should be withdrawn and the Petition granted for the reasons set forth therein and as further explained below.

II. Applicant's Petition Made A Compelling Case for
Withdrawing the Finality of the July 3 Office Action

Applicant's Petition lays out in considerable detail the factual and legal bases for withdrawing the premature finality of the July 3 Office Action, as it introduced new substantive grounds of rejection that were neither necessitated by amendment of the claims, nor based on information submitted in an information disclosure statement. Because the Decision fails to even acknowledge the underlying relevant facts that inextricably lead to that conclusion, let alone consider them, a brief summary of those facts is in order.

As noted in Applicant's Petition, Examiner Kalafut thoroughly reviewed the scientific evidence of record and, based on that review, found this application to be in condition for allowance. Following the controversial withdrawal of this application from issuance, the PTO, through its "Secret Committee," issued a first Office Action, dated September 1, 2000, rejecting all claims under 35 U.S.C. §§ 101 and 112.² Applicant's Response, dated March 1, 2001, noted several deficiencies in that Office Action without amending the claims, particularly the Secret Committee's failure to consider the scientific evidence already made of record and its failure to adequately address supposed shortcomings in Applicant's theory underlying his claimed invention.

² The withdrawal of BlackLight's applications from issue resulted in District Court litigation, which case is pending on appeal at the Federal Circuit. [*BlackLight Power, Inc. v. Q. Todd Dickinson*, No. 00-1530]



The Petition further noted the Secret Committee's attempt—unsuccessful though it was—to overcome those deficiencies in its July 3 Final Office Action. Applicant provided specific examples demonstrating how, in that action, the Committee unfairly raised new substantive grounds of rejection by addressing for the very first time record evidence and other previously submitted technical information that should have been addressed in its first Office Action. Applicant further cited numerous examples of new state-of-the-art books and journals that were relied upon by the Secret Committee and newly-minted arguments that also could have and should have been presented earlier so as to develop a clear issue prior to appeal.

For these and other reasons more fully developed in the Petition, Applicant argued that the finality of the July 3 Office Action was premature and should be withdrawn.

III. The Decision Completely Ignores Relevant Facts and Fails to Respond to the Grounds on Which Applicant's Petition was Based

Incredibly, the Decision does not so much as mention a single relevant fact that formed the basis for Applicant's Petition.³ Rather, the Decision conveniently ignores these facts in arguing that the Final Rejection was proper because it was based on the same statutory grounds as the first Office Action:

In the instant case, no new ground of rejection was applied by the examiner in the final office action. The 35 USC 101 and 112, first paragraph rejections were the same as those in the previous non-final action. . . . [Decision at 2]

That argument, however, is nonsensical and misinterprets the PTO's procedural guidelines on this issue, found in MPEP § 706.07(a), which provide in pertinent part:

³ Inasmuch as the PTO is not disputing any of these facts, they must be accepted as true.



Under present practice, second or any subsequent actions on the merits shall be final, except where the examiner introduces a new ground of rejection that is neither necessitated by applicant's amendment of the claims nor based on information submitted in an information disclosure statement. [Emphasis added.]

The problem with the Decision is that it improperly equates the introduction of a "new ground of rejection" with the raising of a new statutory basis for rejection. That is not the correct standard to be applied in considering whether an Office Action was prematurely made final. The Decision compounds this error by completely ignoring Applicant's Petition arguments showing that the Final Office Action introduced new substantive grounds of rejection under the same statutory provisions, i.e., Sections 101 and 112.

As the PTO well knows, a "new ground of rejection," as referred to in Section 706.07(a), does not require that a new statutory basis be raised. Indeed, the MPEP recognizes situations in which a subsequent Office Action raising a new substantive basis for a rejection, even under precisely the same statutory provision as a prior Office Action, must be made non-final. For example, a second Office Action introducing a rejection under 35 U.S.C. § 103 based upon newly cited art, not necessitated by amendment, would not be made final simply because the claims were previously rejected under that same statutory basis for obviousness. [MPEP § 706.07(a)]

Rejections issued under Sections 101 and 112 are no different and, therefore, should be afforded the same treatment. The PTO's refusal to even consider this aspect of Applicant's Petition is just another example of the arbitrary and capricious way it has handled this case and related applications.

In what seems a desperate grasping at straws, the Decision refers to the fact that the examiner [in actuality the Secret Committee] "specifically referred back to [the] non-final Office action for the reasoning behind the rejections." [Decision at 1.] While that may be technically true, it does not change the fact that additional reasoning was provided as a basis for the final rejection of claims. More significantly, those reasons



were presented for the first time in response to Applicant's specific criticism of the Secret Committee for not providing that reasoning in the first Office Action. Again, that was the basis for Applicant's Petition and simply ignoring these relevant facts will not make them go away.

In apparent recognition that the Final Rejection does in fact present additional reasoning, the Decision asserts that because this reasoning was submitted in response to Applicant's arguments, it should not be considered a new ground of rejection:

The arguments put forth by the examiner do not constitute a new ground of rejection in that they merely respond to arguments presented by Applicant and do not change the basis for the rejections (i.e. the rejections are still based on lack of novelty and enablement as set forth in the previous office action.) [Decision at 2.]

Such argument again simply ignores the fact that among the arguments the Secret Committee addressed for the first time in its Final Rejection were those criticizing its failure to consider the scientific evidence already of record and other technical information. The incredible irony here is that, after acknowledging Applicant's criticisms by supplementing its first Office Action with additional reasoning, the PTO then justifies the finality of this subsequent action by claiming it was merely done in response to Applicant's arguments. While that may be true in a hyper-technical sense, it is simply not a fair representation of the facts in this case.

Applicant further notes that the Decision cites a portion of MPEP § 706.07 that provides: "Before final rejection is in order a clear issue should be developed between the examiner and applicant." The problem with the Decision, however, is that it refuses to even acknowledge, much less analyze, the relevant facts in the case showing that a clear issue had not been developed prior to Final Rejection. The Decision further neglects to cite the additional portion of Section 706.07 providing that:

The examiner should never lose sight of the fact that in every case the applicant is entitled to a full and fair hearing, and that a clear issue between applicant and examiner should be developed, if possible, before appeal.



Application No. 09/009,294
November 19, 2001
Page 6 of 6

The Decision's failure to even address the relevant facts presented as the basis for Applicant's Petition is but another example of the PTO's reluctance to provide such a full and fair hearing.

Please charge any required petition fees to our deposit account No. 50-0687, under order No. 62226.

IV. Conclusion

Based on the foregoing reasons, the Decision on Petition should be reconsidered and modified to grant Applicant's request that the finality of the July 3 Office Action be withdrawn as premature.

Respectfully submitted,
Manelli Denison & Selter PLLC

By 

Jeffrey S. Melcher
Reg. No.: 35,950
Tel. No.: (202) 261-1045
Fax. No.: (202) 887-0336

Customer No. 20736



FROM

Manelli, Denison & Selter PLLC

Customer No. 20736

Telephone: (202) 261-1000

Our Facsimile #: (202) 887-0336

FACSIMILE TRANSMISSION

TO: UNITED STATES PATENT AND TRADEMARK OFFICE

DELIVER TO: **Director Jacqueline M. Stone**

FACSIMILE #: 703.305.3602

No. Pages (Including this page) 7 FAX Opr: JSM

IF YOU DO NOT RECEIVE CLEARLY ALL PAGES, PLEASE CONTACT US IMMEDIATELY

By Telephone **AT: (202) 261-1045** (local)

->->->

USPTO:

PLEASE ACKNOWLEDGE CLEAR RECEIPT OF ALL PAGES
INDICATED ABOVE BY FAXING THIS PAGE BACK TO
ONE OF OUR FACSIMILE NUMBERS STATED ABOVE

In re PATENT APPLICATION of
Inventor(s): Mills

Group Art Unit: 1745

Appln. No.: 09/009,294

Examiner: Kalafut

Filing Date: 1/20/1998

Title: HYDRIDE COMPOUNDS

Name or type of signed paper being transmitted: Amendment

CERTIFICATE OF FACSIMILE TRANSMISSION

I hereby certify that this paper is being facsimile transmitted to the Patent and Trademark Office on the date shown below.

Name Jeff Melcher Sig.  Date November 19, 2001



Confirmation Report - Memory Send

Time : Nov-19-2001 03:20pm
Tel line : +2028870336
Name : MANELLI DENISON + SELTER PLLC

Job number : 264
Date : Nov-19 03:12pm
To : 1045#62226#7033053602
Document pages : 007
Start time : Nov-19 03:16pm
End time : Nov-19 03:20pm
Pages sent : 007
Status : OK

Job number : 264

*** SEND SUCCESSFUL ***

FROM

Manelli, Denison & Selter PLLC
Customer No. 20736
Telephone: (202) 261-1000

Our Facsimile #: (202) 887-0336

FACSIMILE TRANSMISSION

TO: UNITED STATES PATENT AND TRADEMARK OFFICE

DELIVER TO: Director Jacqueline M. Stone

FACSIMILE #: 703.305.3602

No. Pages (Including this page) 7 FAX Opr: JSM

IF YOU DO NOT RECEIVE CLEARLY ALL PAGES, PLEASE CONTACT US IMMEDIATELY
By Telephone AT: (202) 261-1045 (local)

USPTO:

PLEASE ACKNOWLEDGE CLEAR RECEIPT OF ALL PAGES
INDICATED ABOVE BY FAXING THIS PAGE BACK TO
ONE OF OUR FACSIMILE NUMBERS STATED ABOVE

In re PATENT APPLICATION of
Inventor(s): Mills

Group Art Unit: 1745

Appln. No.: 09/009,294

Examiner: Kalafut

Filing Date: 1/20/1998

Title: HYDRIDE COMPOUNDS

Name or type of signed paper being transmitted: Amendment

CERTIFICATE OF FACSIMILE TRANSMISSION

I hereby certify that this paper is being facsimile transmitted to the Patent and Trademark Office on the date shown below.

Name Jeff Melcher Sig. [Signature] Date November 19, 2001



Origin of quantum-mechanical complementarity probed by a 'which-way' experiment in an atom interferometer

S. Dürr, T. Nonn & G. Rempe

Fakultät für Physik, Universität Konstanz, 78457 Konstanz, Germany

BEST AVAILABLE COPY

The principle of complementarity refers to the ability of quantum-mechanical entities to behave as particles or waves under different experimental conditions. For example, in the famous double-slit experiment, a single electron can apparently pass through both apertures simultaneously, forming an interference pattern. But if a 'which-way' detector is employed to determine the particle's path, the interference pattern is destroyed. This is usually explained in terms of Heisenberg's uncertainty principle, in which the acquisition of spatial information increases the uncertainty in the particle's momentum, thus destroying the interference. Here we report a which-way experiment in an atom interferometer in which the 'back action' of path detection on the atom's momentum is too small to explain the disappearance of the interference pattern. We attribute it instead to correlations between the which-way detector and the atomic motion, rather than to the uncertainty principle.

In classical physics, a particle moves along a well-defined trajectory. A quantum object, however, reveals its wave character in interference experiments in which the object seems to move from one place to another along several different paths simultaneously. It is essential that these ways are indistinguishable, because any attempt to observe which way the object actually took unavoidably destroys the interference pattern.

The usual explanation for the loss of interference in a which-way experiment is based on Heisenberg's position-momentum uncertainty relation. This has been illustrated in famous 'gedanken' experiments like Einstein's recoiling 'slit' or Feynman's light microscope¹. In the light microscope, electrons are illuminated with light immediately after they have passed through a double slit with slit separation d . A scattered photon localizes the electron with a position uncertainty of the order of the light wavelength, $\Delta z \approx \lambda_{\text{light}}$. Owing to Heisenberg's position-momentum uncertainty relation, this localization must produce a momentum uncertainty of the order of $\Delta p_z \approx h/\lambda_{\text{light}}$. This momentum uncertainty arises from the momentum kick transferred by the scattered photon. For $\lambda_{\text{light}} < d$, which-way information is obtained, but the momentum kick is so large that it completely washes out the spatial interference pattern.

However, Scully *et al.*² have recently proposed a new gedanken experiment, where the loss of the interference pattern in an atomic beam is not related to Heisenberg's position-momentum uncertainty relation. Instead, the correlations between the which-way detector and the atomic beams are responsible for the loss of interference fringes.

Such correlations had already been studied experimentally. They are, for example, responsible for the lack of ground-state quantum beats in time-resolved fluorescence spectroscopy³. Other examples are neutron interferometers, where which-way information can be stored by selectively flipping the neutron spin in one arm of the interferometer^{4,5}.

Nevertheless, the gedanken experiment of Scully *et al.* was criticized by Storey *et al.*⁶, who argued that the uncertainty relation always enforces recoil kicks sufficient to wash out the fringes. This started a controversial discussion⁴⁻¹¹ about the following question: "Is complementarity more fundamental than the uncertainty

principle?"¹² This motivated Wiseman *et al.*^{13,14} to investigate what constitutes a momentum transfer in a double-slit experiment. They call the usual momentum transfer, like that in Feynman's light microscope, a "classical" kick; in addition, they define the concept of "quantum" momentum transfer. They find that the loss of interference need not be due to "classical" kicks. In this case the "quantum" momentum transfer cannot be less than that required by the uncertainty principle, so that these "quantum" kicks wash out the fringes.

In this context, Eichmann *et al.*¹⁵ performed an experiment with a light interferometer, where the double slit is replaced by two trapped ions, which can store which-way information in internal states. This scheme was criticized¹⁶ because the ions play a double role: they act as sources of elementary waves (just like a double slit) and simultaneously as a which-way detector. Hence the momentum transfer from the double slit and the which-way detector cannot be separated.

Here we report on a which-way experiment with an atom interferometer. A microwave field is used to store the which-way information in internal atomic states. We study the mechanical effect of the which-way detection on the atomic centre-of-mass motion separately, and find that the "classical" momentum kicks are much too small to wash out the interference pattern. Instead, correlations between the which-way detector and the atomic motion destroy the interference fringes. We show that the back action onto the atomic momentum implied by Heisenberg's position-momentum uncertainty relation cannot explain the loss of interference.

The atom interferometer

Figure 1 shows a scheme of our atom interferometer. An incoming beam of atoms passes through two separated standing wave light beams. The detuning of the light frequency from the atomic resonance, $\Delta = \omega_{\text{light}} - \omega_{\text{atom}}$, is large so that spontaneous emission can be neglected. The light fields each create a conservative potential U for the atoms, the so-called light shift, with $U \propto I/\Delta$, where I is the light intensity (see, for example, ref. 13). In a standing wave the light intensity is a function of position, $I(z) = I_0 \cos^2(k_{\text{light}} z)$, where k_{light} is the wavevector of the light. Hence the light shift potential takes the form $U(z) = U_0 \cos^2(k_{\text{light}} z)$, with $U_0 \propto I_0/\Delta$.

The atoms are Bragg-reflected from this periodic potential, if they enter the standing light wave at a Bragg angle (see, for example, ref. 14). This process is similar to Bragg reflection of X-rays from the periodic structure of a solid-state crystal, but with the role of matter and light exchanged. In our experiment, the light creates the periodic structure, from which the matter wave is reflected.

The standing light wave splits the incoming atomic beam A (see Fig. 1) into two beams, a transmitted beam C and a first-order Bragg-reflected beam B. The angle between the beams B and C corresponds to a momentum transfer of exactly $2\hbar k_{\text{light}}$ as determined by the spatial period of $U(z)$. By varying the light intensity, the fraction of reflected atoms can be adjusted to any arbitrary value. In our experiment, the reflectivity of the beam splitter is tuned to $\sim 50\%$.

After switching off the first standing light wave, the two beams are allowed to propagate freely for a time interval t_{sep} . During this time, beam B moves a horizontal distance $d/2$ to the left and beam C moves $d/2$ to the right. The longitudinal velocities (vertical in Fig. 1) of the two beams are not affected by the light field. Then a second standing light wave is switched on, which also serves as a 50% beam splitter. Now two atomic beams D and E are travelling to the left, while beams F and G are travelling to the right. In the far field, each pair of overlapping beams produces a spatial interference pattern. The fringe period is the same as in a double-slit experiment with slit separation d . The relevant wavelength is the de Broglie wavelength associated with the momentum of the atoms. The envelope of the fringe pattern is given by the collimation properties of the initial atomic beam A.

The experiment is performed with the apparatus described in ref. 15. Rb atoms are loaded into a magneto-optical trap (MOT). After trapping and cooling, the cloud of atoms is released and falls freely through the apparatus. The resulting pulsed atomic beam is collimated with a mechanical slit 20 cm below the MOT. The atoms then pass the interaction region with the standing light wave inside a microwave resonator. In the far field of the interaction region, 45 cm below the MOT, the atomic position distribution is observed by exciting the atoms with a resonant laser beam and detecting the fluorescence photons. The interaction time t_{int} of the atoms with the standing light wave is controlled by switching the light on and off. The small atomic velocity of 2 m s^{-1} in the

interaction region allows us to perform the whole interferometer experiment with only one standing light wave, which is switched on and off twice. As compared to ref. 15, only a few changes have been made. The width of the collimation slit was changed to $450 \mu\text{m}$. In order to improve the position resolution, the horizontal waist of the detection laser beam was reduced to $20 \times 50 \mu\text{m}$, and a second collimation slit with a width of $100 \mu\text{m}$ was added 1 cm below the MOT. Finally, the preparation of the internal atomic state was improved by removing atoms in wrong Zeeman sublevels.

Figure 2 shows the spatial fringe pattern in the far field for two different values of t_{sep} . We note that the observed far-field position distribution is a picture of the atomic transverse momentum distribution after the interactions.

Storing which-way information

A second quantum system is now added to the interferometer in order to store the information whether the atom moved along way B

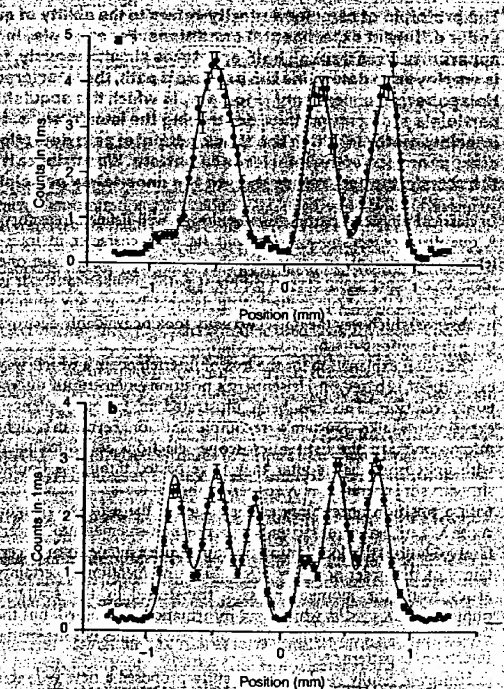


Figure 2 Spatial fringe pattern in the far field of the interferometer. The data were obtained with $t_{\text{sep}} = 45 \mu\text{s}$, and the 50% beam splitter was realized with $|U_0| = \hbar^2 \pi^2 / 2m\lambda^2$. We chose $t_{\text{int}} = 105 \mu\text{s}$ with $d = 1.3 \mu\text{m}$ (a), and $t_{\text{int}} = 255 \mu\text{s}$ with $d = 3.1 \mu\text{m}$ (b). In both cases, the fringe period is in good agreement with the theoretical expectation. Each solid line represents a fit to the experimental data. The best-fit values for the visibilities are $(75 \pm 1)\%$ and $(44 \pm 1)\%$, respectively. The reduced visibility for the case of the narrow fringes is due to the finite position resolution of our apparatus. The dashed lines represent the independently measured beam envelope, which consists of two broad peaks. The right peak is due to beams F and G (see Fig. 1), with a shape determined by the momentum distribution of the initial beam A. The left peak is a combination of beams D and E. It is a Bragg-reflected picture of the right peak. The fringe patterns under these two broad peaks are complementary, that is, the interference maxima in the left peak correspond to interference minima in the right peak, and vice versa.

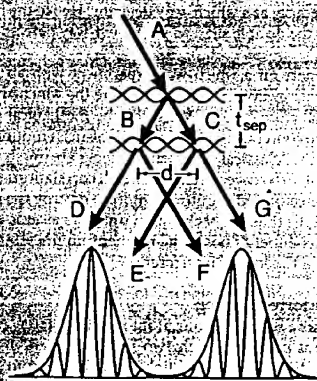


Figure 1 Schematic of the atom interferometer. The incoming atomic beam A is split into two beams: beam C is transmitted and beam B is Bragg-reflected from a standing light wave. The beams are not exactly vertical, because a Bragg condition must be fulfilled. After free propagation for a time t_{sep} , the beams are displaced by a distance d . Then the beams are split again with a second standing light wave. In the far field, a spatial interference pattern is observed.

or C. Two internal electronic states of the atom are used as a which-way detector system. A simplified level scheme of ^{87}Rb is shown in Fig. 3a. Rabi oscillations between states $|2\rangle$ and $|3\rangle$ can be induced by applying a microwave field at ω_{mw} . To describe the information storing process, we first investigate the properties of one single Bragg beam splitter, using a simple model, whose validity will be discussed later. The frequency of the standing light wave ω_{light} is tuned halfway between the $|2\rangle \leftrightarrow |2\rangle$ and $|3\rangle \leftrightarrow |3\rangle$ transitions. Hence the detunings from these transitions, Δ_2 and Δ_3 , have the same absolute value but opposite sign. The reflectivity of the beam splitter (that is, the probability of reflecting an atom) depends on $\hbar\omega_{\text{light}}/U_0$, and it is independent of the internal state.

However, the amplitude of the wavefunction experiences a phase shift which depends on the internal atomic state. A simple analogy for this phase shift can be found in light optics: a light wave reflected from an optically thicker medium experiences a phase shift of π , while reflection from an optically thinner medium or transmission into an arbitrary medium does not cause any phase shift. This argument also applies in atom optics: in our experiment, an atom in $|2\rangle$ sees a negative light shift potential (because $\Delta_2 < 0$), corresponding to an optically thicker medium, while an atom in $|3\rangle$ sees a positive potential (because $\Delta_3 > 0$), corresponding to an optically thinner medium. Hence an atom will experience a π phase shift only if it is reflected in $|2\rangle$.

This phase shift can be converted into a population difference between the hyperfine levels. For that purpose two microwave $\pi/2$ pulses resonant with the hyperfine transition are applied. They form a Ramsey scheme as shown in Fig. 3b. The atom is initially prepared in state $|2\rangle$. Then a microwave $\pi/2$ pulse is applied, converting the internal state to the superposition state $(|3\rangle + |2\rangle)/\sqrt{2}$. After this, the atom interacts with the standing light wave. As explained above, the atom will experience a π phase shift only if it is reflected and in state $|2\rangle$. Thus the internal state of the reflected beam is changed to $(|3\rangle + |2\rangle)/\sqrt{2}$, while the internal state of the transmitted beam is not affected. As a result, there is an entanglement created between the internal and the external degree of freedom of the atom. The state vector of the system becomes:

$$|\psi\rangle \propto |\psi_0\rangle \otimes (|3\rangle - |2\rangle) + |\psi_1\rangle \otimes (|3\rangle + |2\rangle) \quad (1)$$

where $|\psi_0\rangle$ and $|\psi_1\rangle$ describe the centre-of-mass motion for the reflected and transmitted beams (see Fig. 1), respectively. This entanglement is the crucial point for the storage of information. The second microwave pulse acting on both beams (the transmitted and the reflected), converts the internal state of the transmitted beam to state $|3\rangle$, while the reflected beam is converted to state

$|2\rangle$. Thus, the state vector after the pulse sequence shown in Fig. 3b becomes:

$$|\psi\rangle \propto |\psi_0\rangle \otimes |2\rangle + |\psi_1\rangle \otimes |3\rangle \quad (2)$$

We note that momentum transfer from the microwave slightly changes $|\psi_0\rangle$ and $|\psi_1\rangle$, but this has negligible effects, as will be discussed below.

Equation (2) shows that the internal state is correlated with the way taken by the atom. The which-way information can be read out later by performing a measurement of the internal atomic state. The result of this measurement reveals which way the atom took: if the internal state is found to be $|2\rangle$, the atom moved along beam B, otherwise it moved along beam C.

A detailed calculation of the beam splitter reveals an additional phase shift, not discussed so far. It arises because the atoms travel in the light shift potential during $\pi/2$. This creates a phase shift for the atoms proportional to $U_0 \times t_{\text{int}}$, resulting in a relative phase shift between atoms in states $|2\rangle$ and $|3\rangle$. Fortunately, this phase shift is identical for the transmitted and reflected beams and therefore does not affect the storing process in any essential manner. Moreover, a small detuning of the microwave frequency from the atomic resonance allows us to compensate for this effect, so that the simple model discussed above is valid.

Interferometer with which-way information

After considering a single beam splitter, we now return to the complete interferometer. Sandwiching the first Bragg beam splitter between two microwave $\pi/2$ pulses, stores the which-way information in the internal atomic state, as described above. We note that the second Bragg beam splitter does not change the internal state.

Will there still be interference fringes in the farfield when the which-way information is stored? The experimental result is shown in Fig. 4: there are no fringes. The data were recorded with the same parameters as in Fig. 2a. The only difference is that two microwave pulses were added to store the which-way information. Atoms in both hyperfine states were detected, so that the which-way detector was not read out. The mere fact that which-way information is stored in the detector and could be read out already destroys the interference pattern. We have verified experimentally that the fringes also disappear when the which-way detector is read out, that is, when only atoms in state $|2\rangle$ or only atoms in state $|3\rangle$ are detected. Of course, the absolute size of the signal is reduced by a factor of two in these cases.

Mechanical effects

We now discuss whether the loss of interference can be explained by mechanical effects of the which-way detector on the atomic

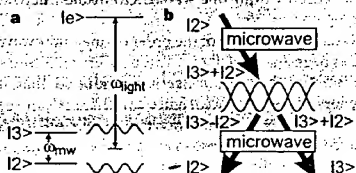


Figure 3 Storage of which-way information. **a**, Left, simplified level scheme of ^{87}Rb . The excited state ($5^2P_{3/2}$) is labelled $|2\rangle$. The ground state ($5^2S_{1/2}$) is split into two hyperfine states with total angular momentum $F = 2$ and $F = 3$, which are labelled $|2\rangle$ and $|3\rangle$, respectively. Right, the standing light wave with angular frequency ω_{light} induces a light shift for both ground states which is drawn as a function of position. **b**, The beam splitter produces a phase shift that depends on the internal and external degree of freedom. A Ramsey scheme, consisting of two microwave $\pi/2$ pulses, converts this phase shift into a population difference (see text).

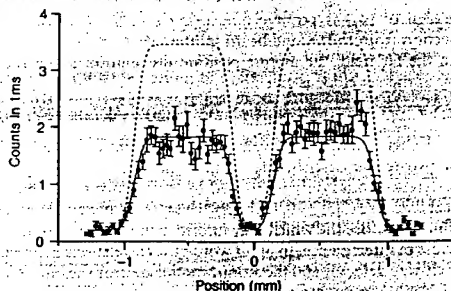


Figure 4 Same as Fig. 2a, but with which-way information stored in the internal atomic state. The interference fringes are lost due to the storage of which-way information.

centre-of-mass motion. Therefore the transverse momentum transfer in the microwave field and the longitudinal displacement of the atomic wavefunction must be investigated.

To wash out the interference fringes, the transverse momentum transfer must have a distribution whose spread must correspond to at least half a fringe period. Such a "classical" momentum transfer distribution would also broaden the envelope of the fringe pattern by the same amount¹¹. Comparing the experimental data in Fig. 2a and Fig. 4, it is obvious that the width of the envelope is not changed. This experimental result clearly shows that there is no significant transfer of transverse momentum in the microwave field.

The momentum transfer during the interaction with the microwave field can also be estimated theoretically. The microwave field is a standing wave diffracting the atomic beam. Because the atoms are travelling much less than a microwave wavelength during the interaction, the Raman-Nath approximation is valid. For a plane atomic wave, the probability to pick up n photon momenta during a $\pi/2$ pulse is $J_n^2(\pi/2)$, where J_n is the n th order Bessel function¹². Hence the probability of transferring more than two microwave photon momenta is less than 1%. The absorption of a single microwave photon shifts the position of the atom in the detector plane by 5 nm. It follows that the mechanical recoils during the interaction with the microwave field can shift the pattern by at most ± 10 nm—too small to be observed. Of course, the transverse width of the atomic beam is much less than a microwave wavelength so that the atomic beam is not a plane wave. However, the atomic beam is a superposition of plane waves. The above Raman-Nath calculation applies for each plane wave component, so that the spread of the atomic beam cannot be larger than for a plane wave.

There is a second mechanical effect that could explain the loss of interference: a longitudinal displacement of the atomic wavefunction, as discussed in ref. 7. In our experiment, this argument does not apply because the whole interaction sequence is pulsed. The atom's potential energy varies as a function of time, not as a function of longitudinal position, so that the interaction does not create any longitudinal forces and displacements.

We conclude that the "classical" mechanical effects of the which-way detector on the atomic centre-of-mass motion are negligible, so that some other mechanism must enforce the loss of interference fringes.

Correlations destroy interference

In order to investigate why the interference is lost, we consider the state vector for the interaction sequence used in Fig. 4. The state vector after the interaction with the first beam splitter sandwiched between the two microwave pulses is given in equation (2). The second beam splitter transforms this state vector into:

$$|\psi\rangle \propto |\psi_D\rangle \otimes |2\rangle + |\psi_C\rangle \otimes |3\rangle + |\psi_A\rangle \otimes |2\rangle + |\psi_B\rangle \otimes |3\rangle \quad (3)$$

The sign of $|\psi_A\rangle$ is positive due to the π phase shift during the reflection from the second beam splitter.

In the far field, the atomic position distribution under the left peak of the envelope is given by:

$$P(z) \propto |\psi_D(z)|^2 + |\psi_C(z)|^2 - \psi_D^*(z)\psi_C(z)2|3\rangle - \psi_C^*(z)\psi_D(z)2|3\rangle \quad (4)$$

because here the spatial wavefunctions $\psi_D(z)$ and $\psi_C(z)$ vanish. The first two terms describe the mean intensity under the envelope. Interference could only be created by the last two terms, but they vanish because $\langle 2|3\rangle = 0$. Precisely the same entanglement that was required to store the which-way information is now responsible for the loss of interference. In other words: the correlations between the which-way detector and the atomic motion destroy the interference, as discussed in ref. 3.

This loss of interference manifests itself as a dramatic change in the momentum distribution when adding the microwave fields to the interferometer, even though the microwave itself does not transfer enough momentum to the atom to wash out the fringes.

However, the addition of the microwave fields modifies the probability for momentum transfer by the light fields. This modification of the momentum transfer probability is due to the correlations between the which-way detector and the atomic motion.

Correlations between the interfering particle and the detector system are produced in any which-way scheme, for example, in the previously mentioned *gedanken* experiments of Einstein's recoiling slit and Feynman's light microscope. But in these experiments "classical" mechanical effects of the detector on the particle's motion can explain the loss of interference as well, so that the effect of the correlations is hidden.

So far, the microwave field has been treated as a classical field; that is, not as a quantized field. At first glance this might seem to be unjustified, because the population difference between the two hyperfine states corresponds to the absorption of one microwave photon, so that the system also becomes entangled with the microwave field. Hence the interference terms in equation (4) must include an additional factor $\langle \alpha|\beta\rangle$, where $|\alpha\rangle$ denotes the initial state of the microwave field, which changes to $|\beta\rangle$ due to the absorption of one photon. In our experiment, the initial state $|\alpha\rangle$ is a coherent state with a large mean photon number, and therefore the spread of the photon number is also large. It follows that $\langle \alpha|\beta\rangle \approx 1$, so that the entanglement with the microwave field has negligible effects, as has already been pointed out in ref. 3.

Uncertainty relation

We now discuss the role of Heisenberg's position-momentum uncertainty relation in our experiment. For this discussion it is essential that the two ways through the interferometer (beams B and C in Fig. 1) have never separated in transverse position space. This is because the beams have a transverse width of 450 μm (as determined by the width of the lower collimation slit), but are shifted transversely only by a few micrometres (given by d) with respect to each other. This has an important consequence: the storage of which-way information does not imply any storage of transverse position information.

Moreover, the atom is not localized with a precision of the order of d at any stage of the experiment. In particular, the atom stays delocalized during its whole passage through the interaction region, regardless of whether the microwave is on or off. Heisenberg's position-momentum uncertainty relation could only be invoked if the atom were localized. Hence the uncertainty relation does not imply any back action onto the transverse momentum, either "classical" or "quantum".

Of course, in every real experiment there are localization effects due to the finite size of the apparatus. This localization leads to a back action onto the momentum. But this back action is not at all related to the fringe separation. For example, in our set-up the atoms are localized within one wavelength of the microwave. The corresponding back action onto the transverse momentum implied by the uncertainty relation is of the order of one microwave photon recoil and has been analysed above. This back action is four orders of magnitude smaller than the fringe separation, so that it cannot explain the loss of interference. Hence correlations can explain the loss of interference while the uncertainty relation cannot. This answers the controversial question cited in the introduction: complementarity is not enforced by the uncertainty relation. This result is not in conflict with the results of Wiseman *et al.*¹³ who considered only experiments in which double-slit interference patterns are destroyed by making a position measurement. In our experiment, no double slit is used and no position measurement is performed, so that the results of ref. 11 do not apply. It is an open question whether the concept of "quantum" momentum transfer can be generalized to schemes without a mechanical double slit. Such a generalization would have to take into account the fact that in our experiment, the amount of momentum transferred by the light fields is always either zero or exactly $2\hbar k$.

Although beams B and C are never separated in transverse position space, they are separated in transverse momentum space. The separation is $2\hbar k_{\text{Bragg}}$ as is required for first-order Bragg reflection. Storing which-way information therefore corresponds to storing transverse momentum information with an accuracy of the order of $\Delta p_{\perp} \approx \hbar k_{\text{Bragg}}$. So the uncertainty relation implies that the storing process must include a back action onto the transverse position of the order of $\Delta z \approx \lambda_{\text{Bragg}}$. This back action is due to the following effect. In the Bragg regime, the interaction time with the standing light wave, τ_{Bragg} , is so long that the atoms move at least a transverse distance of the order of $\lambda_{\text{Bragg}}/2$ within τ_{Bragg} . In a naive picture, the atoms can be Bragg-reflected at the beginning or at the end of this interaction, which implies a transverse position uncertainty of the order of $\Delta z \approx \lambda_{\text{Bragg}}$. But this back action onto the near-field position cannot destroy the far-field fringe pattern. The interference pattern created in the interferometer is a pattern in momentum space, not in position space. The far-field position distribution is simply a picture of the final momentum distribution.

Received 3 February; accepted 15 June 1998

1. Bohr, N. in *Albert Einstein: Philosopher-Scientist* (ed. Schilpp, P. A.) 200–241 (Library of Living Philosophers, Evanston, 1949); reprinted in *Quantum Theory and Measurement* (eds Wheeler, J. A. & Zurek, W. H.) 9–49 (Princeton Univ. Press, 1983).
2. Feynman, R., Leighton, R. & Sands, M. in *The Feynman Lectures on Physics* Vol. III, Ch. 1 (Addison Wesley, Reading, 1965).

3. Scully, M. O., Englert, B. G. & Walther, H. Quantum optical tests of complementarity. *Nature* 351, 111–116 (1991).
4. Harach, S. in *High-Resolution Spectroscopy* (ed. Schawlow, J. L.) 315–318 (Plenum, New York, 1975).
5. Physics, Vol. 43, Springer, 1975; also in *High-Resolution Spectroscopy* (ed. Schawlow, J. L.) 315–318 (Plenum, New York, 1975).
6. Rauch, H. et al. Verification of coherent neutron refraction of Bragg's law. *Phys. Lett. A* 54, 423–427 (1975).
7. Badurek, G., Rauch, H. & Tuppinger, D. Neutron interferometer double-resonance experiment. *Phys. Rev. A* 34, 2600–2608 (1986).
8. Storey, F., Tan, S., Collett, M. & Walls, D. Path detection and the uncertainty principle. *Nature* 367, 626–628 (1994).
9. Englert, B. G., Scully, M. O. & Walther, H. Complementarity and uncertainty. *Nature* 375, 367–368 (1995).
10. Storey, F., Tan, S., Collett, M. & Walls, D. Complementarity and uncertainty. *Nature* 375, 368 (1995).
11. Wiseman, H. & Harrison, F. Uncertainty over complementarity? *Nature* 377, 584 (1995).
12. Wiseman, H. M. et al. Nonlocal momentum transfer in weak-weg measurements. *Phys. Rev. A* 56, 75–78 (1997).
13. Englert, B. G. & Yoon, J. Interference experiment with light scattered from two atoms. *Phys. Rev. Lett.* 70, 2359–2362 (1993).
14. Cohen-Tannoudji, C. Effect of near-resonant irradiation on atomic energy levels. *Metrologia* 15, 161–166 (1977); reprinted in Cohen-Tannoudji, C. *Atoms in Electromagnetic Fields* 343–348 (World Scientific, London, 1994).
15. Künze, S., Dürr, S. & Rempe, G. Bragg scattering of slow atoms from a standing light wave. *Europhys. Lett.* 34, 343–348 (1996).
16. Künze, S. et al. Standing wave diffraction with a beam of slow atoms. *J. Mod. Opt.* 44, 1863–1881 (1997).
17. Bernhardt, A. B. & Shore, B. W. Coherent atomic deflection by resonant standing waves. *Phys. Rev. A* 23, 1290–1301 (1981).

Acknowledgements We thank S. Künze for discussions. This work was supported by the Deutsche Forschungsgemeinschaft. Correspondence and requests for materials should be addressed to G.-J. (e-mail: gerd.jackel@physik.uni-erlangen.de).

A critical window for cooperation and competition among developing retinotectal synapses

Li I. Zhang*, Huizhong W. Tao*, Christine E. Holt†, William A. Harris† & Mu-ming Poo

Department of Biology, University of California at San Diego, La Jolla, California 92093-0357, USA

* These authors contributed equally to this work

In the developing frog visual system, topographic refinement of the retinotectal projection depends on electrical activity. *In vivo* whole-cell recording from developing *Xenopus* tectal neurons shows that convergent retinotectal synapses undergo activity-dependent cooperation and competition following correlated pre- and postsynaptic spiking within a narrow time window. Synaptic inputs activated repetitively within 20 ms before spiking of the tectal neuron become potentiated, whereas subthreshold inputs activated within 20 ms after spiking become depressed. Thus both the initial synaptic strength and the temporal order of activation are critical for heterosynaptic interactions among convergent synaptic inputs during activity-dependent refinement of developing neural networks.

Electrical activity in the developing nervous system plays a crucial role in the establishment of early nerve connections^{1,2}. In the mammalian visual system, both the formation of ocular dominance columns in the primary visual cortex^{3–5} and the segregation of retinal ganglion axons into eye-specific layers in the lateral geniculate nucleus⁶ depend on electrical activity in the visual pathways. The pattern of activity in the optic nerves seems to serve an instructive role, as synchronous stimulation of optic nerves abolishes the formation of ocular dominance columns, whereas asynchronous stimulation leads to sharp ocular dominance columns⁷. Artificially synchronized activity in the optic nerve also disrupts the development of orientation tuning in the visual cortex⁸. In the visual system of frog, chick and fish, retinal axons use activity-independent mechanisms initially to establish a topographic map,

but the initial map is coarse and terminals from each retinal axon arborize over a large portion of the tectum. During development, the map becomes refined as retinal axons progressively restrict their arborizations to a smaller fraction of the tectum^{9,10}. Topographic refinement of the retinotectal projection also depends on activity patterns, as this process is impaired when retinal activity is blocked or uniformly synchronized by raising the animals in strobe light^{11–14}. Thus, throughout the visual system, the refinement of connections depends on the pattern of activity, but the underlying physiological mechanisms are largely unknown.

We have examined quantitatively the effects of activity patterns on the strength of developing central synapses in the *Xenopus* retinotectal system. *In vivo* whole-cell recordings were made from neurons in the optic tectum of young *Xenopus* tadpoles to monitor changes in the strength of retinotectal synapses following repetitive electrical stimulation of retinal neurons in the contralateral eye. By

† Present address: Department of Anatomy, University of Cambridge, Cambridge CB2 3DY, UK.

THIS PAGE BLANK (USPTO)

Recent Developments in the Theory of the Electron

VICTOR F. WEISSKOPF

Massachusetts Institute of Technology, Cambridge, Massachusetts

THE application of the microwave technique to spectroscopy has greatly increased the accuracy of spectroscopic measurements. Recent experiments on the spectrum of hydrogen and other simple elements have revealed that the results are not exactly in agreement with our fundamental theories of the mechanics of the electron within the atom. Small deviations were found in checking the values of the energy levels in hydrogen given by the Sommerfeld formula.¹ The measured value of the magnetic moment of the electron deviated by about 1 in 1000 from the value given by Dirac's fundamental equation of the electron.²

These experimental findings led to a reinvestigation of the theory, and especially of its weakest point—the interaction of the electron with radiation. This interaction was treated by a theory named “quantum electrodynamics” which, since its inception by Dirac in 1926, suffered from some internal inconsistencies connected with the old problem of the internal structure of the electron. These inconsistencies make it impossible in this theory to calculate radiation phenomena in a rigorous way.

In the last years, however, some theoretical work has been carried out³ in an attempt to isolate the unsolved problems and inconsistencies within the theory and to increase the accuracy of the predictions of the theory, in spite of the fact that the structure of the electron and its effects are not understood. The results of this development have been quite successful. The theoretical predictions were in complete agreement with the new experiments. The confidence in the fundamental concepts

of “quantum electrodynamics” was greatly enhanced.

It is attempted in this article to present an account of this new development in a form which, I hope, is understandable to the physicist who is not specialized in this field. Only a qualitative and very incomplete picture of the underlying problems can be given. It seemed advisable not to restrict this report to the newest achievements, but to recapitulate shortly the development of our ideas about the electron beginning with H. A. Lorentz's classical electron theory and including the theory of the positron. The significance of the present problems cannot be evaluated without referring to the most important steps in this development.

I. THE CLASSICAL ELECTRON THEORY

There was hardly any other discovery which led to the understanding of so many and varied phenomena as the discovery of the electron.

Many topics which were thought to be unrelated, as optics, electricity, and chemistry, were understood by the same fundamental mechanism on the basis of the electron theory. It was mainly H. A. Lorentz who brought the classical electron theory into a consistent frame. These were his fundamental assumptions: The electron is an elementary particle with a charge e and a mass m ; the motion of the electrons is determined by classical mechanics if the force acting on the electron is given by the expression:

$$\mathbf{F} = e\mathbf{E} + (e/c)(\mathbf{v} \times \mathbf{H}),$$

where e and \mathbf{v} are the charge and velocity of the electron and \mathbf{E} and \mathbf{H} are the electric and magnetic field strengths. The electromagnetic field in turn is given by the Maxwell equations

$$\begin{aligned} (1/c)(\partial \mathbf{E} / \partial t) - \text{curl} \mathbf{H} &= 4\pi \mathbf{i}, \quad \text{div} \mathbf{E} = 4\pi \rho; \\ (1/c)(\partial \mathbf{H} / \partial t) + \text{curl} \mathbf{E} &= 0, \quad \text{div} \mathbf{H} = 0. \end{aligned}$$

The sources of the field strengths are the charge density ρ and a current density \mathbf{i} , which are produced by the electrons.

In most cases it is possible to consider the electron as a point charge. The field created by the electron can then be expressed in a simple manner. We quote only one trivial example: an electron at rest is surrounded by an electric field

$$\mathbf{E} = e/r^2, \quad (1)$$

¹ W. E. Lamb, Jr., and R. C. Retherford, *Phys. Rev.* **72**, 241 (1947).

² Nafe, Nelson, and Rabi, *Phys. Rev.* **71**, 914 (1947); Nagel, Julian, and Zacharias, *Phys. Rev.* **72**, 971 (1947); P. Kusch and H. M. Foley, *Phys. Rev.* **72**, 1256 (1947).

³ This development started at a conference of theoretical physicists in June, 1947, on Shelter Island, New York, sponsored by the National Academy of Sciences. The same development has been carried out completely independently by a group of Japanese physicists around Professor Tomonaga. The following papers have been published so far: S. Tomonaga, *Prog. Theor. Phys.* **1**, 27 (1946); Koba, Tati, and Tomonaga, *Prog. Theor. Phys.* **2**, 101, 198 (1947); S. Kanesawa and S. Tomonaga, *Prog. Theor. Phys.* **3**, 1 (1948); S. Tomonaga, *Phys. Rev.* **74**, 224 (1948); H. A. Bethe, *Phys. Rev.* **72**, 339 (1947); H. W. Lewis, *Phys. Rev.* **73**, 173 (1948); H. A. Kramers, *Solvay Report*, 1948; J. Schwinger, *Phys. Rev.* **73**, 415 (1948); *Phys. Rev.* **74**, 1439 (1948); *Phys. Rev.* **75**, 651 (1949); R. P. Feynman, *Phys. Rev.* **74**, 939, 1430 (1948); F. J. Dyson, *Phys. Rev.* **73**, 617 (1948); *Phys. Rev.* **75**, 486 (1949); N. M. Kroll and W. Lamb, *Phys. Rev.* **75**, 388 (1949); T. Welton, *Phys. Rev.* **74**, 1157 (1948); J. B. French and V. F. Weisskopf, *Phys. Rev.* **75**, 1240 (1949).

where r is the distance from the electron. The expressions for the field surrounding an electron in motion are somewhat more complicated.

Some additional assumptions had to be made regarding the conditions under which electrons move in matter: Lorentz assumed that there are several electrons in each atom, which are elastically bound to an equilibrium position and thus are able to perform harmonic vibrations with given frequencies. In electric conductors additional electrons were assumed to move freely about. With these fundamental theoretical tools it was possible to explain a great number of phenomena; as for example, the absorption, scattering, and refraction of light by matter, the Zeeman effect, the optical properties of metals for infra-red radiation and many more. In many cases the explanation was only qualitative. Some of the detailed features were not understood. The main assumption of the elastic binding of electrons within atoms was unexplained, especially in view of the planetary structure of the atom. The frequencies of the electron within the atom were neither understood nor determined by the theory.

Lorentz also investigated another fundamental problem: How far is it possible to consider the electron as a point charge? He was forced to make some assumptions about the internal structure of the electron in order to apply the electrodynamic equations within the electron. We quote from his book *The Theory of the Electron*: "While I am speaking so boldly of what goes on in the interior of an electron, as if I had been able to look into these small particles, I fear one will feel inclined to think I had better not try to enter into all these details. My excuse must be, that one can scarcely refrain from doing so, if one wishes to have a perfectly definite system of equations, moreover, as we shall see later on, our experiments can really teach us something about the dimensions of the electrons. In the second place, it may be observed that in those cases in which the internal state of the electrons can make itself felt, speculations like those we have now entered upon, are at all events interesting, be they right or wrong, whereas they are harmless as soon as we may consider the internal state as a matter of little importance."

The main point of interest in the question of the structure of the electron can be formulated very simply today, since the equivalence of mass and energy has become common place: the total energy E_{el} of the electrostatic field (1) of the electron is given by

$$E_{el} = (1/8\pi) \int \mathcal{E}^2 dv,$$

where the integration is extended over the whole space. \mathcal{E} is given by (1) outside of the electron, but

(1) is, of course, no longer valid "inside" the electron; it is convenient to assume that the charge of the electron is concentrated on the surface of a sphere with the radius a . In this case E would vanish inside and we would get:

$$E_{el} = (e^2/2) \int_0^\infty (dr/r^2) = e^2/2a. \quad (2)$$

Any other assumption as to the charge distribution does not change the general character of (2): the energy of the electric field depends critically upon the radius of the electron. It necessarily contributes to the mass m of the electron, and we obtain from the Einstein relation

$$m = m_0 + (E_{el}/c^2) = m_0 + (e^2/2c^2a),$$

where m_0 is the "mechanical" mass of the electron, by which we understand all contributions to the mass which are not of electromagnetic origin. Since the total mass m is known experimentally, there is a lower limit for the radius, corresponding to the assumption that all the mass is of electric origin (we exclude the rather artificial choice of a negative value for m_0):

$$a \geq e^2/2mc^2 = r_0. \quad (3)$$

The electron radius is at least as large as r_0 which is usually called "the classical electron radius." Thus we are forced to abandon the notion of an exact point charge.

Lorentz, Abraham, and Poincaré have studied at length the consequences of this new picture. It is not of very great interest to discuss the detailed consequences of the assumption of a finite classical electron. Later developments have brought into the picture new features which completely overshadow these classical considerations.

One point should be mentioned, however. At what energy should one expect in the classical theory the radius of the electron to change significantly the results expected with a point electron? It is easy to see that scattering cross sections of electrons by electrons, or of electrons by equal charges (as protons), should be influenced if the energy is high enough, so that the particles could approach to distances smaller than a . This would happen at energies larger than $2mc^2$, that is, larger than one Mev. One may remark that the physicists of that time would have been very much surprised if they had been able to perform these experiments. Instead of finding an effect of the finite extension of the electron, they would have observed the creation of electron-positron pairs. The fundamental connection of the pair creation with the problem of the structure of the electron will be discussed later in this article.

II. THE QUANTUM

The problem was soon resolved by the successful application of the electron theory, Bohr's model of the atom, and the properties of development of quantum theory. The interpretation of the energy, position, and the contradictory properties of particles against collision theory is a new theory of the Schrodinger equation.

The success of quantum mechanics is overwhelming. The electron theory stands and collapses, the other facts of mechanics, within the framework of quantum mechanics, to point out the electron could be a phenomenon.

Quantum mechanics to the behavior of electrons as functions of time, asking: How or magnetic fields do a "c" selves?" is explained by its group of the fact that the number of radiation or means of the hypothesis: 1 and absorption or emission or transition whose energy resonance excitation s

Here, and frequency in 2π to as h , $h = 1.0$

II. THE QUANTUM THEORY OF THE ELECTRON

The problems of the structure of the electron were soon removed from the focus of interest by the successful development of the quantum theory of the electron. The discovery of the quantum of action, Bohr's theory of the quantum orbits in the atom, and the duality of wave and particle properties of the electron, led eventually to the development of quantum mechanics. A new interpretation of the mechanical concepts of momentum, energy, position, and velocity was introduced to describe consistently the facts that appear to be contradictory as, for example, the wave and particle properties of the electron, or the stability against collisions of planetary orbits in atoms. The new theory is best known in the mathematical form of the Schrödinger wave equation.

The success of quantum mechanics was overwhelming. Many unsolved problems of classical electron theory were solved. One can now understand and calculate the resonance frequencies of atoms, the stability of electron orbits, and many other facts which cannot be explained in classical mechanics. There is scarcely any phenomenon within the realm of atoms and molecules which, at least in principle, cannot be accounted for by quantum-mechanical description. It is worth while to point out that the quantum theory of the electron could explain all forces between atoms, molecules and electrons as purely electromagnetic phenomena.

Quantum mechanics can answer all questions as to the behavior of the electron (or other particles) in electromagnetic fields, if these fields are given as functions of space and time. Most of the problems in atomic physics can be put into this form by asking: How does the electron move in an electric or magnetic field of a well defined character? Difficulties do arise, however, if the question, "What fields are created by the moving charges themselves?" is asked. For example, it could not be explained by the theory in this stage that an atom in its ground state does not radiate light, in spite of the fact that charges are in rapid motion.

Nevertheless, it was possible to construct a number of unambiguous rules to calculate the radiation of atomic systems. This was done by means of two principles. One is the *light quantum hypothesis*: light of frequency ν can only be emitted and absorbed in quanta of an energy $h\nu$.† Thus its emission or absorption must be accompanied by a transition from one quantum state to another, whose energy difference is $h\nu$. The other is the *correspondence principle*: Quantum states of very high excitation show the same mechanical properties as

† Here, and in what follows, we understand by ν the frequency in 2π seconds, and by h the magnitude usually referred to as h . $h = 1.04 \times 10^{-27}$ g cm² sec⁻¹

one would obtain from a classical calculation of the same problem. Their radiation should then also be equal to the one which is calculated classically. It was possible to derive rules from these two principles with which one could calculate successfully emission, absorption and scattering of light by atomic systems. If the wave-length of light is large compared to the dimensions, a system in a quantum state n is, in many respects, equivalent to an assembly of classical electric oscillators with frequencies given by

$$h\nu_{nk} = (E_n - E_k),$$

where k is some other state of the system. The effective charge e of these oscillators is given by $e^2 = c^2 f_{nk}$ where f_{nk} is the so-called oscillator strength:

$$f_{nk} = (2m/h)\nu_{nk} \left| \int \psi_n^* \mathbf{r} \psi_k d\mathbf{r} \right|^2, \quad (4)$$

where the integral represents the matrix element of \mathbf{r} between the states n and k .

The problem of the structure of the electron does not enter into this theory. The theory admits the construction of an electronic wave packet with arbitrarily small diameter, even smaller than a if only wave-lengths smaller than a are used. The difficulty arising from the field created by such a packet did not arise since the creation of fields by quantum-mechanical systems was not yet clearly defined.

It is worth while mentioning, however, that it is no longer possible to measure effects of an electron radius $a = r_0$ by having two electrons collide with an energy of the order mc^2 . The wave-length corresponding to this energy is h/mc , which is much larger than r_0 . Thus it is impossible at that energy to locate the electron better than within h/mc . During a collision their average distance will be h/mc , and they practically never will be within a distance comparable with the radius.

III. THE RELATIVISTIC WAVE EQUATION AND QUANTUM ELECTRODYNAMICS

The quantum theory of the electron needed improvement in two directions: it needed a generalization for high energies in conformity with the theory of relativity and it needed a consistent treatment of the interaction of matter with radiation. It was Dirac who initiated both steps. He was able to devise a wave equation for the electron which fulfilled the relativistic requirements. He made use of the fact that the electron has an intrinsic spin moment whose state, much like the polarization of light, can always be described as a superposition of a spin parallel and opposite a given direction of reference. Thus, the electron wave had to be considered as a "spinor" wave with two components

corresponding to the two spin directions. Dirac has shown that, for a relativistic wave equation, one has to introduce two more components which, for low velocities, are very much smaller than the others. An electron wave is fully described by giving all four components. Dirac's relativistic wave equation determines the mechanics of this four-component wave. For low kinetic energies (small compared to mc^2) two of the components become very small; the two large ones are themselves solutions of the non-relativistic (Schrödinger) wave equations, each of them corresponding to one of the two directions of the spin.

The non-relativistic theory had to ascribe arbitrarily a magnetic moment μ to the spin, whose value it took from the experimental results. Dirac's relativistic equation contains implicitly an interaction of the spin with a magnetic field. The resulting magnetic moment of the electron $\mu = eh/2mc$ is in almost exact agreement with the experiment.

The relativistic wave equation of the electron exhibits, however, several fundamentally unacceptable features. The equation admits solutions which correspond to states of a particle with negative rest mass. The kinetic energy in these states is negative; the particle moves opposite to the motion in ordinary states. For example: a particle of electronic charge is repelled by the field of a proton. These states are, of course, not realized in nature and the most obvious trouble comes from the fact that their energy is negative and, therefore, below the energy of the actual lowest state with positive rest mass. There should be radiative transitions with the emission of light quanta from the regular states to the irregular ones. No regular state could be stable since there are an infinite number of states of negative energy to which it could go with the emission of a suitable quantum of light.

These states cannot be excluded simply by stating that they do not exist in nature. The regular states alone are not what one calls a complete set of solutions. Physically speaking, if by a certain measurement the electron is put into some arbitrary state, it will very probably be a combination of states containing some of the irregular ones. Especially if an electron is localized in a region smaller than the Compton "wave-length" $\lambda_c = h/mc$, the states of negative mass will be strongly represented.

We now proceed to Dirac's treatment of the radiation. In order to describe in a consistent way the interaction between matter and radiation, it is necessary to "quantize" not only the motion of the material particles, but also the electromagnetic field. We understand by "quantizing," the consistent application of certain rules, which led from classical mechanics to quantum mechanics. It is relatively simple to apply these rules to the electro-

magnetic field in an empty space. The field can be decomposed into its "Fourier components;" it can be thought as a superposition of monochromatic waves. Each of these waves has dynamical properties very much like those of a harmonic oscillator. Thus the "quantization" of the electromagnetic field is equivalent to the quantization of a set of harmonic oscillators and, hence, the energy in one monochromatic wave can change only by multiples of $h\nu$. Thus electromagnetic energy of a frequency ν must appear always in portions of the size $h\nu$. This is the light quantum hypothesis. A further important consequence is the zero-point fluctuations; a harmonic oscillator in its state of lowest energy still has a finite amplitude of vibration. Applying this to the electromagnetic field, we conclude that even in the state of lowest energy the electromagnetic vibrations in space are not zero. The state of lowest energy is the state in which no light quanta are present. Hence, in this state the mean squares of the field strengths do not vanish.

We now give an estimate of the strength of the field fluctuations averaged over a volume V of linear dimensions a : $V = a^3$. The amplitude B of the zero-point oscillation of an oscillator of frequency ν is given by $B \sim (h/2m\nu)^{1/2}$; it corresponds to a vibration with an energy $h\nu/2$. The main contribution to the field fluctuations in the volume a^3 comes from waves of a wave-length $\lambda = c/\nu \sim a$. The amplitude should correspond to an energy of $h\nu/2$, one-half light quantum. Now $(1/4\pi)(\mathcal{E}^2)a^3$ is the field energy content in a^3 ; this must be put equal to $h\nu/2 = hc/2a$, so that we get approximately

$$\mathcal{E}_{\text{fluct}}^2 \sim hc/a^4. \quad (5)$$

It is larger, the smaller the volume chosen.

The interaction between light and matter can now be described as an interaction between two quantized systems: the electromagnetic field, on one hand, and the electron in the atoms, on the other. Such interaction can be treated by the current methods of quantum mechanics. The interaction energy is given by the classical expression:

$$\int (\mathbf{i} \cdot \mathbf{A}) dv,$$

where \mathbf{i} is the current density in the atom and \mathbf{A} is the vector potential in the field. The integral is taken over the space. The two variables \mathbf{i} and \mathbf{A} are now physical magnitudes, which must be dealt with according to the rules of quantum mechanics. Dirac has shown that by this method absorption, emission, and scattering of light can be calculated and that the result is equal to the one which was obtained by the correspondence principle. The

† We use here the term "wave-length" for the length λ which is $1/2\pi$ times the conventional wave-length.

emission of light to the state k described in the $t=0$, the emission and all excited ground states. The probability P of the emission of light is given by

in conformity with oscillator theory.

Dirac's quantum consistent description of the nature and size of the electron field. Let us influence of a field it performs with a displacement of this displacement velocity (\dot{x}, \dot{y}) .

$$\langle x, y \rangle = \frac{1}{2} ($$

The kinetic equations is

where λ is the frequency ν . The field contribution energy. Let us consider a sphere with a wave-length λ and we are allowed the value (\mathcal{E}^2) for the energy point field

In a more precise expression (6), induced by the value \mathcal{E}_0 and the value \mathcal{E} we include the transition into a state \mathcal{E}_{osc} of one

emission of light in a transition from the state n to the state k , for example, in this theory is described in the following way. At a given time, say $t=0$, the emitting atom is in an excited state n and all electromagnetic vibrations are in their ground states. Because of the interaction, the excitation energy $E_n - E_k$ goes over into one of the vibrations; it must, of course, be a vibration whose frequency fulfills the condition $h\nu = E_n - E_k$. The probability P that after a time t the excitation energy has gone into the field turns out to have an exponential time dependence: $P = 1 - e^{-\Gamma t}$. Γ is then the emission probability per unit time. The value of Γ is given by

$$\Gamma = (2e^2\nu_{nk}^2/3mc^2)f_{nk},$$

in conformity with the probability of radiation of an oscillator with the strength f_{nk} , as defined in (4).

Dirac's quantum electrodynamics gave a more consistent derivation of the results of the correspondence principle, but it also brought about a number of new and serious difficulties. The structure and size of the electron appeared again in the theory. The trouble arose from the interaction with the electron of the zero-point fluctuations of the field. Let us consider a free electron under the influence of an oscillatory field strength $\mathcal{E} = \mathcal{E}_0 e^{i\nu t}$: it performs forced oscillations of frequency ν with a displacement x_ν . The average square $\langle x_\nu^2 \rangle_n$ of this displacement and the average square of the velocity $\langle \dot{x}_\nu^2 \rangle_n$ of a free electron are given by

$$\langle x_\nu^2 \rangle_n = \frac{1}{2}(e^2\mathcal{E}_0^2/m^2\nu^4), \quad \langle \dot{x}_\nu^2 \rangle_n = \frac{1}{2}(e^2\mathcal{E}_0^2/m^2\nu^2). \quad (6)$$

The kinetic energy of the electron in these oscillations is

$$E_\nu = \frac{1}{2}m\langle \dot{x}_\nu^2 \rangle_n = e^2\mathcal{E}_0^2\lambda^2/4mc^2, \quad (6a)$$

where λ is the wave-length belonging to the frequency ν . Hence, the zero-point oscillations of the field contribute to the electron a certain amount of energy. Let us assume for a moment that the electron is a sphere with a radius a . Then only waves with a wave-length $\lambda > a$ will act upon the electron; the ones with $\lambda \gg a$ are not very important, so that we are allowed to put in (6a) $\lambda = a$. If we then enter the value (5) for $\langle \mathcal{E}_0^2 \rangle_n$ over a volume a^3 , we obtain for the energy E_{fl} of the electron due to the zero-point field fluctuations:

$$E_{fl} \sim e^2\hbar/4mca^2. \quad (7)$$

In a more accurate calculation we start with expression (6), which gives the effects on the electron induced by an oscillatory field strength of amplitude \mathcal{E}_0 and frequency ν . In order to calculate the value of \mathcal{E}_0^2 for the zero-point oscillations, we include the electromagnetic field and the electron into a big volume Ω . The zero-point amplitude $\mathcal{E}_0 e^{i\nu t}$ of one proper vibration can be calculated by

putting the total energy of the oscillation equal to:

$$(1/8\pi) \int (\mathcal{E}^2 + \mathcal{H}^2) d\Omega = (1/8\pi)\mathcal{E}_0^2\Omega = h\nu/2; \quad \mathcal{E}_0^2 = 4\pi h\nu/\Omega.$$

We use the well-known formula that there are

$$z(\nu)d\nu = \Omega(\nu^2/\pi^2c^2)d\nu$$

proper vibrations in the frequency interval $d\nu$. Since the zero-point oscillations of different frequencies are statistically independent, their contributions to the average square of the displacement and of the velocity add up and we get for the total of these magnitudes:

$$\langle x^2 \rangle_n = \int \langle x_\nu^2 \rangle_n z(\nu) d\nu = (2e^2h/\pi m^2c^2) \int_{\nu_0}^{\infty} (d\nu/\nu), \quad (8)$$

$$\langle \dot{x}^2 \rangle_n = (2e^2h/\pi m^2c^2) \int_{\nu_0}^{\infty} \nu d\nu. \quad (9)$$

The integrals are extended between a lower limit ν_0 and infinity. The frequency ν_0 depends on the state of binding of the electron. $h\nu_0$ is of the order of the binding energy. If the frequency of the field oscillations falls below the frequency ν_0 , the electron can no longer be considered as free and (6) is no longer valid. The resulting effect is equivalent to an omission of the frequencies below ν_0 .

Both expressions (8) and (9) lead to infinite results. This is especially troublesome in the case of the velocity square because it gives rise also to an infinite kinetic energy E_{fl} of the electron due to the zero-point fluctuations:

$$E_{fl} = (m/2)\langle \dot{x}^2 \rangle_n = (e^2h/\pi mc^2) \int_{\nu_0}^{\infty} \nu d\nu. \quad (10)$$

This expression contains a quadratically divergent integral. Since this energy is an inseparable part of the total energy of an electron, it must appear as part of its mass energy mc^2 . In order to keep the mass finite, one therefore is forced to assume some structural properties of the electron which prevent the interaction with high frequencies of the field. We can do this by introducing an upper limit ν_{max} to the interaction which cuts off the integral in (10) at that limit. The fluctuation energy assumes the form

$$E_{fl} = (e^2h/2\pi mc^2)\nu_{max}^2, \quad (7a)$$

and we can determine an upper bound for ν_{max} by setting E_{fl} equal to mc^2 :

$$h\nu_{max} \leq (2\pi\hbar c/e^2)mc^2 \approx 15 \text{ Mev.} \quad (7b)$$

This would remove the interaction with an electron

at rest of a quantum of an energy >15 Mev, a rather improbable result. The introduction of v_{\max} is equivalent to the assumption of an electron radius $a=c/v_{\max}$, which shows the equivalence of (7) and (7a). Equation (7b) gives rise to a value of $a \approx (hc/e^2)^{1/2} r_0$, which is larger than the classical limit (3). Thus the fluctuation energy seemingly pushes the electron radius to even greater values than the one which we obtained from the energy of the electrostatic field. It should be noted, however, that in interactions with light of an energy of more than $2mc^2$, the irregular solutions with negative mass play an essential role. Thus the significance of these states will have an essential bearing upon the problem of the self-energy of the electron.

Dirac's two generalizations of quantum mechanics, the relativistic wave equation and the quantum electrodynamics, were very successful in some respects: the explanation of the magnetic moment of the electron, the derivation of the Sommerfeld fine structure formula, and the consistent derivation of the expressions for the absorption, emission, and scattering of light. Two fundamental difficulties were introduced simultaneously:

(1) The existence of states of the electron of negative mass. They cause an instability of a normal bound state by the emission of a quantum of high energy and subsequent transitions into a state of negative mass. Thus, the "normal" states of the electron have a very strong "resonance" interaction with light quanta of high energy.

(2) The quantization of the electromagnetic field introduces infinite fluctuations of the electron. In order to keep their contribution to the energy within the observed mass energy value, the interaction of the electron with light quanta of an energy $h\nu > (137mc^2)^{1/2}$ would have to be basically altered. It will be shown in the next section that the positron theory removed the first difficulty and completely changes the aspect of the second.

IV. THE POSITRON THEORY

The phenomenon of creation of a positron and an electron by a light quantum introduces a new aspect into the theory of the electron. The fundamental process can be described as follows: a light quantum of an energy larger than $2mc^2$ (1 Mev) can be absorbed by the empty space, in the presence of strong electric fields. The energy is then transformed into a pair consisting of a positive and a negative electron.

Two outstanding facts are shown in this phenomenon: the existence of a positive electron, and the fact that the vacuum has physical properties, which enables it to absorb light and to produce electrons. Hence, the physical description of the

vacuum is bound to be more complicated than hitherto and must contain the latent electron pairs which can be created.

It was again Dirac who, turning a vice into a virtue, used the unacceptable states of negative mass for the description of the vacuum. A reinterpretation of these states gives an almost perfect description of the vacuum and the existence of positrons: the states of negative mass correspond in some respects to the states of a particle of opposite charge since they move in opposite directions in any electromagnetic field. They are, however, still unacceptable because of their negative kinetic energy. The reinterpretation which removes this difficulty can be formulated as follows: According to the Pauli exclusion principle, any state can be either occupied by one single electron, or unoccupied. The occupation of a state of energy E_i increases the total energy of the system by the amount E_i , the removal of an electron from the state decreases the total energy by E_i . Dirac's reinterpretation of the states of negative mass consists in the exchange of "occupation" and "removal." We decide to call an occupied state of negative mass "empty" and an empty state "occupied." The transition from "empty" to "occupied" is then connected with an energy change of $-E_i$. Since E_i is negative itself, the energy actually increases by $+|E_i|$. The trouble with the negative energy is thus removed.

The vacuum can then be described formally by assuming that all states of negative mass are occupied by electrons. They are not "actually" occupied, because of our reinterpretation, so that one need not be bothered by the infinite charge density which one would get if all states of negative mass were really occupied. The wave functions, which represent the absence of positrons are the same functions which would have represented the presence of electrons of negative mass. It is a new feature that the "absence" of a particle is described by a wave function. This is, however, an expression of the fact that the vacuum has the physical properties described above; it is filled with latent electrons.

This reinterpretation removes at once the difficulty which the states of negative mass have introduced. Since in the vacuum these states are occupied, no electron in the regular states can jump into them. Thus the regular states are no longer unstable against decay into the irregular ones. They no longer are in "resonance" interaction with arbitrarily high light quanta.

The pair creation is then described as follows: a light quantum produces a transition from an occupied state of negative mass to a state of positive mass. The result is an electron in a state of positive mass and an unoccupied state of negative mass. The latter must be interpreted as an occupied state

of a positron quantum has negative with

Such trans of external fi momentum c probability c duce exceller opposite pro and a negativ one quantum in the field-f picture as th "unoccupied" sented. This t sion of light c

The new e effect upon t electron. The spect to the analogous to magnetic fie tions of the e in the vacuu when average the Compton sent the late light quanta,

Let us nov uum" in the There will b and the laten exclusion pr electrons ten Two electron than a dista relative mon in the same of one actu some change vacuum: Thi the average which repres slightly reme tron. This cl to the undist to the "actu form of a sp electron, sin pushed away tion shows th classical el $\log(\lambda_e/a)$. H as a better d that fields w act with the The effect even more d

of a positron with positive mass. Thus the light quantum has created two particles positive and negative with positive mass.

Such transition can only occur in the presence of external fields. Without those fields energy and momentum cannot be conserved. The transition probability can be calculated and the results reproduce excellently the experimental material. The opposite process is the annihilation of a positive and a negative electron, with the emission of either one quantum in an electric field or of two quanta in the field-free space. It can be described by our picture as the transition of the electron into the "unoccupied" state by which the positron is represented. This transition is accompanied by the emission of light quanta.

The new aspect of the vacuum has a decisive effect upon the problem of the self-energy of the electron. The properties of the vacuum with respect to the electrons are now, in some aspects, analogous to its properties in respect to the electromagnetic field. There exist also zero-point fluctuations of the electric charge and the electric current in the vacuum. These fluctuations are very small when averaged over a volume of a size larger than the Compton "wave-length" $\lambda_c = h/mc$. They represent the latent electron pairs which, by means of light quanta, could be brought into real existence.

Let us now consider the properties of the "vacuum" in the neighborhood of an actual electron. There will be an interaction between this electron and the latent charges, mainly because of the Pauli exclusion principle. According to this principle, electrons tend to keep distance from one another. Two electrons (of equal spin) do not come nearer than a distance d which is determined by their relative momentum p : $d \sim h/p$. (They must not be in the same cell of the phase space.) The presence of one actual electron in the vacuum introduces some changes in the "charge distribution" of the vacuum. This charge distribution would be zero on the average if undisturbed. The wave functions which represent the electrons of negative mass are slightly removed from the place of the actual electron. This change of charge distribution, compared to the undisturbed vacuum, appears as an addition to the "actual" electron. This manifests itself in form of a spread in the charge distribution of an electron, since the vacuum electrons are slightly pushed away from the actual electron. The calculation shows that this spread is enough to change the classical electrostatic self-energy to $(e^2/hc)mc^2 \log(\lambda_c/a)$. Here a is the "radius" of the electron, or, as a better definition, a is a limit of wave-length so that fields with $\lambda < a$ are no longer assumed to interact with the electron.

The effects of the zero-point field oscillations are even more drastically changed by our new concept

of the vacuum. This comes from the fact that the field oscillations also interact with the latent electron pairs in the vacuum. As long as their frequency is much smaller than $2mc^2/h$ (the minimum frequency of pair creation), the "vacuum" is very little influenced and the old calculation (6) of the displacement $\langle x, z \rangle_n$ and the velocity $\langle \dot{x}, \dot{z} \rangle_n$ are still valid. For frequencies higher than $2mc^2/h$, however, the field oscillations have a strong effect on the latent electron pairs and the induced charge and current fluctuations in the vacuum interfere with the induced fluctuation of the electron itself. This interference is destructive and reduces to some extent values of the induced displacement and velocity. The reduction can be roughly approximated in its main features by a factor $(mc^2/h\nu)^2$ to the expressions (6) for $h\nu > 2mc^2$:

$$\langle x, z \rangle_n = \frac{1}{2}(e^2 \delta^2 / m \nu^4)(mc^2/h\nu)^2 \quad \text{for } h\nu > 2mc^2. \quad (6')$$

$$\langle \dot{x}, \dot{z} \rangle_n = \frac{1}{2}(e^2 \delta^2 / m \nu^2)(mc^2/h\nu)^2$$

This effect is difficult to explain in qualitative language. It is connected with the Pauli exclusion principle, according to which electron have a tendency to keep apart from one another. Thus the charge and current fluctuations of the vacuum in the neighborhood of the electron tend to be in opposite phase to the fluctuations of the electron itself and therefore cause the destructive interference.

These effects represent a definite improvement. The average displacement $\langle x^2 \rangle_n$ does no longer lead to infinities. The divergent integral in (8) converges now because of the reduced contribution (6') of the frequencies above $2mc^2/h$, and we obtain

$$\langle x^2 \rangle_n = (2e^2 h / \pi m^2 c^2) \log(f mc^2 / h \nu_0), \quad (11)$$

where f is a factor of the order unity, which can be determined if the effect of the higher frequencies is exactly taken into account. The average velocity square (9) is still infinite but the divergence is only logarithmic. We get from (6'):

$$\langle \dot{x}^2 \rangle_n \sim (2e^2 h / \pi m^2 c^2) \left[\int_0^{2mc^2/h} \nu d\nu + (mc^2/h)^2 \int_{2mc^2/h}^{\infty} (d\nu/\nu) \right]$$

The fluctuation energy $E_{f1} = (m/2)\langle \dot{x}^2 \rangle_n$ is reduced to $E_{f1} = (e^2/\pi hc)mc^2 \log(fh\nu_{\max}/mc^2)$ where f is a numerical factor and ν_{\max} the cut-off frequency. In order to keep this energy below the total mass energy mc^2 of the electron, it is now sufficient to keep $a = c/\nu_{\max}$ larger than $(h/mc) \exp[-(hc/e^2)]$. This lower limit is very much smaller than any length considered so far. It is no longer necessary to tamper with the interaction of the electron with light quanta of an energy of a few Mev. It is still

unsatisfactory, of course, that the limit cannot be chosen to be infinity without obtaining infinite self-energies; thus the internal structure of the electron will appear somewhere in the theory. However, some changes in the interaction between light and matter are certain to occur at very high energy values where we have good reason to expect the appearance of new phenomena (nuclear or meson type).

So far we have discussed the influence of an actual electron on the vacuum due to the Pauli-exclusion principle. There is also an influence, although weaker, in the form of a displacement of the vacuum electrons due to electric interaction. It is easier to describe this effect, not for an actual electron, but for a *proton*, which is embedded in the vacuum. The wave functions of the states of negative mass are all deformed because of the presence of the proton. Since the vacuum is described by the undeformed states, the difference between the deformed and undeformed ones should give rise to an actual charge density. This is called the polarization of the vacuum by an external charge (the proton).

The proton induces a charge density ρ_i in the vacuum. The calculation shows that $\rho_i(r)$ as function of the location r has the following form:

$$\rho_i(r) = A\rho_0(r) + \int G(r-r')\rho_0(r')dr'. \quad (12)$$

Here $\rho_0(r)$ is the external charge density; in our case, ρ_0 is the charge density of the proton. A is a constant and $G(r-r')$ is a function of the distance between the points r and r' . The integral is extended over all points r' . The expression for the induced charge consists of two parts: the first term is exactly proportional to the inducing charge density ρ_0 ; the second part is an effect at a distance. According to this term a point charge at $r=0$ (like a proton) would give rise to a charge distribution $G(r)$. $G(r)$ is different from zero only over distances up to the Compton wave-length λ_c . The effect is the same as if the dielectric coefficient of the vacuum was different from unity by about $1/137$ over a region of the order λ_c . It is important to note that the first part is unobservable in principle. Its effect is undistinguishable from the original charge density ρ_0 , since it is always induced by it. What is actually measured in nature as the charge of the proton would not be e , but $(1+A)e$. It thus represents nothing but a renormalization of the charge. The second term only has physical significance.

There is one serious difficulty with this interpretation: the factor A turns out to be logarithmically infinite: $A \sim (e^2/\hbar c) \log(\lambda_c/a)$ if the "cut-off" radius a is put equal to zero. This would mean that the external charge ρ_0 of the proton induces a

charge in the vacuum at the same place, which changes its value by an infinite amount. It is true that this change is in itself unobservable, since one always observes the total charge, external plus induced, in nature. However, the fact that the induced charge is infinite for $a=0$ represents a serious difficulty of the theory.

The vacuum is polarized not only by a proton but also by an electron. The situation is somewhat more complicated in this case because of exchange phenomena between the electron and the vacuum electrons. The fact remains, however, that the electron, if considered as a point ($a=0$), also induces a charge in the vacuum which adds an infinite contribution to its original charge. Thus the internal structure of the electron is relevant not only for its mass but also for its charge.

One can make these infinite additions finite without changing the second term in (12) by arbitrarily removing the interaction of the field with electrons whose wave-length is smaller than a . Here, as in the self-energy, the infinity comes from the interaction at very high energies, and there is hope that a future theory will change this interaction so that the constant A remains finite and small.

In spite of these difficulties, the theory of the positron can be regarded as a big step forward in our understanding of the electron: By means of Dirac's reinterpretation of the states of negative mass it was possible to explain the new phenomena of pair creation and annihilation and to remove several fundamental difficulties of the Dirac equation:

- (1) The radiative transitions from the ordinary states into states of negative mass are removed.
- (2) The fluctuation energy is much less sensitive to the structure of the electron because of its logarithmic dependence on the electron radius.
- (3) The average square displacement of the electron by the field fluctuations is finite and independent of the radius or the structure.

V. THE EXPERIMENTAL TEST OF QUANTUM ELECTRODYNAMICS

The quantization of the electromagnetic field so far has not brought much reward. It is true that it made it possible to derive the expressions for the absorption, emission, and scattering of light, which before were based only upon a recipe contrived by means of the correspondence principle. On the other hand, new difficulties came about, all connected with the zero-point oscillations of the electromagnetic field and their effect on the self-energy of the electron. Quantum electrodynamics has not yet shown its superiority over the correspondence principle. On the contrary, its actual expressions for the electromagnetic phenomena be-

come sense the theory electron occurs.

Encouraged by the recently directly confirmed by quantum retical diff separate rest of th can be app the expe within th charge wi Such pro terms and interaction are, there binding o in nature tional ma been shov tion by o of the m complica way. The term be of gre rule as to energy c necessary so that th more exp was per by S. To

There which is due to t frequen condition energy l ing, and Property effect of zero-poi turned o action w strated l in a cas ment, n like ato Let t electron

We ar

Re

come senseless, since a consistent interpretation of the theory would force us to put the mass m of the electron equal to infinity at all places where it occurs.

Encouraged by some new experiments, which will be discussed later on, a new attempt was made recently to find observable effects, which are directly connected with the new features introduced by quantum electrodynamics. The main theoretical difficulty consisted in the problem of how to separate the infinities of mass and charge from the rest of the theory, in order to obtain results that can be applied to nature. This was done by isolating the expressions for the infinite mass and charge within the theory, in the hope that mass and charge will be made finite by a future improvement. Such procedure is possible since the self-energy terms and the infinite charge come mostly from the interaction with very high energy light quanta and are, therefore, largely independent of the state of binding of the electron in fields normally occurring in nature. Hence, they can be split off as an additional mass and charge of the electron. This has been shown already for the charge in the last section by discussing expression (12). The separation of the mass term is mathematically much more complicated but can be performed in an analogous way. The relativistic transformation properties of the terms occurring in the calculation proved to be of great importance for finding an unambiguous rule as to what parts of the expression of the self-energy can be considered as a mass term. It was necessary to reformulate quantum electrodynamics so that the relativistic invariance of the theory was more explicit than before. This very laborious task was performed by J. Schwinger and independently by S. Tomonaga.

There is, however, a small part of the self-energy which is not contained in the mass and which is due to the interaction with oscillations of lower frequencies. This part depends on the external conditions and may give rise to a slight shift of energy levels, depending on the conditions of binding, and a slight change in some of the fundamental properties of the electron. It is due mainly to the effect of the displacement x of the electron by the zero-point oscillations, whose square average $\langle x^2 \rangle_n$ turned out to be finite and due entirely to the interaction with lower frequencies. This can be demonstrated by means of quite elementary calculations⁴ in a case which corresponds to an actual experiment, namely, the shift of the levels in hydrogen-like atoms.

Let us consider a stationary state n of the electron in a Coulomb field, whose wave func-

tion is given by ψ_n . The Coulomb field is described by the potential energy $V(r) = Ze^2/r$, where r is the distance from the nucleus. The average potential energy \bar{V} in the state n can be written in the form

$$\bar{V} = \int V(r) |\psi_n(r)|^2 dv, \quad (13)$$

where $|\psi_n(r)|^2$ is the well-known probability of finding the electron at a point r : the integral is extended over the volume. This expression must be changed in view of the existence of the zero-point oscillations. The effect of these oscillations on the electromagnetic mass is already assumed to be contained in the observed electron mass m . There is, however, also an influence on the potential energy, since the electron is forced to oscillate around the position r . It will be shown that this oscillation changes the average value of the potential energy by a small amount. This change gives rise to a shift of the energy levels.

In order to calculate this change we replace $V(r)$ in (13) by $V(r+x)$, where x is the zero-point oscillation of the electron. We use a Taylor expansion because of the smallness of x .*

$$V(r+x) = V(r) + \text{grad } V \cdot x + \frac{1}{2} \Delta V \cdot (x^2/3), \quad (14)$$

where ΔV is the Laplace operation on V : $\Delta V = [(\partial^2/\partial x^2) + (\partial^2/\partial y^2) + (\partial^2/\partial z^2)]V$. The second term is zero in the average, since x is an oscillation. Thus the addition δE_n to the average potential energy of the state n may be written:

$$\delta E_n = \frac{1}{6} \int \Delta V \cdot \langle x^2 \rangle_n |\psi_n(r)|^2 dv.$$

The Laplacian of the Coulomb potential is proportional to the charge density ρ_0 which produces it: $\Delta V = 4\pi e\rho_0$, ρ_0 is the charge density of the nucleus, which we approximate by a δ -function:** $\rho_0 = Ze\delta(r)$, where Ze is the charge of the nucleus. Hence we obtain for δE_n :

$$\delta E_n = (2\pi/3)Ze^2 |\psi_n(0)|^2 \langle x^2 \rangle_n, \quad (15)$$

where $|\psi_n(0)|^2$ is the intensity of the wave function at the nucleus, and we insert the value (11) which we found for $\langle x^2 \rangle_n$ into (15) to calculate the level shift. The frequency ν_0 which occurs in (11) depends on the binding of the electron and is of the order of the Rydberg frequency ν_R for an electron in a hydrogen-like atom. Since ν_0 appears only under a logarithm, its exact value is not of great importance. It has been shown by Bethe⁴ that, for

* The simple form of the third term in (14) comes from the fact that, in the average: $\langle x_i x_j \rangle_n = 0$, $x_i^2 = x_j^2 = x^2 = \langle x^2 \rangle_n/3$.

** The δ -function $\delta(r)$ is zero everywhere except at $r=0$. It is normalized such that the volume integral $\int \delta(r) dv$ is equal to unity.

(⁴) We are following here a calculation outlined by T. Welton, Phys. Rev. 74, 1157 (1948).

a quantum state n , ν_0 is given by the formula

$$\log h\nu_0 = \frac{\sum_m |\rho_{nm}|^2 (E_m - E_n) \log |(E_m - E_n)|}{\sum_m |\rho_{nm}|^2 (E_m - E_n)},$$

where E_n is the energy of the state n and the sums are extended over all other quantum states m . ρ_{nm} is the matrix element of the momentum between the states n and m .

We observe that $|\psi(0)|^2$ vanishes for all states except S states (states with the orbital angular momentum zero), for which simple relation holds:

$$|\psi_n(0)|^2 = Z^3 |\pi|^2 n^2, \quad (16)$$

where $l = \hbar^2/mc^2$ is the Bohr radius. Thus the level shift vanishes for states with an angular momentum different from zero.

We finally get the level shift for S states from (15), (11), and (16). It is practical to express it in form of a relative shift by dividing δE_n by the energy E_n of the level which is given by the Balmer relation $E_n = Z^2 mc^2 / 2h^2 n^2$:

$$\delta E_n / E_n = (8/3\pi) (e^2/\hbar c)^2 (Z^2/\pi) \log(fmc^2/h\nu_0). \quad (17)$$

The exact calculation for the $2S_1$ term yields the values $\nu_0 = 18\nu_R$, $f = 1.3$. Thus the S levels of hydrogen-like atoms should be shifted upwards (δE_n is positive) by small amounts, relative to the values given by the Sommerfeld formula. This is a direct effect of the zero-point oscillation and its experimental verification constitutes a strong support of quantum electrodynamics.

The polarization of the vacuum by the proton produces also a shift which has to be added to (16). According to the discussions of the last section, the only observable effect is a small polarization around the proton of the extension λ_e . The calculation shows that this causes a line shift $\delta E_n'$:

$$\delta E_n' / E_n = -(8/15\pi) (e^2/\hbar c)^2 Z^2 / n. \quad (18)$$

It amounts to only about 1/40 of the shift δE_n .

The most reliable experiment on the lineshift was performed by Lamb and Retherford¹ on hydrogen. According to the Sommerfeld formula the $2S_1$ level and the $2P_1$ level of the hydrogen atom should coincide in energy, and the $2P_1$ level should lie 10,000 megacycles higher. Lamb and Retherford have measured the $2S_1$ level relative to the two other levels and have found that the $2S_1$ level is shifted upwards by about 1060 mc , a value which is in good agreement with the theoretical formula (17). Similar shifts have been found by J. Mack² and Kopfermann and Paul³ in helium. The present measurements are not accurate enough to prove the existence of shifts as small as the one given by

(18), caused by the polarization of the vacuum. Future experiments will show whether this additional effect can be considered as real.

Another important result obtained by these methods is the correction to the g factor of the electron. According to Dirac's equation, the magnetic moment of the electron μ_e is equal to $\hbar e/2mc$. The ratio between this value and the mechanical moment $\hbar/2$ of the electron is $g(e/2mc)$ with $g=2$, in contrast to the value of this ratio for orbital motions in which $g=1$. If the interaction of the electron with the radiation field is properly taken into account, one obtains the result that g is not accurately equal to 2 but $g=2+e^2/\pi\hbar c$.

Unfortunately, it is impossible to give a qualitative description of this effect along the lines in which the level shift was explained. The spin of the electron is in itself a phenomenon which is not amenable to a simple pictorial understanding. A way to understand the effect may be found by remembering that the magnetic moment of the Dirac electron is due to circular currents of the radius \hbar/mc . The zero-point oscillations of the electromagnetic field influence these currents to a certain extent, and so do the current fluctuations induced in the "vacuum." These interactions cause the slight change of the magnetic moment. The numerical result is in excellent agreement with recent experimental measurements.² The magnetic moment of the electron was determined with great accuracy from the Zeeman effect of some fine structure doublets. Although the correction of the g factor cannot be understood in simple terms, it represents the most important result of quantum electrodynamics since it deals with one of the fundamental properties of the free electron—its magnetic moment.

The great success in these two instances of the quantum-electrodynamical concepts proves that the fundamental ideas must contain a great deal of truth. The main achievement of the recent development consisted in finding an unambiguous and relativistically invariant way of separating those effects of the interaction between light and electron which can be interpreted as additional mass and charge, from the other effects which give rise to observable phenomena. The additional mass and charge are contained in the observed values of m and e and can never be observed independently. It must not be forgotten, however, that these magnitudes are still infinite in this theory. This constitutes a warning that the interaction of the electron with light quanta of very high energy is not yet understood. Somewhere at very high energies, the internal structure of the electron must play an essential role in a future theory in a way which is completely unknown. This structure appears at present in the form of the arbitrary length a which

we have in order to n tron finite

The im in the rec lems deali charge of (meaning to infinity effects, su levels, ma without r structure

There is that the t into a con ducing sor energies. charge of the electro radius r_0 forces. Th tum elect mesons an exists onl

¹ J. Mack, Phys. Rev. 73, 1233 (1948).

² Kopfermann and Paul, Naturwiss. (1948).

vacuum,
his addi-

by these
or of the
the mag-
equal to
and the
 $g(e/2mc)$
ratio for
raction of
properly
ult that g
 $\hbar c$.
a quali-
e lines in
e spin of
ich is not
anding. A
nd by re-
the Dirac
the radius
e electro-
a certain
is induced
cause the
. The nu-
rith recent
netic mo-
with great
some fine
ion of the
e terms, it
quantum
ne of the
ctron—its

ices of the
oves that
eat deal of
recent de-
ambiguous
separating
light and
additional
which give
tional mass
d values of
pendently.
these mag-
This con-
of the elec-
ergy is not
h energies,
ust play an
ay which is
appears at
th a which

we have introduced as a radius of the electron in order to make the mass and the charge of the electron finite magnitudes.

The importance of the recent developments lies in the recognition of the following fact: for problems dealing with atomic energies only mass and charge of the electron are "structure dependent" (meaning dependent on the value of a and going to infinity if a is chosen zero), whereas all other effects, such as scattering cross sections, energy levels, magnetic moments, etc., can be calculated without making any assumption regarding the structure of the electron.

There is perhaps some significance in the fact that the theory of the electron cannot be brought into a completely satisfactory form without introducing some new elements into the theory at high energies. It cannot be a pure accident that the charge of the proton and of the meson is equal to the electronic charge, or that the classical electron radius r_0 is almost equal to the range of nuclear forces. There must be a connection between quantum electrodynamics and the future theory of mesons and of the nuclear forces, which at present exists only in very rudimentary form. The tie

between these theories should be of importance for the electron only at energies of the order of the meson rest mass or higher. This would be high enough (>100 Mev) to leave unchanged the results of the theory for atomic energies. One may hope that the understanding of this tie will solve the problem of the electromagnetic mass and of the induced charge of the electron.

In discussing the classical electron theory, we remarked that a scattering experiment testing the limits of the classical theory would have revealed the existence of positrons, a phenomenon which was of fundamental significance for the further development of the theory. An experiment trying to test the present theory at high energies (100 Mev and over) will probably give rise to meson production. This is perhaps an indication of the important role of the mesons in a future theory of the electron. Future experiments with the new accelerating machines which are now under construction will reach energies of these critical values. It is hoped that the phenomena found by means of these new tools will shed new light upon the fundamental problem of the relation between elementary particles.

BEST AVAILABLE COPY

THIS PAGE BLANK (USPTO)

United States District Court,
District of Columbia.

BLACKLIGHT POWER, INC., Plaintiff,

v.

**Q. Todd DICKINSON, Commissioner of Patents
and Trademarks, Defendant.**

Civil Action No. 00-422(EGS).

Aug. 15, 2000.

Patent applicant challenged Patent Office's decision to withdraw application after payment of issue fee. On cross-motions for summary judgment, the District Court, Sullivan, J., held that: (1) Patent Office had statutory authority to withdraw issued patent after payment of issue fee, and (2) withdrawal was not abuse of discretion.

Plaintiff's motion denied; defendant's motion granted.

West Headnotes

[1] Patents ⇨114.17
291k114.17

Patent Office's interpretation of patent issuance statute is due *Chevron* deference. 35 U.S.C.A. § 151.

[2] Patents ⇨107
291k107

Patent Office had authority, under its statutory mandate to issue only patent to which applicant is entitled, to withdraw application even after applicant has paid issue fee. 35 U.S.C.A. § 151.

[3] Patents ⇨107
291k107

Patent Office regulation authorizing withdrawal of issued patent upon determination of unpatentability was reasonable application of statutory mandate to issue only patent to which applicant was entitled. 35 U.S.C.A. § 151; 37 C.F.R. § 1.313(b).

[4] Patents ⇨112.2
291k112.2

Patent Office decision refusing to rescind notice of patent withdrawal, rather than notice of withdrawal itself, was final agency action, for purposes of judicial review.

[5] Patents ⇨107
291k107

Patent Office decision to withdraw patent application after payment of issue fee, upon determination that it raised substantial question of patentability, was not arbitrary or capricious, even though regulation allowed withdrawal only upon determination of unpatentability; Patent Office was entitled to withdraw application and return it to examiner for determination of patentability. 5 U.S.C.A. § 706(2); 37 C.F.R. § 1.313(b)(3).

Patents ⇨328(2)
291k328(2)

6,024,935. Cited.

*45 Michael H. Selter, Farkas & Manelli, P.L.L.C., Jeffrey Allan Simenauer, Washington, DC, for Plaintiff.

Fred E. Haynes, U.S. Attorney's Office, Washington, DC, Kevin Gerard Baer, Patent & Trademark Office, Office of the Solicitor, Arlington, VA, for Defendant.

MEMORANDUM OPINION AND ORDER

SULLIVAN, District Judge.

I. Introduction

Plaintiff Blacklight Power, Inc., alleges that defendant Q. Todd Dickinson, Commissioner of the Patent and Trademark Office (PTO), violated the Administrative Procedure Act (APA), 5 U.S.C. § 706 *et seq.*, when the PTO withdrew one and threatened to withdraw four others of plaintiff's patents from issue after plaintiff had received a "Notice of Allowance and Issue Fee Due" and payed the issue fee. The issues presented are whether the defendant had the authority to withdraw plaintiff's patent after plaintiff had paid the issue fee, and, if defendant did have the authority, whether that withdrawal was arbitrary and capricious. Plaintiff

claims that defendant's actions were arbitrary and capricious, and that the internal regulation on which defendant relies contravenes the governing patent statute. Pending before the Court are the parties' cross motions for summary judgment. Upon consideration of the parties' motions, memoranda in support, responses in opposition, replies in support, and the arguments at the May 22, 2000 motions hearing, plaintiff's motion for summary judgment [11-1] is **DENIED**, and defendant's motion for summary judgment [13-1] is **GRANTED**.

II. Factual Background

Plaintiff has filed a series of five patent applications for technology that, according to plaintiff, represents a new source of chemical energy from hydrogen. One of these, titled "Lower-Energy Hydrogen Methods and Structure," was filed March 21, 1997. This application was issued as U.S. Patent No. 6,024,935 (the '935 patent) on February 15, 2000. Another of these, Ser. No. 09/009,294 (the '294 application), titled "Hydride Ions," had been filed January 20, 1998. During prosecution of the '294 application, plaintiff cited over 130 prior art articles concerning "cold fusion" and "perpetual motion." When the primary patent examiner raised issues relating to the operability of the '294 technology, plaintiff conducted a personal interview with the examiner to discuss the articles *46 and the operability issues. On October 18, 1999, defendant issued a Notice of Allowance and Issue Fee Due for the '294 application (Notice). The Notice reads:

**THE APPLICATION IDENTIFIED ABOVE
HAS BEEN EXAMINED AND IS ALLOWED
FOR ISSUANCE AS A PATENT.
PROSECUTION ON THE MERITS IS
CLOSED.**

**THE ISSUE FEE MUST BE PAID WITHIN
THREE MONTHS FROM THE MAILING
DATE OF THIS NOTICE ... Pl.'s Mot. for
Summ. J., Ex. 2.**

Plaintiff paid the issue fee three days later, October 21, 1999. See Pl.'s Mot. for Summ. J., Ex. 3. Following payment of the issue fee, the '294 application was set to issue as U.S. Patent No. 6,030,601 on February 29, 2000.

On February 17, 2000, twelve days before the '294 application was to issue, Frances Hicks, a Petitions Examiner with the Office of Petitions, Office of the Deputy Assistant Commissioner for Patent Policy Projects, issued a Notice (February 17 Notice)

informing plaintiff that, by request of the Director of the Special Program Law Office, "the ['294] application ... is being withdrawn from issue pursuant to 37 C.F.R. § 1.313 ... to permit reopening of prosecution." Pl.'s Mot. for Summ. J., Ex. 4. It is uncontested that the '294 application file was not in defendant's possession at the time this Notice was sent.

Upon receiving the February 17 Notice, plaintiff's patent counsel began investigating the circumstances surrounding the withdrawal, contacting different PTO employees by telephone and by mail, including Ms. Hicks, and Director Esther Kepplinger. On February 28, 2000, plaintiff's patent counsel hand-delivered a final letter asking that the withdrawal be reconsidered. Director Kepplinger met with him to receive the letter. She conceded that she still did not have a copy of the '294 application, at which time plaintiff's patent counsel provided her with a copy of his own '294 application file. See Pl.'s Mot. for Summ. J. at 10; Melcher Decl. ¶ 22. In that meeting, Director Kepplinger indicated that she was concerned that the '294 technology involved "cold fusion" and "perpetual motion." [FN1] She also stated that the PTO intended to withdraw from issue four others of plaintiff's patents-in- application. [FN2] See Verified Compl. ¶ 22.

FN1. In plaintiff's motion for summary judgment, plaintiff details that Director Kepplinger indicated that Commissioner Dickinson had telephoned her and told her to re-evaluate the '294 application after receiving communications from undisclosed third-party sources complaining about the '935 patent. See Pl.'s Mot. for Summ. J. at 11. However, at the May 22, 2000 motions hearing, for the purposes of the summary judgment motion, plaintiff's counsel retracted its argument that the withdrawal of the '294 application was in response to pressure outside of the PTO. See May 22, 2000 Hr'g. Tr. at 52.

FN2. The four other patent applications are: Ser. No. 09/008,947, filed January 20, 1998; Ser. No. 09/009,455, filed January 20, 1998; Ser. No. 09/009,678, filed July 7, 1998; and Ser. No. 09/111,160, filed July 7, 1998.

Pursuant to 37 C.F.R. § 1.181(a)(3), defendant treated plaintiff's February 28 letters to the Commissioner, Director Robert Spar, and Director Kepplinger, as a single petition requesting that the Commissioner exercise his supervisory authority and

reverse the PTO's withdrawal decision. In a decision issued March 22, 2000 (March 22 Decision), defendant denied plaintiff's petition, refused to rescind the February 17 Notice, and disallowed plaintiff's patent. See Pl.'s Mot. for Summ. J., Ex. 8. The March 22 Decision indicated that the reason behind the withdrawal of the '294 application was its similarity to the '935 patent, both of which claimed to attain energy levels below the ground state according to a "novel atomic model." See Pl.'s Mot. for Summ. J., Ex. 8 at 2. Both claim that the electron of a hydrogen atom can attain an energy level and orbit below the 'ground state' corresponding to a fractional quantum number. According to defendant, this assertion alarmed the Director, who had *47 examined the '935 patent, and who had learned of the '292 application, because it "did not conform to the known laws of physics and chemistry." *Id.* The March 22 Decision states that the Director "was immediately aware that any pending application embodying such a concept raise [d] a substantial question of patentability of one or more claims which would require reopening prosecution." *Id.*

III. Procedure

Plaintiff filed this lawsuit on March 1, 2000. Plaintiff's complaint consists of two counts. Count I seeks preliminary and permanent injunctive relief directing defendant to issue the five contested patents-in-application as patents. Count II seeks a declaratory judgment that defendant's withdrawal of the patent applications was arbitrary and capricious and contrary to the PTO's own regulations and to the applicable patent issue statute. Plaintiff filed its motion for a temporary restraining order and preliminary injunction on March 2, 2000. At their March 3, 2000 hearing, the parties agreed that plaintiff would withdraw its motion without prejudice, and defendant would not take any Office Action with respect to the patents-in-application. On March 8, 2000, the Court issued an order memorializing that agreement, and setting a briefing schedule. Defendant filed the administrative record on March 22, 2000. The parties filed their cross motions for summary judgment on April 4, 2000. They filed their responses in opposition on April 18, 2000. Plaintiff filed its reply in support on May 1, 2000, and defendant filed its reply in support on May 5, 2000. The Court held a motions hearing on the cross motions for summary judgment on May 22, 2000.

IV. Discussion

The Court must examine several questions to resolve the pending cross motions. First, the Court must determine whether defendant has the authority to withdraw plaintiff's patent after plaintiff has paid the issue fee. If the Court determines that the PTO did possess the requisite authority, then the Court must conclude which PTO issuance, the February 17 Notice or the March 22, 2000 Decision, constitutes final, reviewable agency action. As the last step, the Court must determine whether that final agency action was arbitrary and capricious in contravention of the APA.

A. Whether the PTO Has the Authority To Withdraw Plaintiff's Patent After Payment of the Issue Fee

Plaintiff argues that the PTO does not have the authority to withdraw plaintiff's patent after payment of the issue fee for three reasons: 1) because doing so violates the plain language of the statute, 2) because the PTO regulation on which defendant bases its authority violates the plain language of the statute, and 3) because case law directs defendant to issue the patent upon payment of the fee.

1. Patent Issuance Statute: 35 U.S.C. § 151

The parties interpret 35 U.S.C. § 151, the statute governing the issuance of patents, to support their respective positions by focusing on different sections of the statute. 35 U.S.C. § 151 provides in relevant part:

If it appears that applicant is entitled to a patent under the law, a written notice of allowance of the application shall be given or mailed to the applicant. The notice shall specify a sum, constituting the issue fee or a portion thereof, which shall be paid within three months thereafter. Upon payment of this sum the patent shall issue, but if payment is not timely made, the application shall be regarded as abandoned. 35 U.S.C. § 151 (emphases added).

Plaintiff focuses on the italicized language directing that "[u]pon payment of [the issue fee] the patent shall issue." It is well-established that "shall" is the "language of *48 command." *Boyden v. Commissioner of Patents*, 441 F.2d 1041, 1042 n. 3

(D.C.Cir.1971), *cert. den.*, 404 U.S. 842, 92 S.Ct. 139, 30 L.Ed.2d 77 (1971). Here, it is uncontroverted that the Notice of Allowance for the '294 application stated that the application was "allowed for issuance as a patent" and that "prosecution on the merits is closed." Pl.'s Mot. for Summ. J., Ex. 2. It is also uncontroverted that plaintiff paid the appropriate fees. Accordingly, plaintiff contends that defendant's defalcation is at loggerheads with the statute's clear command.

Defendant argues that if the statute is read *in toto*, see *Dole v. United Steelworkers of America*, 494 U.S. 26, 35, 110 S.Ct. 929, 108 L.Ed.2d 23 (1990), it is clear that the withdrawal of these patent applications is within the PTO's power. Defendant notes that the entire section is premised on whether "it appears that [the] applicant is entitled to a patent under the law." Here, defendant contends, that is not so, because of plaintiff's claims of having attained an energy level and orbit below the hydrogen "ground state" corresponding to a fractional quantum number. Defendant also reminds the Court that even though the word "shall" generally is interpreted as imposing a mandatory duty, "shall" may also be interpreted differently depending on its context. See *LO Shippers Action Committee v. ICC*, 857 F.2d 802, 806 (D.C.Cir.1988). As a result, defendant contends, plaintiff's textual argument is not persuasive.

[1] The parties clash over the appropriate standard of review for the PTO's interpretation of 35 U.S.C. § 151. Plaintiff contends that, since the language of 35 U.S.C. § 151, the patent issuance statute, is unambiguous, the proper statutory construction of § 151 is a question of law that the court decides without deference to the PTO's interpretation. In *In re Portola Packaging Inc.*, 110 F.3d 786, 788 (Fed.Cir.1997), the court held that judicial inquiry is "complete" when the terms of a statute are unambiguous. Plaintiff argues that § 151 is unambiguous because it dictates that the "patent shall issue" upon payment of the issue fee.

Defendant responds that the PTO's interpretation of 35 U.S.C. § 151 is due *Chevron* deference, and should be upheld. See *Chevron U.S.A., Inc. v. Natural Resources Defense Council, Inc.*, 467 U.S. 837, 842-44, 104 S.Ct. 2778, 81 L.Ed.2d 694 (1984). "When faced with a problem of statutory construction, [the reviewing court should] show[]

great deference to the interpretation given the statute by the officers or agency charged with its administration." *Udall v. Tallman*, 380 U.S. 1, 16, 85 S.Ct. 792, 13 L.Ed.2d 616 (1965). The PTO Director is charged with administering 35 U.S.C. § 151. Accordingly, defendant maintains, the Court should grant defendant's interpretation considerable deference. For additional support, defendant cites *Harley v. Lehman*, 981 F.Supp. 9 (D.D.C.1997). The *Harley* court held that the PTO's interpretation of § 151 is due *Chevron* deference, and that the PTO's interpretation was reasonable in light of the agency's "duty to ensure that the patents it issues are valid." *Id.* at 11. The Court is persuaded that the holding of the *Harley* court, which applied to a situation factually and procedurally identical to the present case, applies to the present case. [FN3] Therefore, the Court will accord the PTO's interpretation of 35 U.S.C. § 151 the deference it is due under *Chevron*.

FN3. For a more in-depth discussion of *Harley*, see A.3., "Caselaw."

[2] Examining the parties' interpretations under the by now familiar *Chevron* two-step inquiry, this Court concludes that defendant's interpretation of the plain language 35 U.S.C. § 151 should be upheld. See *Harley*, 981 F.Supp. at 11. The code premises issuance of a patent upon payment of the issue fee "[i]f it appears that applicant is entitled to a patent under the law...." See 35 U.S.C. § 151. These words clearly establish the PTO's mandate *49 to issue valid patents. See *In re Etter*, 756 F.2d 852 (Fed.Cir.1985).

2. PTO's Administrative Regulation: 37 C.F.R. § 1.313(b)

[3] Plaintiff asseverates that 37 C.F.R. § 1.313(b), the PTO regulation implementing § 151, on which the PTO based withdrawal of the '294 application and its proposed withdrawal of the other four allowed applications, is invalid. Plaintiff contends that that regulation violates § 151's mandate that patents shall issue upon payment of the issue fee. 37 C.F.R. § 1.313(b) provides:

When the issue fee has been paid, the application will not be withdrawn from issue for any reasons except:

- (1) a mistake on the part of the Office;
- (2) a violation of § 1.56 [fraud] or illegality in the

application;

(3) *unpatentability of one or more claims* ...

37 C.F.R. § 1.313(b) (emphasis added).

The gravamen of plaintiff's regulatory argument is that the issue before the Court is not whether the PTO is obligated to determine a claim's patentability, but when it must make this determination. Plaintiff argues that § 151 and its legislative history indicate that the PTO must make this determination before issuance of the notice of allowance and payment of the issue fee. [FN4]

FN4. Plaintiff compares § 151 to 35 U.S.C. § 303, the patent reexamination statute, which allows reexamination of a patent only if there is a "substantial new question of patentability." The Federal Circuit, dismissing the PTO's reliance on its Manual of Patent Examining Procedure (MPEP), held that this statute does not allow reexamination of patent claims on ground considered before the patent was issued, even though reexamination might reveal that the requirements for patentability had not been met. *In re Recreative Technologies Corp.*, 83 F.3d 1394, 1397 (Fed.Cir.1996).

Defendant counters that the PTO has long had the discretion to withdraw a patent even after payment of the issue fee on unpatentability grounds. Subsection (3) was added to 37 C.F.R. § 1.313(b) in 1982. However, even before the addition of the "unpatentability" language, the PTO had the discretion to withdraw applications from issue on the basis of "mistake on the part of the Office" or subsection (1). The mistake ground was consistently held to envelop subsequently discovered reasons undermining an application's patentability. *See, e.g., Hull v. Commissioner of Patents*, 9 D.C. (2 MacArth.) 90 (1875)(denying writ of mandamus requesting issue of withdrawn patent). Indeed, defendant argues that the Director has not only the discretion but the duty to withdraw a patent from issue if there is a question about its patentability. *See In re Alappat*, 33 F.3d 1526, 1535 (Fed.Cir.1994)(en banc)(plurality opinion) (holding that the "Commissioner has an obligation to refuse to grant a patent if he believes that doing so would be contrary to law").

As for the standard of review of the PTO's adoption of 37 C.F.R. § 1.313(b), its own regulation, plaintiff offers two arguments to support its contention that the Court's review should be

more searching and less deferential. First, plaintiff argues that 37 C.F.R. § 1.313(b) does not have the force and effect of law, because the PTO does not have substantive rulemaking powers outside of its own regulations, [FN5] and so the regulations are not entitled to the Court's deference.

FN5. 35 U.S.C. § 6 empowers the Commission to "establish regulations, not inconsistent with law, for the conduct of proceedings in the Office." Accordingly, the Commissioner may issue only those regulations concerning the conduct of PTO proceedings.

Alternatively, plaintiff avers that, even if the Court were persuaded that deference is owed § 1.313(b) because it concerns patent proceedings, the regulation still cannot be "inconsistent with law," and under this standard, § 1.313(b) is invalid. Even where an agency's interpretation is entitled to deference, "the courts are the *50 final authority on the issue of statutory construction. They must reject administrative constructions, whether reached by adjudication or by rulemaking, that are inconsistent with the statutory mandate or that frustrate the policy Congress sought to implement." *FEC v. Democratic Senatorial Campaign Comm.*, 454 U.S. 27, 32, 102 S.Ct. 38, 70 L.Ed.2d 23 (1981). Here, plaintiff claims, Congress has explicitly spoken to the salient issue, and so the court "must give effect to the unambiguously expressed intent of Congress." *Brown & Williamson Tobacco Corp.*, 529 U.S. 120, 120 S.Ct. 1291, 1299, 146 L.Ed.2d 121 (2000).

Defendant maintains that *Chevron* deference is appropriate here as well, on several grounds. First, as noted above, defendant argues that this regulation is due great deference because it was propounded pursuant to a statute that the PTO Director is charged with administering. *See Udall v. Tallman*, 380 U.S. 1, 16, 85 S.Ct. 792, 13 L.Ed.2d 616 (1965). Second, defendant argues that the Court must "accord[] considerable weight to the prior long-standing interpretation, if reasonable, of the agency charged with administering a regulatory scheme," *see Craft Machine Works, Inc. v. United States*, 926 F.2d 1110, 1114 (Fed.Cir.1991), and that 35 U.S.C. § 151 and 37 C.F.R. § 1.313(b) have co-existed without incident under that "prior long-standing interpretation." [FN6]

FN6. The PTO has interpreted the "shall issue" language as allowing the withdrawal of a patent

after payment of the issue fee for almost a century. See Rules of Practice in the Patent Office § 165-55 (1888-1848); Rules of Practice of the United States Patent Office in Patent Cases § 313 (1949-1972); and see 37 C.F.R. § 1.313(b) (1973-1996).

This Court is persuaded by defendant's argument. According to the PTO's adoption of 37 C.F.R. § 1.313(b) appropriate deference under *Chevron*, this Court holds that the PTO's regulation is eminently reasonable, in light of the PTO's purpose of issuing valid patents, and contravenes neither the spirit nor the letter of 35 U.S.C. § 151.

3. *Caselaw and Intersection between 35 U.S.C. § 151 and 37 C.F.R. § 1.313(b)*

Plaintiff cites three cases in support of its argument that, once patent fees have been paid, issuance of the patent is a required administrative formality. [FN7] In *Brenner v. Ebbert*, 398 F.2d 762 (D.C.Cir.1968), cert. den., 393 U.S. 926, 89 S.Ct. 259, 21 L.Ed.2d 262 (1968), the D.C. Circuit stated that "if the issue fee is timely tendered, the patent must issue," and that issuance of the patent is "a relatively ministerial act." *Brenner*, 398 F.2d at 764. The *Brenner* plaintiffs failed to pay the issue fee within the statutory three month time period because of an error by their attorney. When plaintiffs tried to pay the fee almost seven months after it was due, defendant PTO rejected the payment. Plaintiffs tried to revive the application. The Commissioner dismissed the petition. Plaintiffs brought suit to reverse the dismissal, compel revival, acceptance of the fee, and issuance of the patent. *Id.* at 763. The court upheld the PTO's dismissal. Defendant notes that, since *Brenner* concerned the timing of payment of the issue fee, and not the PTO's authority to withdraw a patent from issue, the language on which plaintiff relies is dicta. Defendant is correct. In fact, the court expressly set aside meaningful consideration of the patent issuance language, preceding the language on which plaintiff relies with "[c]ongress established a separate statutory framework for what remains--issuance of the patent." Accordingly, the Court is not persuaded by this language.

FN7. Plaintiff also cites Judge Newman's concurring opinion in *Exxon Chem. Patents, Inc. v. Lubrizol Corp.*, 935 F.2d 1263 (Fed.Cir.1991), as persuasive authority in support. Defendant notes that this was only a concurrence, and

therefore "not the law," as Judge Newman herself pointed out in *Pioneer Hi-Bred Int'l, Inc. v. J.E.M. Ag Supply, Inc.*, 200 F.3d 1374, 1378 (Fed.Cir.2000).

*51 Plaintiff also cites *United States Gypsum Co. v. Masonite Corp.*, 21 F.Supp. 551 (D.Del.1937) in support of its mandatory interpretation of the "shall issue" language. In *Gypsum*, the court held that the defendant had a legal right to pay the final patent fee. In interpreting identical "shall issue" language in an earlier version of § 151, the court stated that "the Commissioner is bound by statute to issue the patent" once the final fee has been paid. *United States Gypsum Co. v. Masonite Corp.*, 21 F.Supp. 551, 552 (D.Del.1937). Defendant discounts the *Gypsum* holding by noting that there, as in *Brenner*, the issue before the court was not whether the PTO has the authority to withdraw a patent application from issue after payment of the issue fee; it was whether the district court should enjoin a patent applicant from paying the issue fee on its allowed application. Accordingly, defendant argues, and the Court agrees, this holding has no relevance to the present case. As with *Brenner*, the Court places no reliance on the language plaintiff cites.

Finally, plaintiff cites *Sampson v. Dann*, 466 F.Supp. 965 (D.D.C.1978), which is factually analogous to the present case. In a prior lawsuit, the *Sampson* court had remanded the *Sampson* plaintiff's case to the PTO for the purpose of granting plaintiff a reissue patent. On remand, the PTO examiner completed the patent examination, the PTO sent plaintiff a notice of allowance, and plaintiff timely paid the fee. The PTO mailed plaintiff a notice scheduling the issuance of the patent. Before the patent was issued, however, a defendant in a separate patent infringement action brought by *Sampson* contacted the PTO to inform the PTO of prior art not considered during the review of the original application. In response, PTO officials examined the prior art, and directed that the prior art be withdrawn from issue because the prior art raised doubts about patentability. Plaintiff returned to court and argued that he was entitled to have the patent issued. The court agreed, holding that Congress' command in § 151 that "the patent shall issue" created an enforceable right in *Sampson*. See *Sampson v. Dann*, 466 F.Supp. 965, 972 (D.D.C.1978). The court also postulated that "[t]he Patent and Trademark Office's over-all effectiveness as a protector of that public interest

might well be enhanced by strict and merciful cut-off of Patent and Trademark Office consideration of an individual patent application once notice and payment have been effected, particularly one that has been so prominent and protracted as *Sampson's*." *Id.*

Unlike the *Brenner* and *Gypsum* courts, the *Sampson* court considered the issue presented in the present case: whether defendant has the authority to refuse to issue a patent once the issue fee has been paid. Accordingly, defendant addresses it by citing a more recent case from this court, *Harley v. Lehman*, 981 F.Supp. 9 (D.D.C.1997), which also considered the issue in the present case, but which discounts the *Sampson* case because of a subsequent change in the PTO's implementing regulations.

Harley is factually and procedurally identical to the present case. In *Harley*, plaintiff's application was allowed, plaintiff paid the issue fee, and a patent number and issue date were set. Just five days before the issue date, pursuant to 37 C.F.R. § 1.313(b)(3), the PTO withdrew the application, because a PTO director became concerned about the possible unpatentability of the application's claims. The applicant sued in district court, asserting, as Blacklight does, that the Commissioner lacked the statutory authority to withdraw the patent once the issue fee had been paid. The *Harley* court held that the PTO regulation allowing withdrawal of a patent from issue based on unpatentability was a reasonable interpretation of 35 U.S.C. § 151. The court also noted the historic coexistence of the ostensibly vying statutes as further proof that the PTO's interpretation was reasonable.

*52 The *Harley* court specifically discounted the *Sampson* case. Like Blacklight, the *Harley* plaintiff relied on *Sampson*. The *Harley* court held, however, that "[p]laintiff's reliance on *Sampson v. Dann* ... is misplaced [because] the regulation at issue in this case had not yet been enacted when *Sampson* was decided." [FN8] *Harley*, 981 F.Supp. at 12 n. 3. The *Sampson* court considered the interplay between 35 U.S.C. § 151 and 37 C.F.R. § 1.313(b) before the unpatentability ground, or subsection (3), had been added to the latter provision. Accordingly, the provision allowed the PTO to withdraw the patent after payment of the issue fee only in cases of (1) a mistake on the part of the Office, and (2) a violation of § 1.56 [fraud] or

illegality in the application. The *Sampson* court held that, since there was evidence of neither mistake nor fraud, the PTO was legally bound to issue plaintiff's patent. Defendant's argument on this score, therefore, is double-edged: not only is *Sampson* totally void of persuasive authority here, but *Harley* is controlling. [FN9]

FN8. When *Sampson* was decided in 1978, the PTO's regulations did not expressly allow withdrawal on the basis of unpatentability after payment of the issue fee. The regulation was amended in 1982 specifically to allow withdrawal from issue on the basis of "unpatentability of one or more claims." See 37 C.F.R. § 1.313(b)(3).

FN9. At the May 22, 2000 hearing, plaintiff argued that there actually is no functional difference between the *Sampson* court's consideration of the pre-subsection (3) regulation and the *Harley* court's consideration of the post-subsection (3) regulation. See May 22, 2000 Hr'g Tr. at 63. Plaintiff argued that, in *Harley*, the PTO indicated that they relied on the mistake exception to justify the withdrawal of the *Harley* plaintiff's patent, and that the mistake was the unpatentability of plaintiff's claim. In other words, plaintiff argues defendant slid subsection (3) unpatentability under subsection (1) exception. Therefore, both courts were actually considering the same subsection--subsection (1)--and the fact that subsection (3) had been passed is of no consequence. *Id.* The Court disagrees. The *Harley* opinion clearly indicates that subsection (3), and not subsection (1), was at issue. See *Harley*, 981 F.Supp. at 9, 11.

The Court finds that *Harley*, and not *Sampson*, is the more persuasive authority. First, the *Sampson* opinion, in a crucial section, includes language that effectively approvingly presages the addition of subsection (3):

It may be that fraud by the applicant, or even good cause for the failure by the Patent and Trademark Office to discover the prior art earlier would justify a courtfashioned exception to the statutory command. For example, Patent and Trademark Office custom might have established and Congress might have accepted such an exception. But the Patent and Trademark Office has failed to offer any persuasive proof of such a custom or its acceptance by Congress. Moreover, there is a substantial difference between fraud or other questionable action by an applicant which might justify such an exception and the receipt of prior

art allegations raising routine substantive questions about patentability of a widely known invention claim which is at least ten years old. *Sampson*, 466 F.Supp. at 972-3.

Second, the Court is persuaded that the fact that the *Harley* court squarely considered subsection (3), while the *Sampson* court did not, makes *Harley* more persuasive. Accordingly, this Court finds that, under the applicable caselaw, defendant's interpretation of the governing patent issuance statutes is reasonable.

B. Which PTO Issuance Constituted Reviewable Final Agency Action

[4] The parties disagree over which of the February 17 Notice or the March 22 Decision constituted final, reviewable agency action under the APA. Under 5 U.S.C. § 704, "[a]gency action made reviewable by statute and final agency action for which there is no other adequate remedy in a court are subject to judicial review." For these purposes, " 'agency action' includes the whole or part of an agency rule, order, license, sanction, relief, *53 or the equivalent or denial thereof, or failure to act...." 5 U.S.C. § 551(13). The parties do not dispute whether the February 17 Notice and the March 22 Decision constitute "agency action" under the meaning of the statute; they disagree over which agency action is "final" and therefore "reviewable."

Plaintiff contends that the February 17 Notice is the final, reviewable agency action. See Pl.'s Mot. for Summ. J. at 31-3. Courts must interpret the "finality" element flexibly and practically. See *Abbott Laboratories v. Gardner*, 387 U.S. 136, 149, 87 S.Ct. 1507, 18 L.Ed.2d 681 (1967). Furthermore, in order to be final, the ruling must not have been issued by a subordinate official. See *Franklin v. Massachusetts*, 505 U.S. 788, 797, 112 S.Ct. 2767, 120 L.Ed.2d 636 (1992). Plaintiff argues that the February 17 Notice constitutes the PTO's final action because that Notice effectively vitiated the enforceable right to the '601 patent that arose upon plaintiff's payment of the issue fee. It was definitive action, in that plaintiff's patent counsel's efforts to reverse the Notice were unavailing. And, practically speaking, it had the very concrete effect of delaying Blacklight's planned public offering.

Plaintiff further argues that the February 17 Notice

is the final agency action because the March 22 Decision is merely a post hoc, pretextual rationalization cooked up for litigation purposes. The March 22 Decision was issued after plaintiff filed its lawsuit. Plaintiff characterizes the Decision as a new record made for the reviewing court. See *Consumer Federation of America v. U.S. Department of Health and Human Services*, 83 F.3d 1497, 1506 (D.C.Cir.1996). Accordingly, plaintiff argues, the Court should not consider it the final agency action.

Defendant responds, and the Court agrees, that the March 22 Decision constitutes the "final agency action within the meaning of 5 U.S.C. § 704 for purposes of seeking judicial review." See Pl.'s Mot. for Summ. J., Ex. 8, n. 1.

C. Administrative Procedure Act Claims: Whether the PTO's March 22 Decision Was Arbitrary and Capricious

[5] Plaintiff argues, alternatively, that even if the Court is convinced that § 151 does not forbid the withdrawal of an application from issue after payment of the issue fee, the PTO's withdrawal of the patents-in-application was arbitrary and capricious in violation of the Administrative Procedure Act (APA), 5 U.S.C. § 706 *et seq.* The APA authorizes the Court to issue an injunction to "compel agency action unlawfully withheld," 5 U.S.C. § 706(1), and therefore, plaintiff contends, this Court is authorized to order the PTO to issue the 5 patent applications as patents. The APA also authorizes the Court to "hold unlawful and set aside agency action ... found to be arbitrary, capricious, an abuse of discretion, or otherwise not in accordance with law," or agency action that is "in excess of statutory jurisdiction authority, or limitations, or short of statutory right." 5 U.S.C. § 706(2)(A), (C).

Plaintiff avers that the PTO, in contravention of its own proffered justification for withdrawal of the patents-in-application, did not make the required determination of unpatentability. Here, the March 22 decision upholding the February 17 notice indicated that the PTO relied on 37 C.F.R. § 1.313(b)(3), which allows withdrawal due to the "unpatentability of one or more claims," to justify its withdrawal of the patents-in-application. Plaintiff interprets that regulation to mean that a patent can

be withdrawn only upon a finding of unpatentability, not upon a possibility of unpatentability. But, plaintiff points out, the March 22 decision indicates that the February 17 notice was issued at the PTO Director's request because she believed that Blacklight's applications "raise[d] a substantial question of patentability on one or more claims." March 22 Decision at 2. Therefore, by defendant's *54 own admission, the PTO has not made a final determination on unpatentability, and so acts in violation of its own regulations, and the APA.

Defendant responds that plaintiff makes this argument about PTO regulations without citing any authority. On the other hand, defendant's own Manual of Patent Examining Procedure (MPEP) § 1308.1 makes clear that withdrawal on the basis of unpatentability after payment of the issue fee is a 2-step process: first, "the actual withdrawal will be handled by the Office of Patent Publications and then the application will be returned to the examiner" and the unpatentable claims are rejected. Defendant further points out that this interpretation of the PTO regulation was upheld in *Harley*, in which the applicant's claims were not formally rejected until 6 months after his application had been withdrawn from issue. *Harley*, 981 F.Supp. at 12.

The Court is persuaded by the defendant's argument. The unpatentability subsection functions as a last-chance procedural measure to enable defendant to observe the PTO's central mandate of issuing viable patents. It is not a final pronouncement of unpatentability. The March 22, 2000 Decision informed plaintiff of this posture; it stated that the Director's decision to withdraw the patent from issue did not constitute either a rejection or an adverse action on the ultimate determination of unpatentability. See Pl.'s Mot. for Summ. J., Ex. 8 at 4. Plaintiff has remedies outside this suit and this Court. See May 22, 2000 Hr'g Tr. at 55-59. Those remedies undermine plaintiff's suggested interpretation of the statute. Any subsection (3) determination of unpatentability will necessarily represent only a possibility of unpatentability, since

such a determination, as defendant has made abundantly clear, is not in any way a final rejection. The PTO's withdrawal of plaintiff's patent application in order to reconsider its patentability was neither arbitrary nor capricious. [FN10]

FN10. This Court is troubled by several steps in the PTO's process, however. Defendant claims that the technology of the '294 application contravenes fundamental laws of chemistry and physics, yet the application was approved by a patent examiner, never reviewed by a supervisor, and would have issued as a patent but for the PTO's eleventh hour withdrawal. Defendant conceded at the May 22, 2000 hearing that the '294 application was withdrawn just days before the issuance date without the benefit of any PTO employee's re-evaluating the file. Also, the February 17 Notice, released twelve days before the scheduled issue date, gave no reason for the withdrawal besides a cryptic citation to 37 C.F.R. § 1.313(b)(3). At the May 22, 2000 hearing, defendant represented that these are common occurrences, because of the enormous number of patent applications that need to be addressed each year, and the "tremendous pressure" placed on patent examiners to produce work. See May 22, 2000 Hr'g Tr. at 48. Defendant may be well-advised to examine its patent issuance process so that their normal operations are not compromised by such seemingly suspicious procedures.

V. Conclusion

For the foregoing reasons, it is hereby

ORDERED that defendant's motion for summary judgment [13-1] is **GRANTED**; and it is

FURTHER ORDERED that plaintiff's motion for summary judgment [11-1] is **DENIED**; and it is

FURTHER ORDERED that the Clerk shall enter final judgment in favor of defendant and against plaintiff.

END OF DOCUMENT

THIS PAGE BLANK (USPTO)



washingtonpost

PRINT EDITION

TOP NEWS

WORLD

STYLE

SPORTS

CLASSIFIEDS

MARKETPLACE

NATION

POLITICS

METRO

BUSINESS & TECH

HEALTH

OPINION

WEATHER

Partner Sites:

[Newsweek.com](#)[Britannica Internet Guide](#)**Related Items**[Print Edition](#)[Horizon](#)[Front Page Articles](#)**On Our Site**[Horizon Online](#)[Horizons Archive](#)[Education](#)[Community](#)[Resources](#)

Perpetual Motion: Still Going Around

By Robert L. Park

Special to The Washington Post

Wednesday, January 12, 2000; Page H03

"Every one of you can be disconnected from the central power grid and never pay another electric bill as long as you live!" That's what Dennis Lee promised an audience of several hundred in the gymnasium of a rural high school near Columbus, Ohio, earlier this year.

They were there, and I was there, because of a full-page ad in USA Today. In letters two inches tall, its headline asked:

Tired of High Electric Bills . . . How About NO Electric Bills?

Columbus was just one stop on a tour of 45 cities across the nation to demonstrate the revolutionary new technology that Lee says can provide infinite free electricity. The centerpiece of his three-hour presentation was an odd-looking contraption of belts and pulleys that he calls "counter-rotation technology."

He says it makes use of something called the "Fourth Law of Motion." Presumably, that allows his gizmo to evade the limitations of Newton's Third Law of Motion -- for every action, there is an equal and opposite reaction.

According to Lee, counter-rotation technology, combined with "permanent magnet motors that are more than 200 percent efficient," can produce infinite free electricity.

But there is no Fourth Law of Motion. And a machine that produces more energy than it is required to run it would violate the most fundamental law of physics, the conservation of energy.

Lee is something of a throwback in the free energy game. The various schemes that his company, Better World Technologies, Inc., has promoted over the years are classical perpetual motion devices from a bygone era.

They rely not on exotic new physics but on a misunderstanding of centuries-old physics -- Isaac Newton's laws of motion and Michael Faraday's laws of electromagnetism, among others. Nonetheless, despite centuries of evidence to the contrary, such claims still have the power to bamboozle and have been doing so for a long time.

An Old Dream

In 1618, a London physician named Robert Fludd thought that he had a way to turn a water wheel without depending on nature to provide a millstream. He would use the wheel's rotation to drive a water pump. The water that had turned the wheel would be pumped back to the top, where it could fall again. A mill powered by this device would run indefinitely.

Alas, the amount of energy supplied by a water wheel cannot exceed the weight of the water that hits its paddles multiplied by the distance the water descends in turning the wheel. It would take the same amount of energy to raise the water back to the top of the wheel as the falling water produced in the first place. No energy would be left to grind flour.

Of course, the concept of energy or "work" as a measurable quantity did not exist in the 17th century. Fludd's idea failed, but his failure led others to one of history's greatest scientific insights and helped to pave the way for the industrial revolution.

It would be another 200 years before the flaw in Fludd's machine would be stated in the form of a fundamental law of nature: Energy is neither created nor destroyed. But it is conserved. That is, there is always exactly the same amount of total energy around after something happens than there was before it happened.

Written as a mathematical equation, that is known as the First Law of Thermodynamics. There is no firmer pillar of modern science. It explains why a ball, no matter what it's made of, can never bounce higher than the point from which it's dropped. That's consistent with our everyday experience: You can't get something for nothing.

But Wait, There's More

Even if it ground no flour, Fludd's water wheel still could not be kept turning. Energy losses, including the heat generated by friction in the machinery, are inevitable. That's embodied in the Second Law of Thermodynamics. Our bouncing ball can never bounce quite as high as the point from which it was dropped.

The first law says you can't win; the second law says you can't even break even.

In the 400 years since Fludd's failure, thousands of inventors have tried to beat the laws of thermodynamics. The laws always won. In frustration, and perhaps embarrassment, many inventors have resorted to fraud, constructing complex devices with cleverly concealed sources of energy. Each failure, each fraud exposed, established the laws of thermodynamics more firmly.

In 1911, the U.S. patent commissioner, exasperated by the time wasted on these impossible ideas, ruled that patent applications for

perpetual motion machines could not be submitted until one year after an operating model was filed with the patent office.

If the machine was still running at the end of the year, the application would be accepted. The new ruling seemed to bring an end to patent applications for perpetual motion machines.

In 1983, however, Joseph Newman, a mechanic from Lucedale, Miss., sought to patent an "energy machine" that he said produced more energy than was needed to run it. Newman insisted that his invention was not a perpetual motion machine and asserted that the energy came from conversion of mass into energy according to Einstein's famous equation $E = mc^2$. Nuclear power comes from this conversion, but Newman's was not nuclear power.

Slowly, Newman said, his machine was devouring its own copper wires and iron magnets. Because c^2 (the speed of light squared) is such a huge number, his machine would, for all practical purposes, last forever.

Unimpressed, the patent examiner rejected Newman's application. Not a man to be pushed around, Newman filed suit in federal court to force the Patent and Trademark Office to grant a patent for "an unlimited source of energy."

Could Joe Newman, a simple mechanic, have discovered a way to convert copper and iron into electrical energy? A federal judge ordered Newman to turn his energy machine over to what then was called the National Bureau of Standards for testing. Properly measured, the output power was found to be much less than the input power. Newman lost his suit.

But his failure, like that of Fludd, made a contribution. His suit, *Newman v. Quigg* now is cited as the legal justification for rejecting all patent applications involving perpetual motion. The conservation of energy thus became the law of the land as well as a law of nature.

Beating the System

Nonetheless, plenty of people still claim to have discovered infinite sources of free energy. Indeed, a worldwide network of passionate free energy believers resides just beyond the fringes of the scientific community.

These people generally shun old-fashioned terms such as "perpetual motion." Instead, they speak a language laced with words and symbols drawn from modern cosmology and atomic physics. They may even believe it to be science, just as witches and faith healers may truly believe that they can summon supernatural powers.

Ignored or even ridiculed by other scientists, they dream of redemption when the world finally realizes the truth. They even have their own magazine, *Infinite Energy*, which fills its pages with rosy stories about progress in the quest for free energy, particularly cold fusion. The progress is hard for a nonbeliever to see.

Nevertheless, these claims attract investors.

For example, BlackLight Power of Princeton, N.J., raised \$10 million from power companies on the word of its founder, Randall Mills, that he had discovered a way to produce inexhaustible, low-cost, non-polluting energy from ordinary water. The method: shrinking the hydrogen atoms into an energy state below their ground state. He calls these shrunk hydrogen atoms "hydrinos."

Atoms can absorb energy, much as energy is stored in the spring of an alarm clock when you wind it. As the clock ticks, the energy is released bit by bit in sound waves, friction and the motion of the clockworks. When the clock is fully wound down, a physicist would say it's in its "ground state" -- the state of lowest energy. A state below the ground state is a contradiction of terms.

Mills, whose degree is in medicine and who has no record of accomplishment in physics, describes this as "the most important discovery of all time . . . up there with fire." Could he be right? Could there be a state of hydrogen that other scientists had missed?

No.

The energy states of atoms are studied through their atomic spectra -- light emitted at very specific wavelengths when electrons make a jump from one energy level to another. The exact prediction of the hydrogen spectrum was one of the first great triumphs of quantum theory; it is the platform on which our entire understanding of atomic physics is built. The theory accounts perfectly for every spectral line.

There is no line corresponding to a "hydrino" state. Indeed, there is no credible evidence at all to support Mills' claim.

Weighty Matters

So many companies are claiming to have discovered free energy that additional claims are needed to set one apart from the competition.

James Patterson, an avuncular, white-haired 75-year-old who complains that his wonderful discoveries take time from fishing, says he also can produce unlimited, non-polluting energy from ordinary water with a device similar to the electrolytic cells of BlackLight Power. But he says the Patterson Power Cell also neutralizes radioactivity.

It would be difficult to find a nuclear physicist who would take such a claim seriously. The only way to neutralize radioactivity, to the extent that it can be done at all, is with a nuclear reactor or a powerful nuclear accelerator. Still, Patterson's company, Clean Energy Technologies, Inc., did well for a time after he appeared on ABC's "Good Morning America" in 1996 and again in 1997.

The problem is that we all want to see miracles. Perhaps scientists do more than others. Many of them were drawn to science by its promise

of miracles. Miracles do occur, more all the time, or at least scientific advances that would have seemed like miracles a few years ago. Besides, who could blame venture capitalists for investing in hydrinos when NASA scientists are investing in gravity shields?

NASA has invested about \$1 million to test the 1992 claim of a Russian physicist, Eugene Podkletnov, that objects placed above a spinning superconductive disk showed a decrease in weight of about 2 percent.

Superconductors are materials, in this case a ceramic, that lose all resistance to electric currents when cooled below a critical temperature. Could the Podkletnov gravity shield be another miracle?

"Let your imagination run wild," a NASA spokesman advised in an interview this year with The Columbus Dispatch. "What could you do if you could cut gravity by 50 percent or negate gravity altogether?"

Well, for one thing, you could build a perpetual motion machine. If Robert Fludd had had a gravity shield, he could have raised the water back to the top of the wheel with less energy than the wheel would generate. All that was missing was the shield.

It's still missing.

NASA has tested one Podkletnov shield. Researchers measured a weight change of only 2 parts per million. Any weight reduction would be a revolutionary discovery, but the researchers noted that such a minuscule effect is at the limit of their measurement accuracy.

Podkletnov was brought to the United States to see whether he could help. He said he was puzzled, that it worked for him. But maybe NASA needed a bigger disk. That's what's happening now; they are building a bigger shield.

You can view this two ways: Either you accept the First Law of Thermodynamics, in which case the fact that a gravity shield would let you build a perpetual motion machine becomes proof that such a shield is impossible, or you figure that the First Law might be wrong and begin searching for a gravity shield.

NASA scientists chose the second option. They are betting against the laws of thermodynamics. No one wins that wager.

The gravity shield motor is the simplest example of an unbalanced-wheel perpetual motion machine. There have been hundreds of attempts to build perpetual motion machines that would run off the force of gravity, relying on complicated schemes for shifting weight from one side of a wheel to the other as it turns.

But shifting the weight always costs more energy than the wheel supplies. That was the problem with Fludd's water wheel.

It's also the problem with another another class of perpetual motion

machines that supposedly extract energy from their surroundings. These usually involve a fluid that vaporizes readily at room temperature. The pressure exerted by the expanding vapor is used to drive a piston.

Such machines violate the Second Law of Thermodynamics. It also takes energy to cool the vapor back into the liquid state so it can power a second stroke of the piston. And that takes more energy than the piston can supply.

Dennis Lee was featuring such a machine two years ago when I saw his show in Hackensack, N.J. He called it the "Fisher engine" and described it as the "most important discovery in mechanical history."

Actually, it was an old idea. A remarkably similar machine was sold to the Navy in 1880 by John Gamgee, a professor who called it the "zeromotor." It didn't work then either.

Another popular notion involves devices that somehow can rearrange and condense energy from a wide area to a smaller one, where it can be put to use. This is a hugely appealing idea. After all, there's enough heat energy in the average snowbank to heat your home for quite a while; it just happens to be distributed in inconveniently tiny amounts throughout billions of snowflakes and air pockets.

Even if it could all be gathered, it would take a great deal of energy to do so -- more than you could ever extract from the snow.

Still, an ambient-heat engine recently was described in a full page ad in *Physics Today*, the monthly magazine of the physics community, by a company called Entropy Systems Inc. Physicists who took time to read the ad were either outraged or incapacitated with laughter.

If the authors of the ad had any intention of bamboozling readers, they chose an unlikely publication in which to make their pitch.

It never pays to underestimate the human capacity for self-deception, but at some point, those who claim to have discovered a source of free energy must begin to realize that things aren't working as they expected.

They are faced with a choice. In one direction lies acknowledgment that perhaps they've made a mistake. The more publicly and forcefully they have pressed their claim, the more difficult it will be to take that road.

In the other direction is denial. The farther they travel that road, the less likely it becomes that they will ever turn back. This is the road to fraud because no matter how many laws they've broken by that time, they cannot break the laws of physics.

Robert L. Park, professor of physics at the University of Maryland, is the author of the forthcoming book, *Voodoo Science: The Road from Foolishness to Fraud* (Oxford University Press).



UNITED STATES PATENT and TRADEMARK OFFICE

69
UNDER SECRETARY OF COMMERCE FOR INTELLECTUAL PROPERTY AND
DIRECTOR OF THE UNITED STATES PATENT AND TRADEMARK OFFICE
WASHINGTON, D.C. 20231
WWW.USPTO.GOV

Mailed: NOV 23 1998

Paper Number 37

In re application of
Randell L. Mills.
Serial No. 09/009,294
Filed: January 20, 1998
For: HYDRIDE COMPOUNDS

:
: DECISION ON
: PETITION
:
:

This is a decision on the PETITION UNDER 37 CFR 1.181 TO WITHDRAW THE FINALITY OF THE OFFICE ACTION mailed July 3, 2001.

On September 1, 2000, a non-final office action was mailed to applicant (paper no. 27). The office action contained a rejection of all the claims under 35 USC 101 as lacking utility and 35 USC 112, first paragraph as lacking enablement.

A reply to the office action was filed by Applicant on March 1, 2001. In the reply, no amendments were made to the claims. Applicant presented arguments in an attempt to overcome the aforementioned rejections. Additionally, a declaration under Rule 132 was filed on June 22, 2001.

On July 3, 2001 a final office action was mailed (paper no. 34). All of the previous grounds of rejection were maintained.

Petitioner has argued that the finality of the last office action is improper. Petitioner argues that the finality is premature due to the introduction of new grounds of rejection that were neither necessitated by amendment of the claims, nor based on information submitted in an information disclosure statement. Additionally, it is argued that a clear issue between applicant and examiner has not been developed.

DECISION

The non-final office action mailed September 1 2000 contained rejections over claims 1-299 under 35 USC 101 and 35 USC 112, first paragraph. The office action presented arguments as to why the claims lack utility and enablement under the appropriate statute. Applicant's response to this office action, filed March 1, 2001 attempted to rebut the positions set forth in the September 1, 2000 office action. In the final office action mailed July 3, 2001, the examiner maintained the previous grounds of rejection of claims 1-299 and specifically referred back to non-final Office action for the reasoning behind the rejections (see final office action, page 2, lines 2 and 3). In addition, the examiner responded to Applicant's arguments in a separate section (see final office action - Attachment). In the attachment, the examiner addressed the arguments set forth by Applicant in the response filed March 1, 2001 and the Rule 132 declaration. As to the first issue of premature finality, the MPEP states the following:

706.07(a) Final Rejection, When Proper on Second Action

Under present practice, second or any subsequent actions on the merits shall be final, except where the examiner introduces a new ground of rejection that is neither necessitated by applicant's amendment of the claims nor based on information submitted in an information disclosure statement filed during the period set forth in 37 CFR 1.97(c) with the fee set forth in 37 CFR 1.17(p)

In the instant case, no new ground of rejection was applied by the examiner in the final office action. The 35 USC 101 and 112, first paragraph rejections were the same as those in the previous non-final action (in fact the examiner refers back to the previous office action for the reasoning in making the rejections). The arguments put forth by the examiner do not constitute a new ground of rejection in that they merely respond to arguments presented by applicant and do not change the basis for the rejections (i.e. the rejections are still based on lack of novelty and enablement as set forth in the previous office action).

As to the second issue of premature finality, the MPEP states the following:

Before final rejection is in order a clear issue should be developed between the examiner and applicant.

In the present case, a clear issue has in fact been developed between the examiner and applicant. In the non-final action mailed September 1, 2000, the only grounds of rejection were the 35 USC 101 and 35 USC 112, first paragraph rejections mentioned above. The examiner set forth reasoning to support these rejections. Applicant then replied to the rejections and the positions of the examiner. The rejections were maintained in the final office action and the examiner answered the arguments filed by applicant relating to the issue of whether the claims were lacking in utility and enablement. The issues in the present application are clear - whether the claims lack utility and are enabled to one of ordinary skill in the art.

Accordingly, the examiner properly made the July 3, 2001 Office action final.

The Petition is **DENIED**.



Jacqueline M. Stone, Director
Technology Center 1700
Chemical and Materials Engineering

FARKAS & MANELLI, PLLC
2000 M STREET, N.W.
7TH FLOOR
WASHINGTON, DC 20036-3307

Emission in the Deep Vacuum Ultraviolet from an Incandescently Driven Plasma in a Potassium Carbonate Cell

H. Conrads*, R. Mills**, Th. Wrubel***

* Wolfshovener Strasse 195, 52428 Jülich, Germany

** Black Light Power, Inc., 493 Old Trenton Rd., Cranbury, N.J. 08512, USA

*** Institute for Experimental Physics V, Ruhr University, 44780 Bochum, Germany

Abstract

Electromagnetic radiation in both the visible and vacuum ultraviolet (VUV) spectral ranges was emitted from an incandescently driven plasma in a potassium carbonate cell after the potassium carbonate coated on a titanium mesh was heated to above 750°C in a hydrogen atmosphere. The pressure was between 0.1 and 1 mbar, and the hydrogen was dissociated by a hot tungsten wire. Bright visible light filled the annulus between the coaxial tungsten heater and the titanium mesh. This grid was at a floating potential. The emission of the H_α and H_β transitions as well as the L_α and L_β transitions were recorded and analyzed. In the latter spectral range, the spectra show rotational-vibrational transitions of molecular hydrogen which belong to the Werner-band-system of molecular hydrogen. The plasma generated in the incandescently driven cell has phenomenological similarities to that of low pressure electrical driven discharges such as striations of the plasma or the appearance of unipolar arcs ending on metal surfaces. However, the plasma seemed to be far from thermal equilibrium and dependent on the chemistry of atomic hydrogen with potassium. Details of the chemistry powering a novel VUV-light source could not be revealed within the frame of this contribution.

I. Introduction

Table top sources emitting radiation in the deep ultraviolet spectral range are gaining more and more interest in photochemistry due to the increased functionalization of surfaces, particularly in combination with lithographic processes [1]. The range and complexity of applications are wide and range from simple sterilization of large surfaces to sophisticated nano-patterning in production processes of microelectronics and biotechnology [2]. Well known sources such as electric sparks [3], capillary discharges [4], pseudosparks, hollow cathode discharges [5], laser sparks, and barrier discharges [6], to name a few, are suited for

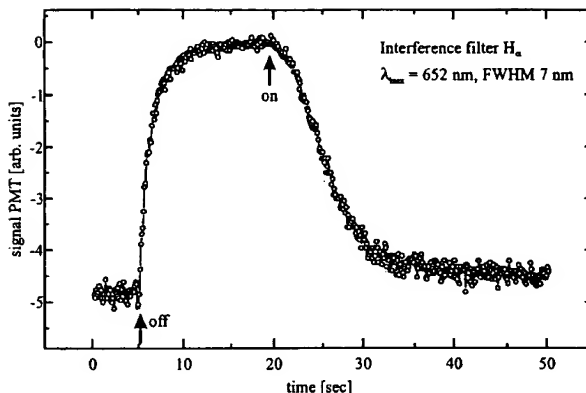


Figure 1: Emission of the cell as a function of time, while the heater current was turned of and on.

such photochemical work and are selected and developed further according to the specifications of the particular application.

Previously reported VUV emission of incandescently driven potassium carbonate cells in hydrogen [7] seemed to depend more on the chemistry of the potassium with hydrogen—with sodium carbonate no VUV emission was observed—and on the temperature of components in the cell than on a particular voltage or current applied to the cell. Figure 1 shows the decay and return of the H_α emission, which is indicative of an associated VUV emission, when the power was turned off and on in several ms. After turning off the heater power, the intensity dropped with a time constant of 2 seconds. With restoration of the original heater power, 10 seconds elapsed before the H_α emission reached its maximum again.

The following paper addresses the plasma and the VUV radiation generated in such a cell. The emission of the first two members of the Balmer and Lyman series were recorded with higher spectral resolution than before [7], and in contrast to earlier investigations, the tungsten wire was heated by external radiation as well as by ohmic heating.

II. Experimental set up

A. The Cell

Three different types of cells were used to investigate the formation of a low-voltage hydrogen plasma and the emitted radiation. One design, type I, was described previously [8]. In the second design, type II, the helical tungsten wire heater was replaced by two commercial 120 V halide bulbs connected in parallel. A tungsten wire was wrapped around the outside of the bulbs to serve as a hydrogen dissociator [9]. The tungsten wire in the type II cell as well as the titanium mesh were at a floating potential. All other components were the same as those of the type I cell. In the third design, type III, the thermal insulation of the quartz tube vacuum vessel of the type I cell was removed and replaced by an oven. An adjacent part of the tube had no insulation in order to allow for "side on" observation of the radiation. The rest of the quartz tube was covered by a brass tube that extended to the cap which provided the different supplies. The voltage supplied to the tungsten wire heater was increased step-wise from 20 V to 70 V. At 70 V, the color of the tungsten wire was similar to the one in the center of the oven.

For the Lyman series measurements, all of the cells were windowless and connected to a VUV spectrometer directly for "end-on" observation. The visible radiation was coupled to the spectrometer by glass fibers for "side-on" observation.

B. The Spectrometers

The light in the visible spectral range was analyzed by a grating spectrometer in Czerny-Turner mounting and recorded by a photomultiplier and oscilloscope as well as by an optical multichannel analyzer (OMA) system. A 1200 lines/mm grating blazed at 1000 nm was used. The light in the vacuum ultraviolet was analyzed by a scanning 1 meter grating spectrometer in Eagle mounting (McPherson, model 225) equipped with a grating of 1200 lines/mm blazed at 120 nm. The spectra were detected by a photomultiplier coated by a p-Terphenyl scintillator and recorded by an oscilloscope. The entrance and exit slits had a width of 50 μm . A pressure gradient was maintained between the cell and the pumped spectrometer.

III. Experimental Results

A. The Cell

The work was started with a type I cell. As soon as the temperature between the quartz wall and the thermal insulation of the cell exceeded 700°C, light was observed from the annulus between the helical tungsten heater and the titanium mesh coated with a thin film of potassium carbonate. The temperature outside of the quartz tube was increased to and held constant at 750°C. The bluish-white-colored emission that lasted for about one hour increased with temperature and was brighter than the glow of the tungsten heater. The experiment was repeated several times until the tungsten heater wire became brittle.

Rather than replace the tungsten wire, a series of experiments was performed next using the type II cell. With an electrically floating tungsten wire wrapped around the outside of the bulbs, the light in the annulus became bright after 10 minutes of heating and was observed to be different in color compared to the bright light emitted from the interior of the bulbs. The bluish-white light was easily observed by eye. The cell wall temperature was again 750°C. The light emission lasted about half an hour. Without the tungsten wire wrapped around the halide bulbs, no bluish-white light emission was observed.

No significant difference in the spectral emission or general performance could be determined between the type I and type II cells. Furthermore, the endurance of the bulbs in type II cell was not significantly better than that of the tungsten heater of the type I cell due to failure of the quartz walls of the bulbs under the resulting high-temperature conditions. The quartz of the bulbs developed plasticity with loss of mechanical stability above 1000°C. This behavior was not observed when the external tungsten wire was absent corresponding to the absence of the generation of the bluish-white light emission from the annulus. Since the operative temperature at the quartz wall of the type II cell was 750°C as well, it was concluded that an exothermic reaction was responsible for the generation of light in the annulus that also required the tungsten to be at a sufficiently high temperature and the presence of potassium carbonate on the titanium mesh.

Next a type III cell was studied. When a current was passed through the tungsten heater of a type III cell, a zone of about 5 – 10 windings was observed to have a significant lower temperature than the other windings as indicated by a difference in color. This cooler zone slowly migrated back and forth along the heater axis. Often several of these lower temperature

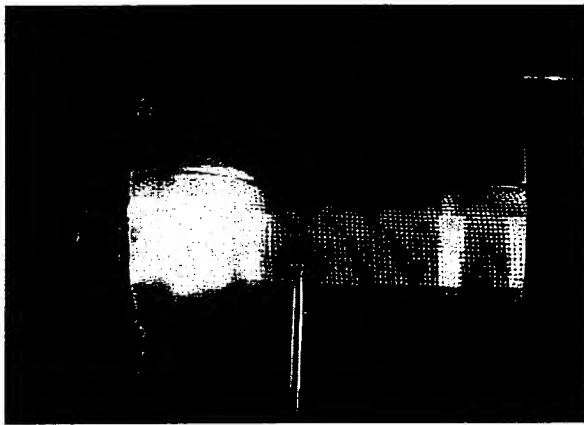


Figure 2: Photograph of the cell (type III). Bluish-white light can be seen at positions up to a few centimeters outside the oven (left) and the brass insulator.

zones were observed. A reasonable explanation for this phenomenon was that an electrical short formed across the zone of the darker windings due to a plasma created around the coil before the bluish emission in the annulus between the tungsten wire and the titanium grid could be visually observed. For the section of the heater that was observable, the voltage across the tungsten windings from one end of the cooler zone to the other was not more than 5 V. The emission of the tungsten wire and the associated voltage inside the insulating brass tube and the oven may have been different.

This segmentation of emission of the tungsten coil also remained active at a later stage when the light emission of the cell was fully developed as evident by the emission of the Balmer series of hydrogen. Then a greenish seam appeared around the dark zone directly pointing to an electrical short by a plasma. At this finally developed stage of the discharge, the bright zones of the tungsten wire shown in Figure 2 pointed to zones of higher axial electric fields. From the inhomogeneous light emission of the tungsten wire, it was concluded that an axial inhomogeneous field was generated in the annulus between the tungsten wire and the titanium mesh.

As shown in Figure 2, bluish light was emitted from the region between the titanium mesh and the quartz wall as well as from the annulus between the tungsten coil and the titanium mesh. A similar pattern was observed for the emission of white light. It was observed that a necessary

condition for this kind of emission was the existence of sufficient potassium carbonate on the titanium mesh, and the intensity of the bluish and white emission was related to the potassium carbonate concentration on the titanium mesh. In addition, it became evident that the temperature of the titanium mesh had to be sufficiently high to enable the emission. This was demonstrated by removing the oven and setting the tungsten coil at the rated voltage of 70 V for a time longer than that required to achieve strong emission. Only the red emission of the tungsten wire was observed. As soon as the oven was slipped over the quartz tube, the bluish and white emission started instantly.

Since the oven heating was sufficient to maintain the temperature of the titanium mesh sufficiently high for emission, the tungsten-coil heater power was reduced by decreasing its voltage. It was possible to sustain VUV light emission down to 20 V corresponding to about 0.2 V per winding and a field of about 0.1 V/cm. The light emission stopped with a voltage just below 20 V and returned at once when the voltage was restored to 20 V. When the voltage was set to zero for a while, the return of the light emission was delayed even when the voltage was quickly increased to 70 V. From these observations, it was concluded that the condition of a minimum tungsten-wire temperature was required in order to trigger the bluish and white light emission, when all of the other conditions were fulfilled. From the experiments with the light bulbs as heaters together with these findings, it was concluded that axial electric fields might be essential for the build up of the plasma and light emission, but an appropriately elevated temperature of the tungsten wire was necessary as well.

Radial plasma striations in the zones of bluish emission (see Figure 2) point to the existence of radial electric fields which might be generated due to chemical potentials in the vicinity of the titanium mesh or due to a Nernst potential because of a strong temperature gradient.

When the pressure in the quartz tube was raised to a couple of mbar, unipolar arcs developed on the titanium mesh. The dependence of this phenomenon on the voltage applied to the tungsten coil was similar to the case described above.

Striations of electric fields and their impact on electron properties in periodic states inside the plasma of a DC-glow-discharge have been analyzed in depth in references [10] and [11]. Since the observed space-resolved visible emission of the AC-driven cell is not very different from that in zones of DC glow discharges, it was concluded that the development of local electric field modulations and distinct non local electron properties may govern this kind of plasma as well. Dark zones in the annulus between tungsten coil and titanium mesh as well as outside the titanium mesh may have been zones of acceleration of free electrons. Electrons

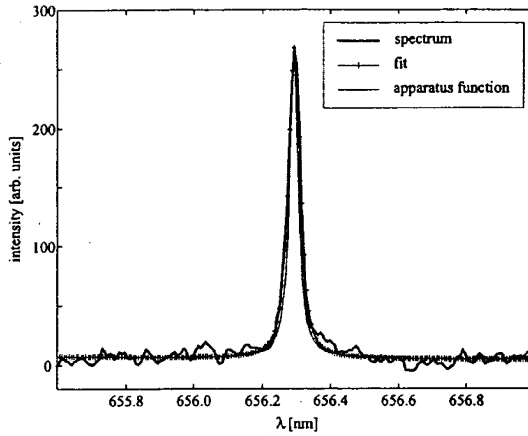


Figure 3: The emission of the H_α measured in second order together with it best fit and the apparatus function.

may have been accelerated axially and/or radially depending on the site in the cell. Inside the bright zones of the plasma the electrons may have lost a part of their energy due to interaction with heavy particles. A local pattern of the velocity distribution of the electrons in periodic states depends on partial pressures of the constituents and the local field distribution [10,11]. Both of these parameters could not be controlled during the reported experiments. It is therefore not too surprising, that the spectral emission such as that in the VUV varied between the different experimental runs as shown in Figures 4a and 4b. The plasma generated by the cell seems to be complex and requires further investigations. These issues are discussed in Sec. IV.

B. The Spectra

For the investigation in the visible spectral range, the wavelength was calibrated using a cold standard lamp that also served for the determination of the apparatus function which was fit by a Voigt profile of 0.96 pixels Gaussian and 3.89 pixels Lorentzian widths. In the first order, the width of the H_α transition ($\lambda = 656.28 \text{ nm}$) corresponds to that of the apparatus profile; whereas, in the second order, a broader and slightly asymmetric H_α profile was observed. Figure 3 shows the emission of the H_α transition measured in the second order with

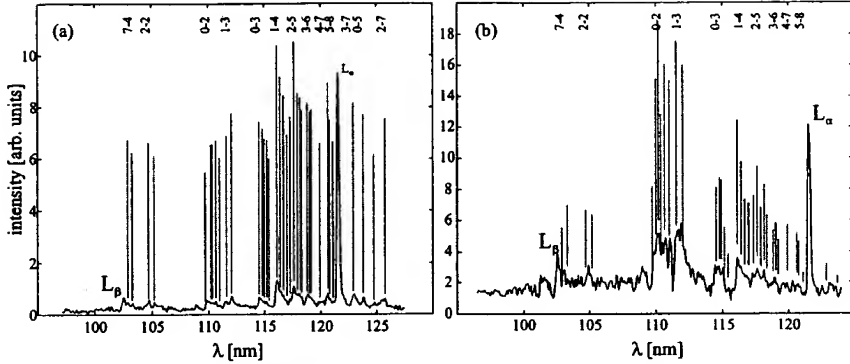


Figure 4: Examples of spectra of the L_α and L_β transitions showing rotational-vibrational transitions belonging to the Werner band system.

a reciprocal dispersion of 7.0 pm/channel together with a least squares fit. The calculated profile consists of three wavelength shifted Gaussian profiles according to the three fine structure transitions of H_α taking into account the intensity ratios given by [12]. The calculated profile is still asymmetric when it is convoluted with the measured apparatus function. Therefore, the asymmetry on the measured spectra can be attributed to the unresolved observation of the fine structure components. The fit gave a Gaussian width of (3.2 ± 0.9) pixels corresponding to (22 ± 0.06) pm. This served for an estimation of an upper limit of the ion temperature of $k_B T_e = (0.1 - 0.32)$ eV.

The H_β transition was identified in the spectra measured in first order. It was not observed in second order because of its low intensity. The intensity ratio of the H_α and H_β transitions was determined to be 15 ± 5 with a relatively high uncertainty due to the low intensity to noise ratio of the H_β transition. By assuming a Maxwell Boltzmann distribution of the level population, an electron temperature of $k_B T_e = (0.30 - 0.43)$ eV was deduced. Since the electron density of the present plasma was small, the assumption of a Maxwell distribution was somewhat questionable. Nevertheless, only a slightly higher temperature of $k_B T_e = (0.32 - 0.48)$ eV was found when a corona model was applied. In both cases, radiation transport was neglected in the calculations so that the temperature given represents an upper limit.

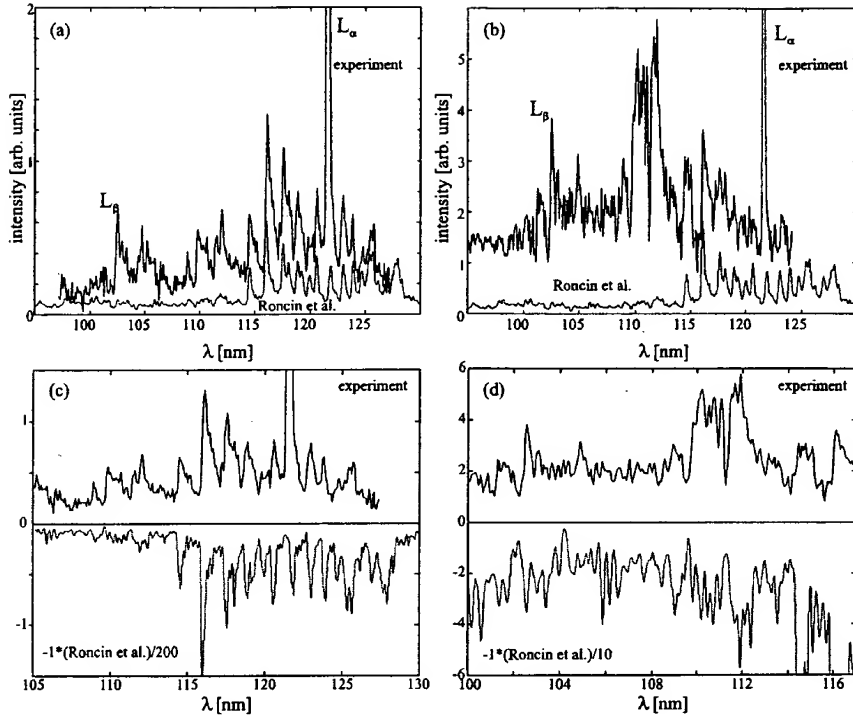


Figure 5: The measured spectra in comparison with a synthetic emission spectrum (intensity-scaled) of molecular hydrogen after /14/. a,c) and b,d) correspond to the experimental spectra in Figure 4a) and 4b), respectively.

Figure 4 shows two scanned spectra in the vacuum ultraviolet spectral range where the emission of the L_α and L_β can easily be seen. Strong emission of bands and lines were also observed in this wavelength region which will be discussed later. The intensity ratio of the L_α and L_β transitions was measured with a higher accuracy to be 16.5. For an optically thin plasma, the corresponding temperature of a Boltzmann level population is 62 eV. This excessive energy may indicate that this model is not applicable possibly because of the large distance of the energy levels. For these series transitions to the ground state, a corona model may be more suitable which gave an upper estimate of the electron temperature of

$k_B T_e = 1.6 \text{ eV}$. Nevertheless, this temperature was also factors higher than the above estimated temperatures indicating that at least the emission of the L_α may have suffered from radiation transport.

In summary, the data indicate that the electron temperature of the present plasma was not higher than $k_B T_e = 0.5 \text{ eV}$. On this basis, it was astonishing that the Lyman alpha and Lyman beta transitions appeared in the spectra since an excitation energy of 10.2 eV and 12.1 eV is required, respectively. The same holds for the Balmer series as well. The Lyman- α energy is a factor of about 20 above the measured thermal energy. The amount of electrons in the Maxwell tail that had enough energy to enhance the Lyman transition was 11 orders of magnitude lower than the total number of electrons.

Figure 5 shows the spectra of Figure 4 together with an emission spectrum of the Werner bands of the hydrogen molecules taken from reference [13]. The experimental spectra in this reference have a coincidence of 95% with theoretical results showing a high level of confidence. About 12,000 transitions were taken into account for the spectrum of Roncin et al. The relative intensities are presented as stated in reference [13], and the lines were convoluted with the measured apparatus profile. It is amazing to see the detailed similarity of the pattern of the energy levels between the experimental and the theoretical spectrum. Not only the vibrational but also numerous rotational transitions were identified in the spectrum of the cell. Similar to atomic emission, electronic transitions in low quantum numbers were preferred by the molecules in the plasma of the cell. However, the relative intensities of the spectrum in Figure 5(b) differed significantly from those of the spectrum of Roncin et al. in the range around 110 nm. This part of the spectrum belongs to a Werner band with $v'=0$ and $v''=1$, respectively.

IV. Discussion

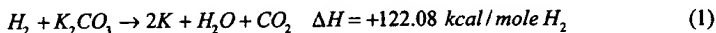
The emission of VUV radiation, and in particular, Lyman series and Werner band emission was observed from a low density plasma of quite moderate temperature similar to that in fluorescence tubes for general lighting. Such a plasma of an incandescently heated cell should not emit VUV radiation. The spectra showed that the plasma was far from thermal equilibrium. This was not too surprising because of the cell components, such as heater and titanium mesh etc., all may have contributed to a bimodal free-electron velocity distribution. But, the relevance of free electrons for the population of electronic levels is questionable

because of the preference for emission from a few specific electronic states of low quantum number. The same applies if a corona equilibrium was assumed.

Only blackbody radiation from the tungsten coil was observed at longer wavelengths. Based on the VUV emission, the plasma was predominately a hydrogen plasma. The ionization of atomic hydrogen requires 13.6 eV. In the cases where plasma was observed, no possible chemical reaction of the tungsten filament, the titanium screen, K_2CO_3 , and low pressure hydrogen at a cell temperature of 750°C could be found which accounted for the generation and sustaining of the plasma. In fact, no known chemical reaction releases enough energy to form an atomic hydrogen plasma as treated in the following discussion.

The enthalpy of formation ΔH_f of potassium hydride is -14.13 kcal/mole [14]. Thus, the formation of potassium hydride releases only 0.59 eV per atom. But, potassium hydride decomposes in this temperature range (288 to 415°C). Thus, it can not account for any emission of the hydrogen plasma.

The reduction of K_2CO_3 by hydrogen calculated from the heats of formation is very endothermic.



The reaction absorbs 2.5 eV per hydrogen atom.

The most energetic reaction possible with oxygen is the reaction of hydrogen to form water which releases 1.48 eV per atom of hydrogen; whereas, the energy of Lyman emission is greater than 10.2 eV per atom.

The dissociation of molecular hydrogen on the filament produces atomic hydrogen which may recombine to release 4.45 eV. Since atomic hydrogen is neutral, no contribution from the electric field of the filament is possible. Thus, excitation with energies of 4.45 eV or less is possible by the transport of thermal energy from the filament due to hydrogen dissociation followed by recombination. But this reaction is not sufficiently energetic to support the observed VUV emission.

Chemical energy may have been transported from regions outside of the annular region where most of the emission was observed. Dense and cold plasmas may have been created close to surfaces such as the titanium mesh due to chemical reactions. In such non ideal plasmas with electron densities close to solid density and temperatures below 0.5 eV, the potential energy of the electrons becomes comparable to their kinetic energy, and energy levels of bound electrons in atoms such as hydrogen are altered such that excitation and ionization energies are lowered [15]. This also applies to other elements of the plasma such as potassium. The electronic energy levels of the different species are further distorted when interacting with

each other. The dissociation of molecules and ionization of both the molecules and atoms may become more probable with more species. However, the lowering of the ionization and excitation energies by the state of "non ideality" in dense plasmas is only about 1 eV even for potassium. Thus, the most energetic chemical source possible, dissociated atomic hydrogen, could not have provided more energy than the Frank-Condon energy of 4.45 eV during recombination. Thus, this mechanism can not explain the hydrogen plasma.

The measured electron temperature, 0.5 eV, is over an order of magnitude too low to account for the hydrogen plasma. The filament electric field as the energy source of the excitation is also eliminated. The emission occurred even when the electric field was set and measured to be zero. The results can not be explained by electric field acceleration of charged species since the estimated external field of the incandescent heater is extremely weak, about 1 V/cm. The electron mean free path at the operating pressure range of 0.1 to 1 mbar is about 0.1 cm corresponding to a mean energy from the acceleration of electrons in the field of about 1 V/cm of under 1 eV. Thus, electron collisional excitation of Lyman emission or hydrogen ionization by a so called 'run-away-situation' of the velocities of free electrons is not probable. However, the observed plasma striations outside the titanium mesh close to the mesh points may have been due to local radial electric fields in the plasma not yet identified, where charged particles were accelerated in the dark zones to energies high enough to excite bound electrons in the brighter zones [11].

Temperature dependent electric fields also arise due to the greater mobility of electrons compared to ions. The generated voltage U for a plasma with a similar ion and electron temperature T is given by

$$U = \frac{kT}{2e} \ln \frac{m_i}{m_e} \quad (2)$$

where m_i is the mass of the ion such as the potassium ion or a proton, m_e is the electron mass, and e is the electron charge. From Eq. (2), the maximum voltage corresponding to the potassium ion is of the order of 1 V.

Multi-collisional processes may be possible [16], but very dense, high-pressure plasmas are required, and given an electron energy of 0.5 eV, about 30 concerted electron collisions would be required within 10^{-8} s—a definite impossibility.

Resonant energy transfer is possible to give predominantly Lyman α and Lyman β emission. Kurunczi, Shah, and Becker [17,18] observed intense emission of Lyman α and Lyman β radiation at 121.6 nm and 102.5 nm, respectively, from microhollow cathode discharges in high-pressure Ne (740 Torr) with the addition of a small amount of hydrogen (up

to 3 Torr). With essentially no molecular emission observed, Kurunczi et al. attributed the anomalous Lyman α emission to the near-resonant energy transfer between the Ne_2^+ excimer and H_2 which leads to formation of $H(n=2)$ atoms, and attributed the Lyman β emission to the near-resonant energy transfer between excited Ne^* atoms (or vibrationally excited neon excimer molecules) and H_2 which leads to formation of $H(n=3)$ atoms. However, the formation of this plasma resulting in Ne_2^+ excimers and excited Ne^* atoms required a field of over 10^4 V/cm; whereas, the field in the heated cells is on the order of 1 V/cm. Thus, this mechanism does not provide a source of energetic photons that may be resonantly transferred.

The titanium-mesh and the tungsten coil were present in all experiments. The emission was not observed with the cell alone, with hydrogen alone, or under identical conditions wherein Na_2CO_3 replaced K_2CO_3 . When the power was interrupted, the emission decayed in about two seconds. Decay was recorded over a time greater than 10,000 times the typical duration of a discharge plasma afterglow [19]. This experiment showed, that plasma emission was occurring even though the voltage between the heater wires was set to and measured to be zero for a time duration which was surprisingly extended. Since the thermal decay time of the filament for dissociation of molecular hydrogen to atomic hydrogen was similar to the plasma afterglow duration of the investigated source which requires the presence of K_2CO_3 , the emission was determined to be due to a reaction of K_2CO_3 with atomic hydrogen. The minimum temperature requirement of the tungsten wire for emission also demonstrated the emission reaction's dependence on atomic hydrogen.

A source of energy other than that provided by the electric field or known chemical reactions must be considered for explaining our experimental findings.

V. Conclusion

The generation of the Lyman and Balmer series and the Lyman Werner bands of molecular hydrogen requires energies significantly greater than 10 eV. The formation of a hydrogen plasma by the cell loaded with K_2CO_3 on titanium and operated in hydrogen required a minimum temperature. The heat from the filament and possibly the weak dipole field from the filament may sustain the hydrogen plasma; but, the latter is not essential because hydrogen lines were emitted during times when this voltage is set to zero. Furthermore, given the observations, free electrons can not excite these states. In the case that the free electrons should have been thermalized, their temperature was too low to contribute to excitation or ionization even from the tail of the velocity distribution. Longer range fields (of the order of mm) were

only about a 1 V/cm. In addition to electron collisional excitation, known chemical reactions, and resonant photon transfer, the lowering of the ionization and excitation energies by the state of "non ideality" in dense plasmas were also rejected as the source of ionization or excitation to form the hydrogen plasma.

The emission from a plasma was observed at low temperatures (e.g. $\approx 10^3$ K) from atomic hydrogen and potassium. The release of energy from hydrogen was evidenced by the hydrogen Lyman and Balmer emission which identified the presence of a hydrogen plasma. The persistence of emission following the removal of all of the power to the cell indicates that an unknown chemical power source is present. The implication is that a new plasma and light source for the vacuum ultraviolet has been discovered.

References

1. U. Kogelschatz, H. Esrom, J. Y. Zhang, I. W. Boyd, "High Intensity Sources of Incoherent UV and UVU Excimer Radiation for Low-Temperature Materials Processing", to be published in Appl. Surf. Sciences 2000/01.
2. A. Ohl, K. Schröder, "Plasma Induced Chemical Micropatterning for Cell Culturing Applications", Surface and Coating Technology, Vol. 116-119, (1999), p. 830.
3. B. Edlen, "Production of Highly Ionized Iron by a Vacuum Spark", Physica, Vol. 13, (1947), p. 545.
4. H. Conrads, "Die Erzeugung eines Rekombinationskontinuums mit Hilfe eines Gleitfunken zur Bestimmung der absoluten Intensität im Vakuum-UV", Z. f. Physik, 200, (1967), p. 444.
5. K. H. Schoenbach, R. Verkeppen, T. Tassow, W. W. Byszewski, "Microhollow Cathode Discharges", Appl. Phys. Lett., Vol. 68, (1996), p. 13.
6. B. Eliasson, U. Kogelschatz, "UV Excimer Radiation from Electrical Barrier Discharges", Appl. Phys. B, Vol. 46, (1988), p. 299.
7. R. Mills, T. Onuma, and Y. Lu, "Formation of a Hydrogen Plasma from an Incandescently Heated Hydrogen-Catalyst Gas Mixture with an Anomalous Afterglow Duration", Int. J. Hydrogen Energy, Vol. 26, No. 7, July, (2001), pp. 749-7628.
8. R. Mills, J. Dong, Y. Lu, "Observation of Extreme Ultraviolet Hydrogen Emission from Incandescently Heated Hydrogen Gas with Certain Catalysts", Int. J. Hydrogen Energy, Vol. 25, (2000), pp. 919-943.

9. N. Ernst, J. H. Block, H. J. Kreuzer, X. Ye, "Thermal Field Desorption Spectroscopy of Chemisorbed Hydrogen for a Single Step Site", *Phys. Rev. Lett.*, Vol. 71, (1993), p. 891.
10. F. Sigeneger, Yu. B. Golubovskii, I. A. Porokhova, R. Winkler, "On the Nonlocal Kinetics in s- and p-Striations of DC Glow Discharge Plasma: I. Electron Establishment in Striation-like Fields", *Plasma Chemistry and Plasma Processing*, Vol. 18, No. 2, (1998), p. 153.
11. F. Sigeneger, and R. Winkler, "On the Nonlocal Electron Kinetics in s and p Striations of a DC Glow Discharge Plasma: II. Electron Properties in Periodic States", *Plasma Chemistry and Plasma Processing*, Vol. 20, No. 4, (2000), p. 429.
12. W. L. Wiese, M. W. Smith, B. M. Glennon, "Atomic Transition Probabilities", *Natl. Bur. Stand. (U.S.) No. NSRDS-NBS 4*, U.S.-GPO, Washington, DC, Vol. I, (1966).
13. J. Y. Roncin, F. Launay, "Vacuum Ultraviolet Emission Spectrum of Molecular Hydrogen", *J. Phys. Chem. Ref. Data*, Monograph 4.
14. W. M. Muller, J. P. Blackledge, G. G. Libowitz, *Metal Hydrides*, Academic Press, New York, (1968), p. 201.
15. H. W. Darwin and P. Felenbok, "Data for Plasmas in Local Thermodynamic Equilibrium", Gauthier-Villars Ed., Paris, (1965).
16. P. Kurunczi, H. Shah, and K. Becker, "Excimer formation in high-pressure microhollow cathode discharge plasmas in helium initiated by low-energy electron collisions", *International Journal of Mass Spectroscopy*, Vol. 205, (2001), pp. 277-283.
17. P. F. Kurunczi, K. H. Becker, "Microhollow Cathode Discharge Plasma: Novel Source of Monochromatic Vacuum Ultraviolet Radiation", *Proc. Hakone VII, Int. Symp. High Pressure, Low Temperature Plasma Chemistry*, Greifswald, Germany, Sept. 10 - 13, (2000), Vol. 2, p. 491.
18. P. Kurunczi, H. Shah, and K. Becker, "Hydrogen Lyman- α and Lyman- β emissions from high-pressure microhollow cathode discharges in $Ne-H_2$ mixtures", *J. Phys. B: At. Mol. Opt. Phys.*, Vol. 32, (1999), L651-L658.
19. A. Surmeian, C. Diplasu, C. B. Collins, G. Musa, I. Lovittz Popescu, *J. Phys. D: Appl. Phys.* Vol. 30, (1997), pp. 1755-1758.

THIS PAGE BLANK (USPTO)

71

Stationary Inverted Lyman Population Formed from Incandescently Heated Hydrogen Gas with Certain Catalysts

Randell L. Mills,* Paresh C. Ray

ABSTRACT

Rb^+ to Rb^{2+} and $2K^+$ to $K+K^{2+}$ each provide a reaction with a net enthalpy equal to the potential energy of atomic hydrogen. The presence of these gaseous ions with thermally dissociated hydrogen formed a plasma having strong VUV emission with a stationary inverted Lyman population. We propose an energetic catalytic reaction involving a resonance energy transfer between hydrogen atoms and Rb^+ or $2K^+$ to form a very stable novel hydride ion. Its predicted binding energy of 3.0468 eV was observed at 4070.0 Å with its predicted bound-free hyperfine structure lines $E_{HF} = j^2 3.0056 \times 10^{-5} + 3.0575 \text{ eV}$ (j is an integer) that matched for $j=1$ to $j=37$ to within a 1 part per 10^5 . This catalytic reaction may pump a cw HI laser.

*Randell L. Mills, BlackLight Power, Inc., 493 Old Trenton Road, Cranbury, NJ 08512, USA,
609-490-1090, 609-490-1066 (fax), rmills@blacklightpower.com

1. Introduction

The Lyman α , β , and γ lines of atomic hydrogen at 121.6 nm, 102.6 nm, and 97.3 nm in the vacuum ultraviolet (VUV) region are due to the transitions from $n=2$, $n=3$, and $n=4$ to $n=1$, respectively. These lines are of great importance in many applications ranging from photochemistry, to laboratory simulations of planetary atmospheres, to astrophysics and plasma physics. In plasma physics, the Lyman series line intensities and their ratios are frequently used in the determination of plasma parameters such as hydrogen number densities and other quantities such as particle fluxes or ion recombination processes [1-2]. For the last four decades, scientist from academia and industry have been searching for lasers using hydrogen plasma [3-6]. Developed sources that provide a usefully intense hydrogen plasma are high powered lasers, arcs and high voltage DC and RF discharges, synchrotron devices, inductively coupled plasma generators, and magnetically confined plasmas. However, the generation of population inversion is very difficult. Recombining expanding plasmas jets formed by methods such as arcs or pulsed discharges is considered one of the most promising methods of realizing an HI laser.

It was reported previously that a new plasma source has been developed that operates by incandescently heating a hydrogen dissociator to provide atomic hydrogen and heats a catalyst such that it becomes gaseous and reacts with the atomic hydrogen to produce a plasma called a resonance transfer or rt-plasma. It was extraordinary, that intense VUV emission was observed by Mills et al. [7-8] at low temperatures (e.g. $\approx 10^3$ K) and an extraordinary low field strength of about 1-2 V/cm from atomic hydrogen and certain atomized elements or certain gaseous ions which singly or multiply ionize at integer multiples of the potential energy of atomic hydrogen, 27.2 eV.

The theory given previously [9-11] is based on applying Maxwell's equations to the Schrödinger equation. The familiar Rydberg equation (Eq. (1)) arises for the hydrogen excited states for $n > 1$ of Eq. (2).

$$E_n = -\frac{e^2}{n^2 8\pi\epsilon_0 a_H} = -\frac{13.598 \text{ eV}}{n^2} \quad (1)$$

$$n = 1, 2, 3, \dots \quad (2)$$

An additional result is that atomic hydrogen may undergo a catalytic reaction with certain atoms and ions which singly or multiply ionize at integer multiples of the potential energy of atomic hydrogen, $m \cdot 27.2 \text{ eV}$ wherein m is an integer. The reaction involves a nonradiative energy transfer to form a hydrogen atom that is lower in energy than unreacted atomic hydrogen that corresponds to a fractional principal quantum number. That is

$$n = \frac{1}{2}, \frac{1}{3}, \frac{1}{4}, \dots, \frac{1}{p}; \quad p \text{ is an integer} \quad (3)$$

replaces the well known parameter $n = \text{integer}$ in the Rydberg equation for hydrogen excited states. The $n=1$ state of hydrogen and the $n = \frac{1}{\text{integer}}$

states of hydrogen are nonradiative, but a transition between two nonradiative states, say $n=1$ to $n=1/2$, is possible via a nonradiative energy transfer. Thus, a catalyst provides a net positive enthalpy of reaction of $m \cdot 27.2 \text{ eV}$ (i.e. it resonantly accepts the nonradiative energy transfer from hydrogen atoms and releases the energy to the surroundings to affect electronic transitions to fractional quantum energy levels). As a consequence of the nonradiative energy transfer, the hydrogen atom becomes unstable and emits further energy until it achieves a lower-energy nonradiative state having a principal energy level given by Eqs. (1) and (3). Processes such as hydrogen molecular bond formation that occur without photons and that require collisions are common [12]. Also, some commercial phosphors are based on resonant nonradiative energy transfer involving multipole coupling [13].

The second ionization energy of potassium is 31.63 eV , and K^+ releases 4.34 eV when it is reduced to K . The combination of reactions K^+ to K^{2+} and K^+ to K , then, has a net enthalpy of reaction of 27.28 eV . Also, the second ionization energy of rubidium is 27.28 eV ; thus, the reaction Rb^+ to Rb^{2+} has a net enthalpy of reaction of 27.28 eV . The catalyst product $H(1/2)$ is predicted to be a highly reactive intermediate which further reacts to form a novel hydride ion $H^-(1/2)$. In this Letter, we report that the population of the level $n=2$ of hydrogen was continuously inverted with respect to $n=3$ and $n=4$ in an rt-plasma formed with K^+ and Rb^+ catalysts. To our knowledge, this is the first report of population inversion in a chemically generated plasma. The plasma was further

characterized by measuring the electron temperature T_e from intensity ratios of alkali lines, the ion temperature and number density from Balmer α line broadening, and the hydride ion product of catalysis by high resolution visible spectroscopy.

2. Experimental

The VUV spectrum (900–1300 Å), the width of the 6563 Å Balmer α line, and the high resolution visible spectrum were recorded on light emitted from a hydrogen microwave discharge performed according to methods reported previously [14] that served as a control for measurements recorded on light emitted from rt-plasmas of hydrogen with KNO_3 or $RbNO_3$. The experimental set up described previously [7-8] comprised a thermally insulated quartz cell with a cap that incorporated ports for gas inlet, outlet, and photon detection. A tungsten filament heater and hydrogen dissociator were in the quartz tube as well as a cylindrical titanium screen that served as a second hydrogen dissociator that was coated with catalysts KNO_3 or $RbNO_3$ and control materials $Mg(NO_3)_2$ or $Al(NO_3)_3$. The titanium screen was electrically floated with 250 W of power applied to the filament. The temperature of the tungsten filament was estimated to be in the range 1100 to 1500 °C. The external cell wall temperature was about 700 °C. The cell was operated with and without an ultrapure hydrogen flow rate of 5.5 sccm maintained at 300 mTorr.

The VUV spectrometer was a normal incidence 0.2 meter monochromator equipped with a 1200 lines/mm holographic grating with a platinum coating that covered the region 20–5600 Å. The VUV spectrum was recorded with a CEM. The wavelength resolution was about 0.2 Å (FWHM) with slit widths of 50 μm . The increment was 2 Å and the dwell time was 500 ms. The VUV spectrum (900–1300 Å) of the rt-plasma cell emission was recorded at about the point of the maximum Lyman α emission to confirm the rt-plasma before the line broadening and high resolution visible spectrum in the region of 4070 Å were recorded. In addition, the visible spectrum 4000–5600 Å was recorded with the normal incidence VUV spectrometer using a PMT and a sodium salicylate scintillator to record K lines.

The electron temperature T_e of the $RbNO_3$ and KNO_3 cell was measured from the ratio of the intensity of the Rb^+ 741.4 Å line to that of the Rb^{2+} 815.3 Å line and the ratio of the K^+ 612.6 Å line to that of the K^{2+} 546.1 Å line, respectively, as described by Griem [15].

The plasma emission from a hydrogen microwave discharge [16] control and each rt-plasma maintained in the filament heated cell was fiber-optically coupled to a high resolution visible spectrometer capable of a resolution of ± 0.06 Å. The slits were set to $20 \mu m$, the step size was 0.1 Å, and the spectra (4000–4090 Å and 6560–6570 Å) were recorded by a PMT in a single accumulation with a 1 second integration time.

3. Results and discussion

A. Hydrogen Lyman series emission

The VUV spectra (900–1300 Å) of the cell emission recorded at about the point of the maximum Lyman α emission from the KNO_3 and $RbNO_3$ gas cell are shown in Figures 1 and 2, respectively, with the superimposed spectrum from the hydrogen microwave plasma. Strong Lyman series VUV emission was observed only with KNO_3 or $RbNO_3$ and hydrogen. The Lyman series lines of the rt-plasma showed population inversion with much greater intensity of atomic hydrogen versus molecular hydrogen compared to the microwave plasma emission. The population density of the excited hydrogen atoms N_α , N_β , and N_γ with principal quantum numbers $n=2,3$, and 4, respectively, were obtained from their intensity integrated over the spectral peaks corrected by their Einstein coefficients. The population ratios, $\frac{N_\beta}{N_\alpha}$ and $\frac{N_\gamma}{N_\alpha}$, for pure H_2 and H_2 with KNO_3 or $RbNO_3$ are given in Table 1.

The important parameter for a lasing medium is the reduced population density $\frac{N}{g}$ given by the population density N divided by the statistical weight g as discussed by Akatsuka et al. [6]. The ratio of $\frac{N}{g}$ for L_β to L_α and L_γ to L_α given in Table 2 demonstrate that with appropriate cavity length and mirror reflection coefficient cw laser oscillations may

be obtained between $n=3$ and $n=2$ since the corresponding $\frac{N_\beta g_\alpha}{N_\alpha g_\beta} > 1$ [6].

For the plasma conditions of this experiment ($T_e \approx 0.7-0.8$ eV, $n_e \approx 10^{11}$ cm $^{-3}$), a threshold reduced overpopulation of $\approx 2 \times 10^8$ cm $^{-3}$ is required for lasing assuming a cavity length of 5 cm and a mirror reflection coefficient of 0.99. Initial modeling results based on the collisional-radiative model [6] suggest that the threshold condition is achieved for these plasmas [17]. Due to the short lifetime of the Balmer α line, an exceptionally monochromatic laser with the possibility of fast switching is anticipated.

In a non-recombining plasma [6], thermal electron collisional mechanisms can not produce the conditions necessary for population inversion. All known sources of excitation were exhausted [18]. The observation, then, of population inversion indicates the presence of free energy in the system. This is further evidence that a new chemical source of energy, greater than 12 eV/atom was present. The only possibility known to the authors is the proposed reaction to form hydrogen states given by Eqs. (1) and (3).

T_e was determined to be 0.84 eV and 0.76 eV for the K^+ and Rb^+ rt-plasma respectively. Similarly, $k_B T_e = (0.30-0.43)$ eV was determined for a K^+ rt-plasma as reported by Conrads et al. [18] with the assumption of a Maxwell Boltzmann distribution of the level population, and a slightly higher temperature of $k_B T_e = (0.32-0.48)$ eV was found when a corona model was applied. The data indicated that the electron temperature was not higher than $k_B T_e = 0.5$ eV. On this basis, it was astonishing that a strong Lyman beta transition appeared in the spectra since an excitation energy of 12.1 eV is required. This energy is a factor of about 25 above the measured thermal energy. The amount of electrons in the Maxwell tail that had enough energy to enhance the Lyman transition was 11 orders of magnitude lower than the total number of electrons. Longer range fields (of the order of mm) were only about a 1 V/cm. In addition to electron collisional excitation, known chemical reactions, resonant photon transfer, and multiphoton absorption, and the lowering of the ionization and excitation energies by the state of "non ideality" in dense plasmas were also rejected as the source of ionization or excitation to form the hydrogen plasma.

A source of energy other than that provided by the electric field or

known chemical reactions must be considered. We propose that the plasma formed chemically rather than electrically and that the product of the energetic chemical reaction of atomic hydrogen with potassium or rubidium ions which serve as catalysts as well as reactants are compounds having hydride ions $H^-(1/p)$; p =integer discussed in Section 3C. Prior related studies that support the possibility of a novel reaction of atomic hydrogen which produces a chemically generated or assisted plasma (rt-plasma) and produces novel hydride compounds include VUV spectroscopy [7-8, 14, 16, 18-27], characteristic emission from catalysts and the hydride ion products [22-25], lower-energy hydrogen emission [14, 19, 21], chemically formed plasmas [7-8, 17-18, 22-27], Balmer α line broadening [16-17, 19, 25, 28], elevated electron temperature [16-17, 19], anomalous plasma afterglow duration [27], power generation [26, 28-29], and analysis of novel chemical compounds [30].

The lines of K^+ , and K^{2+} corresponding to the catalytic reaction were observed as reported previously [23] with the assignments confirmed by a standard potassium plasma spectrum and NIST tables [31-32]. K^{2+} was observed at 510 Å and 550 Å, and K^+ was observed at 620 Å. K was observed at 3447 Å, 4965 Å, and 5084 Å.

The lines of Rb^+ and Rb^{2+} corresponding to the catalytic reaction were observed as reported previously [24] with the assignments confirmed by the NIST tables [32]. Line emission corresponding to Rb^{2+} was observed at 815.9 Å, 591 Å, 581 Å, 556 Å, and 533 Å. Rb^+ was observed at 741.5 Å, 711 Å, 697 Å, and 643.8 Å.

Then the inverted population is explained by a resonance nonradiative energy transfer from the short-lived highly energetic intermediates¹, atoms undergoing catalyzed transitions to states given by Eqs. (1) and (3), to yield $H(n>2)$ atoms directly by multipole coupling [19]

¹ As a consequence of the nonradiative energy transfer of $m \cdot 27.2$ eV to the catalyst, the hydrogen atom becomes unstable and emits further energy until it achieves a lower-energy nonradiative state having a principal energy level given by Eqs. (1) and (3). Thus, these intermediate states also correspond to an inverted population, and the emission from these states with energies of $q \cdot 13.6$ eV where $q=1,2,3,4,6,7,8,9,11,12$ shown in Refs. 14 and 19 may be the basis of a laser in the EUV and soft X-ray, since the excitation of the corresponding relaxed Rydberg state atoms $H(1/(p+m))$ requires the participation of a nonradiative process [18].

and fast $H(n=1)$ atoms. The emission of $H(n=3)$ from fast $H(n=1)$ atoms excited by collisions with the background H_2 has been discussed by Radovanov et al. [33]. Formation of H^+ is also predicted which is far from thermal equilibrium in terms of the ion temperature as discussed in Section 3B. Akatsuka et al. [6] show that it is characteristic of cold recombining plasmas to have the high lying levels in local thermodynamic equilibrium (LTE); whereas, for the low lying levels, population inversion is obtained when T_e becomes low with an appropriate electron density as shown by the Saha-Boltzmann equation.

B. Measurement of hydrogen ion temperature and number density from Balmer line broadening

The method of Videnovic et al. [34] was used to calculate the energetic hydrogen atom densities and energies from the width of the 6563 Å Balmer α line emitted from microwave and rt-plasmas. The full half-width $\Delta\lambda_G$ of each Gaussian results from the Doppler ($\Delta\lambda_D$) and instrumental ($\Delta\lambda_I$) half-widths:

$$\Delta\lambda_G = \sqrt{\Delta\lambda_D^2 + \Delta\lambda_I^2} \quad (4)$$

$\Delta\lambda_I$ in our experiments was 0.06 Å. The temperature was calculated from the Doppler half-width using the formula:

$$\Delta\lambda_D = 7.16 \times 10^{-6} \lambda_0 \left(\frac{T}{\mu} \right)^{1/2} (\text{Å}) \quad (5)$$

where λ_0 is the line wavelength in Å, T is the temperature in K (1 eV = 11,605 K), and μ is the molecular weight (=1 for hydrogen). In each case, the average Doppler half-width that was not appreciably changed with pressure varied by $\pm 5\%$ corresponding to an error in the energy of $\pm 5\%$. The corresponding number densities for noble gas-hydrogen mixtures varied by $\pm 20\%$ depending on the pressure.

The results of the 6563 Å Balmer α line width measured with the high resolution (± 0.06 Å) visible spectrometer on light emitted from rt-plasmas of hydrogen with KNO_3 is shown in Figures 3. Significant line broadening of 17 and 9 eV and an atom density of 4×10^{11} and 6×10^{11} atoms/cm³ were observed from an rt-plasma of hydrogen formed with K^+ and Rb^+ , respectively. A hydrogen microwave plasma

maintained at the same total pressure showed no excessive broadening corresponding to an average hydrogen atom temperature of $\approx 3 \text{ eV}$ and a density of $2 \times 10^{11} \text{ atoms/cm}^3$. These results could not be explained by Stark or thermal broadening or electric field acceleration of charged species since the measured field of the incandescent heater was extremely weak, 1 V/cm, corresponding to a broadening of much less than 1 eV.

C. High resolution visible spectroscopy recorded on rt-plasmas

The catalyst product $H(1/2)$ was predicted to be a highly reactive intermediate which further reacts to form a novel hydride ion $H^-(1/2)$ with a predicted binding energy of 3.0468 eV given by the following formula [9, 25] for the hydride binding energies E_B :

$$E_B = -\frac{\hbar^2 \sqrt{s(s+1)}}{8\mu_e a_0^2 \left[\frac{1 + \sqrt{s(s+1)}}{p} \right]^2} - \frac{\pi\mu_0 e^2 \hbar^2}{m_e^2 a_0^3} \left(1 + \frac{2^2}{\left[\frac{1 + \sqrt{s(s+1)}}{p} \right]^3} \right) \quad (6)$$

where p is an integer greater than one ($1/2$ in this case), $s=1/2$, \hbar is Planck's constant bar, μ_0 is the permeability of vacuum, m_e is the mass of the electron, μ_e is the reduced electron mass, a_0 is the Bohr radius, and e is the elementary charge. The ionic radius is

$$r_1 = \frac{a_0}{p} (1 + \sqrt{s(s+1)}); s = \frac{1}{2} \quad (7)$$

For both the KNO_3 and $RbNO_3$ -rt plasma, this hydride ion was observed by high resolution visible spectroscopy as a broad peak at 4070.0 Å with a FWHM of 1.4 Å as shown in Figure 4 for $RbNO_3$. From the electron g factor, bound-free hyperfine structure lines of $H^-(1/2)$ were predicted with energies E_{HF} given by the sum of the binding energy E_B (Eqs. (6) and (7)), the spin-pairing energy E_{sp} , and the fluxon energy E_Φ that was derived previously [25].

$$E_{HF} = E_\Phi + E_{sp} + E_B = j^2(g-2) \frac{\mu_B}{\sqrt{s(s+1)}} \frac{\mu_0}{r^3} \left(\frac{e\hbar}{2m_e} \right) + g \frac{\mu_0}{r^3} \left(\frac{e\hbar}{2m_e} \right)^2 + E_B \quad (8)$$

$$= j^2 3.0056 \times 10^{-5} + 3.0575 \text{ eV}$$

where j is an integer. The predicted spectrum is an inverse Rydberg-type series that converges at increasing wavelengths and terminates at

3.0575 eV—the hydride spin-pairing energy plus the binding energy. The high resolution visible plasma emission spectra in the region of 4000 Å to 4060 Å show in Figure 4 matched the predicted emission lines for $j=1$ to $j=37$ to 1 part in 10^5 as shown in Figure 5.

4. Conclusion

Rb^+ to Rb^{2+} and $2K^+$ to $K+K^{2+}$ each provide a reaction with a net enthalpy equal to the potential energy of atomic hydrogen, 27.2 eV. The presence of these gaseous ions with thermally dissociated hydrogen formed a plasma having strong VUV emission with an inverted Lyman population. We propose an energetic catalytic reaction involving a resonance energy transfer between hydrogen atoms and Rb^+ or $2K^+$ to form Rb^{2+} and $K+K^{2+}$, respectively, and a hydrogen atom with a Rydberg state $n=1/2$. Emission from Rb^+ , Rb^{2+} and K , K^+ , and K^{2+} were observed. The catalyst product $H(1/2)$ was predicted to be a highly reactive intermediate which further reacts to form a novel hydride ion $H^-(1/2)$. Its predicted binding energy of 3.0468 eV was observed at 4070.0 Å with its predicted bound-free hyperfine structure lines $E_{HF} = j^2 3.0056 \times 10^{-5} + 3.0575 \text{ eV}$ (j is an integer) that matched for $j=1$ to $j=37$ to within a 1 part per 10^5 .

The ionization and population of excited atomic hydrogen levels was attributed to energy provided by atoms undergoing catalyzed transitions to states given by Eqs. (1) and (3). The high ion temperature with a relatively low electron temperature, $T_e < 1 \text{ eV}$, were characteristic of cold recombining plasmas [6]. These conditions of the rt-plasmas favored an inverted population in the lower levels. Thus, the catalysis of atomic hydrogen may pump a cw HI laser. From our results, laser oscillations are expected between $n=3$ and $n=2$.

References

- [1] C. Zimmermann, R. Kallenbach, T. W. Hansch, Phys. Rev. Lett., Vol. 65, (1990), p. 571.
- [2] T. Ibuki, Chem. Phys. Lett., Vol. 94, (1990), p. 169.
- [3] L. I. Gudzenko, L. A. Shelepin, Sov. Phys. JEPT, Vol. 18, (1963), p. 998.

- [4] S. Suckewer, H. Fishman, J. Appl. Phys., Vol. 51, (1980), p. 1922.
- [5] W. T. Silfvast, O. R. Wood, J. Opt. Soc. Am. B, Vol. 4, (1987), p. 609.
- [6] H. Akatsuka, M. Suzuki, Phys. Rev. E, Vol. 49, (1994), pp. 1534-1544.
- [7] R. Mills, J. Dong, Y. Lu, Int. J. Hydrogen Energy, Vol. 25, (2000), pp. 919-943.
- [8] R. Mills and M. Nansteel, P. Ray, IEEE Transactions on Plasma Science, in press.
- [9] R. Mills, *The Grand Unified Theory of Classical Quantum Mechanics*, September 2001 Edition, BlackLight Power, Inc., Cranbury, New Jersey, Distributed by Amazon.com; posted at www.blacklightpower.com.
- [10] R. Mills, Int. J. Hydrogen Energy, in press.
- [11] R. Mills, Int. J. Hydrogen Energy, Vol. 26, No. 10, (2001), pp. 1059-1096.
- [12] N. V. Sidgwick, *The Chemical Elements and Their Compounds*, Volume I, Oxford, Clarendon Press, (1950), p.17.
- [13] M. D. Lamb, *Luminescence Spectroscopy*, Academic Press, London, (1978), p. 68.
- [14] R. Mills, P. Ray, Int. J. Hydrogen Energy, Vol. 27, No. 3, pp. 301-322.
- [15] H. R. Griem, *Principle of Plasma Spectroscopy*, Cambridge University Press, (1987).
- [16] R. L. Mills, P. Ray, B. Dhandapani, J. He, Chem. Phys., submitted.
- [17] R. L. Mills, P. Ray, R. Mayo, IEEE Transactions on Plasma Science, submitted.
- [18] H. Conrads, R. Mills, Th. Wrubel, Plasma Sources Science and Technology, submitted.
- [19] R. L. Mills, P. Ray, B. Dhandapani, J. He, J. of Phys. Chem., submitted.
- [20] R. Mills, Int. J. Hydrogen Energy, Vol. 26, No. 6, (2001), pp. 579-592.
- [21] R. Mills, P. Ray, Int. J. Hydrogen Energy, in press.
- [22] R. Mills, Int. J. Hydrogen Energy, Vol. 26, No. 10, (2001), pp. 1041-1058.
- [23] R. Mills, P. Ray, Int. J. Hydrogen Energy, Vol. 27, No. 2, (2002), pp. 183-192.
- [24] R. L. Mills, P. Ray, Int. J. Hydrogen Energy, in press.
- [25] R. L. Mills, P. Ray, Int. J. Hydrogen Energy, submitted.
- [26] R. Mills, M. Nansteel, and Y. Lu, Int. J. Hydrogen Energy, Vol. 26, No. 4, (2001), pp. 309-326.

- [27] R. Mills, T. Onuma, and Y. Lu, *Int. J. Hydrogen Energy*, Vol. 26, No. 7, July, (2001), pp. 749-762.
- [28] R. Mills, A. Voigt, P. Ray, M. Nanstell, *Int. J. Hydrogen Energy*, in press.
- [29] R. Mills, N. Greenig, S. Hicks, *Int. J. Hydrogen Energy*, in press.
- [30] R. Mills, B. Dhandapani, M. Nansteel, J. He, T. Shannon, A. Echezuria, *Int. J. of Hydrogen Energy*, Vol. 26, No. 4, (2001), pp. 339-367.
- [31] R. Kelly, *Journal of Physical and Chemical Reference Data*, Part I (H-Cr), Volume 16, (1987), Supplement No. 1, Published by the American Chemical Society and the American Institute of Physics for the National Bureau of Standards, pp. 418-422.
- [32] NIST Atomic Spectra Database, www.physics.nist.gov/cgi-bin/AtData/display.ksh.
- [33] S. B. Radovanov, K. Dzierzega, J. R. Roberts, J. K. Olthoff, *Appl. Phys. Lett.*, Vol. 66, No. 20, (1995), pp. 2637-2639.
- [34] I. R. Videnovic, N. Konjevic, M. M. Kuraica, *Spectrochimica Acta*, Part B, Vol. 51, (1996), pp. 1707-1731.

Table 1. The population density ratios $\frac{N_{\beta}}{N_{\alpha}}$ and $\frac{N_{\gamma}}{N_{\alpha}}$ for pure H_2 , KNO_3 , and $RbNO_3$.

| Plasma Gas | $\frac{N_{\beta}}{N_{\alpha}}$ | $\frac{N_{\gamma}}{N_{\alpha}}$ |
|-------------------------|--------------------------------|---------------------------------|
| Pure H_2 ^a | 0.664 | 0.521 |
| KNO_3 | 4.72 | 3.48 |
| $RbNO_3$ | 4.30 | 1.26 |

^a Measured on microwave discharge maintained according to the method of ref. 14.

Table 2. The reduced population density ratios $\frac{N}{g}$ for pure H_2 , KNO_3 , and $RbNO_3$.

| Plasma Gas | $\frac{N_\beta g_\alpha}{N_\alpha g_\beta}$ a | $\frac{N_\gamma g_\alpha}{N_\alpha g_\gamma}$ b |
|-------------------------|---|---|
| Pure H_2 ^c | 0.292 | 0.130 ^c |
| KNO_3 | 2.07 | 0.870 |
| $RbNO_3$ | 1.89 | 0.314 |

a $\frac{g_\alpha}{g_\beta} = 0.444$ where $g = 2n^2$ and n is the principal quantum number

b $\frac{g_\alpha}{g_\gamma} = 0.250$

^c Measured on glow discharge maintained according to the method of ref. 14.

Figure Captions

Figure 1. The VUV spectra (900–1300 Å) of the cell emission from hydrogen microwave plasma (dotted line) and the KNO_3 -hydrogen rt-plasma (solid line) with an inverted Lyman population.

Figure 2. The VUV spectra (900–1300 Å) of the cell emission from hydrogen microwave plasma (dotted line) and the $RbNO_3$ -hydrogen rt-plasma (solid line) with an inverted Lyman population.

Figure 3. The 6563 Å Balmer α line width recorded with a high resolution (± 0.06 Å) visible spectrometer on a rt-plasma formed with K^+ catalyst. Significant broadening was observed corresponding to an average hydrogen atom temperature of 17 eV.

Figure 4. The high resolution visible spectrum in the region of 4000 Å to 4090 Å recorded on the emission of a rt-plasma formed with Rb^+ catalyst from vaporized $RbNO_3$. The $H^-(1/2)$ hydride ion with a predicted binding energy of 3.0468 eV was observed as a broad peak at 4070.0 Å with a FWHM of 1.4 Å. An observed inverse Rydberg-type series of broad emission lines that converged at increasing wavelengths and terminated at about 3.0575 eV—the hydride spin-pairing energy plus the binding energy—matched the theoretical hyperfine energies E_{HF} given by $E_{HF} = j^2 3.0056 \times 10^{-5} + 3.0575$ eV for $j=1$ to $j=37$. Other peaks in the rt-plasma were assigned to molecular hydrogen.

Figure 5. The plot of the theoretical hyperfine energies E_{HF} given by $E_{HF} = j^2 3.0056 \times 10^{-5} + 3.0575$ eV (Eq. (8)) for $j=1$ to $j=37$ and the energies observed for the inverse Rydberg-type series of broad emission lines shown in Figure 4. The agreement was better than within a 1 part per 10^5 .

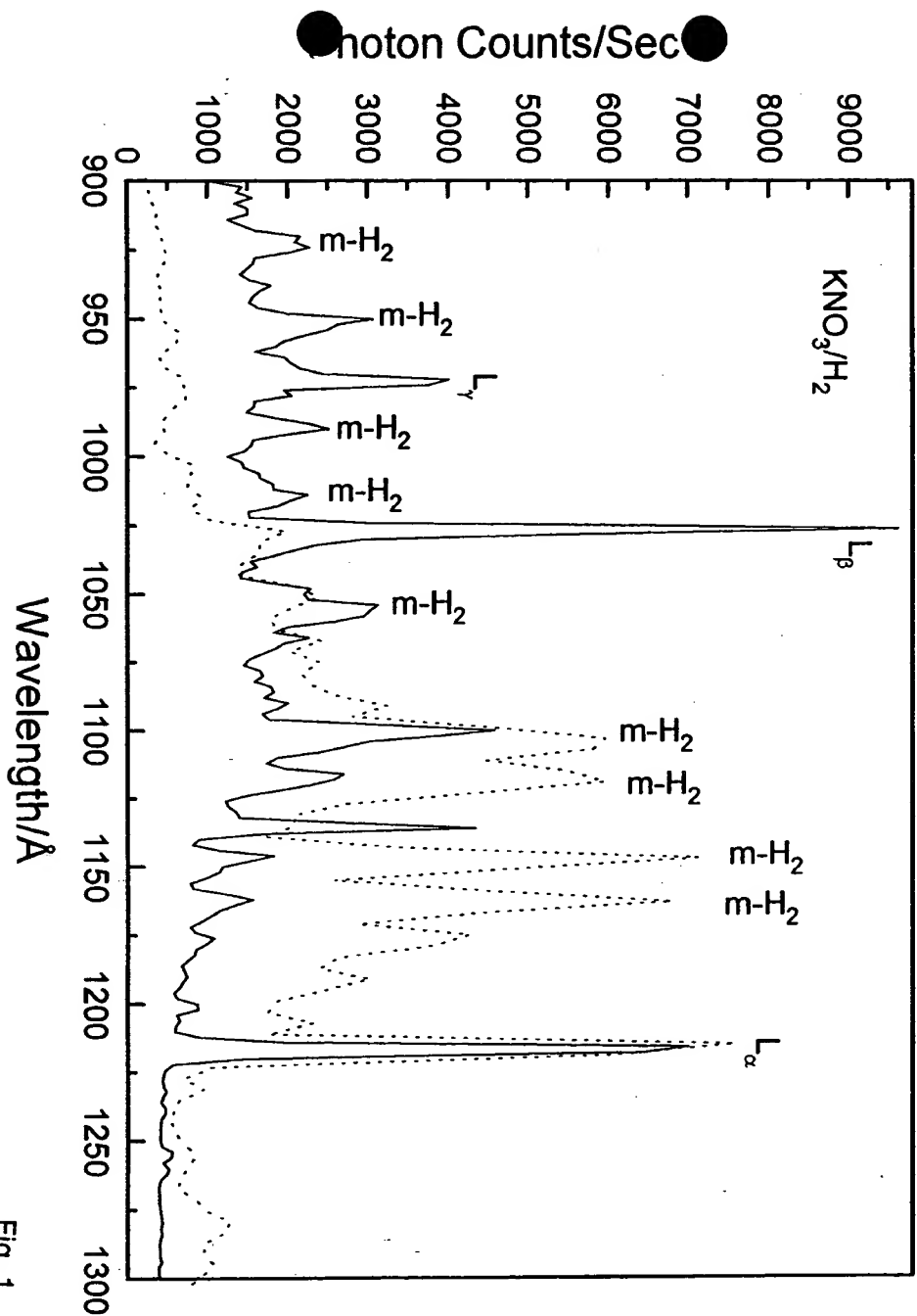


Fig. 1

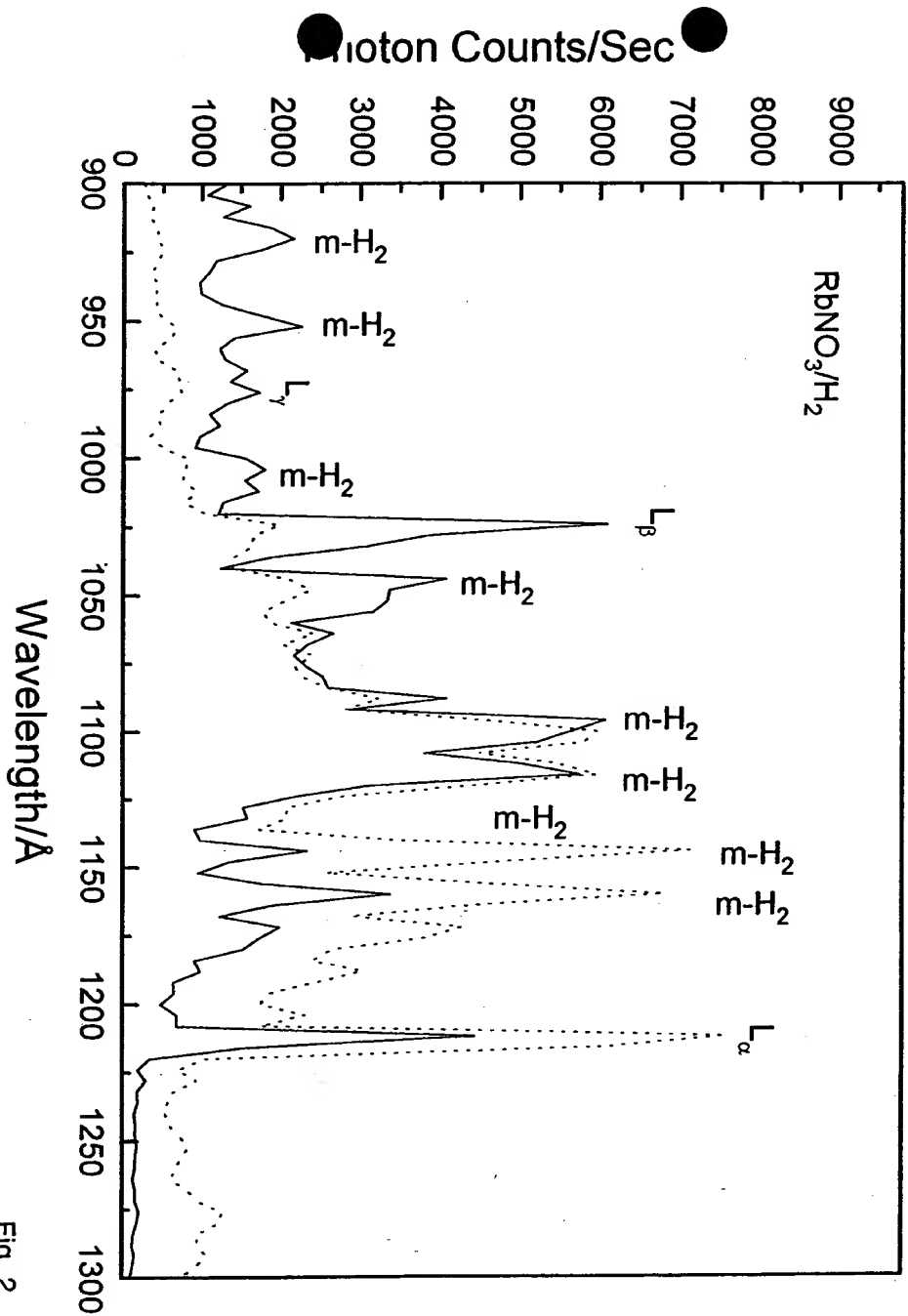


Fig. 2

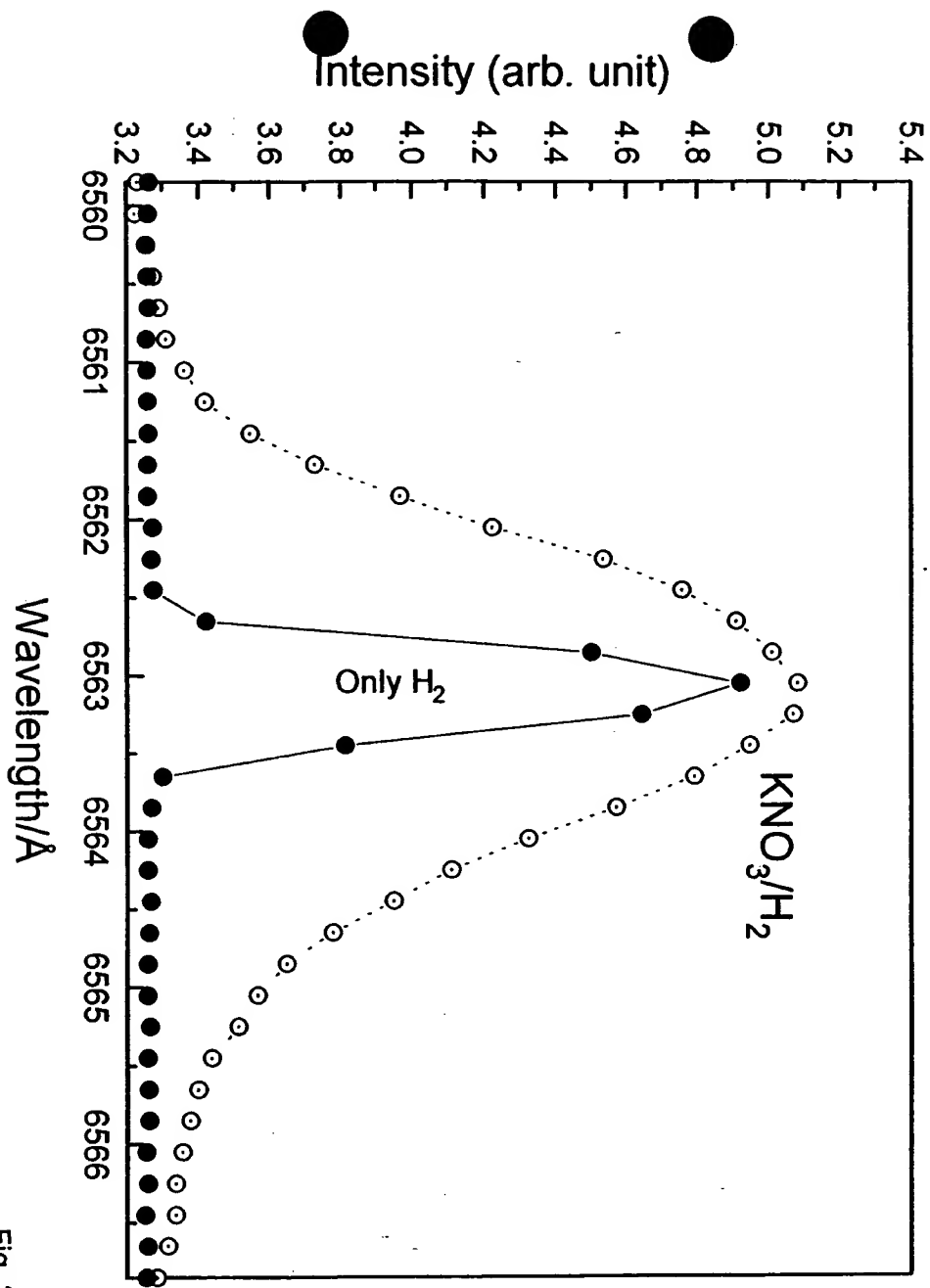


Fig. 3

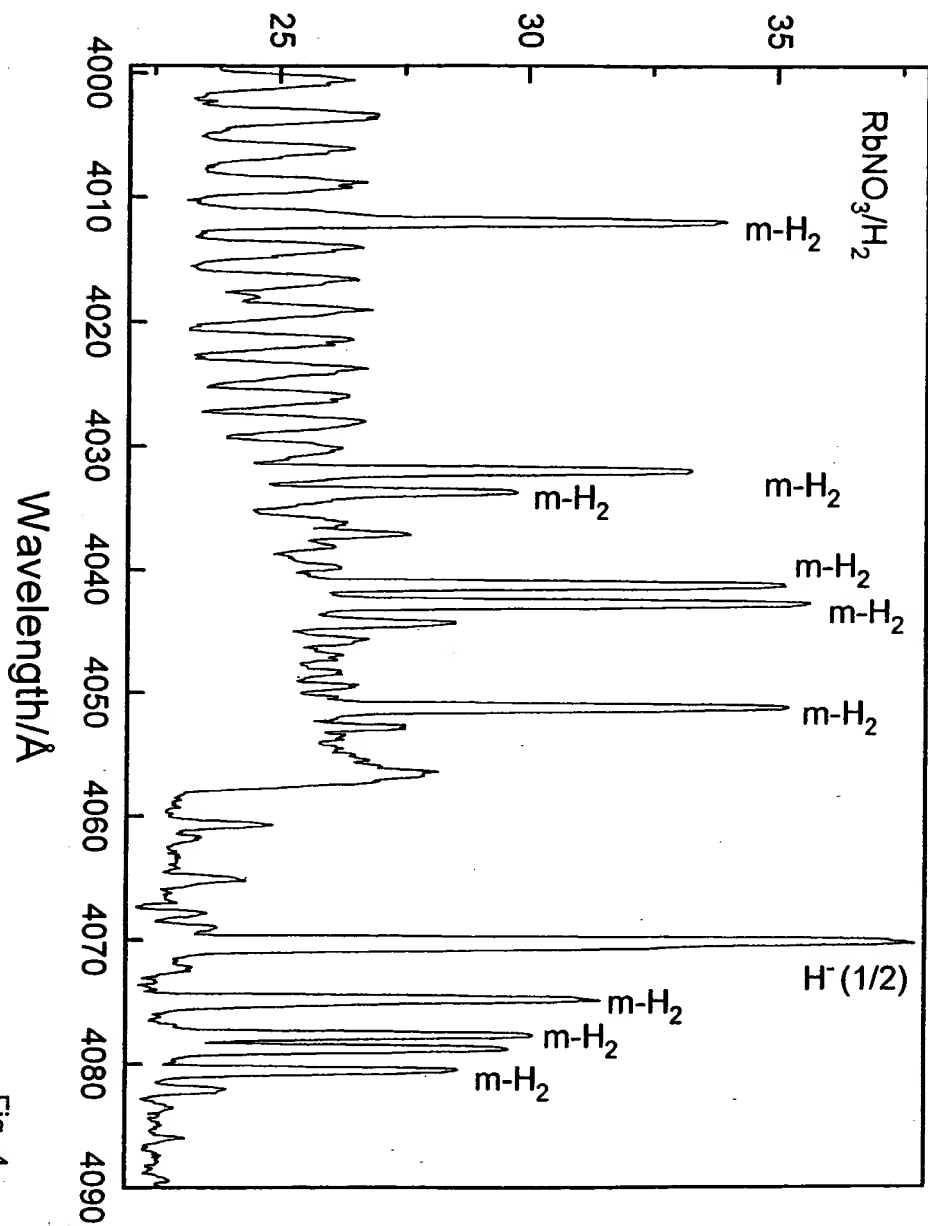
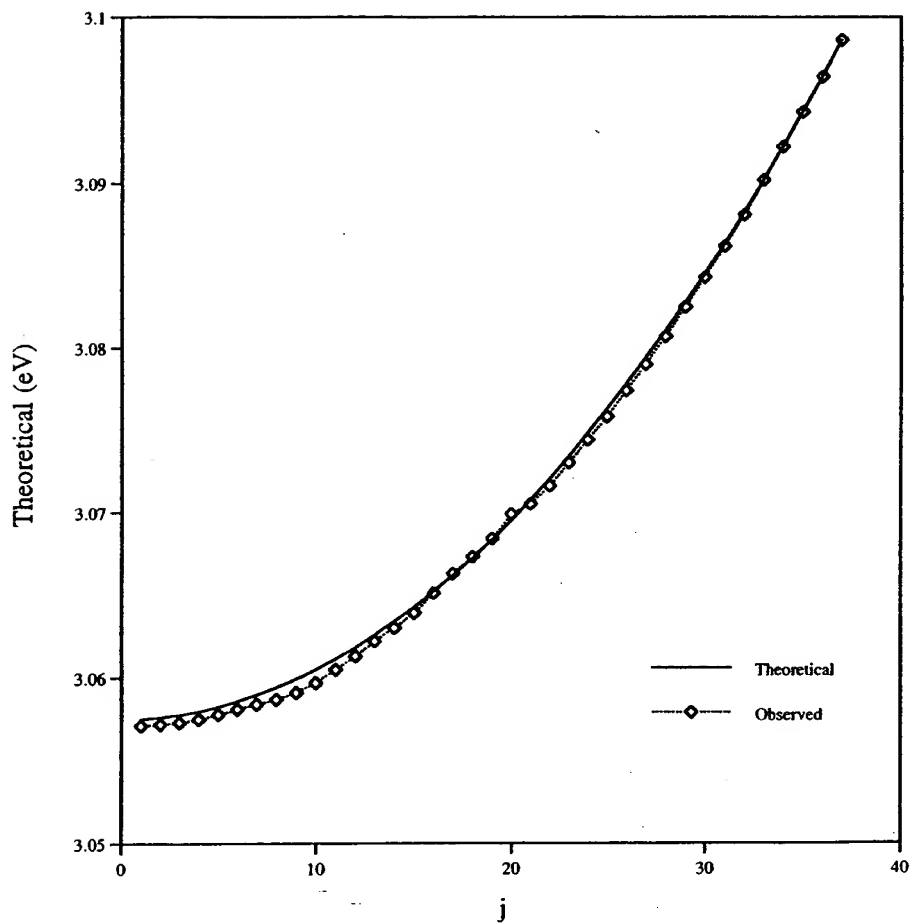


Fig. 4

Figure 5



Synthesis and Characterization of a Highly Stable Amorphous Silicon Hydride

Randell L. Mills

Bala Dhandapani

Jiliang He

BlackLight Power, Inc.
493 Old Trenton Road
Cranbury, NJ 08512

A novel highly stable surface coating $SiH(1/p)$ which comprised high binding energy hydride ions was synthesized by microwave plasma reaction of mixture of silane, hydrogen, and helium wherein it is proposed that He^+ served as a catalyst with atomic hydrogen to form the highly stable hydride ions. Novel silicon hydride was identified by time of flight secondary ion mass spectroscopy and X-ray photoelectron spectroscopy. The ToF-SIMS identified the coatings as hydride by the large SiH^+ peak in the positive spectrum and the dominant H^- in the negative spectrum. XPS identified the H content of the SiH coatings as hydride ions, $H^-(1/4)$, $H^-(1/9)$, and $H^-(1/11)$ corresponding to peaks at 11, 43, and 55 eV, respectively. The silicon hydride surface was remarkably stable to air as shown by XPS. The highly stable amorphous silicon hydride coating may advance the production of integrated circuits and microdevices by resisting the oxygen passivation of the surface and possibly altering the dielectric constant and band gap to increase device performance.

I. INTRODUCTION

Aqueous HF acid etching of silicon surfaces results in the removal of the surface oxide and produces hydrogen terminated silicon surfaces, $Si-H$. HF etching is a key step in producing silicon surfaces which are contamination-free and chemically stable for subsequent processing in the semiconductor industry [1-3]. In fact, chemical oxidation and subsequent HF treatment of Si surfaces are used prior to gate oxidation, where surface contamination (<10 ppm level) and interface control are crucial to device performance. Fluorine termination was initially considered the basis of the chemical stability of HF -treated surfaces. Subsequently, it was found that fluorine is a minor species on the surface and that the remarkable surface passivation achieved by HF is explained by H termination of silicon dangling bonds protecting the surface from chemical attack [3, 4, 5]. However, the replacement of the oxide layer with the H termination of the silicon dangling bonds by HF can be attributed to the increased electronegativity of fluoride ion versus oxide causing an enhanced reactivity of H^+ which attacks the oxide layer. The electron affinity of halogens increases from the bottom of the Group VII elements to the top. Hydride ion may be considered a halide since it possess the same electronic structure. And, according to the binding energy trend, it should have a high binding energy. However, the binding energy is only 0.75 eV which is much lower than the 3.4 eV binding energy of a fluoride ion. And, once the HF is rinsed from the surface, the $Si-H$ layer undergoes rapid oxidation when exposed to oxygen or solvents containing oxygen. An $Si-H$ layer with enhanced stability would be of great value to the semiconductor industry.

Amorphous $Si-H$ films, the active component of important semiconductor devices such as photovoltaics, optoelectronics, and field-effect transistors are formed by plasma enhanced chemical vapor deposition (PECVD) techniques [6]. Typically the film is grown on a silicon wafer substrate exposed to a plasma of silane, hydrogen, and often argon using a reactor with a diode configuration in which the plasma is confined between two parallel electrodes. In this study, we find that the aqueous HF acid etched surface undergoes rapid oxidation when exposed to air and provides little protection from such exposure. Whereas, a

novel highly air stable amorphous $\text{SiH}(1/p)$ surface coating which comprised high binding energy hydride ions was synthesized by microwave plasma reaction of mixture of silane, hydrogen, and helium wherein it is proposed that He^+ served as a catalyst with atomic hydrogen to form the highly stable hydride ions. The novel amorphous Si-H film may advance semiconductor fabrication and devices.

It was reported previously that a new plasma source has been developed that operates by incandescently heating a hydrogen dissociator to provide atomic hydrogen and heats a catalyst such that it becomes gaseous and reacts with the atomic hydrogen to produce a plasma called a resonance transfer or rt-plasma. It was extraordinary, that intense VUV emission was observed by Mills et al. [7] at low temperatures (e.g. $\approx 10^3 \text{ K}$) and an extraordinary low field strength of about 1-2 V/cm from atomic hydrogen and certain atomized elements or certain gaseous ions which singly or multiply ionize at integer multiples of the potential energy of atomic hydrogen, 27.2 eV.

Rb^+ to Rb^{2+} and 2K^+ to $\text{K} + \text{K}^{2+}$ each provide a reaction with a net enthalpy equal to the potential energy of atomic hydrogen, 27.2 eV. Mills et al. have reported an energetic catalytic reaction involving a resonance energy transfer between hydrogen atoms and Rb^+ or 2K^+ to form an rt-plasma with a very stable novel hydride ion product [8-9]. Its predicted binding energy of 3.0468 eV was observed at 407.00 nm with its predicted bound-free hyperfine structure lines $E_{\text{HF}} = j^2 3.0056 \times 10^{-5} + 3.0575 \text{ eV}$ (j is an integer) that matched for $j=1$ to $j=37$ to within a 1 part per 10^5 . Furthermore, each of Cs to Cs^{2+} and Ar^+ to Ar^{2+} each provide a reaction with a net enthalpy of 27.2 eV. The predicted $\text{H}^-(1/2)$ ion due to hydrogen catalysis by each of K^+/K^+ , Rb^+ , Cs , and Ar^+ was also observed by high resolution visible spectroscopy recorded on rt-plasmas and plasma electrolysis cells at 407.00 nm corresponding to its predicted binding energy of 3.0468 eV [10-11]. Hydride ions with high binding energies have been observed by X-ray photoelectron spectroscopy (XPS) and by solid state magic-angle spinning proton nuclear magnetic resonance (^1H MAS NMR) having upfield shifted peaks [11-18]. Additional prior related studies that support the possibility of a novel reaction of atomic hydrogen which produces a chemically generated or assisted plasma (rt-plasma) and produces novel hydride compounds include extreme

ultraviolet (EUV) spectroscopy [7, 9, 19-31], characteristic emission from catalysis and the hydride ion products [8-11, 22-24], lower-energy hydrogen emission [19-21, 27], plasma formation [7-10, 22-26, 32-33], Balmer α line broadening [10, 20, 27-28, 34], elevated electron temperature [20, 27-28], anomalous plasma afterglow duration [32-33], power generation [18, 27, 29-30, 34-35], and analysis of chemical compounds [11-18].

The theory given previously [36-40] is based on applying Maxwell's equations to the Schrödinger equation. The familiar Rydberg equation (Eq. (1)) arises for the hydrogen excited states for $n > 1$ in Eq. (2).

$$E_n = -\frac{e^2}{n^2 8\pi\epsilon_0 a_H} = -\frac{13.598 \text{ eV}}{n^2} \quad (1)$$

$$n = 1, 2, 3, \dots \quad (2)$$

An additional result is that atomic hydrogen may undergo a catalytic reaction with certain atoms and ions which singly or multiply ionize at integer multiples of the potential energy of atomic hydrogen, $m \cdot 27.2 \text{ eV}$ wherein m is an integer. The reaction involves a nonradiative energy transfer to form a hydrogen atom that is lower in energy than unreacted atomic hydrogen that corresponds to a fractional principal quantum number. That is

$$n = \frac{1}{2}, \frac{1}{3}, \frac{1}{4}, \dots, \frac{1}{p}; \quad p \text{ is an integer} \quad (3)$$

replaces the well known parameter $n = \text{integer}$ in the Rydberg equation for hydrogen excited states. The $n=1$ state of hydrogen and the $n = \frac{1}{\text{integer}}$

states of hydrogen are nonradiative, but a transition between two nonradiative states is possible via a nonradiative energy transfer, say $n=1$ to $n=1/2$. Thus, a catalyst provides a net positive enthalpy of reaction of $m \cdot 27.2 \text{ eV}$ (i.e. it resonantly accepts the nonradiative energy transfer from hydrogen atoms and releases the energy to the surroundings to affect electronic transitions to fractional quantum energy levels). As a consequence of the nonradiative energy transfer, the hydrogen atom becomes unstable and emits further energy until it achieves a lower-energy nonradiative state having a principal energy level given by Eqs. (1) and (3). Processes such as hydrogen molecular bond formation that occur without photons and that require collisions are

common [41]. Also, some commercial phosphors are based on resonant nonradiative energy transfer involving multipole coupling [42].

The second ionization energy of helium is 54.417 eV, which is equivalent to 2·27.2 eV. In this case, 54.417 eV is transferred nonradiatively from atomic hydrogen to He^+ which is resonantly ionized. The electron decays to the $n=1/3$ state with the further release of 54.417 eV which may be emitted as a photon. Since the products of the catalysis reaction have binding energies of $m \cdot 27.2$ eV, they may further serve as catalysts. Thus, further catalytic transitions may occur: $n = \frac{1}{3} \rightarrow \frac{1}{4}$, $\frac{1}{4} \rightarrow \frac{1}{5}$, and so on.

The catalyst products $H(1/p)$ were predicted to be a highly reactive intermediates which further react to form a novel hydride ions $H^-(1/p)$ with predicted binding energies E_b given by the following formula [8-9, 36]:

$$E_b = \frac{\hbar^2 \sqrt{s(s+1)}}{8\mu_e a_0^2 \left[\frac{1 + \sqrt{s(s+1)}}{p} \right]^2} - \frac{\pi\mu_0 e^2 \hbar^2}{m_e^2 a_0^3} \left(1 + \frac{2^2}{\left[\frac{1 + \sqrt{s(s+1)}}{p} \right]^3} \right) \quad (4)$$

where p is an integer greater than one, $s=1/2$, \hbar is Planck's constant bar, μ_0 is the permeability of vacuum, m_e is the mass of the electron, μ_e is the reduced electron mass, a_0 is the Bohr radius, and e is the elementary charge. The ionic radius is

$$r_i = \frac{a_0}{p} \left(1 + \sqrt{s(s+1)} \right); s = \frac{1}{2} \quad (5)$$

Extremely stable hydride ions may stabilize a silicon surface to unprecedented time scales to increase the yield in integrated chip fabrication. In this paper, we report the results of the reaction of silane in a helium-hydrogen microwave discharge plasma at the surface of a nickel foil. After the plasma reaction processing, the surface was analyzed by time of flight secondary ion mass spectroscopy (ToF-SIMS) and X-ray photoelectron spectroscopy (XPS).

II. EXPERIMENTAL

Synthesis

Amorphous silicon hydride (α -SiH) films were grown on nickel substrates by their exposure to a low pressure microwave discharge of SiH_4 (2.5%)/He (96.6%)/ H_2 (0.9%). The experimental set up comprising a microwave discharge cell operated under flow conditions is shown in Figure 1. The SiH_4 gas was introduced into a 1000 ml reservoir by a gas/vacuum line where it was mixed with premixed He (99%)/ H_2 (1%) to obtain the reaction mixture SiH_4 (2.5%)/He (96.6%)/ H_2 (0.9%) by controlling the individual gas pressures. Nickel foil (5 X 5 mm and 0.05 mm thick, Alfa Aesar 99+%) substrates were used to avoid charging during ToF-SIMS and XPS characterization. The substrates were placed inside of a quartz tube (1.3 cm in diameter by 15.5 cm long) with vacuum valves at both ends. The tube was fitted with an Ophos coaxial microwave cavity (Evenson cavity) and connected to the gas/vacuum line. The quartz tube and vacuum line were evacuated sufficiently to remove any trace moisture or oxygen. The gas mixture SiH_4 (2.5%)/He (96.6%)/ H_2 (0.9%) was flowed through the quartz tube at a total pressure of 0.7 Torr maintained with a gas flow rate of 40 sccm controlled by a mass flow controller with a readout. The cell pressure was monitored by a 0-10 Torr MKS Baratron absolute pressure gauge. The microwave generator shown in Figure 1 was an Ophos model MPG-4M generator (Frequency: 2450 MHz). The microwave plasma was maintained with a 40 W (forward)/15 W (reflected) power for about 20 min. Yellow-orange coatings formed on the substrates and the wall of the quartz tube. The quartz tube was removed and transferred to a drybox with the samples inside by closing the vacuum valves at both ends and detaching the tube from the vacuum/gas line. The coated substrates were mounted on XPS and ToF-SIMS sample holders under an argon atmosphere in order to prepare samples for the corresponding analyses. One set of samples was analyzed with air exposure limited to 10 minutes and another for 20 minutes while transferring and mounting during the analyses. Separate samples were removed from the drybox and stored in air at room temperature for 48 hours or 10 days before the analyses. Controls comprised a commercial silicon wafer (Alfa Aesar 99.99%) untreated, and HF cleaned silicon wafers exposed to air for 10 minutes.

ToF-SIMS Characterization

The commercial silicon wafer, *HF* cleaned silicon wafer, and α -*SiH* coated nickel foil samples were characterized using Physical Electronics TRIFT ToF-SIMS instrument. The primary ion source was a pulsed $^{69}\text{Ga}^+$ liquid metal source operated at 15 keV. The secondary ions were exacted by a ± 3 keV (according to the mode) voltage. Three electrostatic analyzers (Triple-Focusing-Time-of-Flight) deflect them in order to compensate for the initial energy dispersion of ions of the same mass. The 400 pA dc current was pulsed at a 5 kHz repetition rate with a 7 ns pulse width. The analyzed area was $60\mu\text{m} \times 60\mu\text{m}$ and the mass range was 0-1000 AMU. The total ion dose was $7 \times 10^{11} \text{ ions/cm}^2$, ensuring static conditions. Charge compensation was performed with a pulsed electron gun operated at 20 eV electron energy. In order to remove surface contaminants and expose a fresh surface for analysis, the samples were sputter-cleaned for 30 s using a $80\mu\text{m} \times 80\mu\text{m}$ raster, with 600 pA current, resulting in a total ion dose of $10^{15} \text{ ions/cm}^2$. Three different regions on each sample of $60\mu\text{m} \times 60\mu\text{m}$ were analyzed. The positive and negative SIMS spectra were acquired. Representative post sputtering data is reported. The ToF-SIMS data were treated using 'cadence' software (Physical Electronics), which calculates the mass calibration from well-defined reference peaks.

XPS Characterization

A series of XPS analyses were made on the samples using a Scienta 300 XPS Spectrometer. The fixed analyzer transmission mode and the sweep acquisition mode were used. The angle was 15° . The step energy in the survey scan was 0.5 eV , and the step energy in the high resolution scan was 0.15 eV . In the survey scan, the time per step was 0.4 seconds, and the number of sweeps was 4. In the high resolution scan, the time per step was 0.3 seconds, and the number of sweeps was 30. C1s at 284.5 eV was used as the internal standard.

III. RESULTS AND DISCUSSION

ToF-SIMS

The positive ToF-SIMS spectra ($m/e=0-100$) of the noncoated cleaned commercial silicon wafer and a nickel foil coated with an α -*SiH*

film and exposed to air for 10 min. are shown in Figures 2 and 3, respectively. The positive ion spectrum of the control was dominated by Si^+ , oxides $Si_xO_y^+$, and hydroxides $Si_x(OH)_y^+$; whereas, that of the α -SiH sample contained essentially no oxide or hydride peaks. Rather, it was dominated by Si^+ and a peak at $m/z=29$ which comprised a contribution from SiH^+ and $^{29}Si^+$ which were difficult to separate definitively. However, the contribution due to SiH^+ could be determined by calculating the ratio $R = \frac{^{28}Si}{^{28}SiH + ^{29}Si}$. For comparison, the theoretical ratio of $\frac{^{28}Si}{^{29}Si}$ based on isotopic abundance is 19.6. R for the clean noncoated silicon wafer was 8.1. Whereas, R for the α -SiH sample was 1.15 indicating that the $m/z=29$ peak was overwhelmingly due to SiH^+ .

The positive spectrum ($m/e=0-100$) of a nickel foil coated with an α -SiH film and exposed to air for 10 days before the ToF-SIMS analysis is shown in Figure 4. In this case R was 1.75 demonstrating that the sample was extraordinarily stable to air exposure. In contrast, R was 2.45 in the positive spectrum ($m/e=0-100$) of the HF cleaned silicon wafer exposed to air for only 10 min. before ToF-SIMS analysis as shown in Figure 5.

The negative ion spectra ($m/e=0-100$) of the noncoated cleaned commercial silicon wafer and a nickel foil coated with an α -SiH film and exposed to air for 10 min. before ToF-SIMS analysis are shown in Figures 6 and 7, respectively. The control spectrum was dominated by oxide (O^- $m/z=16$) and hydroxide (OH^- $m/z=17$); whereas, spectrum of the α -SiH film was dominated by hydride ion (H^- $m/z=1$). Very little oxide or hydroxide was observed.

The negative spectrum ($m/e=0-100$) of a nickel foil coated with an α -SiH film and exposed to air for 10 days before the ToF-SIMS analysis is shown in Figure 8. In this case, hydride ion also dominated the negative spectrum demonstrating extraordinary air stability of the α -SiH film. The negative spectrum ($m/e=0-100$) of the HF cleaned silicon wafer exposed to air for only 10 min. before ToF-SIMS analysis shown in Figure 9 also shows a dominant hydride as well as oxide, hydroxide, and some fluoride (F^- $m/z=19$). However, the HF treated surface was not stable with prolonged air exposure. A dominant oxide peak was observed in the negative spectrum ($m/e=0-100$) of the HF

cleaned silicon wafer exposed to air for only 3 hours before ToF-SIMS analysis as shown in Figure 10. Hydride was also observed in lesser amounts and may have resulted as a fragment of the observed hydroxide. Fluoride (F $m/z=19$) was also observed. The ToF-SIMS results from the HF treated surface is consistent with predominantly H termination of silicon dangling bonds as reported previously [3, 4, 5] that has undergone rapid oxidation to form mixed oxides such as $SiOH$.

These results indicate that the plasma reaction formed a highly stable hydrogenated silicon coating in the absence of fluorine observed on the HF treated surface. Remarkably, the $\alpha-SiH$ film was stable even after 10 days; whereas, the HF treated surface showed signs of oxidation over a 1500 times shorter time scale—10 mins. At 3 hours the HF treated surface had similarities to the control untreated silicon wafer which comprised a full oxide coating.

The plasma-reaction-formed $\alpha-SiH$ is proposed to comprise a more stable hydride ion than the H terminated silicon from HF treatment. Thus, the ion production efficiencies in ToF-SIMS analysis could be different making a comparison only qualitative and indicative of relative changes that occurred with timed air exposure. Since the $Si\ 2p$ electron of all samples was equivalent except for energy shifts due to the presence of ordinary H , novel H , or oxide, qualitative analysis was possible as given in the XPS section. As shown in this section, the ToF-SIMS results were confirmed by XPS.

XPS

A survey spectrum was obtained over the region $E_b=0\ eV$ to $1200\ eV$. The primary element peaks allowed for the determination of all of the elements present. The survey spectrum also detected shifts in the binding energies of the $Si\ 2p$ peak which also identified the presence or absence of SiO_2 .

The XPS survey scans of the noncoated cleaned commercial silicon wafer and a nickel foil coated with an $\alpha-SiH$ film and exposed to air for 20 min. before XPS analysis are shown in Figures 11 and 12, respectively. The major species identified in the XPS spectrum of the control sample were silicon, oxygen, and carbon; whereas, the $\alpha-SiH$ sample contained essentially silicon alone with negligible oxygen and carbon present.

The XPS spectra (96-108 eV) in the region of the Si 2*p* peak of the noncoated cleaned commercial silicon wafer and a nickel foil coated with an α -SiH film and exposed to air for 20 min. are shown in Figures 13 and 14, respectively. The XPS spectrum of the control silicon wafer shows a large SiO₂ content at 104 eV as given by Wagner et al. [45]. In contrast the α -SiH sample has essentially no SiO₂. In addition, spin-orbital coupling gives rise to a split Si 2*p* peak in pure silicon, but this peak changed to a single broad peak upon reaction to form the α -SiH film indicative of amorphous silicon.

The XPS spectrum (96-108 eV) in the region of the Si 2*p* peak of a nickel foil coated with an α -SiH film and exposed to air for 48 hours before the XPS analysis is shown in Figure 15. Essentially no SiO₂ was observed at 104 eV demonstrating that the sample was extraordinarily stable to air exposure. Perhaps trace SiOH is present in the region of 102 eV potentially due to less than 100% coverage of the surface with the α -SiH film; rather, some silicon deposition may have occurred. In contrast, the XPS spectrum (96-108 eV) in the region of the Si 2*p* peak of the HF cleaned silicon wafer exposed to air for 10 min. before XPS analysis was essentially fully covered by partial oxides SiO_x such as SiOH. The mixed silicon oxide peak in the region of 101.5-104 eV shown in Figure 16 was essentially the same percentage of the Si 2*p* as that of the SiO₂ peak of the uncleaned wafer shown at 104 eV in Figure 13. In addition, the O 1*s* peak of the α -SiH film exposed to air for 48 hours shown in Figure 17 was negligible; whereas, that of the HF cleaned wafer exposed to air for 10 min. was intense as shown in Figure 18.

The 0-70 eV and the 0-85 eV binding energy region of high resolution XPS spectra of the commercial silicon wafer and a HF cleaned silicon wafer exposed to air for 10 min. before XPS analysis are shown in Figures 19 and 20, respectively. Only a large O 2*s* peak in the low binding energy region was observed in each case. The 0-70 eV binding energy region of a nickel foil coated with an α -SiH film and exposed to air for 20 min. before XPS analysis is shown in Figure 21. By comparison of the α -SiH sample to the controls, novel XPS peaks were identified at 11, 43, and 55 eV. These peaks do not correspond to any of the primary elements, silicon, carbon, or oxygen, shown in the survey scan in Figure 12, wherein the peaks of these elements are given by Wagner et al. [45].

Similarly, hydrogen is the only element which does not have primary element peaks; thus, it is the only candidate to produce the novel peaks and correspond to the H content of the SiH coatings. These peaks closely match and are assigned to hydride ions, $H^-(1/4)$, $H^-(1/9)$, and $H^-(1/11)$, respectively, given by Eqs (4-5). The novel hydride ions are proposed to form by the catalytic reaction of He^+ with atomic hydrogen and subsequent autocatalytic reactions of $H(1/p)$ to form highly stable silicon hydride products $SiH(1/p)$.

These results indicate that the plasma reaction formed a highly stable novel hydrogenated coating; whereas, the control comprised an oxide coating or an ordinary hydrogen terminated silicon surface which rapidly formed an oxide passivation layer. The hydrogen content of the α - SiH coating appears to be novel hydride ions with high binding energies which account for the exceptional air stability.

IV. CONCLUSIONS

Nickel substrates were coated by the reaction product of a low pressure microwave discharge plasma of SiH_4 (2.5%)/ He (96.6%)/ H_2 (0.9%). The ToF-SIMS identified the coatings as hydride by the large SiH^+ peak in the positive spectrum and the dominant H^- in the negative spectrum. XPS identified the H content of the SiH coatings as hydride ions, $H^-(1/4)$, $H^-(1/9)$, and $H^-(1/11)$ corresponding to peaks at 11, 43, and 55 eV, respectively. The novel hydride ions are proposed to form by the catalytic reaction of He^+ with atomic hydrogen and subsequent autocatalytic reactions of $H(1/p)$ to form highly stable silicon hydride products $SiH(1/p)$. The SiH coating was amorphous as indicated by the shape of the $Si\ 2p$ peak and was remarkably stable to air exposure. After a 48 hour exposure to air, essentially no oxygen was observed as evidence by the negligible $O\ 1s$ peak at 531 eV and absence of any SiO_2 $Si\ 2p$ peak in the region of 102-104 eV. The highly stable amorphous silicon hydride coating may advance the production of integrated circuits and microdevices by resisting the oxygen passivation of the surface and possibly altering the dielectric constant and band gap to increase device performance.

REFERENCES

1. W. Kern, *Semicond. Int.*, April, (1984), p. 94.
2. F. J. Grunthaner, P. J. Grunthaner, *Mater. Sci. Rep.*, Vol. 1, (1986), p. 69.
3. M. Grudner, H. Jacob, *Appl. Phys. A*, Vol. 39, (1986), p. 73.
4. H. Ubara, T. Imura, A. Hiraki, *Solid State Comm.*, Vol. 50, (1984), p. 673.
5. E. Yablonovitch, D. L. Allara, C. C. Chang, T. Gmitter, T. B. Bright, *Phys. Rev. Lett.*, Vol. 57, (1986), p. 249.
6. R. A. Street, *Hydrogenated amorphous silicon*, Cambridge University Press, Cambridge, (1991). pp. 18-61.
7. R. Mills, J. Dong, Y. Lu, "Observation of Extreme Ultraviolet Hydrogen Emission from Incandescently Heated Hydrogen Gas with Certain Catalysts", *Int. J. Hydrogen Energy*, Vol. 25, (2000), pp. 919-943.
8. R. L. Mills, P. Ray, "High Resolution Spectroscopic Observation of the Bound-Free Hyperfine Levels of a Novel Hydride Ion Corresponding to a Fractional Rydberg State of Atomic Hydrogen", *Int. J. Hydrogen Energy*, in press.
9. R. L. Mills, P. Ray, "Stationary Inverted Lyman Population Formed from Incandescently Heated Hydrogen Gas with Certain Catalysts", *Chem. Phys. Letts.*, submitted.
10. R. Mills, P. Ray, M. Nansteel, W. Good, P. Jansson, B. Dhandapani, J. He, "Excessive Balmer α Line Broadening, Power Balance, and Novel Hydride Ion Product of Plasma Formed from Incandescently Heated Hydrogen Gas with Certain Catalysts", *Int. J. Hydrogen Energy*, submitted.
11. R. Mills, E. Dayalan, P. Ray, B. Dhandapani, J. He, "Highly Stable Novel Inorganic Hydrides from Aqueous Electrolysis and Plasma Electrolysis, *Japanese Journal of Applied Physics*, submitted.
12. R. Mills, B. Dhandapani, M. Nansteel, J. He, A. Voigt, "Identification of Compounds Containing Novel Hydride Ions by Nuclear Magnetic Resonance Spectroscopy", *Int. J. Hydrogen Energy*, Vol. 26, No. 9, Sept. (2001), pp. 965-979.
13. R. Mills, B. Dhandapani, N. Greenig, J. He, "Synthesis and Characterization of Potassium Iodo Hydride", *Int. J. of Hydrogen Energy*, Vol. 25, Issue 12, December, (2000), pp. 1185-1203.

14. R. Mills, "Novel Inorganic Hydride", *Int. J. of Hydrogen Energy*, Vol. 25, (2000), pp. 669-683.
15. R. Mills, "Novel Hydrogen Compounds from a Potassium Carbonate Electrolytic Cell", *Fusion Technology*, Vol. 37, No. 2, March, (2000), pp. 157-182.
16. R. Mills, B. Dhandapani, M. Nansteel, J. He, T. Shannon, A. Echezuria, "Synthesis and Characterization of Novel Hydride Compounds", *Int. J. of Hydrogen Energy*, Vol. 26, No. 4, (2001), pp. 339-367.
17. R. Mills, "Highly Stable Novel Inorganic Hydrides", *Journal of New Materials for Electrochemical Systems*, in press.
18. R. Mills, W. Good, A. Voigt, Jinquan Dong, "Minimum Heat of Formation of Potassium Iodo Hydride", *Int. J. Hydrogen Energy*, Vol. 26, No. 11, Oct., (2001), pp. 1199-1208.
19. R. Mills, P. Ray, "Spectral Emission of Fractional Quantum Energy Levels of Atomic Hydrogen from a Helium-Hydrogen Plasma and the Implications for Dark Matter", *Int. J. Hydrogen Energy*, Vol. 27 (3), (2002), pp. 301-322.
20. R. L. Mills, P. Ray, B. Dhandapani, J. He, "Spectroscopic Identification of Fractional Rydberg States of Atomic Hydrogen" *J. Phys. Chem. Letts.*, submitted.
21. R. Mills, P. Ray, "Vibrational Spectral Emission of Fractional-Principal-Quantum-Energy-Level Hydrogen Molecular Ion", *Int. J. Hydrogen Energy*, in press.
22. R. L. Mills, P. Ray, "Spectroscopic Identification of a Novel Catalytic Reaction of Rubidium Ion with Atomic Hydrogen and the Hydride Ion Product", *Int. J. Hydrogen Energy*, in press.
23. R. Mills, P. Ray, Spectroscopic Identification of a Novel Catalytic Reaction of Potassium and Atomic Hydrogen and the Hydride Ion Product, *Int. J. Hydrogen Energy*, Vol. 27, No. 2, February, (2002), pp. 183-192.
24. R. Mills, "Spectroscopic Identification of a Novel Catalytic Reaction of Atomic Hydrogen and the Hydride Ion Product", *Int. J. Hydrogen Energy*, Vol. 26, No. 10, (2001), pp. 1041-1058.
25. R. Mills and M. Nansteel, "Argon-Hydrogen-Strontium Discharge Light Source", *IEEE Transactions on Plasma Science*, in press.

26. R. Mills, M. Nansteel, and Y. Lu, "Excessively Bright Hydrogen-Strontium Plasma Light Source Due to Energy Resonance of Strontium with Hydrogen", *European Journal of Physics D*, submitted.
27. R. L. Mills, P. Ray, B. Dhandapani, M. Nansteel, X. Chen, J. He, "New Power Source from Fractional Quantum Energy Levels of Atomic Hydrogen that Surpasses Internal Combustion", *Spectrochimica Acta*, submitted.
28. R. L. Mills, P. Ray, B. Dhandapani, J. He, "Comparison of Excessive Balmer α Line Broadening of Glow Discharge and Microwave Hydrogen Plasmas with Certain Catalysts" *Chem. Phys.*, submitted.
29. R. Mills, J. Dong, W. Good, P. Ray, J. He, B. Dhandapani, Measurement of Energy Balances of Noble Gas-Hydrogen Discharge Plasmas Using Calvet Calorimetry, *Int. J. Hydrogen Energy*, in press.
30. R. Mills, M. Nansteel, and Y. Lu, "Observation of Extreme Ultraviolet Hydrogen Emission from Incandescently Heated Hydrogen Gas with Strontium that Produced an Anomalous Optically Measured Power Balance", *Int. J. Hydrogen Energy*, Vol. 26, No. 4, (2001), pp. 309-326.
31. R. Mills, "Observation of Extreme Ultraviolet Emission from Hydrogen-KI Plasmas Produced by a Hollow Cathode Discharge", *Int. J. Hydrogen Energy*, Vol. 26, No. 6, (2001), pp. 579-592.
32. R. Mills, "Temporal Behavior of Light-Emission in the Visible Spectral Range from a Ti-K₂CO₃-H-Cell", *Int. J. Hydrogen Energy*, Vol. 26, No. 4, (2001), pp. 327-332.
33. R. Mills, T. Onuma, and Y. Lu, "Formation of a Hydrogen Plasma from an Incandescently Heated Hydrogen-Catalyst Gas Mixture with an Anomalous Afterglow Duration", *Int. J. Hydrogen Energy*, Vol. 26, No. 7, July, (2001), pp. 749-762.
34. R. L. Mills, A. Voigt, P. Ray, M. Nansteel, B. Dhandapani, "Measurement of Hydrogen Balmer Line Broadening and Thermal Power Balances of Noble Gas-Hydrogen Discharge Plasmas", *Int. J. Hydrogen Energy*, in press.
35. R. Mills, N. Greenig, S. Hicks, "Optically Measured Power Balances of Anomalous Discharges of Mixtures of Argon, Hydrogen, and Potassium, Rubidium, Cesium, or Strontium Vapor", *Int. J. Hydrogen Energy*, in press.

36. R. Mills, *The Grand Unified Theory of Classical Quantum Mechanics*, September 2001 Edition, BlackLight Power, Inc., Cranbury, New Jersey, Distributed by Amazon.com; posted at www.blacklightpower.com.
37. R. Mills, "The Grand Unified Theory of Classical Quantum Mechanics", Global Foundation, Inc. Orbis Scientiae entitled *The Role of Attractive and Repulsive Gravitational Forces in Cosmic Acceleration of Particles The Origin of the Cosmic Gamma Ray Bursts*, (29th Conference on High Energy Physics and Cosmology Since 1964) Dr. Behram N. Kursunoglu, Chairman, December 14-17, 2000, Lago Mar Resort, Fort Lauderdale, FL, Kluwer Academic/Plenum Publishers, New York, pp. 243-258.
38. R. Mills, "The Grand Unified Theory of Classical Quantum Mechanics", Int. J. of Hydrogen Energy, in press.
39. R. Mills, "The Hydrogen Atom Revisited", Int. J. of Hydrogen Energy, Vol. 25, Issue 12, December, (2000), pp. 1171-1183.
40. R. Mills, The Nature of Free Electrons in Superfluid Helium—a Test of Quantum Mechanics and a Basis to Review its Foundations and Make a Comparison to Classical Theory, Int. J. Hydrogen Energy, Vol. 26, No. 10, (2001), pp. 1059-1096.
41. N. V. Sidgwick, *The Chemical Elements and Their Compounds*, Volume I, Oxford, Clarendon Press, (1950), p.17.
42. M. D. Lamb, *Luminescence Spectroscopy*, Academic Press, London, (1978), p. 68.
43. Microsc. Microanal. Microstruct., Vol. 3, 1, (1992).
44. For recent specifications see PHI Trift II, ToF-SIMS Technical Brochure, (1999), Eden Prairie, MN 55344.
45. C. D. Wagner, W. M. Riggs, L. E. Davis, J. F. Moulder, G. E. Mulilenberg (Editor), *Handbook of X-ray Photoelectron Spectroscopy*, Perkin-Elmer Corp., Eden Prairie, Minnesota, (1997).

Figure Captions

Figure 1. The experimental set up comprising a microwave discharge cell operated under flow conditions.

Figure 2. The positive ion ToF-SIMS spectra ($m/e=0-100$) of a noncoated cleaned commercial silicon wafer (Alfa Aesar 99.9%).

Figure 3. The positive ion ToF-SIMS spectra ($m/e=0-100$) of a nickel foil coated with an α -SiH film and exposed to air for 10 min. that showed a large SiH^+ peak.

Figure 4. The positive ion ToF-SIMS spectrum ($m/e=0-100$) of a nickel foil coated with an α -SiH film and exposed to atmosphere for 10 days before the ToF-SIMS analysis that retained a large SiH^+ peak.

Figure 5. The positive ion ToF-SIMS spectrum ($m/e=0-100$) of the HF cleaned silicon wafer exposed to air for 10 min. before ToF-SIMS analysis.

Figure 6. The negative ion ToF-SIMS spectrum ($m/e=0-100$) of the noncoated cleaned commercial silicon wafer (Alfa Aesar 99.99%).

Figure 7. The negative ion ToF-SIMS spectrum ($m/e=0-100$) of a nickel foil coated with an α -SiH film and exposed to air for 10 min. before ToF-SIMS analysis that was dominated by hydride ion.

Figure 8. The negative ion ToF-SIMS spectrum ($m/e=0-100$) of a nickel foil coated with an α -SiH film and exposed to air for 10 days before the ToF-SIMS analysis that retained the dominant hydride ion peak.

Figure 9. The negative ion ToF-SIMS spectrum ($m/e=0-100$) of the HF cleaned silicon wafer exposed to air for 10 min. before ToF-SIMS analysis.

Figure 10. The negative ion ToF-SIMS spectrum ($m/e=0-100$) of the HF cleaned silicon wafer exposed to air for 3 hours before ToF-SIMS analysis showing a dominant oxide peak.

Figure 11. The XPS survey scan of the noncoated cleaned commercial silicon wafer showing a large amount of oxide and carbon contamination of the surface.

Figure 12. The XPS survey scan of a nickel foil coated with an α -SiH film and exposed to air for 20 min. before XPS analysis showing minimal oxide and carbon.

Figure 13. The XPS spectrum (96-108 eV) in the region of the Si 2p peak of the noncoated cleaned commercial silicon wafer showing a large SiO₂ in the region of 104 eV.

Figure 14. The XPS spectrum (96-108 eV) in the region of the Si 2p peak of a nickel foil with an α -SiH film and exposed to air for 20 min. before XPS analysis showing no oxide in the region of 104 eV.

Figure 15. The XPS spectrum (96-108 eV) in the region of the Si 2p peak of a nickel foil coated with an α -SiH film and exposed to air for 48 hours before the XPS analysis showing no oxide at 104 eV and possibly trace SiOH in the region of 102 eV.

Figure 16. The XPS spectrum (96-108 eV) in the region of the Si 2p peak of the HF cleaned silicon wafer exposed to air for 10 min. before XPS analysis showing a very large SiO₂ peak in the region of 101.5-104 eV.

Figure 17. The XPS spectrum (525-540 eV) in the region of the O 1s peak of a nickel foil coated with an α -SiH film and exposed to air for 48 hours before XPS analysis showing a minimal amount of oxide.

Figure 18. The XPS spectrum (525-540 eV) in the region of the O 1s peak of the HF cleaned silicon wafer exposed to air for 10 min. before XPS analysis showing a very large oxide peak.

Figure 19. The 0-70 eV binding energy region of a high resolution XPS spectrum of the commercial silicon wafer showing only a large O 2s peak in the low binding energy region.

Figure 20. The 0-85 eV binding energy region of a high resolution XPS spectrum of the HF cleaned silicon wafer exposed to air for 10 min. before XPS analysis showing only a large O 2s peak in the low binding energy region.

Figure 21. The 0-70 eV binding energy region of a high resolution XPS spectrum of a nickel foil coated with an α -SiH film and exposed to air for 20 min. before XPS analysis. The novel peaks observed at 11, 43 and 55 eV which could not be assigned to the elements identified by their primary XPS peaks matched and were assigned to H⁻(1/4), H⁻(1/9), and H⁻(1/11). The novel highly stable hydride ions formed by the catalytic reaction of He⁺ and atomic hydrogen may be the basis of the extraordinary stability of the α -SiH film.

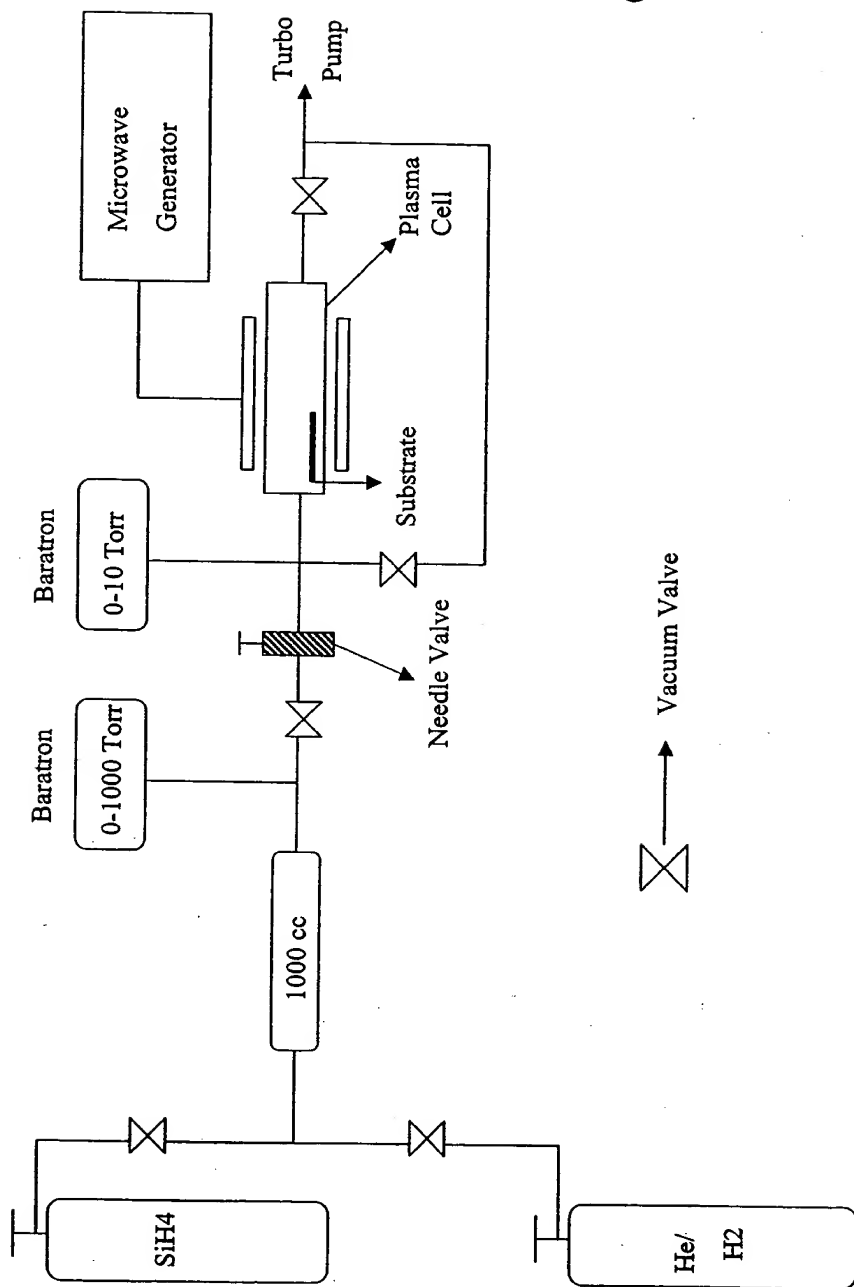


Fig. 1

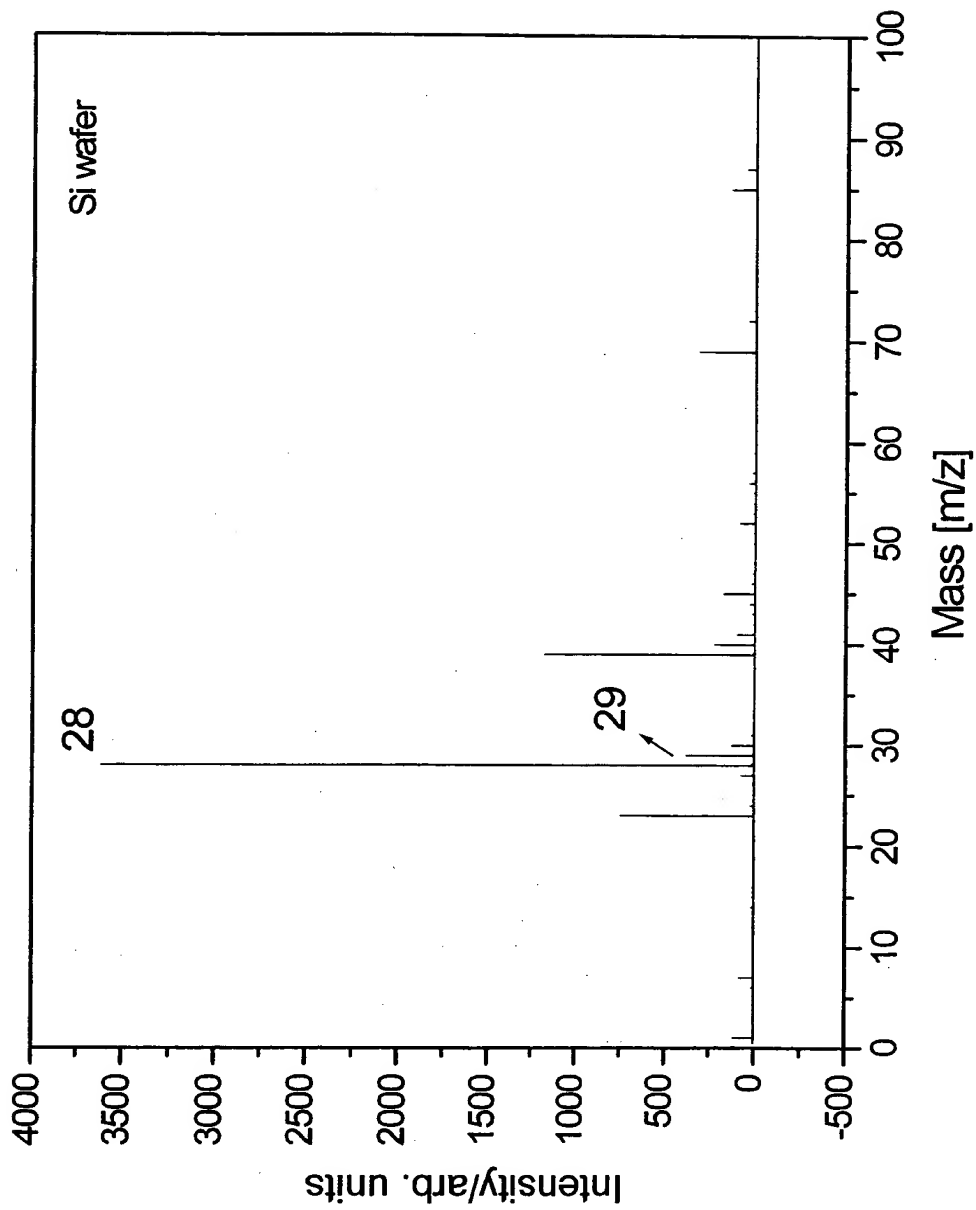


Fig. 2

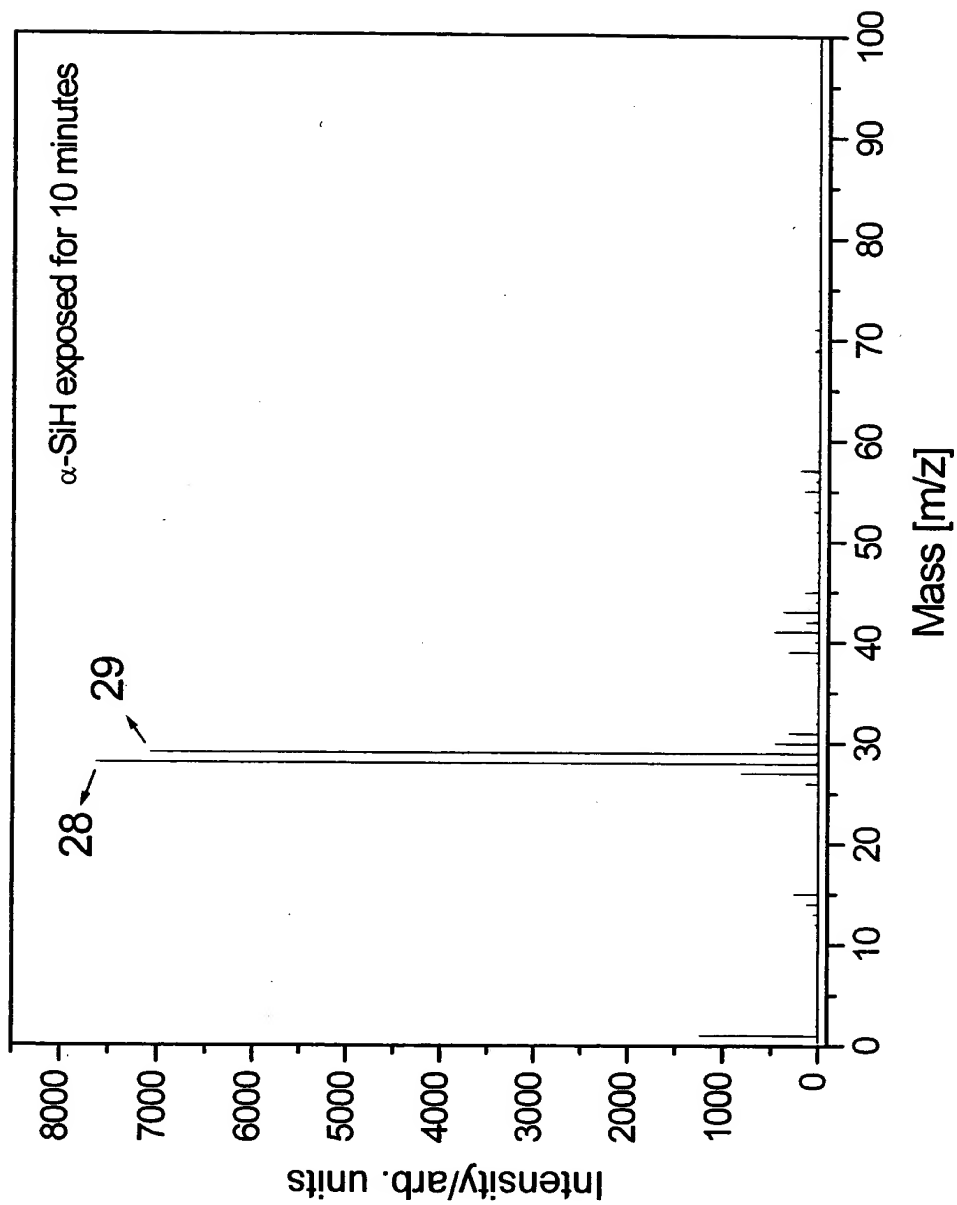


Fig. 3

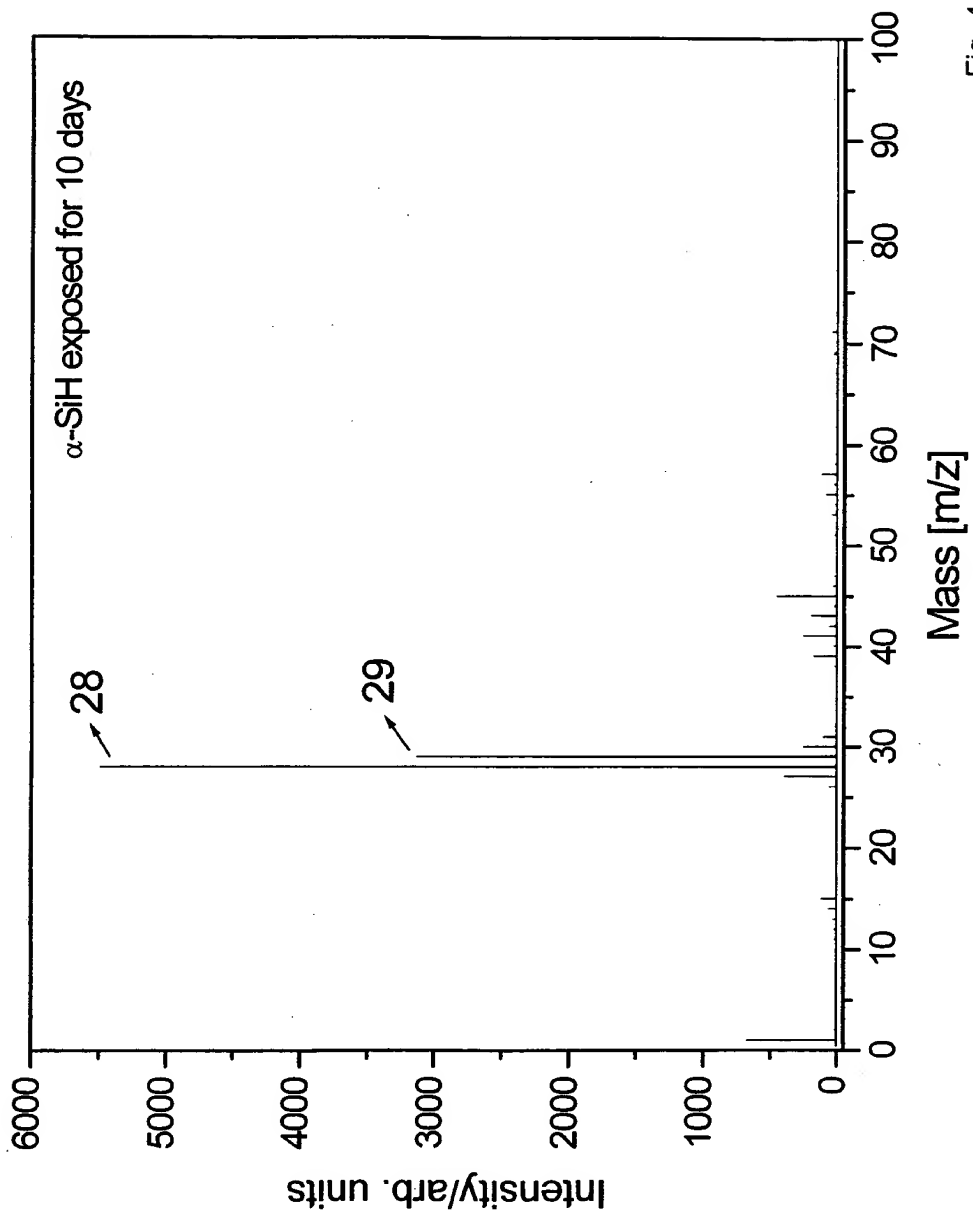


Fig. 4

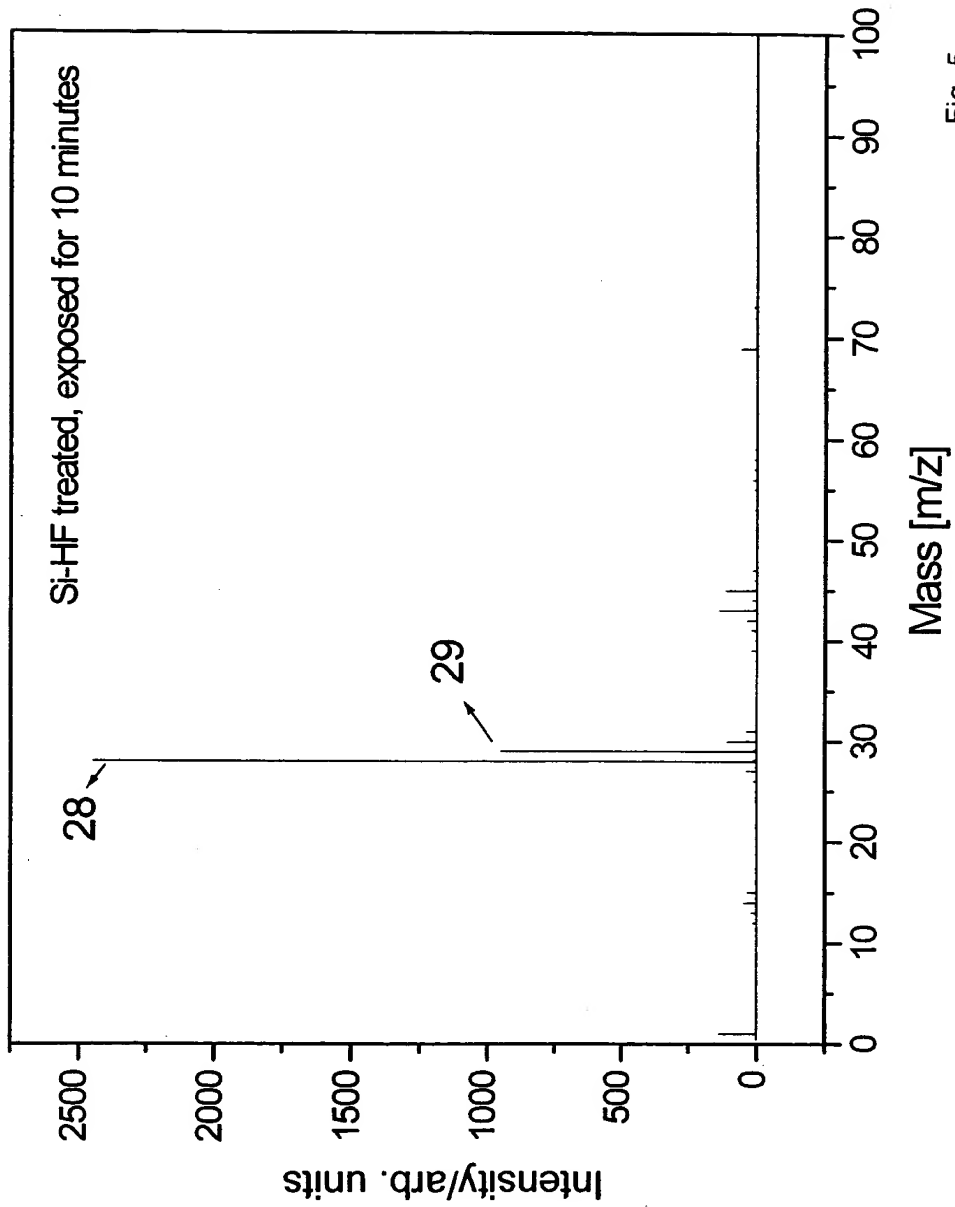


Fig. 5

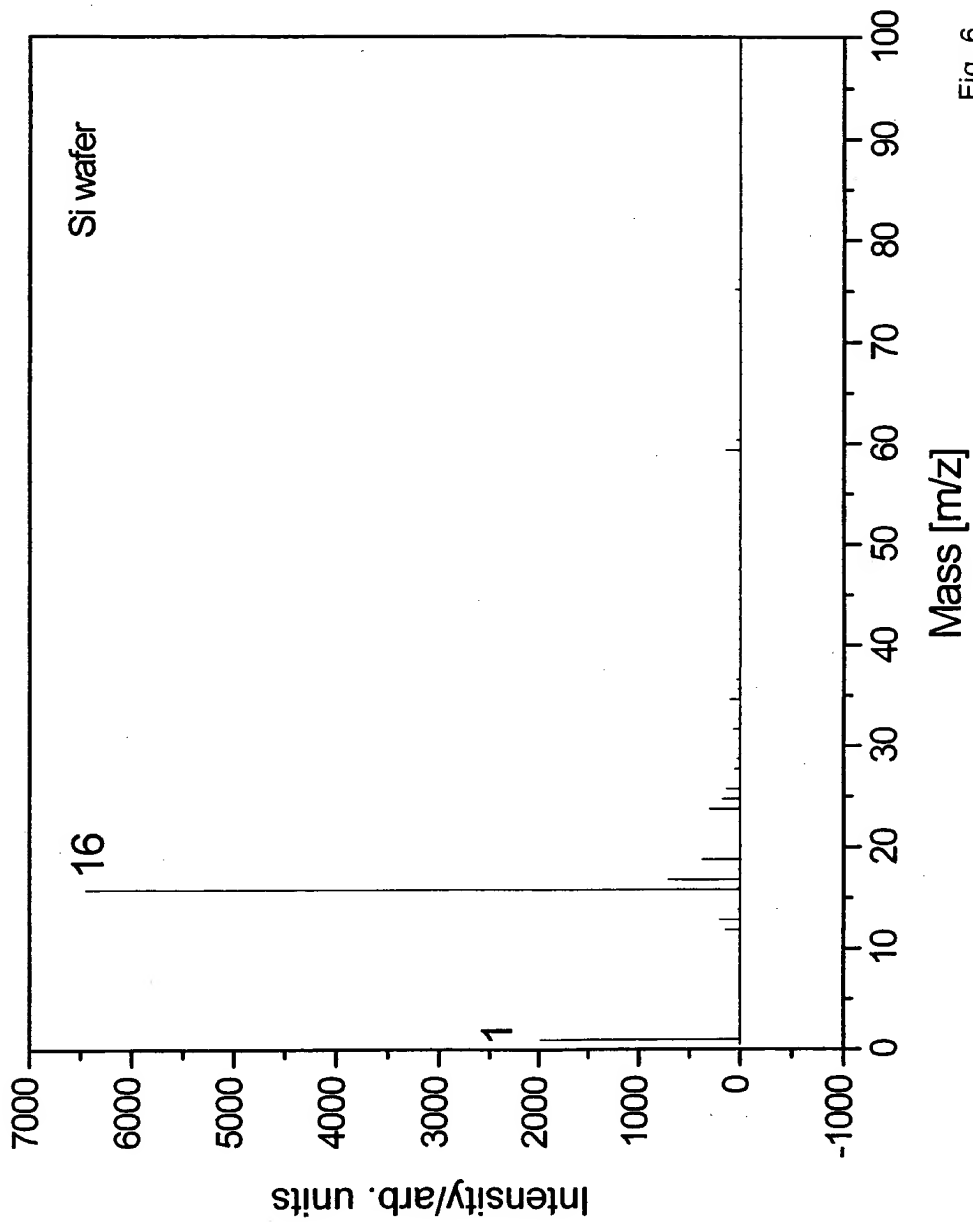


Fig. 6

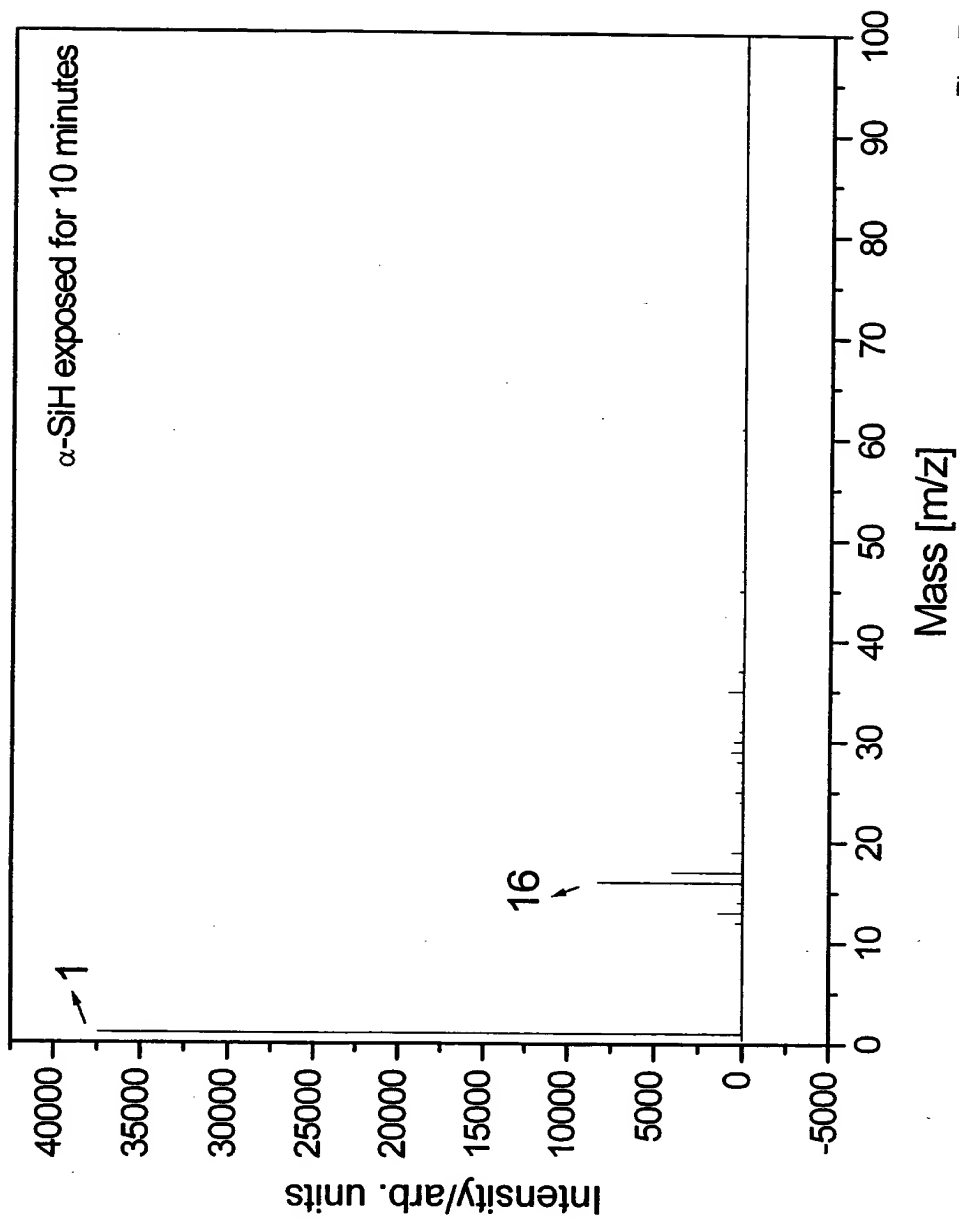


Fig. 7

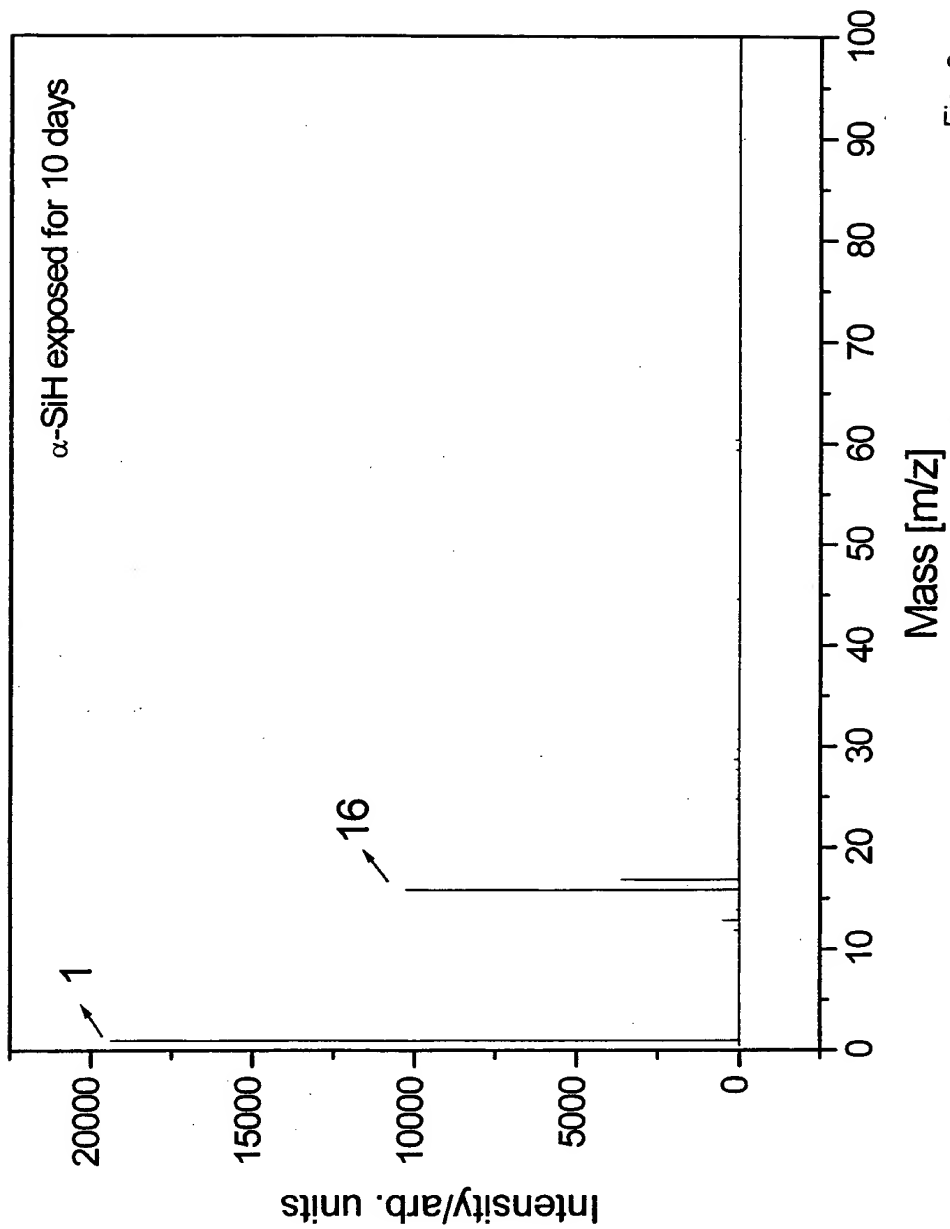


Fig. 8

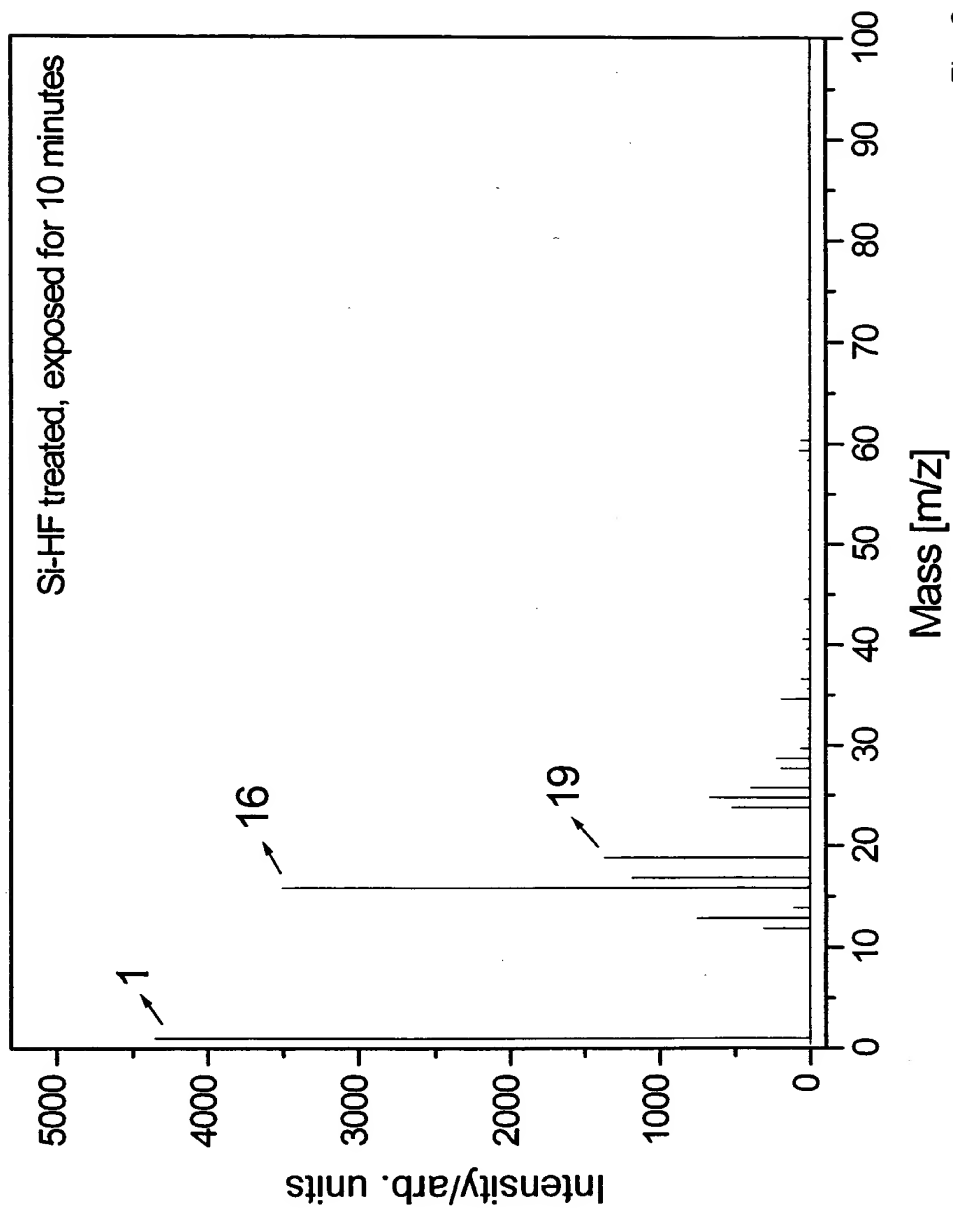


Fig. 9

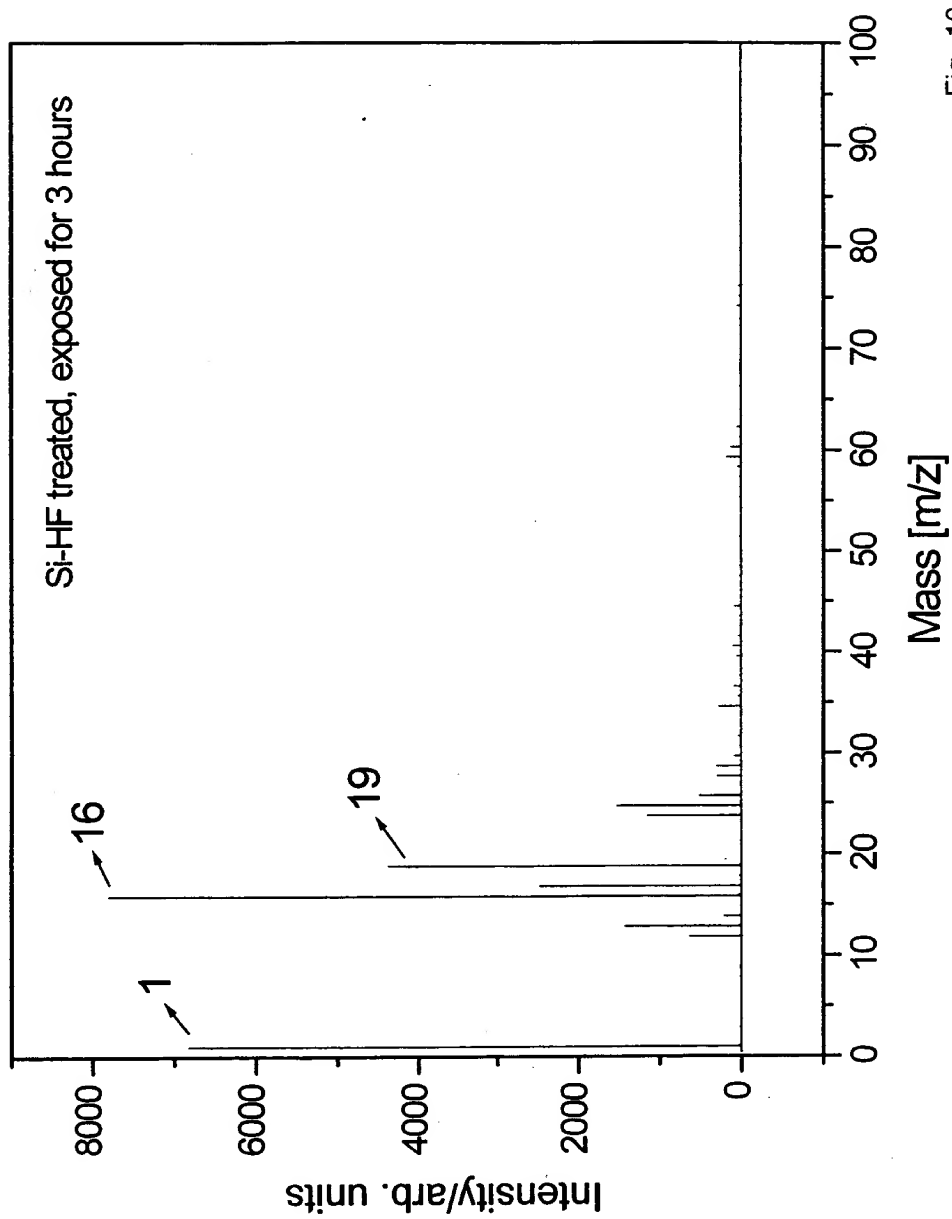


Fig. 10

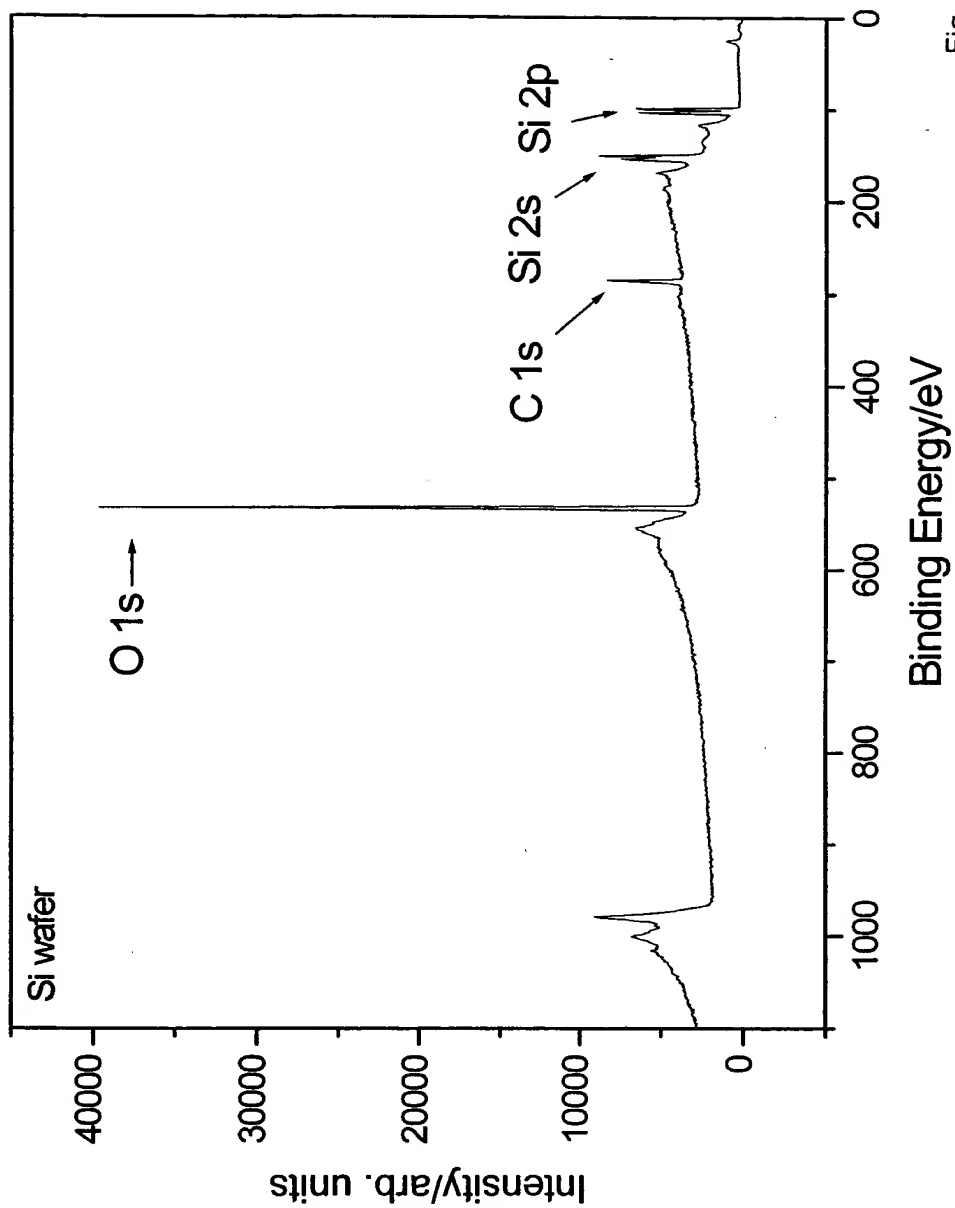


Fig. 11

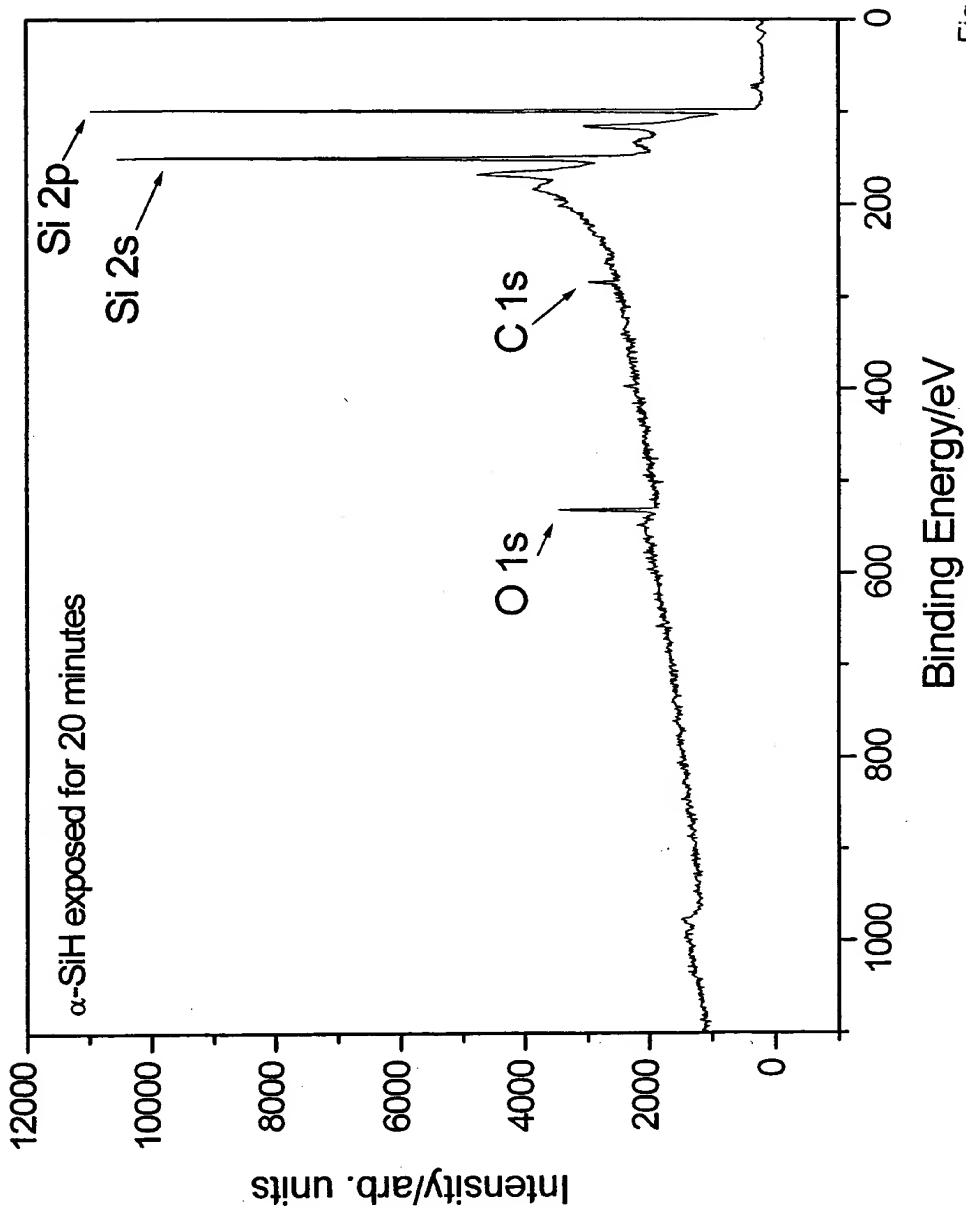


Fig. 12

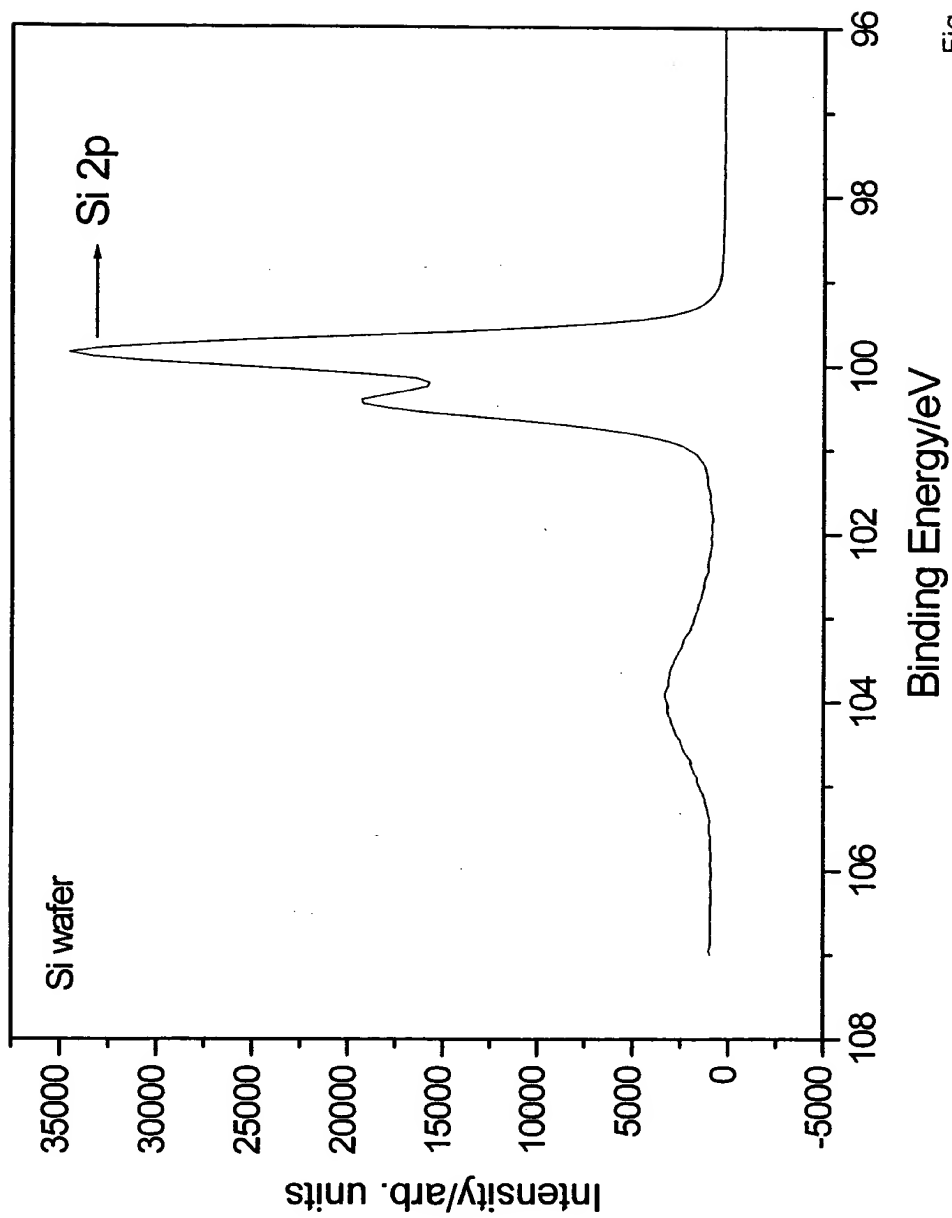


Fig. 13

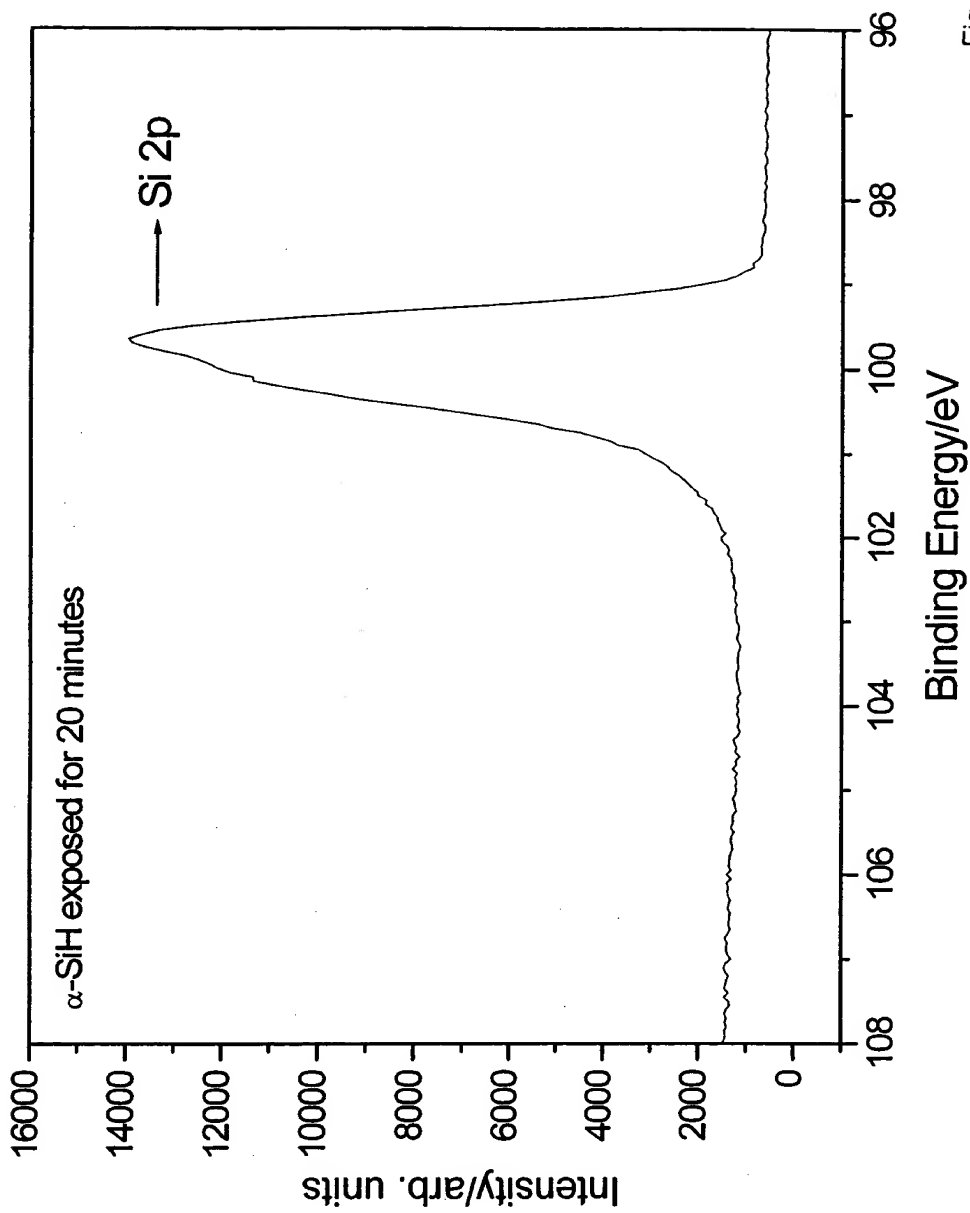


Fig. 14

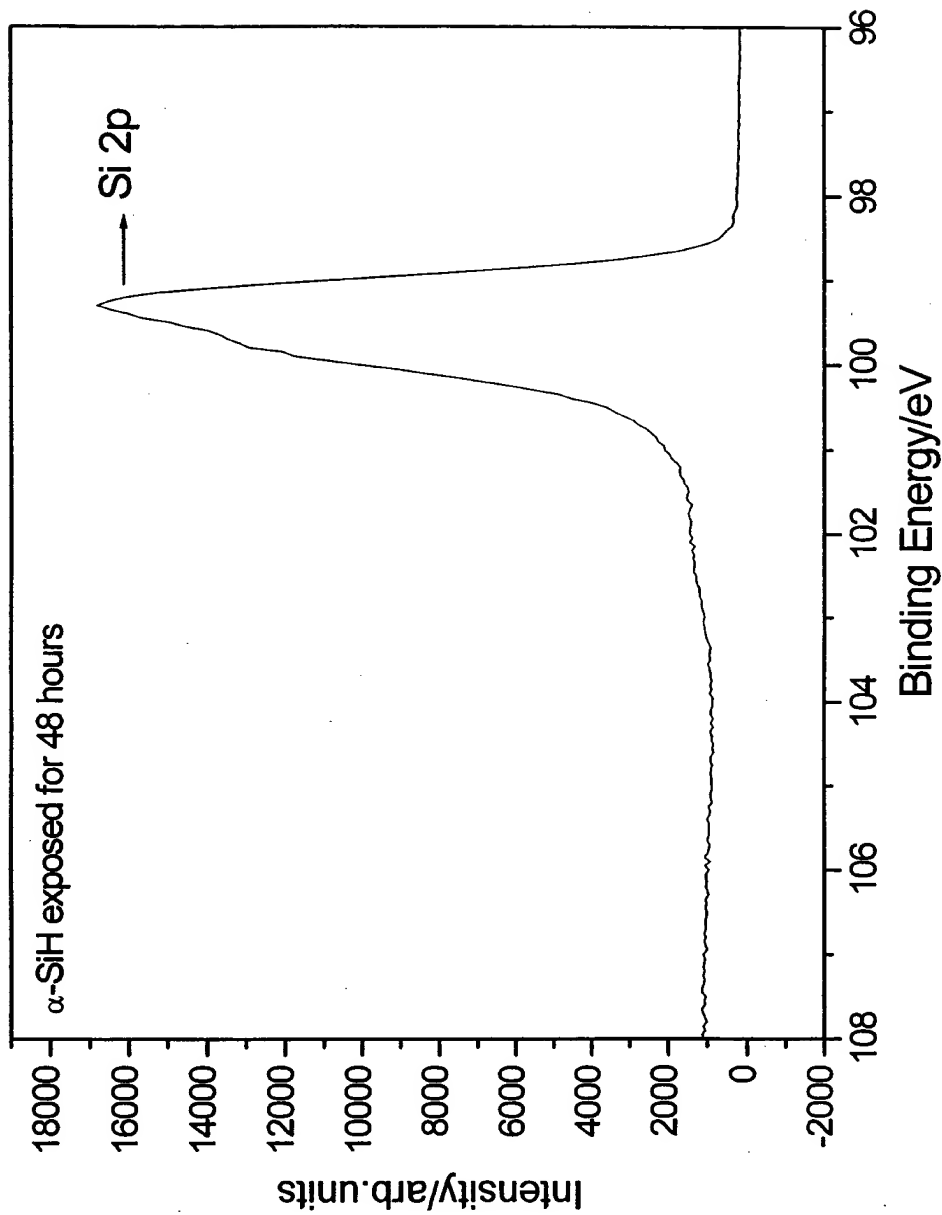


Fig. 15

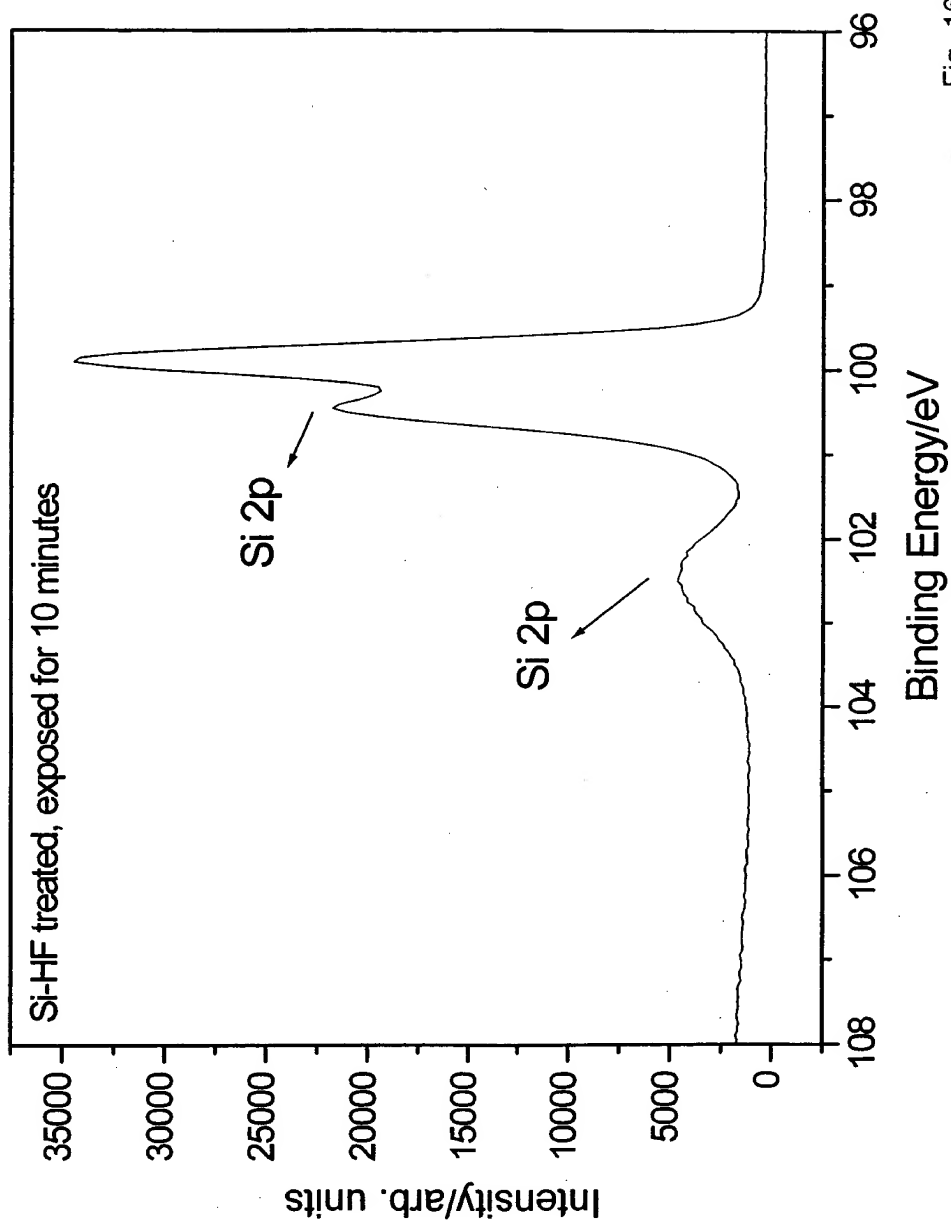


Fig. 16

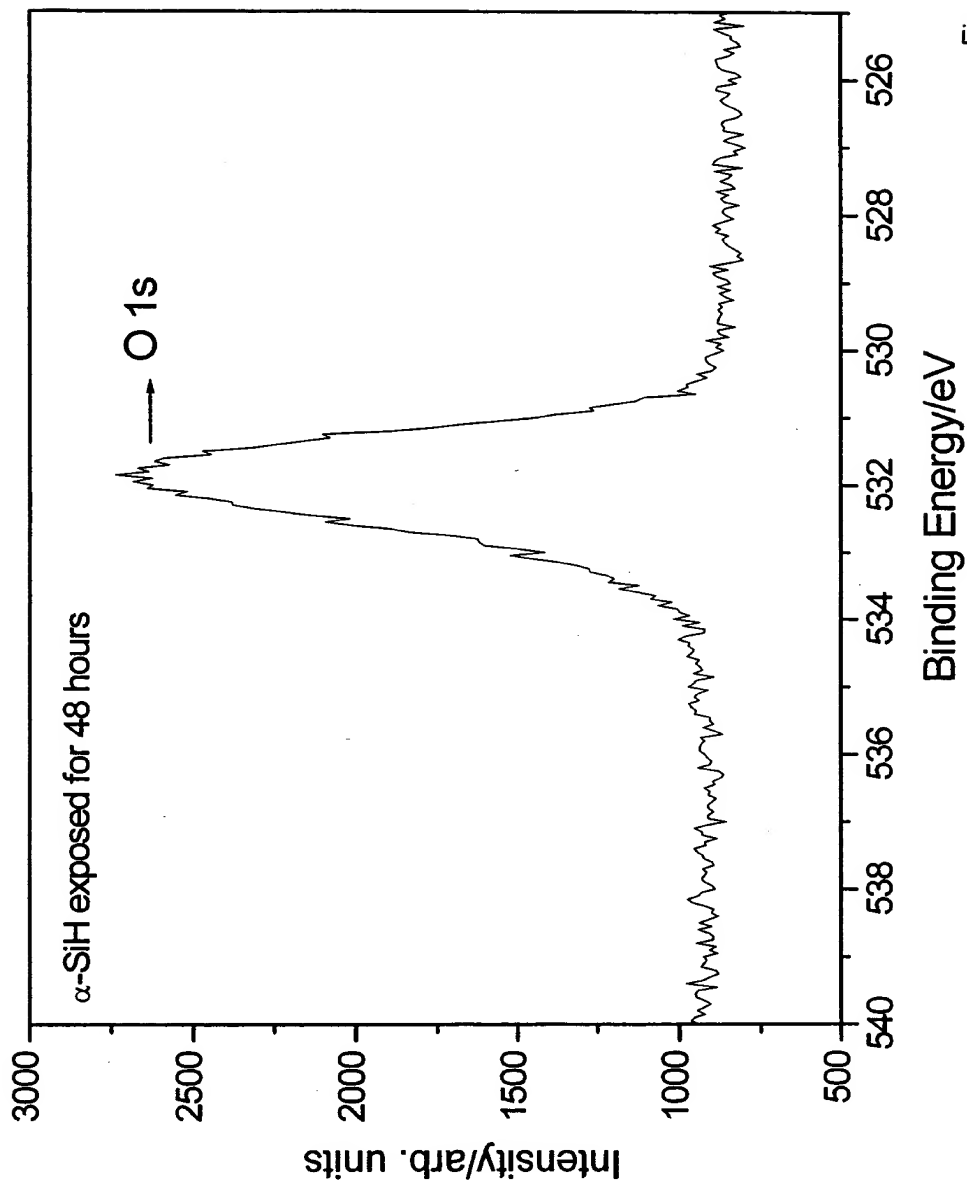


Fig. 17

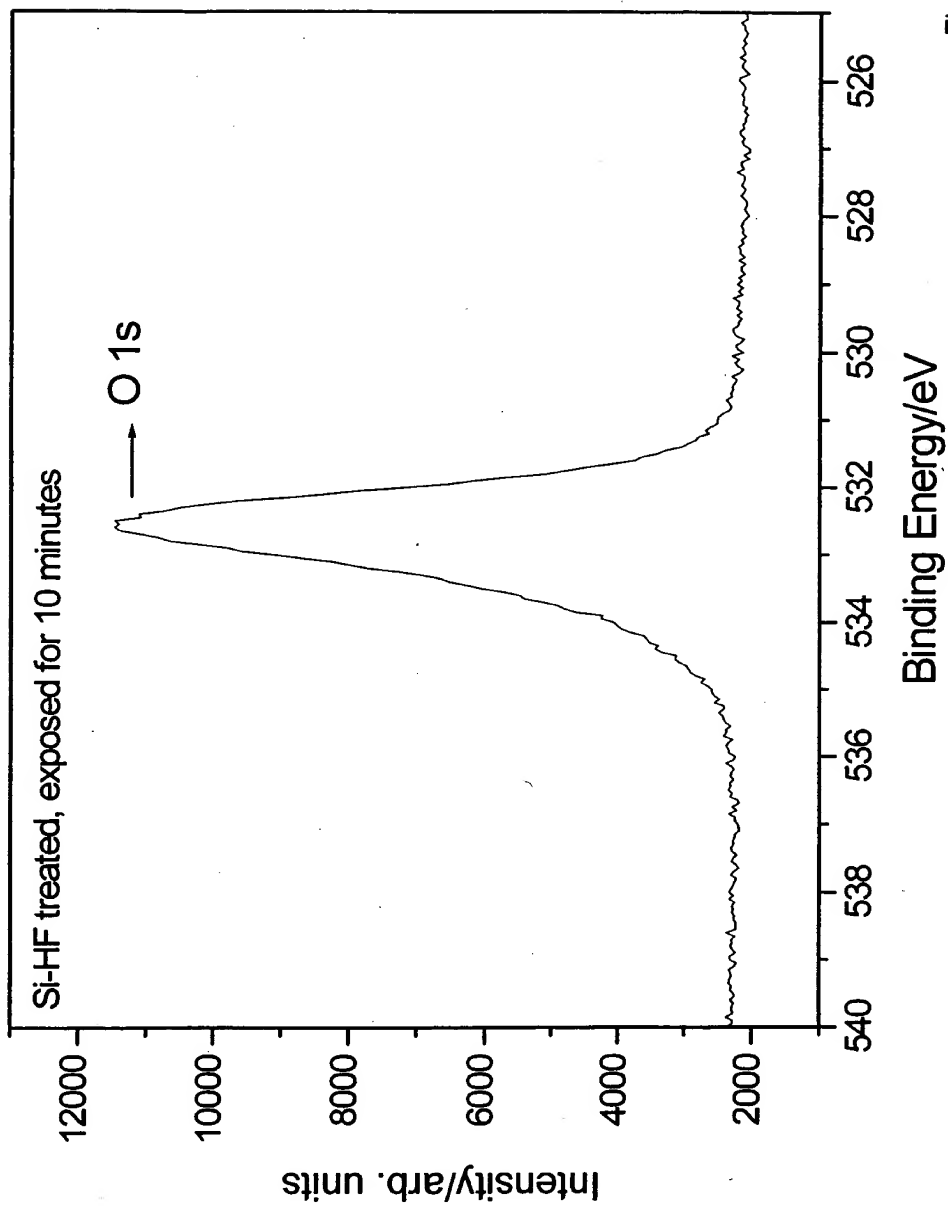


Fig. 18

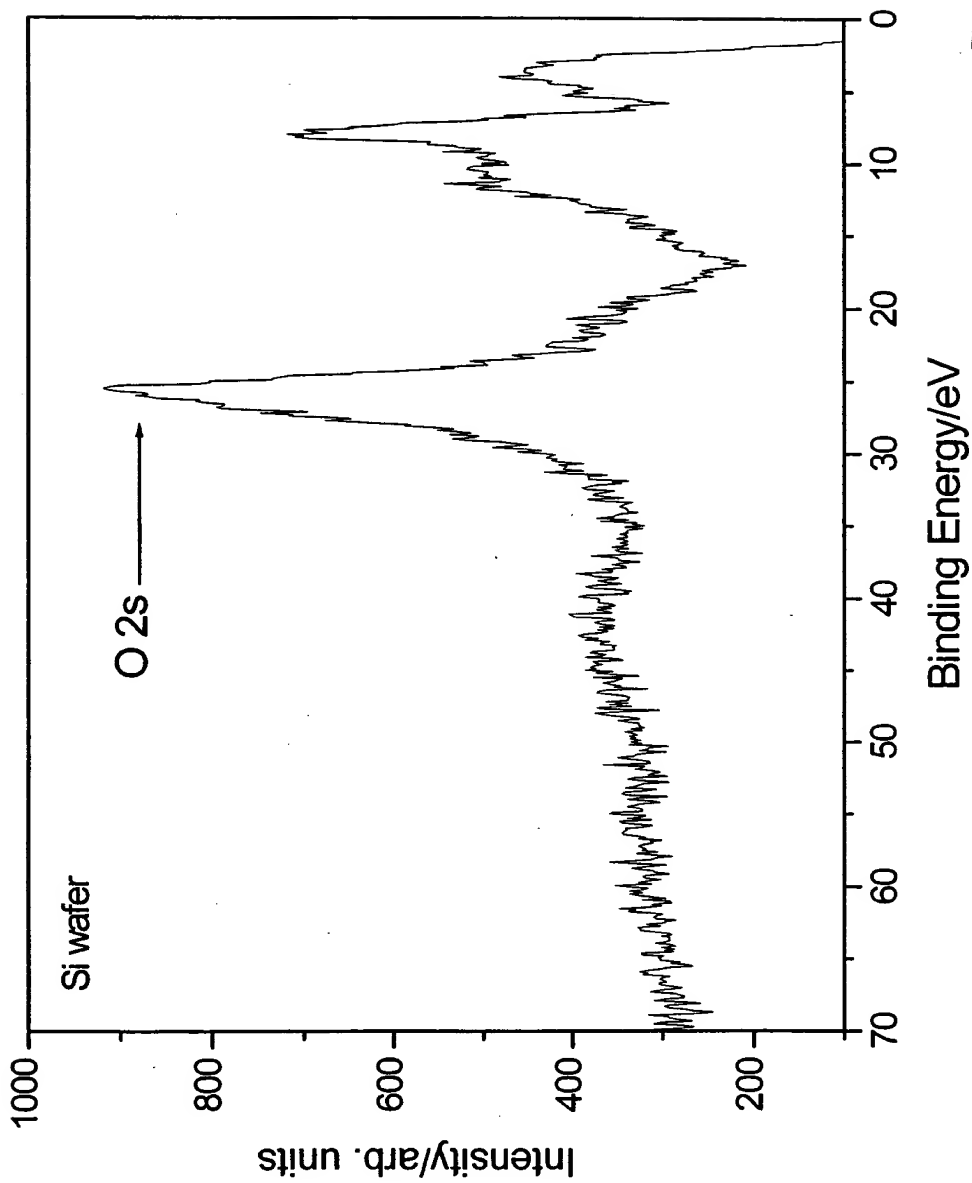


Fig. 19

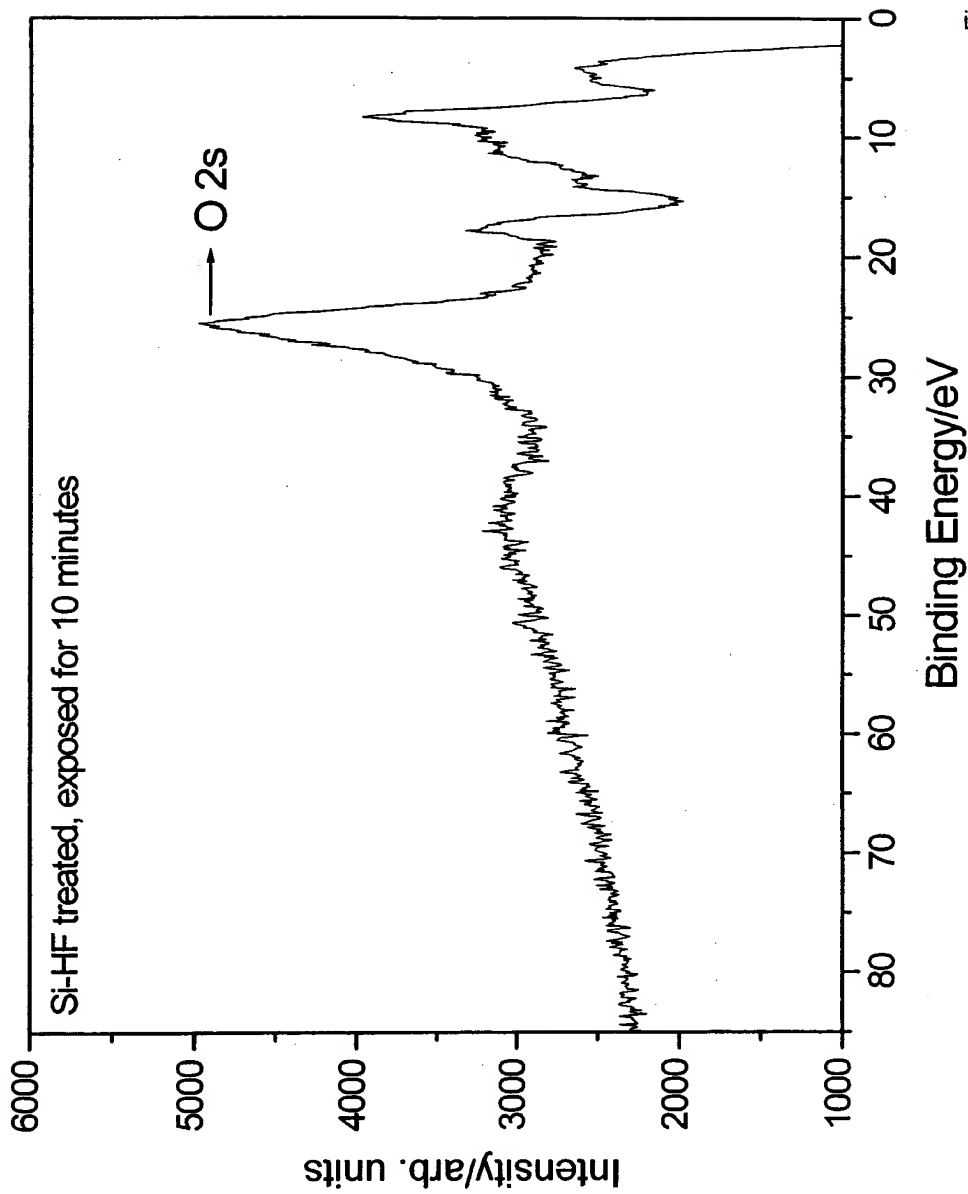


Fig. 20

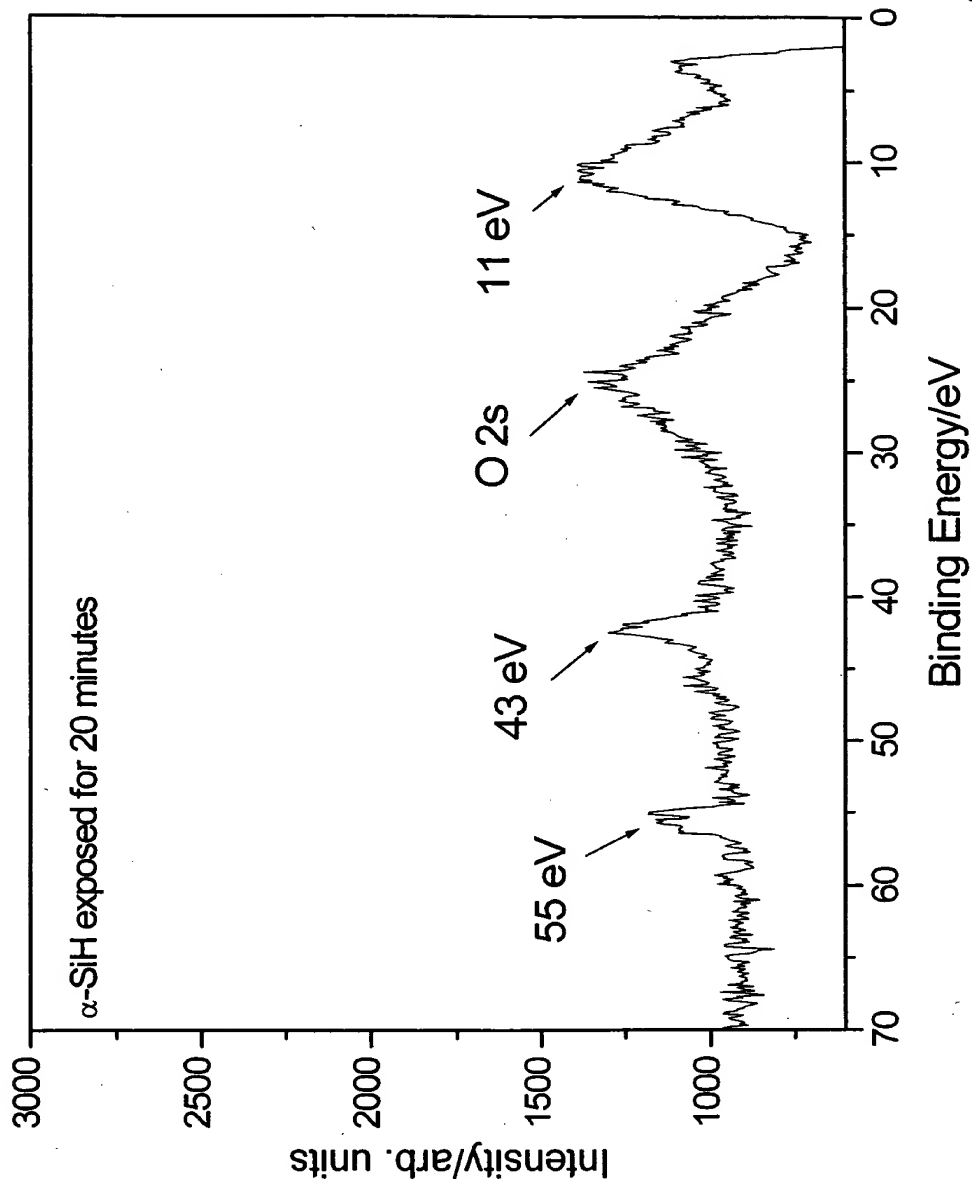


Fig. 21

73

Synthesis and Characterization of Lithium Chloro Hydride

Randell L. Mills
Andreas Voigt
Bala Dhandapani
Jiliang He
Alejandra Echezuria

BlackLight Power, Inc.
493 Old Trenton Road
Cranbury, NJ 08512

A novel inorganic hydride compound lithium chloro hydride, LiHCl , which comprises a high binding energy hydride ion was synthesized by reaction of atomic hydrogen with potassium metal and lithium chloride. Lithium chloro hydride was identified by time of flight secondary ion mass spectroscopy, X-ray photoelectron spectroscopy, ^1H nuclear magnetic resonance spectroscopy, and powder X-ray diffraction. Hydride ions with increased binding energies may form many novel compounds with broad applications such as the oxidant of a high voltage battery.

I. INTRODUCTION

From a solution of a Schrödinger-type wave equation with a nonradiative boundary condition based on Maxwell's equations, Mills predicts that atomic hydrogen may undergo a catalytic reaction with certain atomized elements and ions which singly or multiply ionize at integer multiples of the potential energy of atomic hydrogen, 27.2 eV , $m \cdot 27.2\text{ eV}$ wherein m is an integer [1-47]. The highly exothermic reaction involves a nonradiative energy transfer to form a hydrogen atom that is lower in energy than unreacted atomic hydrogen that corresponds to a fractional principal quantum number ($n = \frac{1}{p} = \frac{1}{\text{integer}}$ replaces the well known parameter $n = \text{integer}$ in the Rydberg equation for hydrogen excited states).

One such atomic catalytic system involves potassium atoms. The first, second, and third ionization energies of potassium are 4.34066 eV , 31.63 eV , and 45.806 eV , respectively. The triple ionization ($t=3$) reaction of K to K^{3+} , then, has a net enthalpy of reaction of 81.7766 eV , which is equivalent to $3 \cdot 27.2\text{ eV}$. It has been reported [21] that intense extreme ultraviolet (EUV) emission was observed from incandescently heated atomic hydrogen and the atomized potassium catalyst that generated an anomalous plasma at low temperatures (e.g. $\approx 10^3\text{ K}$) and an extraordinary low field strength of about $1\text{-}2\text{ V/cm}$. No emission was observed with potassium or hydrogen alone or when sodium replaced potassium with hydrogen.

Emission was observed from K^{3+} that confirmed the resonant nonradiative energy transfer of $3 \cdot 27.2\text{ eV}$ from atomic hydrogen to atomic potassium. The products of the catalysis reaction, lower-energy hydrogen atoms, have binding energies of $m \cdot 27.2\text{ eV}$. Thus, they may further serve as catalysts, and further catalytic transitions may occur: $n = \frac{1}{2} \rightarrow \frac{1}{3}$, $\frac{1}{3} \rightarrow \frac{1}{4}$, $\frac{1}{4} \rightarrow \frac{1}{5}$, and so on. In addition, each lower-energy hydrogen atom is predicted to be highly reactive intermediate to form a novel hydride ion corresponding to the particular atomic energy level. The predicted hydride ion of hydrogen catalysis by atomic potassium is the hydride ion $H^-(1/4)$. This ion was reported to be observed

spectroscopically at 110 nm corresponding to its predicted binding energy of 11.2 eV [21].

A number of independent experimental observations lead to the conclusion that atomic hydrogen can exist in fractional quantum states that are at lower energies than the traditional "ground" ($n=1$) state. Prior related studies that support the possibility of a novel reaction of atomic hydrogen which produces a chemically generated or assisted plasma and produces novel hydride compounds include extreme ultraviolet (EUV) spectroscopy [1, 2, 4, 11-17, 19-21, 24, 28, 32-34, 36, 37], characteristic emission from catalysis and the hydride ion products [4, 6, 9, 10, 16, 21, 24], lower-energy hydrogen emission [12-15, 19, 20], plasma formation [1, 2, 4, 6, 9, 16, 21, 24, 28, 32, 33, 35-37], Balmer α line broadening [2, 4-6, 9, 11-15, 18, 28], elevated electron temperature [2, 5, 11-14], anomalous plasma afterglow duration [1, 35-36], power generation [5, 9, 13-15, 17, 18, 23, 25, 45-47], and analysis of chemical compounds [3, 4, 10, 23, 29, 39-43]. In prior reports [29, 39, 41], novel inorganic alkali and alkaline earth hydrides of the formula MHX and $MHMX$ wherein M is the metal, X , is a singly negatively charged anion, and H comprises a novel high binding energy hydride ion were synthesized in a high temperature gas cell by reaction of atomic hydrogen with a catalyst and MX or MX_2 corresponding to an alkali metal or alkaline earth metal, respectively. We report on the synthesis and characterization of $LiHCl$ which is a new compound of this series.

EXPERIMENTAL

Synthesis

Lithium chloro hydride, $LiHCl$, was prepared in a stainless steel gas cell shown in Figure 1 comprising a Ni screen hydrogen dissociator (Belleville Wire Cloth Co., Inc.), potassium metal catalyst (Aldrich Chemical Company), and $LiCl$ (Aldrich Chemical Company 99.9 %) as the reactant. A 304-stainless steel cell was in the form of a tube having an internal cavity of 359 millimeters in length and 73 millimeters in diameter. The top end of the cell was welded to a high vacuum 4 5/8 inch bored through conflat flange. The mating blank conflat flange contained a single coaxial hole in which was welded a 3/8 inch diameter stainless steel tube that was 100 cm in length and contained an inner

coaxial tube of 1/8 inch diameter. A silver plated copper gasket was placed between the two flanges. The two flanges were held together with 10 circumferential bolts. The bottom of the 3/8 inch tube was flush with the bottom surface of the top flange. The outer tube served as a vacuum line from the cell and the inner tube served as a hydrogen or helium supply line to the cell. The cell was surrounded by four heaters. Concentric to the heaters was high temperature insulation (AL 30 Zircar). Each of the four heaters were individually thermostatically controlled.

The cylindrical wall of the cell was lined with two layers of Ni screen totaling 150 grams. 3 grams of crystalline *LiCl* was poured into the cell. About 0.5 grams of potassium metal was added to the cell under an argon atmosphere. The cell was then continuously evacuated with a high vacuum turbo pump to reach 50 mTorr measured by a pressure gauge (Varian Convectron, Pirani type). The cell was heated by supplying power to the heaters. The heater power of the largest heater was measured using a wattmeter (Clarke -Hess model 259). The temperature of the cell was measured with a type K thermocouple (Omega). The cell temperature was then slowly increased over 2 hours to 300 °C using the heaters that were controlled by a type 97000 controller. The power to the largest heater and the cell temperature and pressure were continuously recorded by a DAS. The vacuum pump valve was closed. Hydrogen was slowly added to maintain a pressure within the range of 1000 Torr to 1500 Torr. The temperature of the cell was then slowly increased to 550 °C over 5 hours. The hydrogen valve was closed except to maintain the pressure at 1500 Torr. After 72 hours, the temperature of the cell was reduced to 400 °C at a rate of 15 °C/hr. The hydrogen supply was switched to helium which was flowed through the inner supply line to the cell while a vacuum was pulled on the outer vacuum line to remove volatilized potassium metal at 400 °C. The cell was then cooled and opened. About 3 grams of light green/brown crystals were observed to have formed in the bottom of the cell.

ToF-SIMS Characterization

The crystalline samples were grounded into powder in a drybox, and then sprinkled onto the surface of a double-sided adhesive tape and characterized using Physical Electronics TRIFT ToF-SIMS instrument. The

primary ion source was a pulsed $^{69}\text{Ga}^+$ liquid metal source operated at 15 keV. The secondary ions were exacted by a ± 3 keV (according to the mode) voltage. Three electrostatic analyzers (Triple-Focusing-Time-of-Flight) deflect them in order to compensate for the initial energy dispersion of ions of the same mass. The 400 pA dc current was pulsed at a 5 kHz repetition rate with a 7 ns pulse width. The analyzed area was $60\mu\text{m} \times 60\mu\text{m}$ and the mass range was 0-1000 AMU. The total ion dose was $7 \times 10^{11} \text{ ions/cm}^2$, ensuring static conditions. Charge compensation was performed with a pulsed electron gun operated at 20 eV electron energy. In order to remove surface contaminants and expose a fresh surface for analysis, the samples were sputter-cleaned for 30 s using a $80\mu\text{m} \times 80\mu\text{m}$ raster, with 600 pA current, resulting in a total ion dose of $10^{15} \text{ ions/cm}^2$. Three different regions on each sample of $60\mu\text{m} \times 60\mu\text{m}$ were analyzed. The positive and negative SIMS spectra were acquired. Representative post sputtering data is reported. The ToF-SIMS data were treated using 'cadence' software (Physical Electronics), which calculates the mass calibration from well-defined reference peaks.

XPS Characterization

A series of XPS analyses of low binding energy region (0 to 100 eV) were made on the crystalline samples using a Scienta 300 XPS Spectrometer. The fixed analyzer transmission mode and the sweep acquisition mode were used. The step energy in the survey scan was 0.5 eV, and the step energy in the high resolution scan was 0.15 eV. In the survey scan, the time per step was 0.4 seconds, and the number of sweeps was 4. In the high resolution scan, the time per step was 0.3 seconds, and the number of sweeps was 30. $\text{C } 1s$ at 284.5 eV was used as the internal standard.

The binding energies and features of core level electrons of control LiCl and the crystals comprising the LiHCl sample were analyzed by a Kratos XSAM-800 spectrometer using nonmonochromatic $\text{Al K}\alpha$ (1468.6 eV) radiation. Samples were crushed in a glove box under argon and mounted on an analysis stub with copper tape. A piece of gold foil was stuck into the sample for calibration. The samples were transferred from glove box to sample treatment chamber under an inert atmosphere. A survey spectrum was run from 1000 eV to 0 eV. For quantitative

analysis, high resolution spectra were run on core level electrons of interest, $\text{Li } 1s$ and $\text{Cl } 2p$ electrons. A high resolution spectrum of the low binding energy region was also run from 120 eV to 0 eV that corresponded to the survey spectrum. Fixed analyzer transmission (FAT) mode was used in all measurements. For the survey scan, a pass energy of 320 eV was employed. A pass energy of 40 eV was used for high resolution scans. In the cases where a charging effect was observed, the spectrum was corrected by using a calibration of $\text{Au } 4f_{7/2}$ peak at 84.0 eV as a first standard and the $\text{Cl } 1s$ peak at 284.5 eV as a second standard.

NMR Spectroscopy

Solid state ^1H MAS NMR was performed on the samples using a custom built spectrometer operating with a Nicolet 1280 computer. Final pulse generation was from a tuned Henry radio amplifier. The ^1H NMR frequency was 270.6196 MHz. A $5 \mu\text{sec}$ pulse corresponding to a 41° pulse length and a 3 second recycle delay were used. The window was $\pm 20 \text{ kHz}$. The spin speed was 4.0 kHz. The number of scans was 600. The offset was 1541.6 Hz, and the magnetic flux was 6.357 T. The samples were handled under a nitrogen atmosphere. Chemical shifts were referenced to external tetramethylsilane (TMS). The reference comprised LiH (Aldrich Chemical Company 99%) and equivalent molar mixtures of LiH (Aldrich Chemical Company 99%) and LiCl (Aldrich Chemical Company 99.99%) prepared in a glove box under argon.

Characterization by X-ray Diffraction (XRD)

The XRD patterns were obtained by IC Laboratories (Amawalk, NY) using a Phillips 547 Diffractometer tuned for Cu K_α (1.540590 \AA) radiation generated at 45 kV and 35 mA. The sample was scanned from 8 to 68 2-theta with a step size of 0.02° and 1 second per step.

RESULTS

ToF-SIMS

The positive ToF-SIMS spectra obtained from LiHCl and LiCl control are shown in Figures 2 and 3, respectively. The positive ion spectrum of LiHCl and that of the LiCl were dominated by the Li^+ ion. $\text{Ga}^+ m/z = 69$, $\text{K}_2^+ m/z = 78$, $\text{K}_2\text{H}^+ m/z = 79$, $\text{K}_2\text{O}^+ m/z = 94$, $\text{K}_2\text{OH}^+ m/z = 95$,

$K(KCl)^+ m/z=113$, $KCO_3^+ m/z=122$, $KHCO_3^+ m/z=123$ and $K_2CO_3^+ m/z=177$ were also observed in the *LiHCl* sample. The presence of K in the *LiHCl* sample was due to the addition of K metal as a catalyst in the synthesis of *LiHCl*.

The negative ion ToF-SIMS of the *LiHCl* shown in Figure 4 was dominated by H^- , O^- and Cl^- peaks. Oxygen contamination was from some air exposure during sample preparation. The Cl^- count was lower than H^- ; whereas, Cl^- dominated the negative ion ToF-SIMS of the *LiCl* control shown in Figure 5. $H^- m/z=1$, and $O^- m/z=16$, were also observed in *LiCl*.

XPS

A survey spectrum was obtained over the region $E_b=0\text{ eV}$ to 1200 eV . The primary element peaks allowed for the determination of all of the elements present in the *LiHCl* and the control *LiCl*. The survey spectrum also detected shifts in the binding energies of the elements which had implications to the identity of the compound containing the elements.

The major species present in control *LiCl* were lithium and chlorine. The XPS survey scan of the *LiHCl* sample obtained on the Scienta instrument is shown in Figure 6. Potassium and oxygen from air exposure of the potassium catalyst during sample preparation was present as well as lithium. Chlorine was observed in the low binding energy region.

The 0-120 eV binding energy region of high resolution XPS spectra of the *LiHCl* sample (solid), the control *LiCl* (dashed), and the 0-30 eV region of an additional control *KCl* obtained on the Scienta instrument are shown in Figure 7. Elements present in the survey scan which could be assigned to peaks in the low binding energy region of the *LiHCl* sample were the $K3p$ and $K3s$ peaks at 19 eV and 35 eV, respectively, the $O2s$ at 24 eV, $Li1s$ at 55 eV, and the $Cl3p$ peak at 6.5 eV.

Accordingly, any other peaks in this region must be due to novel species. The XPS spectrum of the *LiHCl* sample differs from those of *LiCl* and *KCl* by having additional features at 11.2 eV and 14.7 eV. *LiOH* was present in *LiCl* and the *LiHCl* sample as shown by the presence of $O2s$ in Figure 7. Thus, the novel peaks can not be assigned to *LiOH*.

The 0-120 eV binding energy region of high resolution XPS spectra of the *LiHCl* sample (solid) and the control *LiCl* (dashed) obtained on the Scienta instrument is shown in Figure 8. Hydrogen is the only element which does not have primary element peaks; thus, it is the only candidate to produce the novel peaks. The XPS peaks centered at 11.2 eV and 14.7 eV that do not correspond to any other primary element peaks may correspond to the $H^-(n=1/4)E_b = 11.2 \text{ eV}$ hydride ion predicted by Mills [38] (Eqs. (7-8)) in two different chemical environments where E_b is the predicted vacuum binding energy. In this case, the reaction to form $H^-(n=1/4)$ is given by Eqs. (3-5) and Eq. (6). Figure 8 also shows that the *Li* 1s peak of *LiHCl* was shifted about 1.7 eV to lower binding energies relative to the *Li* 1s peak of *LiCl* possibly due to the presence of $H^-(n=1/4)$.

The binding energies and features of core level electrons of control *LiCl* and the *LiHCl* sample were analyzed by XPS. The local structure of *LiCl* and the *LiHCl* sample was investigated by studying the metal *Li* 1s core level electrons and the chloride *Cl* 2p core level electrons. As atomic hydrogen undergoes reaction with potassium catalyst to form a lower-energy hydrogen species which subsequently reacts with the lithium center in *LiCl*, alterations in the electronic structure of lithium such as changes in core level binding energies relative to the starting compound, *LiCl*, were expected.

The XPS spectra of the *Li* 1s core level in *LiCl* and *LiHCl* appear in Figures 9A and 9B respectively. The *Li* 1s binding energy (54.96 eV) in the *LiHCl* sample is about 1.7 eV lower than that of *Li* 1s (56.66 eV) in the control *LiCl*. The full width at half maximum (FWHM) in *Li* 1s from the *LiHCl* sample is about 0.17 eV broader than that from control *LiCl*. The presence of the novel hydride ion shifted the *Li* 1s peaks to lower binding energies relative to the corresponding peaks of *LiCl*. A similar shift in the *Li* 1s core level of the *LiHCl* sample was observed when compared to *Li* 1s of *LiCl* recorded with the Scienta instrument as shown in Figure 8.

The XPS spectra of the *Cl* 2p core level in *LiCl* and *LiHCl* appear in Figures 10A and 10B respectively. In contrast to the *Li* 1s core level, the *Cl* 2p core level FWHM in the *LiHCl* sample is very similar to *LiCl*. Comparing the alterations in the *Li* core level versus the *Cl* core level indicates that the lower-energy hydrogen species is bound to the metal

center of *LiCl*. This binding largely influences the metal core level with little perturbation of the halogen core level.

The XPS data clearly indicates a change in the electronic structure at the *Li* core level and different bonding in *LiHCl* relative to that in the corresponding *LiCl*. It strongly suggests the formation of a novel metal hydride which is consistent with the supporting data provided by XPS given above, NMR and ToF-SIMS given in the respective sections.

The XPS survey scans of *LiCl* and the *LiHCl* sample obtained on the Kratos instrument are shown in Figures 11A-B, respectively. The 0-100 eV binding energy region of high resolution XPS spectra of *LiCl* and the *LiHCl* sample obtained on the Kratos instrument are shown in Figures 12A-B, respectively. Hydrogen is the only element which does not have primary element peaks; thus, it is the only candidate to produce the shifted *Li* 1s peak of the *LiHCl* sample compared to *LiCl* as shown in Figures 12A-B.

NMR

The ^1H MAS NMR spectra of the *LiHCl* sample, the control comprising an equal molar mixture of *LiH* and *LiCl*, and the control *LiH* relative to external tetramethylsilane (TMS) are shown in Figures 13A-C, respectively. Ordinary hydride ion has resonances at 4.2 ppm and 1.1 ppm in the *LiH*/*LiCl* mixture and in *LiH* alone as shown in Figures 13B and 13C, respectively. The presence of *LiCl* does not shift the resonance of ordinary hydride as shown in Figure 13B. The resonance at 4.2 ppm and 1.2 ppm which are assigned to ordinary hydride ion was observed in the spectrum of the *LiHCl* sample as shown in Figure 13A. A large distinct upfield resonance was observed at -15.2 ppm, and features were observed at -1.7 ppm and -9 ppm. These features were not observed in either control. The upfield shifted peaks are consistent with a hydride ion with a smaller radius as compared with ordinary hydride since a smaller radius increases the shielding or diamagnetism. This upfield shifted peak was assigned to a novel hydride ion of *LiHCl* in different chemical environments. The down field shifted peak at 13.3 ppm may have been due to H^+ stabilized by the novel H^- .

XRD

The XRD pattern of *LiHCl* is shown in Figure 14. The identifiable peaks corresponded to a mixture of *LiH*, *LiO* and *LiOH*. In addition, the spectrum contained a number of peaks that could not be assigned. The 2-theta and d-spacings of the unidentified XRD peaks of the *LiHCl* sample are given in Table 1.

DISCUSSION

The ToF-SIMS of the product of the reaction of atomic hydrogen with potassium metal and *LiCl* showed Li^+ and H^- as the dominant peaks with Cl^- present. The potassium metal was oxidized by air exposure during sample preparation. The ToF-SIMS results recorded on the reaction product are consistent with the proposed structure *LiHCl*. The NMR and XPS data indicate that a novel hydride ion was present. The known compounds *LiCl* and *LiH* have the lithium ion in a +1 state. The compound *LiHCl* is unknown and extraordinary. The implied valence of lithium is +2.

The 0-100 eV binding energy region of a high resolution XPS spectrum of the *LiHCl* sample indicates the presence of the hydride ion $\text{H}^-(1/4)$ with binding energies of 11.2 eV and 14.7 eV compared to the predicted binding energy of 11.2 eV. The presence of two peaks may have been due to the presence $\text{H}^-(1/4)$ in two different chemical environments. The XPS data of the core levels clearly indicates a change in the electronic structure and different bonding in *LiHCl* relative to that in the corresponding *LiCl*. This binding influences the metal core level with little perturbation of the halogen core level. Comparing the alterations in the *Li* core levels versus the *Cl* core level indicates that the lower-energy hydrogen species binds to the metal center of *LiCl*. The presence of the novel hydride ion shifts the *Li* 1s peaks to lower binding energies relative to the corresponding peaks of *LiCl*. It strongly suggests the formation of a novel metal hydride which is consistent with the supporting data provided by XPS, NMR and ToF-SIMS.

The resonances in the NMR spectrum of the *LiHCl* at 4.2 ppm and 1.1 ppm were assigned to ordinary hydride ion. The large distinct upfield resonance at -15.2 ppm, and features observed at -1.7 ppm and

-9 ppm identifies a hydride ion with a substantially smaller radius as compared with ordinary hydride since a smaller radius increases the shielding or diamagnetism, and the shift was extraordinary. *LiHCl* was possibly present in different chemical environments as evidenced by the three distinct upfield shifts.

XRD peaks were observed which did not match those known which supported the identification of a novel compound.

CONCLUSIONS

The ToF-SIMS, XPS and NMR results confirmed the identification of *LiHCl* with a hydride ion $H^-(1/4)$ having a high binding energy of 11.2 eV (Eqs. (7-8)) that matched theoretical predictions [38]. Hydride ion ($H^-(1/4)$) may be formed according to Eqs. (3-5) and Eq. (6) which was supported by the XPS and NMR data of the *LiHCl* sample. The identification of compounds containing novel hydride ions is indicative of a new field of hydrogen chemistry. Novel hydride ions may combine with other cations such as other alkali cations and alkaline earth, rare earth, and transition element cations. Numerous novel compounds may be synthesized with extraordinary properties relative to the corresponding compounds having ordinary hydride ions [3, 4, 10, 23, 29, 39-43]. These novel compounds may have a breath of applications. For example, a high voltage battery according to the hydride binding energies in *LiHCl* and previously observed by XPS [3, 10, 23, 39-43] may be possible having projected specifications that are significantly exceed those of the current state of the art [7, 40, 42].

APPENDIX

Mills [38] predicted an exothermic reaction whereby certain atoms or ions serve as catalysts to release energy from hydrogen to produce an increased binding energy hydrogen atom called a hydrino having a binding energy of

$$\text{Binding Energy} = \frac{13.6 \text{ eV}}{\left(\frac{1}{p}\right)^2} \quad (1)$$

where p is an integer greater than 1, designated as $H\left[\frac{a_H}{p}\right]$ where a_H is the radius of the hydrogen atom. Hydrinos were predicted to form by reacting an ordinary hydrogen atom with a catalyst having a net enthalpy of reaction of about

$$m \cdot 27.2 \text{ eV} \quad (2)$$

where m is an integer. This catalysis releases energy from the hydrogen atom with a commensurate decrease in size of the hydrogen atom, $r_n = na_H$. For example, the catalysis of $H(n=1)$ to $H(n=1/2)$ releases 40.8 eV, and the hydrogen radius decreases from a_H to $\frac{1}{2}a_H$.

A catalytic system is provided by the ionization of t electrons from an atom each to a continuum energy level such that the sum of the ionization energies of the t electrons is approximately $m \times 27.2 \text{ eV}$ where m is an integer. One such catalytic system involves potassium. The first, second, and third ionization energies of potassium are 4.34066 eV, 31.63 eV, 45.806 eV, respectively [48]. The triple ionization ($t=3$) reaction of K to K^{3+} , then, has a net enthalpy of reaction of 81.7426 eV, which is equivalent to $m=3$ in Eq. (2).

$$81.7426 \text{ eV} + K(m) + H\left[\frac{a_H}{p}\right] \rightarrow K^{3+} + 3e^- + H\left[\frac{a_H}{(p+3)}\right] + [(p+3)^2 - p^2] \times 13.6 \text{ eV} \quad (3)$$

$$K^{3+} + 3e^- \rightarrow K(m) + 81.7426 \text{ eV} \quad (4)$$

And, the overall reaction is

$$H\left[\frac{a_H}{p}\right] \rightarrow H\left[\frac{a_H}{(p+3)}\right] + [(p+3)^2 - p^2] \times 13.6 \text{ eV} \quad (5)$$

A novel hydride ion having extraordinary chemical properties given by Mills [38] was predicted to form by the reaction of an electron with a hydrino (Eq. (6)). The resulting hydride ion is referred to as a hydrino hydride ion, designated as $H^-(1/p)$.



The hydrino hydride ion is distinguished from an ordinary hydride ion having a binding energy of 0.8 eV. The latter is hereafter referred to as "ordinary hydride ion". The hydrino hydride ion is predicted [38] to comprise a hydrogen nucleus and two indistinguishable electrons at a binding energy according to the following formula:

$$\text{Binding Energy} = \frac{\hbar^2 \sqrt{s(s+1)}}{8\mu_e a_0^2 \left[\frac{1 + \sqrt{s(s+1)}}{p} \right]^2} - \frac{\pi\mu_0 e^2 \hbar^2}{m_e^2 a_0^3} \left(1 + \frac{2^2}{\left[\frac{1 + \sqrt{s(s+1)}}{p} \right]^3} \right) \quad (7)$$

where p is an integer greater than one, $s=1/2$, \hbar is Planck's constant bar, μ_0 is the permeability of vacuum, m_e is the mass of the electron, μ_e is the reduced electron mass, a_0 is the Bohr radius, and e is the elementary charge. The ionic radius is

$$r_1 = \frac{a_0}{p} (1 + \sqrt{s(s+1)}); s = \frac{1}{2} \quad (8)$$

From Eq. (8), the radius of the hydrino hydride ion $H^-(1/p)$; p = integer is $\frac{1}{p}$ that of ordinary hydride ion, $H^-(1/1)$.

REFERENCES

1. H. Conrads, R. Mills, Th. Wrubel, "Emission in the Deep Vacuum Ultraviolet from an Incandescently Driven Plasma in a Potassium Carbonate Cell", Plasma Sources Science and Technology, submitted.
2. R. L. Mills, P. Ray, "Stationary Inverted Lyman Population Formed from Incandescently Heated Hydrogen Gas with Certain Catalysts", Chem. Phys. Letts., submitted.
3. R. L. Mills, B. Dhandapani, J. He, "Synthesis and Characterization of a Highly Stable Amorphous Silicon Hydride", Int. J. Hydrogen Energy, submitted.
4. R. L. Mills, P. Ray, R. Mayo, "CW HI Laser Based on a Stationary Inverted Lyman Population Formed from Incandescently Heated Hydrogen Gas with Certain Catalysts", IEEE Transactions on Plasma Science, submitted.
5. R. L. Mills, P. Ray, "Substantial Changes in the Characteristics of a Microwave Plasma Due to Combining Argon and Hydrogen", New Journal of Physics, submitted.
6. R. L. Mills, P. Ray, " High Resolution Spectroscopic Observation of the Bound-Free Hyperfine Levels of a Novel Hydride Ion Corresponding to a Fractional Rydberg State of Atomic Hydrogen", Int. J. Hydrogen Energy, in press.
7. R. L. Mills, E. Dayalan, "Novel Alkali and Alkaline Earth Hydrides for High Voltage and High Energy Density Batteries", Proceedings of the 17th Annual Battery Conference on Applications and Advances, California State University, Long Beach, CA, (January 15-18, 2002), in press.
8. R. Mayo, R. Mills, M. Nansteel, "On the Potential of Direct and MHD Conversion of Power from a Novel Plasma Source to Electricity for Microdistributed Power Applications", IEEE Transactions on Plasma Science, submitted.
9. R. Mills, P. Ray, J. Dong, M. Nansteel, W. Good, P. Jansson, B. Dhandapani, J. He, "Excessive Balmer α Line Broadening, Power Balance, and Novel Hydride Ion Product of Plasma Formed from Incandescently Heated Hydrogen Gas with Certain Catalysts", Int. J. Hydrogen Energy, submitted.

10. R. Mills, E. Dayalan, P. Ray, B. Dhandapani, J. He, "Highly Stable Novel Inorganic Hydrides from Aqueous Electrolysis and Plasma Electrolysis, Japanese Journal of Applied Physics, submitted.
11. R. L. Mills, P. Ray, B. Dhandapani, J. He, "Comparison of Excessive Balmer α Line Broadening of Glow Discharge and Microwave Hydrogen Plasmas with Certain Catalysts", Chem. Phys., submitted.
12. R. L. Mills, P. Ray, B. Dhandapani, J. He, "Spectroscopic Identification of Fractional Rydberg States of Atomic Hydrogen", J. of Phys. Chem., submitted.
13. R. L. Mills, P. Ray, B. Dhandapani, M. Nansteel, X. Chen, J. He, "New Power Source from Fractional Rydberg States of Atomic Hydrogen", Chem. Phys. Letts., submitted.
14. R. L. Mills, P. Ray, B. Dhandapani, M. Nansteel, X. Chen, J. He, "Spectroscopic Identification of Transitions of Fractional Rydberg States of Atomic Hydrogen", Quantitative Spectroscopy and Energy Transfer, submitted.
15. R. L. Mills, P. Ray, B. Dhandapani, M. Nansteel, X. Chen, J. He, "New Power Source from Fractional Quantum Energy Levels of Atomic Hydrogen that Surpasses Internal Combustion", Spectrochimica Acta, Part A, submitted.
16. R. L. Mills, P. Ray, "Spectroscopic Identification of a Novel Catalytic Reaction of Rubidium Ion with Atomic Hydrogen and the Hydride Ion Product", Int. J. Hydrogen Energy, in press.
17. R. Mills, J. Dong, W. Good, P. Ray, J. He, B. Dhandapani, Measurement of Energy Balances of Noble Gas-Hydrogen Discharge Plasmas Using Calvet Calorimetry, Int. J. Hydrogen Energy, in press.
18. R. L. Mills, A. Voigt, P. Ray, M. Nansteel, B. Dhandapani, "Measurement of Hydrogen Balmer Line Broadening and Thermal Power Balances of Noble Gas-Hydrogen Discharge Plasmas", Int. J. Hydrogen Energy, in press.
19. R. Mills, P. Ray, "Vibrational Spectral Emission of Fractional-Principal-Quantum-Energy-Level Hydrogen Molecular Ion", Int. J. Hydrogen Energy, in press.
20. R. Mills, P. Ray, "Spectral Emission of Fractional Quantum Energy Levels of Atomic Hydrogen from a Helium-Hydrogen Plasma and the

- Implications for Dark Matter", Int. J. Hydrogen Energy, Vol. 27, No. 3, pp. 301-322.
21. R. Mills, P. Ray, "Spectroscopic Identification of a Novel Catalytic Reaction of Potassium and Atomic Hydrogen and the Hydride Ion Product", Int. J. Hydrogen Energy, Vol. 27, No. 2, February, (2002), pp. 183-192.
 22. R. Mills, "BlackLight Power Technology-A New Clean Hydrogen Energy Source with the Potential for Direct Conversion to Electricity", Proceedings of the National Hydrogen Association, 12 th Annual U.S. Hydrogen Meeting and Exposition, *Hydrogen: The Common Thread*, The Washington Hilton and Towers, Washington DC, (March 6-8, 2001), pp. 671-697.
 23. R. Mills, W. Good, A. Voigt, Jinquan Dong, "Minimum Heat of Formation of Potassium Iodo Hydride", Int. J. Hydrogen Energy, Vol. 26, No. 11, Oct., (2001), pp. 1199-1208.
 24. R. Mills, "Spectroscopic Identification of a Novel Catalytic Reaction of Atomic Hydrogen and the Hydride Ion Product", Int. J. Hydrogen Energy, Vol. 26, No. 10, (2001), pp. 1041-1058.
 25. R. Mills, N. Greenig, S. Hicks, "Optically Measured Power Balances of Anomalous Discharges of Mixtures of Argon, Hydrogen, and Potassium, Rubidium, Cesium, or Strontium Vapor", Int. J. Hydrogen Energy, in press.
 26. R. Mills, "The Grand Unified Theory of Classical Quantum Mechanics", Global Foundation, Inc. Orbis Scientiae entitled *The Role of Attractive and Repulsive Gravitational Forces in Cosmic Acceleration of Particles The Origin of the Cosmic Gamma Ray Bursts*, (29th Conference on High Energy Physics and Cosmology Since 1964) Dr. Behram N. Kursunoglu, Chairman, December 14-17, 2000, Lago Mar Resort, Fort Lauderdale, FL, Kluwer Academic/Plenum Publishers, New York, pp. 243-258.
 27. R. Mills, "The Grand Unified Theory of Classical Quantum Mechanics", Int. J. Hydrogen Energy, in press.
 28. R. Mills and M. Nansteel, P. Ray, "Argon-Hydrogen-Strontium Discharge Light Source", IEEE Transactions on Plasma Science, in press.
 29. R. Mills, B. Dhandapani, M. Nansteel, J. He, A. "Voigt, Identification of Compounds Containing Novel Hydride Ions by Nuclear Magnetic

- Resonance Spectroscopy", Int. J. Hydrogen Energy, Vol. 26, No. 9, Sept. (2001), pp. 965-979.
30. R. Mills, "BlackLight Power Technology-A New Clean Energy Source with the Potential for Direct Conversion to Electricity", Global Foundation International Conference on "Global Warming and Energy Policy", Dr. Behram N. Kursunoglu, Chairman, Fort Lauderdale, FL, November 26-28, 2000, Kluwer Academic/Plenum Publishers, New York, pp. 1059-1096.
 31. R. Mills, The Nature of Free Electrons in Superfluid Helium--a Test of Quantum Mechanics and a Basis to Review its Foundations and Make a Comparison to Classical Theory, Int. J. Hydrogen Energy, Vol. 26, No. 10, (2001), pp. 1059-1096.
 32. R. Mills, M. Nansteel, and Y. Lu, "Excessively Bright Hydrogen-Strontium Plasma Light Source Due to Energy Resonance of Strontium with Hydrogen", Plasma Chemistry and Plasma Processing, submitted.
 33. R. Mills, J. Dong, Y. Lu, "Observation of Extreme Ultraviolet Hydrogen Emission from Incandescently Heated Hydrogen Gas with Certain Catalysts", Int. J. Hydrogen Energy, Vol. 25, (2000), pp. 919-943.
 34. R. Mills, "Observation of Extreme Ultraviolet Emission from Hydrogen-KI Plasmas Produced by a Hollow Cathode Discharge", Int. J. Hydrogen Energy, Vol. 26, No. 6, (2001), pp. 579-592.
 35. R. Mills, "Temporal Behavior of Light-Emission in the Visible Spectral Range from a Ti-K₂CO₃-H-Cell", Int. J. Hydrogen Energy, Vol. 26, No. 4, (2001), pp. 327-332.
 36. R. Mills, T. Onuma, and Y. Lu, "Formation of a Hydrogen Plasma from an Incandescently Heated Hydrogen-Catalyst Gas Mixture with an Anomalous Afterglow Duration", Int. J. Hydrogen Energy, Vol. 26, No. 7, July, (2001), pp. 749-762.
 37. R. Mills, M. Nansteel, and Y. Lu, "Observation of Extreme Ultraviolet Hydrogen Emission from Incandescently Heated Hydrogen Gas with Strontium that Produced an Anomalous Optically Measured Power Balance", Int. J. Hydrogen Energy, Vol. 26, No. 4, (2001), pp. 309-326.
 38. R. Mills, *The Grand Unified Theory of Classical Quantum Mechanics*, September 2001 Edition, BlackLight Power, Inc., Cranbury, New Jersey, Distributed by Amazon.com.

39. R. Mills, B. Dhandapani, N. Greenig, J. He, "Synthesis and Characterization of Potassium Iodo Hydride", *Int. J. of Hydrogen Energy*, Vol. 25, Issue 12, December, (2000), pp. 1185-1203.
40. R. Mills, "Novel Inorganic Hydride", *Int. J. of Hydrogen Energy*, Vol. 25, (2000), pp. 669-683.
41. R. Mills, B. Dhandapani, M. Nansteel, J. He, T. Shannon, A. Echezuria, "Synthesis and Characterization of Novel Hydride Compounds", *Int. J. of Hydrogen Energy*, Vol. 26, No. 4, (2001), pp. 339-367.
42. R. Mills, "Highly Stable Novel Inorganic Hydrides", *Journal of New Materials for Electrochemical Systems*, in press.
43. R. Mills, "Novel Hydrogen Compounds from a Potassium Carbonate Electrolytic Cell", *Fusion Technology*, Vol. 37, No. 2, March, (2000), pp. 157-182.
44. R. Mills, "The Hydrogen Atom Revisited", *Int. J. of Hydrogen Energy*, Vol. 25, Issue 12, December, (2000), pp. 1171-1183.
45. R. Mills, W. Good, "Fractional Quantum Energy Levels of Hydrogen", *Fusion Technology*, Vol. 28, No. 4, November, (1995), pp. 1697-1719.
46. R. Mills, W. Good, R. Shaubach, "Dihydrino Molecule Identification", *Fusion Technology*, Vol. 25, 103 (1994).
47. R. Mills and S. Kneizys, *Fusion Technol.* Vol. 20, 65 (1991).
48. David R. Linde, *CRC Handbook of Chemistry and Physics*, 79 th Edition, CRC Press, Boca Raton, Florida, (1998-9), p. 10-175 to p. 10-177.

Table 1. The 2-theta and d-spacings of the unidentified XRD peaks of the *LiHCl* sample.

| Peak Number | 2 - Theta (Deg) | d (Å) |
|-------------|--------------------|----------|
| 2 | 26.60 | 3.3518 |
| 3 | 26.96 | 3.3066 |
| 4 | 30.70 | 2.9128 |
| 11 | 45.71 | 1.9849 |
| 12 | 49.26 | 1.8497 |
| 16 | 62.21 | 1.4923 |

Figure Captions

Figure 1. Stainless steel gas cell.

Figure 2. The positive ToF-SIMS spectrum ($m/e=0-200$) of the *LiHCl* sample that shows Li^+ as the dominate positive ion.

Figure 3. The positive ToF-SIMS spectrum ($m/e=0-200$) of *LiCl* that shows Li^+ as the dominate positive ion.

Figure 4. The negative ToF-SIMS spectrum ($m/e=0-200$) of the *LiHCl* sample that shows H^- as the dominate negative ion.

Figure 5. The negative ToF-SIMS spectrum ($m/e=0-200$) of *LiCl* that shows Cl^- as the dominate negative ion.

Figure 6. The XPS survey scan of the *LiHCl* sample obtained on the Scienta instrument that shows the presence of potassium and oxygen from air exposure of the potassium catalyst during sample preparation as well as lithium.

Figure 7. The 0-120 eV binding energy region of high resolution XPS spectra of the *LiHCl* sample (solid), the control *LiCl* (dashed), and the 0-30 eV region of an additional control *KCl* obtained on the Scienta instrument. The XPS peaks centered at 11.2 eV and 14.7 eV can not be assigned to *LiCl*, *KCl*, or *LiOH*.

Figure 8. The 0-120 eV binding energy region of high resolution XPS spectra of the *LiHCl* sample (solid) and the control *LiCl* (dashed) obtained on the Scienta instrument. The XPS peaks centered at 11.2 eV and 14.7 eV that do not correspond to any other primary element peaks may correspond to the $H^-(n=1/4)E_b=11.2\text{ eV}$ possibly in two different chemical environments where E_b is the predicted vacuum binding energy. The *Li* 1s peak of *LiHCl* is shifted about 1.7 eV to lower binding energies relative to the *Li* 1s peak of *LiCl* possibly due to the presence of $H^-(n=1/4)$.

Figure 9A. The XPS spectrum of the *Li* 1s core level in *LiCl* obtained on the Kratos instrument.

Figure 9B. The XPS spectrum of the *Li* 1s core level in *LiHCl* obtained on the Kratos instrument. The *Li* 1s binding energy (54.96 eV) in the *LiHCl* sample is about 1.7 eV lower than that of *Li* 1s (56.66 eV) in the control *LiCl*. The full width at half maximum (FWHM) in *Li* 1s from the *LiHCl* sample is about 0.17 eV broader than that from control *LiCl*.

Figure 10A. The XPS spectrum of the $Cl\ 2p$ core level in $LiCl$ obtained on the Kratos instrument.

Figure 10B. The XPS spectrum of the $Cl\ 2p$ core level in $LiHCl$ obtained on the Kratos instrument.

Figure 11A. The XPS survey scan of $LiCl$ obtained on the Kratos instrument.

Figure 11B. The XPS survey scan of the $LiHCl$ sample obtained on the Kratos instrument. The $Cl\ 2p$ core level FWHM in the $LiHCl$ sample is very similar to that of $LiCl$.

Figure 12A. The 0-100 eV binding energy region of a high resolution XPS spectrum of $LiCl$ obtained on the Kratos instrument.

Figure 12B. The 0-100 eV binding energy region of a high resolution XPS spectrum of the $LiHCl$ sample obtained on the Kratos instrument. Hydrogen is the only element which does not have primary element peaks; thus, it is the only candidate to produce the shifted $Li\ 1s$ peak.

Figure 13A. The 1H MAS NMR spectrum of $LiHCl$ relative to external tetramethylsilane (TMS). The resonances at 4.2 ppm and 1.1 ppm were assigned to ordinary hydride ion. The large distinct upfield resonance at -15.2 ppm, and features observed at -1.7 ppm and -9 ppm identified a hydride ion with a substantially smaller radius as compared with ordinary hydride since a smaller radius increases the shielding or diamagnetism. The upfield peaks were assigned to a novel hydride ion of $LiHCl$ possibly in different chemical environments.

Figure 13B. The 1H MAS NMR spectrum of the control comprising an equal molar mixture of LiH and $LiCl$ relative to external tetramethylsilane (TMS). Ordinary hydride ion has resonances at 4.2 ppm and 1.1 ppm in the $LiH/LiCl$ mixture and in LiH . The presence of $LiCl$ does not shift the resonance of ordinary hydride as shown in Figure 13C.

Figure 13C. The 1H MAS NMR spectrum of the control LiH relative to external tetramethylsilane (TMS).

Figure 14. The X-ray Diffraction (XRD) pattern of the $LiHCl$ sample. Unidentified XRD peaks of $LiHCl$ are given in Table 1.

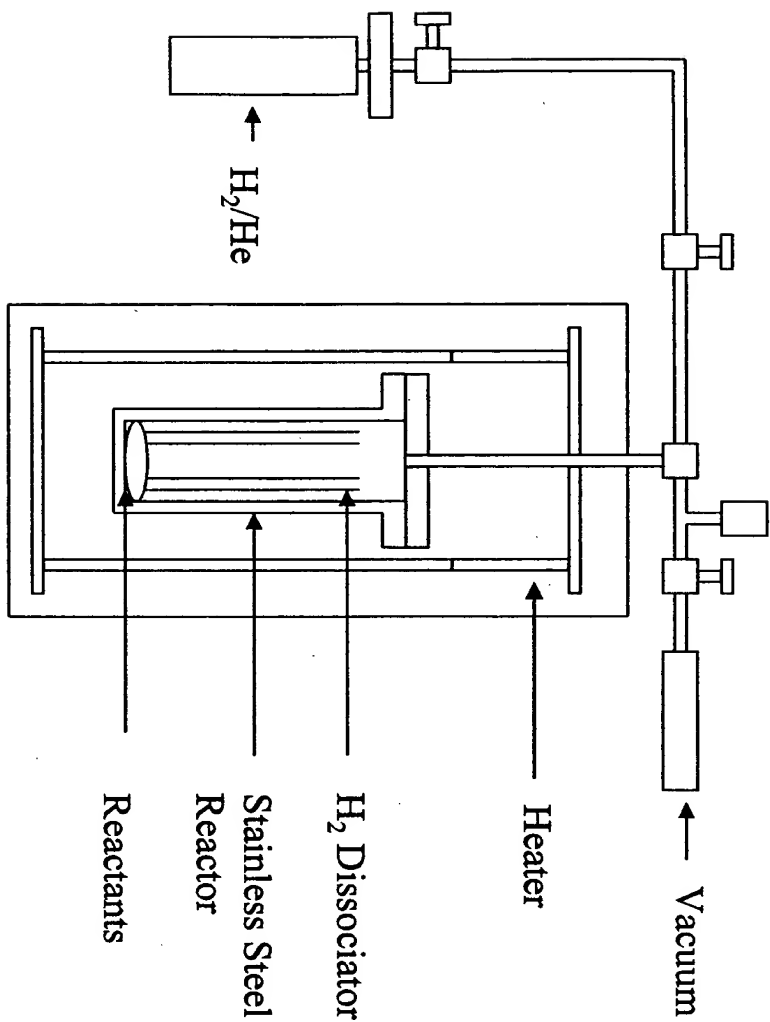


Fig. 1

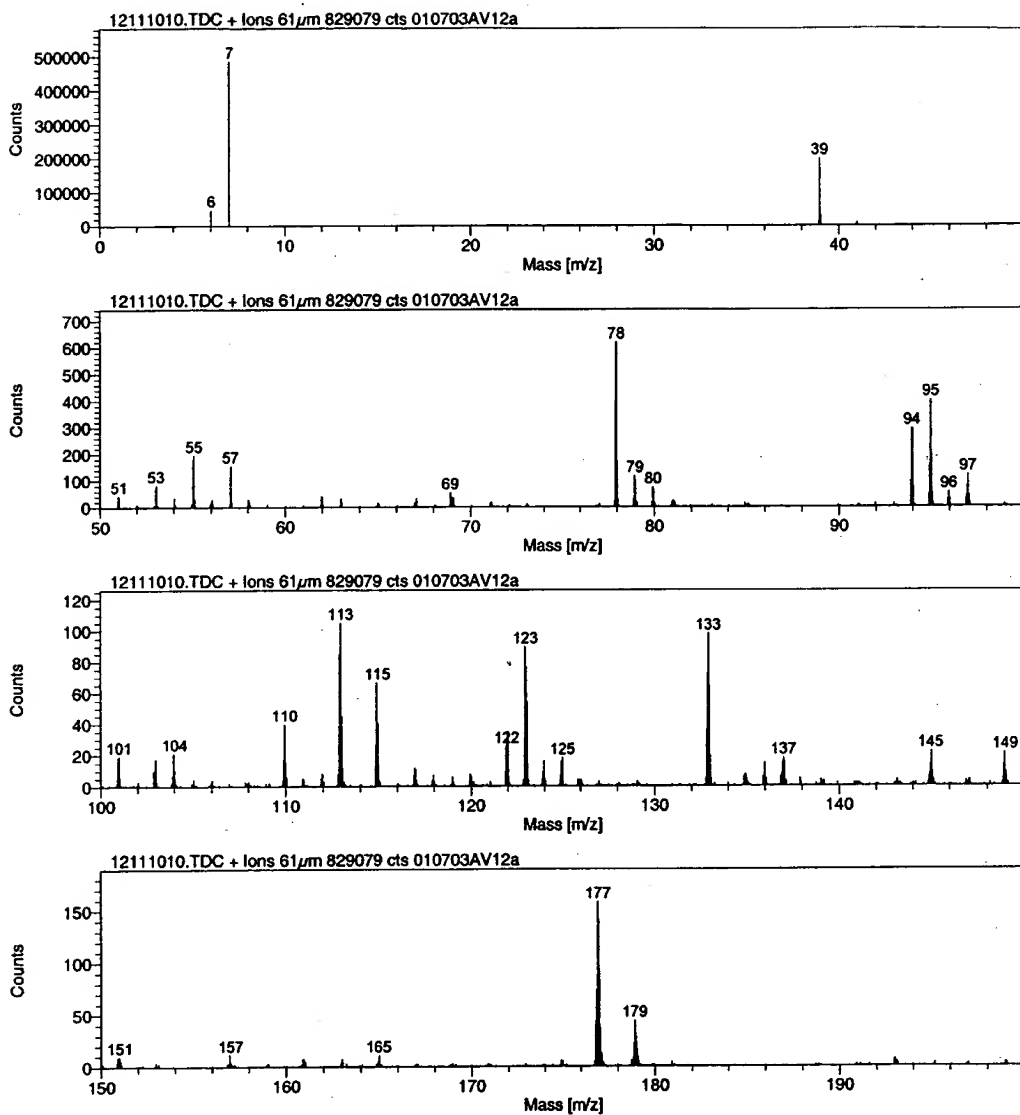


Fig. 2

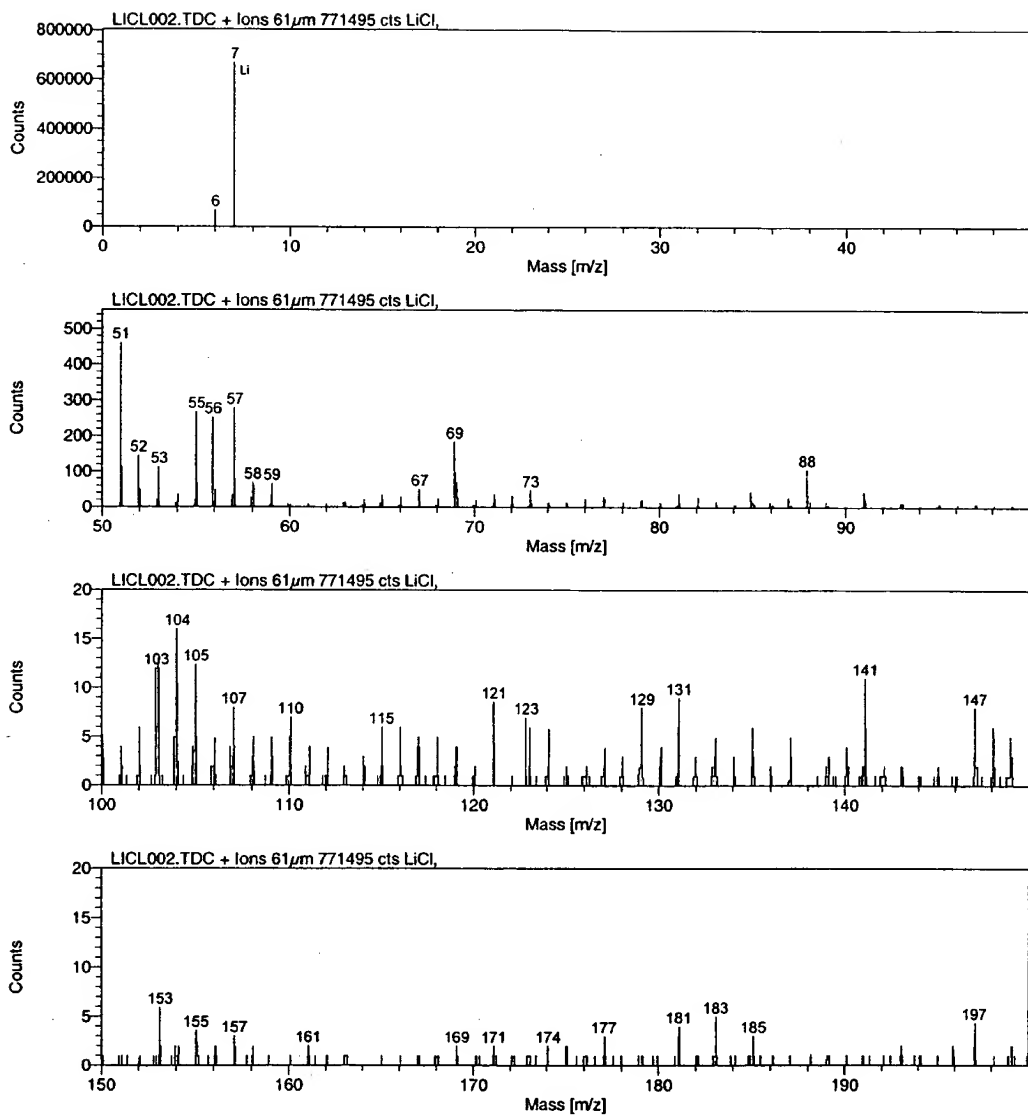


Fig. 3

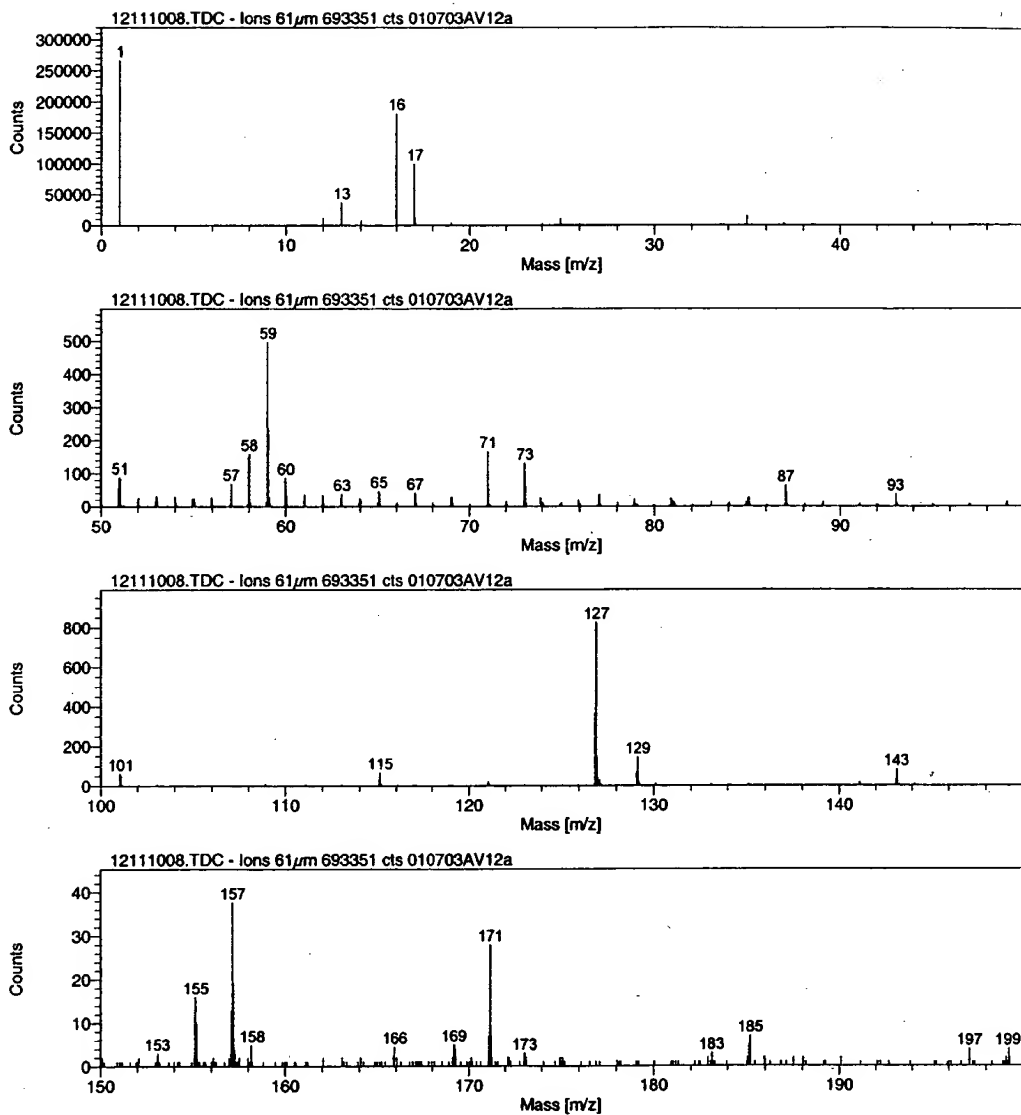


Fig. 4

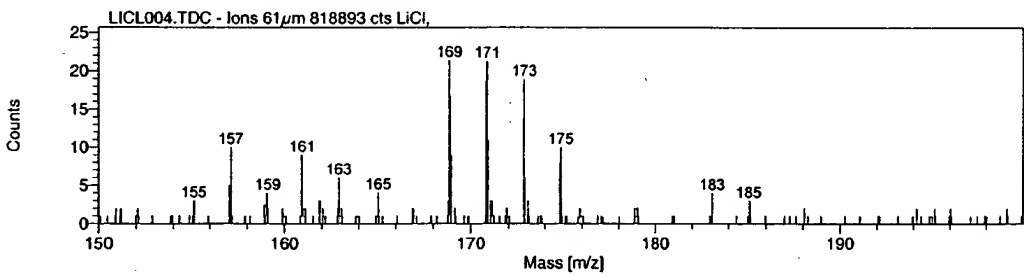
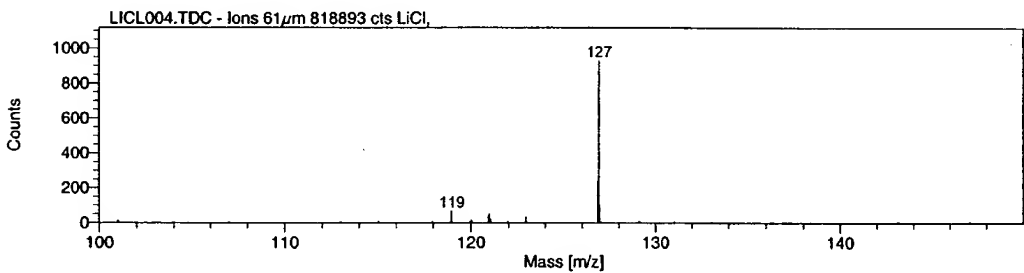
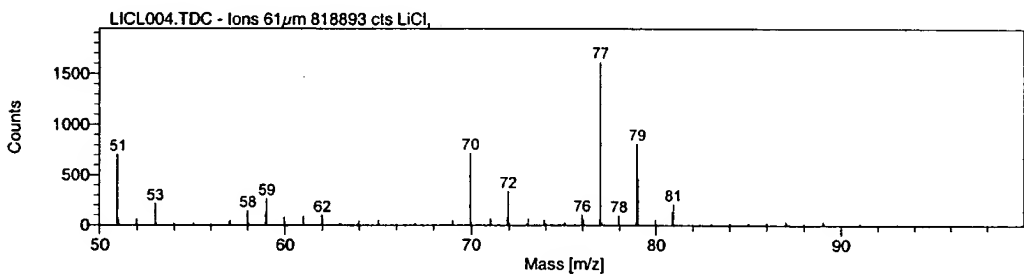
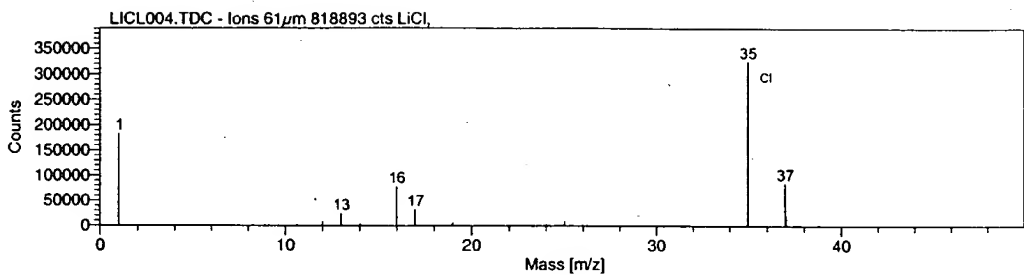


Fig. 5

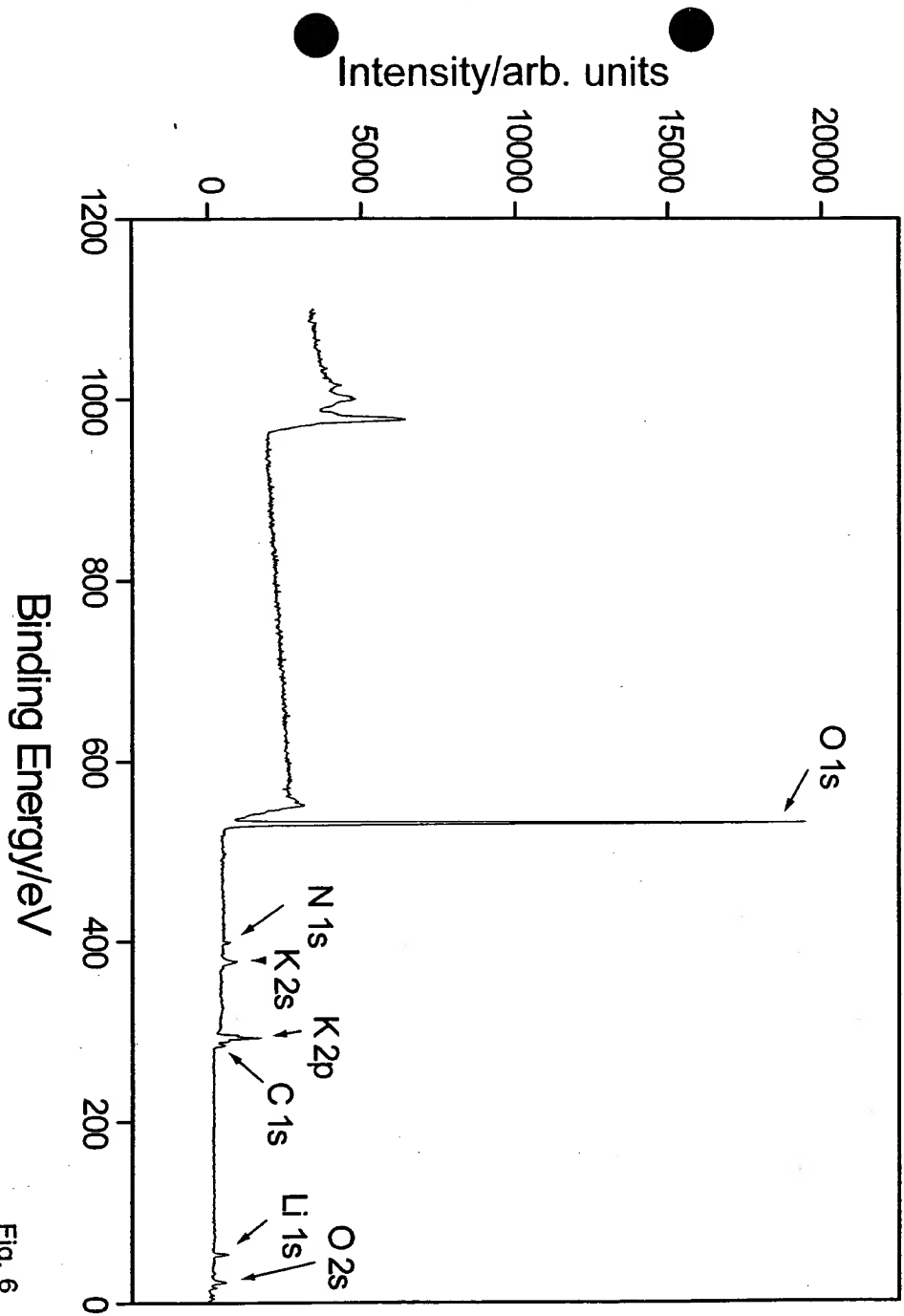


Fig. 6

Binding Energy/eV

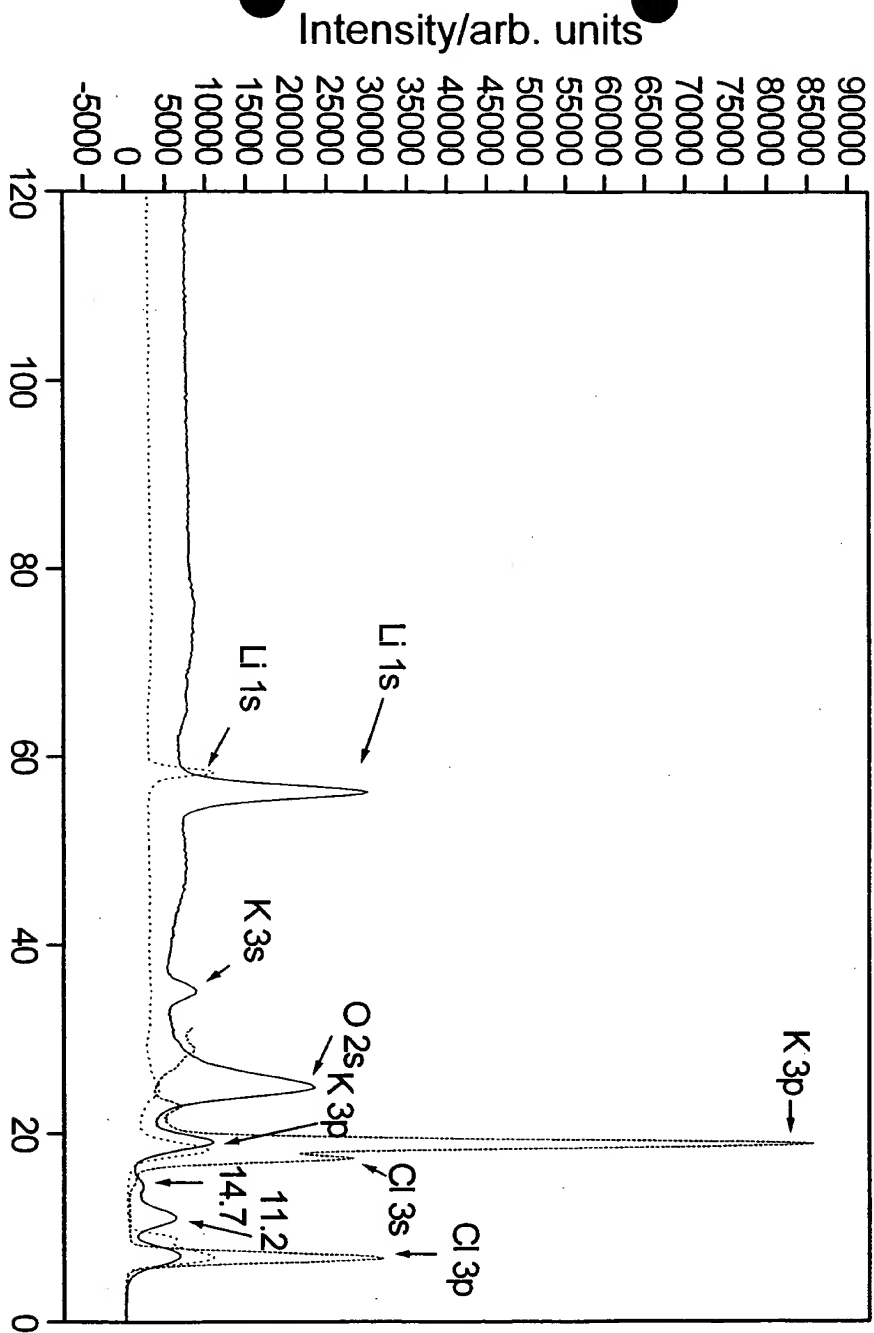


Fig. 7

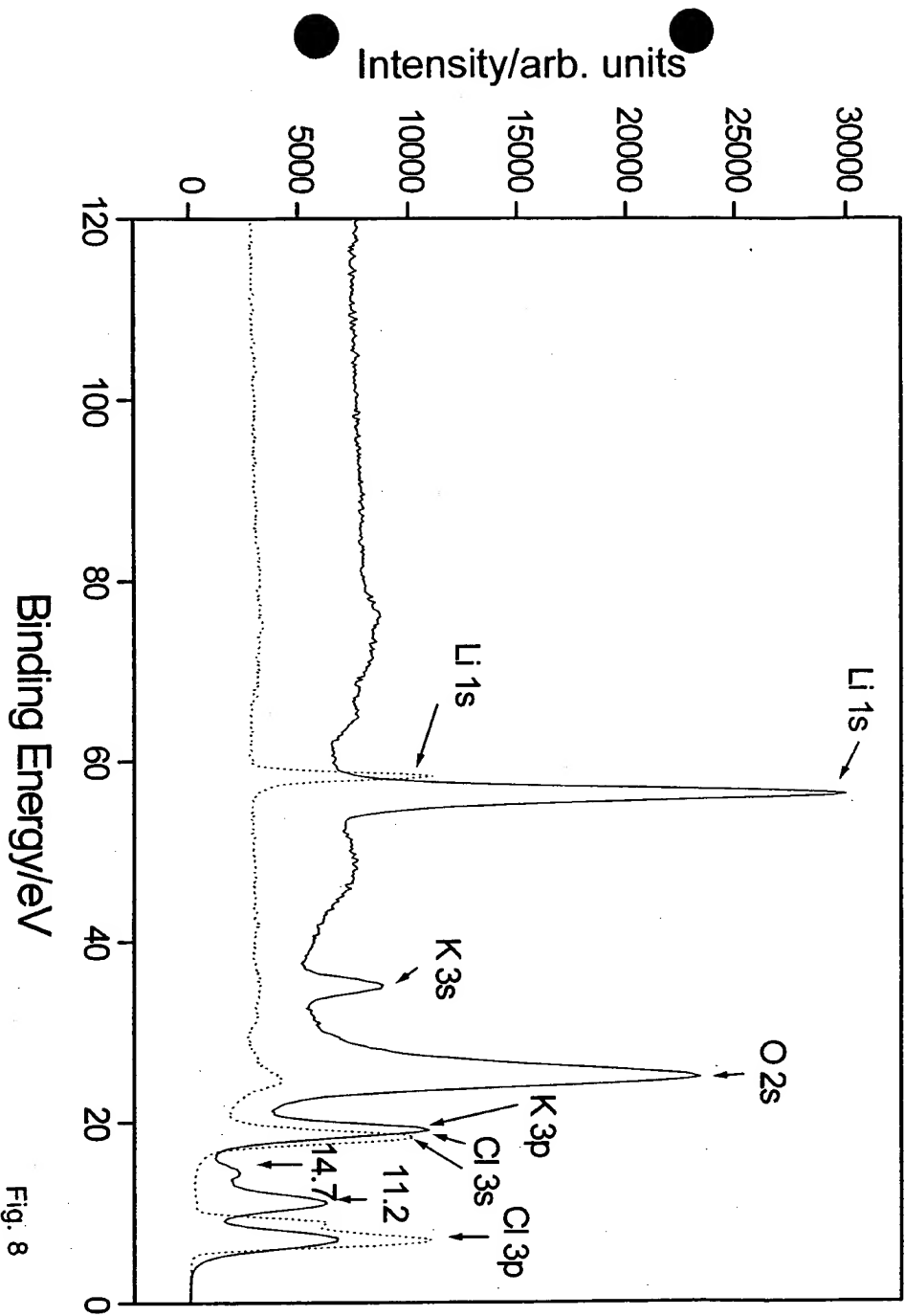


Fig. 8

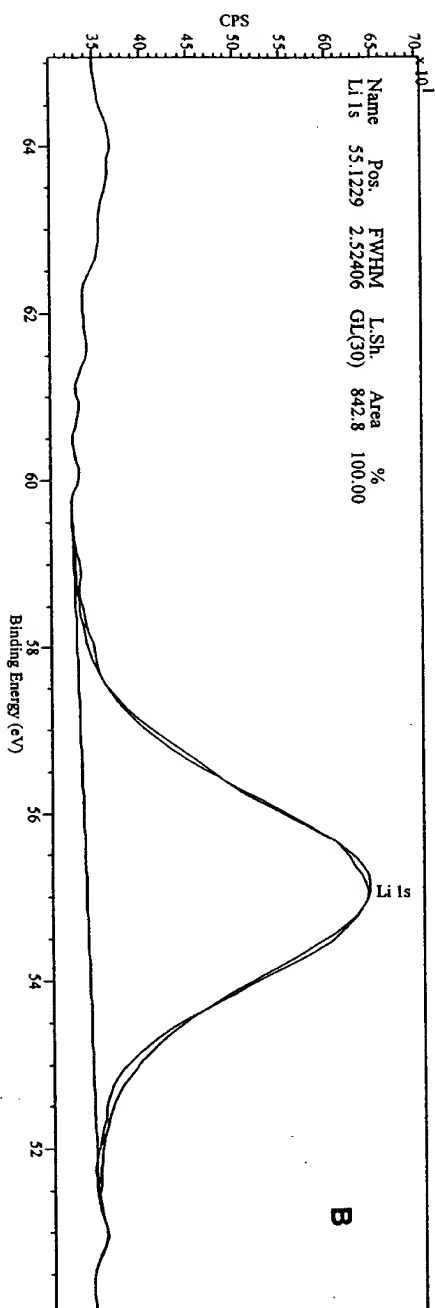
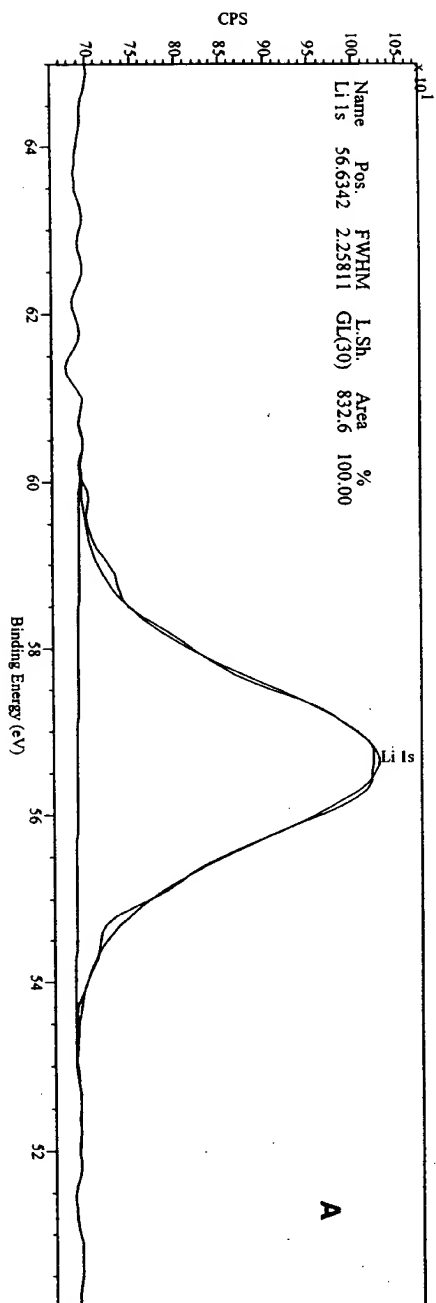


Fig. 9

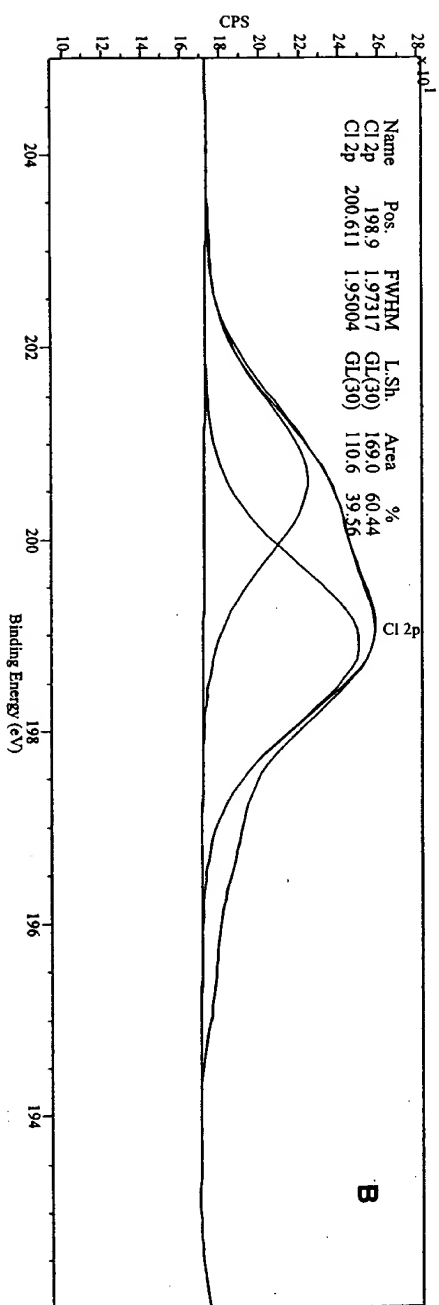
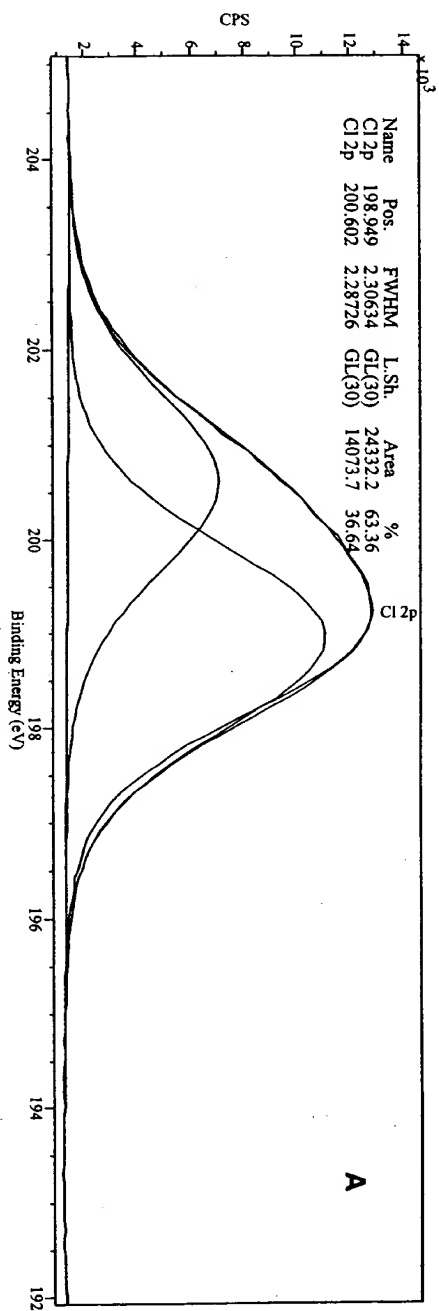


Fig. 10

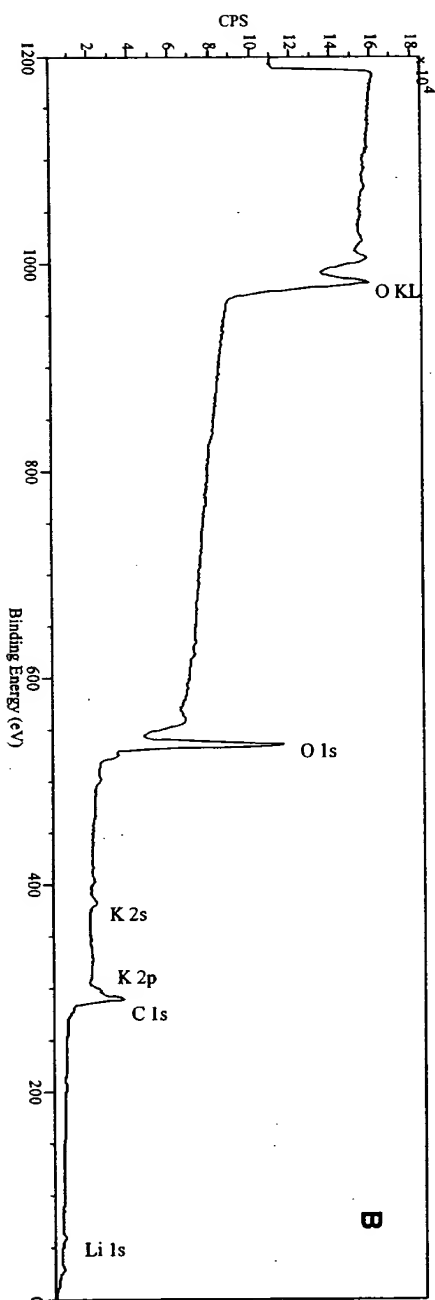
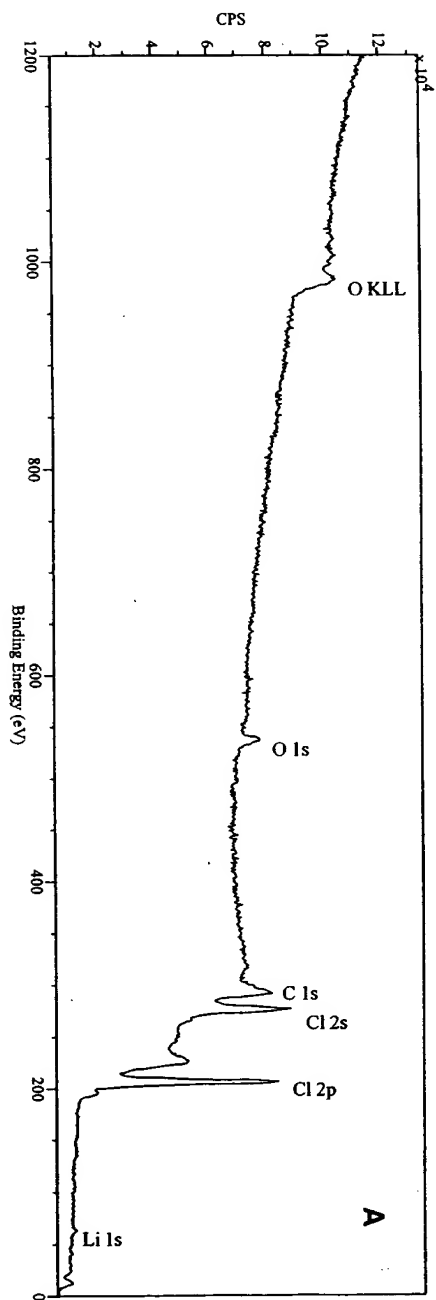


Fig. 11

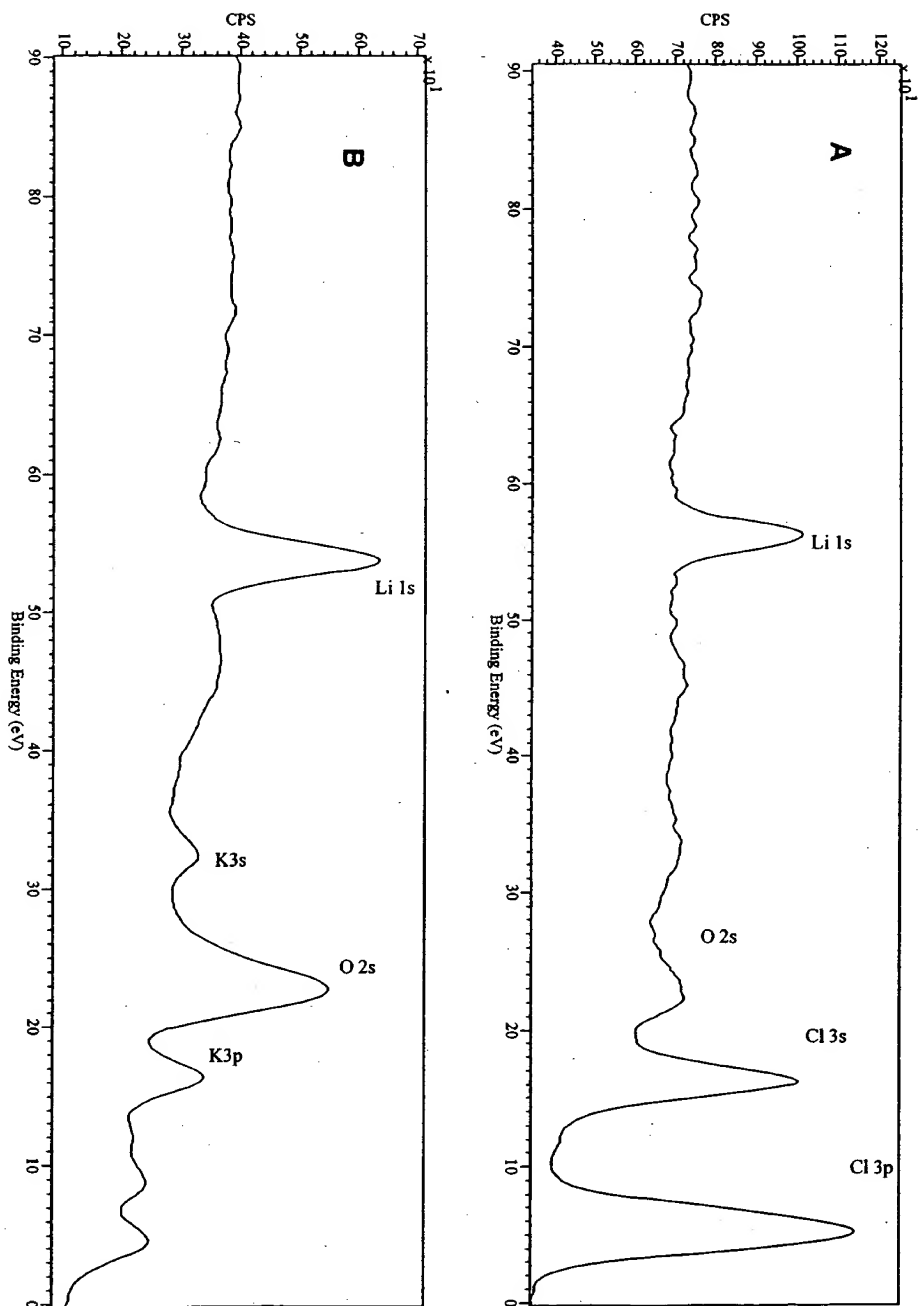


Fig. 12

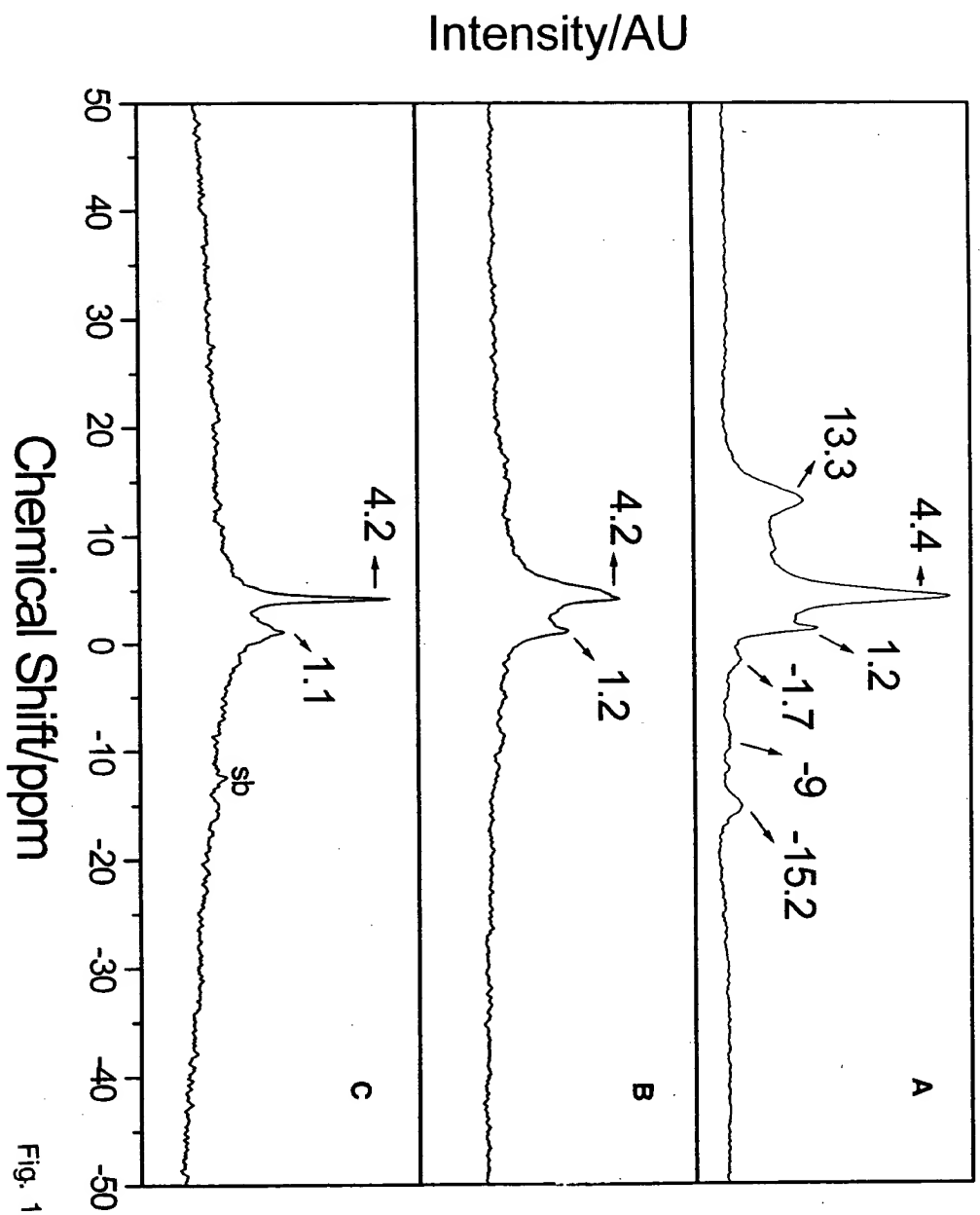


Fig. 13

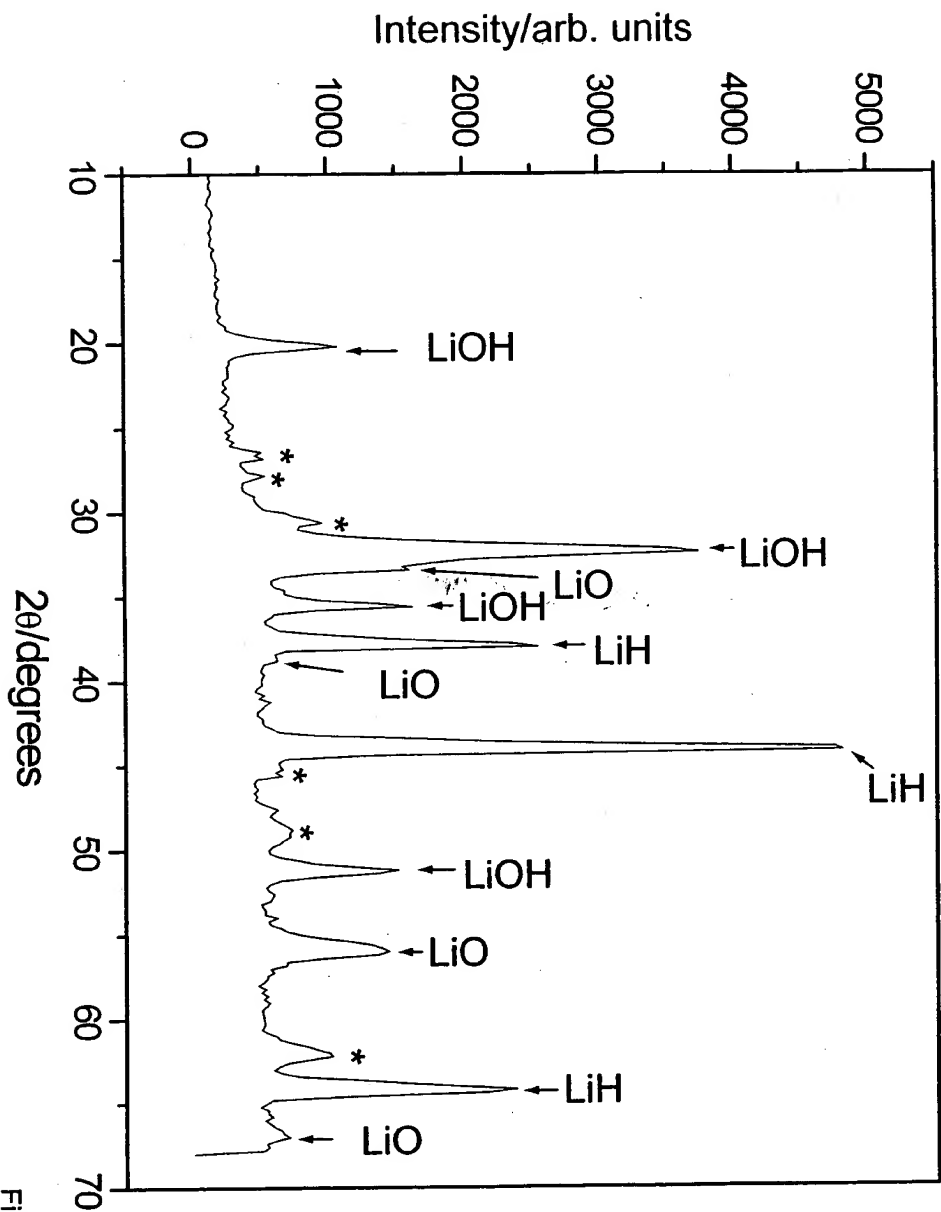


Fig. 14

THIS PAGE BLANK (USPTO)

THIS PAGE BLANK (USPTO)

Substantial Changes in the Characteristics of a Microwave Plasma Due to Combining Argon and Hydrogen

R. L. Mills, P. Ray
BlackLight Power, Inc.
493 Old Trenton Road
Cranbury, NJ 08512

ABSTRACT

Upon the addition of 5% argon to a hydrogen plasma, the Lyman α emission was observed to increase by about an order of magnitude; whereas, xenon control had no effect. With a microwave input power of 40 W, the gas temperature of an argon plasma increased from 400°C to over 750°C with the addition of 3% flowing hydrogen; whereas, the 400°C temperature of a xenon plasma run under identical conditions was essentially unchanged with the addition of hydrogen. The average hydrogen atom temperature of the argon-hydrogen plasma was measured to be 110 - 130 eV versus ≈ 3 eV for pure hydrogen or xenon-hydrogen. Stark broadening or acceleration of charged species due to high fields (e. g. over 10 kV/cm) can not be invoked to explain the results with argon since no high field was observationally present. The electron temperature T_e for the argon-hydrogen and xenon-hydrogen plasmas was $11,600 \pm 5\%$ K and $6500 \pm 5\%$ K, respectively, compared to $4800 \pm 5\%$ K and $4980 \pm 5\%$ K for argon and xenon alone, respectively. The observation of higher temperatures corresponding to three possibly independent plasma parameters for only argon with hydrogen may be explained by the release of energy from atomic hydrogen by a resonant nonradiative energy transfer mechanism.

I. INTRODUCTION

It was reported previously that a new plasma source has been developed that operates by incandescently heating a hydrogen dissociator to provide atomic hydrogen and heats a catalyst such that it becomes gaseous and reacts with the atomic hydrogen to produce a plasma called a resonance transfer or rt-plasma. It was extraordinary, that intense VUV emission was observed by Mills et al. [1-2] at low temperatures (e.g. $\approx 10^3$ K) and an extraordinary low field strength of about 1-2 V/cm from atomic hydrogen and certain atomized elements or certain gaseous ions which singly or multiply ionize at integer multiples of the potential energy of atomic hydrogen, 27.2 eV.

Prior related studies that support the possibility of a novel reaction of atomic hydrogen which produces a chemically generated or assisted plasma (rt-plasma) and produces novel hydride compounds include EUV spectroscopy [1-12, 14], characteristic emission from catalysts and the hydride ion products [8-11], lower-energy hydrogen emission [3-5, 7], chemically formed plasmas [1-2, 6, 8-12], Balmer α line broadening [3-5, 11, 13, 15], elevated electron temperature [3, 5, 13], anomalous plasma afterglow duration [6, 14], power generation [2, 3, 12, 15, 16], and analysis of novel chemical compounds [17]. Argon ions can provide a net enthalpy of a multiple of that of the potential energy of the hydrogen atom. The second ionization energy of argon is 27.63 eV [18]. The reaction Ar^+ to Ar^{2+} has a net enthalpy of reaction of 27.63 eV. Thus, an argon microwave discharge with hydrogen present was anticipated to form an rt-plasma, and the effect of the addition of hydrogen to an argon microwave plasma compared to xenon control was determined. The plasmas were characterized by measuring plasma gas temperature, the ion temperature and number density from Balmer α line broadening, and the electron temperature T_e from intensity ratios of alkali lines.

II. EXPERIMENTAL

A. EUV spectroscopy of hydrogen microwave plasmas with the addition of 5% argon or xenon

Extreme ultraviolet (EUV) spectroscopy was recorded on a hydrogen microwave plasma alone and with the addition of 5% argon or 5% xenon. Due to the short wavelength of this radiation, "transparent" optics do not exist. Therefore, a windowless arrangement was used wherein the microwave discharge cell was connected to the same vacuum vessel as the grating and detectors of the EUV spectrometer. Differential pumping permitted a high pressure in the

cell as compared to that in the spectrometer. This was achieved by pumping on the cell outlet and pumping on the grating side of the collimator that served as a pin-hole inlet to the optics. The spectrometer was continuously evacuated to $10^{-4} - 10^{-6}$ Torr by a turbomolecular pump with the pressure read by a cold cathode pressure gauge. The EUV spectrometer was connected to the cell light source with a 1.5 mm X 5 mm collimator which provided a light path to the slits of the EUV spectrometer. The collimator also served as a flow constrictor of gas from the cell. The cell was operated under gas flow conditions while maintaining a constant gas pressure in the cell.

For spectral measurement, the light emission from microwave plasmas of hydrogen alone, hydrogen-argon (95/5%), and hydrogen-xenon (95/5%) were introduced to a normal incidence McPherson 0.2 meter monochromator (Model 302, Seya-Namioka type) equipped with a 1200 lines/mm holographic grating with a platinum coating. The wavelength region covered by the monochromator was 5 – 560 nm. The UV spectrum (90 – 165 nm) of the cell emission was recorded with a photomultiplier tube (PMT) and a sodium salicylate scintillator. The PMT (Model R1527P, Hamamatsu) used has a spectral response in the range of 185 – 680 nm with a peak efficiency at about 400 nm. The wavelength resolution was about 1 nm (FWHM) with an entrance and exit slit width of 300 μ m. The increment was 0.1 nm and the dwell time was 500 ms.

B. Microwave Emission Spectra

The experimental set up comprising a microwave discharge gas cell light source and an EUV spectrometer which was differentially pumped is shown in Figure 1. Extreme ultraviolet emission spectra were obtained on plasmas of hydrogen alone, hydrogen-argon mixture (95/5%), and hydrogen-xenon mixture (95/5%). Hydrogen or the hydrogen-noble gas mixture was flowed through a half inch diameter quartz tube at 1 Torr that was maintained by flowing hydrogen or the gas mixture while monitoring the pressure with a 10 Torr and 1000 Torr MKS Baratron absolute pressure gauge. The tube was fitted with an Ophos coaxial microwave cavity (Evenson cavity). The microwave generator shown in Figure 1 was an Ophos model MPG-4M generator (Frequency: 2450 MHz). The input power to the plasma was set at 85 watts. The EUV spectrometer was a normal incidence monochromator. (See Section II A).

C. Gas temperature measurements on microwave discharge plasmas

In order to estimate the relative power output [19], the gas temperature of microwave plasmas of argon and xenon alone and each noble gas with 10% hydrogen was measured. The

experimental set up is described in Section II B. Each ultra-pure test gas or mixture was flowed through the half inch diameter quartz tube at 0.3 Torr maintained with a noble gas flow rate of 9.3 sccm or a noble gas flow rate of 8.3 sccm and a hydrogen flow rate of 1 sccm. The light emission was introduced into the normal incidence EUV spectrometer to determine the electron temperature as discussed in Section II E. Balmer α emission from the cell was also recorded with a high resolution visible spectrometer to determine the ion energy and density as discussed in Section II D.

With the input power to the plasma set at 40 watts, the temperature rise and fall was recorded using a K-type thermocouple ($\pm 0.1^\circ\text{C}$) housed in a stainless steel tube that was placed axially inside the center of the 10 cm^3 plasma volume of a quartz microwave cell as hydrogen flow supplied by the mass flow controller was turned on and off. The cell was operated under flow conditions with continuous pumping by the turbopump of the EUV spectrometer.

D. Balmer α line broadening recorded on microwave discharge plasmas

The method of Videnovic et al. [20] was used to calculate the energetic hydrogen atom densities and energies from the width of the 656.3 nm Balmer α line emitted from glow discharge and microwave plasmas. The full half-width $\Delta\lambda_G$ of each Gaussian results from the Doppler ($\Delta\lambda_D$) and instrumental ($\Delta\lambda_I$) half-widths:

$$\Delta\lambda_G = \sqrt{\Delta\lambda_D^2 + \Delta\lambda_I^2} \quad (4)$$

$\Delta\lambda_I$ in our experiments was 0.006 nm . The temperature was calculated from the Doppler half-width using the formula:

$$\Delta\lambda_D = 7.16 \times 10^{-7} \lambda_0 \left(\frac{T}{\mu} \right)^{1/2} \quad (\text{nm}) \quad (5)$$

where λ_0 is the line wavelength in nm, T is the temperature in K ($1\text{ eV} = 11,605\text{ K}$), and μ is the molecular weight ($=1$ for hydrogen). In each case, the average Doppler half-width that was not appreciably changed with pressure varied by $\pm 5\%$ corresponding to an error in the energy of $\pm 5\%$. The corresponding number densities for noble gas-hydrogen mixtures varied by $\pm 20\%$ depending on the pressure.

The width of the 656.3 nm Balmer α line was measured on light emitted from microwave discharges of pure hydrogen alone and a mixture of 10% hydrogen and argon or xenon. The experimental set is described in Section II C. The plasma emission was fiber-optically coupled through a 220F matching fiber adapter positioned 2 cm from the cell wall to a high resolution visible spectrometer with a resolution of $\pm 0.006\text{ nm}$ over the spectral range 190 - 860 nm. The spectrometer was a Jobin Yvon Horiba 1250 M with 2400 groves/mm ion-

etched holographic diffraction grating. The entrance and exit slits were set to $20\ \mu\text{m}$. The spectrometer was scanned between $655.5 - 657\ \text{nm}$ using a $0.005\ \text{nm}$ step size. The signal was recorded by a PMT with a stand alone high voltage power supply (950 V) and an acquisition controller. The data was obtained in a single accumulation with a 1 second integration time.

E. T_e measurements of microwave discharge plasmas

The most commonly used spectroscopic diagnostic method to determine the electron temperature T_e of laboratory plasmas is based on determining the relative intensities of two spectral lines as described by Griem [21]. It may be shown that for two emission lines at wavelengths λ_A and λ_B

$$\frac{I_A}{I_B} = \frac{(\sigma g_2 A_{21})_A}{(\sigma g_2 A_{21})_B} e^{\frac{(E_{2A} - E_{2B})}{kT_e}} \quad (6)$$

where I_A and I_B are the intensities measured at λ_A and λ_B , and $\sigma \propto n^4$ for atomic hydrogen. The frequency ν , the transition probability A , the degeneracy g , and the upper level E are known constants from which T_e was determined.

T_e was measured on microwave plasmas of argon alone and argon-hydrogen mixture (90/10%) from the ratio of the intensity of the Ar 104.8 nm (upper quantum level $n = 3$) line to that of the Ar 420.06 nm ($n = 4$) line. T_e was also measured by the same method on microwave plasmas of pure hydrogen alone, xenon alone, and a mixture of 10% hydrogen and xenon using the ratio of the intensities of two hydrogen or xenon lines in two quantum states.

The experimental set up comprising a microwave discharge gas cell light source and an EUV spectrometer which was differentially pumped is shown in Figure 1. In each case, the microwave plasma cell was run under the conditions given in Section II C. The EUV-UV-VIS spectrum ($20 - 560\ \text{nm}$) of the cell emission was recorded with the Spectrometer described in Section II A. The spectra were repeated five times per experiment and were found to be reproducible within less than $\pm 5\%$.

III. RESULTS AND DISCUSSION

A. Argon-hydrogen microwave emission spectrum

The EUV spectrum ($90 - 165\ \text{nm}$) of the cell emission from the hydrogen plasma (dotted line) and the hydrogen plasma to which 5% argon was added (solid line) is shown in Figure 2. Upon the addition of 5% argon, the hydrogen Lyman α emission intensity was

observed to increase by about an order of magnitude. Essentially no effect was observed for the addition of 5% xenon to the hydrogen plasma. This result indicates that one or more temperatures may be elevated with the addition of argon to a hydrogen plasma.

B. Gas temperature measurements

Due to the high mobility of free electrons, the heat loss of the microwave cell was determined by slow losses from the cell walls with a fast power transfer from the plasma to the wall such that the plasma was isothermal and the inner wall temperature and the plasma gas temperatures were equivalent as discussed by Chen et al. [19]. Since the microwave discharge cell, power input to the plasma, and discharge conditions remained identical between the argon and xenon experiments, the gas temperature may be used to determine the power balance as shown by Chen et al [19].

Essentially no increase in gas temperature was observed with the addition of hydrogen to xenon control as shown in Figure 3. In contrast, With a microwave input power of 40 W, the gas temperature of an argon plasma increased from 400°C to over 750°C with the addition of 3% flowing hydrogen as shown in Figure 4. A conservative estimate of the total output power was determined by taking the ratio of the maximum ΔT , the cell temperature increase above the ambient temperature of $25.0 \pm 0.1^\circ\text{C}$, of the argon-hydrogen plasma compared to that of the argon alone, xenon alone, and xenon-hydrogen plasmas, 1.9, multiplied by the common input. Thus, with a microwave input power of 40 W, the thermal output power was estimated to be 76 W. Since the hydrogen flow rate was 1 sccm, an estimate of the corresponding energy balance was over $-1 \times 10^4 \text{ kJ/mole } H_2$ compared to the enthalpy of combustion of hydrogen of $-241.8 \text{ kJ/mole } H_2$.

C. Line broadening and T_e measurements

The 656.3 nm Balmer α line width recorded with a high resolution ($\pm 0.006 \text{ nm}$) visible spectrometer on microwave discharge plasmas of hydrogen compared with each of xenon-hydrogen (90/10%) and argon-hydrogen (90/10%) are shown in Figures 5 and 6, respectively. The energetic hydrogen atom densities and energies of plasmas of hydrogen alone and the noble gas-hydrogen mixtures were calculated using the method of Videnovic et al. [20]. It was found that the microwave argon-hydrogen plasma showed extraordinary broadening corresponding to an average hydrogen atom temperature of 110 - 130 eV and an atom density of $3.5 \times 10^{14} \text{ atoms/cm}^3$. Whereas, xenon-hydrogen and pure hydrogen showed no excessive broadening corresponding to an average hydrogen atom temperature of 3 - 4 eV for both and

an atom density of only $3 \times 10^{13} \text{ atoms/cm}^3$ and $7 \times 10^{13} \text{ atoms/cm}^3$, respectively, even though 10 times more hydrogen was present for pure hydrogen.

These studies demonstrate excessive line broadening in the absence of an observable effect attributable to an electric field since the hydrogen emission shows no broadening. Since no electric field was present in the microwave plasma, the results can not be explained by Stark broadening or acceleration of charged species due to high fields of over 10 kV/cm as proposed by Videnovic et al. [20] to explain excessive broadening observed in glow discharges. Excessive line broadening was only observed in the cases where Ar^+ was present which could provide a net enthalpy of reaction of an integer multiple of the potential energy of atomic hydrogen. Whereas, plasmas of chemically similar xenon control that do not provide gaseous atoms or ions that have electron ionization energies which are a multiple of 27.2 eV showed no effect with the addition of 10% hydrogen. These results support the rt-plasma mechanism.

Rt-plasmas formed with hydrogen-potassium mixtures have been reported previously [6, 14] wherein the plasma decayed with a two second half-life when the electric field was set to zero. This was the thermal decay time of the filament which dissociated molecular hydrogen to atomic hydrogen. This experiment showed that hydrogen line emission was occurring even though the voltage between the heater wires was set to and measured to be zero, and it indicated that the emission was due to a reaction of potassium atoms with atomic hydrogen. Potassium atoms ionize at an integer multiple of the potential energy of atomic hydrogen, $m \cdot 27.2 \text{ eV}$. The enthalpy of ionization of K to K^{3+} has a net enthalpy of reaction of 81.7426 eV , which is equivalent to $m = 3$. K^{3+} and the formation of the corresponding hydride were detected by EUV spectroscopy recorded on an rt-plasma [9].

Similarly, to the ion measurement, the average electron temperature T_e for the argon-hydrogen plasma was high, $11,600 \pm 5\% \text{ K}$, compared to $4800 \pm 5\% \text{ K}$, $4980 \pm 5\% \text{ K}$, and $6500 \pm 5\% \text{ K}$ for argon alone, xenon alone, and xenon-hydrogen plasmas, respectively.

IV. CONCLUSION

Upon the addition of 5% argon to a hydrogen plasma, the Lyman alpha emission was observed to increase by about an order of magnitude which suggested that one or more of the plasma temperatures may be elevated; whereas, no effect was observed with xenon. Line broadening of the hydrogen Balmer lines provides a sensitive measure of the number and energy of excited hydrogen atoms in a plasma. The width of the 656.3 nm Balmer α line emitted from microwave discharge plasmas having atomized hydrogen from pure hydrogen alone and a mixture of 10% hydrogen and argon or xenon was measured with a high resolution ($\pm 0.006 \text{ nm}$) visible spectrometer. The energetic hydrogen atom density and energies were

determined from the broadening, and it was found that argon-hydrogen showed significant broadening corresponding to an average hydrogen atom temperature of 110 - 130 eV; whereas, pure hydrogen and xenon-hydrogen showed no excessive broadening corresponding to an average hydrogen atom temperature of ≈ 3 eV. Similarly, the average electron temperature T_e for the argon-hydrogen was high, $11,600 \pm 5\%$ K, compared to $4800 \pm 5\%$ K, $4980 \pm 5\%$ K, and $6500 \pm 5\%$ K for argon alone, xenon alone, and xenon-hydrogen plasmas, respectively.

The gas temperature is a means to estimate the power output of the cell. With a microwave input power of 40 W, the gas temperature of an argon plasma increased from 400°C to over 750°C with the addition of 3% flowing hydrogen; whereas, the 400°C temperature of a xenon plasma run under identical conditions was essentially unchanged with the addition of hydrogen. The thermal output power was estimated to be 76 W. Since the hydrogen flow rate was 1 sccm, an estimate of the corresponding energy balance was over -1×10^4 kJ/mole H_2 compared to the enthalpy of combustion of hydrogen of -241.8 kJ/mole H_2 .

The observed excessive line broadening, elevated T_e , and elevated plasma gas temperature were only observed for the case where Ar^+ , an ion which provides a net enthalpy of reaction of a multiple of the potential energy of the hydrogen atom, was present with atomic hydrogen. Nonequilibrium plasma conditions may explain the elevation of one temperature over another [22]; however, the elevation of all three temperatures indicates power dissipation in the plasma in addition to the microwave input. The source of additional power corresponding to the elevated temperatures may be an energetic reaction of atomic hydrogen caused by a resonance energy transfer between hydrogen atoms and Ar^+ .

REFERENCES

1. R. Mills, J. Dong, Y. Lu, "Observation of Extreme Ultraviolet Hydrogen Emission from Incandescently Heated Hydrogen Gas with Certain Catalysts", *Int. J. Hydrogen Energy*, Vol. 25, (2000), pp. 919-943.
2. R. Mills and M. Nansteel, P. Ray, "Argon-Hydrogen-Strontium Discharge Light Source", *IEEE Transactions on Plasma Science*, in press.
3. R. L. Mills, P. Ray, B. Dhandapani, M. Nansteel, X. Chen, J. He, "New Power Source from Fractional Rydberg States of Atomic Hydrogen", *Chem. Phys. Letts.*, submitted.
4. R. Mills, P. Ray, "Spectral Emission of Fractional Quantum Energy Levels of Atomic Hydrogen from a Helium-Hydrogen Plasma and the Implications for Dark Matter", *Int. J. Hydrogen Energy*, Vol. 27 (3), (2002), pp. 301-322.
5. R. L. Mills, P. Ray, B. Dhandapani, J. He, "Spectroscopic Identification of Fractional

- Rydberg States of Atomic Hydrogen", J. of Phys. Chem., submitted.
6. H. Conrads, R. Mills, Th. Wrubel, "Emission in the Deep Vacuum Ultraviolet from an Incandescently Driven Plasma in a Potassium Carbonate Cell", Plasma Sources Science and Technology, submitted.
 7. R. Mills, P. Ray, "Vibrational Spectral Emission of Fractional-Principal-Quantum-Energy-Level Hydrogen Molecular Ion", Int. J. Hydrogen Energy, in press.
 8. R. Mills, "Spectroscopic Identification of a Novel Catalytic Reaction of Atomic Hydrogen and the Hydride Ion Product", Int. J. Hydrogen Energy, Vol. 26, No. 10, (2001), pp. 1041-1058.
 9. R. Mills, P. Ray, "Spectroscopic Identification of a Novel Catalytic Reaction of Potassium and Atomic Hydrogen and the Hydride Ion Product", Int. J. Hydrogen Energy, Vol. 27, No. 2, February, (2002), pp. 183-192.
 10. R. L. Mills, P. Ray, "Spectroscopic Identification of a Novel Catalytic Reaction of Rubidium Ion with Atomic Hydrogen and the Hydride Ion Product", Int. J. Hydrogen Energy, in press.
 11. R. L. Mills, P. Ray, "High Resolution Spectroscopic Observation of the Bound-Free Hyperfine Levels of a Novel Hydride Ion Corresponding to a Fractional Rydberg State of Atomic Hydrogen", Int. J. Hydrogen Energy, submitted.
 12. R. Mills, M. Nansteel, and Y. Lu, "Observation of Extreme Ultraviolet Hydrogen Emission from Incandescently Heated Hydrogen Gas with Strontium that Produced an Anomalous Optically Measured Power Balance", Int. J. Hydrogen Energy, Vol. 26, No. 4, (2001), pp. 309-326.
 13. R. L. Mills, P. Ray, B. Dhandapani, J. He, "Comparison of Excessive Balmer α Line Broadening of Glow Discharge and Microwave Hydrogen Plasmas with Certain Catalysts", Chem. Phys., submitted.
 14. R. Mills, T. Onuma, and Y. Lu, "Formation of a Hydrogen Plasma from an Incandescently Heated Hydrogen-Catalyst Gas Mixture with an Anomalous Afterglow Duration", Int. J. Hydrogen Energy, Vol. 26, No. 7, July, (2001), pp. 749-762.
 15. R. Mills, A. Voigt, P. Ray, M. Nanstell, "Measurement of Hydrogen Balmer Line Broadening and Thermal Power Balances of Noble Gas-Hydrogen Discharge Plasmas", Int. J. Hydrogen Energy, in press.
 16. R. Mills, N. Greenig, S. Hicks, "Optically Measured Power Balances of Anomalous Discharges of Mixtures of Argon, Hydrogen, and Potassium, Rubidium, Cesium, or Strontium Vapor", Int. J. Hydrogen Energy, in press.
 17. R. Mills, B. Dhandapani, M. Nansteel, J. He, T. Shannon, A. Echezuria, "Synthesis and Characterization of Novel Hydride Compounds", Int. J. of Hydrogen Energy, Vol. 26, No.

- 4, (2001), pp. 339-367.
18. David R. Linde, *CRC Handbook of Chemistry and Physics*, 79 th Edition, CRC Press, Boca Raton, Florida, (1998-9), p. 10-175 to p. 10-177.
 19. C. Chen, T. Wei, L. R. Collins, and J. Phillips, "Modeling the discharge region of a microwave generated hydrogen plasma", *J. Phys. D: Appl. Phys.*, Vol. 32, (1999), pp. 688-698.
 20. I. R. Videnovic, N. Konjevic, M. M. Kuraica, "Spectroscopic investigations of a cathode fall region of the Grimm-type glow discharge", *Spectrochimica Acta, Part B*, Vol. 51, (1996), pp. 1707-1731.
 21. H. R. Griem, *Principle of Plasma Spectroscopy*, Cambridge University Press, (1987).
 22. C. K. Chen, Microwave plasma processing of unique ceramic particulate materials, Ph. D. Thesis, The Pennsylvania State University, State College, PA, August, (2001). Chp. 3.

Figure Captions

Figure 1. The experimental set up comprising a microwave discharge gas cell light source and an EUV-UV-VIS spectrometer which was differentially pumped.

Figure 2. The EUV spectrum (90 – 165 nm) of the cell emission from the hydrogen plasma (dotted line) and the hydrogen plasma to which 5% argon was added (solid line).

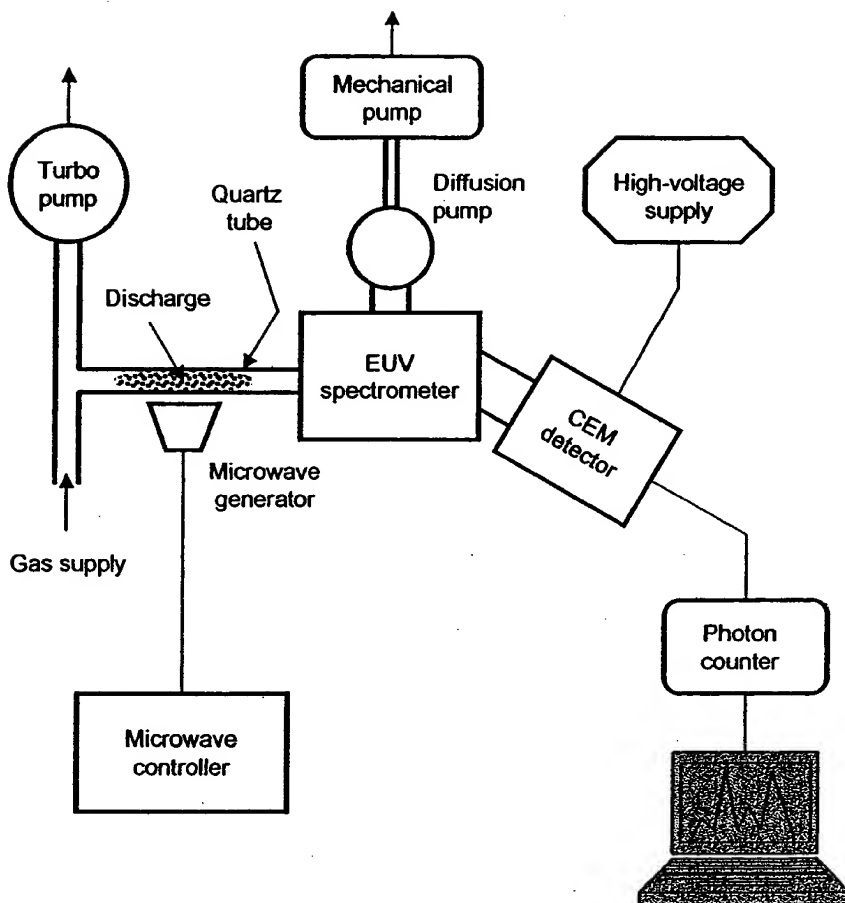
Figure 3. The plasma gas temperature rise as a function of time for xenon alone and the xenon-hydrogen mixture (90/10%) with the microwave input power set at 40 W as the hydrogen flow was turned on and off. The 400°C plasma gas temperature was essentially unchanged with the addition of hydrogen.

Figure 4. The plasma gas temperature rise as a function of time for argon alone and the argon-hydrogen mixture (90/10%) with the microwave input power set at 40 W as the hydrogen flow was turned on and off. The plasma gas temperature reproducibly increased from 400°C to over 750°C with the addition of 3% flowing hydrogen. The thermal output power of the argon-hydrogen plasma was estimated to be 76 W.

Figure 5. The 656.3 nm Balmer α line width recorded with a high resolution (± 0.006 nm) visible spectrometer on a xenon-hydrogen (90/10%) and a hydrogen microwave discharge plasma. No line excessive broadening was observed corresponding to an average hydrogen atom temperature of 3 – 4 eV.

Figure 6. The 656.3 nm Balmer α line width recorded with a high resolution (± 0.006 nm) visible spectrometer on a argon-hydrogen (90/10%) and a hydrogen microwave discharge plasma. Significant broadening was observed corresponding to an average hydrogen atom temperature of 110 - 130 eV.

Fig. 1



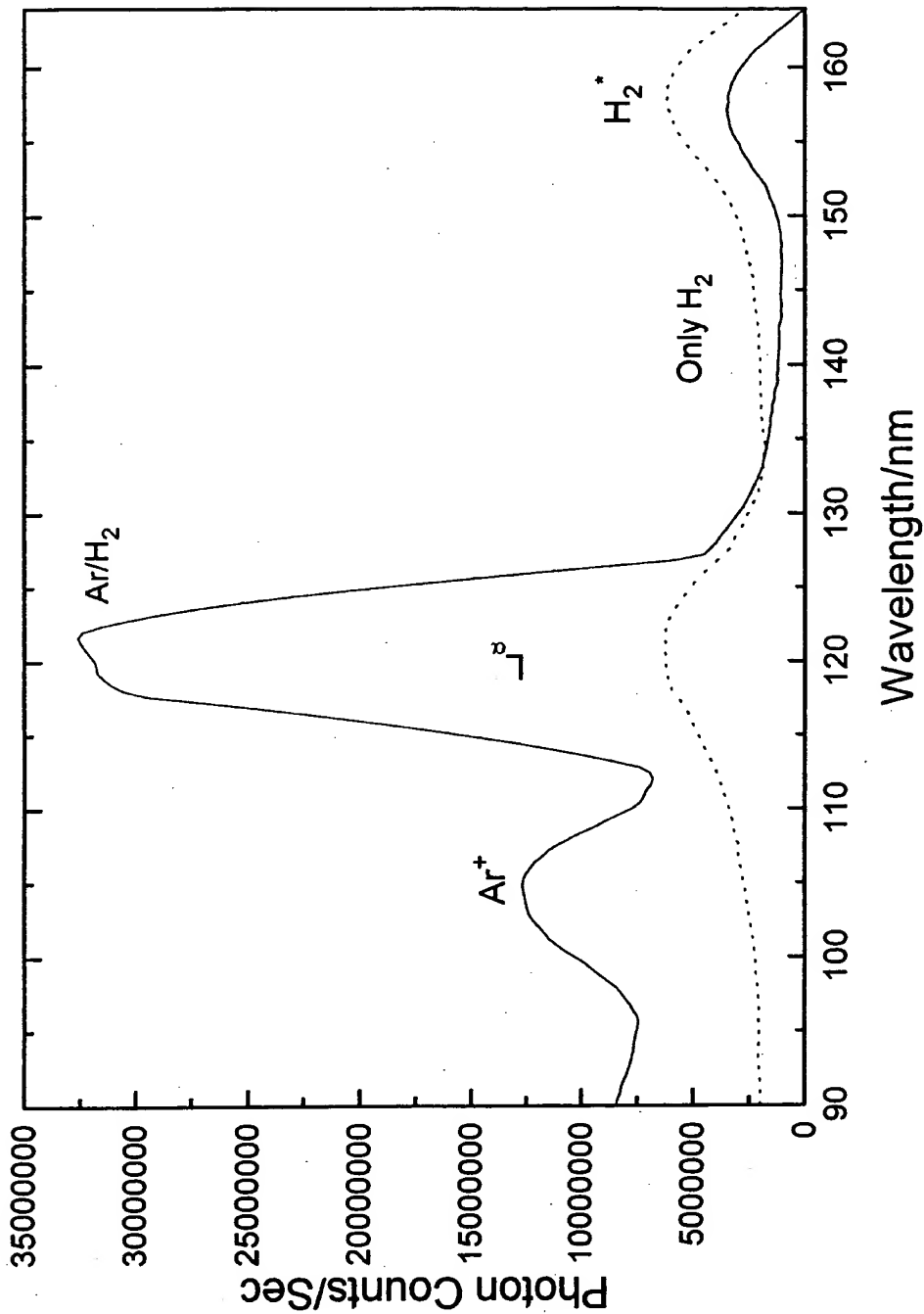


Fig. 2

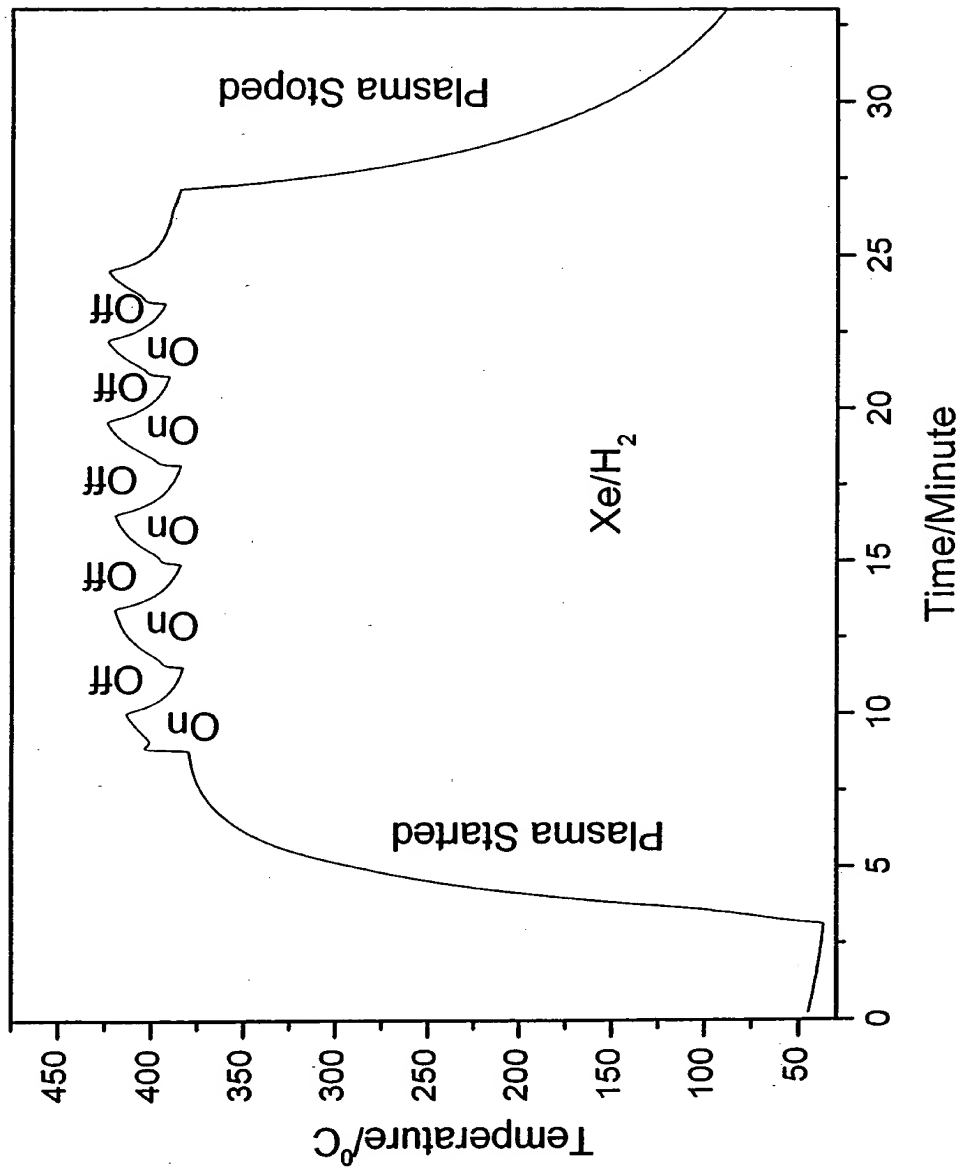


Fig. 3

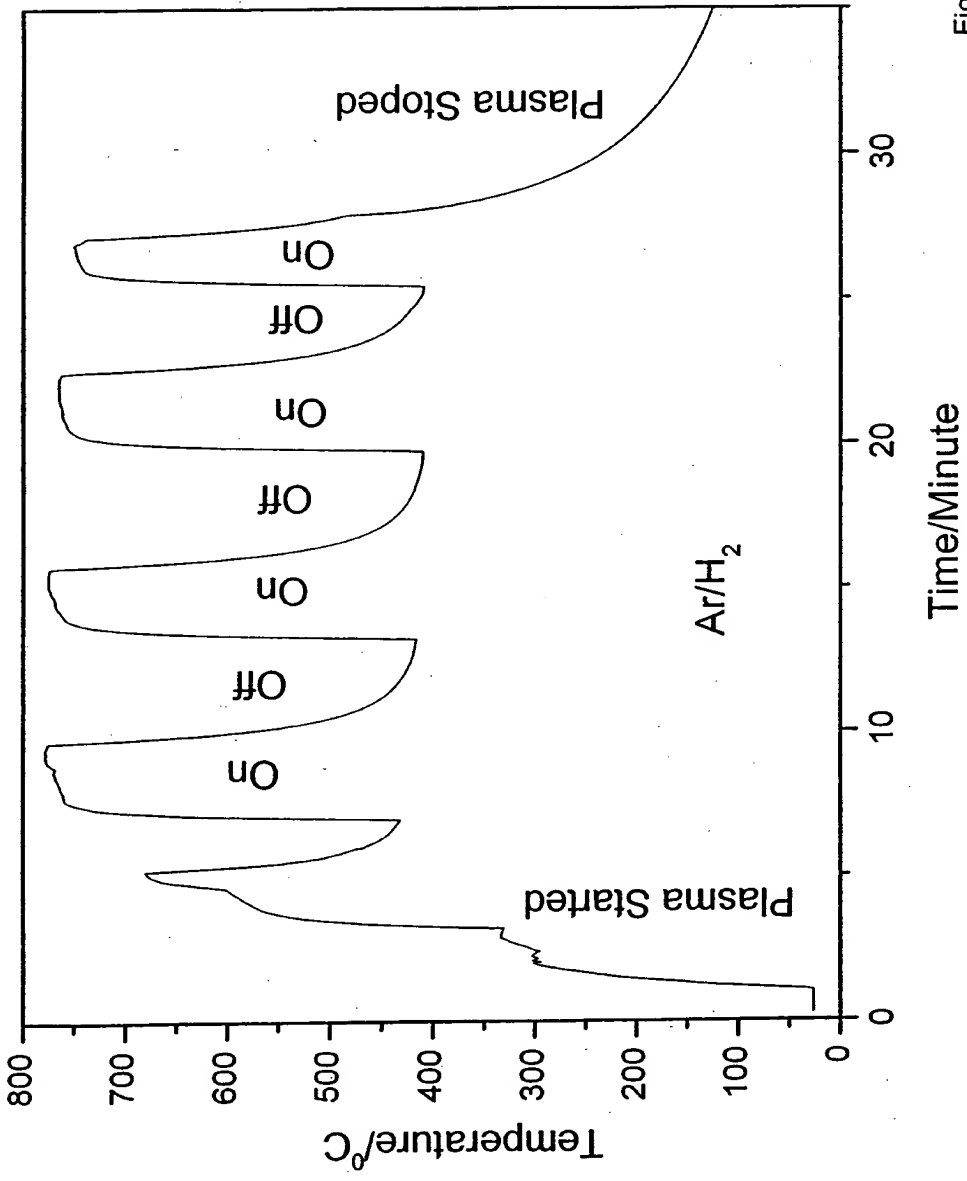


Fig. 4

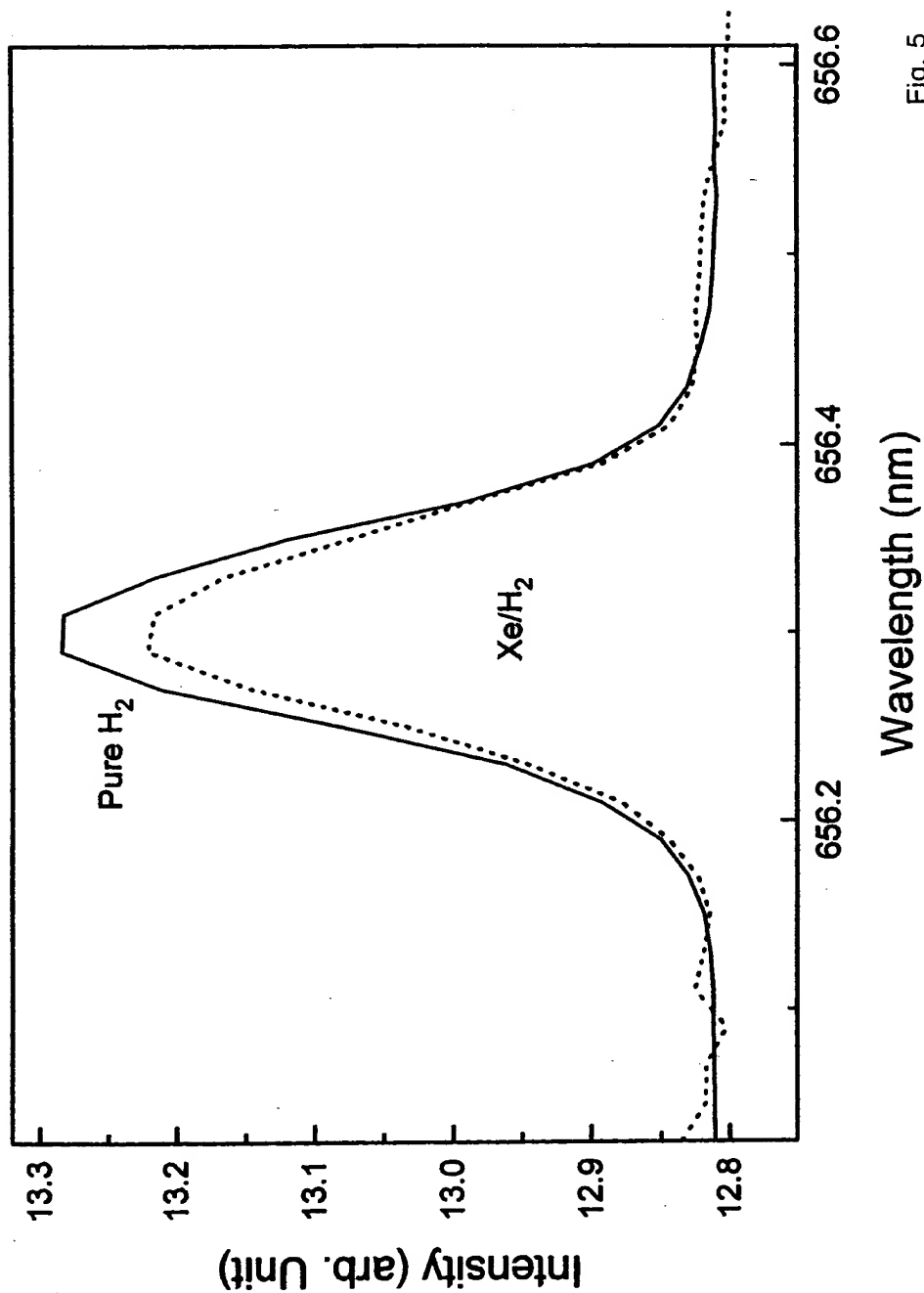


Fig. 5

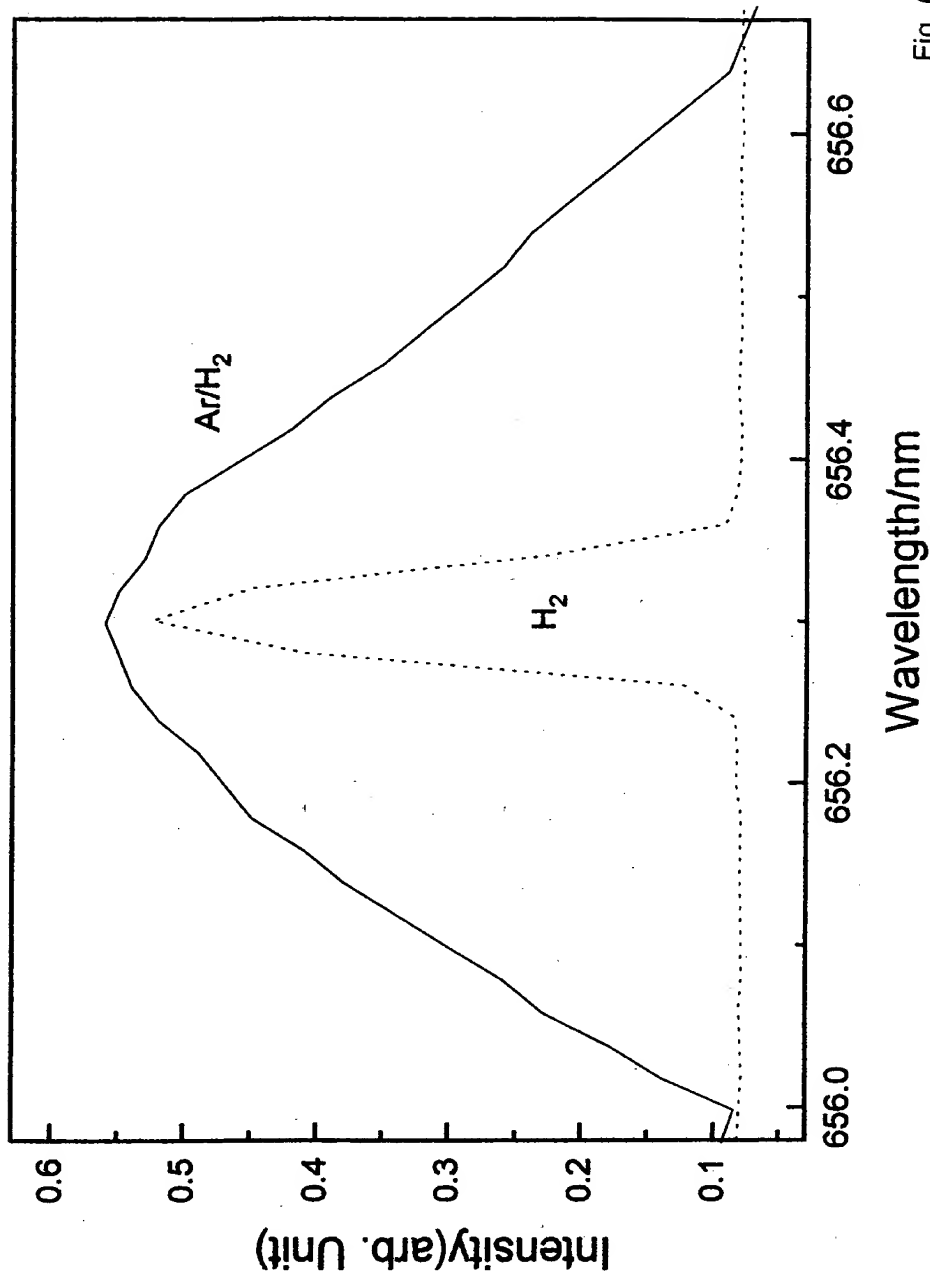


Fig. 6

THIS PAGE BLANK (USPTO)

THIS PAGE BLANK (USPTO)

High Resolution Spectroscopic Observation of the Bound-Free Hyperfine Levels of a Novel Hydride Ion Corresponding to a Fractional Rydberg State of Atomic Hydrogen

R. L. Mills, P. Ray

BlackLight Power, Inc., 493 Old Trenton Road, Cranbury, NJ 08512

From a solution of a Schrödinger-type wave equation with a nonradiative boundary condition based on Maxwell's equations, Mills solves the hydrogen atom, the hydride ion, and predicts corresponding species having fractional principal quantum numbers. Atomic hydrogen may undergo a catalytic reaction with certain atomized elements and ions which singly or multiply ionize at integer multiples of the potential energy of atomic hydrogen, $m \cdot 27.2 \text{ eV}$ wherein m is an integer. The reaction involves a nonradiative energy transfer to form a hydrogen atom $H(1/p)$ that is lower in energy than unreacted atomic hydrogen that corresponds to a fractional principal quantum number ($n = \frac{1}{p} = \frac{1}{\text{integer}}$ replaces the well known parameter $n = \text{integer}$ in the Rydberg equation for hydrogen excited states). The ionization of Rb^+ and an electron transfer between two K^+ ions (K^+/K^+) provide a reaction with a net enthalpy of 27.2 eV which serve as catalysts of atomic hydrogen to form $H(1/2)$. Intense extreme ultraviolet (EUV) emission was observed from incandescently heated atomic hydrogen and each of atomized potassium and rubidium ions that generated a plasma called a resonance transfer or rt-plasma at low temperatures (e.g. $\approx 10^3 \text{ K}$) and an extraordinary low field strength of about $1\text{--}2 \text{ V/cm}$. For further characterization, the width of the 6562 \AA Balmer α line was recorded. Significant line broadening of 17 and 9 eV was observed from a rt-plasma of hydrogen with K^+/K^+ and Rb^+ respectively. These results could not be explained by Stark or thermal broadening or electric field acceleration of charged species since the measured field of the incandescent heater was extremely weak, 1 V/cm , corresponding to a broadening of much less than 1 eV . Rather the source of the excessive line broadening is consistent with that of the observed EUV emission, an energetic reaction caused by a resonance energy transfer between hydrogen atoms and K^+/K^+ or Rb^+ . The catalyst product $H(1/2)$ was predicted to be a highly reactive intermediate which further reacts to form a novel hydride ion $H^-(1/2)$. This hydride ion with a predicted binding energy of 3.0468 eV was observed by high resolution visible spectroscopy as a broad peak at 4070.0 \AA with a FWHM of 1.4 \AA . From the electron g factor, bound-free hyperfine structure lines of $H^-(1/2)$ were predicted with energies E_{HF} given by $E_{HF} = j^2 3.0056 \times 10^{-5} + 3.0575 \text{ eV}$ (j is an integer) as an inverse Rydberg-type series that converges at increasing wavelengths and terminates at 3.0575 eV —the hydride spin-pairing energy plus the binding energy. The high resolution visible plasma emission spectra in the region of 4000 \AA to 4060 \AA matched the predicted emission lines for $j = 1$ to $j = 37$.

I. INTRODUCTION

A. Background

J. J. Balmer showed in 1885 that the frequencies for some of the lines observed in the emission spectrum of atomic hydrogen could be expressed with a completely empirical relationship. This approach was later extended by J. R. Rydberg, who showed that all of the spectral lines of atomic hydrogen were given by the equation:

$$\bar{\nu} = R \left(\frac{1}{n_f^2} - \frac{1}{n_i^2} \right) \quad (1)$$

where $R = 109,677 \text{ cm}^{-1}$, $n_f = 1, 2, 3, \dots$, $n_i = 2, 3, 4, \dots$, and $n_i > n_f$.

Niels Bohr, in 1913, developed a theory for atomic hydrogen that gave the energy levels in agreement with Rydberg's equation. An identical equation, based on a totally different theory for the hydrogen atom, was developed by E. Schrödinger, and independently by W. Heisenberg, in 1926.

$$E_n = -\frac{e^2}{n^2 8\pi\epsilon_0 a_H} = -\frac{13.598 \text{ eV}}{n^2} \quad (2a)$$

$$n = 1, 2, 3, \dots \quad (2b)$$

where a_H is the Bohr radius for the hydrogen atom (52.947 pm), e is the magnitude of the charge of the electron, and ϵ_0 is the vacuum permittivity.

The excited energy states of atomic hydrogen are given by Eq. (2a) for $n > 1$ in Eq. (2b). The $n=1$ state is the "ground" state for "pure" photon transitions (the $n=1$ state can absorb a photon and go to an excited electronic state, but it cannot release a photon and go to a lower-energy electronic state). However, an electron transition from the ground state to a lower-energy state may be possible by a nonradiative energy transfer such as multipole coupling or a resonant collision mechanism. Processes such as hydrogen molecular bond formation that occur without photons and that require collisions are common [1]. Also, some commercial phosphors are based on resonant nonradiative energy transfer involving multipole coupling [2].

We propose that atomic hydrogen may undergo a catalytic reaction with certain atomized elements and ions which singly or multiply ionize

at integer multiples of the potential energy of atomic hydrogen, $m \cdot 27.2 \text{ eV}$ wherein m is an integer. The theory and supporting data was given previously [3-37]. The reaction involves a nonradiative energy transfer to form a hydrogen atom that is lower in energy than unreacted atomic hydrogen called a *hydrino* that corresponds to a fractional principal quantum number. That is

$$n = \frac{1}{2}, \frac{1}{3}, \frac{1}{4}, \dots, \frac{1}{p}; \quad p \text{ is an integer} \quad (2c)$$

replaces the well known parameter $n = \text{integer}$ in the Rydberg equation for hydrogen excited states. The $n=1$ state of hydrogen and the $n = \frac{1}{\text{integer}}$

states of hydrogen are nonradiative, but a transition between two nonradiative states is possible via a nonradiative energy transfer, say $n=1$ to $n=1/2$. In these cases, during the transition the electron couples to another electron transition, electron transfer reaction, or inelastic scattering reaction which can absorb the exact amount of energy that must be removed from the hydrogen atom to cause the transition. Thus, a catalyst provides a net positive enthalpy of reaction of $m \cdot 27.2 \text{ eV}$ (i.e. it absorbs $m \cdot 27.2 \text{ eV}$ where m is an integer). Certain atoms or ions serve as catalysts which resonantly accept the nonradiative energy transfer from hydrogen atoms and release the energy to the surroundings to affect electronic transitions to fractional quantum energy levels. As a consequence of the nonradiative energy transfer, the hydrogen atom becomes unstable and emits further energy until it achieves a lower-energy nonradiative state having a principal energy level given by Eqs. (2a) and (2c).

B. rt-plasma

It was reported previously that a new plasma source has been developed that operates by incandescently heating a hydrogen dissociator to provide atomic hydrogen and heats a catalyst such that it becomes gaseous and reacts with the atomic hydrogen to produce a rt-plasma. It was extraordinary, that intense EUV emission was observed by Mills et al. [11, 13-15, 23-24, 26-27] at low temperatures (e.g. $\approx 10^3 \text{ K}$) from atomic hydrogen and certain atomized elements or certain gaseous

ions which singly or multiply ionize at integer multiples of the potential energy of atomic hydrogen, 27.2 eV that comprise catalysts. The only pure elements that were observed to emit EUV were those wherein the ionization of t electrons from an atom to a continuum energy level is such that the sum of the ionization energies of the t electrons is approximately

$$m \cdot 27.2\text{ eV} \quad (3)$$

where t and m are each an integer. Alternatively, a catalyst depended on the transfer of t electrons between participating ions such that the transfer of t electrons from one ion to another ion provides a net enthalpy of reaction whereby the sum of the ionization energy of the electron donating ion minus the ionization energy of the electron accepting ion equals approximately $m \cdot 27.2\text{ eV}$.

Since Ar^+ and strontium each ionize at an integer multiple of the potential energy of atomic hydrogen, a discharge with one or more of these species present with hydrogen was anticipated to form a rt-plasma wherein the plasma forms by a resonance transfer mechanism involving the species providing a net enthalpy of a multiple of 27.2 eV and atomic hydrogen.

Mills and Nansteel [11, 16-17, 23] have reported that strontium atoms each ionize at an integer multiple of the potential energy of atomic hydrogen and caused emission. (The enthalpy of ionization of Sr to Sr^{5+} has a net enthalpy of reaction of 188.2 eV , which is equivalent to $m=7$.) The emission intensity of the plasma generated by atomic strontium increased significantly with the introduction of argon gas only when Ar^+ emission was observed. Whereas, no emission was observed when chemically similar atoms that do not ionize at integer multiples of the potential energy of atomic hydrogen (sodium, magnesium, or barium) replaced strontium with hydrogen, hydrogen-argon mixtures, or strontium alone.

Mills and Nanstell [16-17, 23] measured the power balance of a gas cell having vaporized strontium and atomized hydrogen from pure hydrogen or argon-hydrogen mixture (77/23%) by integrating the total light output corrected for spectrometer system response and energy over the visible range. Hydrogen control cell experiments were identical except that sodium, magnesium, or barium replaced strontium. In the case of hydrogen-sodium, hydrogen-magnesium, and hydrogen-barium

mixtures, 4000, 7000, and 6500 times the power of the hydrogen-strontium mixture was required, respectively, in order to achieve that same optically measured light output power. With the addition of argon to the hydrogen-strontium plasma, the power required to achieve that same optically measured light output power was reduced by a factor of about two. The power required to maintain a plasma of equivalent optical brightness with strontium atoms present was 8600 and 6300 times less than that required for argon-hydrogen and argon control, respectively. A plasma formed at a cell voltage of about 250 V for hydrogen alone and sodium-hydrogen mixtures, 140-150 V for hydrogen-magnesium and hydrogen-barium mixtures, 224 V for an argon-hydrogen mixture, and 190 V for argon alone; whereas, a plasma formed for hydrogen-strontium mixtures and argon-hydrogen-strontium mixtures at extremely low voltages of about 2 V and 6.6 V, respectively.

It was reported [15] that characteristic emission was observed from a continuum state of Ar^{2+} which confirmed the resonant nonradiative energy transfer of 27.2 eV from atomic hydrogen Ar^+ . The transfer of 27.2 eV from atomic hydrogen to Ar^+ in the presence of a electric weak field resulted in its excitation to a continuum state. Then, the energy for the transition from essentially the Ar^{2+} state to the lowest state of Ar^+ was predicted to give a broad continuum radiation in the region of 456 Å. This broad continuum emission was observed. This emission was dramatically different from that given by an argon microwave plasma wherein the entire Rydberg series of lines of Ar^+ was observed with a discontinuity of the series at the limit of the ionization energy of Ar^+ to Ar^{2+} . The observed Ar^+ continuum in the region of 456 Å confirmed the rt-plasma mechanism of the excessively bright, extraordinarily low voltage discharge. The product hydride ion with Ar^+ as a reactant was predicted to have a binding energy of 3.05 eV and was observed spectroscopically at 4070 Å [11, 15].

A number of independent experimental observations lead to the conclusion that atomic hydrogen can exist in fractional quantum states that are at lower energies than the traditional "ground" ($n=1$) state. Prior related studies that support the possibility of a novel reaction of atomic hydrogen which produces a chemically generated or assisted plasma (rt-plasma) and produces novel hydride compounds include extreme

ultraviolet (EUV) spectroscopy [8-11, 13-17, 19-20, 23-25], characteristic emission from catalysis and the hydride ion products [11-15], lower-energy hydrogen emission [6, 8, 9-10, 19], plasma formation [11, 13-15, 23-24, 26-27], Balmer α line broadening [9, 11, 16-17, 19-21], elevated electron temperature [9, 20], anomalous plasma afterglow duration [26-27], power generation [9, 11, 16-19, 21-23, 34], and analysis of chemical compounds [28-34]. Furthermore, mobility and spectroscopy data of individual electrons in liquid helium shows direct experimental confirmation that electrons may have fractional principal quantum energy levels [7].

C. Catalysts

a. Potassium Ions

Potassium ions can provide a net enthalpy of a multiple of that of the potential energy of the hydrogen atom. The second ionization energy of potassium is 31.63 eV; and K^+ releases 4.34 eV when it is reduced to K . The combination of reactions $K^+ \rightarrow K^{2+}$ and $K^+ \rightarrow K$, then, has a net enthalpy of reaction of 27.28 eV, which is equivalent to $m=1$ in Eq. (3).

$$27.28 \text{ eV} + K^+ + K^+ + H\left[\frac{a_H}{p}\right] \rightarrow K + K^{2+} + H\left[\frac{a_H}{(p+1)}\right] + [(p+1)^2 - p^2] \times 13.6 \text{ eV} \quad (4)$$



The overall reaction is

$$H\left[\frac{a_H}{p}\right] \rightarrow H\left[\frac{a_H}{(p+1)}\right] + [(p+1)^2 - p^2] \times 13.6 \text{ eV} \quad (6)$$

Alkali metal nitrates are extraordinarily volatile and can be distilled at 350-500 °C [38]. Gaseous potassium ions were provided by heating KNO_3 .

b. Potassium atom

An atomic catalytic system involves potassium atoms. The first, second, and third ionization energies of potassium are 4.34066 eV, 31.63 eV,

45.806 eV, respectively [39]. The triple ionization ($t=3$) reaction of K to K^{3+} , then, has a net enthalpy of reaction of 81.7766 eV, which is equivalent to $m=3$ in Eq. (3).

$$81.7766 \text{ eV} + K(m) + H\left[\frac{a_H}{p}\right] \rightarrow K^{3+} + 3e^- + H\left[\frac{a_H}{(p+3)}\right] + [(p+3)^2 - p^2]X13.6 \text{ eV} \quad (7)$$

$$K^{3+} + 3e^- \rightarrow K(m) + 81.7766 \text{ eV} \quad (8)$$

And, the overall reaction is

$$H\left[\frac{a_H}{p}\right] \rightarrow H\left[\frac{a_H}{(p+3)}\right] + [(p+3)^2 - p^2]X13.6 \text{ eV} \quad (9)$$

Vaporized atomic potassium was formed by hydrogen reduction and thermal decomposition of KNO_3 .

c. Rubidium ion

Rubidium ions can also provide a net enthalpy of a multiple of that of the potential energy of the hydrogen atom. The second ionization energy of rubidium is 27.28 eV. The reaction Rb^+ to Rb^{2+} has a net enthalpy of reaction of 27.28 eV, which is equivalent to $m=1$ in Eq. (3).

$$27.28 \text{ eV} + Rb^+ + H\left[\frac{a_H}{p}\right] \rightarrow Rb^{2+} + e^- + H\left[\frac{a_H}{(p+1)}\right] + [(p+1)^2 - p^2]X13.6 \text{ eV} \quad (10)$$

$$Rb^{2+} + e^- \rightarrow Rb^+ + 27.28 \text{ eV} \quad (11)$$

The overall reaction is

$$H\left[\frac{a_H}{p}\right] \rightarrow H\left[\frac{a_H}{(p+1)}\right] + [(p+1)^2 - p^2]X13.6 \text{ eV} \quad (12)$$

$RbNO_3$ was the favored candidate for providing gaseous Rb^+ ions due to its volatility [38].

D. Classical Quantum Theory of the Atom Based on Maxwell's Equations Predicts Hyperfine Levels of Novel Hydride Ions

a. One Electron Atoms

A theory of classical quantum mechanics (CQM), derived from first principles, that successfully applies physical laws on all scales was given previously [3-7]. One-electron atoms include the hydrogen atom, He^+ , Li^{2+} , Be^{3+} , and so on. The mass-energy and angular momentum of the electron are constant; this requires that the equation of motion of the electron be temporally and spatially harmonic. Thus, the classical wave equation applies and

$$\left[\nabla^2 - \frac{1}{v^2} \frac{\partial^2}{\partial t^2} \right] \rho(r, \theta, \phi, t) = 0 \quad (13)$$

where $\rho(r, \theta, \phi, t)$ is the time dependent charge density function of the electron in time and space. In general, the wave equation has an infinite number of solutions. To arrive at the solution which represents the electron, a suitable boundary condition must be imposed. It is well known from experiments that each single atomic electron of a given isotope radiates to the same stable state. Thus, the physical boundary condition of nonradiation of the bound electron was imposed on the solution of the wave equation for the time dependent charge density function of the electron [3, 5, 7]. The condition for radiation by a moving point charge given by Haus [40] is that its spacetime Fourier transform does possess components that are synchronous with waves traveling at the speed of light. Conversely, it is proposed that the condition for nonradiation by an ensemble of moving point charges that comprises a current density function is

For non-radiative states, the current-density function must NOT possess spacetime Fourier components that are synchronous with waves traveling at the speed of light.

The time, radial, and angular solutions of the wave equation are separable. The motion is time harmonic with frequency ω_n . A constant angular function is a solution to the wave equation. The solution for the

radial function which satisfies the boundary condition is a radial delta function

$$f(r) = \frac{1}{r^2} \delta(r - r_n) \quad (14)$$

which defines a constant charge function on a spherical shell where $r_n = nr_1$. Given time harmonic motion and a radial delta function, the relationship between an allowed radius and the electron wavelength is given by

$$2\pi r_n = \lambda_n \quad (15)$$

Using the observed de Broglie relationship for the electron mass where the coordinates are spherical,

$$\lambda_n = \frac{h}{p_n} = \frac{h}{m_e v_n} \quad (16)$$

and the magnitude of the velocity for *every* point on the spherical shell is

$$v_n = \frac{\hbar}{m_e r_n} \quad (17)$$

The sum of the L_i , the magnitude of the angular momentum of each infinitesimal point of the shell of mass m_i , must be constant. The constant is \hbar .

$$\sum |L_i| = \sum |\mathbf{r} \times m_i \mathbf{v}| = m_e r_n \frac{\hbar}{m_e r_n} = \hbar \quad (18)$$

Thus, an electron is a spinning, two-dimensional spherical surface, called an *electron orbitsphere*, that can exist in a bound state at only specified distances from the nucleus as shown in Figure 1¹. The corresponding current function shown in Figure 2 which gives rise to the phenomenon of *spin* is derived in the Spin Function section of Ref. 3.

Nonconstant functions are also solutions for the angular functions. To be a harmonic solution of the wave equation in spherical coordinates,

¹ Mobility measurements and spectroscopy directly show that electrons may be trapped in superfluid helium as autonomous electron bubbles interloped between helium atoms that have been excluded from the space occupied by the bubble. Electrons bubbles in superfluid helium reveal that the electron is real and that a physical interpretation of the wavefunction is necessary. The electron orbitsphere representation matches the data identically and is also in agreement with scattering experiments, another direct determination of the nature of the electron [7].

these angular functions must be spherical harmonic functions. A zero of the spacetime Fourier transform of the product function of two spherical harmonic angular functions, a time harmonic function, and an unknown radial function is sought. The solution for the radial function which satisfies the boundary condition is also a delta function given by Eq. (14). Thus, bound electrons are described by a charge-density (mass-density) function which is the product of a radial delta function, two angular functions (spherical harmonic functions), and a time harmonic function.

$$\rho(r, \theta, \phi, t) = f(r)A(\theta, \phi, t) = \frac{1}{r^2} \delta(r - r_n)A(\theta, \phi, t); \quad A(\theta, \phi, t) = Y(\theta, \phi)k(t) \quad (19)$$

In these cases, the spherical harmonic functions correspond to a traveling charge density wave confined to the spherical shell which gives rise to the phenomenon of orbital angular momentum. The orbital functions which modulate the constant "spin" function shown graphically in Figure 3 are given in the "Angular Functions" section of Ref. 3 and 5.

b. Spin Function

The orbitsphere spin function comprises a constant charge density function with moving charge confined to a two-dimensional spherical shell. The current pattern of the orbitsphere spin function comprises an infinite series of correlated orthogonal great circle current loops wherein each point moves time harmonically with angular velocity

$$\omega_n = \frac{\hbar}{m_e r_n^2} \quad (20)$$

The current pattern is generated over the surface by a series of nested rotations of two orthogonal great circle current loops where the coordinate axes rotate with the two orthogonal great circles. Half of the pattern is generated as the z-axis rotates to the negative z-axis during a 1st set of nested rotations. The mirror image, second half of the pattern is generated as the z-axis rotates back to its original direction during a 2nd set of nested rotations.

Points on Great Circle Current Loop One:

$$\begin{bmatrix} x_1 \\ y_1 \\ z_1 \end{bmatrix} = \begin{bmatrix} \cos(\Delta\alpha) & -\sin^2(\Delta\alpha) & -\sin(\Delta\alpha)\cos(\Delta\alpha) \\ 0 & \cos(\Delta\alpha) & -\sin(\Delta\alpha) \\ \sin(\Delta\alpha) & \cos(\Delta\alpha)\sin(\Delta\alpha) & \cos^2(\Delta\alpha) \end{bmatrix} \begin{bmatrix} x_1' \\ y_1' \\ z_1' \end{bmatrix} \quad (21)$$

and $\Delta\alpha' = -\Delta\alpha$ replaces $\Delta\alpha$ for $\sum_{n=1}^{\frac{\sqrt{2}\pi}{\Delta\alpha}} \Delta\alpha = \sqrt{2}\pi$; $\sum_{n=1}^{\frac{\sqrt{2}\pi}{|\Delta\alpha'|}} |\Delta\alpha'| = \sqrt{2}\pi$

Points on Great Circle Current Loop Two:

$$\begin{bmatrix} x_2 \\ y_2 \\ z_2 \end{bmatrix} = \begin{bmatrix} \cos(\Delta\alpha) & -\sin^2(\Delta\alpha) & -\sin(\Delta\alpha)\cos(\Delta\alpha) \\ 0 & \cos(\Delta\alpha) & -\sin(\Delta\alpha) \\ \sin(\Delta\alpha) & \cos(\Delta\alpha)\sin(\Delta\alpha) & \cos^2(\Delta\alpha) \end{bmatrix} \begin{bmatrix} x_2' \\ y_2' \\ z_2' \end{bmatrix} \quad (22)$$

and $\Delta\alpha' = -\Delta\alpha$ replaces $\Delta\alpha$ for $\sum_{n=1}^{\frac{\sqrt{2}\pi}{\Delta\alpha}} \Delta\alpha = \sqrt{2}\pi$; $\sum_{n=1}^{\frac{\sqrt{2}\pi}{|\Delta\alpha'|}} |\Delta\alpha'| = \sqrt{2}\pi$

The orbitsphere is given by reiterations of Eqs. (21) and (22). The output given by the non primed coordinates is the input of the next iteration corresponding to each successive nested rotation by the infinitesimal angle where the summation of the rotation about each of the x-axis and

the y-axis is $\sum_{n=1}^{\frac{\sqrt{2}\pi}{\Delta\alpha}} \Delta\alpha = \sqrt{2}\pi$ (1st set) and $\sum_{n=1}^{\frac{\sqrt{2}\pi}{|\Delta\alpha'|}} |\Delta\alpha'| = \sqrt{2}\pi$ (2nd set). The current pattern corresponding to great circle current loop one and two shown with 8.49 degree increments of the infinitesimal angular variable $\Delta\alpha(\Delta\alpha')$ of Eqs. (21) and (22) is shown from the perspective of looking along the z-axis in Figure 2. The true orbitsphere current pattern is given as $\Delta\alpha(\Delta\alpha')$ approaches zero. This current pattern gives rise to the phenomenon corresponding to the spin quantum number of the electron.

c. Magnetic Field Equations of the Electron

The orbitsphere is a shell of negative charge current comprising correlated charge motion along great circles. For $\mathbf{l} = 0$, the orbitsphere gives rise to a magnetic moment of 1 Bohr magneton [41].

$$\mu_B = \frac{e\hbar}{2m_e} = 9.274 \times 10^{-24} \text{ JT}^{-1}, \quad (23)$$

The magnetic field of the electron shown in Figure 4 is given by

$$\mathbf{H} = \frac{e\hbar}{m_e r_n^3} (\mathbf{i}_r \cos \theta - \mathbf{i}_\theta \sin \theta) \quad \text{for } r < r_n \quad (24)$$

$$\mathbf{H} = \frac{e\hbar}{2m_e r^3} (\mathbf{i}_r 2 \cos \theta - \mathbf{i}_\theta \sin \theta) \quad \text{for } r > r_n \quad (25)$$

The energy stored in the magnetic field of the electron is

$$E_{\text{mag}} = \frac{1}{2} \mu_0 \int_0^{2\pi} \int_0^\pi \int_0^\infty H^2 r^2 \sin \theta dr d\theta d\Phi \quad (26)$$

$$E_{\text{mag total}} = \frac{\pi \mu_0 e^2 \hbar^2}{m_e^2 r_1^3} \quad (27)$$

d. Stern-Gerlach Experiment

The Stern-Gerlach experiment implies a magnetic moment of one Bohr magneton and an associated angular momentum quantum number of $1/2$. Historically, this quantum number is called the spin quantum number, s ($s = \frac{1}{2}$; $m_s = \pm \frac{1}{2}$). The superposition of the vector projection of the orbitsphere angular momentum on to an axis S that precesses about the z -axis called the spin axis at an angle of $\theta = \frac{\pi}{3}$ and an angle of $\phi = \pi$ with respect to $\langle \mathbf{L}_{xy} \rangle_{\Sigma \Delta \alpha}$ is

$$S = \pm \sqrt{\frac{3}{4}} \hbar \quad (28)$$

S rotates about the z -axis at the Larmor frequency. $\langle S_z \rangle$, the time averaged projection of the orbitsphere angular momentum onto the axis of the applied magnetic field is

$$\langle \mathbf{L}_z \rangle_{\Sigma \Delta \alpha} \pm \frac{\hbar}{2}. \quad (29)$$

e. Electron g Factor

Conservation of angular momentum of the orbitsphere permits a discrete change of its "kinetic angular momentum" ($\mathbf{r} \times m\mathbf{v}$) by the applied magnetic field of $\frac{\hbar}{2}$, and concomitantly the "potential angular momentum" ($\mathbf{r} \times e\mathbf{A}$) must change by $-\frac{\hbar}{2}$.

$$\Delta\mathbf{L} = \frac{\hbar}{2} - \mathbf{r} \times e\mathbf{A} \quad (30)$$

$$= \left[\frac{\hbar}{2} - \frac{e\phi}{2\pi} \right] \hat{z} \quad (31)$$

In order that the change of angular momentum, $\Delta\mathbf{L}$, equals zero, ϕ must be $\Phi_0 = \frac{h}{2e}$, the magnetic flux quantum. The magnetic moment of the electron is parallel or antiparallel to the applied field only. During the spin-flip transition, power must be conserved. Power flow is governed by the Poynting power theorem,

$$\nabla \cdot (\mathbf{E} \times \mathbf{H}) = -\frac{\partial}{\partial t} \left[\frac{1}{2} \mu_0 \mathbf{H} \cdot \mathbf{H} \right] - \frac{\partial}{\partial t} \left[\frac{1}{2} \epsilon_0 \mathbf{E} \cdot \mathbf{E} \right] - \mathbf{J} \cdot \mathbf{E} \quad (32)$$

Eq. (33) gives the total energy of the flip transition which is the sum of the energy of reorientation of the magnetic moment (1st term), the magnetic energy (2nd term), the electric energy (3rd term), and the dissipated energy of a fluxon trading the orbitsphere (4th term), respectively,

$$\Delta E_{mag}^{spin} = 2 \left(1 + \frac{\alpha}{2\pi} + \frac{2}{3} \alpha^2 \left(\frac{\alpha}{2\pi} \right) - \frac{4}{3} \left(\frac{\alpha}{2\pi} \right)^2 \right) \mu_B B \quad (33)$$

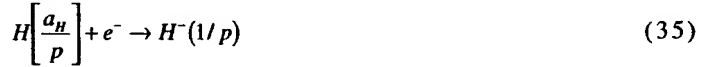
$$\Delta E_{mag}^{spin} = g \mu_B B \quad (34)$$

where the stored magnetic energy corresponding to the $\frac{\partial}{\partial t} \left[\frac{1}{2} \mu_0 \mathbf{H} \cdot \mathbf{H} \right]$ term increases, the stored electric energy corresponding to the $\frac{\partial}{\partial t} \left[\frac{1}{2} \epsilon_0 \mathbf{E} \cdot \mathbf{E} \right]$ term increases, and the $\mathbf{J} \cdot \mathbf{E}$ term is dissipative. The spin-flip transition can be considered as involving a magnetic moment of g times that of a Bohr magneton. The g factor is redesignated the fluxon g factor as opposed to the anomalous g factor. The calculated value of $\frac{g}{2}$ is

1.001 159 652 137 [3]. The experimental value of $\frac{g}{2}$ is 1.001 159 652 188(4) [42].

f. Hydride Ion

A novel hydride ion having extraordinary chemical properties given by Mills [3] is predicted to form by the reaction of an electron with a hydrino (Eq. (35)). The resulting hydride ion is referred to as a hydrino hydride ion, designated as $H^-(1/p)$.



The hydrino hydride ion is distinguished from an ordinary hydride ion having a binding energy of 0.8 eV for $p=1$. The hydrino hydride ion is predicted [3] to comprise a hydrogen nucleus and two indistinguishable electrons at a binding energy according to the following formula:

$$\text{Binding Energy} = \frac{\hbar^2 \sqrt{s(s+1)}}{8\mu_e a_0^2 \left[\frac{1 + \sqrt{s(s+1)}}{p} \right]^2} - \frac{\pi\mu_0 e^2 \hbar^2}{m_e^2 a_0^3} \left(1 + \frac{2^2}{\left[\frac{1 + \sqrt{s(s+1)}}{p} \right]^3} \right) \quad (36)$$

where p is an integer greater than one, $s=1/2$, π is pi, \hbar is Planck's constant bar, μ_0 is the permeability of vacuum, m_e is the mass of the electron, μ_e is the reduced electron mass, a_0 is the Bohr radius, and e is the elementary charge. The ionic radius is

$$r_1 = \frac{a_0}{p} \left(1 + \sqrt{s(s+1)} \right); s = \frac{1}{2} \quad (37)$$

From Eq. (37), the radius of the hydrino hydride ion $H^-(1/p)$; p =integer is $\frac{1}{p}$ that of ordinary hydride ion, $H^-(1/1)$. From Eq. (37) radius of $H^-(1/2)$ is

$$r_1 = 0.93301a_0 \quad (38)$$

where $p=2$. From Eq. (36), the binding energy E_b of $H^-(1/2)$ is

$$E_b = 3.0468 \text{ eV } (4069.4 \text{ \AA}) \quad (39)$$

The radius of $H^-(1/4)$ is

$$r_1 = 0.46651a_0 \quad (40)$$

where $p=2$, and the binding energy E_b of $H^-(1/4)$ is

$$E_b = 11.232 \text{ eV } (1103.8 \text{ \AA}) \quad (41)$$

g. Hydride Ion Hyperfine Lines

For ordinary hydride ion H^- , a continuum is observed at shorter wavelengths of the ionization or binding energy referred to as the bound-free continuum. For typical conditions in the photosphere, Figure 5 shows the continuous absorption coefficient $\kappa_c(\lambda)$ of the Sun [43]. In the visible and infrared, the hydride ion H^- is the dominant absorber. Its free-free continuum starts at $\lambda = 1.645 \mu m$, corresponding to the ionization energy of 0.745 eV for H^- with strongly increasing absorption towards the far infrared. The ordinary hydride spectrum recorded on the Sun is representative of the hydride spectrum in a very hot plasma.

Hydride ions formed by the reaction of hydrogen or hydrino atoms with free electrons with a kinetic energy distribution give rise to the bound-free emission band to shorter wavelengths than the ionization or binding energy due to the release of the electron kinetic energy and the hydride ion binding energy. As shown by Eq. (36), the energies for the formation of hydrino hydride ions are much greater, and with sufficient spectroscopic resolution, it may be possible to resolve hyperfine structure in the corresponding bound-free band due to interactions of the free and bound electrons. The derivation of the hyperfine lines follows.

Consider a free electron binding to a hydrino atom to form a hydrino hydride ion. The total angular momentum of an electron is \hbar . During binding of the free electron, the bound electron produces a magnetic field at the free electron given by Eq. (25). Thus, for radial distances greater than the radius of the hydride ion, the magnetic field is equivalent to that of a magnetic dipole of a Bohr magneton at the origin. The energy of interaction of a magnetic dipole with the magnetic field of the bound electron E_{ss} , the spin-spin energy, is given by Eq. (34)—the product of the electron g factor given by Eq. (33), the magnetic moment of the free electron, a Bohr magneton given by Eq. (23), and the magnetic flux which follows from Eq. (25).

$$E_{ss} = g\mu_B\mu_0 H = g\mu_B B = g \frac{\mu_0}{r^3} \left(\frac{e\hbar}{2m_e} \right)^2 \quad (42)$$

where μ_0 is the permeability of free space, r is the radius of hydride ion $H^-(n=1/p)$ given by Eq. (37), and p is an integer. E_{ss} for $H^-(1/2)$ is given

by

$$E_{\text{a}} = 0.011223 \text{ eV} \quad (43)$$

where the radius is given by Eq. (38). When a free electron binds to the hydrino atom $H(1/2)$ to form a hydride ion $H^-(1/2)$, a photon is emitted with a minimum energy equal to the binding energy ($E_b = 3.0468 \text{ eV}$). Any kinetic energy that the free electron possess must increase the energy of the emitted photon. The interaction of the two electrons quantizes this emission by the same mechanism as that observed in the Stern Gerlach experiment—quantization of flux linkage. Superconducting Quantum Interference Devices (SQUIDs) or wire loops linked to SQUIDs also show quantization of flux and the corresponding energies as shown in Chp 37 of Ref. 3.

In the Stern-Gerlach experiment, a magnetic field is applied along the z-axis called the spin axis. S , the projection of the angular momentum of an electron onto an axis which precesses about the z-axis, is $\pm\sqrt{\frac{3}{4}}\hbar$. S rotates about the z-axis at the Larmor frequency, and $\langle S_z \rangle$, the time averaged projection of the electron angular momentum onto the axis of the applied magnetic field is $\pm\frac{\hbar}{2}$ [3]. As given in Sec. I D e, the electron links flux in units of the magnetic flux quantum $\Phi_0 = \frac{h}{2e}$ during a Stern-Gerlach transition which conserves the angular momentum of the electron of \hbar . Due to the field of the bound electron, the free electron possessing kinetic energy will precess with a precessional angular momentum as well as an intrinsic angular momentum of $\pm\sqrt{s(s+1)}\hbar = \pm\sqrt{\frac{3}{4}}\hbar$.

In order to conserve angular momentum of both electrons as the bound electron links an integer number of fluxons due to the free electron, the total angular momentum of the free electron must have a magnitude that is an integer number of $\frac{\hbar}{\sqrt{s(s+1)}}$. The corresponding fluxon energy E_{ϕ}

follows from Eq. (33) derived previously [3] wherein the angular momentum corresponding to the Bohr magneton, \hbar , is replaced by $j\frac{\hbar}{\sqrt{s(s+1)}}$, and the magnetic flux density B is given by the ratio of the flux to the area.

$$\begin{aligned}
E_{\Phi} &= j(g-2) \frac{\mu_B}{\sqrt{s(s+1)}} B = j(g-2) \frac{\mu_B}{\sqrt{s(s+1)}} \left(\frac{j\Phi_0}{A} \right) = j^2(g-2) \frac{\mu_B}{\sqrt{s(s+1)}} B \\
&= j^2(g-2) \frac{\mu_B}{\sqrt{s(s+1)}} \frac{\mu_0}{r^3} \left(\frac{e\hbar}{2m_e} \right)
\end{aligned} \tag{44}$$

where j is an integer, $s=1/2$, and A is the area linked by the integer number of fluxons as given previously [3]. With the radius given by Eq. (38), the fluxon energy E_{Φ} of $H^-(1/2)$ is given by

$$E_{\Phi} = j^2(g-2) \frac{\mu_B}{\sqrt{s(s+1)}} \frac{\mu_0}{r^3} \left(\frac{e\hbar}{2m_e} \right) = j^2 3.0056 \times 10^{-5} \text{ eV} \tag{45}$$

The energies of the hyperfine lines E_{HF} , are given by the sum of the binding energy (Eqs. (36) and (39)), the spin-spin energy (Eqs. (42) and (43)), and the fluxon energy (Eqs. (44) and (45)).

$$E_{HF} = E_{\Phi} + E_s + E_b = j^2 3.0056 \times 10^{-5} + 0.011223 + 3.0468 \text{ eV}$$

$$(j \text{ is an integer}) \tag{46}$$

$$= j^2 3.0056 \times 10^{-5} + 3.0580 \text{ eV}$$

h. Spectroscopic Determination of the Bound-Free Hyperfine Levels of $H^-(1/2)$

Extreme ultraviolet (EUV) spectra recorded on microwave discharges of helium with 2% hydrogen were previously reported [8, 9, 19]. He^+ ionizes at 54.417 eV which is 2.27.2 eV, and novel emission lines were observed with energies of $q \cdot 13.6 \text{ eV}$ where $q=1,2,3,4,6,7,8,9,11,12$ or these lines inelastically scattered by helium atoms wherein 21.2 eV was absorbed in the excitation of $He(1s^2)$ to $He(1s^1 2p^1)$. These lines were identified as hydrogen transitions to electronic energy levels below the "ground" state corresponding to fractional quantum numbers. The hydrino catalysis product may further react with a source of electrons to form the corresponding hydride ion. Each of K^+/K^+ , Rb^+ , Cs , and Ar^+ are predicted to catalyze hydrogen to form $H\left[\frac{a_H}{2}\right]$ which reacts with an electron to form $H^-(1/2)$. A potassium atom is predicted to catalyze hydrogen to form $H\left[\frac{a_H}{4}\right]$ which reacts with an electron to form $H^-(1/4)$. Several studies including EUV and high resolution visible spectroscopy on rt-plasmas from several salt or metal catalysts confirmed the catalyst

mechanism and the predicted novel hydride ions. Exemplary studies include:

1.) the observation of continuum state emission of Cs^{2+} and Ar^{2+} at 533 Å and 456 Å, respectively, with the absence of the other corresponding Rydberg series of lines from these species which confirmed the resonant nonradiative energy transfer of 27.2 eV from atomic hydrogen to the catalysts atomic Cs or Ar^+ [15],

2.) the spectroscopic observation of the predicted hydride ion $H^-(1/2)$ of hydrogen catalysis by either Cs atom or Ar^+ catalyst at 4070 Å corresponding to its predicted binding energy of 3.05 eV [11, 15],

3.) the observation of characteristic emission from K^{3+} which confirmed the resonant nonradiative energy transfer of 3.27.2 eV from atomic hydrogen to atomic K [14],

4.) the spectroscopic observation of the predicted $H^-(1/4)$ ion of hydrogen catalysis by K catalyst at 1100 Å corresponding to its predicted binding energy of 11.2 eV [14],

5.) the observation of characteristic emission from Rb^{2+} which confirmed the resonant nonradiative energy transfer of 27.2 eV from atomic hydrogen to Rb^+ [13],

6.) the spectroscopic observation of the predicted $H^-(1/2)$ ion of hydrogen catalysis by Rb^+ catalyst at 4070 Å corresponding to its predicted binding energy of 3.05 eV [11, 13],

7.) the high resolution visible spectroscopic observation from rt-plasmas and plasma electrolysis cells of the predicted $H^-(1/2)$ ion of hydrogen catalysis by each of K^+/K^+ , Rb^+ , Cs, and Ar^+ at 4070 Å corresponding to its predicted binding energy of 3.05 eV [11-12],

Evidence was also previously presented that emission from lower-energy hydrogen atoms and molecules, as well as hydride ions was

observed from the Sun and interstellar medium [3, 6, 8, 10].

According to Eq. (42) and (44), the predicted electron interactions for $H^-(1/2)$ are 8 times more energetic than those of ordinary hydride ion. Identification of the $H^-(1/2)$ hydride ion was sought using high resolution spectroscopy of rt-plasma cell emission from Rb^+ and K^+/K^+ catalysts which were each predicted to form $H(1/2)$ which further reacts to form $H^-(1/2)$. The spectrometer had a sufficiently high resolution ($\pm 0.06 \text{ \AA}$) to determine whether the predicted hyperfine structure due to bound-free electron-electron interactions occurred during the formation of the hydride $H^-(1/2)$ in rt-plasma formed by K^+/K^+ and Rb^+ catalysts.

II. EXPERIMENTAL

A. EUV spectroscopy recorded on rt-plasmas

EUV spectra, 6562 \AA Balmer α line width measurements, and high resolution visible spectra were recorded on light emitted from rt-plasmas of hydrogen with KNO_3 and $RbNO_3$. The experimental set up shown in Figure 6 comprised a quartz cell which was 500 mm in length and 50 mm in diameter. The entire quartz cell was enclosed in an Alumina insulation package. Several K-type thermocouples were located in the insulation. The thermocouples were monitored with a multichannel computer data acquisition system. A Pyrex cap sealed to the quartz cell with a Viton O ring and a C-clamp incorporated ports for gas inlet, outlet, and photon detection. A tungsten filament (0.508 mm in diameter and 800 cm in length, total resistance $\sim 2.5 \text{ ohm}$) heater and hydrogen dissociator were in the quartz tube as well as a cylindrical titanium screen (300 mm long and 40 mm in diameter) that served as a second hydrogen dissociator. The filament was coiled on a grooved ceramic tube support to maintain its shape when heated. The return lead passed through the inside of the ceramic tube. The nitrate test materials were coated on a titanium screen dissociator by the method of wet impregnation. The screen was coated by dipping it in a 0.6 M $KNO_3/10\% H_2O_2$ or 0.6 M $RbNO_3/10\% H_2O_2$, and the crystalline material was dried on the surface by heating for 12 hours in a drying oven at 130 $^\circ\text{C}$. A new dissociator was used for each experiment. The titanium screen was electrically floated with power applied to the

filament. In each test, power was applied to the filament by a DC power supply which was controlled by a constant power controller. The power applied to the filament was 300 W. The voltage across the filament was about 40 V and the current was about 6.25 A at 250 W. The temperature of the tungsten filament was estimated to be in the range 1100 to 1500 °C. The external cell wall temperature was about 700 °C.

The cell was operated under gas flow conditions while maintaining a constant gas pressure in the cell. The hydrogen gas was ultrahigh purity. The gas pressure inside the cell was maintained at about 300 mtorr with a hydrogen flow rate of 5.5 sccm controlled by a 0-20 sccm range mass flow controller (MKS 1179A21CS1BB) with a readout (MKS type 246). The cell pressure was monitored by a 0-10 torr MKS Baratron absolute pressure gauge.

The light emission was introduced to an EUV spectrometer for spectral measurement. The spectrometer was a McPherson 0.2 meter monochromator (Model 302, Seya-Namioka type) equipped with a 1200 lines/mm holographic grating with a platinum coating. The wavelength region covered by the monochromator was 50–5600 Å. A channel electron multiplier (CEM) was used to detect the EUV light. The wavelength resolution was about 2 Å (FWHM) with an entrance and exit slit width of 10 μ m. The vacuum inside the monochromator was maintained below 5×10^{-4} Torr by a turbo pump. The Lyman α emission was recorded as a function of time after the filament was turned on. In each case, the EUV spectrum (900–1300 Å) of the rt-plasma cell emission was recorded at about the point of the maximum Lyman α emission to confirm the rt-plasma before the line broadening and high resolution visible spectrum in the region of 4070.0 Å were recorded. The EUV spectrum was also recorded on light emitted from a hydrogen glow discharge maintained according to methods reported previously [8] that served as a control for measurements recorded on light emitted from rt-plasmas of hydrogen with KNO_3 .

B. Balmer α line broadening and high resolution visible spectroscopy recorded on rt-plasmas

The plasma emission from each rt-plasma maintained in the

filament heated cell was fiber-optically coupled through a 220F matching fiber adapter positioned 2 cm from the cell wall to a high resolution visible spectrometer with a resolution of $\pm 0.06 \text{ \AA}$ over the spectral range 1900-8600 \AA . The spectrometer was a Jobin Yvon Horiba 1250 M with 2400 grooves/mm ion-etched holographic diffraction grating. The entrance and exit slits were set to $20 \mu\text{m}$. The spectrometer was scanned between 6555-6570 \AA using a 0.1 \AA step size. The signal was recorded by a PMT with a stand alone high voltage power supply (950 V) and an acquisition controller. The data was obtained in a single accumulation with a 1 second integration time. In addition, the high resolution visible spectrum of each rt-plasma was recorded over the range 4000-4200 \AA using the same methods as those of the line broadening measurements.

The width of the 6562 \AA Balmer α line and the high resolution visible spectrum (4000-4200 \AA) were also recorded on light emitted from a hydrogen glow discharge cell maintained according to methods reported previously [21]. The light introduced into the 220F matching fiber adapter positioned 2 cm from a sapphire window in the discharge cell wall served as a control for measurements recorded on light emitted from rt-plasmas of hydrogen with KNO_3 and RbNO_3 .

III. RESULTS AND DISCUSSION

A. EUV Spectroscopy

The intensity of the Lyman α emission as a function of time from the gas cell at a cell temperature of 700°C comprising a tungsten filament, a titanium dissociator, and 300 mtorr hydrogen with a flow rate of 5.5 sccm was tested for hydrogen alone and with potassium catalyst formed by hydrogen reduction and thermal decomposition of KNO_3 . The cell was run with hydrogen but without any test material present to establish the baseline of the spectrometer. The intensity of the Lyman α emission as a function of time was measured for three hours, and no emission was observed. The intensity of the Lyman α emission as a function of time with vaporized potassium from KNO_3 was recorded. Strong EUV emission was observed from vaporized potassium catalyst only with hydrogen present.

The EUV spectrum (900–1300 Å) of the cell emission of a control hydrogen glow discharge is shown in Figure 7. The EUV spectrum (900–1300 Å) of the potassium rt-plasma cell emission recorded at about the point of the maximum Lyman α emission is shown in Figure 8. No emission was observed in the absence of hydrogen, and no emission occurred until the catalyst was vaporized as indicated by the appearance of KNO_3 crystals and a metal coating in the cap of the cell over the course of the experiment. Potassium is predicted to form the hydride $H^-(1/4)$ with emission in the region of 1100 Å (Eq. (41)). Molecular hydrogen has peaks in this region as shown in Figure 7. The broad peak in the region of 1100 Å was assigned to $H^-(1/4)$ based on comparison of the ratio of the intensity of this peak and nearby hydrogen molecular lines to the ratio at the same wavelengths from the control as described previously [14]. The novel 1100 Å continuum peak was observed only with potassium and atomic hydrogen present over an extended reaction time. As shown in Figures 7 & 8, the Lyman β and Lyman δ lines of the potassium gas cell at 1026 Å and 973 Å, respectively, have a much greater intensity relative to Lyman α line at 1216 Å than those of the hydrogen glow discharge. For example, the rt-plasma Lyman β to α ratio was very high—1.3 versus 0.13 for the control which indicates a high plasma temperature. These results are consistent with the formation of $H^-(1/4)$ from the catalysis of atomic hydrogen by $K(m)$.

The hydride ion $H^-(1/4)$ has been reported previously [29]. KHI containing $H^-(1/4)$ was synthesized by reaction of potassium metal, atomic hydrogen, and KI . The XPS spectrum of the product blue crystals differed from that of KI by having additional features at 9.1 eV and 11.1 eV. The XPS peaks centered at 9.0 eV and 11.1 eV that did not correspond to any other primary element peaks were assigned to the $H^-(n=1/4) E_b = 11.2 \text{ eV}$ hydride ion (Eq. (41)) in two different chemical environments where E_b is the predicted vacuum binding energy. Furthermore, the reported minimum heats of formation of KHI by the catalytic reaction of potassium with atomic hydrogen and KI were over $-2000 \text{ kJ/mole } H_2$ compared to the enthalpy of combustion of hydrogen of $-241.8 \text{ kJ/mole } H_2$ [34].

B. Balmer α line broadening recorded on rt-plasmas

Line broadening of the hydrogen Balmer lines provides a sensitive measure of the number and energy of excited hydrogen atoms in a plasma. To further characterize the plasma parameters of rt-plasmas, the width of the 6562 Å Balmer α line was recorded on light emitted from rt-plasmas formed from hydrogen with a gaseous atom or ion which ionizes at integer multiples of the potential energy of atomic hydrogen. The results of the 6562 Å Balmer α line width measured with a high resolution (± 0.06 Å) visible spectrometer on light emitted from rt-plasmas of hydrogen with KNO_3 and $RbNO_3$ are shown in Figures 9 and 10, respectively. To illustrate the method of displaying each line broadening result as an unsmoothed curve, the corresponding raw data points are also shown that further show the scatter in the data. The Balmer α line width and energetic hydrogen atom densities and energies given in Table 1 were calculated from the broadening using the method of Videnocic et al. [44]. Significant line broadening of 17 and 9 eV and an atom density of 4×10^{11} and 6×10^{11} atoms/cm³ were observed from rt-plasmas of hydrogen formed with K^+/K^+ and Rb^+ catalysts, respectively. Whereas, a glow discharge of hydrogen maintained at the same total pressure with an electric field strength that was at least two order of magnitude greater than the 1 V/cm field of the filament cell showed no excessive broadening corresponding to an average hydrogen atom temperature of ≈ 3 eV.

In the characterization of the plasmas of Grimm-type discharges with a hollow anode, Videnocic et al. [44] and M. Kuraica and N. Konjevic [45] analyzed the broadening data in terms of Stark and Doppler effects wherein acceleration of charges such as H^+ , H_2^+ , and H_3^+ in the high fields (e. g. over 10 kV/cm) which were present in the cathode fall region was used to explain the Doppler component. In our experiments, the results could not be explained by Stark or thermal broadening or electric field acceleration of charged species since the measured field of the incandescent heater was extremely weak, 1 V/cm, corresponding to a broadening much less than 1 eV. Rather the source of the excessive line broadening is consistent with that of EUV emission, an energetic reaction caused by a resonance energy transfer between hydrogen atoms and

K^+/K^+ or Rb^+ catalyst.

Rt-plasmas formed with hydrogen-potassium mixtures have been reported previously [26-27] wherein the plasma decayed with a two second half-life when the electric field was set to zero. This was the thermal decay time of the filament which dissociated molecular hydrogen to atomic hydrogen. This experiment showed that hydrogen line emission was occurring even though the voltage between the heater wires was set to and measured to be zero and indicated that the emission was due to a reaction of potassium atoms with atomic hydrogen. Potassium atoms ionize at an integer multiple of the potential energy of atomic hydrogen, $m \cdot 27.2 \text{ eV}$. The enthalpy of ionization of K to K^{3+} has a net enthalpy of reaction of 81.7426 eV , which is equivalent to $m=3$.

An excessive afterglow duration was observed for rt-plasmas of hydrogen and certain alkali ions that were recorded via EUV spectroscopy and the hydrogen Balmer and alkali line emissions in the visible range [27]. The observed plasma formed at low temperatures (e.g. $\approx 10^3 \text{ K}$) from atomic hydrogen generated at a tungsten filament that heated a titanium dissociator and one of potassium, rubidium, cesium, and their carbonates and nitrates. These atoms and ions ionize to provide a net enthalpy of reaction of an integer multiple of the potential energy of atomic hydrogen ($m \cdot 27.2 \text{ eV}$, $m = \text{integer}$) to within 0.17 eV and comprise only a single ionization in the case of a potassium or rubidium ion. Whereas, the chemically similar atoms of sodium and sodium and lithium carbonates and nitrates which do not ionize with these constraints caused no emission. To test the electric dependence of the emission, the weak electric field of about 1 V/cm was set and measured to be zero in $< 0.5 \times 10^{-6} \text{ sec}$. An afterglow duration of about one to two seconds was recorded in the case of potassium, rubidium, cesium, K_2CO_3 , $RbNO_3$, and $CsNO_3$. Hydrogen line or alkali line emission was occurring even though the voltage between the heater wires was set to and measured to be zero. These atoms and ions ionize to provide a net enthalpy of reaction of an integer multiple of the potential energy of atomic hydrogen to within less than the thermal energies at $\approx 10^3 \text{ K}$ and comprise only a single ionization in the case of a potassium or rubidium ion. Since the thermal decay time of the filament for dissociation of molecular hydrogen to atomic hydrogen was similar to the rt-plasma

afterglow duration, the emission was determined to be due to a reaction of atomic hydrogen with each of the atoms or ions that did not require the presence of an electric field to be functional.

C. High resolution visible spectroscopy recorded on rt-plasmas

The high resolution visible spectra (4000-4060 Å) and (4060-4090 Å) recorded on the emission of a control hydrogen glow discharge plasma are shown in Figures 11 and 12, respectively. Only weak hydrogen molecular peaks were observed.

The high resolution visible spectrum in the region of 4000 Å to 4090 Å recorded on the emission of a rt-plasma formed with K^+/K^+ catalyst from vaporized KNO_3 is shown in Figure 13 with the expanded views of the 4000-4060 Å and 4060-4090 Å regions shown in Figures 14 and 15, respectively. A broad peak consistent with a hydride ion was observed at 4070.0 Å with a FWHM of 1.4 Å. This peak overlaps the predicted threshold for binding energy of $H^-(1/2)$ given by Eq. (39). The 4070.0 Å peak was not observed in the hydrogen glow discharge plasma as shown in Figures 11 and 12. O II lines at 4069.623, 4069.881, and 4071.238 Å were eliminated due to the absence of O I lines at 3947.29, 3947.48, 3947.58, 3954.60, and 4054.77 Å. C III lines at 4070.26 and 4068.916 Å were eliminated due to the absence of C I lines which were outside of the region of 4070 Å or C II lines at 3918.96 and 3920.68 Å. Furthermore, the presence of the O II or C III lines would be extraordinary since the ionization energy required for O II is above the first ionization energy of 13.62 eV, and the energies required for C III are above the sum of the first and second ionization energies of 11.26 eV and 24.38 eV, respectively [39]. The novel 4070.0 Å peak which could not be assigned to a known peak was assigned to $H^-(1/2)$. Other peaks in the rt-plasma that partially covered some of the hyperfine peaks were assigned to molecular hydrogen and K I. In addition, K II was observed outside this region at 4829 Å which confirmed the presence of the catalyst K^+/K^+ .

Since the $H^-(1/2)$ peak is broad, it consequently contributes to the broadening of the hyperfine lines. Thus, a better determination of the hyperfine energies under experimental conditions is to use the maximum

of the hydride peak as the parameter E_b in Eq. (46). Substitution of the energy, 3.0463 eV, corresponding to the wavelength of the maximum of the observed hydride peak, 4070.0 Å, into Eq. (46) for E_b gives

$$E_{HF} = E_\phi + E_s + E_b = j^2 3.0056 \times 10^{-5} + 0.011223 + 3.0463 \text{ eV} \quad (j \text{ is an integer}) \quad (47)$$

$$= j^2 3.0056 \times 10^{-5} + 3.0575 \text{ eV}$$

The predicted inverse Rydberg-type series that converges at increasing wavelengths and terminates at 3.0575 eV was observed as shown in Figures 13 and 14.

The inverse Rydberg-type series of broad emission lines was not observed in the hydrogen glow discharge plasma as shown in Figures 11 and 12. Other possibilities such as rotational transitions of diatomic molecules were also eliminated. Emission in the 4000-4060 Å region could only correspond to an electronic transition with emission from vibrational as well as rotational levels. No vibrational or other related electronic bands were observed. Diatomic molecules other than H_2 have equally spaced rotational levels which may have $\approx 10^{-3}$ energies, but the observed lines matched a second order integer relationship as opposed to a linear one. Furthermore, the system was run under hydrogen flow conditions with continuous pumping which made improbable the presence of a detectable concentration of gaseous molecules other than hydrogen. And, the possible diatomic molecules, NO, N_2 , O_2 , and OH, were further eliminated as the source of the Rydberg-type series based on their known spectra such as those shown in Figure 3 of Refs. 46-47. No emission was observed from these molecules as well as from oxygen or nitrogen atoms over the 900-1300 Å and 4000-4200 Å regions.

The high resolution visible spectrum in the region of 4000 Å to 4090 Å recorded on the emission of a rt-plasma formed with Rb^+ catalyst from vaporized $RbNO_3$ is shown in Figure 16 with the expanded views of the 4000-4060 Å and 4060-4090 Å regions are shown in Figures 17 and 18, respectively. The $H^-(1/2)$ hydride ion with a predicted binding energy of 3.0468 eV was observed as a broad peak at 4070.0 Å with a FWHM of 1.4 Å as shown in Figures 16 and 18. An inverse Rydberg-type series of broad emission lines shown in Figures 16 and 17 that converged at increasing wavelengths and terminated at about 3.0575 eV—the hydride spin-pairing energy plus the binding energy—matched the theoretical

hyperfine energies E_{HF} given by $E_{HF} = j^2 3.0056 \times 10^{-5} + 3.0575 \text{ eV}$ for $j=1$ to $j=37$. The results are presented in Table 2. Other peaks in the rt-plasma that partially covered some of the hyperfine peaks were assigned to molecular hydrogen. In addition to hydrogen molecular lines, a Rb II peak was observed in Figure 18 which confirmed the presence of the catalyst Rb^+ .

The emission spectra of the $H^-(1/2)$ hydride ion and the corresponding hyperfine lines were very reproducible. Three matching EUV spectra (4000-4060Å) of Rb^+ rt-plasmas that were equivalent to the spectrum of the K^+/K^+ and the Rb^+ rt-plasmas shown in Figures 14 and 17, respectively, are shown in Figure 19. The theoretical hyperfine energies, the observed energies, and the difference between the two are given in Table 2. The remarkable agreement is further evident in Figure 20 which shows the energies of the observed peaks overlaid on the plot of the theoretical energies given by Eq. (47).

IV. CONCLUSION

Each of an electron transfer between two K^+ ions and the ionization of a potassium atom or Rb^+ provide a reaction with a net enthalpy of an integer multiple of the potential energy of atomic hydrogen. The presence of each of the corresponding reactants formed the low applied temperature, extremely low voltage plasma called a resonance transfer or rt-plasma. For further characterization, the width of the 6562 Å Balmer α line was recorded on light emitted from rt-plasmas. Significant line broadening of 17 and 9 eV and an atom density of 4×10^{11} and $6 \times 10^{11} \text{ atoms/cm}^3$ were observed from a rt-plasma of hydrogen formed with potassium or K^+/K^+ and Rb^+ catalysts, respectively. These results could not be explained by Stark or thermal broadening or electric field acceleration of charged species since the measured field of the incandescent heater was extremely weak, 1 V/cm, corresponding to a broadening much less than 1 eV. Rather, the source of the excessive line broadening is consistent with that of EUV emission, an energetic reaction caused by a resonance energy transfer between hydrogen atoms and the catalyst.

The predicted $H^-(1/4)$ hydride ion of hydrogen catalysis by

potassium catalyst given by Eqs. (7-9) and Eq. (36) was observed spectroscopically at 1100 Å corresponding to its predicted binding energy of 11.2 eV.

The K^+/K^+ and Rb^+ catalysis product, $H(1/2)$, given by Eqs. (4-6), and (10-12) respectively, was predicted to form hydride ion $H^-(1/2)$ given by Eq. (36). This hydride ion with a predicted binding energy of 3.0465 eV was observed by high resolution visible spectroscopy as a broad peak at 4070.0 Å with a FWHM of 1.4 Å. From the electron g factor, bound-free hyperfine structure lines of $H^-(1/2)$ were predicted with energies E_{HF} given by $E_{HF} = j^2 3.0022 \times 10^{-5} + 3.0582 \text{ eV}$ (j is an integer) as an inverse Rydberg-type series that converges at increasing wavelengths and terminates at 3.0582 eV—the hydride spin-pairing energy plus the binding energy. Remarkable agreement between theory and experiment was observed for the lines corresponding to $j=1$ to $j=37$. Since the hyperfine lines of ordinary hydride ion are not sufficiently energetic to be resolved; whereas, those of $H^-(1/2)$ are, this is the first report of the observation of hyperfine energy levels of a hydride ion.

The release of energy from hydrogen as evidenced by the EUV emission must result in a lower-energy state of hydrogen. The present study identified the formation of novel hydride ions, $H^-(1/2)$ and $H^-(1/4)$. The formation of novel compounds based on novel hydride ions would be substantial evidence supporting catalysis of hydrogen as the mechanism of the observed EUV emission and further support the present spectroscopic identification of $H^-(1/2)$ and $H^-(1/4)$. Compounds containing novel hydride ions have been isolated as products of the reaction of atomic hydrogen with atoms and ions identified as catalysts in the present study and previously reported EUV studies [28-34]. The novel hydride compounds were identified analytically by techniques such as time of flight secondary ion mass spectroscopy, X-ray photoelectron spectroscopy, and 1H nuclear magnetic resonance spectroscopy. For example, the time of flight secondary ion mass spectroscopy showed a large hydride peak in the negative spectrum. The X-ray photoelectron spectrum showed large metal core level shifts due to binding with the hydride as well as novel hydride peaks. The 1H nuclear magnetic resonance spectrum showed significantly upfield shifted peaks which corresponded to and identified novel hydride ions as shown in Figure 21

reported previously [28].

The identification of novel hydride ions is indicative of a new field of hydrogen chemistry. Novel hydride ions may combine with other cations such as other alkali cations and alkaline earth, rare earth, and transition element cations. Numerous novel compounds may be synthesized with unique properties such as high stability relative to the corresponding compounds having ordinary hydride ions wherein the enthalpy of formation is very exothermic—at least 43.9 eV/Hatom and 215.2 eV/Hatom for $\text{H}^-(1/2)$ and $\text{H}^-(1/4)$, respectively, compared to the enthalpy of combustion of 1.48 eV/Hatom .

Since the net enthalpy released may be at least one hundred times that of combustion, the catalysis of atomic hydrogen represents a new source of energy with H_2O as the source of hydrogen fuel. Moreover, rather than air pollutants or radioactive waste, novel hydride compounds with potential broad commercial applications are the products [28-34]. Since the power is in the form of a plasma, direct high-efficiency, low cost energy conversion may be possible, thus, avoiding a heat engine such as a turbine [35-37] or a reformer-fuel cell system. Significantly lower capital costs and lower commercial operating costs than that of any known competing energy source are anticipated.

ACKNOWLEDGMENT

Special thanks to Alex Echezuria for preparing filament cells for plasma experiments and Bala Dhandapani for assisting with logistics and reviewing this manuscript.

REFERENCES

1. N. V. Sidgwick, *The Chemical Elements and Their Compounds*, Volume I, Oxford, Clarendon Press, (1950), p.17.
2. M. D. Lamb, *Luminescence Spectroscopy*, Academic Press, London, (1978), p. 68.
3. R. Mills, *The Grand Unified Theory of Classical Quantum Mechanics*, January 2000 Edition, BlackLight Power, Inc., Cranbury, New Jersey, Distributed by Amazon.com; September 2001 Edition posted at

www.blacklightpower.com.

4. R. Mills, "The Grand Unified Theory of Classical Quantum Mechanics", Global Foundation, Inc. Orbis Scientiae entitled *The Role of Attractive and Repulsive Gravitational Forces in Cosmic Acceleration of Particles The Origin of the Cosmic Gamma Ray Bursts*, (29th Conference on High Energy Physics and Cosmology Since 1964) Dr. Behram N. Kursunoglu, Chairman, December 14-17, 2000, Lago Mar Resort, Fort Lauderdale, FL, Kluwer Academic/Plenum Publishers, New York, pp. 243-258.
5. R. Mills, "The Grand Unified Theory of Classical Quantum Mechanics", Int. J. of Hydrogen Energy, in press.
6. R. Mills, "The Hydrogen Atom Revisited", Int. J. of Hydrogen Energy, Vol. 25, Issue 12, December, (2000), pp. 1171-1183.
7. R. Mills, The Nature of Free Electrons in Superfluid Helium—a Test of Quantum Mechanics and a Basis to Review its Foundations and Make a Comparison to Classical Theory, Int. J. Hydrogen Energy, Vol. 26, No. 10, (2001), pp. 1059-1096.
8. R. Mills, P. Ray, "Spectral Emission of Fractional Quantum Energy Levels of Atomic Hydrogen from a Helium-Hydrogen Plasma and the Implications for Dark Matter", Int. J. Hydrogen Energy, in press.
9. R. L. Mills, P. Ray, B. Dhandapani, J. He, "Spectroscopic Identification of Fractional Rydberg States of Atomic Hydrogen" J. Phys. Chem. Letts., submitted.
10. R. Mills, P. Ray, "Vibrational Spectral Emission of Fractional-Principal-Quantum-Energy-Level Hydrogen Molecular Ion", Int. J. Hydrogen Energy, in press.
11. R. Mills, P. Ray, M. Nansteel, W. Good, P. Jansson, B. Dhandapani, J. He, "Excessive Balmer α Line Broadening, Power Balance, and Novel Hydride Ion Product of Plasma Formed from Incandescently Heated Hydrogen Gas with Certain Catalysts", Int. J. Hydrogen Energy, submitted.
12. R. Mills, E. Dayalan, P. Ray, B. Dhandapani, J. He, "Highly Stable Novel Inorganic Hydrides from Aqueous Electrolysis and Plasma Electrolysis, submitted.
13. R. L. Mills, P. Ray, "Spectroscopic Identification of a Novel Catalytic Reaction of Rubidium Ion with Atomic Hydrogen and the Hydride Ion Product", Int. J. Hydrogen Energy, submitted.

14. R. Mills, P. Ray, Spectroscopic Identification of a Novel Catalytic Reaction of Potassium and Atomic Hydrogen and the Hydride Ion Product, *Int. J. Hydrogen Energy*, in press.
15. R. Mills, "Spectroscopic Identification of a Novel Catalytic Reaction of Atomic Hydrogen and the Hydride Ion Product", *Int. J. Hydrogen Energy*, Vol. 26, No. 10, (2001), pp. 1041-1058.
16. R. Mills and M. Nansteel, "Argon-Hydrogen-Strontium Plasma Light Source", *IEEE Transactions on Plasma Science*, submitted.
17. R. Mills, M. Nansteel, and Y. Lu, "Excessively Bright Hydrogen-Strontium Plasma Light Source Due to Energy Resonance of Strontium with Hydrogen", *European Journal of Physics D*, submitted.
18. R. Mills, J. Dong, W. Good, P. Ray, J. He, B. Dhandapani, Measurement of Energy Balances of Noble Gas-Hydrogen Discharge Plasmas Using Calvet Calorimetry, *Int. J. Hydrogen Energy*, submitted.
19. Randell L. Mills, P. Ray, B. Dhandapani, M. Nansteel, X. Chen, J. He, "New Power Source from Fractional Quantum Energy Levels of Atomic Hydrogen that Surpasses Internal Combustion", *Spectrochimica Acta*, submitted.
20. R. L. Mills, P. Ray, B. Dhandapani, J. He, "Comparison of Excessive Balmer α Line Broadening of Glow Discharge and Microwave Hydrogen Plasmas with Certain Catalysts" *J. Phys. Chem.*, submitted.
21. R. L. Mills, A. Voigt, P. Ray, M. Nansteel, B. Dhandapani, "Measurement of Hydrogen Balmer Line Broadening and Thermal Power Balances of Noble Gas-Hydrogen Discharge Plasmas", *Int. J. Hydrogen Energy*, in press.
22. R. Mills, N. Greenig, S. Hicks, "Optically Measured Power Balances of Anomalous Discharges of Mixtures of Argon, Hydrogen, and Potassium, Rubidium, Cesium, or Strontium Vapor", *Int. J. Hydrogen Energy*, in press.
23. R. Mills, M. Nansteel, and Y. Lu, "Observation of Extreme Ultraviolet Hydrogen Emission from Incandescently Heated Hydrogen Gas with Strontium that Produced an Anomalous Optically Measured Power Balance", *Int. J. Hydrogen Energy*, Vol. 26, No. 4, (2001), pp. 309-326.
24. R. Mills, J. Dong, Y. Lu, "Observation of Extreme Ultraviolet Hydrogen Emission from Incandescently Heated Hydrogen Gas with Certain Catalysts", *Int. J. Hydrogen Energy*, Vol. 25, (2000), pp. 919-943.

25. R. Mills, "Observation of Extreme Ultraviolet Emission from Hydrogen-KI Plasmas Produced by a Hollow Cathode Discharge", *Int. J. Hydrogen Energy*, Vol. 26, No. 6, (2001), pp. 579-592.
26. R. Mills, "Temporal Behavior of Light-Emission in the Visible Spectral Range from a Ti-K₂CO₃-H-Cell", *Int. J. Hydrogen Energy*, Vol. 26, No. 4, (2001), pp. 327-332.
27. R. Mills, T. Onuma, and Y. Lu, "Formation of a Hydrogen Plasma from an Incandescently Heated Hydrogen-Catalyst Gas Mixture with an Anomalous Afterglow Duration", *Int. J. Hydrogen Energy*, Vol. 26, No. 7, July, (2001), pp. 749-762.
28. R. Mills, B. Dhandapani, M. Nansteel, J. He, A. Voigt, "Identification of Compounds Containing Novel Hydride Ions by Nuclear Magnetic Resonance Spectroscopy", *Int. J. Hydrogen Energy*, Vol. 26, No. 9, Sept. (2001), pp. 965-979.
29. R. Mills, B. Dhandapani, N. Greenig, J. He, "Synthesis and Characterization of Potassium Iodo Hydride", *Int. J. of Hydrogen Energy*, Vol. 25, Issue 12, December, (2000), pp. 1185-1203.
30. R. Mills, "Novel Inorganic Hydride", *Int. J. of Hydrogen Energy*, Vol. 25, (2000), pp. 669-683.
31. R. Mills, "Novel Hydrogen Compounds from a Potassium Carbonate Electrolytic Cell", *Fusion Technology*, Vol. 37, No. 2, March, (2000), pp. 157-182.
32. R. Mills, B. Dhandapani, M. Nansteel, J. He, T. Shannon, A. Echezuria, "Synthesis and Characterization of Novel Hydride Compounds", *Int. J. of Hydrogen Energy*, Vol. 26, No. 4, (2001), pp. 339-367.
33. R. Mills, "Highly Stable Novel Inorganic Hydrides", *Journal of New Materials for Electrochemical Systems*, in press.
34. R. Mills, W. Good, A. Voigt, Jinquan Dong, "Minimum Heat of Formation of Potassium Iodo Hydride", *Int. J. Hydrogen Energy*, Vol. 26, No. 11, Oct., (2001), pp. 1199-1208.
35. R. Mills, "BlackLight Power Technology-A New Clean Hydrogen Energy Source with the Potential for Direct Conversion to Electricity", *Proceedings of the National Hydrogen Association, 12 th Annual U.S. Hydrogen Meeting and Exposition, Hydrogen: The Common Thread*, The Washington Hilton and Towers, Washington DC, (March 6-8, 2001), pp. 671-697.

36. R. Mills, "BlackLight Power Technology-A New Clean Energy Source with the Potential for Direct Conversion to Electricity", Global Foundation International Conference on "Global Warming and Energy Policy", Dr. Behram N. Kursunoglu, Chairman, Fort Lauderdale, FL, November 26-28, 2000, Kluwer Academic/Plenum Publishers, New York, pp. 1059-1096.
37. R. Mayo, R. Mills, M. Nansteel, "On the Potential of Direct and MHD Conversion of Power from a Novel Plasma Source to Electricity for Microdistributed Power Applications", IEEE Transactions on Plasma Science, submitted.
38. C. J. Hardy, B. O. Field, J. Chem. Soc., (1963), pp. 5130-5134.
39. David R. Linde, *CRC Handbook of Chemistry and Physics*, 79 th Edition, CRC Press, Boca Raton, Florida, (1998-9), p. 10-175 to p. 10-177.
40. H. A. Haus, On the radiation from point charges, *American Journal of Physics*, 54, 1126-1129 (1986).
41. D. A. McQuarrie, *Quantum Chemistry*, University Science Books, Mill Valley, CA, (1983), pp. 238-241.
42. R. S. Van Dyck, Jr., P. Schwinberg, H. Dehmelt, "New high precision comparison of electron and positron g factors", Phys. Rev. Lett., Vol. 21, (1987), p. 26-29.
43. M. Stix, *The Sun*, Springer-Verlag, Berlin, (1991), p. 136.
44. I. R. Videnovic, N. Konjevic, M. M. Kuraica, "Spectroscopic investigations of a cathode fall region of the Grimm-type glow discharge", Spectrochimica Acta, Part B, Vol. 51, (1996), pp. 1707-1731.
45. M. Kuraica, N. Konjevic, "Line shapes of atomic hydrogen in a plane-cathode abnormal glow discharge", Physical Review A, Volume 46, No. 7, October (1992), pp. 4429-4432.
46. C. O. Laux, R. J. Gessman, C. H. Kruger, "Measurements and modeling of the absolute spectral emission of air plasmas between 185 and 800 nm", Journal of Quantitative Spectroscopy and Radiative Transfer, (2001), submitted.
47. C. O. Laux, C. H. Kruger, R. N. Zare, "Diagnostics of atmospheric pressure air plasmas", www-krf.stanford.edu/kruger.html.

Table 1. Energetic hydrogen atom densities and energies for rt-plasmas determined from the 6562 Å Balmer α line width.

| Plasma Gas | Hydrogen Atom Density ^a (10^{11} atoms/cm ³) | Hydrogen Atom Energy ^b (eV) |
|---------------------------|---|---|
| H_2 | 2 | 2-3 ^c |
| K and $K^+ / K^+ / H_2$ | 4 | 15-18 |
| Rb^+ / H_2 | 6 | 8-10 |

^a Approximate Calculated [44].

^b Calculated [44].

^c Measured on glow discharge according to method of Ref. 21.

Table 2. Calculated hyperfine emission lines of bound-free plasma emission of $H^-(1/2)$ and the observed lines.

| Hyperfine Quantum Number j | Calculated Emission (eV) Eq. (47) | Calculated Emission (Å) Eq. (47) | Observed Lines (eV) | Observed Lines (Å) | Difference between Experimental and Calculated (eV) |
|------------------------------------|--|---|---------------------------|--------------------------|---|
| 1 | 3.0575 | 4055.1 | 3.0571 | 4055.6 | -0.00041 |
| 2 | 3.0576 | 4055.0 | 3.0572 | 4055.5 | -0.00039 |
| 3 | 3.0578 | 4054.8 | 3.0573 | 4055.4 | -0.00045 |
| 4 | 3.0580 | 4054.5 | 3.0575 | 4055.2 | -0.00052 |
| 5 | 3.0583 | 4054.1 | 3.0578 | 4054.7 | -0.00044 |
| 6 | 3.0586 | 4053.7 | 3.0581 | 4054.4 | -0.00051 |
| 7 | 3.0590 | 4053.2 | 3.0584 | 4054.0 | -0.00062 |
| 8 | 3.0594 | 4052.6 | 3.0587 | 4053.5 | -0.00072 |
| 9 | 3.0599 | 4051.9 | 3.0591 | 4053.0 | -0.00084 |
| 10 | 3.0605 | 4051.1 | 3.0597 | 4052.2 | -0.00080 |
| 11 | 3.0611 | 4050.3 | 3.0605 | 4051.2 | -0.00068 |
| 12 | 3.0618 | 4049.4 | 3.0613 | 4050.1 | -0.00055 |
| 13 | 3.0626 | 4048.4 | 3.0622 | 4048.9 | -0.00038 |
| 14 | 3.0634 | 4047.3 | 3.0630 | 4047.9 | -0.00044 |
| 15 | 3.0643 | 4046.2 | 3.0639 | 4046.6 | -0.00033 |
| 16 | 3.0652 | 4044.9 | 3.0651 | 4045.1 | -0.00012 |
| 17 | 3.0662 | 4043.6 | 3.0663 | 4043.5 | 0.00010 |
| 18 | 3.0672 | 4042.2 | 3.0673 | 4042.1 | 0.00011 |
| 19 | 3.0684 | 4040.8 | 3.0684 | 4040.7 | 0.00006 |
| 20 | 3.0695 | 4039.2 | 3.0699 | 4038.8 | 0.00033 |
| 21 | 3.0708 | 4037.6 | 3.0705 | 4037.9 | -0.00022 |
| 22 | 3.0720 | 4035.9 | 3.0716 | 4036.5 | -0.00045 |
| 23 | 3.0734 | 4034.1 | 3.0730 | 4034.6 | -0.00038 |
| 24 | 3.0748 | 4032.3 | 3.0744 | 4032.8 | -0.00039 |
| 25 | 3.0763 | 4030.4 | 3.0758 | 4031.0 | -0.00053 |
| 26 | 3.0778 | 4028.3 | 3.0774 | 4028.9 | -0.00042 |
| 27 | 3.0794 | 4026.3 | 3.0790 | 4026.8 | -0.00043 |
| 28 | 3.0811 | 4024.1 | 3.0807 | 4024.6 | -0.00038 |
| 29 | 3.0828 | 4021.9 | 3.0825 | 4022.3 | -0.00032 |
| 30 | 3.0846 | 4019.6 | 3.0843 | 4019.9 | -0.00026 |
| 31 | 3.0864 | 4017.2 | 3.0862 | 4017.5 | -0.00023 |
| 32 | 3.0883 | 4014.7 | 3.0881 | 4014.9 | -0.00013 |
| 33 | 3.0902 | 4012.2 | 3.0902 | 4012.2 | -0.00004 |
| 34 | 3.0922 | 4009.6 | 3.0922 | 4009.6 | -0.00001 |
| 35 | 3.0943 | 4006.9 | 3.0943 | 4006.9 | -0.00003 |
| 36 | 3.0965 | 4004.1 | 3.0964 | 4004.2 | -0.00005 |
| 37 | 3.0986 | 4001.3 | 3.0986 | 4001.4 | -0.00007 |

Figure Captions

Figure 1. The orbitsphere is a two dimensional spherical shell with the Bohr radius of the hydrogen atom.

Figure 2. The current pattern of the orbitsphere from the perspective of looking along the z-axis. The current and charge density are confined to two dimensions at $r_n = nr_1$. The corresponding charge density function is uniform.

Figure 3. The orbital function modulates the constant (spin) function (shown for $t = 0$; cross-sectional view).

Figure 4. The magnetic field of an electron orbitsphere.

Figure 5. Continuum absorption coefficient (per particle) in the solar atmosphere showing a discontinuity at $1.645 \mu\text{m}$, the wavelength corresponding to the ordinary hydride ion H^- ionization energy, and the bound-free continuum of H^- at shorter wavelengths.

Figure 6. The experimental set up comprising a filament gas cell light source and an EUV spectrometer which was differentially pumped.

Figure 7. The EUV spectrum (900–1300 Å) of the cell emission of a control hydrogen glow discharge.

Figure 8. The EUV spectrum (900–1300 Å) of the potassium rt-plasma cell emission. The increase in intensity at 1100 Å compared to hydrogen emission alone was assigned to a contribution from $H^-(1/4)$. The Lyman β to α ratio was also very high—1.3 versus 0.13 for the control.

Figure 9. The 6562 Å Balmer α line width recorded with a high resolution (± 0.06 Å) visible spectrometer on a rt-plasma formed with K^+/K^+ catalyst. Significant broadening was observed corresponding to an average hydrogen atom temperature of 17 eV.

Figure 10. The 6562 Å Balmer α line width recorded with a high resolution (± 0.06 Å) visible spectrometer on a rt-plasma formed with Rb^+ catalyst from $RbNO_3$. Significant broadening was observed corresponding to an average hydrogen atom temperature of 9 eV.

Figure 11. The high resolution visible spectrum in the region of 4000 Å to 4060 Å recorded on the emission of a control hydrogen glow discharge plasma. Only weak hydrogen molecular peaks were observed.

Figure 12. The high resolution visible spectrum in the region of

4060 Å to 4090 Å recorded on the emission of a control hydrogen glow discharge plasma. Only weak hydrogen molecular peaks were observed.

Figure 13. The high resolution visible spectrum in the region of 4000 Å to 4090 Å recorded on the emission of a rt-plasma formed with K^+/K^+ catalyst from vaporized KNO_3 . The $H^-(1/2)$ hydride ion with a predicted binding energy of 3.0468 eV was observed as a broad peak at 4070.0 Å with a FWHM of 1.4 Å. An observed inverse Rydberg-type series of broad emission lines that converged at increasing wavelengths and terminated at about 3.0575 eV—the hydride spin-pairing energy plus the binding energy—matched the theoretical hyperfine energies E_{HF} given by $E_{HF} = j^2 3.0056 \times 10^{-5} + 3.0575 \text{ eV}$ for $j=1$ to $j=37$ as given in Table 2. Other peaks in the rt-plasma that partially covered some of the hyperfine peaks were assigned to K I and molecular hydrogen.

Figure 14. The 4000 Å to 4060 Å region of the Figure 13 spectrum to show an expanded view of the $H^-(1/2)$ emission hyperfine lines. Other peaks in the rt-plasma that partially covered some of the hyperfine peaks were assigned to K I and molecular hydrogen.

Figure 15. The 4060 Å to 4090 Å region of the Figure 13 spectrum to show an expanded view of the $H^-(1/2)$ binding energy emission. Other peaks in the rt-plasma were assigned to molecular hydrogen.

Figure 16. The high resolution visible spectrum in the region of 4000 Å to 4090 Å recorded on the emission of a rt-plasma formed with Rb^+ catalyst from vaporized $RbNO_3$. The $H^-(1/2)$ hydride ion with a predicted binding energy of 3.0468 eV was observed as a broad peak at 4070.0 Å with a FWHM of 1.4 Å. An observed inverse Rydberg-type series of broad emission lines that converged at increasing wavelengths and terminated at about 3.0575 eV—the hydride spin-pairing energy plus the binding energy—matched the theoretical hyperfine energies E_{HF} given by $E_{HF} = j^2 3.0056 \times 10^{-5} + 3.0575 \text{ eV}$ for $j=1$ to $j=37$ as given in Table 2. Other peaks in the rt-plasma were assigned to molecular hydrogen.

Figure 17. The 4000 Å to 4060 Å region of the Figure 16 spectrum to show an expanded view of the $H^-(1/2)$ emission hyperfine lines. Other peaks in the rt-plasma were assigned to molecular hydrogen.

Figure 18. The 4060 Å to 4090 Å region of the Figure 16 spectrum to show an expanded view of the $H^-(1/2)$ binding energy emission. Other peaks in the rt-plasma were assigned to Rb II and molecular hydrogen.

Figure 19. The three matching EUV spectra (4000-4060 Å) of Rb^+ rt-plasmas that were equivalent to the spectrum shown in Figure 17.

Figure 20. The plot of the theoretical hyperfine energies E_{HF} given by $E_{HF} = j^2 3.0056 \times 10^{-5} + 3.0575 \text{ eV}$ (Eq. (47)) for $j=1$ to $j=37$ and the energies observed for the inverse Rydberg-type series of broad emission lines shown in Figure 17 as given in Table 2. The agreement was remarkable.

Figure 21. (A) The 1H MAS NMR spectrum of KH^*Cl relative to external tetramethylsilane (TMS). The resonance at 1.3 ppm was assigned to ordinary hydride ion. The large distinct upfield resonance at -4.4 identifies a hydride ion (H^*) with a substantially smaller radius as compared with ordinary hydride since a smaller radius increases the shielding or diamagnetism, and it was assigned to a novel hydride ion of KH^*Cl . (B) The 1H MAS NMR spectrum of the control comprising an equal molar mixture of KH and KCl relative to external tetramethylsilane (TMS). Ordinary hydride ion has a resonance at 1.1 ppm and 0.8 ppm in the KH/KCl mixture and in KH . The presence of KCl does not shift the resonance of ordinary hydride as shown in Figure 21C. (C) The 1H MAS NMR spectrum of the control KH relative to external tetramethylsilane (TMS).

Fig. 1

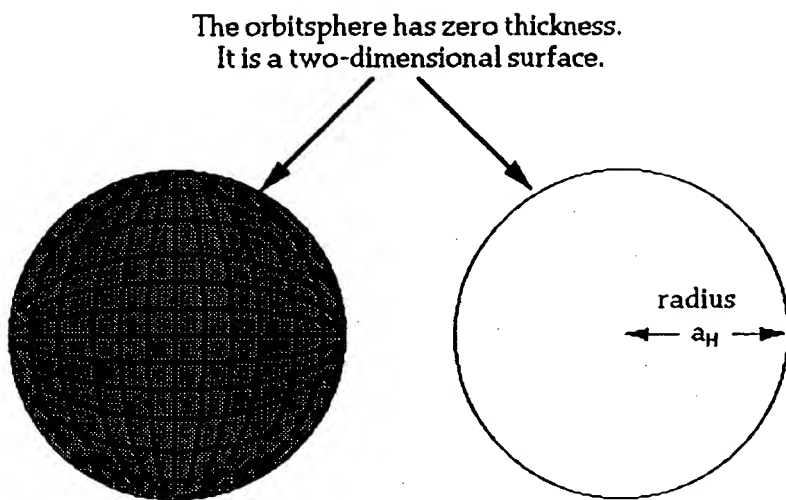


Fig. 2

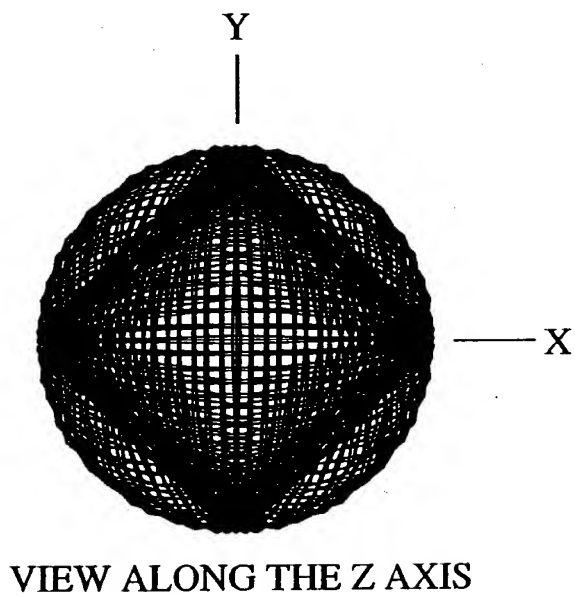


Fig. 3

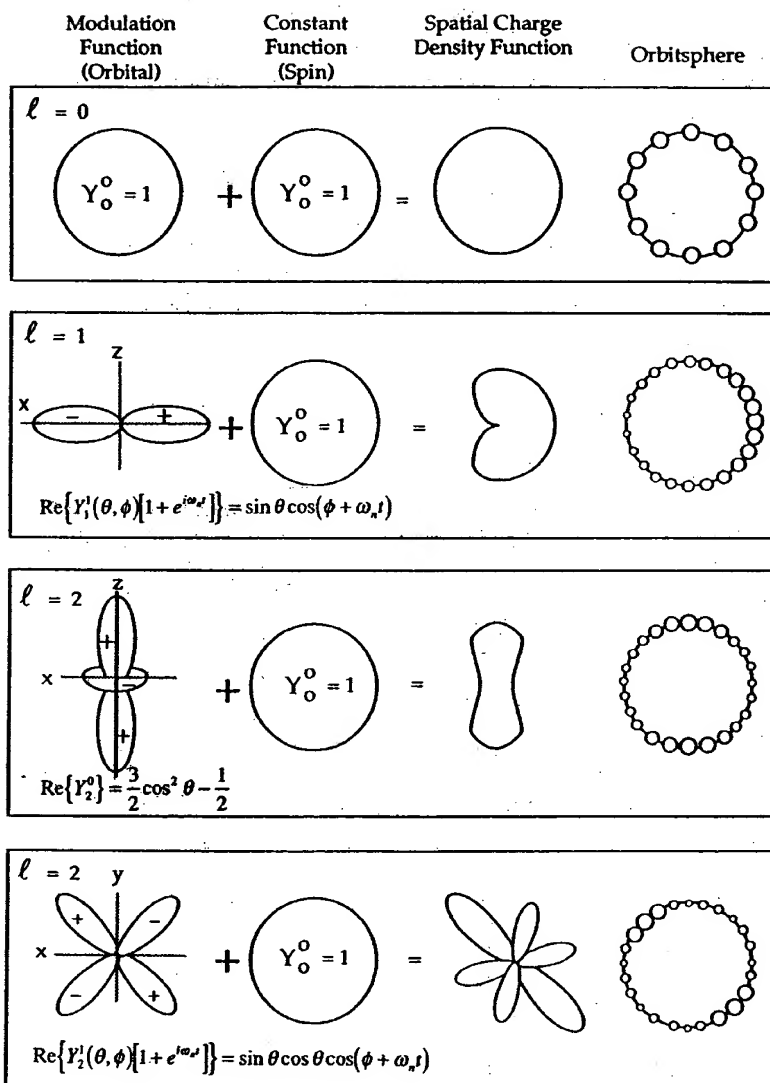
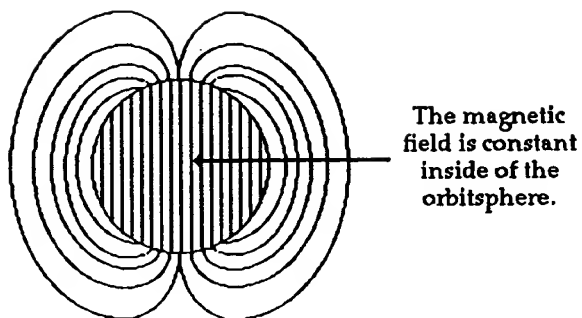


Fig. 4



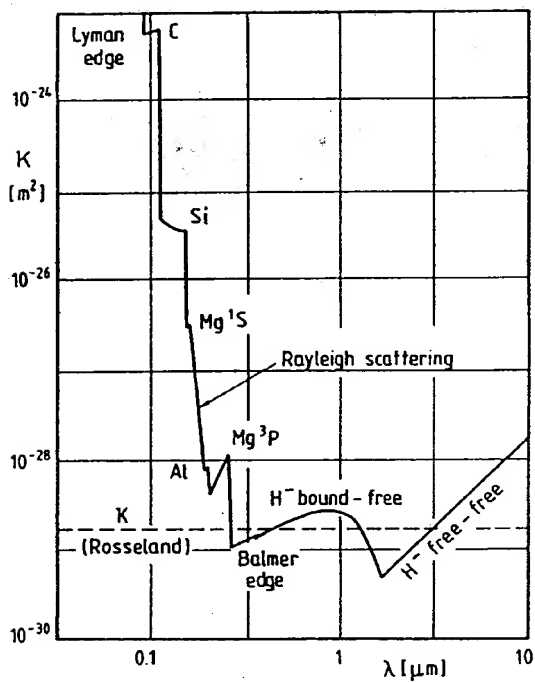


Fig. 5

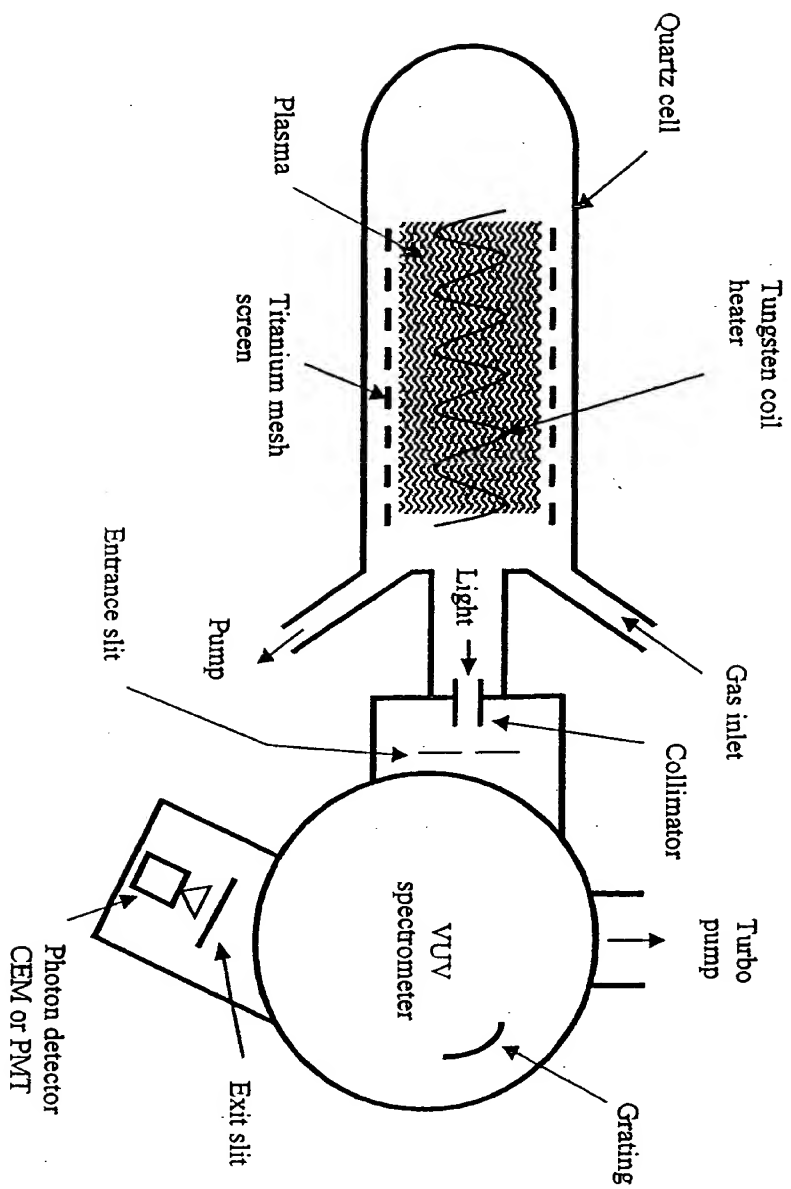


Fig. 6

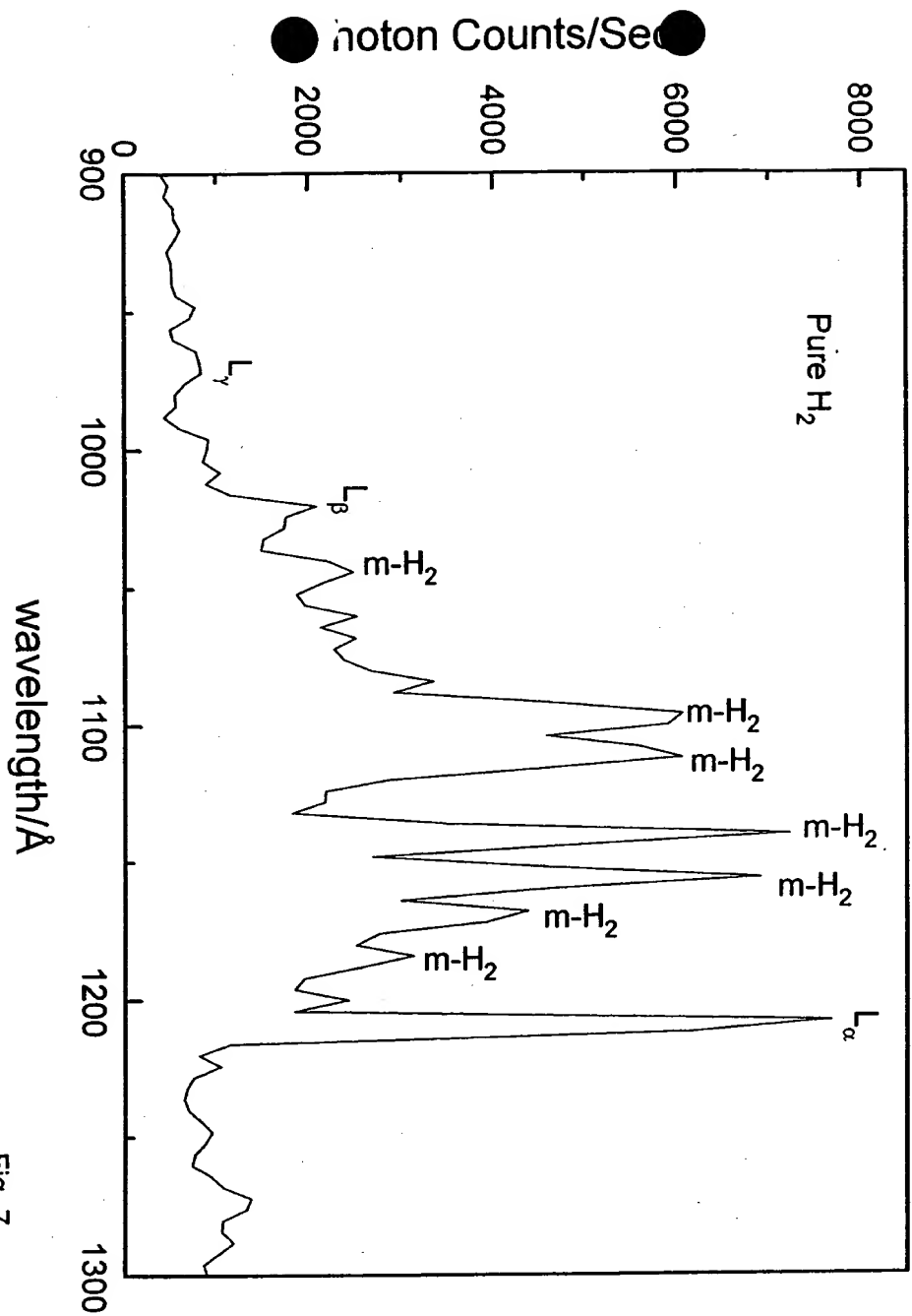


Fig. 7

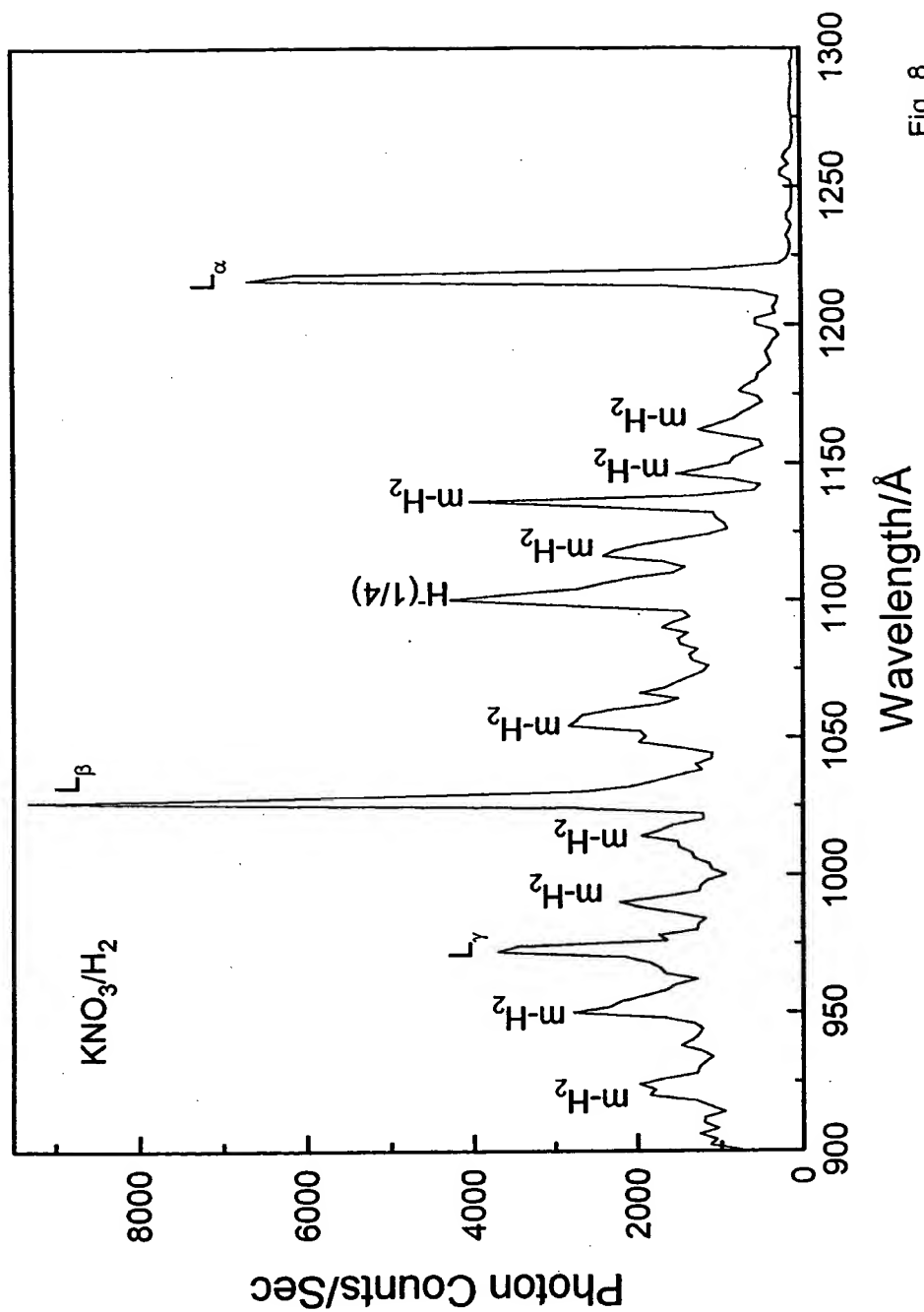


Fig. 8

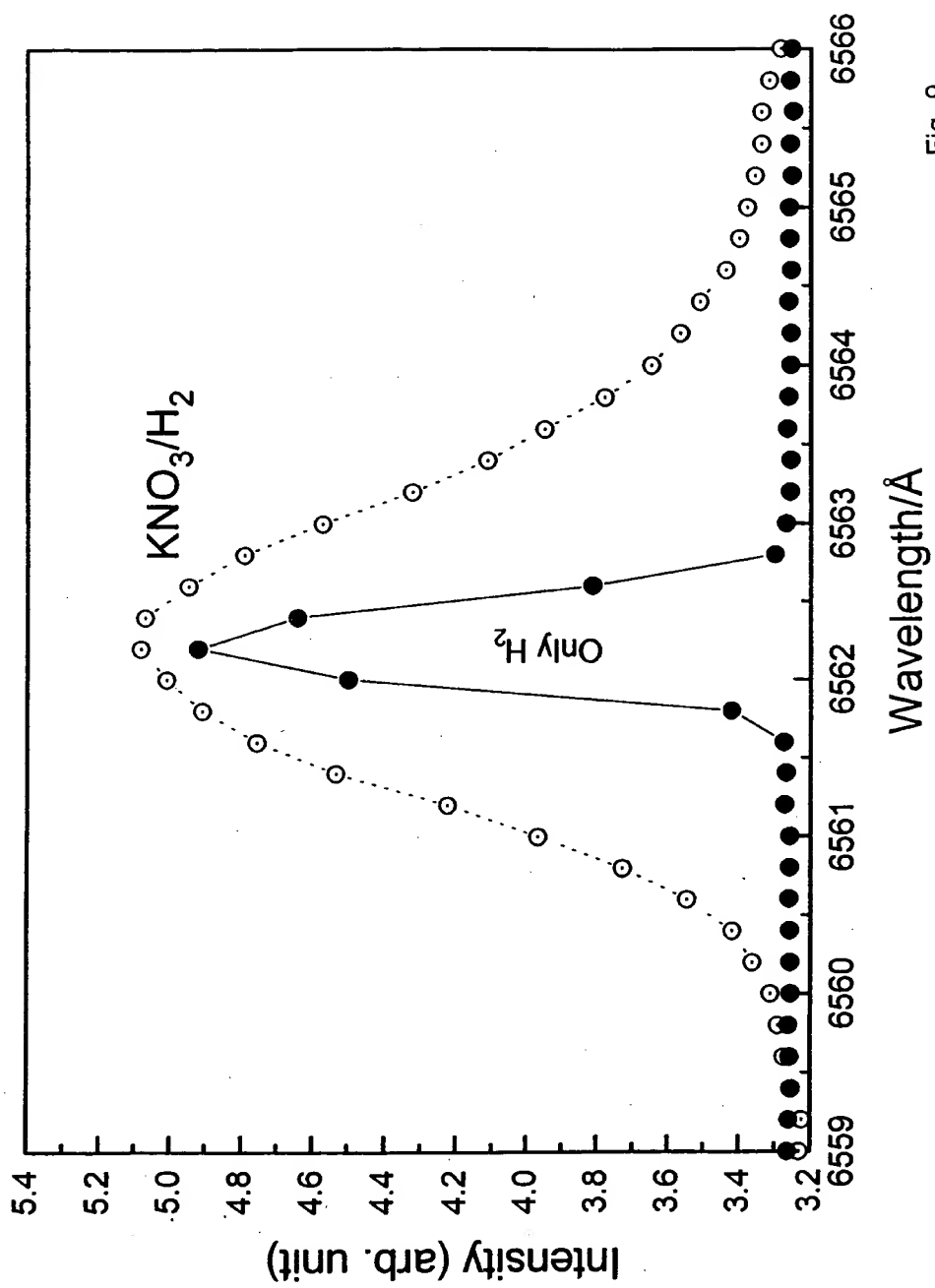


Fig. 9

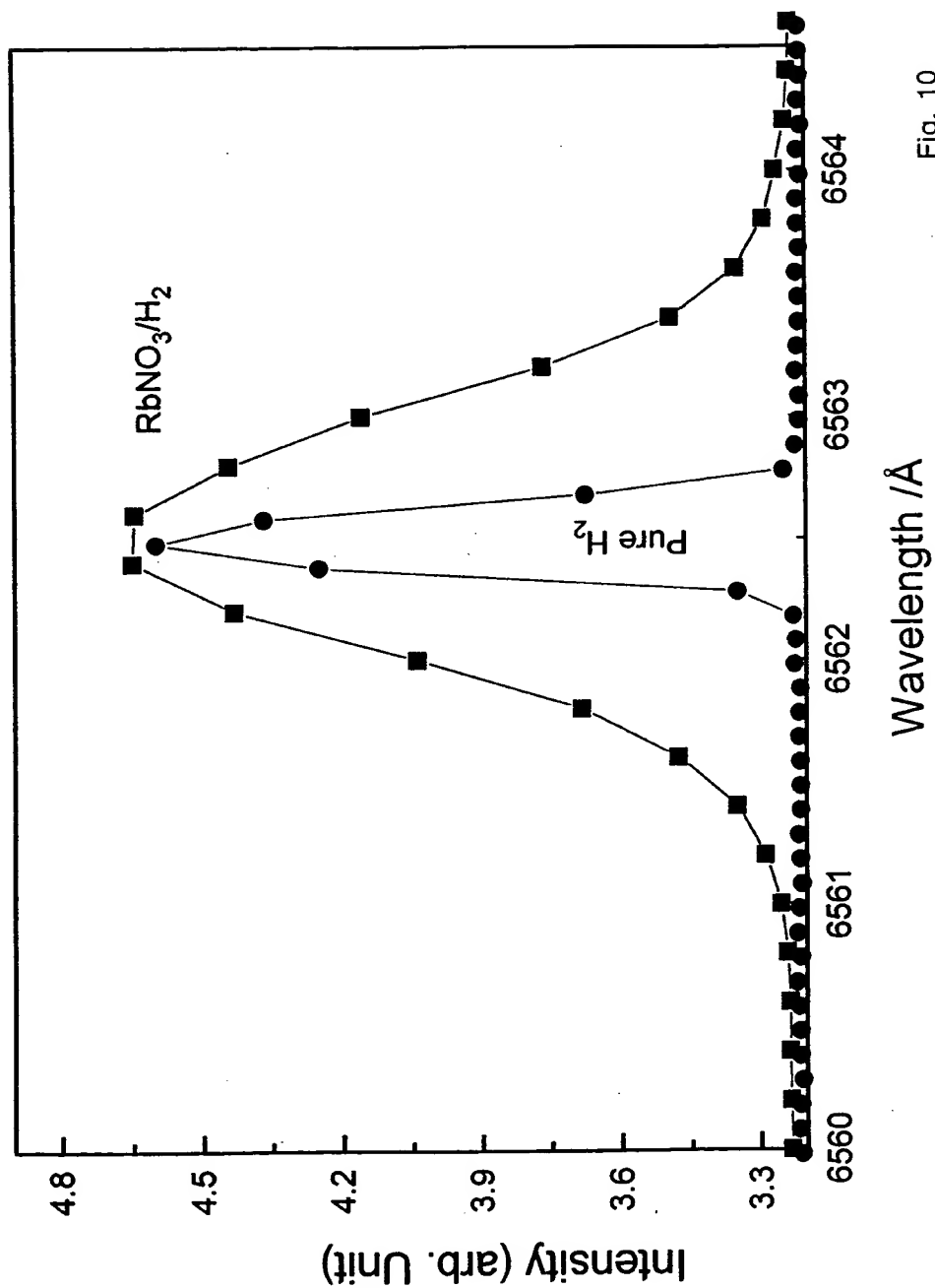


Fig. 10

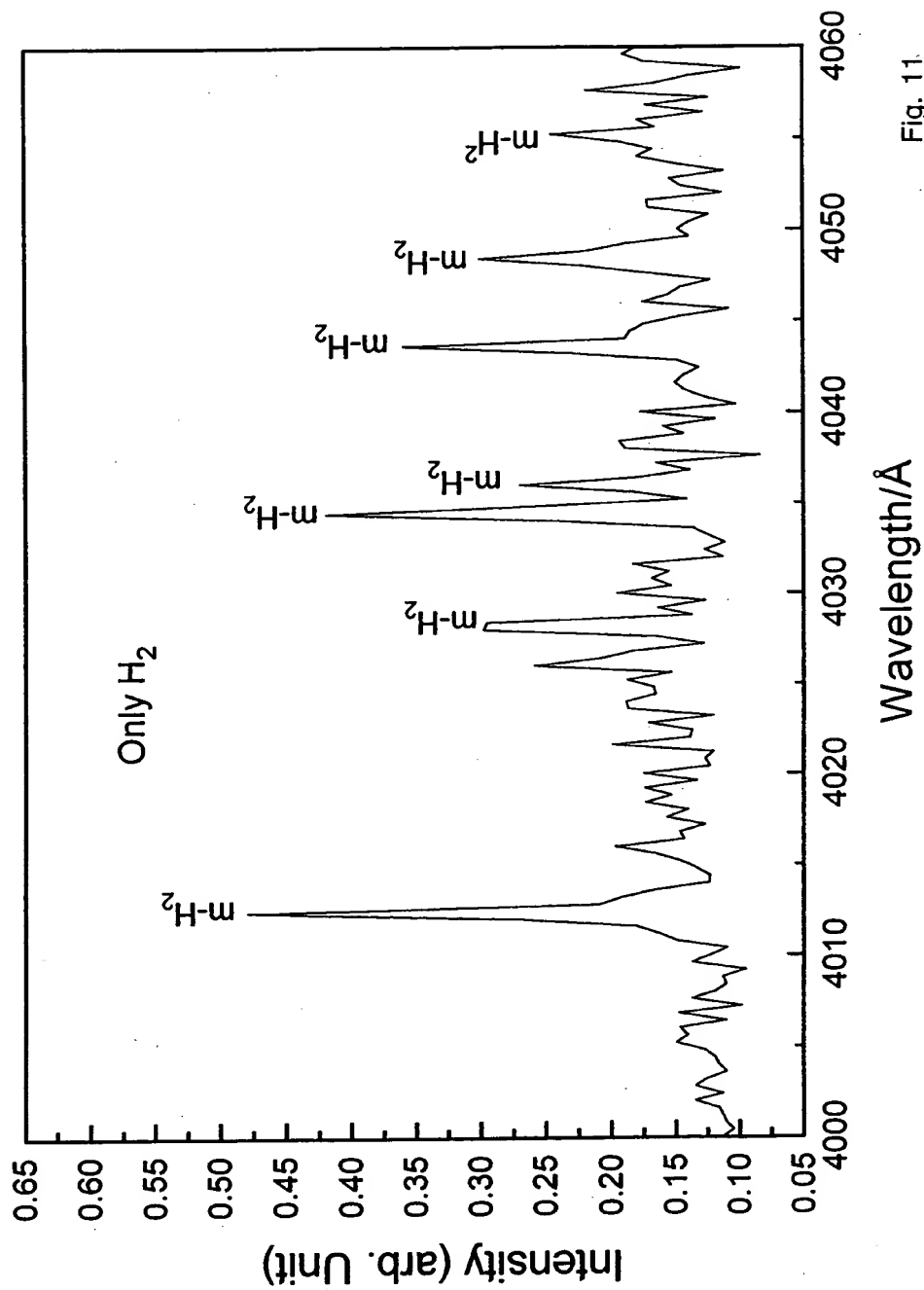


Fig. 11.

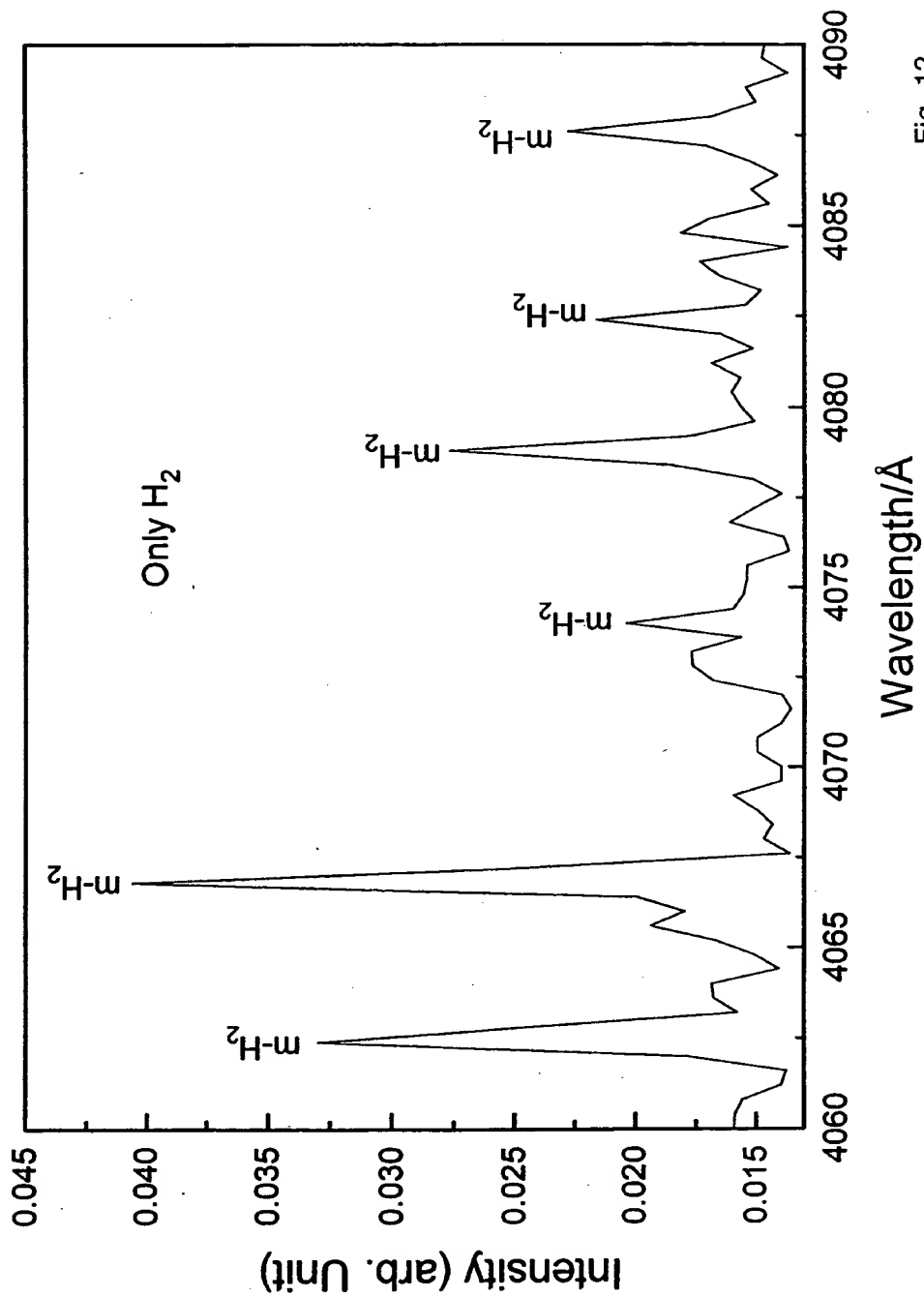


Fig. 12

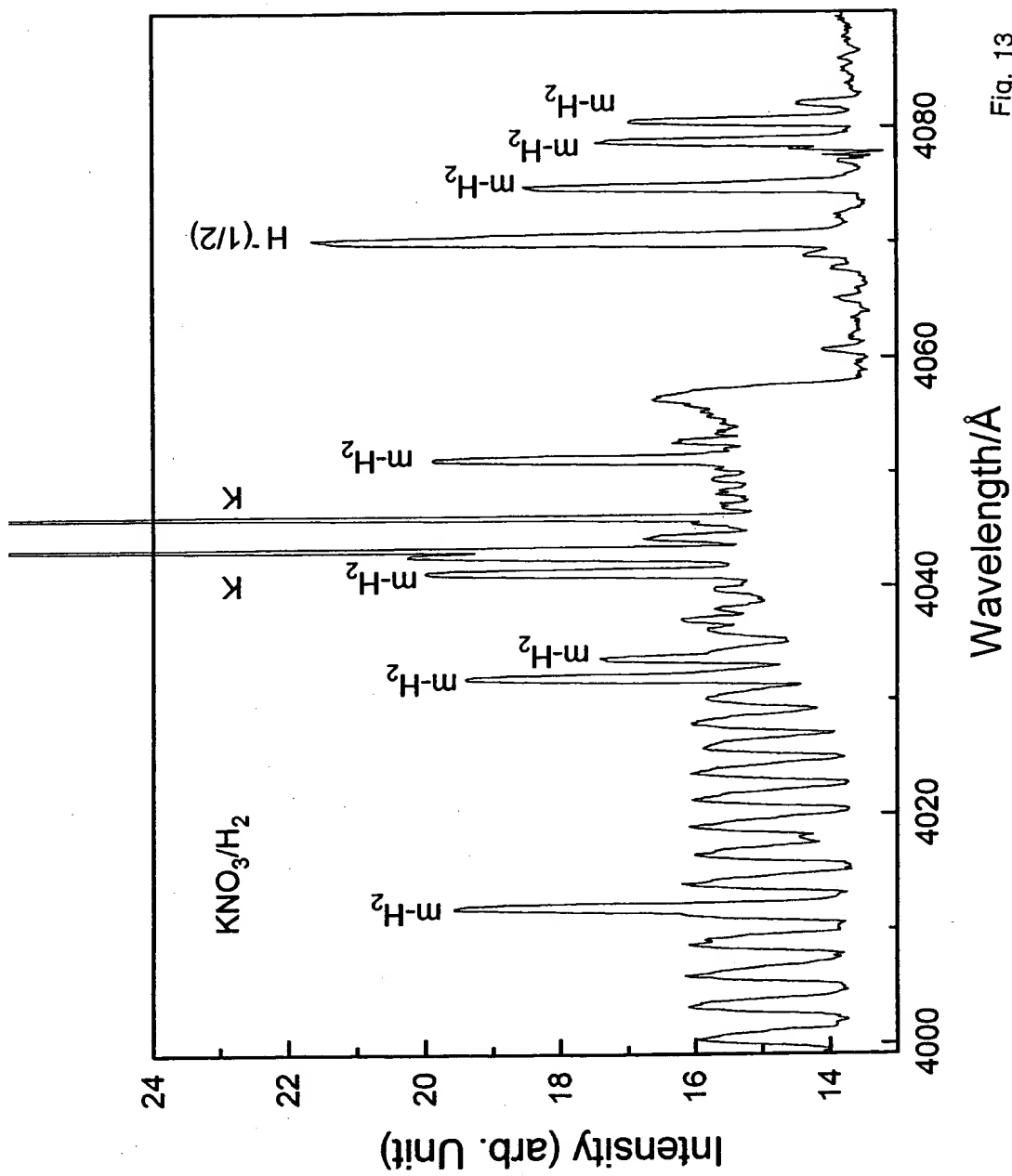


Fig. 13

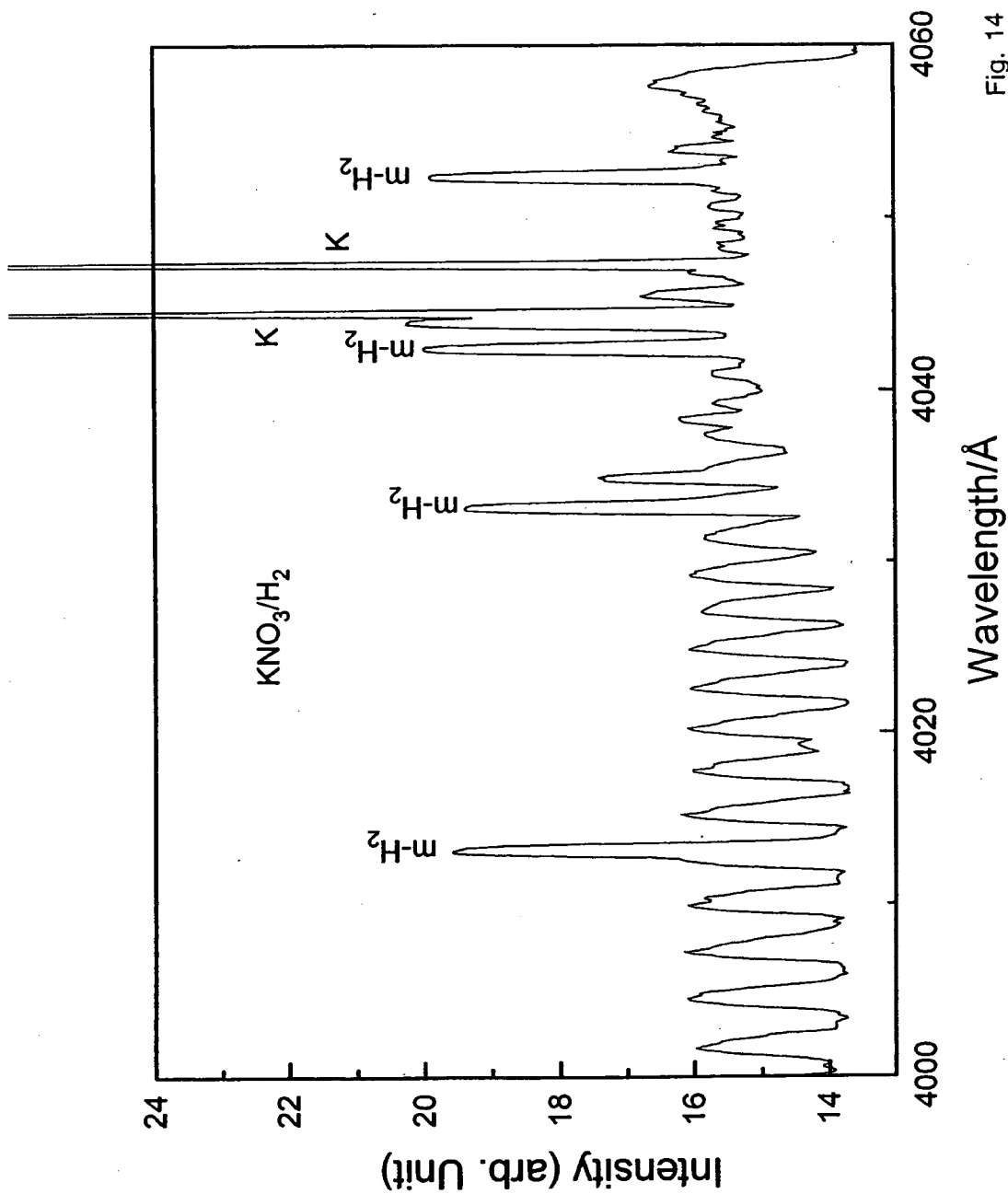


Fig. 14

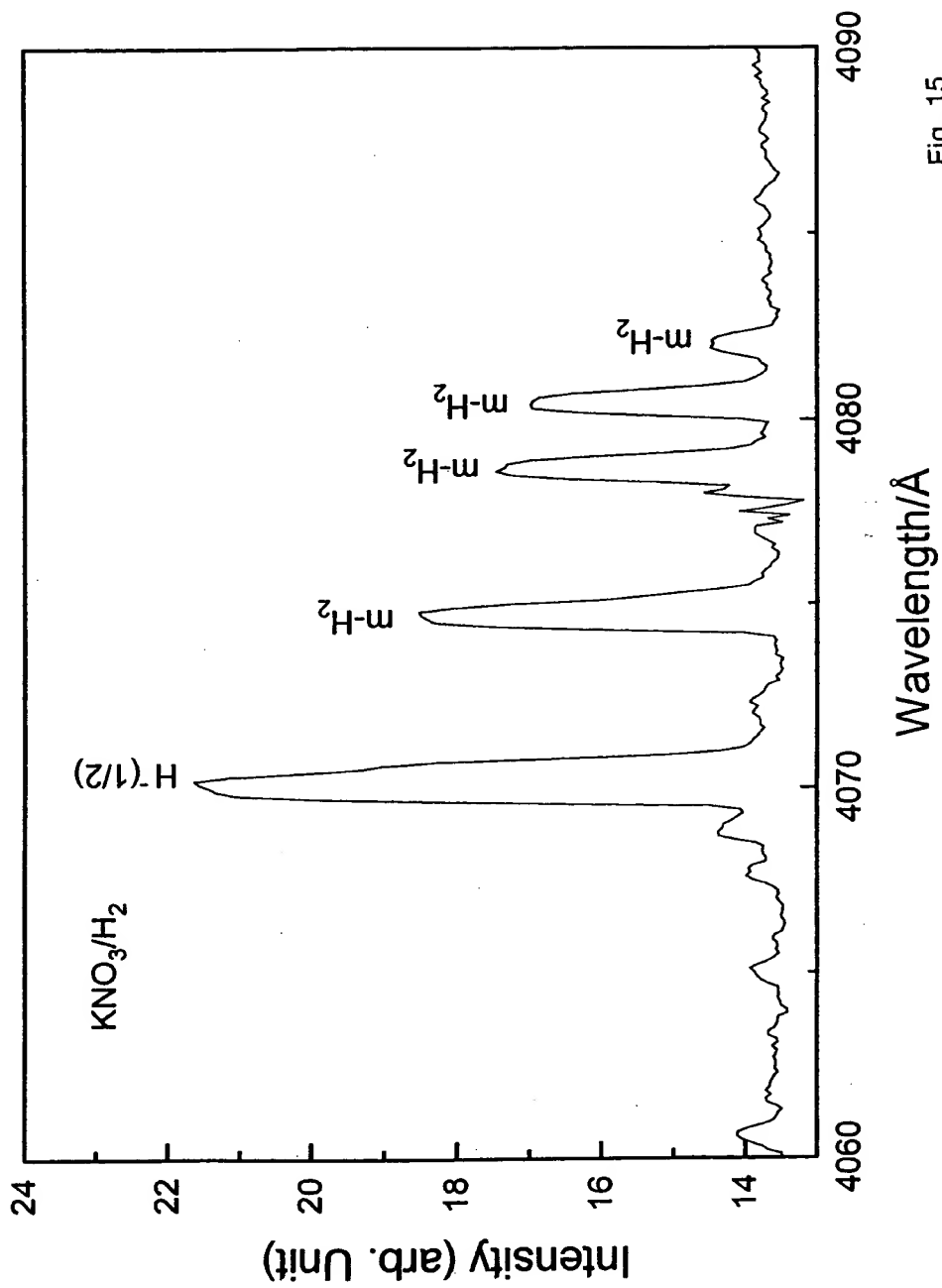
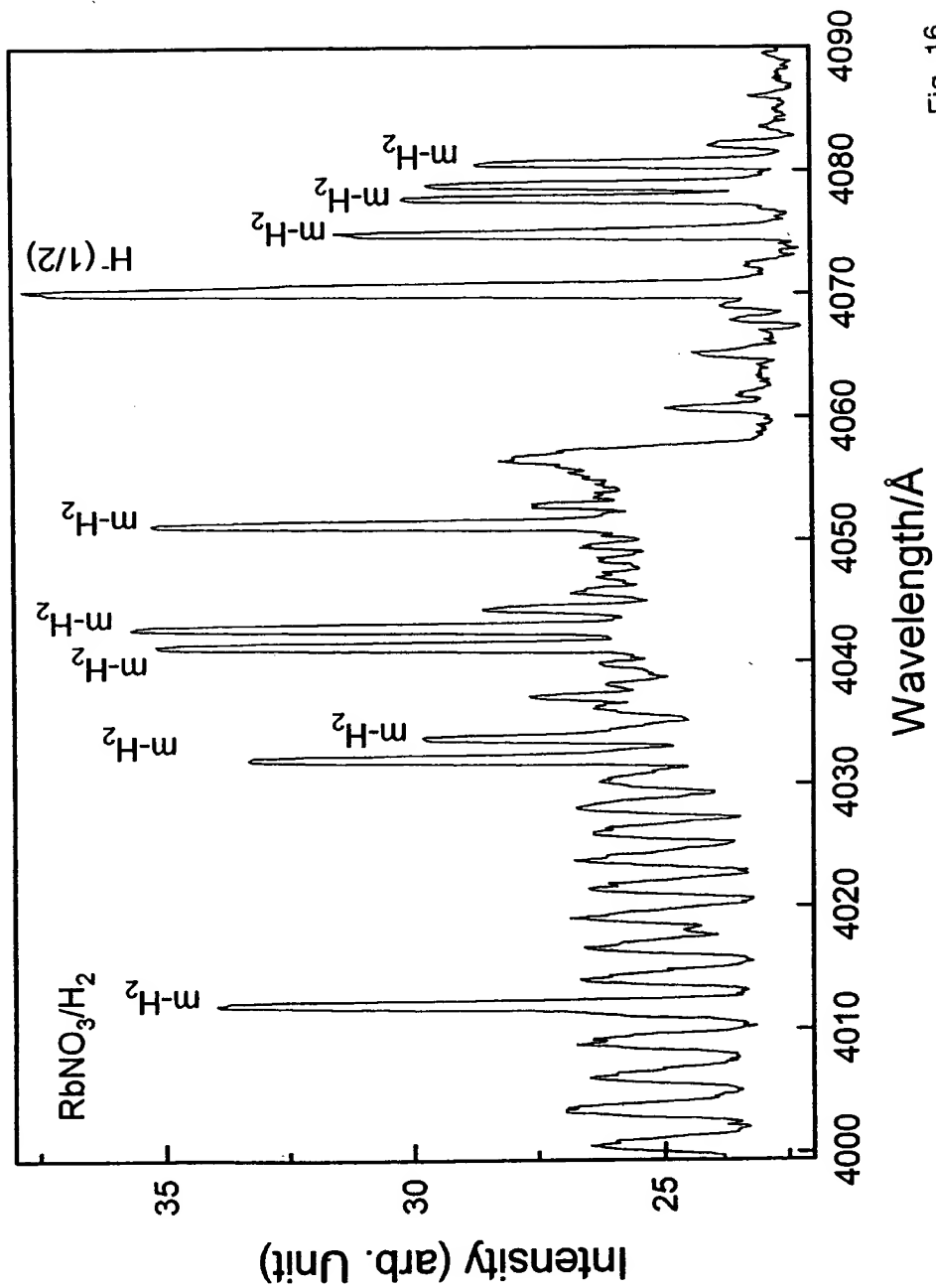


Fig. 15



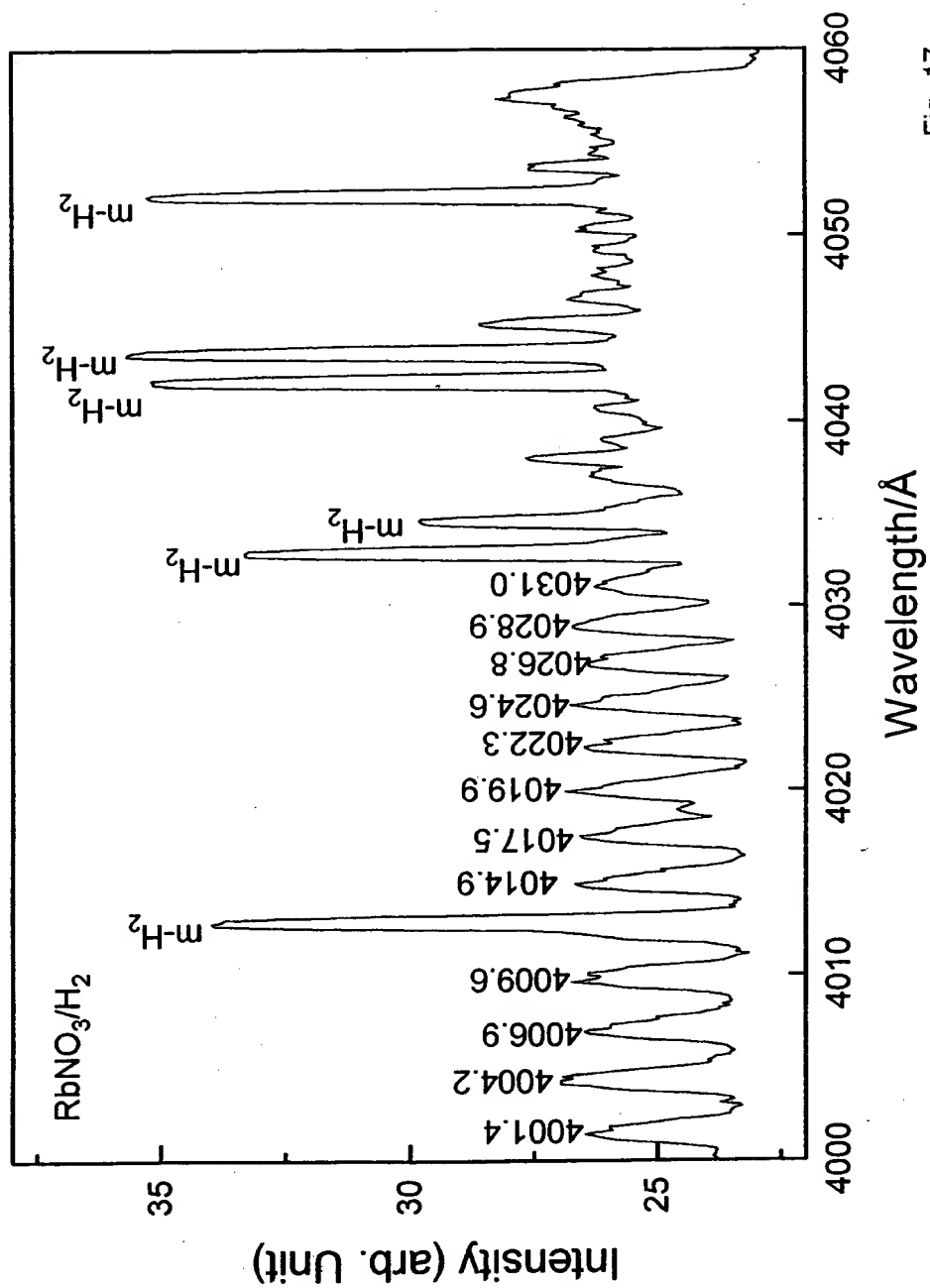


Fig. 17

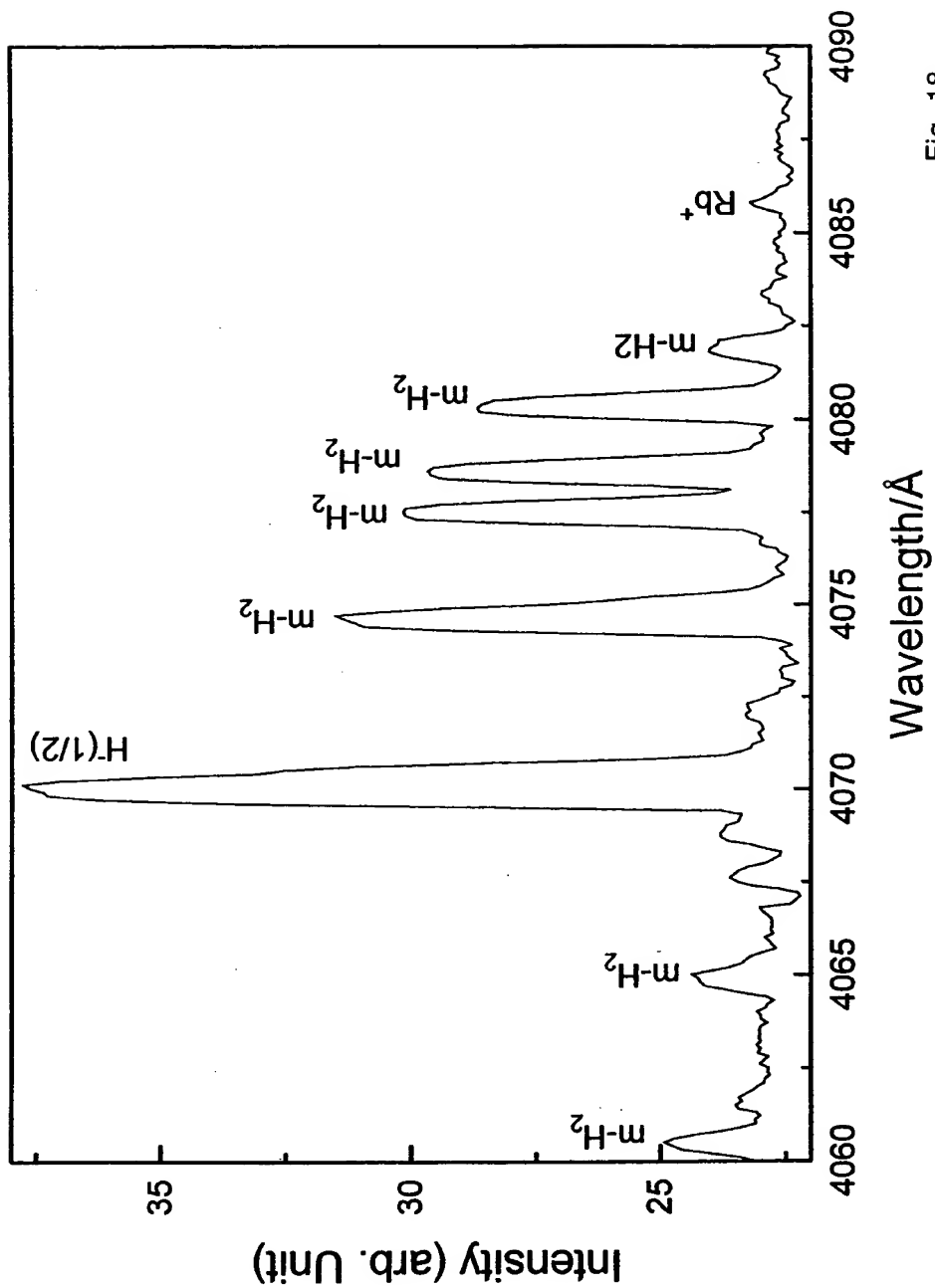


Fig. 18

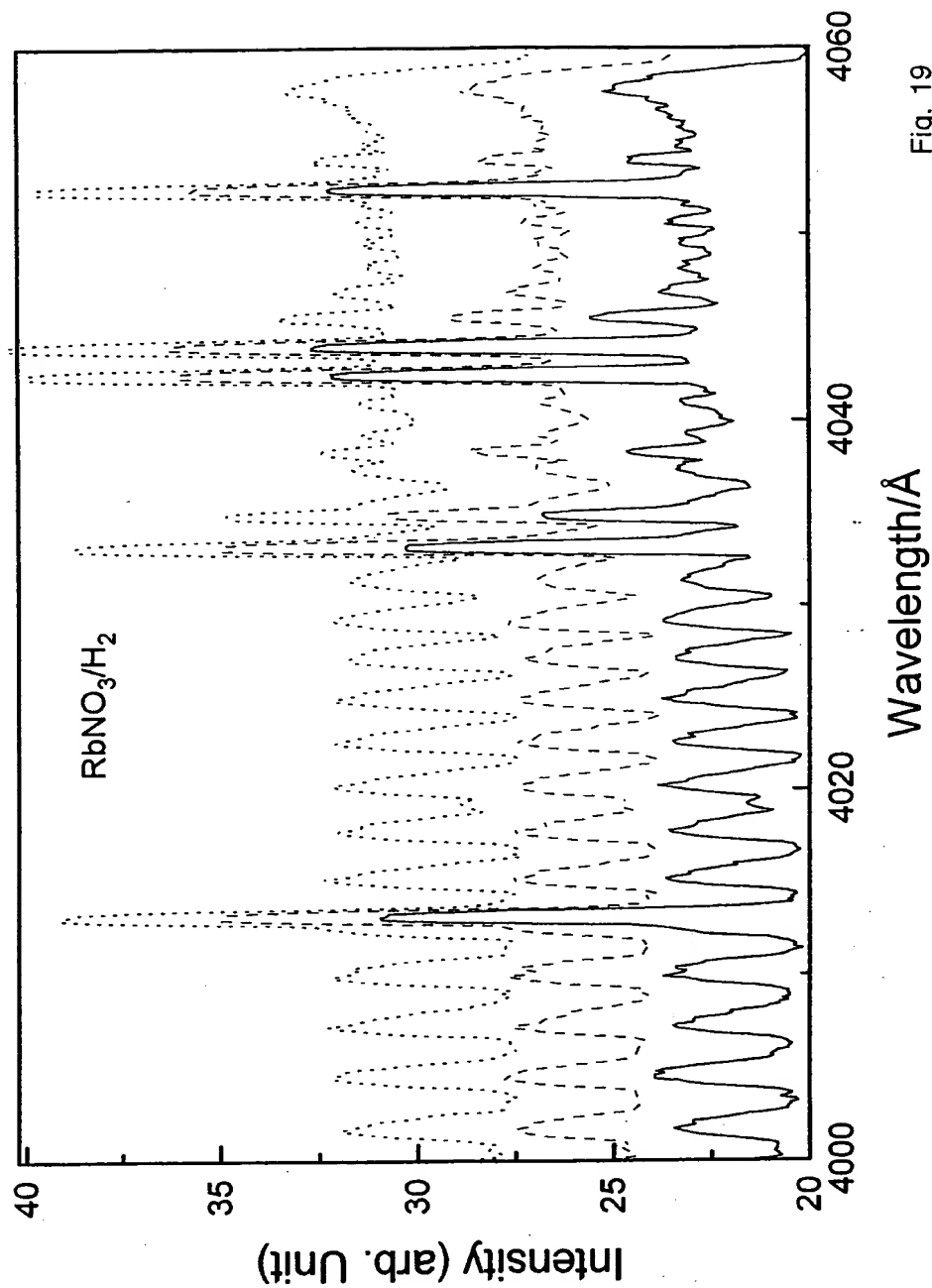
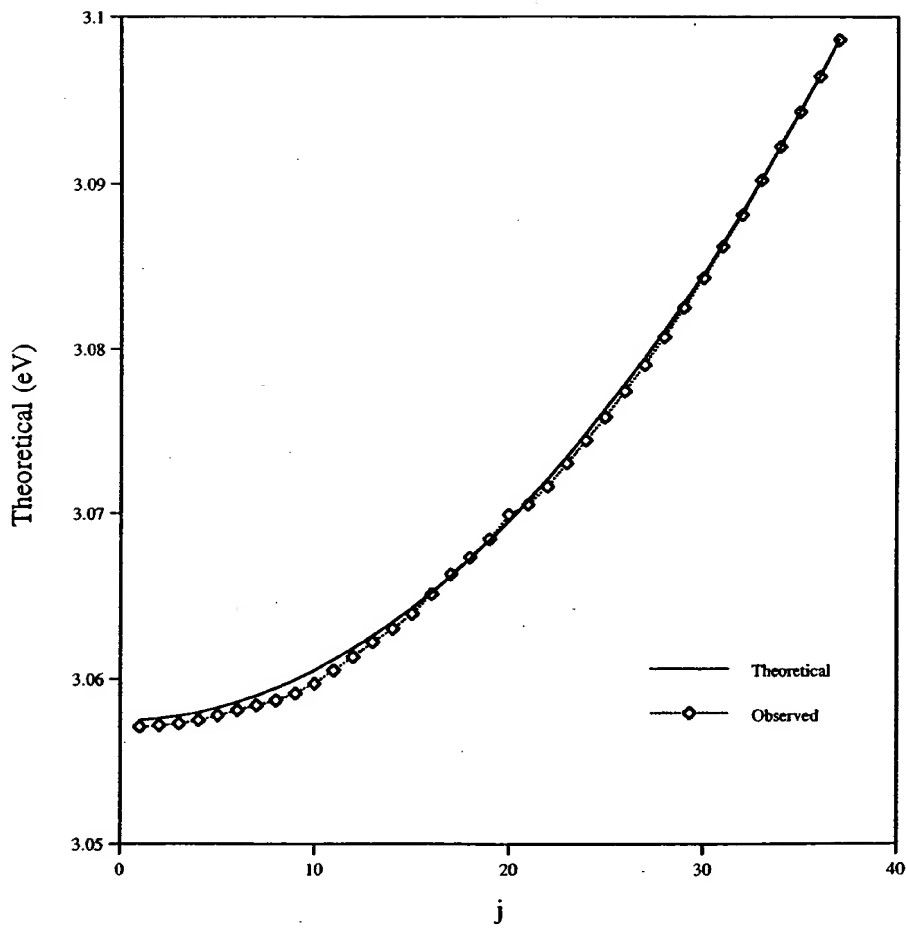


Fig. 19

Figure 20



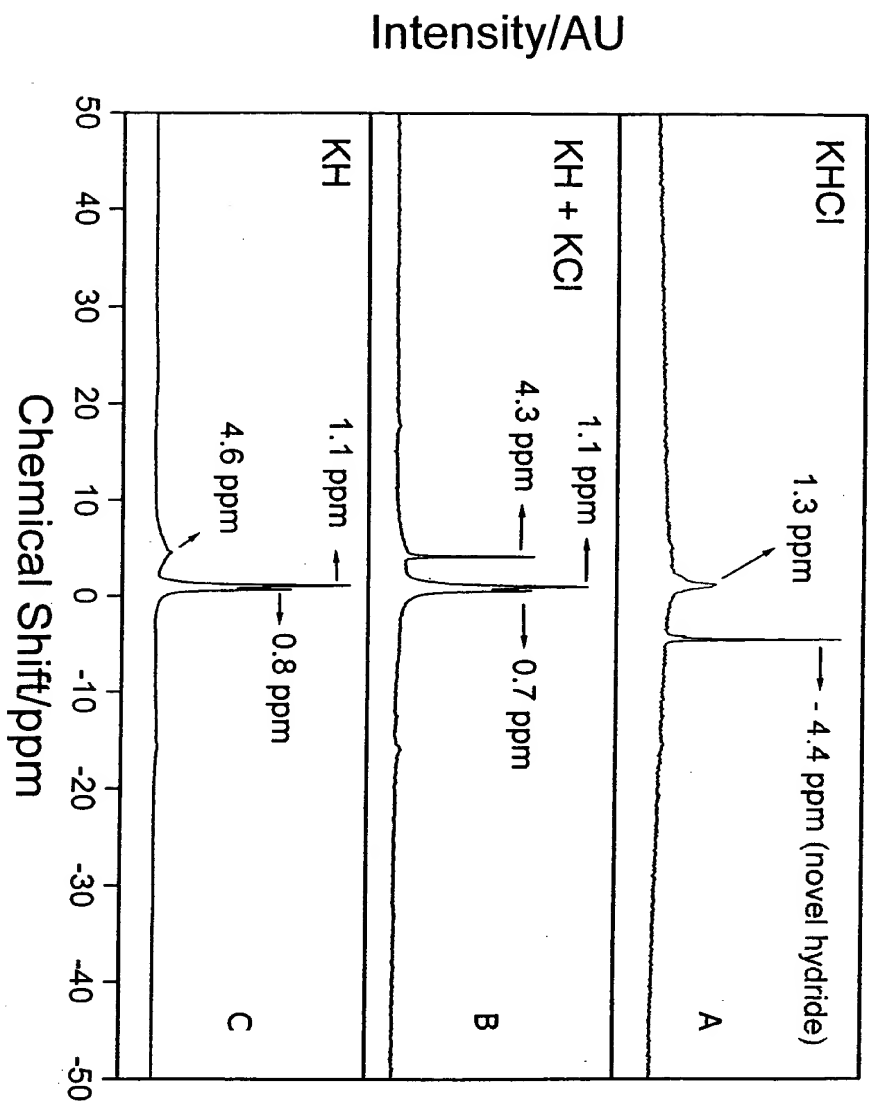


Fig. 21

THIS PAGE BLANK (USPTO)

Novel Alkali and Alkaline Earth Hydrides for High Voltage and High Energy Density Batteries

Randell Mills and Ethirajulu Dayalan
BlackLight Power, Inc., 493 Old Trenton Road, Cranbury, NJ 08512

ABSTRACT

BlackLight Power, Inc. (BLP) of Cranbury, New Jersey, is developing a revolutionary technology based on novel hydrogen chemistry. More explicitly, energy is catalytically released as the electrons of atomic hydrogen are induced to undergo transitions to lower energy levels corresponding to fractional quantum numbers with the production of plasma, light, and novel hydrogen compounds (*I-35*). The Company uses a chemically generated or assisted plasma to form atomic hydrogen and a catalyst which react through a nonradiative energy transfer to form lower-energy hydrogen atoms called hydrinos. Since hydrinos have energy levels much lower than uncatalyzed hydrogen atoms, the energy release is intermediate between chemical and nuclear energies. The net enthalpy released may be over several hundred times that of combustion. Thus, the catalysis of atomic hydrogen represents a new source of energy with H_2O as the source of hydrogen fuel obtained by diverting a fraction of the output energy of the process to split water into its elemental constituents. Moreover, rather than air pollutants or radioactive waste, the products are novel compounds having hydride ions with increased binding energies that may be the basis of a high voltage battery. Such a high voltage battery would have the advantages of much greater power and much higher energy density where the limitations of battery chemistry attributed to the binding energy of the anion of the oxidant are addressed. The concept of our novel hydride battery and some preliminary results will be discussed during the presentation.

THEORY AND INTRODUCTION

J. J. Balmer showed in 1885 that the frequencies for some of the lines observed in the emission spectrum of atomic hydrogen could be expressed with a completely empirical relationship. This approach was later extended by J. R. Rydberg, who showed that all of the spectral lines of atomic hydrogen were given by the equation:

$$\frac{1}{\nu} = R \left(\frac{1}{n_f^2} - \frac{1}{n_i^2} \right) \quad (1)$$

where

$$R = 109,677 \text{ cm}^{-1}, n_f = 1, 2, 3, \dots, n_i = 2, 3, 4, \dots, \text{ and } n_i > n_f.$$

Niels Bohr, in 1913, developed a theory for atomic hydrogen that gave the energy levels in agreement with Rydberg's equation. An identical equation, based on a totally different theory for the hydrogen atom, was developed by E. Schrödinger, and independently by W. Heisenberg, in 1926.

$$E_n = -\frac{e^2}{n^2 8 \pi \epsilon_0 a_H} = -\frac{13.598 \text{ eV}}{n^2} \quad (2a)$$

$$n = 1, 2, 3, \dots \quad (2b)$$

where a_H is the Bohr radius for the hydrogen atom (52.947 pm), e is the magnitude of the charge of the electron, and ϵ_0 is the vacuum permittivity.

The excited energy states of atomic hydrogen are given by Eq. (2a) for $n > 1$ in Eq. (2b). The $n = 1$ state is the "ground" state for "pure" photon transitions (the $n = 1$ state can absorb a photon and go to an excited electronic state, but it cannot release a photon and go to a lower-energy electronic state). However, an electron transition from the ground state to a lower-energy state may be possible by a nonradiative energy transfer such as multipole coupling or a resonant collision mechanism. Processes such as hydrogen molecular bond formation that occur without photons and that require collisions are common (36). Also, some commercial phosphors are based on resonant nonradiative energy transfer involving multipole coupling (37).

We propose that atomic hydrogen may undergo a catalytic reaction with certain atomized elements and ions which singly or multiply ionize at integer multiples of the potential energy of atomic hydrogen, $m \cdot 27.2 \text{ eV}$ wherein m is an integer. The theory and supporting data was given previously (*I-35*). The reaction involves a nonradiative energy transfer to form a hydrogen atom that is lower in energy than unreacted atomic hydrogen that corresponds to a fractional principal quantum number. That is

$$n = \frac{1}{2}, \frac{1}{3}, \frac{1}{4}, \dots, \frac{1}{p}; p \text{ is an integer} \quad (2c)$$

replaces the well known parameter $n = \text{integer}$ in the Rydberg equation for hydrogen excited states. The $n=1$ state of hydrogen and the $n = \frac{1}{\text{integer}}$ states of hydrogen are nonradiative, but a transition between two nonradiative states

is possible via a nonradiative energy transfer, say $n=1$ to $n=1/2$. In these cases, during the transition the electron couples to another electron transition, electron transfer reaction, or inelastic scattering reaction which can absorb the exact amount of energy that must be removed from the hydrogen atom to cause the transition. Thus, a catalyst provides a net positive enthalpy of reaction of $m \cdot 27.2 \text{ eV}$ (i.e. it absorbs $m \cdot 27.2 \text{ eV}$ where m is an integer). Certain atoms or ions serve as catalysts which resonantly accept the nonradiative energy transfer from hydrogen atoms and release the energy to the surroundings to affect electronic transitions to fractional quantum energy levels. As a consequence of the nonradiative energy transfer, the hydrogen atom becomes unstable and emits further energy until it achieves a lower-energy nonradiative state having a principal energy level given by Eqs. (2a) and (2c).

EXPERIMENTAL OBSERVATIONS

A number of independent experimental observations lead to the conclusion that atomic hydrogen can exist in fractional quantum states that are at lower energies than the traditional "ground" ($n=1$) state. Prior related studies that support the possibility of a novel reaction of atomic hydrogen which produces a chemically generated or assisted plasma (rt-plasma) and produces novel hydride compounds include extreme ultraviolet (EUV) spectroscopy (6-9, 11-15, 17, 18, 21-23), characteristic emission from catalysis and the hydride ion products (9-13), lower-energy hydrogen emission (4, 6, 7-8, 17), plasma formation (9, 11-13, 21-22, 24-25), Balmer α line broadening (7, 9, 14, 15, 17-19), elevated electron temperature (7, 18), anomalous plasma afterglow duration (24, 25), power generation (7, 9, 14-17, 19-21, 32), and analysis of chemical compounds (26-32). Exemplary studies include:

- 1) the observation of intense extreme ultraviolet (EUV) emission at low temperatures (e.g. $\approx 10^3 \text{ K}$) from atomic hydrogen and only those atomized elements or gaseous ions which provide a net enthalpy of reaction of approximately $m \cdot 27.2 \text{ eV}$ via the ionization of t electrons to a continuum energy level where t and m are each an integer (e.g. K , Cs , and Sr atoms and Rb^+ ion ionize at integer multiples of the potential energy of atomic hydrogen and caused emission; whereas, the chemically similar atoms, Na , Mg , and Ba , do not ionize at integer multiples of the potential energy of atomic hydrogen and caused no emission) (9, 11-13, 21, 22, 24, 25),
- 2) the observation of novel EUV emission lines from microwave and glow discharges of helium with 2% hydrogen with energies of $q \cdot 13.6 \text{ eV}$ where $q = 1, 2, 3, 4, 6, 7, 8, 9, 11, 12$ or these lines inelastically scattered by helium atoms in the excitation of $He(1s^2)$ to $He(1s^1 2p^1)$ that were identified as hydrogen transitions to electronic energy levels below the "ground" state corresponding to fractional quantum numbers as shown in Figure A(6, 7, 17),

- 3) the observation of novel EUV emission lines from microwave and glow discharges of helium with 2% hydrogen at 44.2 nm and 40.5 nm with energies of of

$$q \cdot 13.6 + \left(\frac{1}{n_f} - \frac{1}{n_i} \right) \cdot 13.6 \text{ eV} \quad \text{where } q=2 \quad \text{and}$$

$n_f = 2, 4, \quad n_i = \infty$ that corresponded to multipole coupling to give two photon emission from a continuum excited state atom and an atom undergoing fractional Rydberg state transition (7),

- 4) the identification of transitions of atomic hydrogen to lower energy levels corresponding to lower-energy hydrogen atoms in the extreme ultraviolet emission spectrum from interstellar medium and the sun (1, 4, 6, 8),

- 5) the EUV spectroscopic observation of lines by the Institut für Niedertemperatur-Plasmaphysik e.V. that could be assigned to transitions of atomic hydrogen to lower energy levels corresponding to fractional principal quantum numbers and the emission from the excitation of the corresponding hydride ions (23),

- 6) the recent analysis of mobility and spectroscopy data of individual electrons in liquid helium which shows direct experimental confirmation that electrons may have fractional principal quantum energy levels (5),

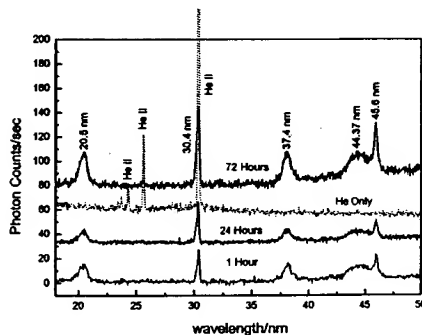


Figure A. The EUV spectra (15–50 nm) of the microwave cell emission of the helium-hydrogen mixture (98/2%) recorded at 1, 24, and 72 hours with a normal incidence EUV spectrometer and a CEM, and control helium (dotted curve) recorded with a 4° grazing incidence EUV spectrometer and a CEM. The pressure was maintained at 20 torr. Only known He I and He II peaks were observed with the helium control. Reproducible novel emission lines that increased with time were observed at 45.6 nm and 30.4 nm with energies of $q \cdot 13.6 \text{ eV}$ where $q = 2$ or 3 and at 37.4 nm and 20.5 nm with energies of $q \cdot 13.6 \text{ eV}$ where $q = 4$ or 6 that were inelastically scattered by helium atoms wherein 21.2 eV (58.4 nm) was absorbed in the excitation of $He(1s^3)$.

7) the observation of novel EUV emission lines from microwave discharges of argon or helium with 10% hydrogen that matched those predicted for vibrational transitions of $H_2^+[n=1/4; n^*=2]^+$ with energies of $\nu \cdot 1.185 \text{ eV}$, $\nu = 17$ to 38 that terminated at the predicted dissociation limit, E_D , of $H_2[n=1/4]^+$, $E_D = 42.88 \text{ eV}$ (28.92 nm) (8),

8) the observation of continuum state emission of Cs^{2+} and Ar^{2+} at 53.3 nm and 45.6 nm, respectively, with the absence of the other corresponding Rydberg series of lines from these species which confirmed the resonant nonradiative energy transfer of 27.2 eV from atomic hydrogen to the catalysts atomic Cs or Ar^+ (13),

9) the spectroscopic observation of the predicted hydride ion $H^-(1/2)$ of hydrogen catalysis by either Cs atom or Ar^+ catalyst at 407 nm corresponding to its predicted binding energy of 3.05 eV (13),

10) the observation of characteristic emission from K^{3+} which confirmed the resonant nonradiative energy transfer of 3-27.2 eV from atomic hydrogen to atomic K (12),

11) the spectroscopic observation of the predicted $H^-(1/4)$ ion of hydrogen catalysis by K catalyst at 110 nm corresponding to its predicted binding energy of 11.2 eV (12),

12) the observation of characteristic emission from Rb^{2+} which confirmed the resonant nonradiative energy transfer of 27.2 eV from atomic hydrogen to Rb^+ (11),

13) the spectroscopic observation of the predicted $H^-(1/2)$ ion of hydrogen catalysis by Rb^+ catalyst at 407 nm corresponding to its predicted binding energy of 3.05 eV (11),

14) the observation by the Institut für Niedertemperatur-Plasmaphysik e.V. of an anomalous plasma and plasma afterglow duration formed with hydrogen-potassium mixtures (24),

15) the observation of anomalous afterglow durations of plasmas formed by catalysts providing a net enthalpy of reaction within thermal energies of $m \cdot 27.28 \text{ eV}$ (24, 25),

16) the observation of Lyman series in the EUV that represents an energy release about 10 times that of hydrogen combustion which is greater than that of any possible known possible chemical reaction (9, 11-13, 21, 22, 24, 25),

17) the observation of line emission by the Institut für Niedertemperatur-Plasmaphysik e.V. with a 4° grazing incidence EUV spectrometer that was 100 times more energetic than the combustion of hydrogen (23),

18) the observation of anomalous plasmas formed with Sr and Ar^+ catalysts at 1% of the theoretical or prior known voltage requirement with a light output per unit power input up to 8600 times that of the control standard light source (14, 15, 20, 21),

19) the observation that the optically measured output power of gas cells for power supplied to the glow discharge increased

by over two orders of magnitude depending on the presence of less than 1% partial pressure of certain catalysts in hydrogen gas or argon-hydrogen gas mixtures, and an excess thermal balance of 42 W was measured for the 97% argon and 3% hydrogen mixture versus argon plasma alone (20),

20) the observation that glow discharge plasmas of the catalyst-hydrogen mixtures of strontium-hydrogen, helium-hydrogen, argon-hydrogen, strontium-helium-hydrogen, and strontium-argon-hydrogen showed significant Balmer α line broadening corresponding to an average hydrogen atom temperature of 25-45 eV; whereas, plasmas of the noncatalyst-hydrogen mixtures of pure hydrogen, krypton-hydrogen, xenon-hydrogen, and magnesium-hydrogen showed no excessive broadening corresponding to an average hydrogen atom temperature of $\approx 3 \text{ eV}$ (17-19),

21) the observation that microwave helium-hydrogen and argon-hydrogen plasmas having catalyst Ar^+ or He^{2+} showed extraordinary Balmer α line broadening due to hydrogen catalysis corresponding to an average hydrogen atom temperature of 110-130 eV and 180-210 eV, respectively; whereas, plasmas of pure hydrogen, neon-hydrogen, krypton-hydrogen, and xenon-hydrogen showed no excessive broadening corresponding to an average hydrogen atom temperature of $\approx 3 \text{ eV}$ (7, 18),

22) the observation that microwave helium-hydrogen and argon-hydrogen plasmas showed average electron temperatures that were high, 28,000 K and 11,600 K, respectively; whereas, the corresponding temperatures of helium and argon alone were only 6800 K and 4800 K, respectively (7, 18),

23) the observation of significant Balmer α line broadening of 17, 9, 11, 14, and 24 eV from rt-plasmas of incandescently heated hydrogen with K^+/K^+ , Rb^+ , cesium, strontium, and strontium with Ar^+ catalysts, respectively, wherein the results could not be explained by Stark or thermal broadening or electric field acceleration of charged species since the measured field of the incandescent heater was extremely weak, 1 V/cm, corresponding to a broadening of much less than 1 eV (9),

24) calorimetric measurement of excess power of 20 mW/cc on rt-plasmas formed by heating hydrogen with K^+/K^+ and Ar^+ as catalysts (9),

25) the high resolution visible spectroscopic observation from rt-plasma and plasma electrolysis cells of the predicted $H^-(1/2)$ ion of hydrogen catalysis by each of K^+/K^+ , Rb^+ , Cs, and Ar^+ at 407 nm corresponding to its predicted binding energy of 3.05 eV as shown in Figure B(9, 10),

26) the isolation of novel inorganic hydride compounds such as $KHKHCO_3$ and KH following each of the electrolysis and plasma electrolysis of a K_2CO_3 electrolyte which comprised high binding energy hydride ions that were stable in water with their identification by methods such as (i)

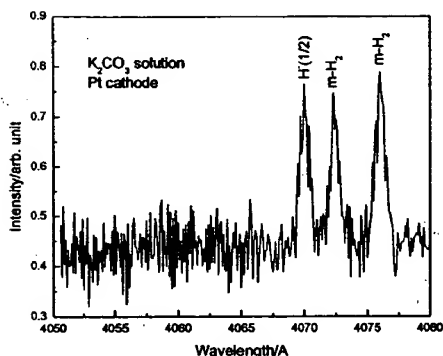


Figure B1. The high resolution visible spectrum in the region of 407 nm recorded on the emission of K_2CO_3 plasma electrolysis cell.

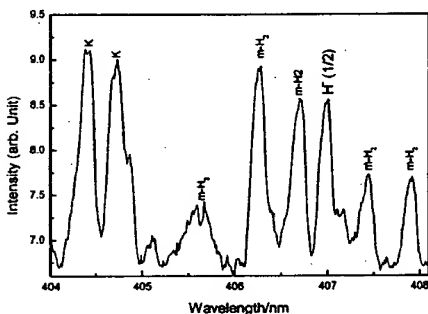


Figure B2. The high resolution visible spectrum in the region of 407 nm recorded on the emission of the rt-plasma formed by atomic hydrogen and gaseous potassium ion catalyst generated by a filament heater. In both cases, the novel 407.0 nm peak which could not be assigned to a known peak was assigned to $H(1/2)$.

ToF-SIMS on KH_2KCO_3 , which showed inorganic hydride clusters $K[KH_2KCO_3]$, and a negative ToF-SIMS dominated by hydride ion, (ii) X-ray photoelectron spectroscopy which showed novel peaks corresponding to high binding energy hydride ions, and (iii) proton nuclear magnetic resonance spectroscopy which showed upfield shifted peaks corresponding to more diamagnetic, high-binding-energy hydride ions (10, 28, 29, 31),

27) the observation that the power output exceeded the power supplied to a hydrogen glow discharge plasmas by 35–184 W depending on the presence of catalysts helium or argon and less than 1% partial pressure of strontium metal in noble gas-hydrogen mixtures; whereas, the chemically similar noncatalyst krypton had no effect on the power balance (19),

28) the Calvet calorimetry measurement of an energy balance of over $-151,000 \text{ kJ/mole } H_2$ with the addition of 3% hydrogen to a plasma of argon having the catalyst Ar^+ compared to the enthalpy of combustion of hydrogen of $-241.8 \text{ kJ/mole } H_2$; whereas, under identical conditions no change in the Calvet voltage was observed when hydrogen was added to a plasma of noncatalyst krypton (16),

29) the observation that upon the addition of 10% hydrogen to a helium microwave plasma maintained with a constant microwave input power of 40 W, the thermal output power was measured to be at least 400 W corresponding to a reactor temperature rise from room temperature to 1200°C within 150 seconds, a power density of 40 MW/m^3 , and an energy balance of at least $-5 \times 10^5 \text{ kJ/mole } H_2$ compared to the enthalpy of combustion of hydrogen of $-241.8 \text{ kJ/mole } H_2$ (17),

30) the differential scanning calorimetry (DSC) measurement of minimum heats of formation of KHI by the catalytic reaction of K with atomic hydrogen and KI that were over $-2000 \text{ kJ/mole } H_2$ compared to the enthalpy of combustion of hydrogen of $-241.8 \text{ kJ/mole } H_2$ (32),

31) the isolation of novel hydrogen compounds as products of the reaction of atomic hydrogen with atoms and ions which formed an anomalous plasma as reported in the EUV studies (26–32),

32) the identification of novel hydride compounds by a number of analytic methods as such as (i) time of flight secondary ion mass spectroscopy which showed a dominant hydride ion in the negative ion spectrum, (ii) X-ray photoelectron spectroscopy which showed novel hydride peaks and significant shifts of the core levels of the primary elements bound to the novel hydride ions, (iii) 1H nuclear magnetic resonance spectroscopy (NMR) which showed extraordinary upfield chemical shifts compared to the NMR of the corresponding ordinary hydrides, and (iv) thermal decomposition with analysis by gas chromatography, and mass spectroscopy which identified the compounds as hydrides (26–32),

33) the NMR identification of novel hydride compounds MH^*X wherein M is the alkali or alkaline earth metal, X, is a halide, and H^* comprises a novel high binding energy hydride ion identified by a large distinct upfield resonance as shown in Figure C (26–31),

34) the replication of the NMR results of the identification of novel hydride compounds by large distinct upfield resonances at Spectral Data Services, University of Massachusetts Amherst, University of Delaware, Grace Davison, and National Research Council of Canada (26),

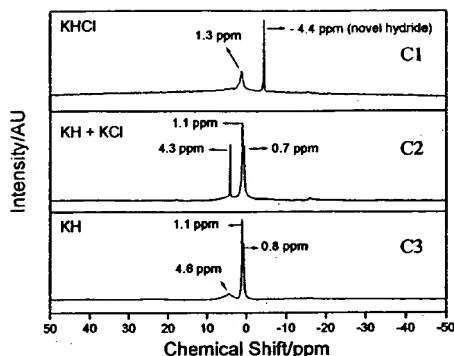


Figure C. (1) The ^1H MAS NMR spectrum of KH^*Cl relative to external tetramethylsilane (TMS). The resonance at 1.3 ppm was assigned to ordinary hydride ion. The large distinct upfield resonance at -4.4 identifies a hydride ion with a substantially smaller radius as compared with ordinary hydride since a smaller radius increases the shielding or diamagnetism, and it was assigned to a novel hydride ion of KH^*Cl . (2) The ^1H MAS NMR spectrum of the control comprising an equal molar mixture of KH and KCl relative to external tetramethylsilane (TMS). Ordinary hydride ion has a resonance at 1.1 ppm and 0.8 ppm in the KH/KCl mixture and in KH . The presence of KCl does not shift the resonance of ordinary hydride as shown in Figure C3. (3) The ^1H MAS NMR spectrum of the control KH relative to external tetramethylsilane (TMS).

35) the NMR identification of novel hydride compounds MH^* and MH_2^* wherein M is the alkali or alkaline earth metal and H^* comprises a novel high binding energy hydride ion identified by a large distinct upfield resonance that proves the hydride ion is different from the hydride ion of the corresponding known compound of the same composition (26).

HYDRIDE ION BATTERY

Hydride ions formed by the catalysis of atomic hydrogen having extraordinary binding energies may stabilize a cation M^{*+} in an extraordinarily high oxidation state such as +2 in the case of lithium. Thus, these hydride ions may be used as the basis of a high voltage battery of a rocking chair design wherein the hydride ion moves back and forth between the cathode and anode half cells during discharge and charge cycles. Exemplary reactions for a cation M^{*+} are shown in Figure D.

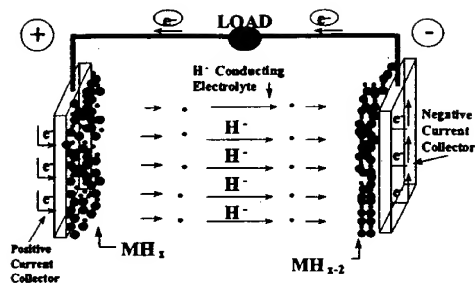


Figure D. The schematic of a hydride ion battery comprising the reactions for a cation M^{*+} of:

Cathode reaction: $\text{MH}_x + e^- \rightarrow \text{MH}_{x-1} + \text{H}^-$

Anode reaction: $\text{MH}_{x-2} + \text{H}^- \rightarrow \text{MH}_{x-1} + e^-$

Overall reaction: $\text{MH}_x + \text{MH}_{x-2} \rightarrow 2\text{MH}_{x-1}$

REFERENCES

1. R. Mills, *The Grand Unified Theory of Classical Quantum Mechanics*, January 2000 Edition, BlackLight Power, Inc., Cranbury, New Jersey, Distributed by Amazon.com; Sept. 2001 Edition posted at www.blacklightpower.com.
2. R. Mills, "The Grand Unified Theory of Classical Quantum Mechanics," Global Foundation, Inc. Orbis Scientiae entitled *The Role of Attractive and Repulsive Gravitational Forces in Cosmic Acceleration of Particles The Origin of the Cosmic Gamma Ray Bursts*, (29th Conference on High Energy Physics and Cosmology Since 1964) Dr. Behram N. Kursunoglu, Chairman, Dec. 14-17, 2000, Lago Mar Resort, Ft Lauderdale, FL, Kluwer: New York, pp. 243-258.
3. R. Mills, "The Grand Unified Theory of Classical Quantum Mechanics," Int. J. of Hydrogen Energy, in press.
4. R. Mills, "The Hydrogen Atom Revisited," Int. J. of Hydrogen Energy, Vol. 25, No. 12, (2000), pp. 1171-1183.
5. R. Mills, *The Nature of Free Electrons in Superfluid Helium—a Test of Quantum Mechanics and a Basis to Review its Foundations and Make a Comparison to Classical Theory*, Int. J. Hydrogen Energy, Vol. 26, No. 10, (2001), pp. 1059-1096.
6. R. Mills, P. Ray, "Spectral Emission of Fractional Quantum Energy Levels of Atomic Hydrogen from a Helium-Hydrogen Plasma and the Implications for Dark Matter," Int. J. Hydrogen Energy, in press.
7. R. L. Mills, P. Ray, B. Dhandapani, J. He, "Spectroscopic Identification of Fractional Rydberg States of Atomic Hydrogen" J. Phys. Chem. Letts., submitted.
8. R. Mills, P. Ray, "Vibrational Spectral Emission of Fractional-Principal-Quantum-Energy-Level Hydrogen Molecular Ion," Int. J. Hydrogen Energy, in press.

9. R. Mills, P. Ray, M. Nansteel, W. Good, P. Jansson, B. Dhandapani, J. He, "Excessive Balmer α Line Broadening, Power Balance, and Novel Hydride Ion Product of Plasma Formed from Incandescently Heated Hydrogen Gas with Certain Catalysts," *Int. J. Hydrogen Energy*, submitted.
10. R. Mills, E. Dayalan, P. Ray, B. Dhandapani, J. He, "Highly Stable Novel Inorganic Hydrides from Aqueous Electrolysis and Plasma Electrolysis, submitted.
11. R. L. Mills, P. Ray, "Spectroscopic Identification of a Novel Catalytic Reaction of Rubidium Ion with Atomic Hydrogen and the Hydride Ion Product," *Int. J. Hydrogen Energy*, submitted.
12. R. Mills, P. Ray, Spectroscopic Identification of a Novel Catalytic Reaction of Potassium and Atomic Hydrogen and the Hydride Ion Product, *Int. J. Hydrogen Energy*, in press.
13. R. Mills, "Spectroscopic Identification of a Novel Catalytic Reaction of Atomic Hydrogen and the Hydride Ion Product," *Int. J. Hydrogen Energy*, Vol. 26, No. 10, (2001), pp. 1041-58.
14. R. Mills and M. Nansteel, "Argon-Hydrogen-Strontium Plasma Light Source," *IEEE Transactions on Plasma Science*, submitted.
15. R. Mills, M. Nansteel, and Y. Lu, "Excessively Bright Hydrogen-Strontium Plasma Light Source y Resonance of Strontium with Hydrogen," *European Journal of Physics D*, submitted.
16. R. Mills, J. Dong, W. Good, P. Ray, J. He, B. Dhandapani, Measurement of Energy Balances of Noble Gas-Hydrogen Discharge Plasmas Using Calvet Calorimetry, *Int. J. Hydrogen Energy*, submitted.
17. Randell L. Mills, P. Ray, B. Dhandapani, M. Nansteel, X. Chen, J. He, "New Power Source from Fractional Quantum Energy Levels of Atomic Hydrogen that Surpasses Internal Combustion," *Spectrochimica Acta*, submitted.
18. R. L. Mills, P. Ray, B. Dhandapani, J. He, "Comparison of Excessive Balmer α Line Broadening of Glow Discharge and Microwave Hydrogen Plasmas with Certain Catalysts" *J. Phys. Chem.*, submitted.
19. R. L. Mills, A. Voigt, P. Ray, M. Nansteel, B. Dhandapani, "Measurement of Hydrogen Balmer Line Broadening and Thermal Power Balances of Noble Gas-Hydrogen Discharge Plasmas," *Int. J. Hydrogen Energy*, in press.
20. R. Mills, N. Greenig, S. Hicks, "Optically Measured Power Balances of Anomalous Discharges of Mixtures of Argon, Hydrogen, and Potassium, Rubidium, Cesium, or Strontium Vapor," *Int. J. Hydrogen Energy*, in press.
21. R. Mills, M. Nansteel, and Y. Lu, "Observation of Extreme Ultraviolet Hydrogen Emission from Incandescently Heated Hydrogen Gas with Strontium that Produced an 'Anomalous Optically Measured Power Balance,'" *Int. J. Hydrogen Energy*, Vol. 26, No. 4, (2001), pp. 309-326.
22. R. Mills, J. Dong, Y. Lu, "Observation of Extreme Ultraviolet Hydrogen Emission from Incandescently Heated Hydrogen Gas with Certain Catalysts," *Int. J. Hydrogen Energy*, Vol. 25, (2000), pp. 919-943.
23. R. Mills, "Observation of Extreme Ultraviolet Emission from Hydrogen-KI Plasmas Produced by a Hollow Cathode Discharge," *Int. J. Hydrogen Energy*, Vol. 26, No. 6, (2001), pp. 579-592.
24. R. Mills, "Temporal Behavior of Light-Emission in the Visible Spectral Range from a Ti-K₂CO₃-H-Cell," *Int. J. Hydrogen Energy*, Vol. 26, No. 4, (2001), pp. 327-332.
25. R. Mills, T. Onuma, and Y. Lu, "Formation of a Hydrogen Plasma from an Incandescently Heated Hydrogen-Catalyst Gas Mixture with an Anomalous Afterglow Duration," *Int. J. Hydrogen Energy*, Vol. 26, No. 7, (2001), pp. 749-762.
26. R. Mills, B. Dhandapani, M. Nansteel, J. He, A. Voigt, "Identification of Compounds Containing Novel Hydride Ions by Nuclear Magnetic Resonance Spectroscopy," *Int. J. Hydrogen Energy*, Vol. 26, No. 9, (2001), pp. 965-979.
27. R. Mills, B. Dhandapani, N. Greenig, J. He, "Synthesis and Characterization of Potassium Iodo Hydride," *Int. J. of Hydrogen Energy*, Vol. 25, No. 12, (2000), pp. 1185-1203.
28. R. Mills, "Novel Inorganic Hydride," *Int. J. of Hydrogen Energy*, Vol. 25, (2000), pp. 669-683.
29. R. Mills, "Novel Hydrogen Compounds from a Potassium Carbonate Electrolytic Cell," *Fusion Technology*, Vol. 37, No. 2, March, (2000), pp. 157-182.
30. R. Mills, B. Dhandapani, M. Nansteel, J. He, T. Shannon, A. Echezuria, "Synthesis and Characterization of Novel Hydride Compounds," *Int. J. of Hydrogen Energy*, Vol. 26, No. 4, (2001), pp. 339-367.
31. R. Mills, "Highly Stable Novel Inorganic Hydrides," *Journal of New Materials for Electrochemical Systems*, in press.
32. R. Mills, W. Good, A. Voigt, Jinquan Dong, "Minimum Heat of Formation of Potassium Iodo Hydride," *Int. J. Hydrogen Energy*, Vol. 26, No. 11, (2001), pp. 1199-1208.
33. R. Mills, "BlackLight Power Technology-A New Clean Hydrogen Energy Source with the Potential for Direct Conversion to Electricity," *Proceedings of the National Hydrogen Association, 12 th Annual U.S. Hydrogen Meeting and Exposition, Hydrogen: The Common Thread*, The Washington Hilton and Towers, Washington DC, (March 6-8, 2001), pp. 671-697.
34. R. Mills, "BlackLight Power Technology-A New Clean Energy Source with the Potential for Direct Conversion to Electricity," *Global Foundation International Conference on "Global Warming and Energy Policy," Dr. Behram N. Kursunoglu, Chairman, Fort Lauderdale, FL, November 26-28, 2000, Kluwer: New York, pp. 1059-1096.*
35. R. Mayo, R. Mills, M. Nansteel, "On the Potential of Direct and MHD Conversion of Power from a Novel Plasma Source to Electricity for Microdistributed Power Applications," *IEEE Transactions on Plasma Science*, submitted.
36. N. V. Sidgwick, *The Chemical Elements and Their Compounds*, Vol. I, Oxford, Clarendon Press, (1950), p.17.
37. M. D. Lamb, *Luminescence Spectroscopy*, Academic Press, London, (1978), p. 68.

On the Potential of Direct and MHD Conversion of Power from a Novel Plasma Source to Electricity for Microdistributed Power Applications

R. M. Mayo,^{a)} R. L. Mills, and M. Nansteel

BLP Inc.,

Cranbury, NJ 08512

The generation of electricity using direct electrostatic and magnetohydrodynamic (MHD) conversion of the plasma particle energy of small to mid-size chemically assisted microwave or glow discharge plasmas (CA-plasma) power sources in the range of a few hundred Watts to several 10's of kW for microdistributed commercial applications (e.g. household, automotive, light industry, and space based power) is studied for the first time. In the determination of the effect of plasma parameters on conversion efficiency, careful attention was paid to the unique plasma conditions of low pressure, low ionization fraction, and nonthermal ion energies that are much greater than that of the thermal ions of traditional MHD but much lower than those of a fully ionized plasma typically generated for fusion experiments. The density of plasma ions and neutrals and their cross sections for processes such as charge exchange were also considered. The most important parameters were found to be charged particle density and energy, as well as the large inventory of neutral gas atoms and molecules. Momentum and charge exchange of plasma ions with the large background fraction of neutrals represents a limitation to conversion efficiency. Two conversion technologies were examined in some detail. We considered the possibility of converting a CA-plasma using adaptations of a member of the broad category of electromagnetic direct converters previously developed for recovery and conversion of the high energy particles lost from tandem mirror and magnetically confined plasmas, and an MHD converter previously developed for conversion of high pressure combustion gases to electricity. While it was found that both conversion techniques performed well under ideal conditions for conversion of plasma to electricity showing conversion efficiencies of $> 50\%$, the tight coupling of plasma cell and converter, size limitations, particle energy, and the substantial inventory of relatively low energy neutrals eliminate direct electrostatic converters

as practical converters under these conditions. However, MHD conversion of CA-plasmas appears feasible at ~50% efficiency with a simple compact design.

I. INTRODUCTION

Central station generation and distribution, the mainstay of electrical power production for the last 100 years worldwide, is now being supplemented in an increasing number of areas by smaller power units closer to the end-user group. Most distributed-generation units are in the capacity range of 100 kW-3 MW (electric), but some could be as large as 250 MW (electric). Distributed generation solves some of centralized power's inherent problems of transmission and distribution line losses, electromagnetic pollution fears from high-tension lines, cost and difficulty of transmission-line maintenance, and inefficiencies in load factor design of power plants (wherein the use of a 20% capacity safety factor is still a common industry practice when estimating peak loading).

The microdistributed market emerged with uninterruptable power supplies (UPS) which serve the premium power market including businesses where brief electrical outages can cause severe monetary loss: telecommunication sites, computer centers, server hotels, e-commerce centers, semiconductor fabrication facilities, and others. With a suitable technology, market conditions exist to extend the trend away from central power with the expansion of microdistributed power into the broader electricity market. The broader market which includes hundreds of millions of homes and businesses in the US, Europe, and Japan will be drawn by significant cost savings and increasing unreliability of the grid with a lack of viable microdistributed alternatives. The market is already moving in that direction. Plug Power¹ is developing a home fuel cell unit for the U.S. market, and in Japan, Matsushita plans to introduce a 1 kW fuel-cell system costing \$10,000 where the price of electricity is 20 /kW-hr for microdistributed power.² The current price for government subsidized green distributed power in Germany is even higher, 50 /kW hr.³ The populace of the third world, particularly Asia, represents a further enormous market opportunity for a technology with low capital and O&M costs and no requirement of an electrical grid infrastructure.

The automotive market is also currently at a crossroads with many different options being considered for the next generation of automobile. Evidence of the changing landscape for automobiles can be found in the recent increase in research into the next generation of automobiles. But, the fact that there is no clear front-runner in the technological race to replace the internal combustion

(IC) engine can be attested to by the divergent approaches taken by the major automobile companies. Programs include various approaches to hybrid vehicles, alternative fueled vehicles such as dual-fired engines that can run on gasoline or compressed natural gas, and a natural gas-fired engine. Serious efforts are also being put into a number of alternative fuels such as ethanol, methanol, propane, and reformulated gasoline. To date, the most favored approach is an electric vehicle based on fuel cell technology or advanced battery technology such as sodium nickel chloride, nickel-metal hydride, and lithium-ion batteries.⁴ Although billions of dollars are being spent to develop an alternative to the IC engine, there is no technology in sight that can match the performance of an IC engine system.⁵

A chemically generated or assisted plasma (CA-plasma) as a novel power source using hydrogen as the fuel has been reported previously.⁶⁻¹¹ Since the power is in the form of a plasma, high-efficiency, low-cost direct energy conversion may be possible, thus, avoiding a heat engine such as a turbine^{12,13} or a reformer-fuel-cell system. Significantly lower capital costs and lower commercial operating costs than that of any known competing energy source are anticipated.

High temperature plasmas possess a substantial inventory of energy stored in the thermal and/or kinetic components of plasma ions, electrons, and in some cases neutral gas particles in some weakly ionized plasmas. There is obvious incentive then in devising methods and technologies to efficiently extract this energy and convert it to a more useful form. Most often, conversion to electrical energy is desired as this form is readily stored and transmitted, and is efficiently converted to mechanical work at the delivery site.

A number of conversion schemes have been studied in the four plus decades of controlled thermonuclear fusion research. At high temperature (as that produced in the blanket material of high power D-T fusion reactor) a thermal steam cycle^{14,15} is usually considered the most practical energy extraction means as the bulk (80%) of the energy release is in the form of chargeless neutrons. Thermal steam cycles are robust, reliable, proven technologies, and are well established as the work horse of modern electrical power delivery. Yet, the conversion efficiency is limited and high coolant temperatures are required. Furthermore, costs are prohibitive for the use of steam cycles in small, distributed power sources.

Direct conversion of plasma charged particle kinetic to electric energy¹⁶ may represent an attractive alternative to the steam cycle for at least several plasma systems of great interest including: (a) the D-T fusion reactor (as a "topping" unit to extract the 20% of fusion energy in high energy charged particles), (b) advanced, a-neutronic fueled fusion reactors, and (c) CA-plasma cells. In fusion reactors, the fully ionized, high temperature (up to 10-15 keV) plasma energy may be readily extracted by direct, electrostatic means, thereby converting charged particle kinetic energy to electrostatic potential energy via decelerating electrodes.¹⁶ Whereas for CA-plasma cell devices, possessing only weakly ionized and relatively cold plasmas, conversion methods more compatible with a fluid environment like MHD converters may be required to extract stored energy.

A number and variety of direct energy conversion techniques have been studied over the years.¹⁶ Many of these may be loosely grouped into the following broad categories. (1) Electrostatic Direct Converters: Electrostatic direct devices convert directed ion kinetic energy to electrical potential energy via an electrode (or set of electrodes) electrically biased to decelerate ions extant from the plasma source. The most well studied of such converter devices are the *venetian blind*^{17,18} and *periodic focused*¹⁹ converters. These devices appear to hold great promise as very efficient (80-90%) direct converters for large scale (on the order of 1000 MW) generating stations. In these devices, plasma particles are electrostatically separated before deceleration and collection at the electrodes. Separation incurs space charge limitations which are particularly troublesome for all but very high energy particles. Reasonable currents are achievable only at very high energy (several to 100s of keV). Particles of these energy levels are not present in appreciable numbers in CA-plasma cells. Furthermore, to mitigate the effects of high heat loading,^{20,21} such devices require plasma expansion and become enormous in linear scale (10's-100's of meters).

(2) Electromagnetic Direct (Crossed Field or Drift) Converters: The guiding center drift of charged particles in magnetic and crossed electric fields may be exploited to separate and collect charge without the necessity to do so electrostatically. Space charge complications are to a large degree eliminated. Dimensions can often be reduced (for low power converters) by many orders (perhaps to the ion gyro-scale). Natural mating of the converter magnetic field to a guide field is a further advantage. As the devices extract particle energy perpendicular to the magnetic field, expansion

may not be necessary and is often undesirable. The performance characteristics of an idealized $\vec{E} \times \vec{B}$ converter which relies on the inertial difference between ions and electrons, is analyzed in sec. III. Timofeev^{22,23} devised a high efficiency conversion device based on combined $\vec{E} \times \vec{B}$ and $\nabla \vec{B}$ drift collection. This particular device is again designed for high-power fusion energy conversion and is quite large in dimension, and requires expansion and end plug fields to prevent plasma leakage. In addition, collisions among energetic ions and neutral particles in a low power plasma cell will likely interrupt the drift trajectory required for efficient energy conversion. As an example, Ar^+ ions in a 1 T field have a gyro-frequency of $\omega_{ci} \sim 2.4 \times 10^6 \text{ s}^{-1}$ and a collision frequency with neutral Ar atoms of $\nu_{in} \sim 6 \times 10^7 \text{ s}^{-1}$ at 40 eV, making the ion magnetization parameter $\Omega = \omega_c/\nu \sim 0.04$. (For H^+ ions under the same conditions the magnetization parameter is 0.27). Ions then are readily interrupted in their drift trajectory and will not reach the desired collection electrode in the $\nabla \vec{B} \times \vec{B}$ direction.

(3) MHD Converter: In MHD a highly conducting plasma, flowing at velocity \vec{u} in a direction across a magnetic field \vec{B} gives rise to an electric field $\vec{E} = -\vec{u} \times \vec{B}$. This electric field may be intercepted at the boundary of a plasma device by electrodes and exploited to drive electric current through an external load. Mechanical flow energy of the conducting fluid is then converted to electrical energy. In the presence of a load to complete the circuit, the density of electric current, \vec{j} , is given by the plasma Ohm's law

$$\vec{j} = \sigma(\vec{E} + \vec{u} \times \vec{B}) \quad (1)$$

where σ is the plasma electrical conductivity. The term $\vec{u} \times \vec{B}$ is referred to as the MHD electric field or MHD term in Ohm's law.

The performance of an MHD power conversion system is impacted strongly by the value of σ attained in the plasma region of the MHD converter. As such, collisions among charge carriers or between charge carriers and neutral gas atoms play a crucial role. Collisions, however, are not as disruptive in MHD converters as they are in direct conversion. MHD converters operate on fluid plasmas where collisions are frequent and the trajectories of individual plasma particles are relatively unimportant. The conductivity is also affected strongly by the strength of applied magnetic field in plasma. A more detailed discussion of this subject is presented in sec. IV. MHD

Power conversion devices acting on alkali metal seeded, high-pressure (at or above atmospheric) combustion gases have been extensively studied²⁴⁻²⁹ including MHD concepts to deliver AC power directly from the converter.^{30,31} Prior studies also include plasmas generated in shock tubes or arc jets for high power electric generation. Little effort has been made in studying MHD conversion in hotter, more tenuous plasmas for low power applications. The work described herein is intended to initiate such a dialogue.

II. PROPERTIES OF CA-PLASMA CELLS & CONVERTER CONCERNS

A. Plasma Parameters

Plasma cells operating at about 1 Torr total pressure in the glow or microwave discharge regime producing output power significantly greater than the input power due to catalytic release of energy from supplied hydrogen have been reported previously.⁶⁻¹¹ Results from studies on ca-plasmas of hydrogen with strontium, argon or helium with 3-10% hydrogen and strontium with these latter mixtures include:

1. the observation that glow discharge plasmas of the catalyst-hydrogen mixtures of strontium-hydrogen, helium-hydrogen, argon-hydrogen, strontium-helium-hydrogen, and strontium-argon-hydrogen showed significant Balmer- α line broadening corresponding to an average hydrogen atom temperature of 25-45 eV; whereas, plasmas of the noncatalyst-hydrogen mixtures of pure hydrogen, krypton-hydrogen, xenon-hydrogen, and magnesium-hydrogen showed no excessive broadening corresponding to an average hydrogen atom temperature of ~ 3 eV,^{10,11}
2. the observation that microwave helium-hydrogen and argon-hydrogen plasmas having catalyst Ar^+ or He^{2+} showed extraordinary Balmer- α line broadening due to hydrogen catalysis corresponding to an average hydrogen atom temperature of 110-130 eV and 180-210 eV, respectively; whereas, plasmas of pure hydrogen, neon-hydrogen, krypton-hydrogen, and xenon-hydrogen showed no excessive broadening corresponding to an average hydrogen atom temperature of ~ 3 eV,^{7,10}

3. the observation that microwave helium-hydrogen and argon-hydrogen plasmas showed average electron temperatures that were high, 28,000 K and 11,600 K, respectively; whereas, the corresponding temperatures of helium and argon alone were only 6800 K and 4800 K, respectively,^{7,10}
4. the observation that the optically measured output power of gas cells for power supplied to the glow discharge increased by over two orders of magnitude depending on the presence of less than 1% partial pressure of certain catalysts in hydrogen gas or argon-hydrogen gas mixtures, and an excess thermal balance of 42 W was measured for the 97% argon and 3% hydrogen mixture versus argon plasma alone,⁶
5. the observation that the power output exceeded the power supplied to a hydrogen glow discharge plasmas by 35-184 W depending on the presence of catalysts helium or argon and less than 1% partial pressure of strontium metal in noble gas-hydrogen mixtures; whereas, the chemically similar noncatalyst krypton had no effect on the power balance,¹¹
6. the Calvet calorimetry measurement of an energy balance of over -151,000 kJ/mole-H₂ with the addition of 3% hydrogen to a plasma of argon having the catalyst Ar⁺ compared to the enthalpy of combustion of hydrogen of -241.8 kJ/mole-H₂; whereas, under identical conditions no change in the Calvet voltage was observed when hydrogen was added to a plasma of noncatalyst krypton,⁸
7. the observation that upon the addition of 10% hydrogen to a helium microwave plasma maintained with a constant microwave input power of 40 W, the thermal output power was measured to be at least 400 W corresponding to a reactor temperature rise from room temperature to 1200 °C within 150 seconds, a power density of 40 MW/m³, and an energy balance of at least -5×10^5 kJ/mole-H₂ compared to the enthalpy of combustion of hydrogen of -241.8 kJ/mole-H₂,⁹

Plasma parameters of a CA-plasma of an argon-hydrogen mixture (97/3%) which are very conservative in terms of their impact on the potential for conversion of plasma power to electricity are given in table 1 along with fill gas parameters at ~ 1 Torr.

B. Device Scale

Practical design parameters were established for the magnetic field strength B of 1 T and a converter physical scale L of 1 m to determine the performance of the converter. Fields on this order are readily produced with Weiss electromagnets³² with iron or rare-earth cores and without active cooling. The choice of converter length is considered a reasonable upper limit in an initial analysis of micro-distributed power devices without a detailed cost analysis. At times, the parameters B and L will be treated as independent variables for the purpose of optimization or parameterization; although, it is always recognized that practical considerations limit these to be of the order prescribed above.

C. Energy Content and Power Flow

To gauge the power scales involved, initial energy content and power flow estimates were made. At $T_e \sim 10$ eV, $T_i \sim 40$ eV, and $n_{e,i} = 10^{12}$ cm⁻³, for a 1 liter plasma cell, the stored thermal energy is

$$U_T = n_{e,i} V (kT_e + kT_i) \sim 8 \text{ mJ} \quad (2)$$

independent of ion species, where V is the plasma volume. Power flow can be estimated presuming the ability to extract this stored energy at an acoustic rate. At 40 eV, H⁺ ions have an acoustic speed of $\sim 6 \times 10^4$ m/s, while that for Ar⁺ ions is $\sim 10^4$ m/s. For a 10 cm drift path through the cell, this makes the drift time for H⁺ and Ar⁺ ions $t \sim 1.67 \mu\text{s}$ and $\sim 10 \mu\text{s}$, respectively. Assuming a particle replacement to maintain steady conditions of $n\nu A$, where $n\nu$ is the particle outflux and A is the flow channel cross section, thermal energy can then be extracted at a rate $U_T/t \sim 4.78$ kW for H⁺ and 0.8 kW for Ar⁺. This analysis is identical to setting the power output equal to the kinetic energy flow rate, $m\nu^2(n\nu A)/2$. A similar argument can be made by considering the rate at which work is done on the fluid as it is expelled from the cell, $P = \partial W/\partial t \simeq F\nu$ for constant F . For $F \sim pA$, then $P = p\nu A = n k T \nu A$ for an ideal gas. All of the aforementioned arguments, of course, require that steady conditions are maintained while extracting energy at the estimated rate. To do this, plasma particles must be replaced at the rate $n\nu A$ and heated to steady temperature T at the rate kT/t per particle.

D. Converter Concerns

It is considered convention in the direct conversion of plasma to electrical energy that a conversion system must perform the following tasks. (1) A well defined plasma stream is extracted from the plasma confinement or reactor chamber. (2) Neutral particles must be trapped or otherwise diverted from the plasma flow to ensure high quality plasma and reduce the deleterious effects of neutral interactions including elastic scattering and charge exchange recombination. (3) The extant plasma stream must be expanded to reduce the heat loading on converter surfaces such as electrodes and grids, and convert plasma thermal energy to flow energy, thereby enhancing converter performance. (4) Charge separation is performed usually by electrostatic means. Ions and electrons are separated very early in the converter region. Before being individually collected, substantial space charge is developed which can severely limit performance especially at low energy (below a few keV). (5) Charged particles are decelerated at high voltage electrodes and collected. For high efficiency, many electrodes may be required, each set at a different bias voltage to intercept ions with kinetic energy nearly equal to the bias potential. (6) To meet the needs of the application, direct converter power (usually high voltage DC) must be conditioned to the requirements at the delivery site.

These are all challenging engineering issues for direct conversion. Neutral trapping incurs the need for diverting the plasma flow and a differential pumping system to remove the neutral inventory. Extraction may require a separate extraction chamber and additional magnetic field coils for guide fields. Expansion increases the physical dimensions and cost of the converter and supporting systems. Charge separation introduces the inevitable and sometimes fatal complication of space charge limitations.

Fortunately, however, many of these requirements are dictated by the high power and high energies per particle associated with the nuclear fusion origins of direct conversion. At lower particle energies, many of these constraints can be relaxed. For example, wall loading is not considered a materials concern at the relatively low power typical of CA-plasma cell devices. Therefore, expansion may not be necessary unless there is a compelling conversion advantage (i.e. greatly increased conversion efficiency). Collecting plasma thermal or flow energy directly (as in the $\vec{E} \times \vec{B}$

or MHD conversion techniques) rather than first converting this energy to directed individual particle energy, eliminates the need for charge separation. This represents an enormous advantage and, in many cases, an enabling condition for CA-plasma power converters. Space charge would otherwise pose an insurmountable obstacle. As an example, consider an infinitely wide (so that transverse space charge effects are neglected) beam of H^+ ions at 10 eV and 1.6 kA/m². This beam dictates a longitudinal space charge limitation on the maximum collector length of ~ 0.5 mm, an obviously impractical constraint. The complications associated with plasma extraction and neutral trapping may also be eliminated by considering conversion strategies that allow the immersion of electrodes in-situ or allow a collector region to be closely coupled to the plasma cell to provide a natural flow path from cell to collector as in the case of $\vec{E} \times \vec{B}$ and MHD converters. Flow or collection interruption by neutral particles must still be considered, however.

E. Recombination

In low temperature plasmas, the recombination of free charge is often an important consideration in determining the concentration and distribution of charge states. This is especially true of low temperature plasmas that possess high neutral concentration and low ionization fraction. Three principle reactions dominate in the parameter range of interest, radiative and dielectronic recombination, and resonant charge exchange (CX). Estimating the rate of dielectric and radiative recombination is important for any plasma-to-electric conversion scheme since these processes remove free charge from the inventory intended for collection. Though the CX reaction does not alter the net concentration of ions in the plasma, it has the deleterious effect for conversion technologies relying on flow like MHD by removing energetic ions from the flow stream and replacing them with energetic neutral particles, leaving behind cold ions.

CX may occur among particles of the same species or among different species so long as the ionization energetics permits. In CA-plasma cells comprising Ar-H mixtures at low pressure in which the H minority concentration is not insignificant ($\gtrsim 3\%$), H^+ is expected to be the majority charge carrier as it is energetically favorable for ionized Ar to ionize H through CX.

The relevant recombination reactions then are those involving H^+ . Radiative recombination in H^+ occurs with a rate coefficient of $\sim 10^{13} \text{ cm}^3/\text{s}$. In plasma of electron density of 10^{12} cm^{-3} , this yields a recombination frequency of 0.1 s^{-1} or a 10 s recombination time. The recombination mean free path at 40 eV is then in excess of 600 km, a completely negligible process. CX, on the other hand, occurs at a much higher rate. The CX cross section for H^+ on H^0 is $\sim 10^{-16} \text{ cm}^2$. At 5% neutral H concentration, the CX mean path is then on the order of 10 cm. This is a reasonable dimension for the length of a small scale converter for a CA-plasma power cell.

III. $\vec{E} \times \vec{B}$ DIRECT CONVERTER

To illustrate an example of direct conversion for small to mid-scale power applications, the kinematics expressions and conversion efficiency are derived for the simple $\vec{E} \times \vec{B}$ converter with both ion and electron collectors. The zero order behavior of an ideal converter is described to retain an analytically tractable formalism. In the absence of significant expansion, the impact of collisions cannot be underestimated. As briefly mentioned in the introduction section, collisions may significantly reduce the efficiency of such devices by interrupting ion trajectories to the collector.

A schematic of a converter based on $\vec{E} \times \vec{B}$ collection is shown in Fig. 1. Here a rectangular arrangement of electrodes is chosen for simplicity with plasma particles incident from the left and drifting along guide field, \vec{B} . When both ions and electrons enter the collector region and experience the applied crossed fields, \vec{E} and \vec{B} , they will immediately assume a guiding center drift in the direction perpendicular to both \vec{E} and \vec{B} and with speed $\vec{v}_E = \vec{E} \times \vec{B}$. Though this speed is identical for ions and electrons, ions having greatly reduced translational speed parallel to \vec{B} (for $T_i = T_e$), will be turned and deflected to the upper electrode before electrons. For the same transit time, high-speed electrons will then be intercepted by the end electrode. The addition of electron collection increases direct power conversion.

Direct electromagnetic conversion like $\vec{E} \times \vec{B}$ offers distinct advantage over electrostatic conversion for a number of reasons. Perhaps the single most important aspect is that, like all fluid drift conversion processes, $\vec{E} \times \vec{B}$ conversion acts on the entire neutral plasma. The necessity to separate charge is thereby removed as are the space-charge complications that arise therefrom. Coupling to

the plasma source and expander (if necessary) are quite natural in an converter with its applied guide field. Furthermore, expansion may be unnecessary in this concept since the energy extraction in crossed field concepts is perpendicular to both \vec{B} and the direction of plasma extraction from the source. In the absence of expansion, dimensions can be greatly reduced. Collisions and end losses remain the principle obstacles to high efficiency conversion.

To assess the benefit of expansion in an $\vec{E} \times \vec{B}$ converter, an analysis is performed on expansion kinematics and collection efficiency. All plasma and field parameters before the flow enters the expander are identified with the subscript 1, and those upon exiting the expander and entering the converter are identified with subscript 2. For plasma particles initially at total energy $W_1 = W_{\parallel} + W_{\perp}$, equipartition requires that $W_{\perp} = 2W_{\parallel}$, where \perp and \parallel refer to directions perpendicular and parallel to the guide field, respectively, so that

$$v_{\parallel} = \sqrt{\frac{kT_1}{M}}, \quad v_{\perp} = \sqrt{\frac{2kT_1}{M}} \quad (3)$$

where M is the species mass. An expander region must conserve magnetic flux so that for cross sections of linear dimension d_1 and d_2 at the inlet and outlet of the expander respectively, we have

$$B_1 d_1^2 = B_2 d_2^2 \quad (4)$$

Assigning $d_1 = ad_2$, where a is a dimensionless, inverse expansion ratio, flux conservation can be expressed as $B_2 = a^2 B_1$. By conserving the adiabatic invariant $\mu = W_{\perp}/B$, expressions for the post expansion particle speed are obtained

$$v_{\perp 2} = a \sqrt{\frac{2kT_1}{M}}, \quad v_{\parallel 2} = \left(\frac{3}{2} - a^2\right)^{1/2} \sqrt{\frac{2kT_1}{M}} \quad (5)$$

Note that when $a = 1$ (the no expansion limit) then $v_{\perp 2} = v_{\perp 1}$ and $v_{\parallel 2} = v_{\parallel 1}$.

Conserving mass flow nvA (where A is the channel cross section at any position) determines the particle density change across the expander section

$$\frac{n_2}{n_1} = \frac{a^2}{(3 - 2a^2)^{1/2}} \quad (6)$$

Coupling this result to an adiabatic expansion requirement ($pV^\gamma = \text{const.}$) and the ideal gas law ($p = nkT$), dictates a temperature difference across the expander region

$$\frac{T_2}{T_1} = (3 - 2a^2)^{1/2} \left(\frac{h}{l}\right)^\gamma a^{2\gamma-2} \quad (7)$$

where h and l are the lengths of the cell and expander regions, respectively. At $a = 1/2$, $h/l = 1/2$, and $\gamma = 5/3$, the relative temperature decrease is found to be $T_2/T_1 \sim 0.2$.

Ion energy extraction requires that ions drift to the ion collector at $\vec{E} \times \vec{B}$. The rate of ion collection is then

$$R_i = n_2 \vec{v}_{E \times B} l \Delta \quad (8)$$

where $\Delta \sim 2d_2$ is the width of the collector electrodes. Since ions bring only perpendicular energy $W_{\perp 2}$ to collection, the rate of energy collection is

$$P_i = n_2 \vec{v}_{E \times B} l \Delta W_{\perp 2} = \frac{a^4}{(3 - 2a^2)^{1/2}} n_1 k T_1 \frac{E}{B_2} l \Delta \quad (9)$$

Electrons by contrast bring $W_{\parallel 2}$ to the electron collector since they drift parallel to B . Ambipolar considerations require electrons to reach their collector at the same rate that ions reach the ion collector, so that

$$n_2 \vec{v}_{E \times B} l \Delta = n_2 v_{\parallel 2e} \Delta^2 \quad (10)$$

so that the electron drift speed is limited to $v_{\parallel 2e} = (l/\Delta) \vec{v}_{E \times B}$. The collected electron power is then

$$P_e = n_2 v_{\parallel 2e} \Delta^2 \left(\frac{1}{2} m v_{\parallel 2e}^2 \right) = \frac{a^2 n_1}{(3 - 2a^2)^{1/2}} \frac{m l^3}{2 \Delta} \left(\frac{E}{B_2} \right)^3 \quad (11)$$

Combining ion and electron power, the total collected power is

$$P = \frac{a^3 n_1}{(3 - 2a^2)^{1/2}} l d_1 \frac{E}{B_2} \left[2kT_1 + \frac{m l^2}{4 d_1^2} \left(\frac{E}{B_2} \right)^2 \right] \quad (12)$$

For $l/d_1 \gg 1$, P peaks at $a \sim \sqrt{3/2}$. Since the maximum for the inverse expansion ratio is 1, expansion is not desirable in this situation. At $a = 1$, there is no adiabatic change in fluid parameters across the expander region, and

$$P = n l d \frac{E}{B} (2kT) \left[1 + \frac{m l^2}{8kT d^2} \left(\frac{E}{B} \right)^2 \right] \quad (13)$$

separating the ion and electron contributions, respectively, within the square brackets.

The power input to the converter has two contributions. Thermal flow power from the cell is estimated

$$P_{flow} = 3n k T \sqrt{\frac{kT}{M} \frac{\pi \Delta^2}{4}} \quad (14)$$

and in addition, there is a contribution from the work required of an external agent (power supply) to maintain the electric field in the converter in the presence of particle drifts

$$P_E - n\bar{v}_{E \times B} \Delta l \left(\frac{1}{2} M \bar{v}_{E \times B}^2 \right) \quad (15)$$

By the mass ratio $M \gg m$, the ion contribution is the only important contribution to this component of input power.

The converter efficiency is defined $\eta = P/P_{in}$ where $P_{in} = P_{flow} + P_E$. Defining a new parameter as the dimensionless drift-to-thermal-speed-ratio, $\alpha = \bar{v}_{E \times B}/v_{thi}$, the efficiency expression is parameterized as

$$\eta = \frac{1 + \frac{m}{8M} \left(\frac{l}{d} \right)^2 \alpha^2}{\frac{3\pi}{2} \frac{d}{\alpha l} + \frac{\alpha^2}{2}} \quad (16)$$

With $l/d \sim 5$ the conversion efficiency peaks at $\eta \sim 70\%$ near $\alpha \sim 1$. This is demonstrated in Fig. 2 as a parameterization of η vs. α with $l/d \sim 5$.

Some additional conditions should be considered. First, to avoid transverse ion loss, it is necessary to ensure $r_{Li} < \Delta/2$ — the ion gyro-scale fits within the channel dimensions. This requires $B > \sqrt{2kT}/qd \sim 45$ G for 10 eV H^+ ions at $d = 10$ cm, a trivial requirement. More limiting is ensuring a drift time much larger than the ion gyro-time to allow fully developed ion drift flow to intercept the upper electrode $(\Delta VB/E) > \omega_{ci}^{-1}$. This places an upper limit on $E < \Delta q B^2/M$ of $E, 7600$ V/m when $B = 200$ G. Since $l/d > 1$ is required for $v_{||ze} > \bar{v}_{E \times B}$, this forces $l \sim 1/2$ –1 m. The condition for equal ion and electron contributions to output power is

$$E = \frac{2\sqrt{2}}{5} B \sqrt{\frac{kT}{M}} \sim 15,000 \text{ V/m} \quad (17)$$

again for 10 eV and 200 G. This is superseded by the gyro-time requirement. It is more reasonable then to fix the electric field to a lower value near $\alpha \sim 1$. For example, at $E = 1000$ V/m (e.g. $V = 200$ V for $\Delta = 20$ cm) and $B = 200$ G at 10 eV, one finds $\alpha \sim 1.6$ and $\eta \sim 54\%$ (from Eq. (16)). The power output under these conditions (and with $n_e \sim 10^{12} \text{ cm}^{-3}$), is $P \sim 4.7$ kW.

A reasonable quantity of electric power may be extracted in such a converter design provided, of course, that collisional effects are not important. The effect of collisions has not been considered here. One may estimate, however, as done in the introduction (sec. I) that the magnetization

parameter is quite low for ions, $\Omega_i \ll 1$. This is found even at very high field approaching 1 T. The majority of ions in the stream are then not expected to complete an uninterrupted trajectory to the ion collector. For this reason alone, the success of direct collection in a compact, low power converter would be suspect.

IV. MHD CONVERTER

The MHD converter exploits the Lorentz action on a flowing magnetofluid across a magnetic field to generate an electrical potential difference. A schematic illustrating the basic components of an MHD system interfaced with a CA-plasma cell device is shown in Fig. 3. Magnetofluid flow is extant from the CA-plasma cell (labeled *Plasma Tube-Reactor*) at flow velocity \vec{u} . As the flow enters the MDH converter/expansion region, it experiences flow-crossed magnetic field \vec{B} . In the absence of an external load, an open-circuit electric field $\vec{E}_o = -\vec{u} \times \vec{B}$ is generated. This is a direct expression of the plasma Ohm's Law when the flow of electric current is prevented. When the system supports the flow of electric current, the relationship between electric current density \vec{j} and \vec{E} (Ohm's law) is given in Eq. (1) where σ is the electrical conductivity of the magnetofluid. The circuit is completed through the external load which reduces the electrode voltage so that $\vec{E} = \kappa \vec{E}_o = -\kappa \vec{u} \times \vec{B}$ where $\kappa < 1$, so that the magnitude of the current density becomes

$$j = \sigma(1 - \kappa)uB \quad (18)$$

The continuous appearance of an MHD voltage, $V = Ed$, (where d is the electrode separation) and electric current flow is predicated upon continuous fluid flow through the channel defined by the separation of the converter electrodes. The flow may be maintained via a pressure drop, ∇P , across the channel so that the plasma component of the fluid is in dynamic equilibrium with the applied field

$$\nabla p = \vec{j} \times \vec{B} \quad (19)$$

or $\Delta p = jBL$ for a linear pressure drop (i.e. constant B, j) across a channel of length L . The converter length required to support the fluid at fixed Δp can then be written

$$L = \frac{\Delta p}{\sigma(1 - \kappa)uB^2} \quad (20)$$

indicating a reduction in scale for concomitant increases in u , B , or σ . When the field magnitude and flow speed are fixed by power and materials limitations, there is a premium on a high degree of conductivity for the fluid. The electrical conductivity in plasma is determined by a number of factors including species, charge, average thermal speed, collision cross section,³³ and B . A detailed analysis on conduction in partially ionized gases will follow (sec. A).

In order to maintain a pressure drop, and hence flow, evacuation of the fluid extant from the converter is required in conventional MHD, but may be unnecessary in the CA-plasma case. Three possible scenarios are presented. (1) The plasma cell and converter may be directly coupled and open to atmosphere in a once-through, *open* system. The pressure drop is maintained by a vacuum pump or by operating at greater than atmospheric pressure. (2) The cell and converter may be arranged in a *closed* configuration which utilizes a recirculating pump to accumulate the converter effluent and divert it back to an injection reservoir in the plasma cell. Neither of the pump scenarios presented in (1) or (2) are beneficial in an energy conversion system since the pumping power required to maintain Δp and hence \bar{u} would necessarily be greater than that converted to electrical power by the flow. This follows directly from the requirement that the energy extracted as electricity is a direct consequence of a high enthalpy fluid expending flow energy in crossing \vec{B} . (3) Hot plasma generated in the CA-plasma cell and expanding outward therefrom into the converter region, may introduce an adverse pressure gradient which may be filled by backflow of neutral gas from the converter region returning to the cell. A *natural convection* like pattern may be established providing both continuous flow and refueling simultaneously. The CA-plasma cell and converter may then be coupled in a simply closed configuration without need for pumping.

Power flow through an external load at MHD supported \vec{j} and \vec{E} can be computed

$$P = \vec{j} \cdot \vec{E} = \sigma \kappa (1 - \kappa) u^2 B^2 \quad (21)$$

This is optimized at $\kappa = 1/2$, which simply represents the impedance matching condition where half the open-circuit voltage drop appears across the load.

A. Electrical Conductivity in an Applied Magnetic Field

As the electrical performance of the MHD converter is a strong function of the electrical conductivity, the accuracy of quantitative determination of σ is of paramount importance. Indeed, when the high concentration of neutral particles is in flow and thermal equilibrium with plasma ions and electrons, it is noted²⁹ that the MHD efficiency of conversion in historical applications is limited to the ionization fraction. This is a rather debilitating limitation as the ion fraction may be quite low, perhaps at only a few percent or less. However, in the low pressure CA-plasma case, no such equilibrium exists. The greatly reduced collisionality afforded by low density somewhat decouples the plasma species from neutral particles. Input power then is not required to heat the large inventory of neutrals, nor is it required to drive flow in this component so that the input power requirements may be much reduced and the electrical efficiency much greater.

The strong applied magnetic field, on the other hand, does have a dramatic influence on conduction.^{34,35} This can be directly ascertained from the electron momentum equation. Under the limiting, yet illustrative, conditions of constant and uniform plasma and flow with $\vec{B} = B\hat{z}$ and $\nabla T_e = 0$, the electron equation of motion yields the familiar expression for the transverse electron speed

$$\vec{v}_e = \frac{\Omega_e^2}{1 + \Omega_e^2} \frac{E_y}{B} + \frac{\Omega_e^2}{1 + \Omega_e^2} \frac{kT_e}{eB} \frac{\nabla_y n_e}{n_e} - \frac{\mu_e}{1 + \Omega_e^2} E_z - \frac{D_e}{1 + \Omega_e^2} \frac{\nabla_z n_e}{n_e} \quad (22)$$

where $\mu_e = e/(m_e \nu_e)$ is the electron mobility, $D_e = kT_e/(m_e \nu_e)$ is the electron mass diffusivity, and $\Omega_e = \omega_{ce} = eB/(m_e \nu_e) = \mu_e B$ is the electron magnetization parameter. For $\Omega_e \gg 1$, the electron fluid is magnetized and strongly influenced by \vec{B} . When $\Omega_e \ll 1$, the applied field has much less influence than particle collisions on electron transport. The first two terms in Eq. (22) are the familiar electric and diamagnetic drift terms perpendicular to \vec{B} . The last two terms represent electrostatic mobility and diffusive transport, yet the magnitude of the transport coefficients is reduced by the factor $1 + \Omega_e^2$, so that

$$\mu_{e\perp} = \frac{\mu_e}{1 + \Omega_e^2}, \quad D_{e\perp} = \frac{D_e}{1 + \Omega_e^2} \quad (23)$$

which may represent a significant reduction for large \vec{B} . Alternatively, the effective collisionality is increased

$$\nu_{e\perp} = \nu_e(1 + \Omega_e^2), \quad \eta_{e\perp} = \eta_e(1 + \Omega_e^2) \quad (24)$$

Because of the mass difference, ions and electrons are influenced by collisions and \vec{B} to differing degrees. Table 2 shows ion and electron collision frequencies with all species present (e, H^+, Ar^o neutrals) for a low power plasma cell possessing conditions of table 1 with 40 eV ions, 10^{12} cm^{-3} plasma density, and a Coulomb logarithm of 20. Charge neutral collisions are among ions or electrons with neutral Ar atoms at 1 Torr total pressure. Coulomb collisions are self ($i-i$ or $e-e$) or cross ($i-e$ or $e-i$) involving electrons and H^+ ions as the dominant ionized species. Conduction for both ions and electrons is limited by collisions with neutral particles due principally to the large inventory of neutrals at 1 Torr. These mechanisms (*i.e.* ν_{en}, ν_{in}) will then be considered the only important collisional effects.

In weak magnetic fields ($\Omega_{i,e} \ll 1$), both ions and electrons are relatively unaffected by the presence of \vec{B} . Electrons, then, due to their higher mobility, dominate electrical conduction. When the magnetic field strength increases such that $\Omega_{i,e} \gg 1$ (the strong field limit), both ions and electrons are magnetized and electrical conduction perpendicular to \vec{B} is dominated by ion flow. For intermediate fields, as for our test case near $B \sim 1 \text{ T}$, both ions and electrons conduct electrical current. To see this, a conductivity ratio can be estimated

$$\frac{\sigma_{e\perp}}{\sigma_{i\perp}} = \frac{\sigma_e(1 + \Omega_i^2)}{\sigma_i(1 + \Omega_e^2)} \quad (25)$$

At 1 T, $\Omega_e \sim 29.3$ and $\Omega_i \sim 0.27$ (H^+ ions) while $\sigma_e/\sigma_i = \mu_e/\mu_i \sim 85.7$. The conduction ratio perpendicular to \vec{B} then becomes $\sigma_{e\perp}/\sigma_{i\perp} \sim 0.1$ so that electrons carry only about 10% of the electrical current in the converter.

B. Sample MHD Converter Performance

MHD converter performance can be illustrated by examining a test case with $B \sim 1 \text{ T}$, $\kappa = 1/2$, $\Delta p = 1 \text{ Torr}$, and $u = 1.36 \times 10^4 \text{ m/s}$ (ion acoustic speed at neutral Ar inertia). For $\nu_{e\perp} = 0.1\nu_{i\perp}$, and $n_e = 10^{12} \text{ cm}^{-3}$, the plasma conductivity perpendicular to \vec{B} is estimated at 0.048 mho/m or

$\eta_{\perp} \sim 21 \Omega\text{-m}$. Then employing Eq. (20), a converter length of only ~ 40 cm is found. This is a modest requirement and suggests that such large fields may not be necessary. The MHD electric field generated in this case is $E = \kappa u B \sim 6.8$ kV/m, providing a voltage drop of 680 V across a 10 cm converter gap. The electric current density can then be estimated from Eq. (18) to be ~ 326 A/m² so that the MHD output power becomes ~ 8.8 kW.

Sample converter performance is shown in Figs. 4 and 5 illustrating MHD current density and power as functions of applied field, B , from 0–40 T at constant L and u . Though the upper limit on B is clearly impractical, the range encompasses all the relevant MHD physics. Under these constraints the MHD voltage and EMF are linear functions of B . The electric current density (Fig. 4), however, shows much more interesting behavior. There are two peaks in the curve, one at $B \sim 1/\mu_e$ and another at $B \sim 1/\mu_i$, before asymptotically decreasing to zero as $B \rightarrow \infty$. This behavior is explained by considering the perpendicular conductivity or mobility of charges in strong B . At low field ($B < 1/\mu_e$), electrons easily conduct under the influence of E , and j increases linearly with B since the MHD E increases with B . As B approaches $1/\mu_e = 0.034$ T, electrons become magnetized and are greatly impeded in their flow perpendicular to B , so that j decreases rapidly. This situation is sometimes referred to as the *ion slip condition*²⁷ since ions continue to slip through the applied field whereas electrons are trapped. In the region of B parameter space between $1/\mu_e$ and $1/\mu_i$, there is a competition between conductivity reduction and increasing EMF with B . At $B = 1/\mu_i \sim 3.7$ T, ions now become magnetized, and the current once again peaks. Beyond this field strength, the current is a continuously decreasing function of B . The MHD power (Fig. 5) is a continuously increasing function of B in spite of the variation in j with B , since E is continuously increasing. The power function reaches an asymptotic value ($P_{\infty} = \kappa(1 - \kappa)d^2 L u^2 e n / \mu_i \sim 110$ kW for this case) at high field since the E increase is linearly with B and j decreases like B^{-1} at large B .

Though the output power can approach appreciable levels, the quantity of total electric current remains low, $I \leq 25$ A (and $j \leq 600$ A/m²) so that induced fields remain negligible in comparison with the applied field. The magnetic Reynolds number $R_m = \mu_0 \sigma_{\perp} u d \sim 10^{-5}$ determines the scale

of flow interactions with the applied field. Since $R_m \ll 1$, the complications usually associated with flow-field distortion, hydromagnetic waves, and instabilities can be avoided.

C. Channel Hydrodynamics

The hydrodynamics of one dimensional, steady channel flow ($\vec{u} = u\hat{x}$) in crossed field ($\vec{B} = B\hat{z}$) is examined by considering the conservation equations of hydrodynamics

$$\begin{aligned} \text{energy : } \rho u \frac{d}{dx} \left(\frac{u^2}{2} + C_p T \right) &= \vec{j} \cdot \vec{E} \\ \text{momentum : } \rho \vec{u} \frac{du}{dx} + \nabla p &= \vec{j} \times \vec{B} \\ \text{continuity : } \dot{m} = \rho u A &= \text{const.} \end{aligned} \quad (26)$$

for a fluid of mass density ρ in a channel of cross section A . If constant flow ($u = \text{const.}$) is considered, the hydrodynamics equations simplify to

$$\begin{aligned} \text{energy : } \rho u \frac{d}{dx} (C_p T) &= \vec{j} \cdot \vec{E} \quad \text{or} \quad \frac{dh}{dx} = \frac{\vec{j} \cdot \vec{E}}{\rho u} \\ \text{momentum : } \nabla p &= \vec{j} \times \vec{B} \\ \text{continuity : } \rho A &= \text{const.} \end{aligned} \quad (27)$$

where h is the specific enthalpy.

In considering a constant applied field and disregarding flow distortion of the applied field as indicated by the tiny order of the magnetic Reynolds number, the pressure profile must be linear. By integrating the momentum

$$p(x) = 2j_y B L [1 - x/2L] \quad (28)$$

on $0 \leq x \leq L$. Given the pressure profile above and ideal gas behavior, $p = nkT$, the energy equation can be integrated to find the temperature profile

$$T(x)/T_o = [1 - x/2L]^{-\frac{kE}{\eta m B C_p}} \quad (29)$$

where T_o is the channel inlet temperature. Since $E = \kappa u B$, the exponent reduces to $\kappa k/mC_p \sim 0.33$ using the properties of Ar as the bulk species. At the channel exit we find $T(L)/T_o \sim 1.26$. The

temperature increase along the channel is attributed to Joule heating of the plasma by the MHD current and field.

Since the temperature and pressure profiles are determined, the density profile can be found

$$\begin{aligned} n(x) &= \frac{2j_y B L}{k T_o} [1 - x/2L]^{1 + \frac{k B}{u_m B c_p}} \\ &= n_o [1 - x/2L]^{1.33} \end{aligned} \quad (30)$$

The extant flow (at $x = L$) then has density reduction $n(L)/n_o \sim 0.4$.

By mass conservation, the channel cross section must widen to support constant flow while the density decreases, $A \sim 1/\rho$. Then it is readily determined

$$\begin{aligned} A(x) &= \frac{m k T_o}{2 j_y B L} [1 - x/2L]^{-(1 + \frac{k B}{u_m B c_p})} \\ &= A_o [1 - x/2L]^{-1.33} \end{aligned} \quad (31)$$

As the flow exits the channel, the gap must widen to $A(L)/A_o \sim 2.5$ or $d(L)/d_o \sim 1.6$ to accommodate constant flow.

D. Generator Efficiency and the Hall Effect

The preceding analysis considers only the idealized behavior of an MHD converter, that is the electrodynamic and hydrodynamic behavior in the absence of heat and particle losses, and Hall currents. Collisions, on the other hand, are fully accounted for through the explicit determination of collision frequency and its implementation in the Ohm's Law (Eq. (1)). In this context, the MHD efficiency may be quantified by considering the following. The output power density is determined by the rate at which specific enthalpy in the flow is converted to electrical energy

$$\rho u \frac{dh}{dx} = \vec{j} \cdot \vec{E} = j_y E \quad (32)$$

The rate at which energy is expended is attributed to work done by the fluid in expanding through the applied magnetic field

$$h \frac{dp}{dx} = u j_y B \quad (33)$$

The ratio of these two expressions is the MHD efficiency

$$\eta_{MHD} = \frac{E}{uB} = \kappa \quad (34)$$

This quantity is a constant ($\kappa = 1/2$) in the heretofore provided formalism since no physical effects other than impedance matching are considered.

At high applied field strength, however, the Hall effect may play an important role in channel dynamics.³⁶⁻³⁸ The Hall effect in plasma is a consequence of electric current interaction with applied magnetic fields just as that experienced in metallic conductors. In plasma, though, this effect can have significant impact on plasma impedance and dynamics. The Hall effect is quantified via the generalized Ohm's Law

$$\vec{E} + \vec{u} \times \vec{B} = \frac{1}{\sigma} \vec{j} + \frac{1}{en} (\vec{j} \times \vec{B} - \nabla p_e) \quad (35)$$

where the last two terms were omitted in the form previously employed (Eq. 1). The $\vec{j} \times \vec{B}$ term on the right side is the Hall term. The last term represents the electrodynamic influence of electron pressure gradients and is ignorable when $\beta_e = 2\mu_0 kT_e/B^2 \ll 1$. For CA-plasma cell conditions $\beta_e \sim 10^{-6}$ at 1 T so that neglecting electron pressure is well justified.

The Hall contribution, however, is most often not negligible. It can have quite a strong influence on plasmadynamics, electrodynamics, and energy balance in MHD plasmas.³⁶⁻³⁸ Via the Hall term, a component of electric current and field perpendicular to B is introduced. For the cartesian MHD channel described earlier with $\vec{B} = (0, 0, B)$ and $\vec{u} = (u, 0, 0)$ resulting in MHD fields E_y and j_y , the Hall contribution appears in the $-\hat{x}$ direction and is given by

$$E_{hall} = E_x = \frac{1}{\sigma} j_x + \frac{1}{en} j_y B \quad (36)$$

where j_x is the Hall current. Lacking experimental guidance or further theoretical constraints on j_x , parameterization is provided by the Morozov^{37,38} Hall parameter

$$\Xi = j_x / enu \quad (37)$$

The MHD efficiency expression is then suitably modified to incorporate the rate at which energy is expended in driving Hall currents

$$\eta_{MHD} = \kappa \frac{1}{1 + \frac{j_x E_x}{u j_y B}} \quad (38)$$

No credit is taken here for the potential for power conversion of the Hall current component. This has enhanced performance been suggested elsewhere^{27,29} and should be considered further to improve the overall performance of the converter. Figure 6 displays the MHD efficiency including Hall losses as a function of the applied field for $\Xi = 0.1, 0.3, 1.0$. A smaller Hall parameter is clearly desirable here. As Ξ is increased, a greater fraction of converter power is diverted to drive Hall currents. The effect is increased with increasing B since $E_{\text{hall}} \sim B$ for large B .

E. Flow

In the absence of spontaneous plasma flow from the hot CA-plasma cell to the relatively cold MHD converter section, a directional plasma flow may also be formed by using a magnetic mirror. A magnetic mirror has a magnetic field gradient in the desired direction of ion flow where the initial parallel velocity of plasma particles increases as the orbital velocity decreases with conservation of kinetic energy and adiabatic invariant $\mu = W_{\perp}/B$, the linear energy being drawn from that of orbital motion. The adiabatic invariance of flux through the orbit of an ion is a means to form a flow of ions along the field with the conversion of W_{\perp} to W_{\parallel} .

Plasma is selectively generated in the center region of the CA-plasma power cell. A magnetic mirror located in the center region causes electrons and ions to be forced from a homogeneous distribution of velocities at the cell center to a preferential velocity along the axis of the magnetic mirror. Thus, the plasma ions have a preferential velocity along the field and propagate into the MHD power converter. By preserving the adiabatic invariant, the parallel velocity at any position along the z -axis is given by

$$v_{\parallel 0}^2 = v_o^2 - v_{\perp o}^2 \frac{B}{B_o} \quad (39)$$

where the zero subscript represents the initial condition at the cell center. In the case that $v_{\parallel o}^2 = v_{\perp o}^2 = 0.5v_o^2$ and $\frac{B}{B_o} = 0.1$ at the MHD power converter, the particle velocity is 95% parallel to the field at the converter.

V. CONCLUSIONS

Preliminary investigation has been made on plasma-to-electric conversion technologies for small to mid-scale CA-plasma cells. Direct electromagnetic and MHD conversion technologies have been considered in some detail for the unique parameter range of CA-plasma cells. The plasma conditions inherent in these devices (intermediate temperature and ionization fraction, high neutral inventory) pose unique challenges to conversion. An $\vec{E} \times \vec{B}$ direct converter is considered in detail showing quite promising ideal performance with conversion efficiency up to $\sim 70\%$. However, in light of the large neutral inventory present, direct conversion including $\vec{E} \times \vec{B}$, other drift concepts, as well as electrostatic collection should be considered as impractical as plasma-to-electric conversion technologies. Collisional interruption of ion trajectories become the most serious shortcoming. However, fluid conversion strategies, like MHD, appear to be much better suited to cell conditions. These conversion technologies do not require charge separation, nor is expansion required in most cases. It is discussed herein that ion acoustic flow at 40 eV can generate up to several kW of electrical power in a 1 T field with conversion efficiency approaching 50% including Hall losses.

References

- ¹www.plugpower.com.
- ²Energy Information Administration, *International Electricity Prices for Households*, October 20, 2000 (www.eia.doe.gov/emeu/iea/elecprh.html).
- ³P. Maycock, *PV News* **19**, 3 (April, 2000).
- ⁴I. Uehara, T. Sakai, and H. Ishikawa, *J. Alloy Comp.* **253/254**, 635 (1997).
- ⁵J. Glanz, *New Scientist*, 32 (April 15, 1995).
- ⁶R. L. Mills, N. Greening, and S. Hicks, Optically measured power balances of glow discharges of mixtures of argon, hydrogen, potassium, rubidium, cesium, or strontium vapor, submitted to *Int. J. Hydrogen Energy*, 2001.
- ⁷R. L. Mills, P. Ray, B. Dhandapani, and J. He, Spectroscopic identification of fractional rydberg states of atomic hydrogen, submitted to *J. Phys. Chem. Letts.*, 2001.
- ⁸R. Mills, J. Dong, W. Good, P. Ray, J. He, and B. Dhandapani, Measurement of energy balances of noble gas-hydrogen discharge plasmas using calvet calorimetry, submitted to *Int. J. Hydrogen Energy*, 2001.
- ⁹R. L. Mills, P. Ray, B. Dhandapani, M. Nansteel, X. Chen, and J. He, New power source from fractional quantum energy levels of atomic hydrogen that surpasses internal combustion, *Spectrochimica Acta*, in progress, 2001.
- ¹⁰R. L. Mills, P. Ray, B. Dhandapani, and J. He, Comparison of excessive balmer line broadening of glow discharge and microwave hydrogen plasmas with certain catalysts, submitted to *J. Phys. Chem.*, 2001.
- ¹¹R. L. Mills, A. Voigt, P. Ray, M. Nansteel, and B. Dhandapani, Measurement of hydrogen balmer line broadening and thermal power balances of noble gas-hydrogen discharge plasmas, *Int. J. Hydrogen Energy*, in press, 2001.

- ¹²R. L. Mills, Blacklight power technology-a new clean energy source with the potential for direct conversion to electricity, in *Global Foundation International Conference on Global Warming and Energy Policy*, Fort Lauderdale, FL, 2000, Kluwer Academic/Plenum Publishers, New York.
- ¹³R. L. Mills, Blacklight power technology-a new clean hydrogen energy source with the potential for direct conversion to electricity, in *Proceedings of the National Hydrogen Association, 12th Annual U.S. Hydrogen Meeting and Exposition, Hydrogen: The Common Thread*, Washington, DC, 2001.
- ¹⁴R. G. Mills, *Nucl. Fusion* **7**, 223 (1967).
- ¹⁵D. L. Rose, *Nucl. Fusion* **9**, 183 (1969).
- ¹⁶G. H. Miley, *Fusion Energy Conversion*, American Nuclear Society, La Grange, IL, 1976.
- ¹⁷R. W. Moir, W. L. Barr, and G. A. Carlson, Direct conversion of plasma energy to electricity for mirror fusion reactors, in *Proc. 5th IAEA Conference on Plasma Physics and Controlled Nuclear Fusion Research*, Japan, 1974, 1975, IAEA, IAEA Pub., Vienna.
- ¹⁸R. W. Moir and W. L. Barr, *Nucl. Fusion* **13**, 35 (1973).
- ¹⁹R. P. Freis, *Nucl. Fusion* **13**, 247 (1973).
- ²⁰J. D. Lee, *J. Nucl. Mater.* **53**, 76 (1974).
- ²¹R. W. Moir, W. L. Barr, and G. H. Miley, *J. Nucl. Mater.* **53**, 86 (1974).
- ²²A. V. Timofeev, *Sov. J. Plasma Phys.* **4**, 464 (1978).
- ²³V. M. Glagolev and A. V. Timofeev, *Plasma Phys. Rep.* **19**, 745 (1994).
- ²⁴S. Way, *Westinghouse Eng.* **20**, 105 (1960).
- ²⁵M. Sakuntala, B. E. Clotfelter, W. B. Edwards, and R. G. Fowler, *J. Appl. Phys.* **30**, 1669 (1959).
- ²⁶H. P. Pain and P. R. Smy, *J. Fluid Mech.* **10**, 51 (1961).

- ²⁷R. J. Rosa, *Phys. Fluids* **4**, 182 (1961).
- ²⁸R. J. Rosa, *J. Appl. Phys.* **31**, 735 (1961).
- ²⁹C. Manna and N. W. Mather, *Engineering Aspects of Magnetohydrodynamics*, Columbia University Press, NY, 1962.
- ³⁰R. B. Clark, D. T. Swift-Hook, and J. K. Wright, *Brit. J. Appl. Phys.* **14**, 10 (1963).
- ³¹P. R. Smy, *J. Appl. Phys.* **32**, 1946 (1961).
- ³²P. Bitter, *Rev. Sci. Instrum.* **7**, 479 (1936).
- ³³S. C. Brown, *Basic Data of Plasma Physics*, The Technology Press of The Massachusetts Institute of Technology and John Wiley and Sons, Inc., New York, 1959.
- ³⁴H. J. Pain and P. R. Smy, *J. Fluid Mech.* **9**, 390 (1960).
- ³⁵M. Sakuntala, A. von Engel, and R. G. Fowler, *Phys. Rev.* **118**, 1459 (1960).
- ³⁶D. C. Black, R. M. Mayo, and R. W. Caress, *Phys. Plasmas* **4**, 2820 (1997).
- ³⁷D. C. Black, R. M. Mayo, R. A. Gerwin, K. F. Schoenberg, J. T. Scheuer, R. P. Hoyt, and I. Henins, *Phys. Plas.* **1**, 3115 (1994).
- ³⁸K. F. Schoenberg, R. A. Gerwin, I. Henins, R. M. Mayo, J. T. Scheuer, and G. Wurden, *IEEE Trans. Plas. Sci.* **21**, 625 (1993).
- ³⁹Electronic mail: rmayo@blacklightpower.com

Table 1: Typical plasma conditions in Ar-H CA-plasma cell with 5% minority H concentration.

| | | |
|--------------------------|-------------|--------------------------------------|
| Electron Temperature | T_e | 10 eV |
| Ion Temperature | T_i | 30–40 eV |
| Plasma Density | $n_e = n_i$ | $10^{12} - 10^{14} \text{ cm}^{-3}$ |
| Majority Neutral Density | n_{Ar} | $3 \times 10^{16} \text{ cm}^{-3}$ |
| Minority Neutral Density | n_H | $1.5 \times 10^{15} \text{ cm}^{-3}$ |

Table 2: Ion and electron collision frequencies in a CA-plasma cell having the conditions of table 1 with 40 eV H^+ ions, 10^{12} cm^{-3} plasma density, and Coulomb logarithm of 20.

| | Neutrals | Electrons | Ions |
|-----------|---------------------------|---------------------------|---------------------------|
| | $\nu_{xn} \text{ s}^{-1}$ | $\nu_{xe} \text{ s}^{-1}$ | $\nu_{xi} \text{ s}^{-1}$ |
| Electrons | 6×10^9 | 2.7×10^6 | 2.7×10^6 |
| Ions | 3.8×10^8 | 2×10^3 | 7.8×10^3 |

Figures

FIG. 1. $\vec{E} \times \vec{B}$ type direct converter schematic.

FIG. 2. Ideal efficiency for an $\vec{E} \times \vec{B}$ converter as a function of drift to thermal ratio α with $l/d \sim 5$.

FIG. 3. Schematic of an MHD converter interfaced to a CA-plasma cell, labeled *Plasma Tube-Reactor*. A magnetic mirror coil provides a guide field for the plasma flow extant from the cell region.

FIG. 4. MHD converter current density for sample converter as a function of applied magnetic field strength.

FIG. 5. MHD converter power density for sample converter as a function of applied magnetic field strength.

FIG. 6. MHD converter efficiency as a function of applied magnetic field strength including Hall losses for $\Xi = 0.1, 0.3, 1.0$.

ExB Converter

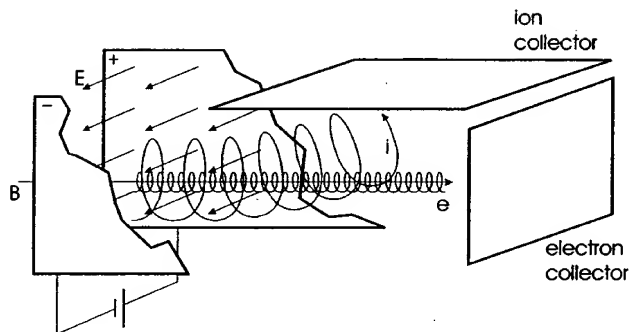


Figure 1

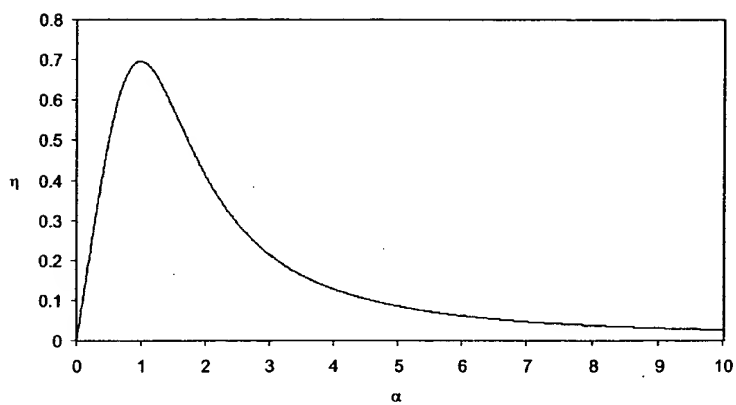


Figure 2

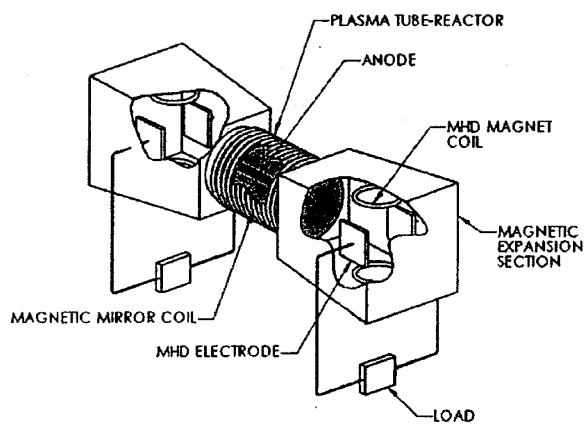


Figure 3

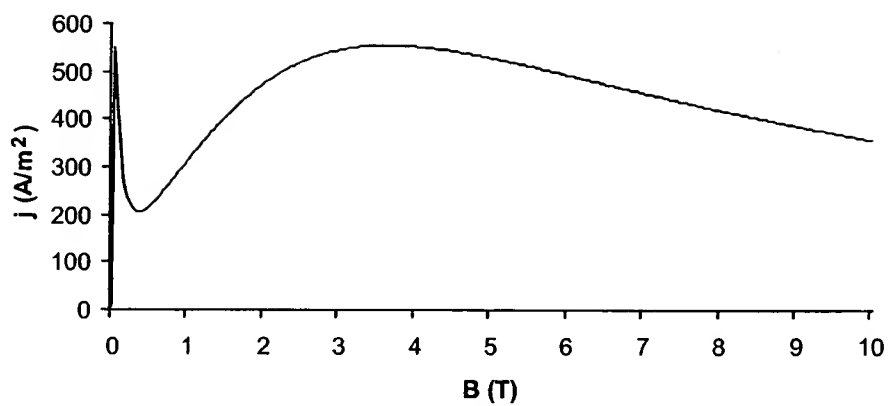


Figure 4

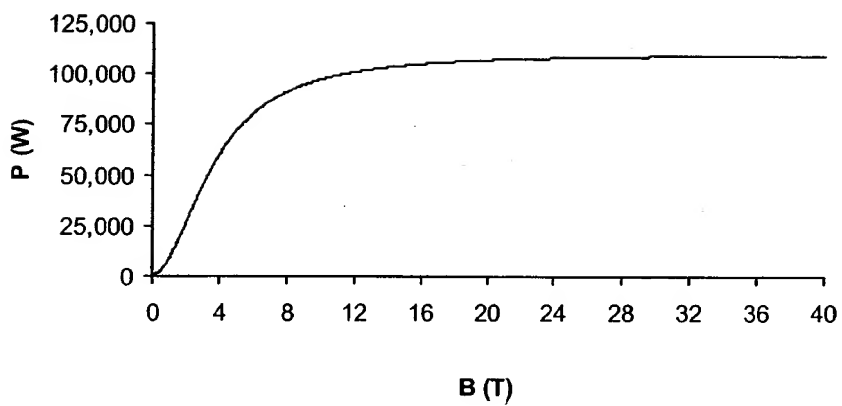


Figure 5

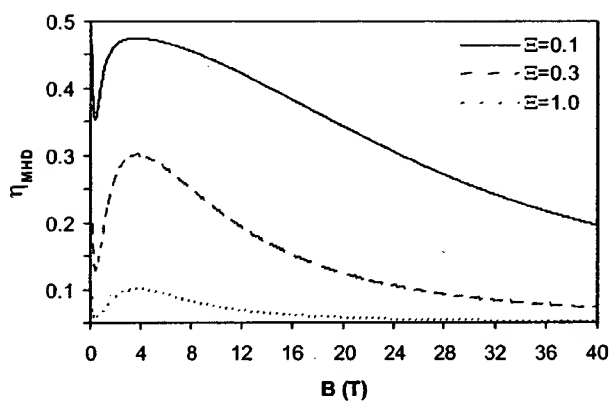


Figure 6

Excessive Balmer α Line Broadening, Power Balance, and Novel Hydride Ion Product of Plasma Formed from Incandescently Heated Hydrogen Gas with Certain Catalysts

Randell Mills, Paresh Ray, Jinquan Dong, Mark Nansteel, William Good,
Peter Jansson, Bala Dhandapani, Jiliang He

BlackLight Power, Inc.

493 Old Trenton Road

Cranbury, NJ 08512

ABSTRACT

Typically the emission of vacuum ultraviolet light from hydrogen gas is achieved using discharges at high voltage, synchrotron devices, high power inductively coupled plasma generators, or a plasma is created and heated to extreme temperatures by RF coupling (e.g. $> 10^6$ K) with confinement provided by a toroidal magnetic field. Observation of intense extreme ultraviolet (EUV) emission at low temperatures (e.g. $\approx 10^3$ K) from atomic hydrogen generated at a tungsten filament that heated a titanium dissociator and certain gaseous atoms or ions vaporized by filament heating has been reported previously [R. Mills, J. Dong, Y. Lu, "Observation of Extreme Ultraviolet Hydrogen Emission from Incandescently Heated Hydrogen Gas with Certain Catalysts", *Int. J. Hydrogen Energy*, Vol. 25, (2000), pp. 919-943]. Each of the ionization of potassium, cesium, strontium, and Rb^+ and an electron transfer between two K^+ ions (K^+ / K^+) provide a reaction with a net enthalpy of an integer multiple of the potential energy of atomic hydrogen. The presence of each of the corresponding reactants formed the low applied temperature, extremely low voltage plasma called a resonance transfer or rt-plasma having strong EUV emission. Similarly, the ionization energy of Ar^+ is 27.63 eV, and the emission intensity of the plasma generated by atomic strontium increased significantly with the introduction of argon gas only when Ar^+ emission was observed [R. Mills, "Spectroscopic Identification of a Novel Catalytic Reaction of Atomic Hydrogen and the Hydride Ion Product", *Int. J. Hydrogen Energy*, Vol. 26, No. 10, (2001), pp. 1041-1058.]. In contrast, the chemically similar atoms, sodium, magnesium and barium, do not ionize at integer multiples of the potential energy of atomic hydrogen did not form a plasma and caused no emission. For further characterization, we recorded the width of the 656.2 nm Balmer α line on light emitted from rt-plasmas. Significant line broadening of 17, 9, 11, 14, and 24 eV was observed from a rt-plasma of hydrogen with K^+ / K^+ , Rb^+ , cesium, strontium, and strontium with Ar^+ , respectively. These results could not be explained by Stark or thermal broadening or electric field acceleration of charged species since the measured field of the incandescent heater was extremely weak, 1 V/cm, corresponding to a broadening of much less than 1 eV. Rather the

source of the excessive line broadening is consistent with that of the observed EUV emission, an energetic reaction caused by a resonance energy transfer between hydrogen atoms and K^+ / K^+ , Rb^+ , cesium, strontium, or Ar^+ . Since line broadening is a measure of temperature, the excess power was measured calorimetrically on rf-plasmas formed by K^+ / K^+ and Ar^+ as catalysts. The product hydride ion with each of K^+ / K^+ , Rb^+ , Cs, and Ar^+ as the catalyst was predicted to have a binding energy of 3.05 eV and was observed by high resolution visible spectroscopy at 407 nm.

I. INTRODUCTION

Glow discharge devices have been developed over decades as light sources, ionization sources for mass spectroscopy, excitation sources for optical spectroscopy, and sources of ions for surface etching and chemistry [1-3]. A Grimm-type glow discharge is a well established excitation source for the analysis of conducting solid samples by optical emission spectroscopy [4-6]. Despite extensive performance characterizations, data was lacking on the plasma parameters of these devices. M. Kuraica and N. Konjevic [7] and Videnocic et al. [8] have characterized these plasma by determining the excited hydrogen atom concentrations and energies by measuring line broadening of the 656.2 nm Balmer α line. The data was analyzed in terms of Stark and Doppler effects wherein acceleration of charges such as H^+ , H_2^+ , and H_3^+ in the high fields (e. g. over 10 kV/cm) which were present in the cathode fall region was used to explain the Doppler component.

More recently, microhollow glow discharges have been spectroscopically studied as candidates for the development of an intense monochromatic EUV light source (e.g. Lyman α) for short wavelength lithograph for production of the next generation of integrated circuits. A neon-hydrogen microhollow cathode glow discharge has been proposed as a source of predominantly Lyman α radiation. Kurunczi, Shah, and Becker [9] observed intense emission of Lyman α and Lyman β radiation at 121.6 nm and 102.5 nm, respectively, from microhollow cathode discharges in high-pressure Ne (740 Torr) with the addition of a small amount of hydrogen (up to 3 Torr). With essentially no molecular emission observed, Kurunczi et al. attributed the anomalous Lyman α emission to the near-resonant energy transfer between the Ne_2^+ excimer

and H_2 which leads to formation of $H(n=2)$ atoms, and attributed the Lyman β emission to the near-resonant energy transfer between excited Ne^* atoms (or vibrationally excited neon excimer molecules) and H_2 which leads to formation of $H(n=3)$ atoms. Despite the emission characterization of this source, data is lacking about plasma parameters.

For analyses of solids, direct current (dc) glow discharge sources have been successfully complemented by radio-frequency (rf) discharges [10]. The use of dc discharges is limited to metals; whereas, rf discharges are applicable to non-conducting materials. Other developed sources that provide a usefully intense plasma are synchrotron devices, inductively coupled plasma generators [11], and magnetically confined plasmas. Plasma characterization data on these sources is also limited.

A new plasma source has been developed that operates by incandescently heating a hydrogen dissociator to provide atomic hydrogen and heats a catalyst such that it becomes gaseous and reacts with the atomic hydrogen to produce a plasma [12-45]. It was extraordinary, that intense EUV emission was observed by Mills et al. [21-25, 31-32, 34-35] at low temperatures (e.g. $\approx 10^3$ K) from atomic hydrogen and certain atomized elements or certain gaseous ions which singly or multiply ionize at integer multiples of the potential energy of atomic hydrogen, 27.2 eV that comprise catalysts. The only pure elements that were observed to emit EUV were those wherein the ionization of i electrons from an atom to a continuum energy level is such that the sum of the ionization energies of the i electrons is approximately $m \cdot 27.2$ eV where i and m are each an integer.

Since Ar^+ , He^+ , and strontium each ionize at an integer multiple of the potential energy of atomic hydrogen, a discharge with one or more of these species present with hydrogen is anticipated to form a plasma called a resonance transfer (rt) plasma. The plasma forms by a resonance transfer mechanism involving the species providing a net enthalpy of a multiple of 27.2 eV and atomic hydrogen.

Mills and Nansteel [24-25, 31] have reported that strontium atoms each ionize at an integer multiple of the potential energy of atomic hydrogen and caused emission. (The enthalpy of ionization of Sr to Sr^{3+} has a net enthalpy of reaction of 188.2 eV, which is equivalent to $m=7$.) The emission intensity of the plasma generated by atomic strontium

increased significantly with the introduction of argon gas only when Ar^+ emission was observed. Whereas, no emission was observed when chemically similar atoms that do not ionize at integer multiples of the potential energy of atomic hydrogen (sodium, magnesium, or barium) replaced strontium with hydrogen, hydrogen-argon mixtures, or strontium alone.

Mills and Nanstell [24-25, 31] measured the power balance of a gas cell having vaporized strontium and atomized hydrogen from pure hydrogen or argon-hydrogen mixture (77/23%) by integrating the total light output corrected for spectrometer system response and energy over the visible range. Hydrogen control cell experiments were identical except that sodium, magnesium, or barium replaced strontium. In the case of hydrogen-sodium, hydrogen-magnesium, and hydrogen-barium mixtures, 4000, 7000, and 6500 times the power of the hydrogen-strontium mixture was required, respectively, in order to achieve that same optically measured light output power. With the addition of argon to the hydrogen-strontium plasma, the power required to achieve that same optically measured light output power was reduced by a factor of about two. The power required to maintain a plasma of equivalent optical brightness with strontium atoms present was 8600 and 6300 times less than that required for argon-hydrogen and argon control, respectively. A plasma formed at a cell voltage of about 250 V for hydrogen alone and sodium-hydrogen mixtures, 140-150 V for hydrogen-magnesium and hydrogen-barium mixtures, 224 V for an argon-hydrogen mixture, and 190 V for argon alone; whereas, a plasma formed for hydrogen-strontium mixtures and argon-hydrogen-strontium mixtures at extremely low voltages of about 2 V and 6.6 V, respectively.

It was reported [23] that characteristic emission was observed from a continuum state of Ar^{2+} which confirmed the resonant nonradiative energy transfer of 27.2 eV from atomic hydrogen Ar^+ . The transfer of 27.2 eV from atomic hydrogen to Ar^+ in the presence of a electric weak field resulted in its excitation to a continuum state. Then, the energy for the transition from essentially the Ar^{2+} state to the lowest state of Ar^+ was predicted to give a broad continuum radiation in the region of 45.6 nm. This broad continuum emission was observed. This emission was dramatically different from that given by an argon microwave plasma

wherein the entire Rydberg series of lines of Ar^+ was observed with a discontinuity of the series at the limit of the ionization energy of Ar^+ to Ar^{2+} . The observed Ar^+ continuum in the region of 45.6 nm confirmed the rt-plasma mechanism of the excessively bright, extraordinarily low voltage discharge. The product hydride ion with Ar^+ as a reactant was predicted to have a binding energy of 3.05 eV and was observed spectroscopically at 407 nm [23].

He^+ ionizes at 54.417 eV which is 2·27.2 eV, and novel EUV emission lines were observed from microwave and glow discharges of helium with 2% hydrogen [18-19, 27]. The observed energies were $q \cdot 13.6 \text{ eV}$ ($q=1,2,3,4,6,7,8,9, \text{ or } 11$) or these energies less 21.2 eV due to inelastic scattering of the lines by helium atoms in the excitation of $He(1s^2)$ to $He(1s'2p')$. These lines can be explained by the resonance transfer of $m \cdot 27.2 \text{ eV}$.

The plasma parameters of rt-plasmas were previously studied by EUV spectroscopy [18-25, 31-35], characteristic emission from catalysis and the hydride ion products [21-23], lower-energy hydrogen emission [16, 18-20], plasma formation [21-25, 31-32, 34-35], Balmer α line broadening [19, 28-29], elevated electron temperature [19, 28], anomalous plasma afterglow duration [34-35], power generation [24-31, 42], and analysis of chemical compounds [36-42]. To further characterize these plasmas, the width of the 656.2 nm Balmer α line was recorded on light emitted from rt-plasmas formed from hydrogen with K^+/K^+ , Rb^+ , Cs , Sr , or Ar^+ . Since line broadening is a measure of temperature, the power balance of rt-plasmas formed with K^+/K^+ and $Sr-Ar^+$ catalysts were measured calorimetrically. The product hydride ion with each of K^+/K^+ , Rb^+ , Cs , and Ar^+ as the catalyst was predicted to have a binding energy of 3.05 eV corresponding to emission at 407 nm. Thus, the high resolution visible spectra covering the region of 407 nm was recorded.

II. EXPERIMENTAL

A. Balmer line broadening and high resolution visible spectroscopy recorded on rt-plasmas

The width of the 656.2 nm Balmer α line was recorded on light

emitted from a hydrogen glow discharge performed according to methods reported previously [29] that served as a control for measurements recorded on light emitted from rt-plasmas of hydrogen with K_2CO_3 , KNO_3 , $RbNO_3$, Cs_2CO_3 , strontium or strontium with an argon-hydrogen mixture (97/3%). The experimental set up shown in Figure 1 comprised a quartz cell which was 500 mm in length and 50 mm in diameter. The entire quartz cell was enclosed in an Alumina insulation package. Several K-type thermocouples were located in the insulation. The thermocouples were monitored with a multichannel computer data acquisition system. A Pyrex cap sealed to the quartz cell with a Viton O ring and a C-clamp incorporated ports for gas inlet, outlet, and photon detection. A tungsten filament (0.508 mm in diameter and 800 cm in length, total resistance ~2.5 ohm) heater and hydrogen dissociator were in the quartz tube as well as a cylindrical titanium screen (300 mm long and 40 mm in diameter) that served as a second hydrogen dissociator in the case of experiments with carbonates and nitrates. The filament was coiled on a grooved ceramic tube support to maintain its shape when heated. The return lead passed through the inside of the ceramic tube. The inorganic test materials were coated on a titanium screen dissociator by the method of wet impregnation. The screen was coated by dipping it in a 0.6 M K_2CO_3 /10% H_2O_2 , 0.6 M KNO_3 /10% H_2O_2 , 0.6 M $RbNO_3$ /10% H_2O_2 , 0.6 M Cs_2CO_3 /10% H_2O_2 , or 0.6 M $SrCO_3$ /10% H_2O_2 , and the crystalline material was dried on the surface by heating for 12 hours in a drying oven at 130 °C. A new dissociator was used for each experiment. The titanium screen was electrically floated with power applied to the filament. In a repeat of the rt-plasma formed with strontium, the titanium screen was removed, and about 1 g of strontium metal (Alfa Aesar 99.95%) was placed in the center of the cell under one atmosphere of dry argon in a glovebox. The cell was sealed, removed from the glovebox, and connected to an EUV spectrometer. Strontium was vaporized by the filament heater. In each test, power was applied to the filament by a DC power supply which was controlled by a constant power controller. The power applied to the filament was 300 W. The voltage across the filament was about 55 V and the current was about 5.5 A at 300 W. The temperature of the tungsten filament was estimated to be in the range 1100 to 1500 °C. The external cell wall temperature was about 700 °C.

The cell was operated under gas flow conditions while maintaining a constant gas pressure in the cell. Each gas was ultrahigh purity. The gas pressure inside the cell was maintained at about 300 mtorr with a hydrogen flow rate of 5.5 sccm or an argon flow rate of 5.2 sccm and a hydrogen flow rate of 0.3 sccm. Each gas flow was controlled by a 0-20 sccm range mass flow controller (MKS 1179A21CS1BB) with a readout (MKS type 246). The cell pressure was monitored by a 0-10 torr MKS Baratron absolute pressure gauge.

The light emission was introduced to an EUV spectrometer for spectral measurement. The spectrometer was a McPherson 0.2 meter monochromator (Model 302, Seya-Namioka type) equipped with a 1200 lines/mm holographic grating with a platinum coating. The wavelength region covered by the monochromator was 30–560 nm. A channel electron multiplier (CEM) was used to detect the EUV light. The wavelength resolution was about 1 nm (FWHM) with an entrance and exit slit width of 300 μ m. The vacuum inside the monochromator was maintained below 5×10^{-4} Torr by a turbo pump. The Lyman α emission was recorded as a function of time after the filament was turned on. In each case, the EUV spectrum (40–160 nm) of the rt-plasma cell emission was recorded at about the point of the maximum Lyman α emission to confirm the rt-plasma before the line broadening and high resolution visible spectrum in the region of 407 nm were recorded.

The plasma emission from the hydrogen glow discharge and each rt-plasma maintained in the filament heated cell was fiber-optically coupled through a 220F matching fiber adapter positioned 2 cm from the sapphire window or cell wall, respectively, to a high resolution visible spectrometer with a resolution of ± 0.006 nm over the spectral range 190–860 nm. The spectrometer was a Jobin Yvon Horiba 1250 M with 2400 grooves/mm ion-etched holographic diffraction grating. The entrance and exit slits were set to 20 μ m. The spectrometer was scanned between 655.5–657 nm using a 0.01 nm step size. The signal was recorded by a PMT with a stand alone high voltage power supply (950 V) and an acquisition controller. The data was obtained in a single accumulation with a 1 second integration time.

In addition, the high resolution visible spectrum of each rt-plasma was recorded over the range 400–410 nm using the same methods as those

of the line broadening measurements. The emission from a control hydrogen microwave discharge plasma maintained by the methods given previously [18] was also recorded.

B. Calvet calorimeter methods for the power balance measurement of a rt-plasma formed with K^+/K^+

The power balance of a rt-plasma formed with K^+/K^+ was measured calorimetrically using Calvet calorimeter as shown in Figure 2. The instrument used to measure the heat of reaction comprises a cylindrical heat flux calorimeter (International Thermal Instrument Co., Model CA-100-1). The cylindrical calorimeter walls contain a thermopile structure composed of two sets of thermoelectric junctions. One set of junctions is in thermal contact with the internal calorimeter wall, at temperature T_i , and the second set of thermal junctions is in thermal contact with the external calorimeter wall at T_e which is held constant by a forced convection oven. When heat is generated in the calorimeter cell, the calorimeter radially transfers a constant fraction of this heat into the surrounding heat sink. As heat flows a temperature gradient, $(T_i - T_e)$, is established between the two sets of thermopile junctions. This temperature gradient generates a voltage which is compared to the linear voltage versus power calibration curve to give the power of the reaction. The calorimeter was calibrated with a filament that served as a joule heater and a fixed power source at power levels representative of the power of reaction of the catalyst runs. The calibration constant of the Calvet calorimeter is not sensitive to the flow of hydrogen over the range of conditions of the tests. A chemically resistant cylindrical reactor, machined from 304 stainless steel to fit inside the calorimeter, was used to contain the reaction. To maintain an isothermal reaction system and improve baseline stability, the calorimeter was placed inside a commercial forced convection oven (Precision Scientific 625 S) capable of operating from room temperature to 616 K. Also, the calorimeter and reactor were enclosed within a cubic insulated box filled with aluminasilicate insulation to further dampen thermal oscillations in the oven. A more complete description of the instrument and methods are given by Bradford, Phillips, and Klanchar [46].

C. Gas Cell for Calvet Calorimeter

Since KNO_3 is volatile at a temperature much less than that at which it decomposes [47], it was used as the source of K^+/K^+ catalyst at a temperature at which it was volatile. The cylindrical stainless steel filament cell and Calvet instrument for power balance studies with hydrogen and gaseous KNO_3 compared to gaseous KNO_3 alone is shown in Figure 2. The cell schematic is shown in Figure 3. The cell comprised a 20 cc stainless steel vessel. The cell was maintained at a constant isothermal temperature of 250 °C by the forced convection oven. The cell was used in the vertical position and was inserted into a thermopile. The flange was sealed with a copper gasket. The flange had a two hole Conax-Buffalo gland for the leads of a 0.25 mm diameter by 10, 20, or 30 cm length Pt (Aldrich 99.99%) filament wound in a coil that radiatively heated a 0.7 ml volume, cylindrical flat base Alumina crucible (Alfa 15.2 mm high X 10 mm OD X 8 mm ID) which contained 250 mg of KNO_3 (Aldrich 99.999% pure). The filament served to dissociate hydrogen and to slowly vaporize the KNO_3 by heating. The filament also served as a precision resistor to calibrate the cell. The filament was powered by a constant power supply (Pennsylvania State University 0-20 W \pm 1%), and the power dissipated in the filament was recorded with a watt meter (Clarke-Hess Model 259 V-A-W Meter \pm 0.03 W).

The flange also had a 6.4 mm vacuum port through which a 1.6 mm OD inlet for hydrogen passed. The hydrogen gas was ultrahigh pure grade or higher (Praxair). The 1.6 mm OD inlet was connected to a 6.4 mm OD stainless steel tube which connected to a Tee, a needle valve, a pressure gauge, and then the gas supply. The elbow port of the Tee was attached to a vacuum gauge, a needle valve, a meter valve, and then a vacuum pump. The gas pressure was controlled manually by adjusting the supply through the inlet versus the amount pumped away at the outlet where the pressure was monitored in the outlet tube by the vacuum gauge. The hydrogen pressure and flow rate were adjusted to maximize the output power. The optimal pressure was about 0.2 torr maintained by an estimated flow rate of about 0.1 sccm. The data was recorded with a data acquisition system.

The cell was calibrated by measuring the steady state Calvet response to constant power into the filament over the power range 1-16 W with hydrogen at 0.2 Torr pressure without KNO_3 . At a constant oven temperature of 250 °C, the experiment was repeated by allowing the Calvet voltage to reach steady state with KNO_3 alone present and constant power applied to the filament. Hydrogen was then maintained at 0.2 Torr with flow. The experiment was performed for a filament length of 10, 20, or 30 cm at a constant filament input power of 7.02, 9.82, and 15.01 W, respectively.

D. Calvet power balance measurements

Since the ambient temperature was held constant, the general form of the power balance equation for the Calvet cell in steady state is:

$$0 = P_{in} + P_{ex} - P_{loss} \quad (1)$$

where P_{in} is the input power to the filament, P_{ex} is the excess power generated from the hydrogen catalysis reaction, and P_{loss} is the thermal power loss from the cell. The Calvet voltage response to input power for hydrogen without KNO_3 was determined over the constant input power range of 1 W to 16 W. The data was recorded after the cell had reached a thermal steady state with each increase in the input power to the filament which typically occurred in about 6 hours. At this point, the power lost from the cell P_{loss} was equal to the total power P_T supplied to the cell P_{in} plus any excess power P_{ex} .

$$P_T = P_{in} + P_{ex} = P_{loss} \quad (2)$$

Since the heat transfer was dominated by conduction, the output voltage of the cell V was modeled by a linear curve

$$V = aP_T + C \quad (3)$$

where a and C are constants for the least square curve fit of the Calvet voltage response to power input for the control experiments ($P_{ex} = 0$). V was recorded as a function of input power P_{in} for hydrogen without KNO_3 catalyst as the input power was varied. The higher voltage produced with hydrogen and catalyst compared with hydrogen and no catalyst was representative of the excess power. In the case of the catalysis run, the total output power P_T was determined by solving Eq. (3) using the measured V . The excess power P_{ex} was determined from Eq. (2). The

integral of the excess power P_{ex} over time gave the excess energy E_{ex} .

E. Filament cell apparatus and procedure for power balance measurement of an Ar⁺ rt-plasma

The power balance of a rt-plasma of strontium with argon-hydrogen mixture (95/5%) was measured with the experimental setup shown in Figure 4. The power balances of argon-hydrogen-strontium rt-plasmas maintained in a one-liter cylindrical stainless steel cell fitted with a heated tungsten filament shown in Figure 5 were measured by heat loss calorimetry (determining the power balance from the temperature at steady state relative to that of a control power source) as the input power to the filament was varied. The relationship between the rate of heat loss from the cell and the cell temperature was determined from a control experiment in which both strontium catalyst and plasma were absent.

The 304-stainless steel cylindrical cell was 9.21 cm in diameter and 14.5 cm in height. The base of the cell contained a welded-in stainless steel thermocouple well (1 cm OD) which housed a thermocouple in the cell interior approximately 3 cm from the cell axis. The upper end of the cell was welded to a high vacuum 15 cm diameter conflat flange. A silver-plated copper gasket was used to seal the cell flange to a mating flange. The two flanges were clamped together with 10 circumferential bolts. The mating flange contained two penetrations comprising a stainless steel thermocouple well (1 cm OD), which also housed a thermocouple in the cell interior approximately 3.5 cm from the cell axis, and a centered high voltage feedthrough. The body of the cell included two radial penetrations. One was a 9.5 mm OD tube for gas fill and evacuation, the other was a tube which housed a 1.5 cm diameter UV-grade sapphire viewport. The cell interior was fitted with a 27 mm OD grooved Alumina tube which was 60 mm in length. The tube was tightly wrapped with approximately 330 cm of 0.25 mm tungsten wire. The tube was suspended on the cell axis by connecting the ends of the tungsten filament to the central electrode and the cell body (ground) as shown in Figure 5. AC power at 60 Hz was supplied to the filament through a variac. True rms voltage and current, and also power

dissipation in the filament were monitored by a digital volt-amp-watt meter (Clarke-Hess Model 259 V-A-W Meter) shown in Figure 4. Gas pressure in the cell was monitored with a 0-10 Torr MKS Baratron absolute pressure gauge.

Approximately 1.2 g of strontium metal (Alfa Aesar 99.95%) was placed on the base of the cell under one atmosphere of dry argon in a glovebox. After sealing the cell it was heated in a temperature-controlled kiln to 465°C while evacuating the system. At this condition the strontium vapor pressure was approximately 1 mTorr. After reaching thermal equilibrium, the cell was pressurized with 190 mTorr of argon and then an additional 10 mTorr of hydrogen to yield a argon-hydrogen mixture (95/5%) at 200 mTorr. Hydrogen was periodically added during the course of the experiment in order to maintain 200 mTorr pressure. It was observed that a substantial amount of hydrogen was absorbed during addition which was attributed to formation of strontium hydride. Ultrahigh purity grade argon and hydrogen were used. Approximately 50 V was applied to the filament corresponding to about 100 W. Plasma formation resulted after several minutes of heating the cell with the filament. Strong strontium and argon plasma line emission were observed in the visible and near-infrared with a visible spectrometer (Ocean Optics S2000). Electric power input to the cell was varied in the range 110-245 W. At each power setting, 2.5-3 hours was allowed for the cell to reach thermal equilibrium. The cell temperature was then computed by averaging the temperatures of the two thermocouples. In the control experiment, this procedure was repeated with the same cell except that both strontium and the resulting rt-plasma were absent.

G. Filament cell power balance measurements

Heat loss from the cell was primarily by radiation. Because the temperature of the kiln was fixed, the rate of heat loss from the cell, $P_T = P_{loss}$, was a function of the cell temperature:

$$P_T = f(T) \quad (4)$$

This relationship was determined from the argon-hydrogen control experiments in which $P = P_{in}$ was the electric power input. In the argon-hydrogen-strontium rt-plasma experiments, the rate of heat loss from

the cell exceeded the electric power input by the excess power P_{ex}

$$P_T = P_{in} + P_{ex} = f(T) \quad (5)$$

The excess power was then

$$P_{ex} = P_T - P_{in} = f(T) - P_{in} \quad (6)$$

Using the measured cell temperature and the input power, the excess power of each argon-hydrogen-strontium rt-plasma was computed from Eq. (6).

III. RESULTS

A. Balmer line broadening and high resolution visible spectroscopy recorded on rt-plasmas

The results of the 656.2 nm Balmer α line width measured with a high resolution (± 0.006 nm) visible spectrometer on light emitted from rt-plasmas of hydrogen with K_2CO_3 , $RbNO_3$, Cs_2CO_3 , and $SrCO_3$, and $SrCO_3$ with an argon-hydrogen mixture (97/3%) are shown in Figures 6-10, respectively. The spectrum of the KNO_3 cell was the same as that of the K_2CO_3 cell except that the intensity was higher. To illustrate the method of displaying each line broadening result as an unsmoothed curve, the corresponding raw data points are also shown in Figures 9 and 10 that further show the scatter in the data. The Balmer α line width and energetic hydrogen atom densities and energies given in Table 1 were calculated using the method of Videnović et al. [8]. Significant line broadening of 17, 9, 11, 14, and 24 eV and an atom density of 4×10^{11} , 6×10^{11} , 4×10^{11} , 8×10^{11} , and 4×10^{11} atoms/cm³ were observed from a rt-plasma of hydrogen formed with K^+/K^+ , Rb^+ , cesium, strontium, and strontium with Ar^+ catalysts, respectively. A glow discharge of hydrogen maintained at the same total pressure showed no excessive broadening corresponding to an average hydrogen atom temperature of ≈ 3 eV. The superposition of the 656 nm Balmer α line width recorded with a high resolution (± 0.006 nm) visible spectrometer on a hydrogen-strontium rt-plasma and a hydrogen-strontium rt-plasma intensified by argon ion catalyst is shown in Figure 11. By comparison to the strontium rt-plasma, significant broadening attributable to argon ion was observed corresponding to an average hydrogen atom temperature of 24 eV versus

14 eV. The atom density was also very high in the argon rt-plasma given that the hydrogen concentration was 30 times less than that of the strontium-pure-hydrogen rt-plasma.

The high resolution visible spectra in the region of 407 nm from the hydrogen rt-plasma formed using K_2CO_3 , $RbNO_3$, Cs_2CO_3 , and strontium metal with argon are shown in Figures 12-15, respectively. In each case, a peak was observed at 407 nm which could not be assigned to hydrogen, alkali or alkaline earth atom or ion. The known peaks of these atoms and ions in the region of 407 nm were separated as indicated in the figures. The spectrum of the KNO_3 cell was the same as that of the K_2CO_3 cell.

The 407.0 nm peak was not observed in an intense hydrogen microwave discharge plasma as shown in Figure 16. O II lines at 406.9623, 406.9881, and 407.1238 nm were eliminated due to the absence of O I lines at 394.729, 394.748, 394.758, 395.460, and 405.477 nm. C III lines at 407.026 and 406.8916 nm were eliminated due to the absence of C I lines which were outside of the region of 407 nm or C II lines at 391.896 and 392.068 nm. The observation of the 407.0 peak with KNO_3 , $RbNO_3$, and with strontium metal and argon also eliminated carbon as the source of the novel peak. Furthermore, the presence of the O II or C III lines would be extraordinary since the ionization energy required for O II is above the first ionization energy of 13.62 eV, and the energies required for C III are above the sum of the first and second ionization energies of 11.26 eV and 24.38 eV, respectively [48].

The emission intensity and the Balmer α line broadening of the hydrogen rt-plasma formed using strontium metal or $SrCO_3$ increased significantly with the introduction of argon gas only when Ar^+ emission was observed as shown in Figure 11. In both cases, the 407 nm peak of the argon-hydrogen-strontium rt-plasma was not observed with hydrogen alone—the presence of Ar^+ was required. The 407 nm peak shown in Figure 15 was formed using argon with strontium metal with no oxygen or carbon present which further eliminated oxygen and carbon lines as possible sources.

B. Power balance of a K^+/K^+ rt-plasma

The Calvet voltage as a function of the power applied to the

filament heater at 0.2 Torr hydrogen pressure was plotted for the input power range of 0.5 W to 16 W as shown in Figure 17. The least squares fit of the V response to unit input power calculated from the control (Eq. (3)) was determined to be

$$V = -0.061 + 0.233 \times P_T \quad (7)$$

A constant filament input power of 7.02, 9.82, and 15.01 W was maintained for a filament length of 10, 20, or 30 cm, respectively. The Calvet voltage was allowed to reach steady state with KNO_3 alone. The Calvet voltage significantly increased upon the addition of hydrogen, and the output signal was permitted to reach a second steady state as shown in Figure 18 for the case of 9.82 W input to a 20 cm long filament with a typical voltage and current of 4.16 V and 2.36 A, respectively. The excess power in each case was determined from Eq. (7) and Eq. (2). The results are shown in Table 2.

The sources of error were the error in the calibration curve (± 0.05 W) and the power measurement of the watt meter (± 0.03 W) in the power range of 0-16 W which was independent of the errors of the voltage (± 0.025 V) and current (± 1 mA) measurements due to any power factor. The propagated error of the calibration and power measurements was ± 0.06 W.

C. Power balance of an Ar^+ rt-plasma

Power input to the cell is plotted versus the cell temperature for the argon-hydrogen-strontium rt-plasma and also for the argon-hydrogen control in Figure 19. The relation between cell temperature and the rate of heat loss from the cell, found from the argon-hydrogen control data, is of the form

$$P_T = f(T) = A(T^4 - T_0^4) \quad (8)$$

where $A = 2.74 \times 10^{-9} \text{ W/K}^4$ and $T_0 = 465^\circ\text{C} = 738.2 \text{ K}$ is the kiln temperature. Deviations of the control data from this expression are less than 2 W. Using Eq. (8) in Eq. (6) yields the excess power generated in the argon-hydrogen-strontium rt-plasma for each power input condition. Power input and excess power are tabulated in Table 3. The excess power ranged from 13.3 W at 110 W input to 26.0 W at 245 W input. The average excess power over the range was about 20 W. This

corresponded to an excess power density of approximately 20 mW/cc in the one-liter cell.

The error in the temperature measurement over the range of 70 °C was ± 0.5 °C for the type K thermocouples. However, the excess power was measured as the difference in filament power to the control to achieve the same temperature as the argon-hydrogen-strontium rt-plasma. Thus, the sources of error were the error in the calibration curve ± 2 W and the power measurement of the watt meter (± 1 W) in the power range of 100-300 W which was independent of the errors of the voltage (± 0.25 V) and current (± 10 mA) measurements due to any power factor. The propagated error of the calibration and power measurements was ± 2.2 W.

IV. DISCUSSION

Line broadening of the hydrogen Balmer lines provides a sensitive measure of the number and energy of excited hydrogen atoms in a plasma. To further characterize the plasma parameters of rt-plasmas, the width of the 656.2 nm Balmer α line was recorded on light emitted from rt-plasmas formed from hydrogen with a gaseous atom or ion which ionizes at integer multiples of the potential energy of atomic hydrogen. The energetic hydrogen atom density and energies were determined from the broadening, and it was found that significant line broadening of 17, 9, 11, 14, and 24 eV and an atom density of 4×10^{11} , 6×10^{11} , 4×10^{11} , 8×10^{11} , and 4×10^{11} atoms/cm³ were observed from a rt-plasma of hydrogen formed with K^+/K^+ , Rb^+ , cesium, strontium, and strontium with Ar^+ catalysts, respectively. Whereas, a glow discharge of hydrogen maintained at the same total pressure with an electric field strength that was at least two order of magnitude greater than the 1 V/cm field of the filament cell showed no excessive broadening corresponding to an average hydrogen atom temperature of ≈ 3 eV.

In the characterization of the plasmas of Grimm-type discharges with a hollow anode, M. Kuraica and N. Konjevic [7] and Videnocic et al. [8] analyzed the broadening data in terms of Stark and Doppler effects wherein acceleration of charges such as H^+ , H_2^+ , and H_3^+ in the high fields (e. g. over 10 kV/cm) which were present in the cathode fall region was

used to explain the Doppler component. In our experiments, the results could not be explained by Stark or thermal broadening or electric field acceleration of charged species since the measured field of the incandescent heater was extremely weak, 1 V/cm, corresponding to a broadening much less than 1 eV. Rather the source of the excessive line broadening is consistent with that of EUV emission, an energetic reaction caused by a resonance energy transfer between hydrogen atoms and K^+/K^* , Rb^+ , cesium, strontium, or Ar^+ catalysts.

Rt-plasmas formed with hydrogen-potassium mixtures have been reported previously [34-35] wherein the plasma decayed with a two second half-life when the electric field was set to zero. This was the thermal decay time of the filament which dissociated molecular hydrogen to atomic hydrogen. This experiment showed that hydrogen line emission was occurring even though the voltage between the heater wires was set to and measured to be zero and indicated that the emission was due to a reaction of potassium atoms with atomic hydrogen. Potassium atoms ionize at an integer multiple of the potential energy of atomic hydrogen, $m \cdot 27.2 \text{ eV}$. The enthalpy of ionization of K to K^{3+} has a net enthalpy of reaction of 81.7426 eV, which is equivalent to $m=3$.

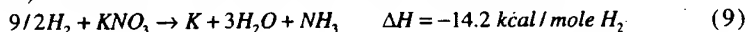
A rt-plasma of hydrogen and certain alkali ions formed at low temperatures (e.g. $\approx 10^3 \text{ K}$) as recorded via EUV spectroscopy and the hydrogen Balmer and alkali line emissions in the visible range [35]. The observed plasma formed at low temperatures (e.g. $\approx 10^3 \text{ K}$) from atomic hydrogen generated at a tungsten filament that heated a titanium dissociator and one of potassium, rubidium, cesium, and their carbonates and nitrates. These atoms and ions ionize to provide a net enthalpy of reaction of an integer multiple of the potential energy of atomic hydrogen ($m \cdot 27.2 \text{ eV}$, $m=\text{integer}$) to within 0.17 eV and comprise only a single ionization in the case of a potassium or rubidium ion. Whereas, the chemically similar atoms of sodium and sodium and lithium carbonates and nitrates which do not ionize with these constraints caused no emission. To test the electric dependence of the emission, the weak electric field of about 1 V/cm was set and measured to be zero in $< 0.5 \times 10^{-6} \text{ sec}$. An afterglow duration of about one to two seconds was recorded in the case of potassium, rubidium, cesium, K_2CO_3 , $RbNO_3$, and $CsNO_3$. Hydrogen line or alkali line emission was occurring even though

the voltage between the heater wires was set to and measured to be zero. These atoms and ions ionize to provide a net enthalpy of reaction of an integer multiple of the potential energy of atomic hydrogen to within less than the thermal energies at $\approx 10^3$ K and comprise only a single ionization in the case of a potassium or rubidium ion. Since the thermal decay time of the filament for dissociation of molecular hydrogen to atomic hydrogen was similar to the rt-plasma afterglow duration, the emission was determined to be due to a reaction of atomic hydrogen with each of the atoms or ions that did not require the presence of an electric field to be functional.

Each of K^+/K^+ , Rb^+ , Cs , and Ar^+ as the catalyst are predicted to catalyze hydrogen to form $H\left[\frac{a_H}{2}\right]$ which reacts with an electron to form $H^-(1/2)$. The predicted $H^-(1/2)$ hydride ion of hydrogen catalysis by these catalysts was observed spectroscopically at 407 nm corresponding to its predicted binding energy of 3.05 eV. The hydride reaction product formed over time.

The release of energy from hydrogen as evidenced by the EUV emission must result in a lower-energy state of hydrogen. The present study identified the formation of a novel hydride ion, $H^-(1/2)$. The formation of novel compounds based on novel hydride ions would be substantial evidence supporting catalysis of hydrogen as the mechanism of the observed EUV emission and further support the present spectroscopic identification of $H^-(1/2)$. Compounds containing novel hydride ions have been isolated as products of the reaction of atomic hydrogen with atoms and ions identified as catalysts in the present study and previously reported EUV studies [18-25, 31-42]. The novel hydride compounds were identified analytically by techniques such as time of flight secondary ion mass spectroscopy, X-ray photoelectron spectroscopy, and 1H nuclear magnetic resonance spectroscopy. For example, the time of flight secondary ion mass spectroscopy showed a large hydride peak in the negative spectrum. The X-ray photoelectron spectrum showed large metal core level shifts due to binding with the hydride as well as novel hydride peaks. The 1H nuclear magnetic resonance spectrum showed significantly upfield shifted peaks which corresponded to and identified novel hydride ions.

Balmer α line broadening and the predicted 407 nm peak corresponding to the hydride ion product $H^-(1/2)$ was observed in the case of potassium ions as the catalyst. Thus, the power balance of a rt-plasma formed with KNO_3 which is volatile under the measurement conditions of 250 °C was determined using Calvet calorimetry. The steady state Calvet voltage significantly increased upon the addition of atomic hydrogen to vaporized KNO_3 . With constant power per unit length to the filament to maintain a constant filament temperature, the power was observed to be linear in filament length, and therefore filament area. This result is consistent with the dissociation of hydrogen as a rate limiting mechanism. Given a flow rate of 0.1 sccm and an excess power of 2.07 W, energy balances of over -28,000 kJ/mole H_2 (145 eV/H atom) were measured. The reduction of KNO_3 to water, potassium metal, and NH_3 calculated from the heats of formation only releases -14.2 kcal/mole H_2 (0.3 eV/H atom) which can not account for the observed heat.



The most energetic reaction possible was the reaction of hydrogen to form water which releases -241.8 kJ/mole H_2 (1.48 eV/H atom) which is about 100 times less than that observed. The results indicate that once a hydrino atom is formed by a catalyst, further catalytic transitions: $n = \frac{1}{2} \rightarrow \frac{1}{3}, \frac{1}{3} \rightarrow \frac{1}{4}, \frac{1}{4} \rightarrow \frac{1}{5}$, and so on occur to a substantial extent. This is consistent with the previously given theory [12, 18, 20, 27], the reported series of lower-energy hydrogen lines with energies of $q \cdot 13.6 \text{ eV}$ where $q = 1, 2, 3, 4, 6, 7, 8, 9$, or 11 [18-19, 27], and previous studies which show very large energy balances [26-27, 29-30].

Similarly, the emission intensity of the plasma generated by atomic strontium increased significantly with the introduction of argon gas only when Ar^+ emission was observed. And, an increase in the Balmer α line broadening and the predicted 407 nm peak corresponding to the hydride ion product $H^-(1/2)$ was observed with Ar^+ present as the catalyst. Thus, the power balance of a rt-plasma formed with Ar^+ as the catalyst was measured by heat loss calorimetry. The steady state temperature of a rt-plasma formed with strontium and increased by Ar^+ was significantly higher than heated argon which did not form a rt-plasma. A maximum excess power of 26 W was observed. The enthalpy of formation ΔH_f of

strontium hydride is -47.59 kcal/mole (1.0 eV/H atom) [49]. Thus, the energy for hydriding all of the 1.2 g (13 mmoles) of strontium would be 0.65 kcal compared to the energy released over the minimum three hours to steady state of 280 kcal.

IV. CONCLUSION

Each of the ionization of Rb^+ , cesium, strontium and Ar^+ , and an electron transfer between two K^+ ions provide a reaction with a net enthalpy of an integer multiple of the potential energy of atomic hydrogen. The presence of each of the corresponding reactants formed the low applied temperature, extremely low voltage plasma called a resonance transfer or rt-plasma. For further characterization, the width of the 656.2 nm Balmer α line was recorded on light emitted from rt-plasmas. Significant line broadening of 17, 9, 11, 14, and 24 eV was observed from a rt-plasma of hydrogen formed with K^+/K^+ , Rb^+ , Cs, and Ar^+ catalysts, respectively. These results could not be explained by Stark or thermal broadening or electric field acceleration of charged species since the measured field of the incandescent heater was extremely weak, 1 V/cm, corresponding to a broadening much less than 1 eV. Rather, the source of the excessive line broadening is consistent with that of EUV emission, an energetic reaction caused by a resonance energy transfer between hydrogen atoms and the catalyst. Since line broadening is a measure of temperature, the excess power of about 20 mW/cc was measured calorimetrically on K^+/K^+ and Ar^+ catalyzed rt-plasmas corresponding to an energy balance of about 100 times that of the combustion of the hydrogen. The product hydride ion with each of K^+/K^+ , Rb^+ , Cs, and Ar^+ as the catalyst was predicted to have a binding energy of 3.05 eV and was observed by high resolution visible spectroscopy at the corresponding 407 nm.

Since the net enthalpy released may be at least one hundred times that of combustion, the catalysis of atomic hydrogen represents a new source of energy with H_2O as the source of hydrogen fuel. Moreover, rather than air pollutants or radioactive waste, novel hydride compounds with potential commercial applications are the products [36-42]. Since the power is in the form of a plasma, direct high-efficiency, low cost

energy conversion may be possible, thus, avoiding a heat engine such as a turbine [43-45] or a reformer-fuel cell system. Significantly lower capital costs and lower commercial operating costs than that of any known competing energy source are anticipated.

ACKNOWLEDGMENT

Special thanks to Alex Echezuria for preparing filament cells for plasma experiments.

REFERENCES

1. P. W. J. M. Boumans, *Spectrochim. Acta Part B*, 46 (1991) 711.
2. J. A. C. Broekaert, *Appl. Spectrosc.*, 49, (1995) 12A.
3. P. W. J. M. Boumans, J. A. C. Broekaert, and R. K. Marcus, Eds., *Spectrochim. Acta Part B*, 46 (1991) 457.
4. M. Dogan, K. Laqua, and H. Massmann, "Spektrochemische Analysen mit einer Glimmentladungslampe als Lichtquelle—I," *Spectrochim. Acta*, Volume 26B, (1971) 631-649.
5. M. Dogan, K. Laqua, and H. Massmann, "Spektrochemische Analysen mit einer Glimmentladungslampe als Lichtquelle—II," *Spectrochim. Acta*, Volume 27B, (1972) 65-88.
6. J. A. C. Broekaert, *J. Anal. At. Spectrom.*, 2 (1987) 537.
7. M. Kuraica, N. Konjevic, "Line shapes of atomic hydrogen in a plane-cathode abnormal glow discharge", *Physical Review A*, Volume 46, No. 7, October (1992), pp. 4429-4432.
8. I. R. Videnocic, N. Konjevic, M. M. Kuraica, "Spectroscopic investigations of a cathode fall region of the Grimm-type glow discharge", *Spectrochimica Acta, Part B*, Vol. 51, (1996), pp. 1707-1731.
9. P. Kurunczi, H. Shah, and K. Becker, "Hydrogen Lyman- α and Lyman- β emissions from high-pressure microhollow cathode discharges in $Ne-H_2$ mixtures", *J. Phys. B: At. Mol. Opt. Phys.*, Vol. 32, (1999), L651-L658.
10. M. Parker and R. K. Marcus, *Appl. Spectrosc.*, 48, (1994) 623.
11. J. A. R. Sampson, *Techniques of Vacuum Ultraviolet Spectroscopy*, Pied

- Publications, (1980), pp. 94-179.
12. R. Mills, *The Grand Unified Theory of Classical Quantum Mechanics*, January 2000 Edition, BlackLight Power, Inc., Cranbury, New Jersey, Distributed by Amazon.com; September 2001 Edition posted at www.blacklightpower.com.
 13. R. Mills, "The Grand Unified Theory of Classical Quantum Mechanics", Global Foundation, Inc. Orbis Scientiae entitled *The Role of Attractive and Repulsive Gravitational Forces in Cosmic Acceleration of Particles The Origin of the Cosmic Gamma Ray Bursts*, (29th Conference on High Energy Physics and Cosmology Since 1964) Dr. Behram N. Kursunoglu, Chairman, December 14-17, 2000, Lago Mar Resort, Fort Lauderdale, FL.
 14. R. Mills, "The Grand Unified Theory of Classical Quantum Mechanics", Global Foundation, Inc. Orbis Scientiae entitled *The Role of Attractive and Repulsive Gravitational Forces in Cosmic Acceleration of Particles The Origin of the Cosmic Gamma Ray Bursts*, (29th Conference on High Energy Physics and Cosmology Since 1964) Dr. Behram N. Kursunoglu, Chairman, December 14-17, 2000, Lago Mar Resort, Fort Lauderdale, FL, Kluwer Academic/Plenum Publishers, New York, pp. 243-258.
 15. R. Mills, "The Grand Unified Theory of Classical Quantum Mechanics", Int. J. of Hydrogen Energy, in press.
 16. R. Mills, "The Hydrogen Atom Revisited", Int. J. of Hydrogen Energy, Vol. 25, Issue 12, December, (2000), pp. 1171-1183.
 17. R. Mills, The Nature of Free Electrons in Superfluid Helium—a Test of Quantum Mechanics and a Basis to Review its Foundations and Make a Comparison to Classical Theory, Int. J. Hydrogen Energy, Vol. 26, No. 10, (2001), pp. 1059-1096.
 18. R. Mills, P. Ray, "Spectral Emission of Fractional Quantum Energy Levels of Atomic Hydrogen from a Helium-Hydrogen Plasma and the Implications for Dark Matter", Int. J. Hydrogen Energy, in press.
 19. R. L. Mills, P. Ray, B. Dhandapani, J. He, "Spectroscopic Identification of Fractional Rydberg States of Atomic Hydrogen" J. Phys. Chem., submitted.
 20. R. Mills, P. Ray, "Vibrational Spectral Emission of Fractional-Principal-Quantum-Energy-Level Hydrogen Molecular Ion", Int. J. Hydrogen Energy, in press.

21. R. L. Mills, P. Ray, "Spectroscopic Identification of a Novel Catalytic Reaction of Rubidium Ion with Atomic Hydrogen and the Hydride Ion Product", *Int. J. Hydrogen Energy*, submitted.
22. R. Mills, P. Ray, Spectroscopic Identification of a Novel Catalytic Reaction of Potassium and Atomic Hydrogen and the Hydride Ion Product, *Int. J. Hydrogen Energy*, in press.
23. R. Mills, "Spectroscopic Identification of a Novel Catalytic Reaction of Atomic Hydrogen and the Hydride Ion Product", *Int. J. Hydrogen Energy*, Vol. 26, No. 10, (2001), pp. 1041-1058.
24. R. Mills and M. Nansteel, "Argon-Hydrogen-Strontium Plasma Light Source", *IEEE Transactions on Plasma Science*, submitted.
25. R. Mills, M. Nansteel, and Y. Lu, "Excessively Bright Hydrogen-Strontium Plasma Light Source Due to Energy Resonance of Strontium with Hydrogen", *European Journal of Physics D*, submitted.
26. R. Mills, J. Dong, W. Good, P. Ray, J. He, B. Dhandapani, Measurement of Energy Balances of Noble Gas-Hydrogen Discharge Plasmas Using Calvet Calorimetry, *Int. J. Hydrogen Energy*, submitted.
27. Randell L. Mills, P. Ray, B. Dhandapani, M. Nansteel, X. Chen, J. He, "New Power Source from Fractional Quantum Energy Levels of Atomic Hydrogen that Surpasses Internal Combustion", *Spectrochimica Acta*, submitted.
28. R. L. Mills, P. Ray, B. Dhandapani, J. He, "Comparison of Excessive Balmer α Line Broadening of Glow Discharge and Microwave Hydrogen Plasmas with Certain Catalysts" *J. Phys. Chem.*, submitted.
29. R. L. Mills, A. Voigt, P. Ray, M. Nansteel, B. Dhandapani, "Measurement of Hydrogen Balmer Line Broadening and Thermal Power Balances of Noble Gas-Hydrogen Discharge Plasmas", *Int. J. Hydrogen Energy*, in press.
30. R. Mills, N. Greenig, S. Hicks, "Optically Measured Power Balances of Anomalous Discharges of Mixtures of Argon, Hydrogen, and Potassium, Rubidium, Cesium, or Strontium Vapor", *Int. J. Hydrogen Energy*, in press.
31. R. Mills, M. Nansteel, and Y. Lu, "Observation of Extreme Ultraviolet Hydrogen Emission from Incandescently Heated Hydrogen Gas with Strontium that Produced an Anomalous Optically Measured Power Balance", *Int. J. Hydrogen Energy*, Vol. 26, No. 4, (2001), pp. 309-326.

32. R. Mills, J. Dong, Y. Lu, "Observation of Extreme Ultraviolet Hydrogen Emission from Incandescently Heated Hydrogen Gas with Certain Catalysts", *Int. J. Hydrogen Energy*, Vol. 25, (2000), pp. 919-943.
33. R. Mills, "Observation of Extreme Ultraviolet Emission from Hydrogen-KI Plasmas Produced by a Hollow Cathode Discharge", *Int. J. Hydrogen Energy*, Vol. 26, No. 6, (2001), pp. 579-592.
34. R. Mills, "Temporal Behavior of Light-Emission in the Visible Spectral Range from a Ti-K₂CO₃-H-Cell", *Int. J. Hydrogen Energy*, Vol. 26, No. 4, (2001), pp. 327-332.
35. R. Mills, T. Onuma, and Y. Lu, "Formation of a Hydrogen Plasma from an Incandescently Heated Hydrogen-Catalyst Gas Mixture with an Anomalous Afterglow Duration", *Int. J. Hydrogen Energy*, Vol. 26, No. 7, July, (2001), pp. 749-762.
36. R. Mills, B. Dhandapani, M. Nansteel, J. He, A. Voigt, "Identification of Compounds Containing Novel Hydride Ions by Nuclear Magnetic Resonance Spectroscopy", *Int. J. Hydrogen Energy*, Vol. 26, No. 9, Sept. (2001), pp. 965-979.
37. R. Mills, B. Dhandapani, N. Greenig, J. He, "Synthesis and Characterization of Potassium Iodo Hydride", *Int. J. of Hydrogen Energy*, Vol. 25, Issue 12, December, (2000), pp. 1185-1203.
38. R. Mills, "Novel Inorganic Hydride", *Int. J. of Hydrogen Energy*, Vol. 25, (2000), pp. 669-683.
39. R. Mills, "Novel Hydrogen Compounds from a Potassium Carbonate Electrolytic Cell", *Fusion Technology*, Vol. 37, No. 2, March, (2000), pp. 157-182.
40. R. Mills, B. Dhandapani, M. Nansteel, J. He, T. Shannon, A. Echezuria, "Synthesis and Characterization of Novel Hydride Compounds", *Int. J. of Hydrogen Energy*, Vol. 26, No. 4, (2001), pp. 339-367.
41. R. Mills, "Highly Stable Novel Inorganic Hydrides", *Journal of New Materials for Electrochemical Systems*, in press.
42. R. Mills, W. Good, A. Voigt, Jinquan Dong, "Minimum Heat of Formation of Potassium Iodo Hydride", *Int. J. Hydrogen Energy*, Vol. 26, No. 11, Oct., (2001), pp. 1199-1208.
43. R. Mills, "BlackLight Power Technology-A New Clean Hydrogen Energy Source with the Potential for Direct Conversion to Electricity", *Proceedings of the National Hydrogen Association, 12 th Annual U.S.*

Hydrogen Meeting and Exposition, *Hydrogen: The Common Thread*, The Washington Hilton and Towers, Washington DC, (March 6-8, 2001), pp. 671-697.

44. R. Mills, "BlackLight Power Technology-A New Clean Energy Source with the Potential for Direct Conversion to Electricity", Global Foundation International Conference on "Global Warming and Energy Policy", Dr. Behram N. Kursunoglu, Chairman, Fort Lauderdale, FL, November 26-28, 2000, Kluwer Academic/Plenum Publishers, New York, pp. 1059-1096.
45. R. Mayo, R. Mills, M. Nansteel, "On the Potential of Direct and MHD Conversion of Power from a Novel Plasma Source to Electricity for Microdistributed Power Applications", IEEE Transactions on Plasma Science, submitted.
46. M. C. Bradford, J. Phillips, J. Klanchar, Rev. Sci. Instrum., 66, (1), January, (1995), pp. 171-175.
47. C. J. Hardy, B. O. Field, J. Chem. Soc., (1963), pp. 5130-5134.
48. David R. Linde, *CRC Handbook of Chemistry and Physics*, 79 th Edition, CRC Press, Boca Raton, Florida, (1998-9), p. 10-175 to p. 10-177.
49. W. M. Muller, J. P. Blackledge, G. G. Libowitz, *Metal Hydrides*, Academic Press, New York, (1968), p 201.

Table 1. Energetic hydrogen atom densities and energies for rt-plasmas determined from the 656.2 nm Balmer α line width.

| Plasma Gas | Hydrogen Atom Density ^a (10^{11} atoms/cm ³) | Hydrogen Atom Energy ^b (eV) |
|---------------|--|--|
| H_2 | 2 | 2-3 ^c |
| K/H_2 | 4 | 15-18 |
| Rb^+/H_2 | 6 | 8-10 |
| Cs/H_2 | 4 | 10-12 |
| Sr/H_2 | 8 | 13-15 |
| $Sr/Ar^+/H_2$ | 4 | 22-26 |

^a Approximate Calculated [8].

^b Calculated [8].

^c Measured on glow discharge according to method ref. 29.

Table 2. Input and excess power for a rt-plasma formed with K^+/K^+ catalyst.

| Filament Length (cm) | Input Power (W) | Total Power (W) ^a | Excess Power (± 0.06 W) ^b |
|----------------------------|-----------------------|------------------------------------|---|
| 10 | 7.02 | 7.64 | 0.62 |
| 20 | 9.82 | 10.63 | 0.81 |
| 30 | 15.01 | 17.08 | 2.07 |

^a Eq. (7)

^b Eq. (2)

Table 3. Input and excess power for argon-hydrogen-strontium rt-plasma.

| Voltage (V) | Current (A) | Input Power (W) | Cell Temp. (K) | Total Power (W) ^a | Excess Power (± 2.2 W) ^b |
|----------------|----------------|-----------------------|----------------------|------------------------------------|--|
| 40.4 | 2.73 | 110 | 764.7 | 123.3 | 13.3 |
| 41.7 | 3.04 | 125 | 768.2 | 140.6 | 15.6 |
| 43.0 | 3.46 | 140 | 772.1 | 160.1 | 20.1 |
| 43.4 | 3.57 | 155 | 775.3 | 176.3 | 21.3 |
| 44.4 | 3.85 | 170 | 778.6 | 193.3 | 23.3 |
| 45.7 | 4.27 | 185 | 780.7 | 204.2 | 19.2 |
| 46.2 | 4.48 | 200 | 783.7 | 219.9 | 19.9 |
| 46.8 | 4.70 | 215 | 786.5 | 234.8 | 19.8 |
| 47.7 | 4.83 | 230 | 789.3 | 249.8 | 19.8 |
| 48.4 | 5.17 | 245 | 793.2 | 271.0 | 26.0 |

^a Eq. (8)

^b Eq. (6)

Figure Captions

Figure 1. The experimental set up comprising a filament gas cell light source and an EUV spectrometer which was differentially pumped.

Figure 2. The Calvet instrument for power balance studies with hydrogen and gaseous KNO_3 compared hydrogen alone.

Figure 3. Schematic of the gas cell and the cross sectional view of the Calvet calorimeter used to measure the power balance of a rt-plasma formed with K^+/K^+ catalyst. 1—1.6 mm OD stainless steel tube (to hydrogen supply), 2—stainless steel tee union, 3—6.4 mm OD stainless steel tube (to vacuum manifold), 4—cell lid, 5—filament leads, 6—Conax-Buffalo gland, 7—0.1 mm OD Pt filament, 8—copper ring gasket, 9—cell body, 10—Calvet calorimeter, 11—thermopile signal output, 12—thermal shunt, 13—thermopile, 14—insulated calorimeter base, 15—Alumina crucible KNO_3 reservoir.

Figure 4. The experimental setup for generating a argon-hydrogen-strontium rt-plasma and for measuring the power balance.

Figure 5. The one-liter cylindrical stainless steel cell fitted with a heated tungsten filament used to measure the power balances of argon-hydrogen-strontium rt-plasmas as a function of input power to the filament.

Figure 6. The 656 nm Balmer α line width recorded with a high resolution (± 0.006 nm) visible spectrometer on a rt-plasma formed with K^+/K^+ catalyst. Significant broadening was observed corresponding to an average hydrogen atom temperature of 17 eV.

Figure 7. The 656 nm Balmer α line width recorded with a high resolution (± 0.006 nm) visible spectrometer on a rt-plasma formed with Rb^+ catalyst. Significant broadening was observed corresponding to an average hydrogen atom temperature of 9 eV.

Figure 8. The 656 nm Balmer α line width recorded with a high resolution (± 0.006 nm) visible spectrometer on a cesium-hydrogen rt-plasma. Significant broadening was observed corresponding to an average hydrogen atom temperature of 11 eV.

Figure 9. The 656 nm Balmer α line width recorded with a high resolution (± 0.006 nm) visible spectrometer on a hydrogen-strontium rt-plasma. Significant broadening was observed corresponding to an

average hydrogen atom temperature of 14 eV.

Figure 10. The 656 nm Balmer α line width recorded with a high resolution (± 0.006 nm) visible spectrometer on a hydrogen-strontium rt-plasma intensified by argon ion catalyst. Significant broadening was observed corresponding to an average hydrogen atom temperature of 24 eV.

Figure 11. The superposition of the 656 nm Balmer α line width recorded with a high resolution (± 0.006 nm) visible spectrometer on a hydrogen-strontium rt-plasma and a hydrogen-strontium rt-plasma intensified by argon ion catalyst. By comparison to the strontium rt-plasma, significant broadening attributable to argon ion was observed corresponding to an average hydrogen atom temperature of 24 eV versus 14 eV.

Figure 12. The high resolution visible spectrum in the region of 407 nm recorded on the emission of a rt-plasma formed with K^+/K^+ catalyst. The novel 407 nm peak which could not be assigned to a known peak was assigned to $H^-(1/2)$.

Figure 13. The high resolution visible spectrum in the region of 407 nm recorded on the emission of a rt-plasma formed with Rb^+ catalyst. The novel 407 nm peak which could not be assigned to a known peak was assigned to $H^-(1/2)$.

Figure 14. The high resolution visible spectrum in the region of 407 nm recorded on the emission of a cesium-hydrogen rt-plasma. The novel 407 nm peak which could not be assigned to a known peak was assigned to $H^-(1/2)$.

Figure 15. The high resolution visible spectrum in the region of 407 nm recorded on the emission of a argon-hydrogen-strontium rt-plasma. The novel 407 nm peak which could not be assigned to a known peak was assigned to $H^-(1/2)$.

Figure 16. The high resolution visible spectrum in the region of 407 nm recorded on the emission of a hydrogen microwave discharge plasma. The 407.0 nm peak was not observed.

Figure 17. The Calvet voltage as a function of the power applied to the 20 cm long filament with hydrogen alone at 0.2 Torr total pressure plotted for the input power range of 1 W to 16 W.

Figure 18. With 9.82 W input to the 20 cm filament, the Calvet cell

was allowed to reach a steady Calvet voltage with KNO_3 alone. The Calvet voltage significantly increased upon the addition of hydrogen, and the output signal showed 0.81 W of excess power at the second steady state.

Figure 19. Plot of power input to the cell versus the cell temperature for the argon-hydrogen-strontium plasma and also for the argon-hydrogen control.

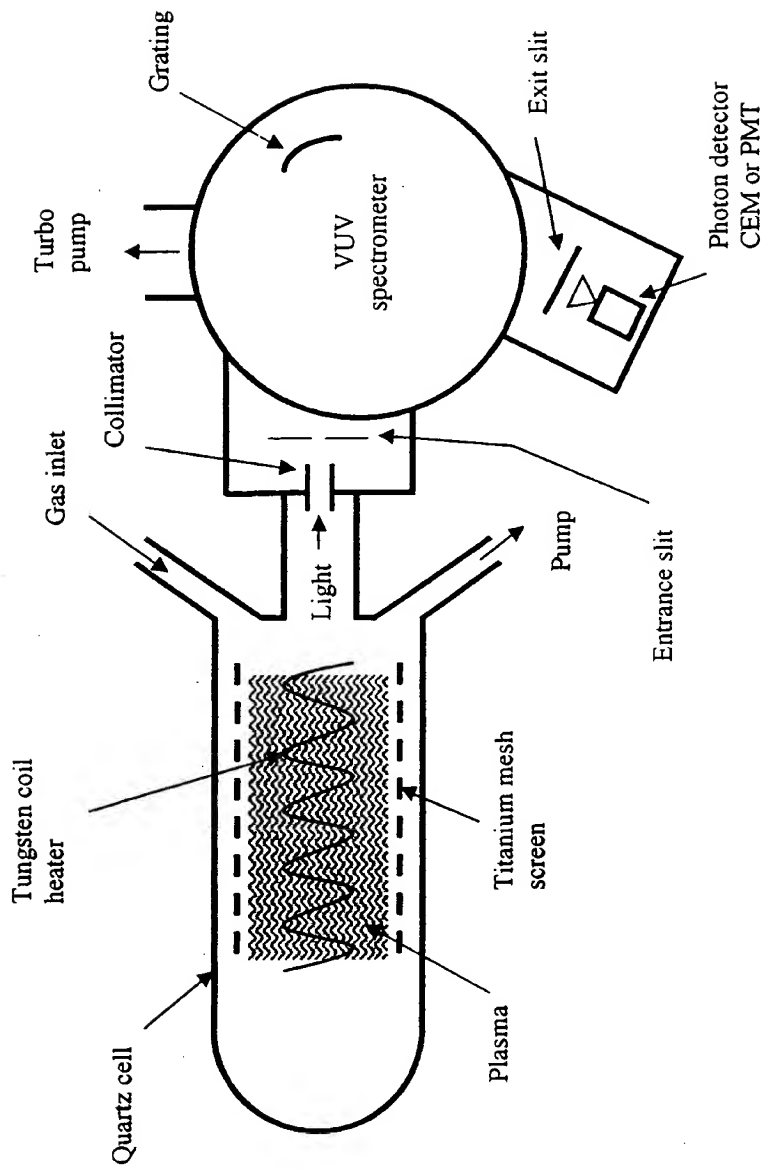


Fig. 1

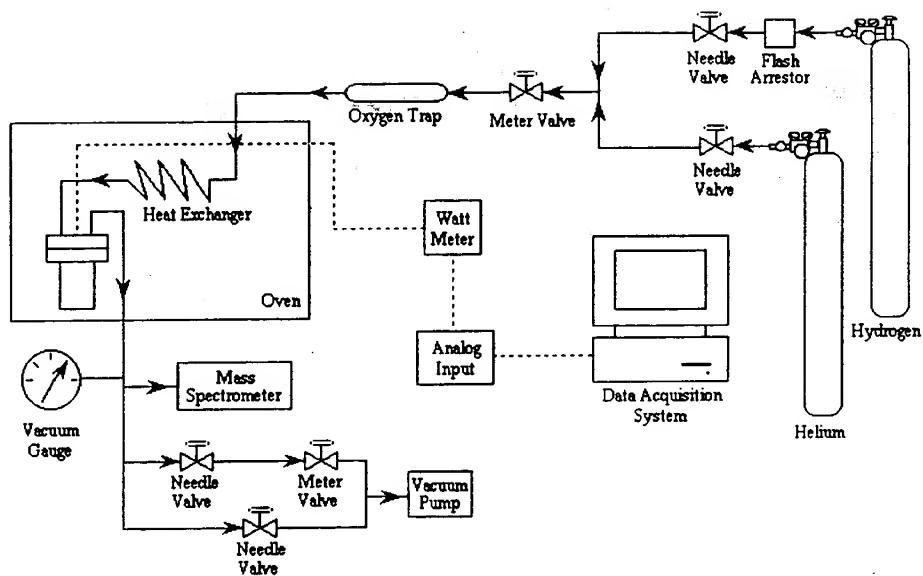


Fig. 2

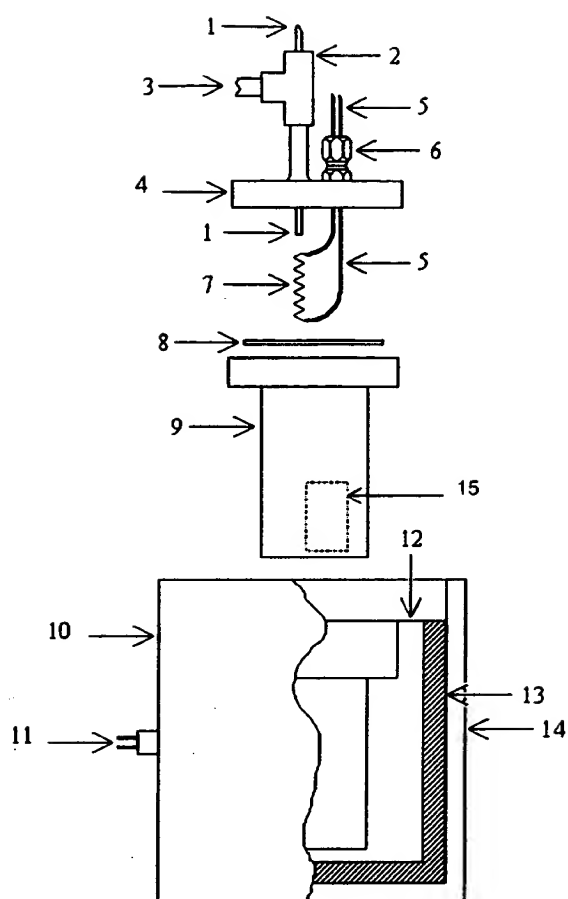


Fig. 3

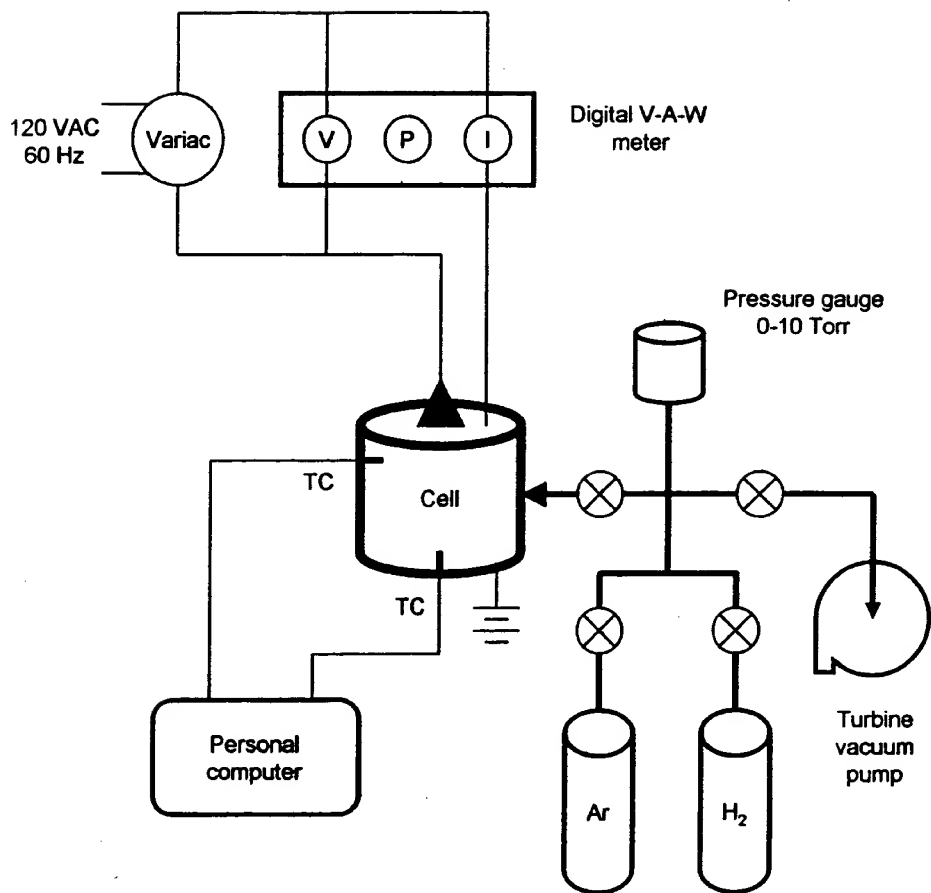


Fig. 4

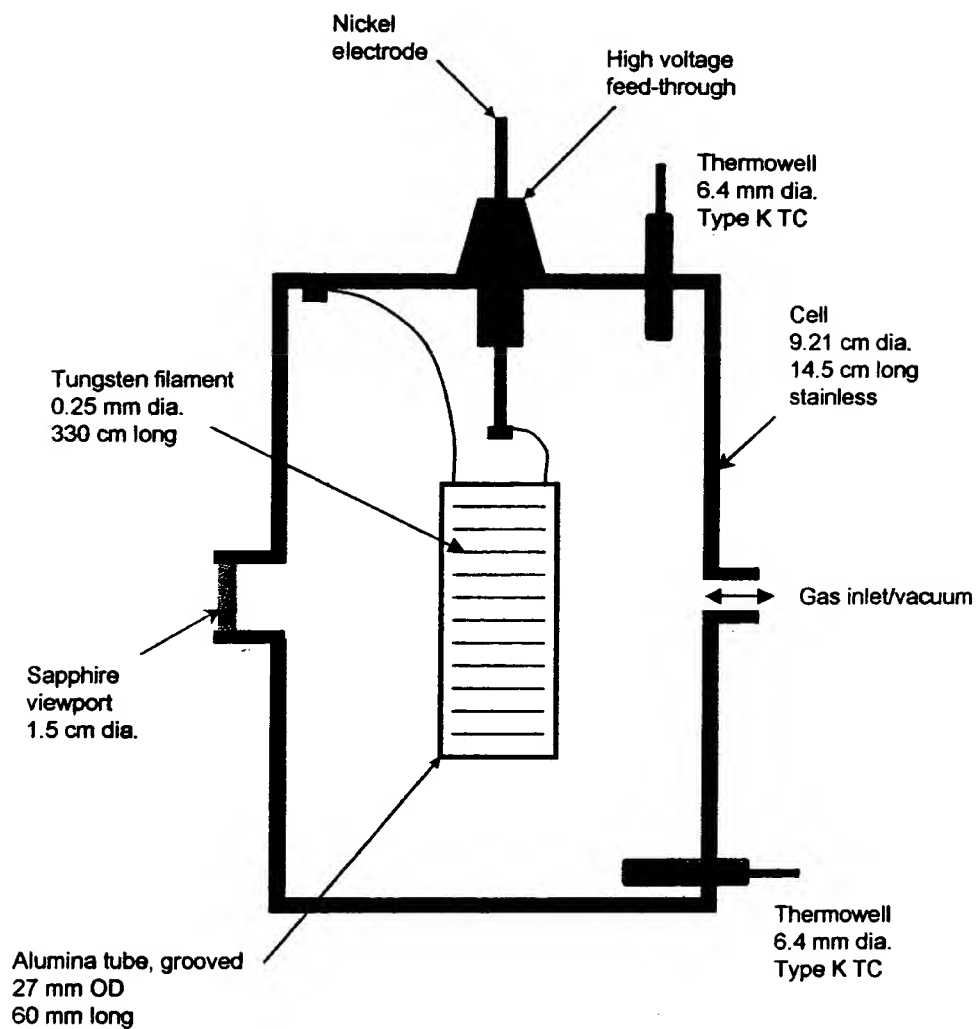


Fig. 5

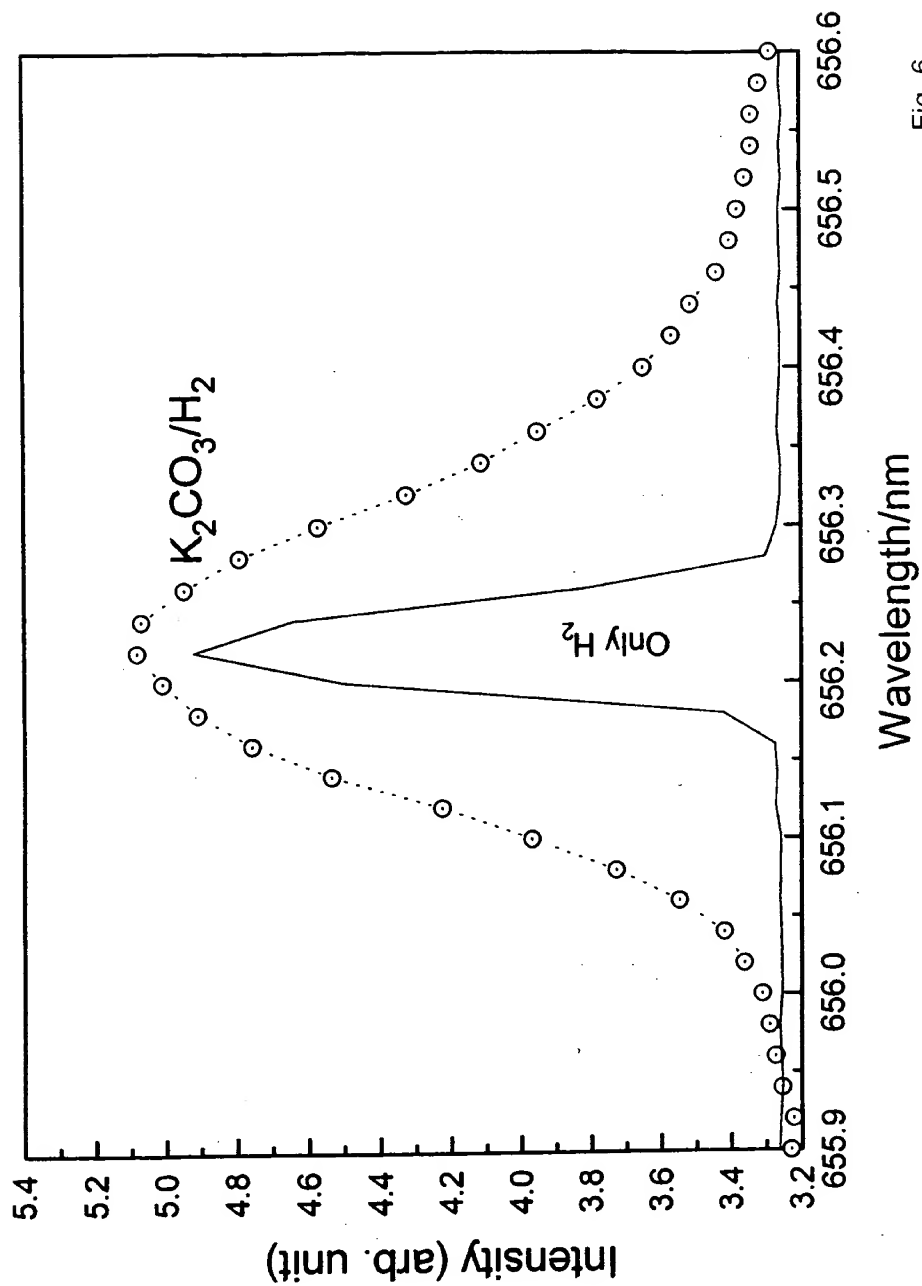


Fig. 6

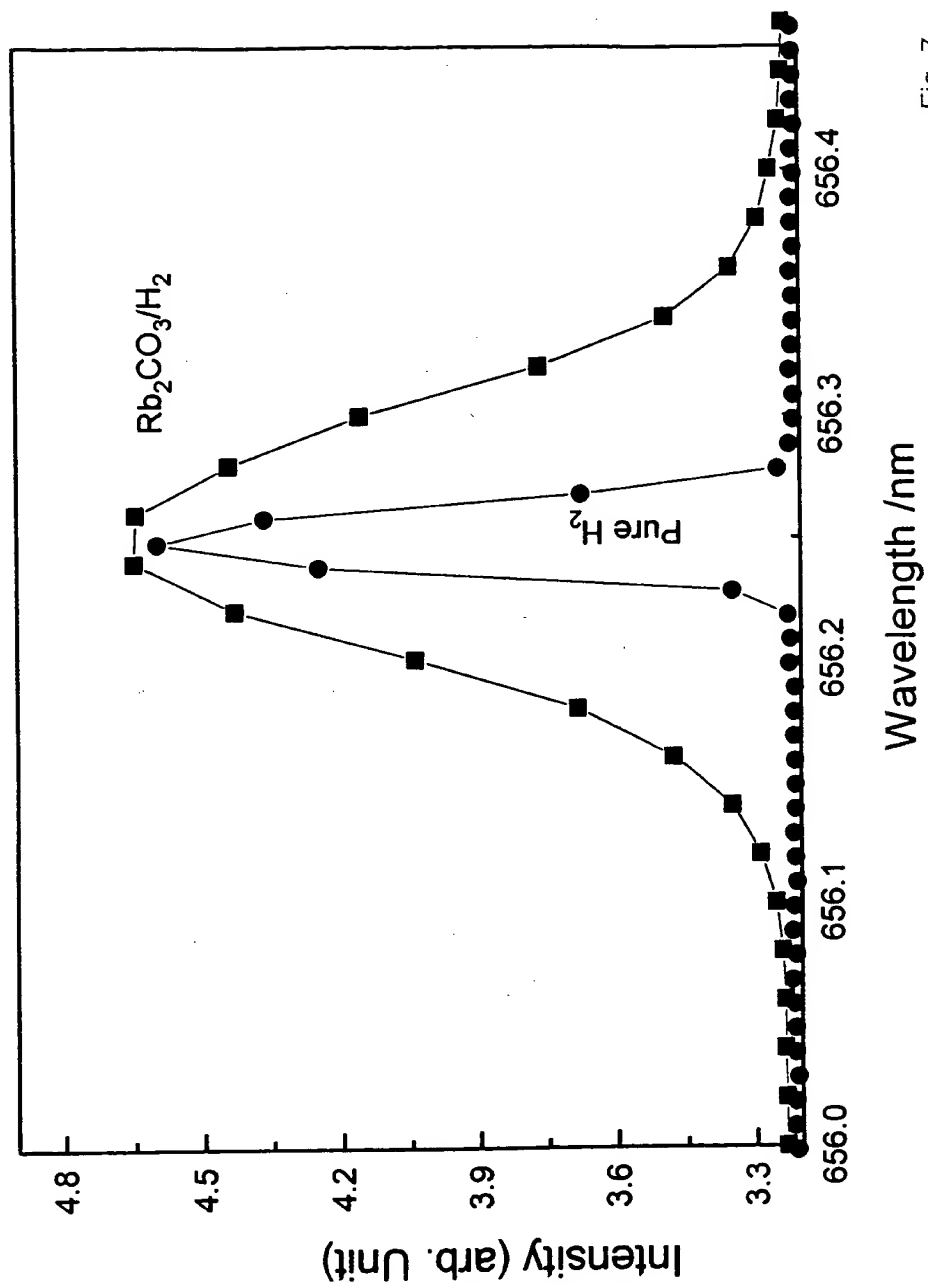


Fig. 7

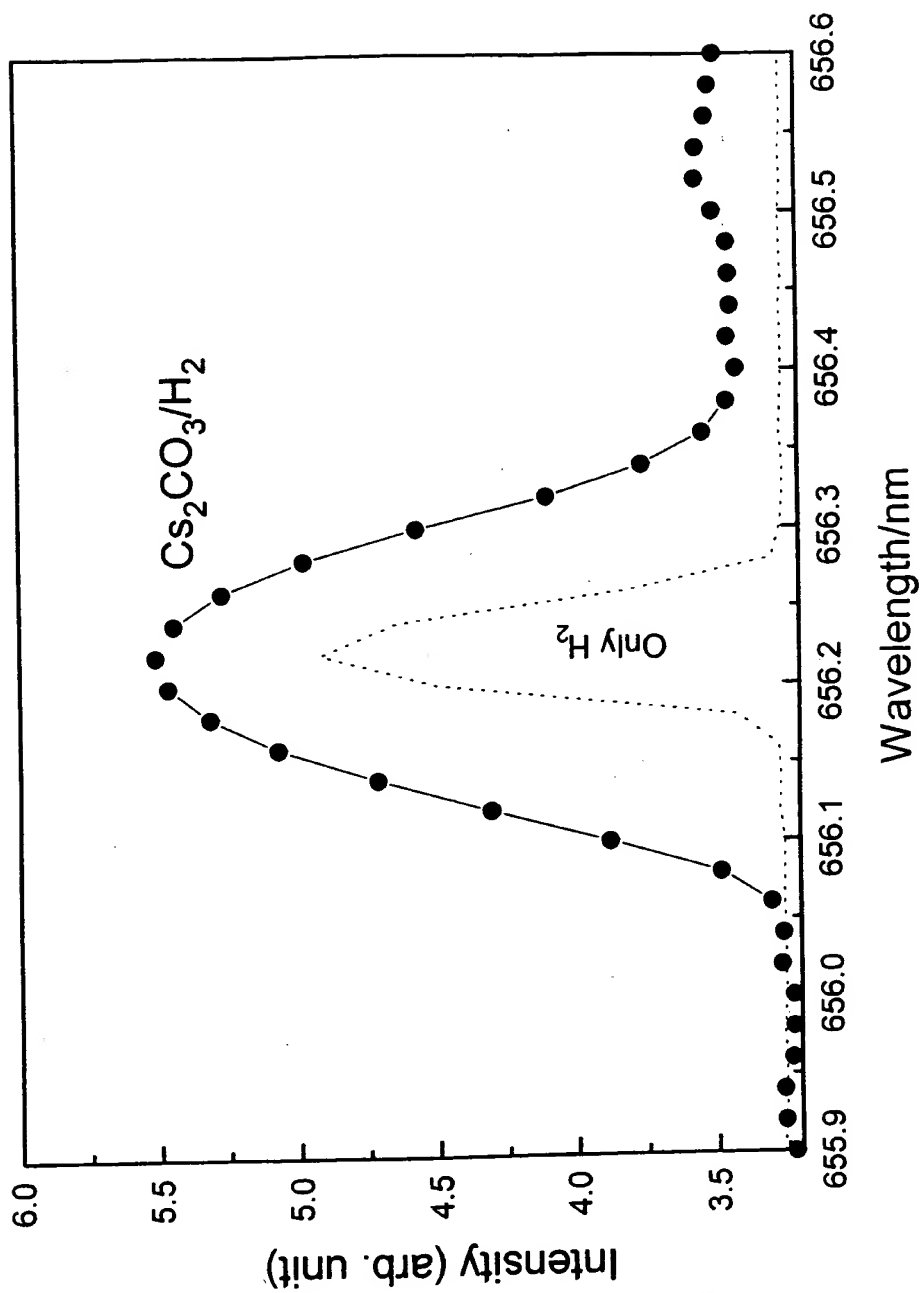


Fig. 8

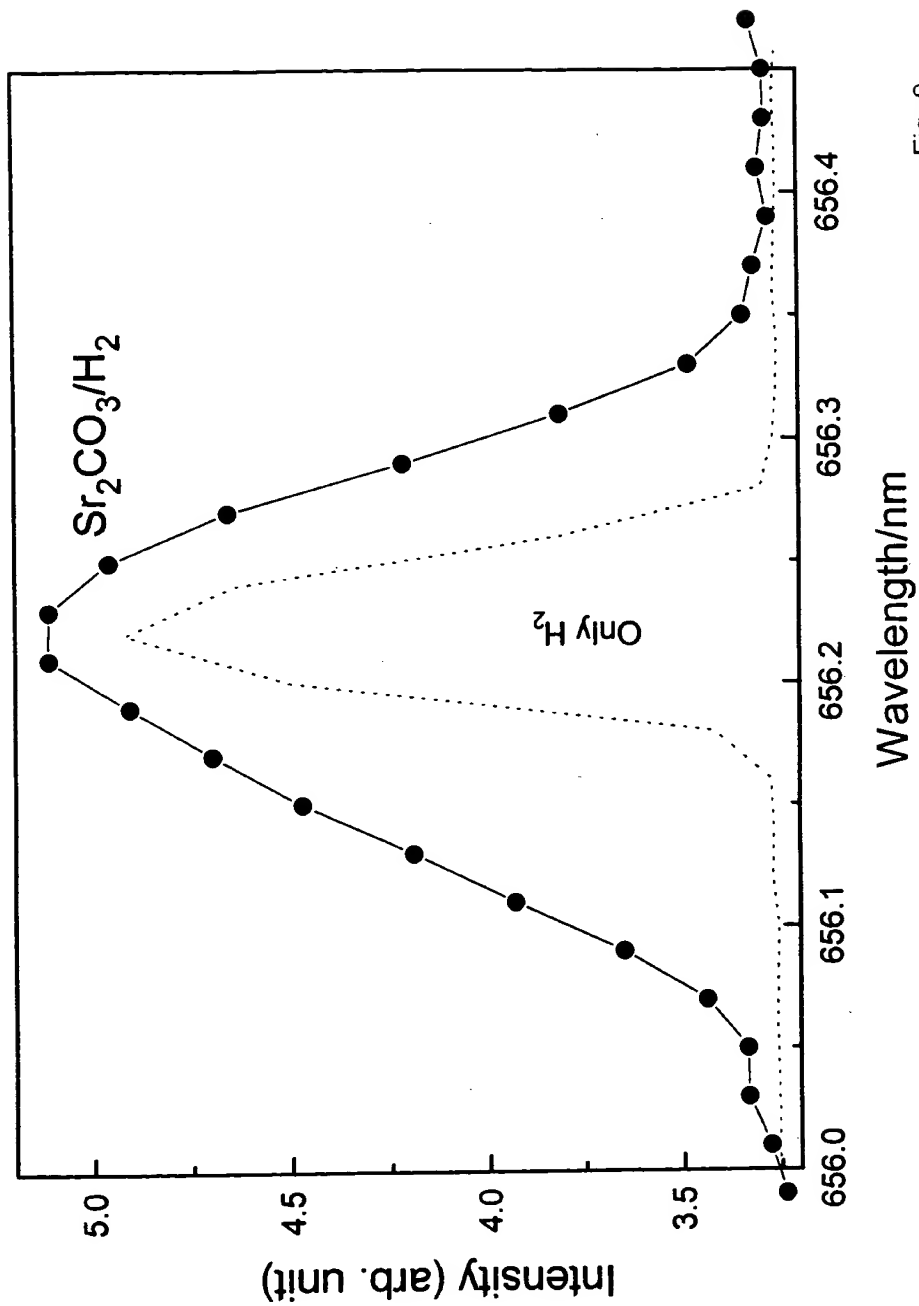


Fig. 9

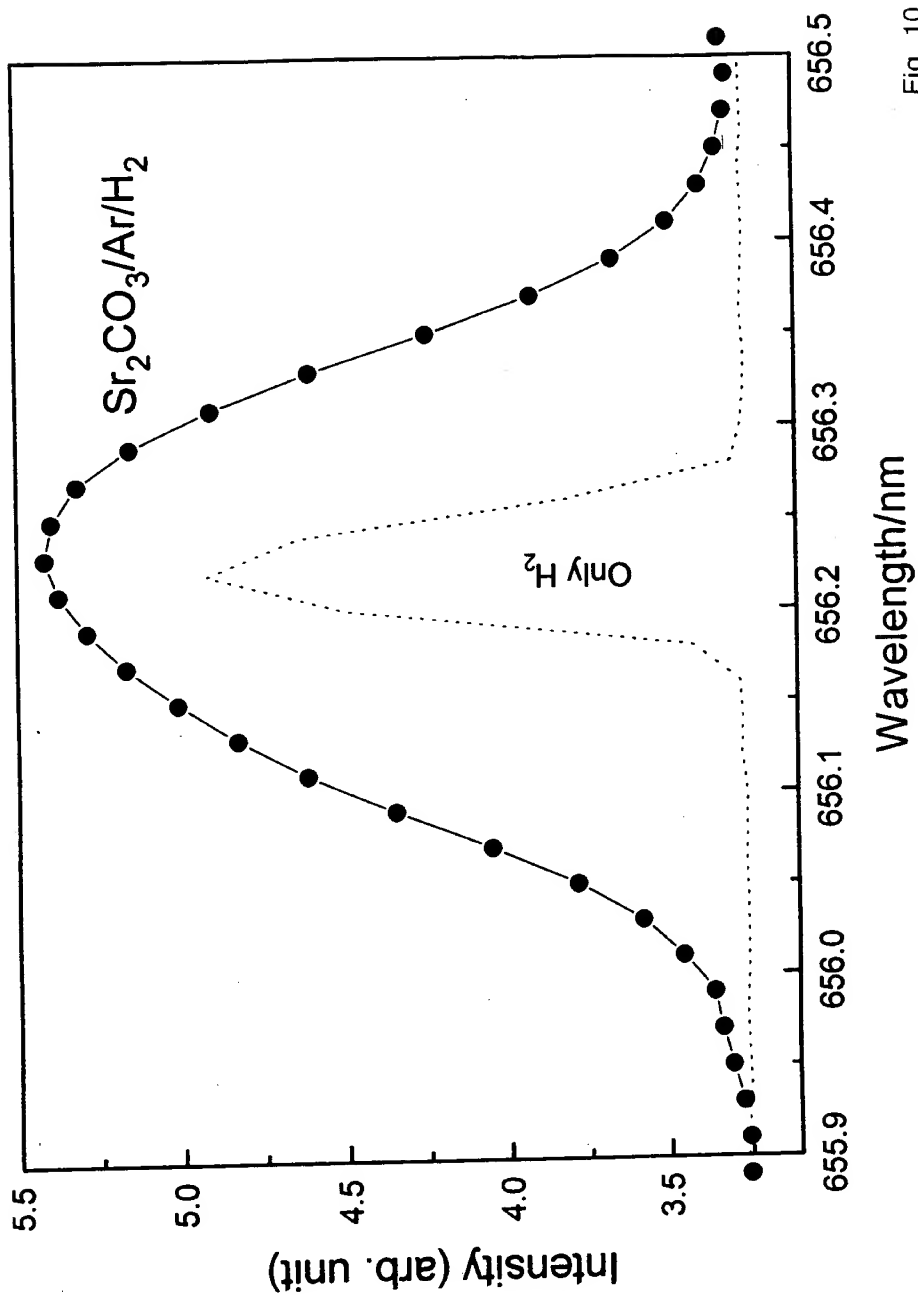


Fig. 10

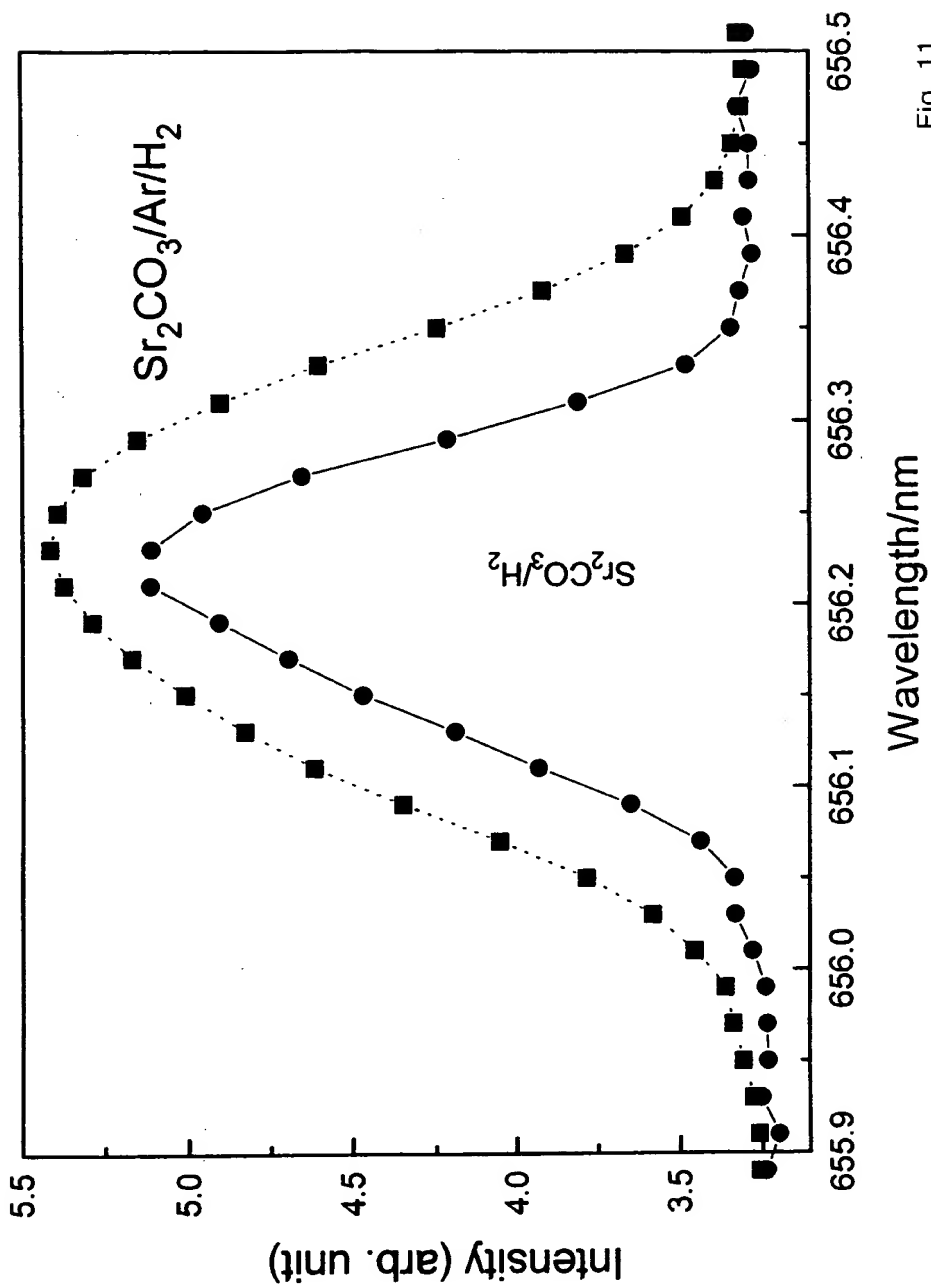


Fig. 11

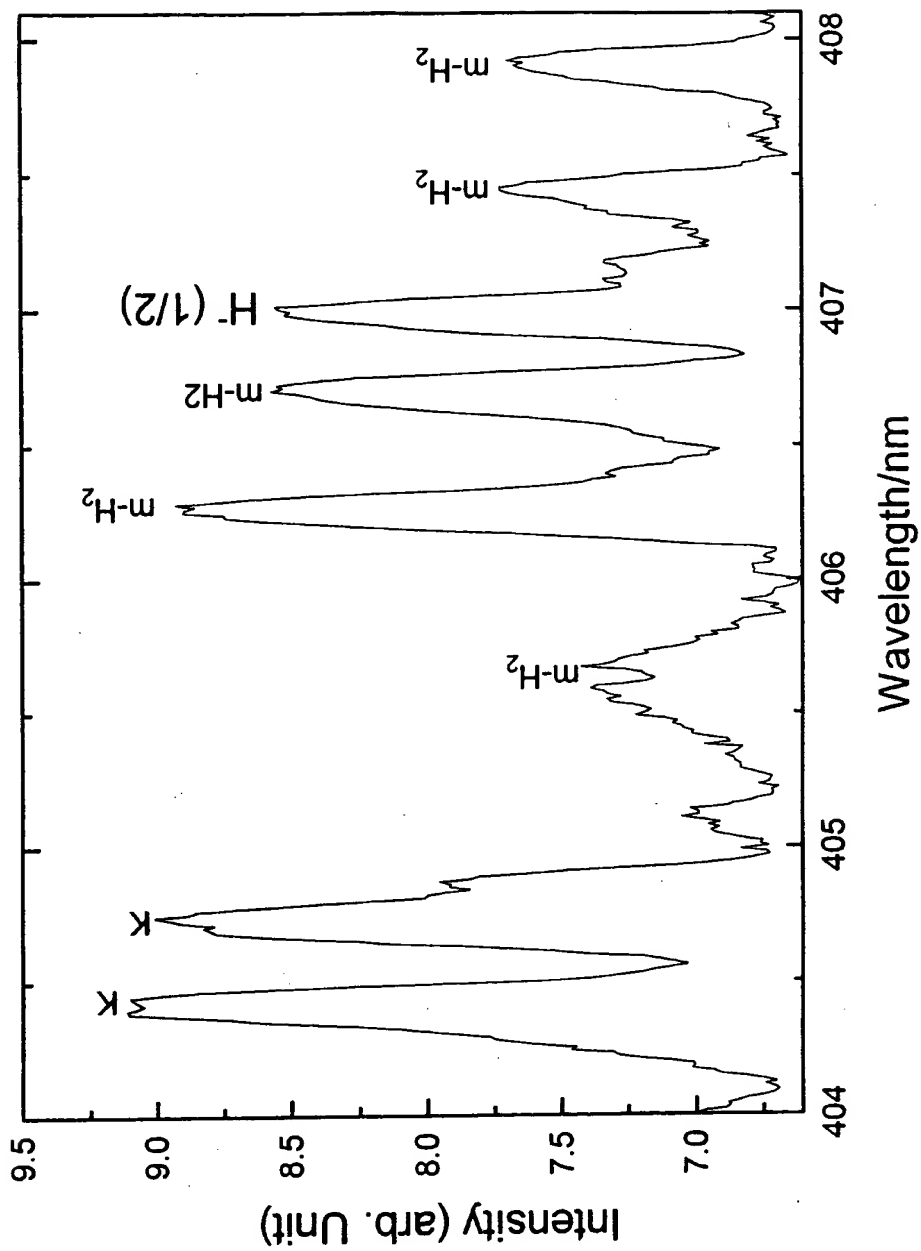


Fig. 12

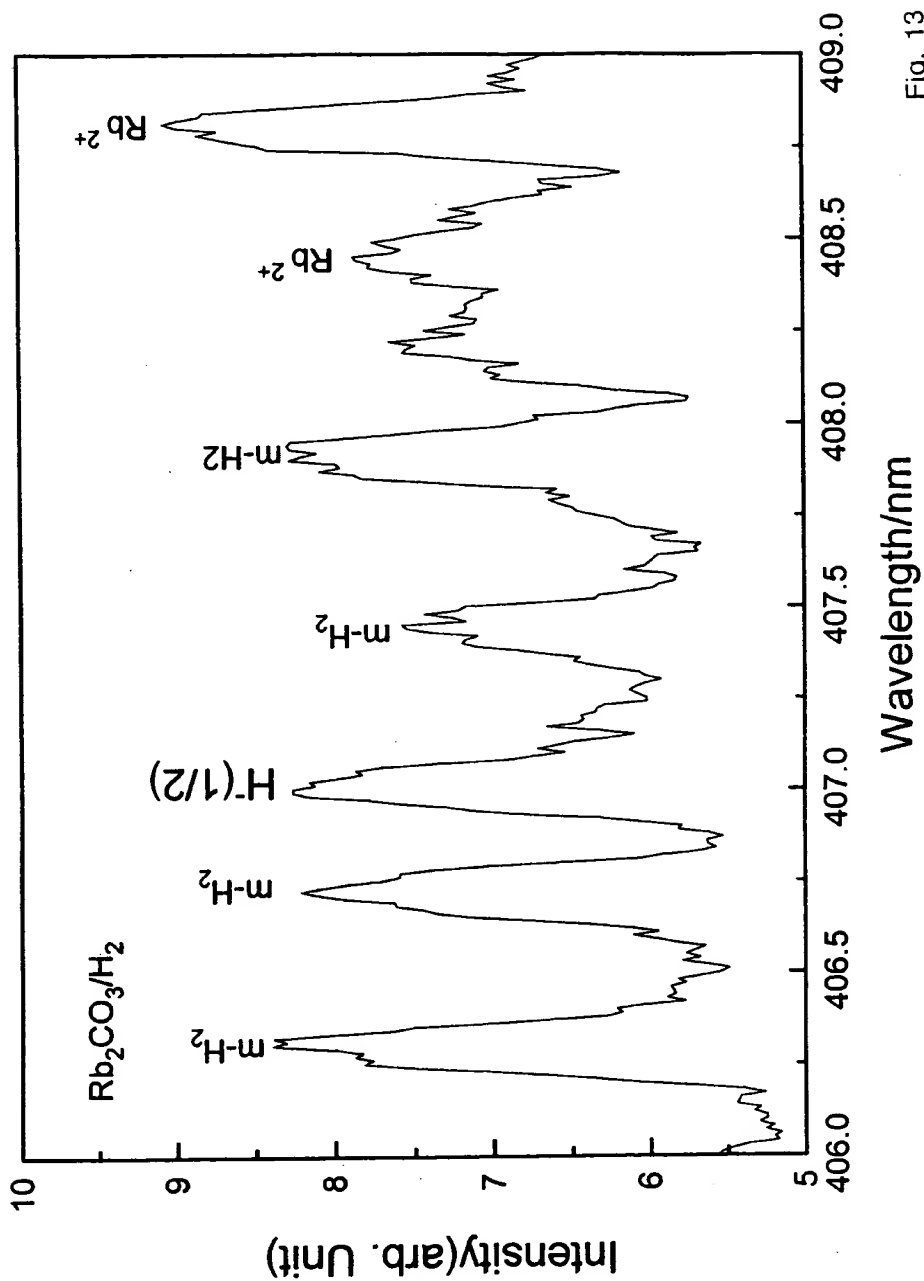


Fig. 13

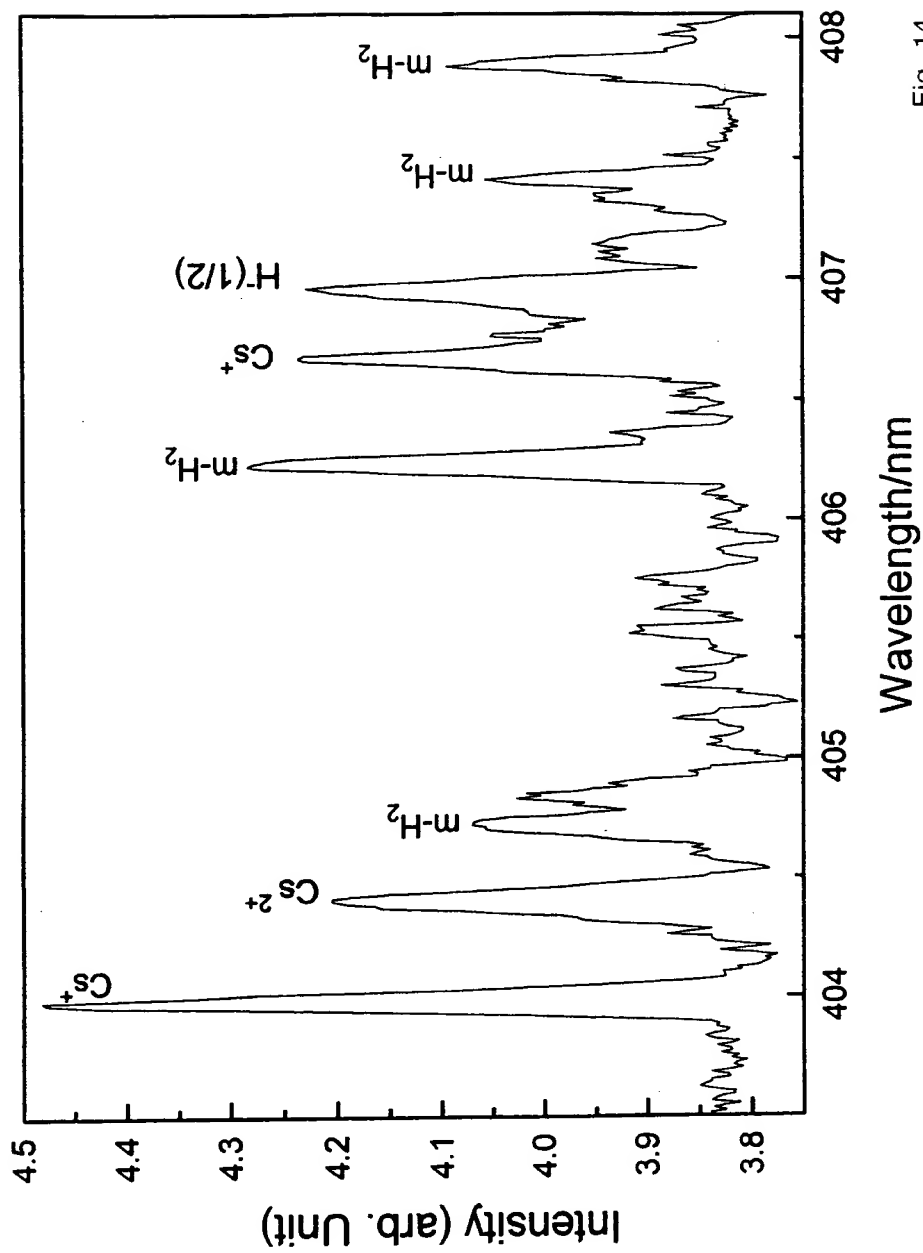


Fig. 14

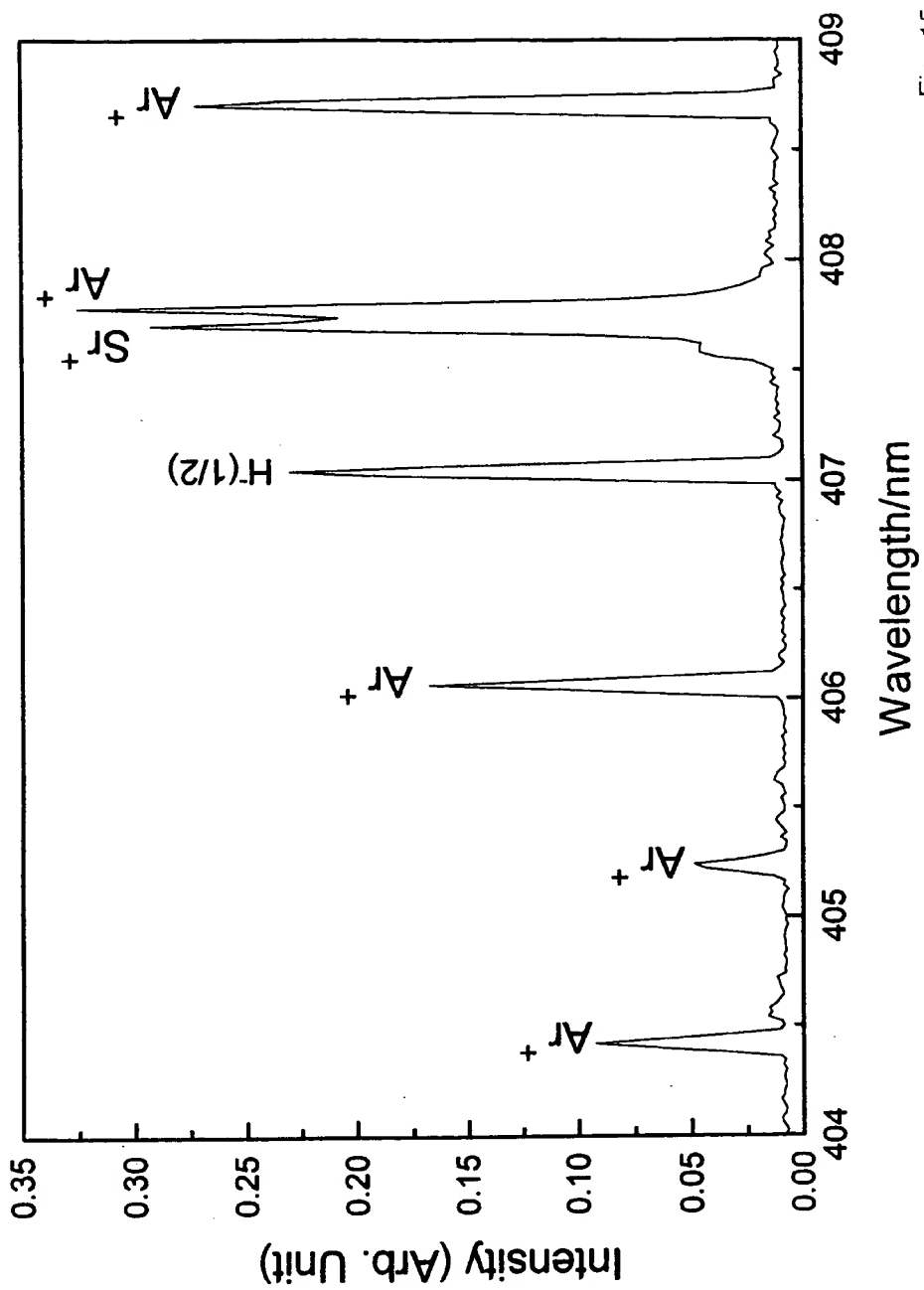


Fig. 15

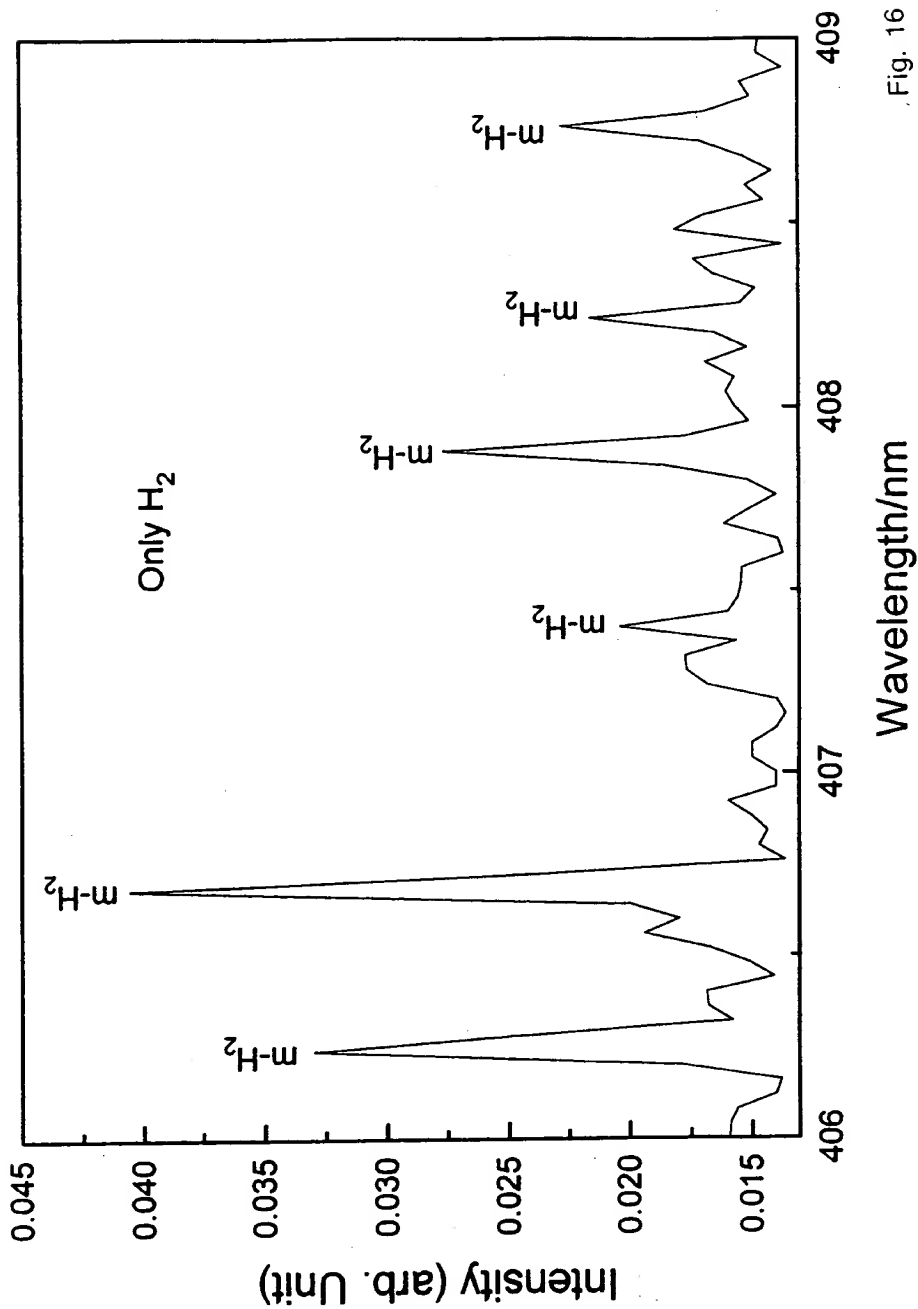


Fig. 16

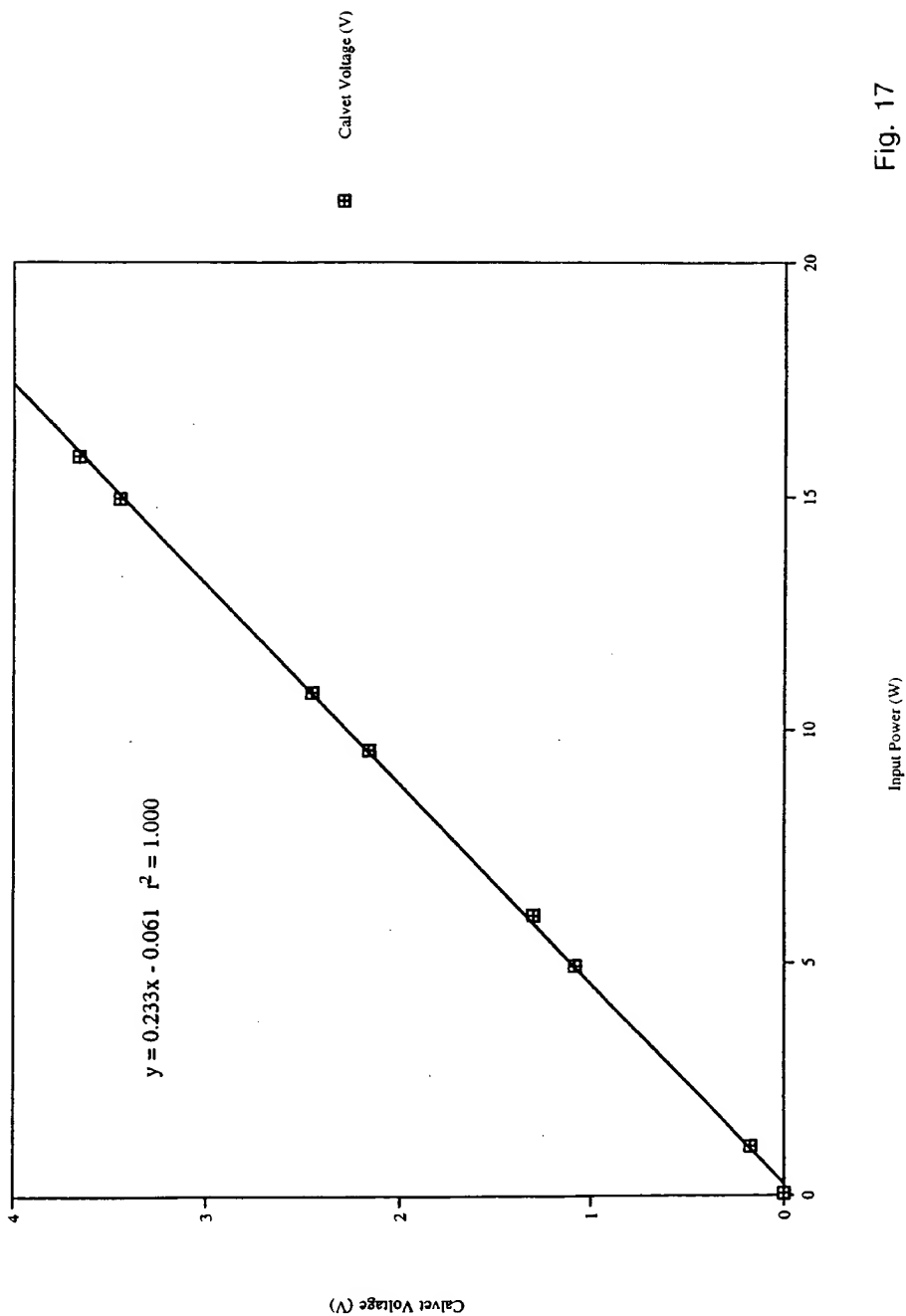


Fig. 17

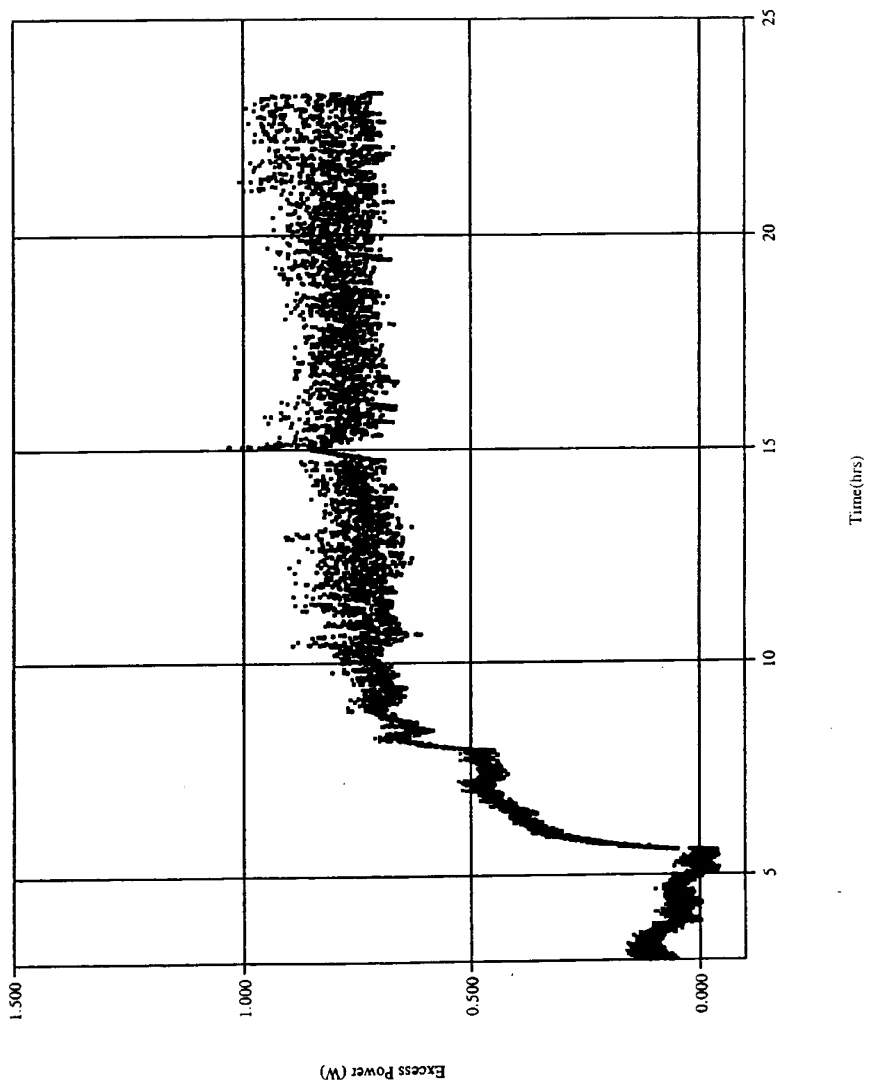


Fig. 18

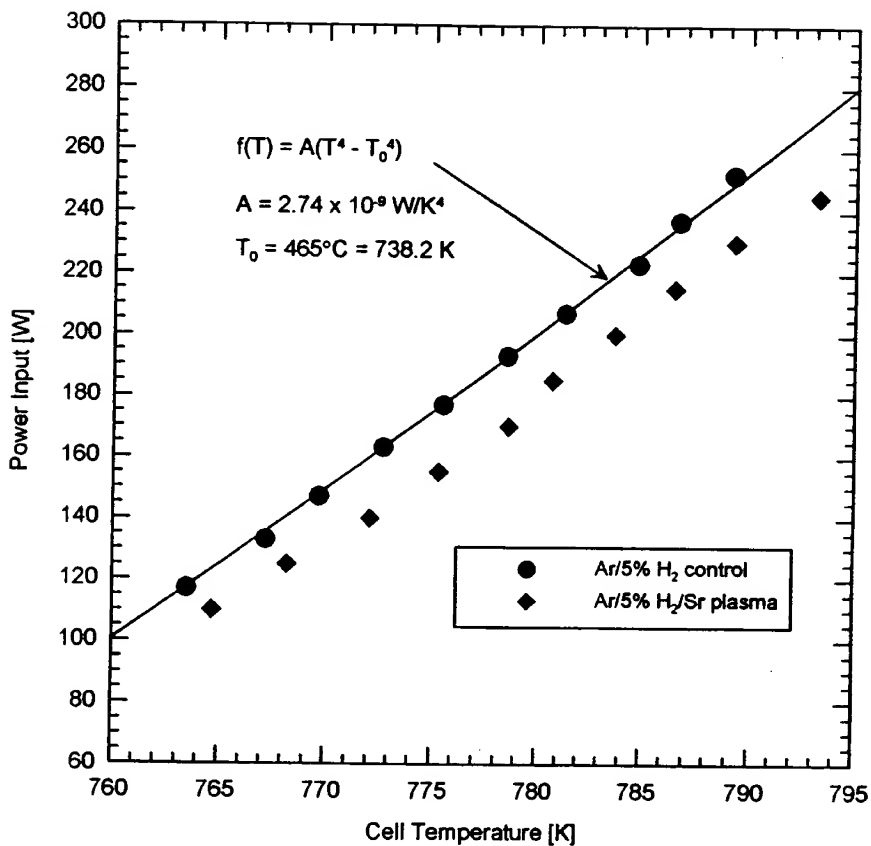


Fig. 19

79

Highly Stable Novel Inorganic Hydrides from Aqueous Electrolysis and Plasma Electrolysis

Randell Mills,* Bala Dhandapani, Ethirajulu Dayalan, Jiliang He, Paresh Ray

BlackLight Power, Inc., 493 Old Trenton Road, Cranbury, NJ 08512, USA

(Received)

ABSTRACT

Each of the ionization of potassium, cesium, and Rb^+ and an electron transfer between two K^+ ions (K^+ / K^+) provide a reaction with a net enthalpy of an integer multiple of the potential energy of atomic hydrogen and catalyze the exothermic formation of lower-energy hydrogen. For each of K^+ / K^+ , Rb^+ , and cesium, the net enthalpy of reaction of the catalyst is about 27.2 eV, and the lower-energy hydrogen atom catalysis product is predicted to be a highly reactive intermediate which further reacts to form a novel hydride ion $H^-(1/2)$. This ion formed by plasma electrolysis of a K_2CO_3 , Rb_2CO_3 , or Cs_2CO_3 electrolyte was observed by high resolution visible spectroscopy at 407.0 nm corresponding to its predicted binding energy of 3.05 eV. Furthermore, novel inorganic hydride compounds such as $KHKHCO_3$ and KH were isolated following the electrolysis of a K_2CO_3 electrolyte and identified by ToF-SIMS. The existence of novel hydride ions was determined using X-ray photoelectron spectroscopy and proton nuclear magnetic resonance spectroscopy. Applications include high voltage batteries.

KEYWORDS: plasma electrolysis, novel hydride ion, highly stable hydride compounds, high voltage battery, catalytic hydride synthesis

*rmills@blacklightpower.com

1. INTRODUCTION

1.1. Background

Evidence of the changing landscape for automobiles can be found in the recent increase in research into the next generation of automobiles. But, the fact that there is no clear front-runner in the technological race to replace the internal combustion (IC) engine can be attested to by the divergent approaches taken by the major automobile companies. Programs include various approaches to hybrid vehicles, alternative fueled vehicles such as dual-fired engines that can run on gasoline or compressed natural gas, and a natural gas-fired engine. Serious efforts are also being put into a number of alternative fuels such as ethanol, methanol, propane, and reformulated gasoline. To date, the most favored approach is an electric vehicle based on fuel cell technology or advanced battery technology such as sodium nickel chloride, nickel-metal hydride, and lithium-ion batteries ¹⁾. Although billions of dollars are being spent to develop an alternative to the IC engine, there is no technology in sight that can match the specifications of an IC engine system ²⁾.

Fuel cells have advantages over the IC engine because they convert hydrogen to water at about 70% efficiency when running at about 20% below peak output ³⁾. But, hydrogen is difficult and dangerous to store. Cryogenic, compressed gas, and metal hydride storage are the main options. In the case of cryogenic storage, liquefaction of hydrogen requires an amount of electricity which is at least 30% of the lower heating value of liquid hydrogen ⁴⁾. Compressed hydrogen, and metal hydride storage are less viable since the former requires an unacceptable volume, and the latter is heavy and has difficulties supplying hydrogen to match a load such as a fuel cell ⁴⁾. The main challenge with hydrogen as a replacement to gasoline is that a hydrogen production and refueling infrastructure would have to be built. Hydrogen may be obtained by reforming fossil fuels. However, in practice fuel cell vehicles would probably achieve only 10 to 45 percent efficiency because the process of reforming fossil fuel into hydrogen and carbon dioxide requires energy ³⁾. Presently, fuel cells are also impractical due to their high cost as well as the lack of inexpensive reforming technology ⁵⁾.

In contrast, batteries are attractive because they can be recharged wherever electricity exists which is ubiquitous. The cost of mobile energy from a battery powered car may be less than that from a fossil fuel powered car. For example, the cost of energy per mile of a nickel metal hydride battery powered car is 25% of that of a IC powered car ⁶⁾. However, current battery technology is trying to compete with something that it has little chance of imitating. Whichever battery technology proves to be superior, no known electric power plant will match the versatility and power of an internal combustion engine. A typical IC engine yields more

than 10,000 watt-hours of energy per kilogram of fuel, while the most promising battery technology yields 200 watt-hours per kilogram ²⁾.

A high voltage battery would have the advantages of much greater power and much higher energy density. The limitations of battery chemistry may be attributed to the binding energy of the anion of the oxidant. For example, the 2 volts provided by a lead acid cell is limited by the 1.46 eV electron affinity of the oxide anion of the oxidant PbO_2 . An increase in the oxidation state of lead such as $Pb^{2+} \rightarrow Pb^{3+} \rightarrow Pb^{4+}$ is possible in a plasma. Further oxidation of lead could also be achieved in theory by electrochemical charging. However, higher lead oxidation states are not achievable because the oxide anion required to form a neutral compound would undergo oxidation by the highly oxidized lead cation. An anion with an extraordinary binding energy is required for a high voltage battery. One of the highest voltage batteries known is the lithium fluoride battery with a voltage of about 6 volts. The voltage can be attributed to the higher binding energy of the fluoride ion. The electron affinity of halogens increases from the bottom of the Group VII elements to the top. Hydride ion may be considered a halide since it possess the same electronic structure. And, according to the binding energy trend, it should have a high binding energy. However, the binding energy is only 0.75 eV which is much lower than the 3.4 eV binding energy of a fluoride ion.

1.2. Catalysis of Hydrogen to Form Novel Hydrides

Atomic hydrogen may undergo a catalytic reaction with certain atomized elements and ions which singly or multiply ionize at integer multiples of the potential energy of atomic hydrogen, $m \cdot 27.2 \text{ eV}$ wherein m is an integer. The theory and supporting data were given previously ⁷⁻⁴²⁾. The reaction involves a nonradiative energy transfer to form a hydrogen atom, "hydrino" designated by $H(1/p)$, that is lower in energy than unreacted atomic hydrogen that corresponds to a fractional principal quantum number ($n = \frac{1}{p} = \frac{1}{\text{integer}}$ replaces the well known parameter $n = \text{integer}$ in the Rydberg equation for hydrogen excited states). A number of independent experimental observations lead to the conclusion that atomic hydrogen can exist in fractional quantum states that are at lower energies than the traditional "ground" ($n = 1$) state. Prior related studies that support the possibility of a novel reaction of atomic hydrogen which produces a chemically generated or assisted plasma (rt-plasma) and produces novel hydride compounds include extreme ultraviolet (EUV) spectroscopy ^{12-14,16,18-25,28-30)}, characteristic emission from catalysis and the hydride ion products ¹⁵⁻²⁰⁾, lower-energy atomic and molecular hydrogen emission ^{12-14,24)}, plasma formation ^{15,16,18-22,28,29,31,32)}, Balmer α line broadening ^{13,15,16,21,22,24-26)}, elevated electron temperature ^{13,24)}, anomalous plasma afterglow

duration^{31,32}), power generation^{13,15,21-24,26-28,39}), and analysis of chemical compounds³³⁻³⁹). Furthermore, mobility and spectroscopy data of individual electrons in liquid helium shows direct experimental confirmation that electrons may have fractional principal quantum energy levels¹¹).

An atomic catalytic system to produce a rt-plasma involves helium ions. The second ionization energy of helium is 54.4 eV⁴³); thus, the ionization reaction of He^+ to He^{2+} has a net enthalpy of reaction of 54.4 eV which is equivalent to $2 \cdot 27.2$ eV. Thus, it may serve as a catalyst to form $H(1/3)$. The products of the catalysis reaction may accept energy nonradiatively in multiples of the potential energy of atomic hydrogen and may further serve as catalysts. Thus, once a hydrino atom is formed by a catalyst, further catalytic transitions $n = \frac{1}{3} \rightarrow \frac{1}{4}, \frac{1}{4} \rightarrow \frac{1}{5}$, and so on occur to a substantial extent.

Extreme ultraviolet (EUV) spectra recorded on microwave discharges of helium with 2% hydrogen were previously reported^{12,13,24}). Novel emission lines were observed with energies of $q \cdot 13.6$ eV where $q = 1, 2, 3, 4, 6, 7, 8, 9, 11, 12$ or these lines inelastically scattered by helium atoms wherein 21.2 eV was absorbed in the excitation of $He(1s^2)$ to $He(1s^1 2p^1)$. These lines were identified as hydrogen transitions to electronic energy levels below the "ground" state corresponding to fractional quantum numbers. The hydrino catalysis product may further react with a source of electrons to form the corresponding hydride ion.

Each of K^+/K^+ , Rb^+ , Cs , and Ar^+ are predicted to catalyze hydrogen to form $H\left[\frac{a_H}{2}\right]$ which reacts with an electron to form $H^-(1/2)$. A potassium atom is predicted to catalyze hydrogen to form $H\left[\frac{a_H}{4}\right]$ which reacts with an electron to form $H^-(1/4)$. Several studies including EUV and high resolution visible spectroscopy on rt-plasmas from several salt or metal catalysts confirmed the catalyst mechanism and the predicted novel hydride ions.

$H^-(1/2)$, the hydride ion catalyst product of K^+/K^+ or Rb^+ , was observed by high resolution visible spectroscopy as a broad peak at 407.00 nm with a FWHM of 0.14 nm corresponding to its predicted binding energy of 3.0468 eV. From the electron g factor, bound-free hyperfine structure lines of $H^-(1/2)$ were predicted with energies E_{HF} given by $E_{HF} = j^2 3.0056 \times 10^{-5} + 3.0575$ eV (j is an integer) as an inverse Rydberg-type series that converges at increasing wavelengths and terminates at 3.0575 eV—the hydride spin-pairing energy plus the binding energy. The high resolution visible plasma emission spectra in the region of 400.0 nm to 406.0 nm matched the predicted emission lines for $j = 1$ to $j = 37$ ¹⁶) to within a 1 part per 10^5 .

Further exemplary studies include:

1.) the observation of continuum state emission of Cs^{2+} and Ar^{2+} at 53.3 nm and 45.6 nm, respectively, with the absence of the other corresponding Rydberg series of lines from these species which confirmed the resonant nonradiative energy transfer of 27.2 eV from atomic hydrogen to the catalysts atomic Cs or Ar^{+20} ,

2.) the spectroscopic observation of the predicted hydride ion $H^{-}(1/2)$ of hydrogen catalysis by either Cs atom or Ar^{+} catalyst at 407.0 nm corresponding to its predicted binding energy of 3.05 eV^{15-17, 20},

3.) the observation of characteristic emission from K^{3+} which confirmed the resonant nonradiative energy transfer of 3 · 27.2 eV from atomic hydrogen to atomic K¹⁹,

4.) the spectroscopic observation of the predicted $H^{-}(1/4)$ ion of hydrogen catalysis by K catalyst at 110 nm corresponding to its predicted binding energy of 11.2 eV¹⁹,

5.) the observation of characteristic emission from Rb^{2+} which confirmed the resonant nonradiative energy transfer of 27.2 eV from atomic hydrogen to Rb^{+18} ,

6.) the spectroscopic observation of the predicted $H^{-}(1/2)$ ion of hydrogen catalysis by Rb^{+} catalyst at 407.0 nm corresponding to its predicted binding energy of 3.05 eV¹⁵⁻¹⁸,

7.) the high resolution visible spectroscopic observation from rt-plasmas of the predicted $H^{-}(1/2)$ ion of hydrogen catalysis by each of K^{+}/K^{+} , Rb^{+} , Cs, and Ar^{+} at 407.0 nm corresponding to its predicted binding energy of 3.05 eV¹⁵⁻²⁰,

The formation of novel compounds having hydrino hydride ions would be substantial evidence supporting catalysis of hydrogen as the mechanism of observed rt-plasmas and further support the spectroscopic identification of $H^{-}(1/p)$ (p is an integer). Compounds containing novel hydride ions have been isolated as products of the reaction of atomic hydrogen with atoms and ions identified as catalysts in previously reported EUV studies³³⁻³⁹. The novel hydride compounds were identified analytically by techniques such as time of flight secondary ion mass spectroscopy, X-ray photoelectron spectroscopy, and ¹H nuclear magnetic resonance spectroscopy. For example, the time of flight secondary ion mass spectroscopy showed a large hydride peak in the negative spectrum. The X-ray photoelectron spectrum showed large metal core level shifts due to binding with the hydride as well as novel hydride

peaks. The ^1H nuclear magnetic resonance spectrum showed significantly upfield-shifted peaks which corresponded to and identified novel hydride ions ³³).

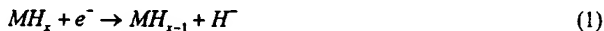
In this article we report that novel inorganic hydride compounds having the formula KHKHCO_3 and KH were isolated from an aqueous K_2CO_3 electrolytic cell reactor. KH was stable at elevated temperature (600°C). Inorganic hydride clusters $\text{K}[\text{KHKHCO}_3]_n$ were identified by positive ToF-SIMS of KHKHCO_3 . The negative ToF-SIMS was dominated by hydride ion. The positive and negative ToF-SIMS of KH showed essentially K^+ and H^- only, respectively. A hydride ion with a binding energy of 22.8 eV has been observed by X-ray photoelectron spectroscopy (XPS) of KHKHCO_3 having upfield shifted solid state magic-angle spinning proton nuclear magnetic resonance (^1H MAS NMR) peaks. Moreover, a polymeric structure is indicated by Fourier transform infrared (FTIR) spectroscopy. Hydride ions with binding energies of 22.8 eV and 69.2 eV have been observed by XPS of KH . $\text{H}^- (1/2)$, the predicted hydride ion product with each of K^+ / K^+ , Rb^+ , and Cs as the catalyst, has a binding energy of 3.05 eV corresponding to a 407.0 nm emission that was observed by high resolution visible spectroscopy on the emission from plasma electrolysis cells.

1.3. Hydride Ion Battery

The discovery of novel hydride ions with high binding energies has implications for a new field of hydride chemistry with applications such as a high voltage battery. Such extremely stable hydride ions may stabilize positively charged ions in an unprecedented highly charged state. A battery may be possible having projected specifications and environmental advantages that may be competitive with the internal combustion engine.

Hydride ions having extraordinary binding energies may stabilize a cation M^{n+} in an extraordinarily high oxidation state such as $+2$ in the case of lithium. Thus, these hydride ions may be used as the basis of a high voltage battery of a rocking chair design wherein the hydride ion moves back and forth between the cathode and anode half cells during discharge and charge cycles. Exemplary reactions for a cation M^{n+} are:

Cathode reaction:



Anode reaction:



Overall reaction:



2. EXPERIMENTAL

2.1. Synthesis

2.1.1. Potassium Hydride Potassium Hydrogen Carbonate, $KH K H C O_3$, Synthesis with an Electrolytic Cell

An electrolytic cell comprising a K_2CO_3 electrolyte, a nickel wire cathode, and platinized titanium anodes was used to synthesize the $KH K H C O_3$ sample. Briefly, the cell vessel comprised a 37.85 liter (83.82 cm x 38.1 cm) Nalgene tank. An outer cathode comprised 5000 meters of 0.5 mm diameter clean, cold drawn nickel wire (NI 200 0.5 mm, HTN36NOAG1, A-1 Wire Tech, Inc., 840-39th Ave., Rockford, Illinois, 61109) wound on a polyethylene cylindrical support. A central cathode comprised 5000 meters of the nickel wire wound in a toroidal shape. The central cathode was inserted into a cylindrical, perforated polyethylene container that was placed inside the outer cathode with an anode array between the central and outer cathodes. The anode comprised an array of 15 platinized titanium anodes (ten - Engelhard Pt/Ti mesh 4.06 cm x 20.32 cm with one 1.91 cm x 17.78 cm stem attached to the 4.06 cm side plated with 100 U Pt series 3000; and 5 - Engelhard 2.54 cm diameter x 20.32 cm length titanium tubes with one 1.91 cm x 17.78 cm stem affixed to the interior of one end and plated with 100 U Pt series 3000). Before assembly, the anode array was cleaned in 3 M HCl for 5 minutes and rinsed with distilled water. The cathode was cleaned by placing it in a tank of 0.57 M K_2CO_3 /3% H_2O_2 for 6 hours and then rinsing it with distilled water. The anode was placed in the support between the central and outer cathodes, and the electrode assembly was placed in the tank containing electrolyte. The electrolyte solution comprised 28 liters of 0.57 M K_2CO_3 (Alfa K_2CO_3 99%). Electrolysis was performed at 20 amps constant current with a constant current ($\pm 0.02\%$) power supply for 15 months with water add-back to maintain the 28 liters constant.

Samples were isolated from the electrolytic cell by concentrating the K_2CO_3 electrolyte about six fold using a rotary evaporator at 50°C until a yellow white polymeric suspension formed. Precipitated crystals of the suspension were then grown over three weeks by allowing

the saturated solution to stand in a sealed round bottom flask at 25°C. Control samples utilized in the following experiments contained K_2CO_3 (99%), $KHCO_3$ (99.99%), KNO_3 (99.99%), KI (99.99%), KOH (99.9%), and KH (99%).

2.1.2. Potassium Hydrino Hydride, KH , Synthesis with an Electrolytic Cell

An electrolytic cell comprising a K_2CO_3 electrolyte, a nickel wire cathode, and platinized titanium anodes was also used to synthesize potassium hydride, KH . The cell was equivalent to that described *supra*, except that it lacked the additional central cathode.

After 3 months of operation, the cathode wire obtained a graphite colored coating. The cathode was placed in 37.85 liter (83.82 cm x 38.1 cm) Nalgene tank of 0.57 M K_2CO_3 /3% H_2O_2 for 6 hours. A very vigorous exothermic reaction was observed during the six hours. The cathode was removed and placed in a second 37.85 liter (83.82 cm x 38.1 cm) Nalgene tank of distilled water. NiO was observed to precipitate in the tank containing 0.57 M K_2CO_3 /3% H_2O_2 . The coat was observed to be removed from the cathode when it was pulled from the distilled water bath. A white polymeric solid floated to the top of the water bath over 2 weeks. The solid was collected by scooping it with a 250 ml beaker. The polymeric material was stable in water indefinitely (over a year with no observable change). The material was pure white and appeared like cotton suspended in water. Other samples were obtained which were thin films. The density was less than that of water. The material was observed to be weakly ferromagnetic. It collapsed along the magnet field lines and was attracted to a magnet in solution. It could be pulled out of water with a strong magnet. It was poured onto an evaporation dish, dried, and analyzed.

2.2. ToF-SIMS Characterization

The crystalline samples were sprinkled onto the surface of double-sided adhesive tapes and characterized using a Physical Electronics TFS-2000 ToF-SIMS instrument. The primary ion gun utilized a $^{69}Ga^+$ liquid metal source. In order to remove surface contaminants and expose a fresh surface, the samples were sputter cleaned for 30 seconds using a 40 μm X 40 μm raster. The aperture setting was 3, and the ion current was 600 pA resulting in a total ion dose of 10^{15} ions/ cm^2 .

During acquisition, the ion gun was operated using a bunched (pulse width 4 ns bunched to 1 ns) 15 kV beam⁴⁴⁻⁴⁵. The total ion dose was 10^{12} ions/ cm^2 . Charge neutralization was active, and the post accelerating voltage was 8000 V. Three different

regions on each sample of $(12\mu\text{m})^2$, $(18\mu\text{m})^2$, and $(25\mu\text{m})^2$ were analyzed. The positive and negative SIMS spectra were acquired. Representative post sputtering data is reported.

2.3. XPS Characterization

A series of XPS analyses were made on the crystalline samples each mounted on a silicon wafer using a Scienta 300 XPS Spectrometer. The fixed analyzer transmission mode and the sweep acquisition mode were used. A survey spectrum was obtained over the region $E_b = 0 \text{ eV}$ to 1200 eV . The primary element peaks allowed for the determination of all of the elements present in each sample isolated from the K_2CO_3 electrolyte. The survey spectrum also detected shifts in the binding energies of potassium and oxygen which had implications as to the identity of the compound containing the elements. A high resolution XPS spectrum was also obtained of the low binding energy region ($E_b = 0 \text{ eV}$ to 100 eV) to determine the presence of novel XPS peaks. The step energy in the survey scan was 0.5 eV , and the step energy in the high resolution scan was 0.15 eV . In the survey scan, the time per step was 0.4 seconds, and the number of sweeps was 4. In the high resolution scan, the time per step was 0.3 seconds, and the number of sweeps was 30. $C 1s$ of trace graphitic carbon contamination at 284.6 eV was used as the internal standard.

2.4. NMR Spectroscopy

1H MAS NMR was performed on the crystalline samples. The data were obtained on a custom built spectrometer operating with a Nicolet 1280 computer. Final pulse generation was from a tuned Henry radio amplifier. The 1H NMR frequency was 270.6196 MHz. A $2 \mu\text{sec}$ pulse corresponding to a 15° pulse length and a 3 second recycle delay were used. The window was $\pm 31 \text{ kHz}$. The spin speed was 4.5 kHz. The number of scans was 1000. The offset was 1527.12 Hz, and the magnetic flux was 6.357 T. Chemical shifts were referenced to external TMS.

2.5. FTIR Spectroscopy

Samples were transferred to an infrared transmitting substrate and analyzed by FTIR spectroscopy using a Nicolet Magna 550 FTIR Spectrometer with a NicPlan FTIR microscope. The number of scans was 500 for both the sample and background. The resolution was 8 cm^{-1} . A dry air purge was applied.

2.6. Thermal Decomposition with Analysis by Mass Spectroscopy²

Mass spectroscopy was performed on the gases released from the thermal decomposition of the samples. One end of a 4 mm ID fritted capillary tube containing about 5 mg of sample was sealed with a 6.35 mm in. Swagelock union and plug (Swagelock Co., Solon, OH). The other end was connected directly to the sampling port of a Dycor System 1000 Quadrapole Mass Spectrometer (Model D200MP, Ametek, Inc., Pittsburgh, PA with a HOVAC Dri-2 Turbo 60 Vacuum System). The capillary was heated with a Nichrome wire heater wrapped around the capillary. The mass spectrum was obtained at the ionization energy of 70 eV at a sample temperature of 600°C with the detection of hydrogen indicated by a $m/e = 2$ peak.

The control hydrogen gas was ultrahigh purity (MG Industries).

2.7. High Resolution Visible Spectroscopy of Plasma Electrolysis Cells

The plasma electrolysis cell shown in Fig. 1 comprised a 800 ml glass beaker covered with a Teflon lid with a gas outlet and 4 penetrations for electrodes, a thermometer, and a circulating water cold finger for cooling. The electrolyte comprised 600 ml of 0.15 M aqueous $\text{Na}_2\text{CO}_3 \cdot \text{H}_2\text{O}$ (99.5% Alfa Aesar), K_2CO_3 (99% Fluka), Rb_2CO_3 (99% Alfa Aesar), or Cs_2CO_3 (99% Alfa Aesar). The cathode that was sufficiently durable for long duration electrolysis was a 0.3 cm diameter tungsten rod with 3 cm immersed in the electrolyte. To eliminate the possibility of tungsten emission lines in the region of 407 nm, the experiments were repeated with the tungsten cathode replaced by a 0.1 cm diameter platinum wire cathode. The anode was a 20 cm^2 platinum wire gauze. The high voltage electrolysis power was supplied by two Xantrex XFR 100-28 (0-100 V, 0-28 A) DC power supplies connected in series. The electrolysis was carried out at about 160 V and about 3A. Using water cooling, the cell was maintained under bright cathode plasma conditions corresponding to a temperature of about 90°C.

The high resolution visible spectrum of each electrolysis plasma was recorded over the range 400 – 410 nm to search for the 407.0 nm emission of $\text{H}^-(1/2)$. Other regions were scanned to eliminate known elements as discussed in Sec. IIIG. The plasma emission was fiber-optically coupled through a 220F matching fiber adapter positioned at the wall of the beaker just opposite to the cathode to a high resolution visible spectrometer with a resolution of ± 0.006 nm over the spectral range 190 - 860 nm. The spectrometer was a Jobin Yvon Horiba 1250 M with 2400 groves/mm ion-etched holographic diffraction grating. The entrance and exit slits were set to 20 μm . The spectrometer was scanned between 400 – 410 nm using a

0.001 nm step size. The signal was recorded by a PMT with a stand alone high voltage power supply (950 V) and an acquisition controller. The data was obtained in a single accumulation with a 1 second integration time.

In addition, a low resolution spectrum of each electrolysis plasma was recorded over the range 400 – 900 nm to identify the emitting species such as hydrogen and alkali species. The spectrometer system comprised a 100 μ m optical fiber and visible spectrometer (Ocean Optics S2000). To correct for the nonuniform response of the spectrometer system as a function of wavelength, the system was calibrated against a reference light source (Ocean Optics LS-1-CAL), and the count rate data at each wavelength was corrected by the spectral calibration factor.

3. RESULTS AND DISCUSSION

3.1. ToF-SIMS

3.1.1. ToF-SIMS of Potassium Hydride Potassium Hydrogen Carbonate, KH KHCO₃, Electrolytic Cell Sample

The positive ToF-SIMS spectrum obtained from the KHCO₃ control is shown in Figs. 2 and 3. In addition, the positive ToF-SIMS of a sample isolated from the electrolytic cell is shown in Figs. 4 and 5. The respective hydride compounds and mass assignments appear in Table I. In both the control and electrolytic samples, the positive ion spectrum are dominated by the K⁺ ion. Two series of positive ions {K[K₂CO₃]⁺, m/z = (39 + 138n) and K₂OH[K₂CO₃]⁺, m/z = (95 + 138n)} are observed in the KHCO₃ control. Other peaks containing potassium include KC⁺, K₂O₂⁺, K₂O₂H₂⁺, KCO⁺, and K₂²⁺. However, in the electrolytic cell sample, three new series of positive ions are observed at {K[KH KHCO₃]⁺, m/z = (39 + 140n), K₂OH[KH KHCO₃]⁺, m/z = (95 + 140n), and K₃O[KH KHCO₃]⁺, m/z = (133 + 140n)}. These ions correspond to inorganic clusters containing novel hydride combinations (i.e. KH KHCO₃ units plus other positive fragments).

The comparison of the positive ToF-SIMS spectrum of the KHCO₃ control with the electrolytic cell sample shown in Figs. 2 and 3 and Figs. 4 and 5, respectively, demonstrates that the ³⁹K⁺ peak of the electrolytic cell sample may saturate the detector and give rise to a peak that is atypical of the natural abundance of ⁴¹K. The natural abundance of ⁴¹K is 6.7%; whereas, the observed ⁴¹K abundance from the electrolytic cell sample is 57%. This atypical abundance was also confirmed using Electrospray-Ionization-Time-of-Flight-Mass-

Spectroscopy (ESIToFMS). The high resolution mass assignment of the $m/z = 41$ peak of the electrolytic sample was consistent with ^{41}K , and no peak was observed at $m/z = 42.98$ ruling out $^{41}\text{KH}_2^+$. Moreover, the natural abundance of ^{41}K was observed in the positive ToF-SIMS spectra of KHCO_3 , KNQ_3 , and KI standards that were obtained with an ion current such that the ^{39}K peak intensity was an order of magnitude higher than that given for the electrolytic cell sample. The saturation of the ^{39}K peak of the positive ToF-SIMS spectrum by the electrolytic cell sample is indicative of a unique crystalline matrix ⁴⁶.

The negative ToF-SIMS spectrum ($m/e = 0 - 50$) of the KHCO_3 (99.99%) sample and the negative ToF-SIMS spectrum ($m/e = 0 - 30$) of the electrolytic cell sample are shown in Figs. 6 and 7, respectively. The negative ion ToF-SIMS of the electrolytic cell sample was dominated by H^- , O^- , and OH^- peaks. A series of nonhydride containing negative ions $\{\text{KCQ}_3[\text{K}_2\text{CO}_3]^- \quad m/z = (99 + 138n)\}$ was also present which implies that H_2 was eliminated from KHKHCO_3 during fragmentation of the compound KHKHCO_3 . Comparing the H^- to O^- ratio of the electrolytic cell sample to that of the KHCO_3 control sample, the H^- peak was about an order of magnitude higher in the electrolytic cell sample.

3.1.2. ToF-SIMS of Potassium Hydrino Hydride, KH, Electrolytic Cell Sample

The positive ToF-SIMS spectrum obtained from the KH electrolytic cell sample is shown in Fig. 8. The positive spectrum was dominated by the potassium peak $\text{K}^+ \quad m/z = 39$ followed by the proton peak. Small silicon, sodium, and hydrocarbon fragment peaks such as $\text{C}_2\text{H}_3^+ \quad m/z = 27$ and $\text{C}_2\text{H}_5^+ \quad m/z = 29$, $\text{K}_2^+ \quad m/z = 87$, $\text{K}(\text{KO})^+ \quad m/z = 94$, and $\text{K}(\text{KOH})^+ \quad m/z = 95$ were also observed.

The positive spectrum of the KHCO_3 control shown in Figs. 2 and 3 was also dominated by the potassium peak $\text{K}^+ \quad m/z = 39$. Two series of positive ions $\{\text{K}[\text{K}_2\text{CO}_3]^- \quad m/z = (39 + 138n) \text{ and } \text{K}_2\text{OH}[\text{K}_2\text{CO}_3]^- \quad m/z = (95 + 138n)\}$ were observed in the KHCO_3 control. Other peaks containing potassium included $\text{KC}^+ \quad m/z = 51$, K_2O^+ , $\text{K}_2\text{O}_2\text{H}^+$, $\text{KCO}^+ \quad m/z = 67$, and $\text{K}_2^+ \quad m/z = 78$.

The negative ion ToF-SIMS of KH shown in Fig. 9 was dominated by H^- . $\text{O}^- \quad m/z = 16$ and $\text{OH}^- \quad m/z = 17$ dominated the negative ion ToF-SIMS of the KHCO_3 control as shown in Fig. 6. These peaks were present in the case of KH, but they were very small in comparison to the KHCO_3 control. For both samples smaller hydrocarbon fragment peaks such as $\text{C}^- \quad m/z = 12$ and $\text{CH}^- \quad m/z = 13$ were observed. A series of negative ions $\{\text{KCQ}_3[\text{K}_2\text{CO}_3]^- \quad m/z = (99 + 138n)\}$ was also present in the control which were not observed

in the *KH* sample. A hydride peak probably due to OH^- $m/z = 17$ which was significantly smaller than the O^- $m/z = 16$ peak was observed in the control.

3.2. XPS

3.2.1. XPS of Potassium Hydride Potassium Hydrogen Carbonate, $KH KHCO_3$, Electrolytic Cell Sample

The 0 to 80 eV binding energy region of a high resolution XPS spectrum of the $KH KHCO_3$ electrolytic cell sample is shown in Fig. 10. The XPS survey spectrum the $KH KHCO_3$ electrolytic cell sample with the primary elements identified is shown in Fig. 11. No elements were present in the survey scans which can be assigned to peaks in the low binding energy region with the exception of a small variable contaminant of sodium at 63 eV and 31 eV, potassium at 16.2 eV and 32.1 eV, and oxygen at 23 eV. Accordingly, any other peaks in this region must be due to novel species. The $K 3s$ and $K 3p$ are shown in Fig. 10 at 16.2 eV and 32.1 eV, respectively. A weak $Na 2s$ is observed at 63 eV. The $O 2s$ which is weak compared to the potassium peaks of K_2CO_3 , is typically present at 23 eV, but is broad or obscured in Fig. 10.

Peaks centered at 22.8 eV and 38.8 eV which do not correspond to any other primary element peaks were observed. The relative intensities and shift of each peak match $K 3s$ and $K 3p$ peaks shifted to higher binding energies. Hydrogen is the only element which does not have primary element peaks; thus, it is the only candidate to produce the shifted peaks. These peaks may be shifted by a highly binding hydride ion with a binding energy of 22.8 eV as observed in other compounds by Mills et al.^{15-20, 33-39} that bonds to potassium $K 3p$ and shifts the peak to this energy. In this case, the $K 3s$ is similarly shifted. These peaks were not present in the case of the XPS of matching samples isolated from an identical electrolytic cell except that Na_2CO_3 replaced K_2CO_3 as the electrolyte.

XPS further confirmed the ToF-SIMS data by showing shifts of the primary elements. The splitting of the principal peaks of the survey XPS spectrum is indicative of multiple forms of bonding involving the atom of each split peak. For example, the XPS survey spectrum shown in Fig. 11 shows extraordinary potassium and oxygen peak shifts. All of the potassium primary peaks are shifted to about the same extent as that of the $K 3s$ and $K 3p$. In addition, extraordinary $O 1s$ peaks of the electrolytic cell sample were observed at 537.5 eV and 547.8 eV; whereas, a single $O 1s$ was observed in the XPS spectrum of K_2CO_3 at 532.0 eV. The results are not due to uniform charging as the internal standard $C 1s$ remains the same at 284.6 eV. The results are not due to differential charging because the peak shapes of carbon

and oxygen are normal, and no tailing of these peaks was observed. The binding energies of the K_2CO_3 control and the $KH/KHCO_3$ electrolytic cell sample are shown in Table II. The range of literature ⁴⁷⁾ values of the binding energies of the peaks of interest are given in the final row of Table II. The $K 3p$, $K 3s$, $K 2p_{3/2}$, $K 2p_{1/2}$, and $K 2s$ XPS peaks and the $O 1s$ XPS peaks shifted to an extent greater than those of known compounds may correspond to and identify $KH/KHCO_3$.

3.2.2. XPS of Potassium Hydride, KH, Electrolytic Cell Sample

The XPS survey scan of the KH electrolytic cell sample is shown in Fig. 12. $C 1s$ at 284.5 eV was used as the internal standard for the KH sample and the control K_2CO_3 . The major species present in the control are potassium and carbon and oxygen. The major species present in the KH sample was potassium. Large silicon, oxygen and graphitic and hydrocarbon carbon peaks were also seen that originated from the silicon wafer sample mount. Nitrogen was present, and trace magnesium and sodium may be present. The identifying peaks of the primary elements and their binding energies are: $Na 1s$ at 1072.2 eV, $O 1s$ at 532.0 eV, $Na KL_{23}L_{23}$ at 496.6 eV, $N 1s$ at 399.3 eV, $K 2s$ at 377.2 eV, $Mg KL_{23}L_{23}$ at 305.9 eV, $K 2p_{1/2}$ at 295.4 eV, $K 2p_{3/2}$ at 292.5 eV, $C 1s$ at 285.5 and 284.6 eV, $Si 2p_{3/2}$ at 156.7 eV and 153.4 eV, $Si 2s$ at 105.7 eV and 102.1 eV, and $Mg 2s$ at 88.5 eV.

No elements were present in the survey scan which could be assigned to peaks in the low binding energy region with the exception of the $K 3p$ at 16.8 eV, $K 3s$ at 33.0 eV, $O 2s$ at 26.2 eV, and $Mg 2p$ at 49.6 eV. Accordingly, any other peaks in this region must be due to novel species. The 0-80 eV binding energy region of a high resolution XPS spectrum of the KH electrolytic cell sample is shown in Fig. 13. Peaks of interest were observed in the valance band at 3.8 eV, 9.95 eV, and 13.7 eV which may be due to nitrogen, carbon, and oxygen, but the assignment can not be made with certainty. A 62.8 peak may be assigned to $Na 2s$. However, no peak is detectable above baseline at 29.8 eV which corresponds to $Na 2p_{1/2}$. Since the intensity of the $Na 2p_{1/2}$ peak is less than $Na 2s$, and the $Na 2s$ peak is weak, the $Na 2p_{1/2}$ may not be seen. So, the assignment is uncertain. Novel peaks were observed in the KH sample at 19.5 eV, 36.0 eV, and 68.0 eV. The 68.0 eV peak may be assigned to $Ni 3p$, but the shape is incorrect. And, if the $Ni 2p_{3/2}$ at about 860 eV is present, it is smaller than the proposed $Ni 3p$. Thus, the 68.0 eV can not be assigned to $Ni 3p$.

The XPS peaks at 19.5 eV, 36.0 eV, and 68.0 eV do not correspond to any other primary element peaks. The 68.0 eV peak may correspond to a hydride ion with a binding energy of 69.2 eV as observed in other compounds by Mills et al. ^{15-20, 33-39)}. Peaks at 19.5 eV and 36.0 eV which do not correspond to any other primary element peaks were observed. The

relative intensities and shift of each peak match $K 3s$ and $K 3p$ peaks shifted to higher binding energies. Hydrogen is the only element which does not have primary element peaks; thus, it is the only candidate to produce the shifted peaks. These peaks may be shifted by a highly binding hydride ion with a binding energy of 22.8 eV ^{15-20, 33-39} that bonds to potassium $K 3p$ and shifts the peak to this energy. In this case, the $K 3s$ is similarly shifted. The shift of about 3 eV is greater than that of known potassium compounds. These peaks were not present in the case of the XPS of matching samples isolated from an identical electrolytic cell except that Na_2CO_3 replaced K_2CO_3 as the electrolyte.

The KH electrolytic cell sample was observed to be weakly ferromagnetic. The origin of the magnetism is from nonmetallic elements which were most likely potassium and hydrogen.

3.3. NMR

The signal intensities of the 1H MAS NMR spectrum of the K_2CO_3 reference were relatively low. It contained a water peak at 1.208 ppm , a peak at 5.604 ppm , and very broad weak peaks at 13.2 ppm , and 16.3 ppm . The 1H MAS NMR spectrum of the $KHCO_3$ reference contained a large peak at 4.745 with a small shoulder at 5.150 ppm , a broad peak at 13.203 ppm , and small peak at 1.2 ppm .

The 1H MAS NMR spectra of the $KH/KHCO_3$ electrolytic cell sample is shown in Fig. 14. The peak assignments are given in Table III. The reproducible peaks assigned to $KH/KHCO_3$ in Table III were not present in the controls except for the peak assigned to water at $+5.066 \text{ ppm}$. The novel peaks could not be assigned to hydrocarbons. Hydrocarbons were not present in the electrolytic cell sample based on the ToF-SIMS spectrum and FTIR spectra which were also obtained (see below). The novel peaks without identifying assignment are consistent with $KH/KHCO_3$. The NMR peaks of the reference KH (Aldrich Chemical Company 99%) were observed at 0.8 and 1.1 ppm relative to TMS. The upfield peaks of Fig. 14 are assigned to novel hydride ion of the potassium hydride species (KH^-) in different environments. The down field peaks are assigned to the proton of the potassium hydrogen carbonate species in different chemical environments ($-KHCO_3$).

3.4. FTIR

The FTIR spectra of K_2CO_3 (99%) and $KHCO_3$ (99.99%) were compared with that of the $KH/KHCO_3$ electrolytic cell sample. A spectrum of a mixture of the bicarbonate and the carbonate was produced by digitally adding the two reference spectra. The two standards alone

and the mixed standards were compared with that of the electrolytic cell sample. From the comparison, it was determined that the electrolytic cell sample contained potassium carbonate but did not contain potassium bicarbonate. The unknown component could be a bicarbonate other than potassium bicarbonate. The spectrum of potassium carbonate was digitally subtracted from the spectrum of the electrolytic cell sample as shown in Fig. 15. Several bands were observed including bands in the $1400 - 1600\text{ cm}^{-1}$ region. Some organic nitrogen compounds (e.g. acrylamides, pyrrolidinones) have strong bands in the region 1660 cm^{-1} ⁴⁸. However, the lack of any detectable $C - H$ bands ($\approx 2800 - 3000\text{ cm}^{-1}$) and the bands present in the 700 to 1100 cm^{-1} region indicate an inorganic material ⁴⁹. Peaks that are not assignable to potassium carbonate were observed at 3294 , 3077 , 2883 , 1100 cm^{-1} , 2450 , 1660 , 1500 , 1456 , 1423 , 1300 , 1154 , 1023 , 846 , 761 , and 669 cm^{-1} .

The overlap FTIR spectrum of the electrolytic cell sample and the FTIR spectrum of the reference potassium carbonate appears in Fig. 16. In the 700 to 2500 cm^{-1} region, the peaks of the electrolytic cell sample closely resemble those of potassium carbonate, but they are shifted about 50 cm^{-1} to lower frequencies. The shifts are similar to those observed by replacing potassium (K_2CO_3) with rubidium (Rb_2CO_3) as demonstrated by comparing their IR spectra ⁵⁰. The shifted peaks may be explained by a polymeric structure for the compound KH_2KCO_3 , wherein the vibrational frequency is inversely proportional to the square root of the mass. The polymeric structure is supported by the observation of multimers of $140n$ in the positive ToF-SIMS spectrum of the electrolytic cell sample.

3.5. Mass Spectroscopy (MS)

The KH electrolytic cell sample did not decompose upon heating to 600°C . Essentially no hydrogen was observed by mass spectroscopy. The sample changed very little which indicates no decomposition and extraordinary stability for a compound mainly comprised of hydrogen.

3.6. Further Analytical Tests

X-ray diffraction (XRD), elemental analysis, and Raman spectroscopy were also performed on the KH_2KCO_3 electrolytic sample. The XRD data indicated that the diffraction pattern of the electrolytic cell sample does not match that of either KH , $KHCO_3$, K_2CO_3 , or KOH . The elemental analysis (Galbraith Laboratories) showed a wt % of potassium, carbon, and hydrogen of 43.65 , 7.91 , and 1.43 , respectively. Oxygen could not be obtained. The corresponding high hydrogen atomic percentage supports KH_2KCO_3 . Unidentified Raman

peaks at 1685 cm^{-1} and 835 cm^{-1} were present in addition to the known peaks of KHCO_3 and a small peak assignable to K_2CO_3 .

Results from gaseous reactions at elevated temperature demonstrate that KHKHCO_3 may also be formed by a reaction of gaseous KI with atomic hydrogen in the presence of K_2CO_3 ³⁷. In addition to the previous analytical studies, the fragment KK_2CO_3^+ corresponding to KHKHCO_3 was observed by ESIToFMS as a chromatographic peak on a C18 liquid chromatography column typically used to separate organic compounds. No chromatographic peaks were observed in the case of inorganic compound controls KI , KHCO_3 , K_2CO_3 , and KOH .

3.7. Insitu High Resolution Visible Spectroscopy

The low resolution spectrum of each electrolysis plasma was recorded over the range 400 – 900 nm to identify emitting species such as hydrogen and alkali species as demonstrated by the low resolution spectrum of the K_2CO_3 electrolysis plasma shown in Fig. 17. In each case, strong alkali metal, Balmer α , and molecular hydrogen emission was observed. In addition, weaker alkali metal ion emission was observed for each plasma except for the Na_2CO_3 plasma. The alkali emission lines are given in Table IV.

The high resolution visible spectrum in the region of 407 nm was recorded on the emission from each of the plasma electrolysis cells. A peak at 407.0 nm was observed in each case except for the Na_2CO_3 cell. To eliminate tungsten emission as the source of the 407.0 nm peak, each plasma electrolysis was repeated with a platinum cathode.

The high resolution visible spectra in the region of 407 nm from the Na_2CO_3 , K_2CO_3 , Rb_2CO_3 , and Cs_2CO_3 plasma electrolysis cells each with a platinum cathode are shown in Figs. 18–21, respectively. The only peaks observed from the Na_2CO_3 plasma were known peaks of molecular hydrogen; whereas, in each case of the K_2CO_3 , Rb_2CO_3 , and Cs_2CO_3 plasma, a peak was observed at 407.0 nm which could not be assigned to hydrogen, the alkali or alkaline earth atom or ion, or platinum. The known peaks of molecular hydrogen in the region of 407 nm were separated as indicated in Figs. 18–21.

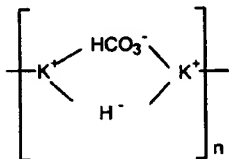
Since the novel 407.0 nm peak was also only observed for the K_2CO_3 , Rb_2CO_3 , and Cs_2CO_3 plasma electrolysis cells, but not for the Na_2CO_3 cell when the tungsten cathode was replaced by a platinum cathode, cathode metal lines were eliminated as the source of the novel 407.0 nm peak. O II lines at 406.9623, 406.9881, and 407.1238 nm were also eliminated due to the absence of O I lines at 394.729, 394.748, 394.758, 395.460, and 405.477 nm. C III lines at 407.026 and 406.8916 nm were eliminated due to the absence of C I lines which were outside of the region of 407.0 nm or C II lines at 391.896 and 392.068 nm. Furthermore, the

presence of the O II or C III lines would be extraordinary since the ionization energy required for O II is above the first ionization energy of 13.62 eV, and the energies required for C III are above the sum of the first and second ionization energies of 11.26 eV and 24.38 eV, respectively ⁴³⁾.

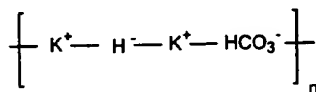
4. DISCUSSION

Alkali and alkaline earth hydrides react violently with water to release hydrogen gas which subsequently ignites due to the exothermic reaction with water. Typically metal hydrides decompose upon heating at a temperature in the range of 250-1000°C. These saline hydrides, so called because of their saltlike or ionic character, are the monohydrides of the alkali metals and the dihydrides of the alkaline-earth metals, with the exception of beryllium. BeH_2 appears to be a hydride with bridge type bonding rather than an ionic hydride. Highly polymerized molecules held together by hydrogen-bridge bonding is exhibited by boron hydrides and aluminum hydride. Based on the known structures of these hydrides, the ToF-SIMS hydride clusters such as $K[KH K H C O_3]_n$, the XPS peaks observed at 22.8 eV and 38.8 eV, upfield NMR peaks assigned to hydride ion, and the shifted FTIR peaks, the present novel hydride compound of the $KH K H C O_3$ electrolytic cell sample may be a polymer, $[K H K H C O_3]_n$, with a structural formula which is similar to boron and aluminum hydrides. The reported novel compound appeared polymeric in the concentrated electrolytic solution and in distilled water. $[K H K H C O_3]_n$ is extraordinarily stable in water, whereas, potassium hydride reacts violently with water.

As an example of the structures of this compound, the $K[KH K H C O_3]_n$, $m/z = (39 + 140n)$ series of fragment peaks is tentatively assigned to novel hydride bridged or linear potassium bicarbonate compounds having a general formula such as $[K H K H C O_3]_n$, $n = 1, 2, 3, \dots$. General structural formulas may be



and



Liquid chromatography/ESIToFMS studies are in progress to support the polymer assignment.

KH was stable at elevated temperature (600°C). The positive and negative ToF-SIMS of the *KH* electrolytic sample showed essentially K^+ and H^- only, respectively. Hydride ions with binding energies of 22.8 eV and 69.2 eV have been observed by XPS of *KH*. The former hydride ion with a binding energy of 22.8 eV was observed by X-ray photoelectron spectroscopy (XPS) of the *KH KHCO₃* electrolytic sample. These compounds appear polymeric in aqueous solution. *KH* was observed to be weakly ferromagnetic; whereas, *KH KHCO₃* was diamagnetic. The magnetism of *KH* may be due to mixed oxidation states due to the presence of two hydride ions with a substantially reduced radii to permit spin correlation.

Each of K^+ / K^\bullet , Rb^+ , and Cs as the catalyst was predicted to catalyze hydrogen to form $H\left[\frac{a_H}{2}\right]$ which reacts with an electron to form $H^-(1/2)$. The predicted $H^-(1/2)$ hydride ion of hydrogen catalysis by these catalysts was observed spectroscopically at 407.0 nm corresponding to its predicted binding energy of 3.05 eV. The hydride reaction product formed over time and was stable in water. The formation of hydride novel compounds observed by ToF-SIMS provided substantial evidence supporting catalysis of hydrogen to form $H^-(1/2)$ and its spectroscopic identification.

5. CONCLUSION

The ToF-SIMS, XPS, and NMR results of products from a K_2CO_3 electrolytic cell with K^+ / K^\bullet as the catalyst confirm the identification of *KH KHCO₃* and *KH* with new states of hydride ions. $H^-(1/2)$, the predicted hydride ion product with each of K^+ / K^\bullet , Rb^+ , and Cs as the catalyst, has a binding energy of 3.05 eV corresponding to a 407 nm emission. Metal and/or metal ion peaks corresponding to the electrolyte (K, Rb, Cs, Na^+), molecular hydrogen, and atomic hydrogen were observed by high resolution visible spectroscopy in plasma electrolysis cells. The $H^-(1/2)$ peak at 407.0 nm was observed in all of the electrolytes except Na_2CO_3 which cannot form $H^-(1/2)$. It was remarkable that the hydride ion formed in aqueous solution which is indicative of its stability and potential novel chemistry.

The chemical structure and properties of the novel compounds having hydride ions with high binding energies are indicative of a new field of hydride chemistry. The novel hydride ions may combine with other cations such as other alkali cations and alkaline earth, rare earth, and transition element cations. Thousands of novel compounds may be synthesized with extraordinary properties relative to the corresponding compounds having ordinary hydride ions. These novel compounds may have a breadth of applications. For example, a high voltage battery (eqs. (1)–(3)) according to the hydride binding energies of 22.8 eV and

69.2 eV observed by XPS may be possible having projected specifications and environmental advantages that may be competitive with the internal combustion engine.

ACKNOWLEDGMENTS

Special thanks to F. Becker for assistance with the power electronics and monitoring systems.

REFERENCES

- 1) I. Uehara, T. Sakai, H. Ishikawa: *J. Alloy Comp.* **253/254** (1997) No. 1/2, 635.
- 2) J. Glanz: *New Scientist*. **146** (1995) No. 1973, 32.
- 3) D. Mulholland: *Defense News*. **14** (1999) No. 10, 1 and 34.
- 4) S. M. Aceves, G. D. Berry, and G. D. Rambach: *Int. J. Hydrogen Energy*. **23** (1998) No. 7, 583.
- 5) J. Ball: Auto Makers Are Racing to Market "Green" Cars Powered by Fuel Cells published in *The Wall Street Journal*. March 15, (1999) p. 1.
- 6) US Office of Technology Assessment: *Advanced Automotive Technology: Visions of a Super-Efficient Family Car*, National Technical Information Service, US Department of Commerce, PB96-109202, OTA-ETI-638 (1995).
- 7) R. Mills: *The Grand Unified Theory of Classical Quantum Mechanics* (BlackLight Power, Inc.: Cranbury, New Jersey, 2000, Distributed by Amazon.com; September 2001 Edition posted at www.blacklightpower.com.)
- 8) R. Mills: *Proc. 29th Conference on High Energy Physics and Cosmology, 2000* (Kluwer Academic/Plenum Publishers, New York, 2001) p. 243.
- 9) R. Mills: *The Grand Unified Theory of Classical Quantum Mechanics* to be published in *Int. J. of Hydrogen Energy*. (2002).
- 10) R. Mills: *Int. J. of Hydrogen Energy*. **25** (2000) 1171.
- 11) R. Mills: *Int. J. Hydrogen Energy* **26** (2001) 1059.
- 12) R. Mills and P. Ray: Spectral Emission of Fractional Quantum Energy Levels of Atomic Hydrogen from a Helium-Hydrogen Plasma and the Implications for Dark Matter to be published in *Int. J. Hydrogen Energy*. (2002).
- 13) R. L. Mills, P. Ray, B. Dhandapani and J. He: Spectroscopic Identification of Fractional Rydberg States of Atomic Hydrogen submitted to *J. Phys. Chem. Letts*.
- 14) R. Mills and P. Ray: Vibrational Spectral Emission of Fractional-Principal-Quantum-Energy-Level Hydrogen Molecular Ion to be published in *Int. J. Hydrogen Energy*. (2002).
- 15) R. Mills, P. Ray, M. Nansteel, W. Good, P. Jansson, B. Dhandapani and J. He: Excessive Balmer α Line Broadening, Power Balance, and Novel Hydride Ion Product of Plasma Formed from Incandescently Heated Hydrogen Gas with Certain Catalysts submitted to *Int. J. Hydrogen Energy*.
- 16) R. L. Mills and P. Ray: High Resolution Spectroscopic Observation of the Bound-Free Hyperfine Levels of a Novel Hydride Ion Corresponding to a Fractional Rydberg State of Atomic Hydrogen submitted to *Int. J. Hydrogen Energy*.

- 17) R. L. Mills and E. Dayalan: *Proc. 17th Annual Battery Conference on Applications and Advances, 2002*, (California State University, Long Beach, 2002.)
- 18) R. L. Mills and P. Ray: Spectroscopic Identification of a Novel Catalytic Reaction of Rubidium Ion with Atomic Hydrogen and the Hydride Ion Product submitted to *Int. J. Hydrogen Energy*.
- 19) R. Mills and P. Ray: *Int. J. Hydrogen Energy*. **27** (2002) 183.
- 20) R. Mills: *Int. J. Hydrogen Energy*. **26** (2001) 1041.
- 21) R. Mills and M. Nansteel: Argon-Hydrogen-Strontium Plasma Light Source submitted to *IEEE Transactions on Plasma Science*.
- 22) R. Mills, M. Nansteel, and P. Ray: Excessively Bright Hydrogen-Strontium Plasma Light Source Due to Energy Resonance of Strontium with Hydrogen submitted to *European Journal of Physics D*.
- 23) R. Mills, J. Dong, W. Good, P. Ray, J. He, and B. Dhandapani: Measurement of Energy Balances of Noble Gas-Hydrogen Discharge Plasmas Using Calvet Calorimetry submitted to *Int. J. Hydrogen Energy*.
- 24) Randell L. Mills, P. Ray, B. Dhandapani, M. Nansteel, X. Chen and J. He: New Power Source from Fractional Quantum Energy Levels of Atomic Hydrogen that Surpasses Internal Combustion submitted to *Spectrochimica Acta Part A*.
- 25) R. L. Mills, P. Ray, B. Dhandapani and J. He: Comparison of Excessive Balmer α Line Broadening of Glow Discharge and Microwave Hydrogen Plasmas with Certain Catalysts submitted to *J. Phys. Chem*.
- 26) R. L. Mills, A. Voigt, P. Ray, M. Nansteel and B. Dhandapani: Measurement of Hydrogen Balmer Line Broadening and Thermal Power Balances of Noble Gas-Hydrogen Discharge Plasmas to be published in *Int. J. Hydrogen Energy*. (2002).
- 27) R. Mills, N. Greenig and S. Hicks: Optically Measured Power Balances of Anomalous Discharges of Mixtures of Argon, Hydrogen, and Potassium, Rubidium, Cesium, or Strontium Vapor to be published in *Int. J. Hydrogen Energy*. (2002).
- 28) R. Mills, M. Nansteel, and Y. Lu: *Int. J. Hydrogen Energy*. **26** (2001) 309.
- 29) R. Mills, J. Dong and Y. Lu: *Int. J. Hydrogen Energy*. **25** (2000) 919.
- 30) R. Mills: *Int. J. Hydrogen Energy*. **26** (2001) 579.
- 31) R. Mills: *Int. J. Hydrogen Energy*, **26** (2001) 327.
- 32) R. Mills, T. Onuma, and Y. Lu: *Int. J. Hydrogen Energy*. **26** (2001) 749.
- 33) R. Mills, B. Dhandapani, M. Nansteel, J. He and A. Voigt: *Int. J. Hydrogen Energy*. **26** (2001) 965.
- 34) R. Mills, B. Dhandapani, N. Greenig and J. He: *Int. J. of Hydrogen Energy*. **25** (2000) 1185.

- 35) R. Mills: *Int. J. of Hydrogen Energy*. **25** (2000) 669.
- 36) R. Mills: *Fusion Technology*. **37** (2000) No. 2, 157.
- 37) R. Mills, B. Dhandapani, M. Nansteel, J. He, T. Shannon and A. Echezuria: *Int. J. of Hydrogen Energy*. **26** (2001) 339.
- 38) R. Mills: *Highly Stable Novel Inorganic Hydrides to be published in Journal of New Materials for Electrochemical Systems*. (2002).
- 39) R. Mills, W. Good, A. Voigt, J. Dong: **26** (2001) 1199.
- 40) R. Mills: *Proc. National Hydrogen Association, 12th Annual U.S. Hydrogen Meeting and Exposition, Hydrogen: The Common Thread, 2001*. (National Hydrogen Association, Washington, DC, 2001) p. 671.
- 41) R. Mills: *Proceedings of Global Foundation International Conference on Global Warming and Energy Policy, 2001*. (Kluwer Academic/Plenum Publishers, New York) p. 1059.
- 42) R. Mayo, R. Mills and M. Nansteel: On the Potential of Direct and MHD Conversion of Power from a Novel Plasma Source to Electricity for Microdistributed Power Applications submitted to *IEEE Transactions on Plasma Science*.
- 43) David R. Linde, *CRC Handbook of Chemistry and Physics*, 79 th Edition, CRC Press, Boca Raton, Florida, (1998-9), p. 10-175-10-177.
- 44) *Microsc. Microanal. Microstruct.* **3** (1992) No. 1.
- 45) For recent specifications see PHI Trift II, ToF-SIMS Technical Brochure, (1999), Eden Prairie, MN 55344.
- 46) D. Briggs, M. P. Seah, eds.: *Practical Surface Analysis, 2E., Vol. 2, Ion and Neutral Spectroscopy*. (Wiley & Sons, New York, 1992).
- 47) C. D. Wagner, W. M. Riggs, L. E. Davis, J. F. Moulder: *Handbook of X-ray Photoelectron Spectroscopy*, ed. G. E. Mullenberg (Perkin-Elmer Corp., Eden Prairie, Minnesota, 1997).
- 48) D. Lin-Vien, N. B. Colthup, W. G. Fateley and J. G. Grasselley: *The Handbook of Infrared and Raman Characteristic Frequencies of Organic Molecules* (Academic Press, Inc., San Diego, CA, 1991).
- 49) R. A. Nyquist and R. O. Kagel, eds.: *Infrared Spectra of Inorganic Compounds* (Academic Press, New York, 1971).
- 50) M. H. Brooker and J. B. Bates: *Spectrochimica Acta Part A—Molecular and Biomolecular Spectroscopy*. **A 30** (1974) 2211.

Figure Captions

Figure 1. Plasma electrolysis cell for synthesis of novel hydride compounds and as a source of light from the cathodic plasma for high resolution visible spectroscopy.

Figure 2. The positive ToF-SIMS spectrum ($m/e = 0 - 200$) of $KHCO_3$ (99.99%) where HC = hydrocarbon.

Figure 3. The positive ToF-SIMS spectrum ($m/e = 200 - 1000$) of $KHCO_3$ (99.99%) where HC = hydrocarbon.

Figure 4. The positive ToF-SIMS spectrum ($m/e = 0 - 200$) of the $KH KHCO_3$ electrolytic cell sample where HC = hydrocarbon.

Figure 5. The positive ToF-SIMS spectrum ($m/e = 200 - 1000$) of the $KH KHCO_3$ electrolytic cell sample where HC = hydrocarbon.

Figure 6. The negative ToF-SIMS spectrum ($m/e = 0 - 50$) of the $KHCO_3$ (99.99%) sample.

Figure 7. The negative ToF-SIMS spectrum ($m/e = 0 - 30$) of the $KH KHCO_3$ electrolytic cell sample.

Figure 8. The positive ToF-SIMS spectrum ($m/e = 0 - 400$) of the KH electrolytic cell sample.

Figure 9. The negative ToF-SIMS spectrum ($m/e = 0 - 400$) of the KH electrolytic cell sample.

Figure 10. The 0 to 80 eV binding energy region of a high resolution XPS spectrum of the $KH KHCO_3$ electrolytic cell sample.

Figure 11. The XPS survey spectrum of the $KH KHCO_3$ electrolytic cell sample with the primary elements identified.

Figure 12. The XPS survey scan of the KH electrolytic cell sample.

Figure 13. The 0-80 eV binding energy region of a high resolution XPS spectrum of the KH electrolytic cell sample.

Figure 14. The magic angle spinning proton NMR spectrum of the $KH KHCO_3$ electrolytic cell sample.

Figure 15. The spectrum of potassium carbonate digitally subtracted from the spectrum of the electrolytic cell sample.

Figure 16. The overlap FTIR spectrum of the $KH KHCO_3$ electrolytic cell sample and the FTIR spectrum of the reference potassium carbonate.

Figure 17. The low resolution spectrum (400 – 800 nm) of the K_2CO_3 electrolysis plasma cell showing the emission from atomic hydrogen, molecular hydrogen, potassium metal, and K^+ .

Figure 18. The high resolution visible spectrum in the region of 407 nm recorded on the emission of Na_2CO_3 plasma electrolysis cell with a platinum cathode. All of the peaks could be assigned to known lines of molecular hydrogen.

Figure 19. The high resolution visible spectrum in the region of 407 nm recorded on the emission of K_2CO_3 plasma electrolysis cell with a platinum cathode. The novel 407.0 nm peak which could not be assigned to a known peak was assigned to $H^-(1/2)$.

Figure 20. The high resolution visible spectrum in the region of 407 nm recorded on the emission of Rb_2CO_3 plasma electrolysis cell with a platinum cathode. The novel 407.0 nm peak which could not be assigned to a known peak was assigned to $H^-(1/2)$.

Figure 21. The high resolution visible spectrum in the region of 407 nm recorded on the emission of Cs_2CO_3 plasma electrolysis cell with a platinum cathode. The novel 407.0 nm peak which could not be assigned to a known peak was assigned to $H^-(1/2)$.

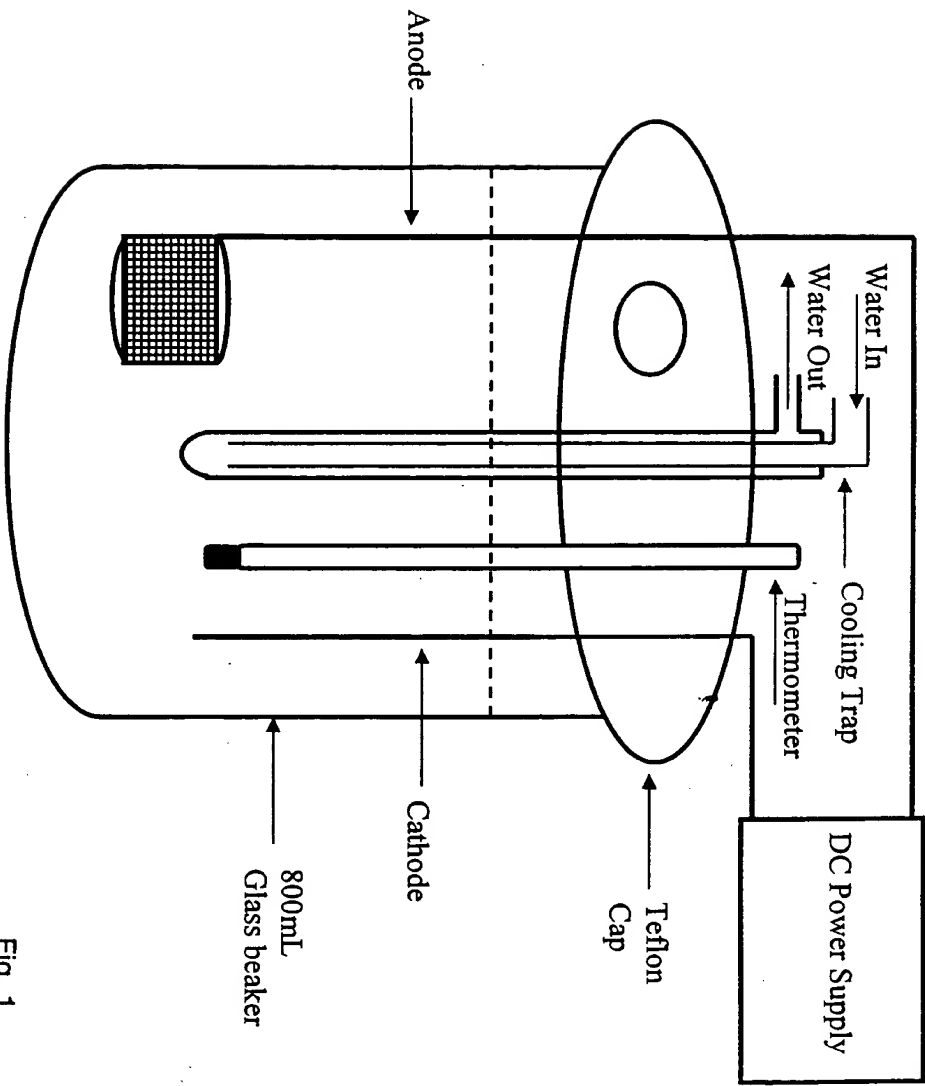


Fig. 1

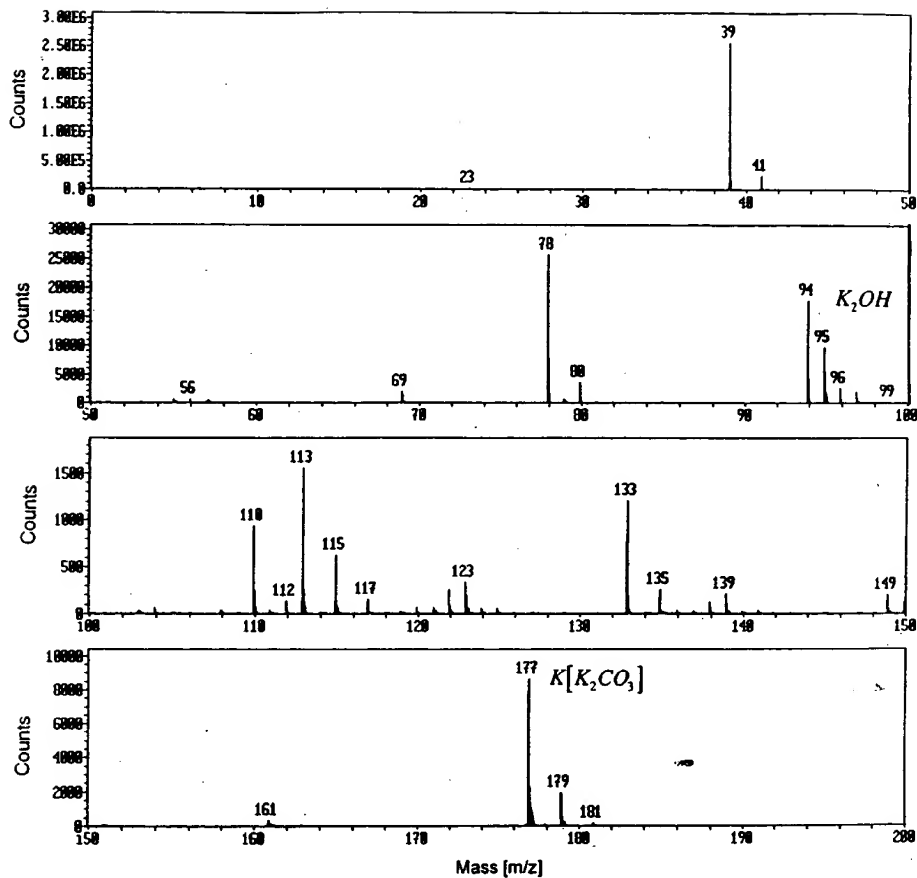


Fig. 2

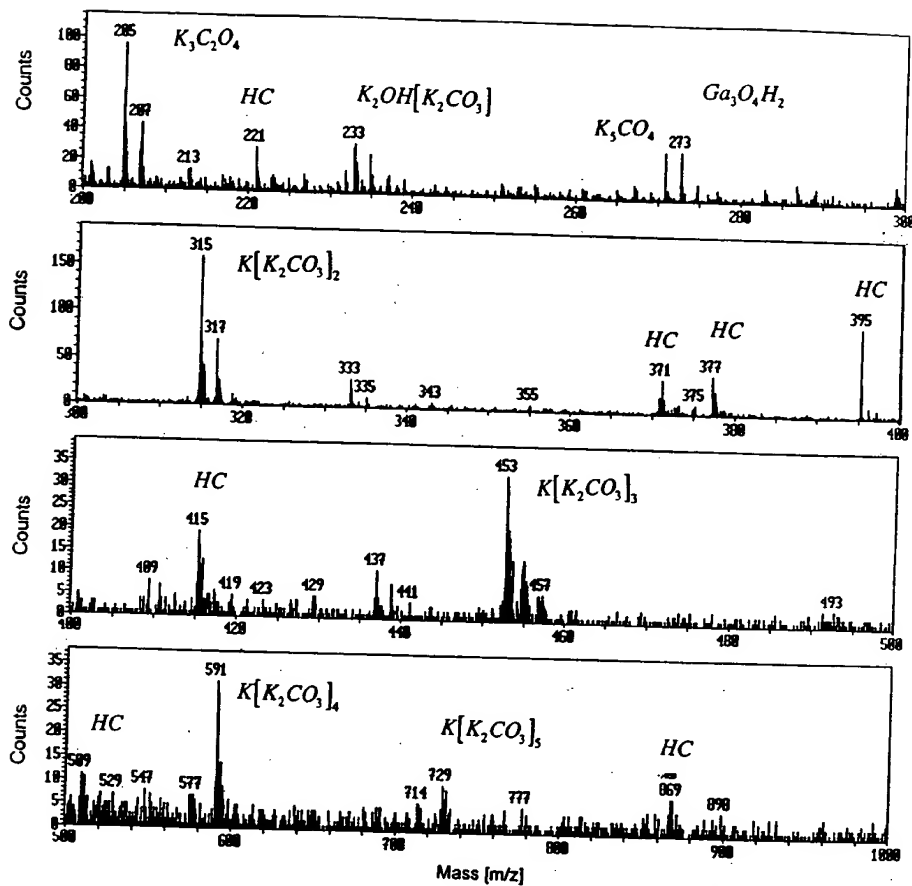


Fig. 3

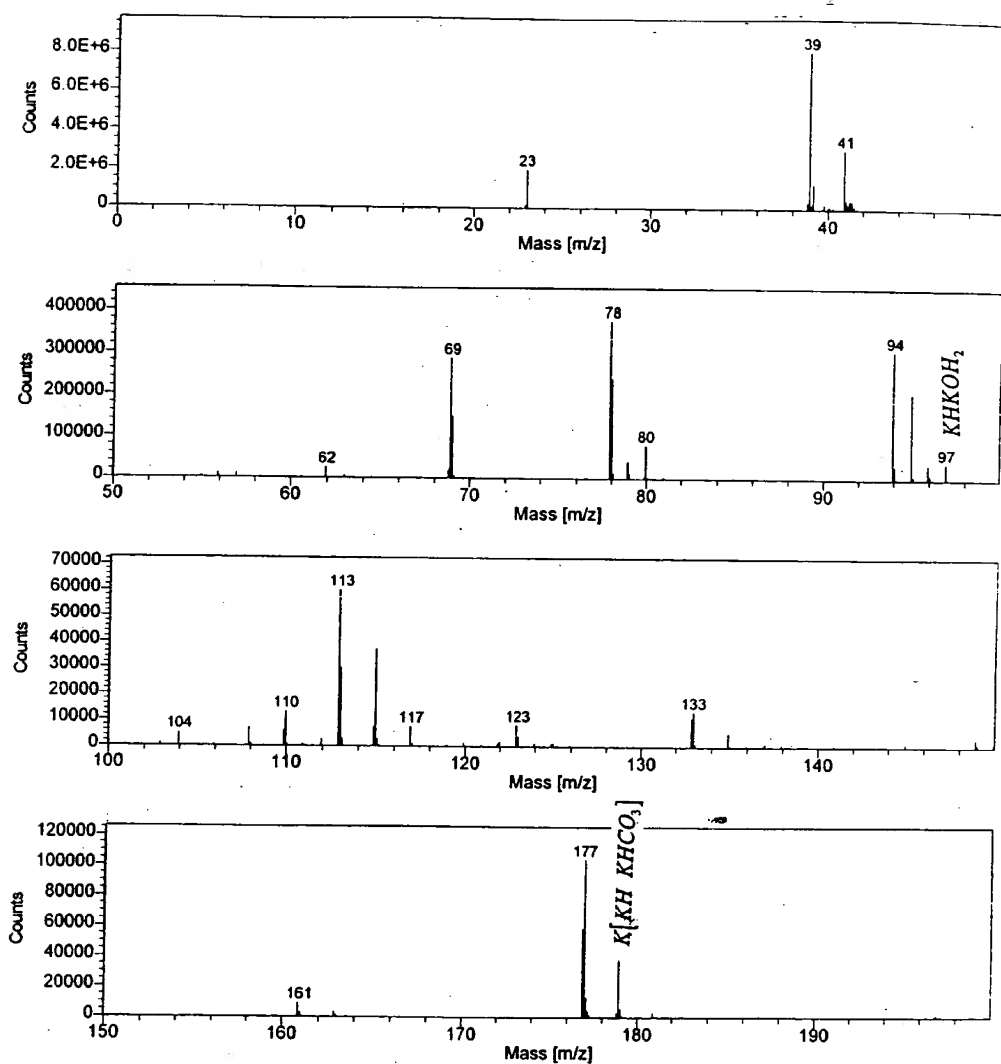


Fig. 4

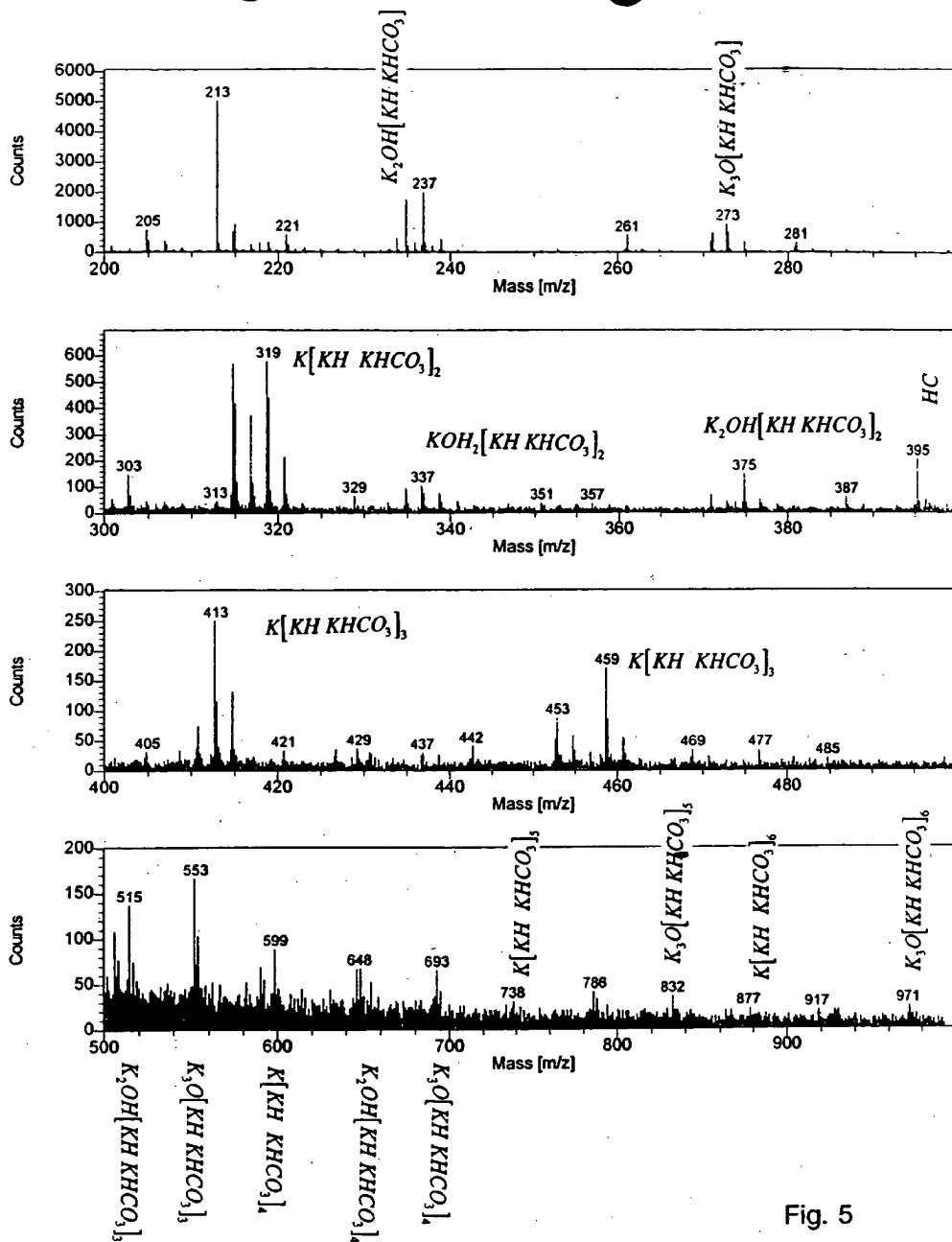


Fig. 5

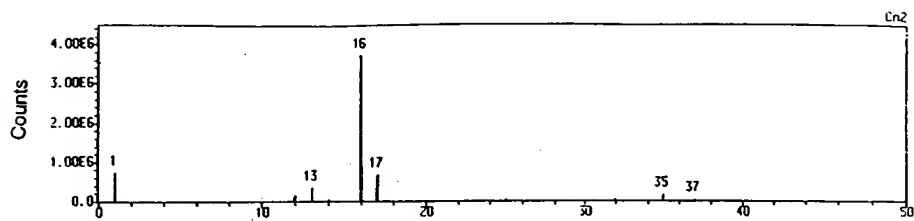


Fig. 6

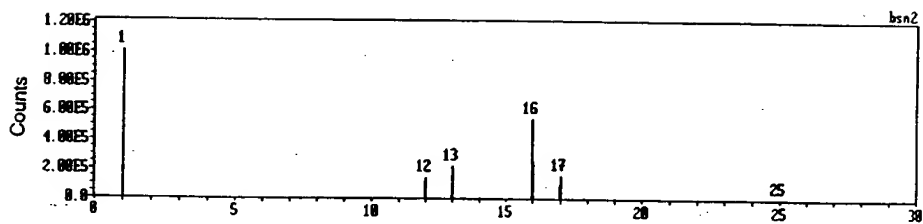


Fig. 7

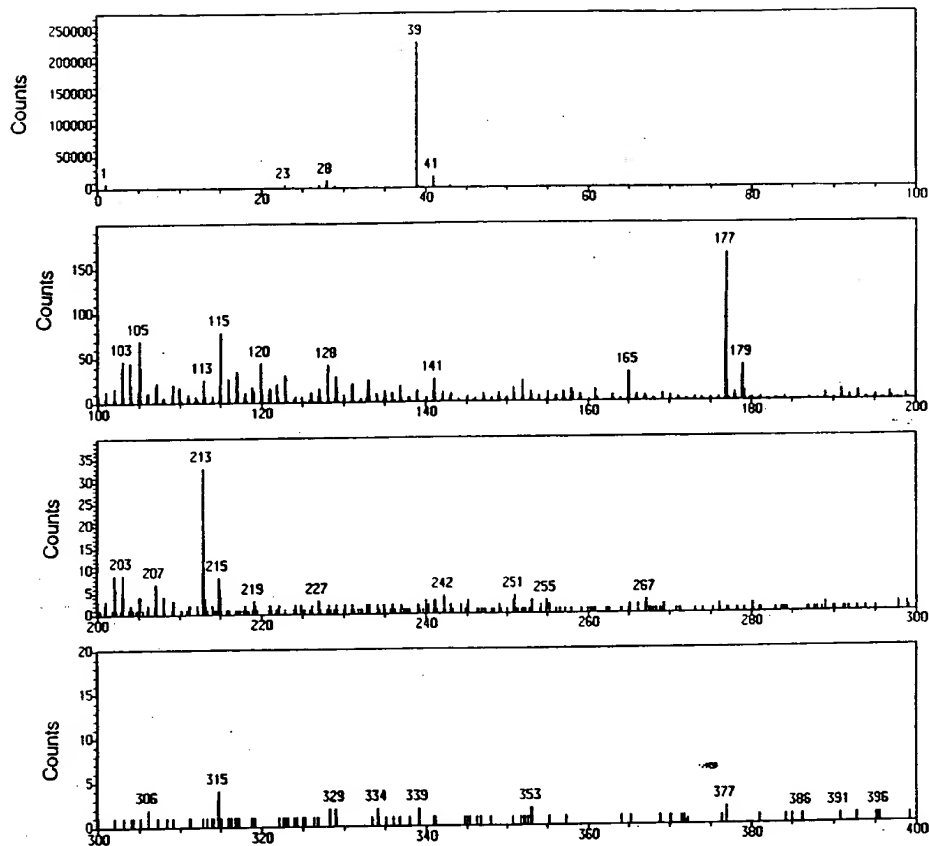


Fig. 8

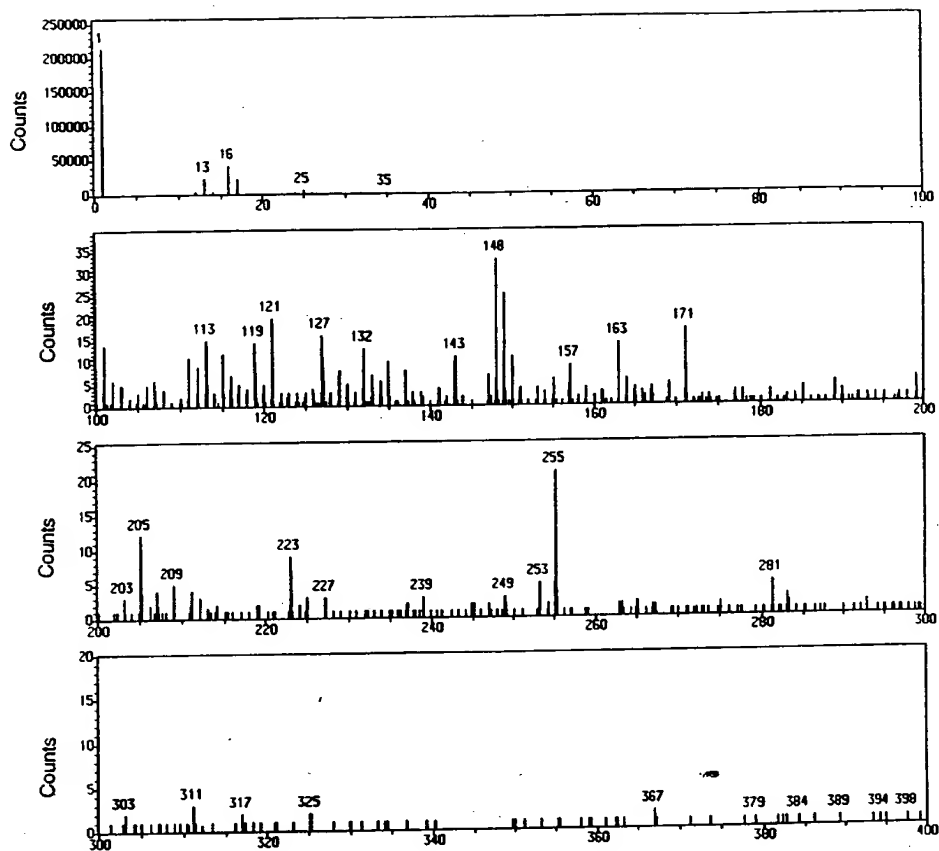


Fig. 9

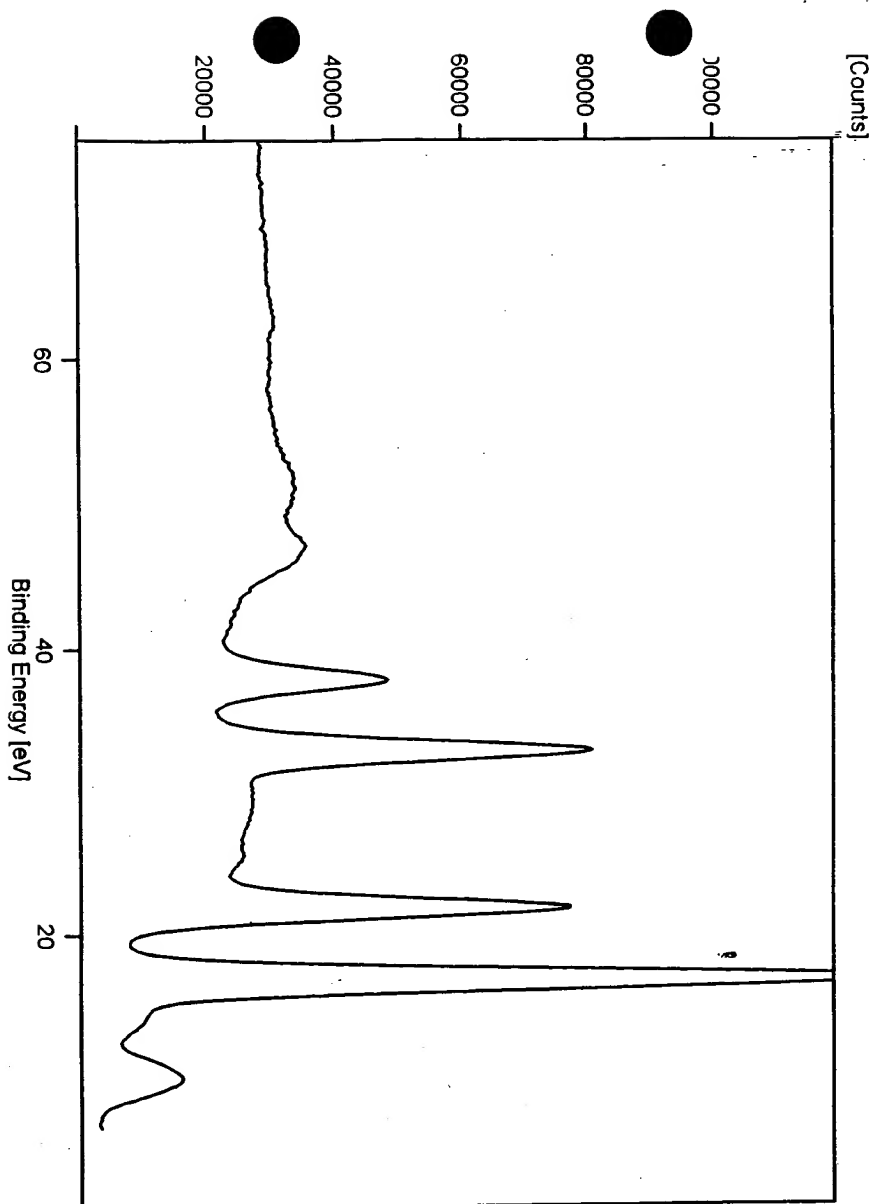


Fig. 10

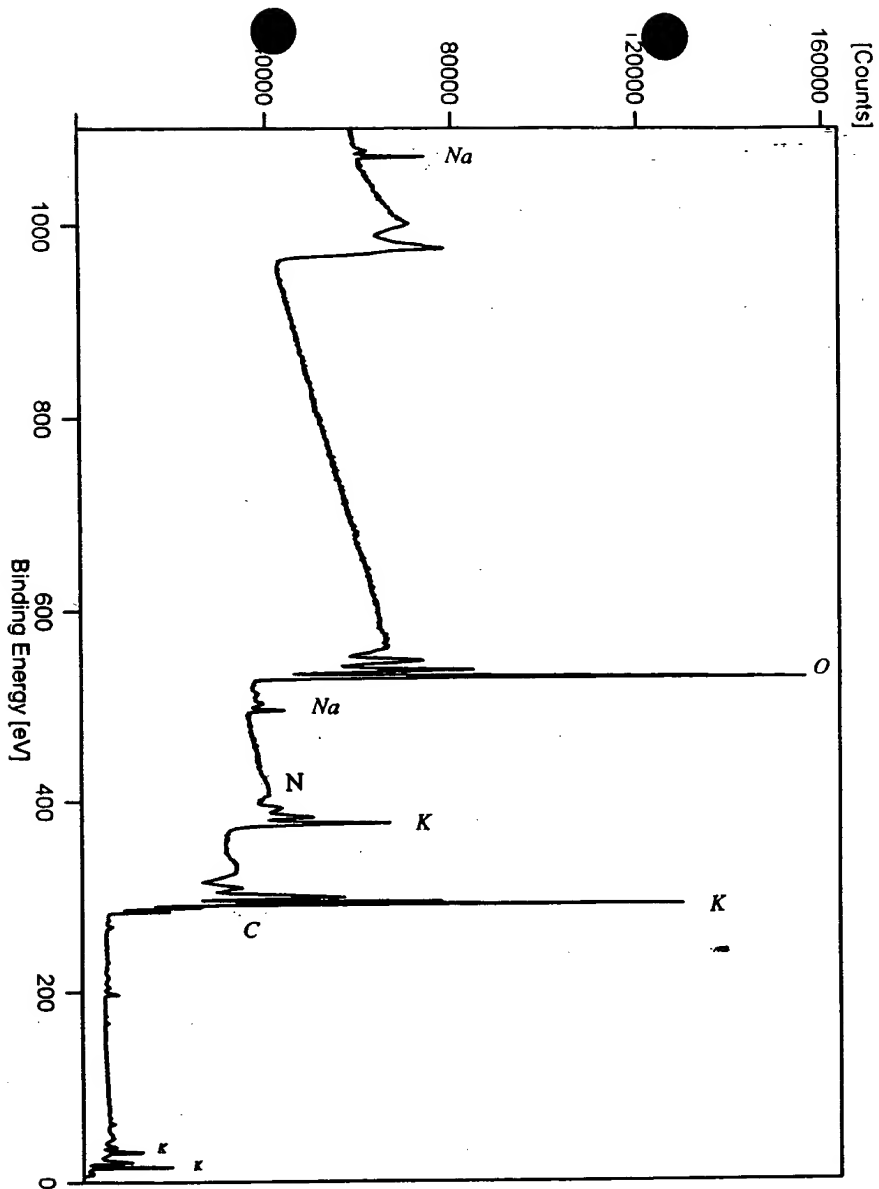


Fig. 11

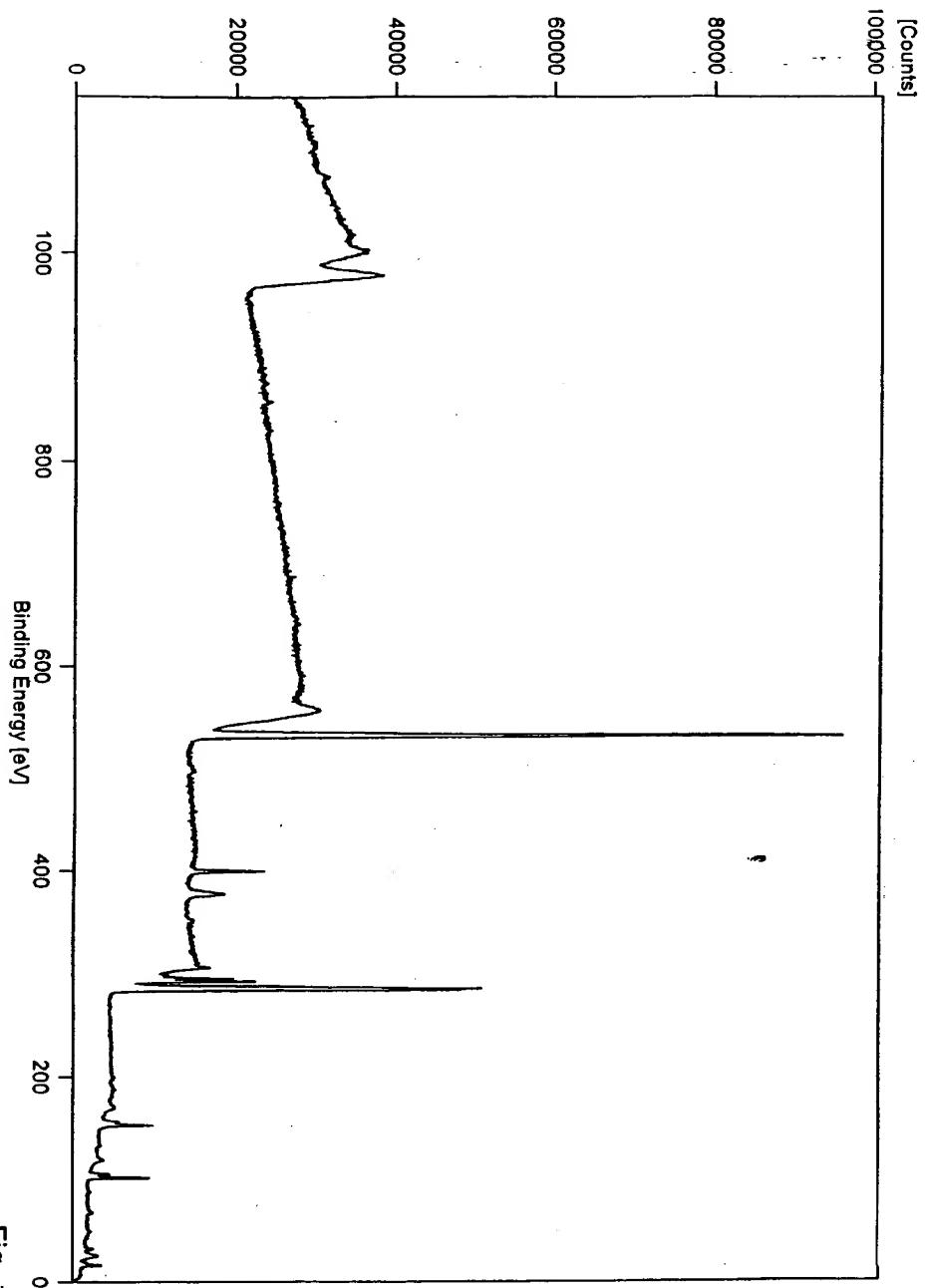


Fig. 12

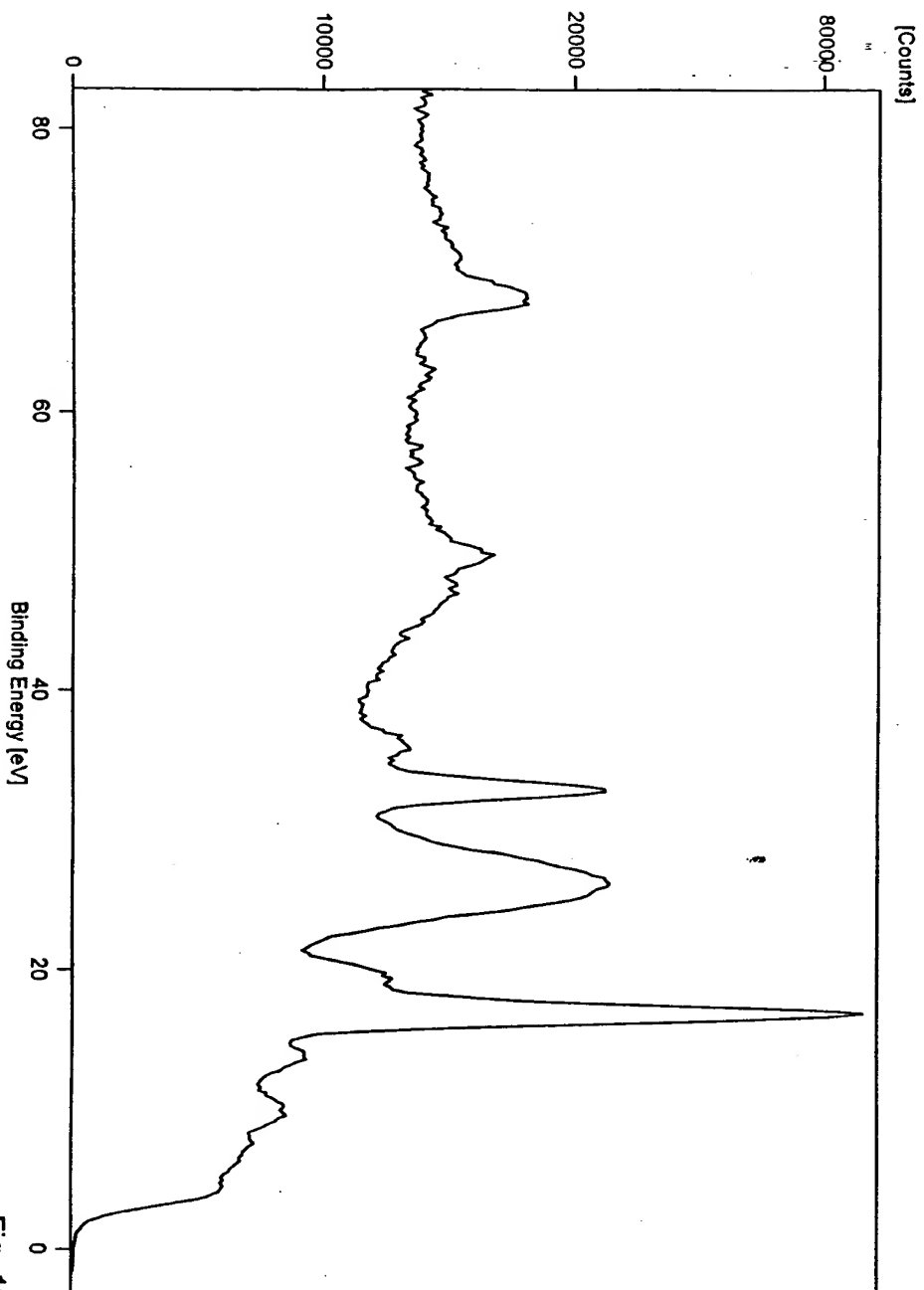


Fig. 13

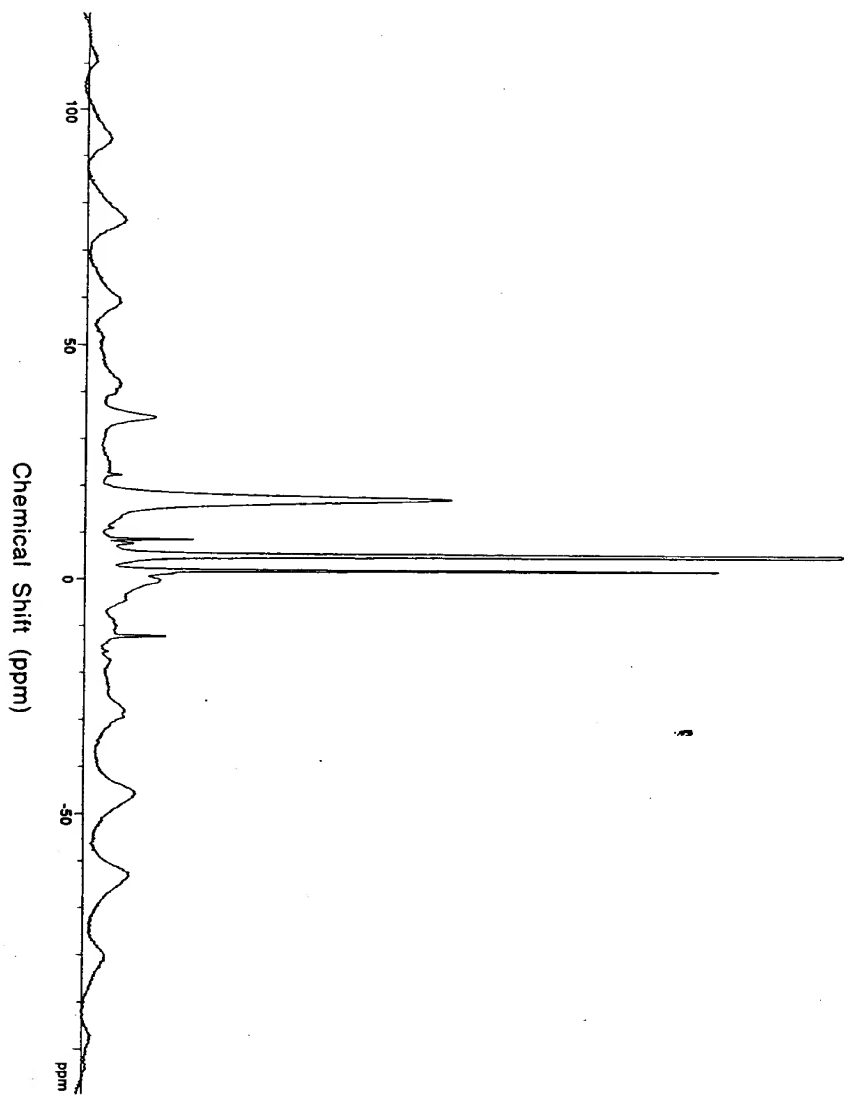


Fig. 14

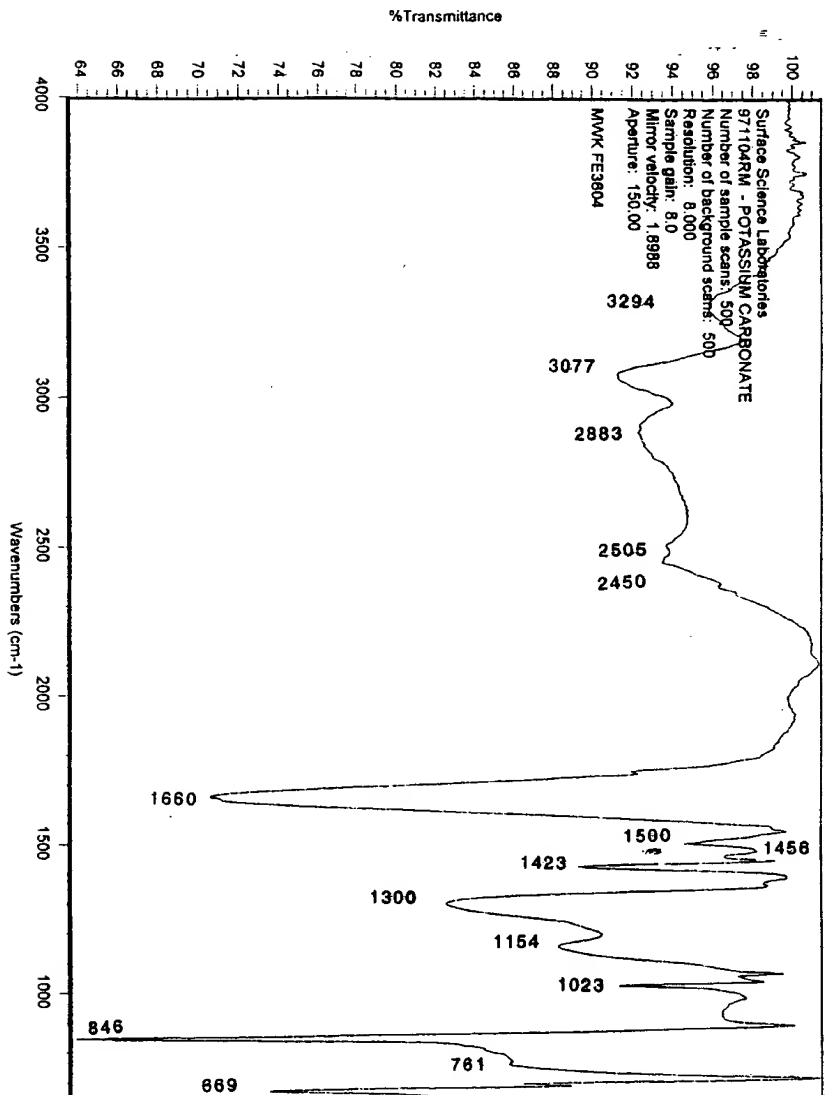


Fig. 15

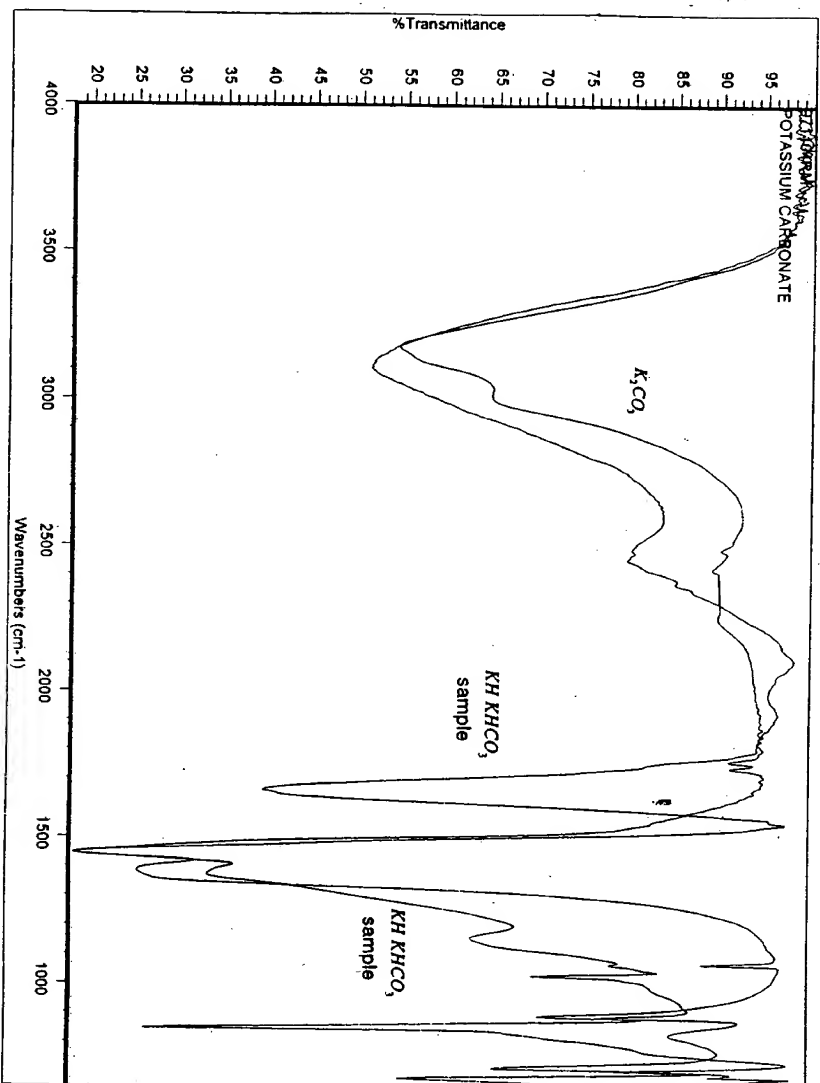


Fig. 16

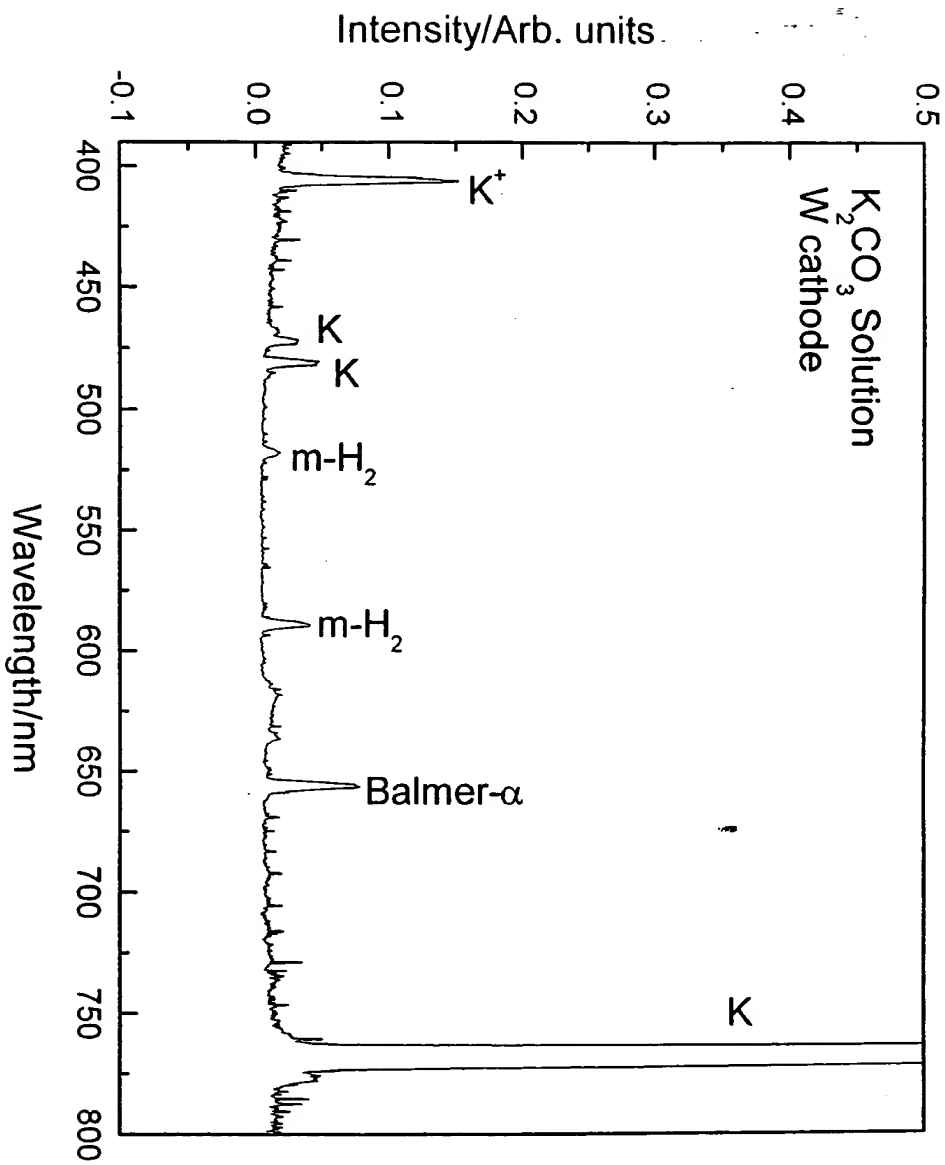


Fig. 17

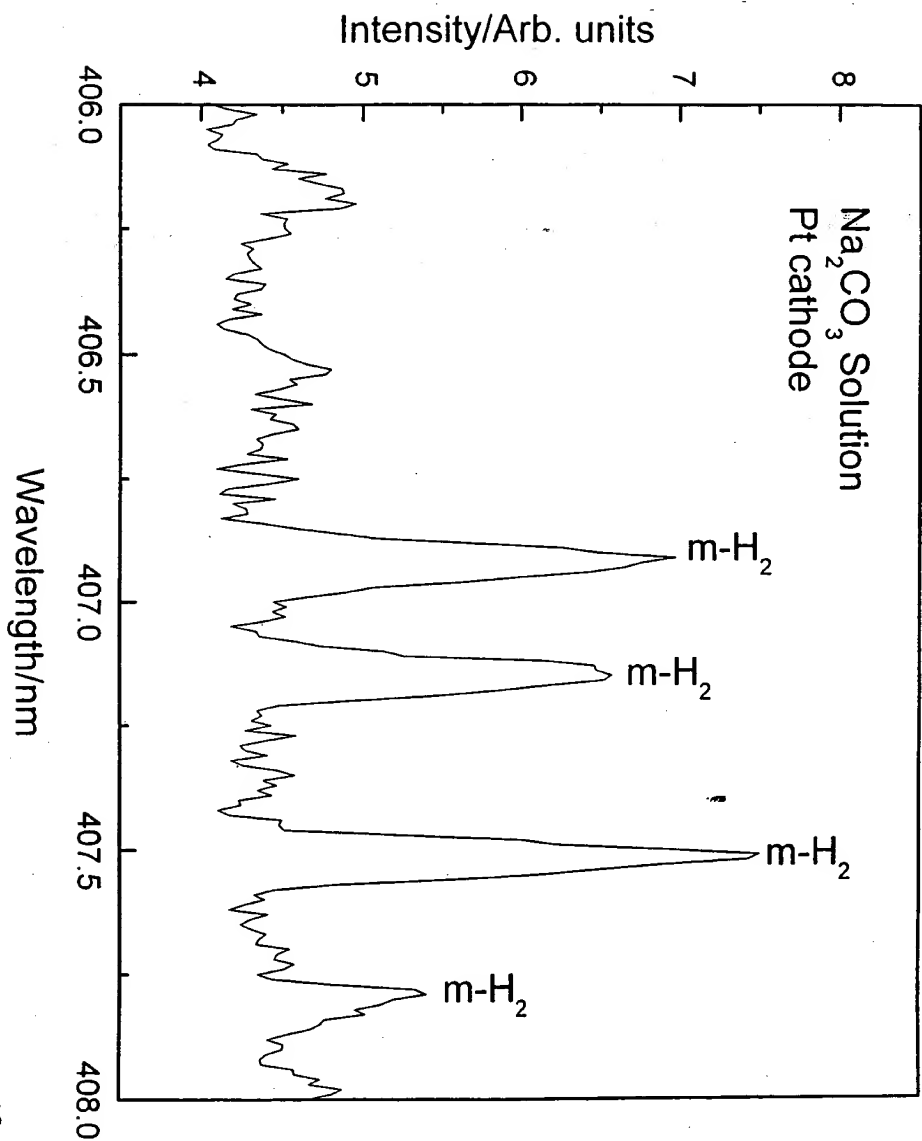


Fig. 18

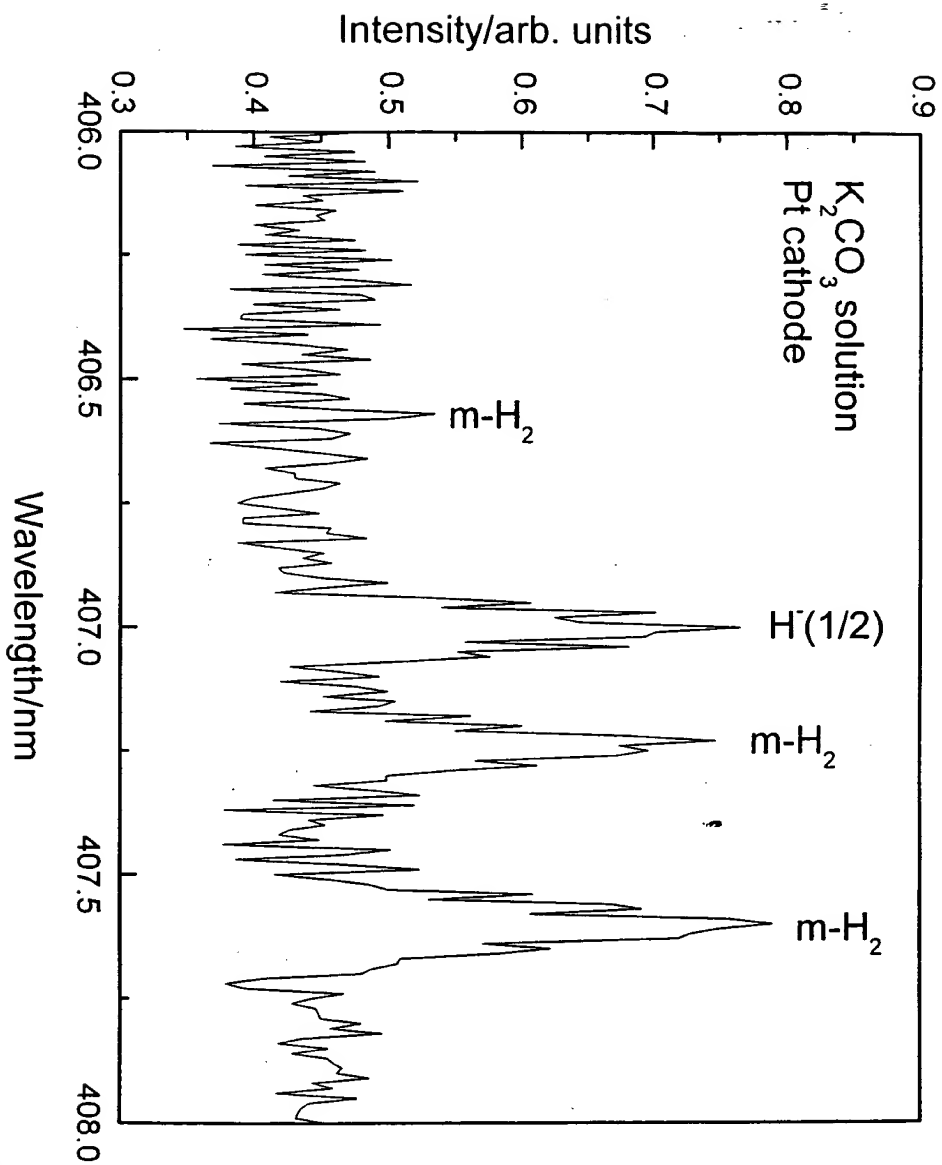


Fig. 19

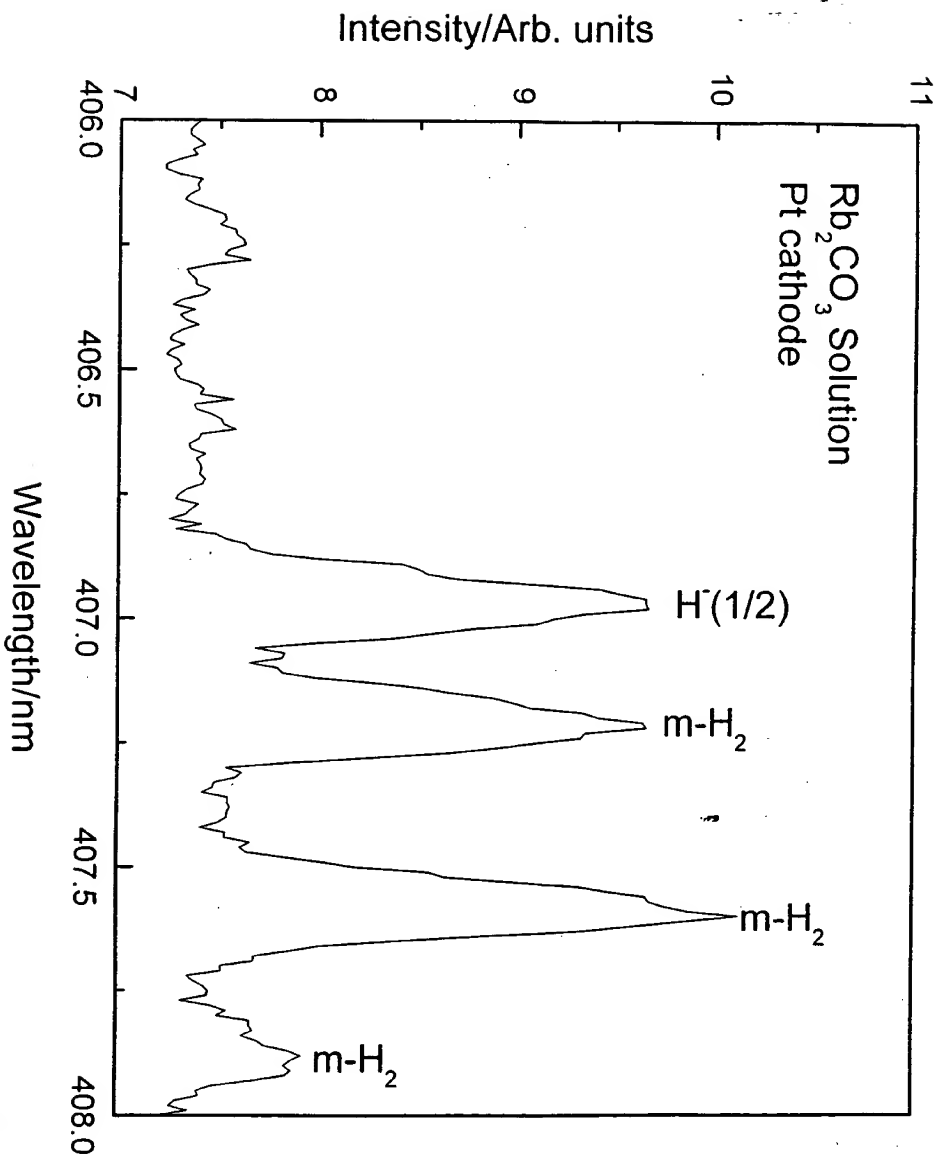


Fig. 20

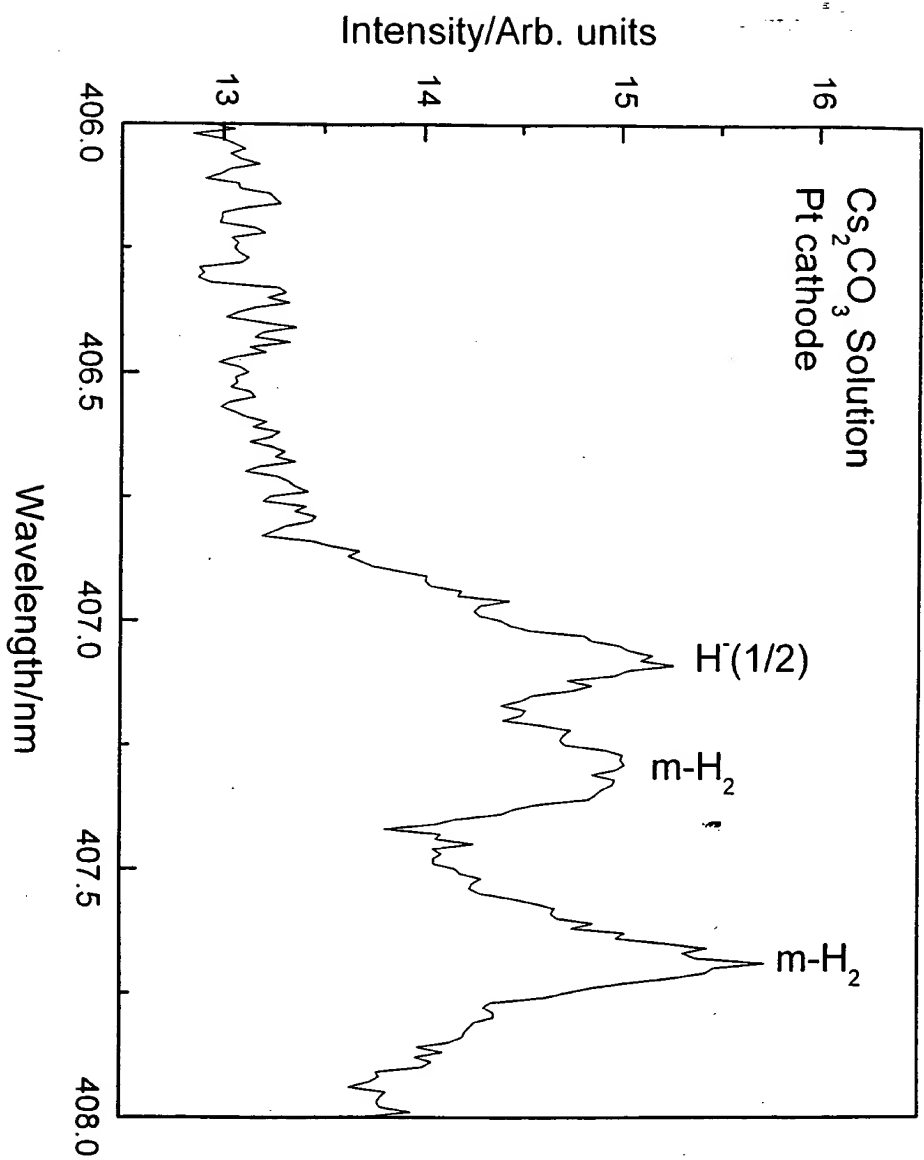


Fig. 21

Table I. The respective hydride compounds and mass assignments (m/z) of the positive ToF-SIMS of the $KH K H C O_3$ electrolytic cell sample.

| Hydrino Hydride Compound or Fragment | Nominal Mass m/z | Observed m/z | Calculated m/z | Difference Between Observed and Calculated m/z |
|--|--------------------------|-------------------|---------------------|--|
| KH | 40 | 39.97 | 39.971535 | 0.0015 |
| K_2H | 79 | 78.940 | 78.935245 | 0.004 |
| $(KH)_2$ | 80 | 79.942 | 79.94307 | 0.001 |
| $KHKOH_2$ | 97 | 96.945 | 96.945805 | 0.0008 |
| $KH_2(KH)_2$ | 121 | 120.925 | 120.92243 | 0.003 |
| $KH K H C O_2$ | 124 | 123.925 | 123.93289 | 0.008 |
| $KH_2 K H O_4$ | 145 | 144.92 | 144.930535 | 0.010 |
| $K(KOH)_2$ | 151 | 150.90 | 150.8966 | 0.003 |
| $KH(KOH)_2$ | 152 | 151.90 | 151.904425 | 0.004 |
| $KH_2(KOH)_2$ | 153 | 152.90 | 152.91225 | 0.012 |
| $K[KH K H C O_3]$ | 179 | 178.89 | 178.8915 | 0.001 |
| $KCO(KH)_3$ | 187 | 186.87 | 186.873225 | 0.003 |
| $K_2OHKHKOH$ | 191 | 190.87 | 190.868135 | 0.002 |
| $KH_2KOHKHKOH$ | 193 | 192.89 | 192.883785 | 0.006 |
| $K_3O(H_2O)_4$ | 205 | 204.92 | 204.92828 | 0.008 |
| $K_2OH[KH K H C O_3]$ | 235 | 234.86 | 234.857955 | 0.002 |
| $K[H_2CO_4 K H K H C O_3]$ | 257 | 256.89 | 256.8868 | 0.003 |
| $K_3O[KH K H C O_3]$ | 273 | 272.81 | 272.81384 | 0.004 |
| $[KH_2CO_3]_3$ | 303 | 302.88 | 302.89227 | 0.012 |
| $K[KH K H C O_3 K_2CO_3]$ | 317 | 316.80 | 316.80366 | 0.004 |
| $K[KH K H C O_3]_2$ | 319 | 318.82 | 318.81931 | 0.001 |
| $KH_2[KH KOH]_3$ | 329 | 328.80 | 328.7933 | 0.007 |
| $KOH_2[KH K H C O_3]_2$ | 337 | 336.81 | 336.82987 | 0.020 |
| $KH KO_2$ $[KH K H C O_3][K H C O_3]$ | 351 | 350.81 | 350.80913 | 0.001 |
| $KKHK_2CO_3$ $[KH K H C O_3]$ | 357 | 356.77 | 356.775195 | 0.005 |

| | | | | |
|--|-----|--------|------------|-------|
| $KKH[KH KHC O_3]_2$ | 359 | 358.78 | 358.790845 | 0.011 |
| $K_2OH[KH KHC O_3]_2$ | 375 | 374.78 | 374.785755 | 0.005 |
| $K_2OH[KHKOH]_2$ $[KHC O_3]$ | 387 | 386.75 | 386.76238 | 0.012 |
| $KKH_3KH_3[KH KHC O_3]_2$ | 405 | 404.79 | 404.80933 | 0.019 |
| $K_3O[K_2CO_3]$ $[KH KHC O_3]$ or $K[KH KOH(K_2CO_3)_2]$ | 411 | 410.75 | 410.72599 | 0.024 |
| $K_3O[KH KHC O_3]_2$ | 413 | 412.74 | 412.74164 | 0.002 |
| $K \begin{bmatrix} KH KOH \\ (KH KHC O_3)_2 \end{bmatrix}$ | 415 | 414.74 | 414.75729 | 0.017 |
| $KH_2OKHC O_3[KH KHC O_3]_2$ | 437 | 436.81 | 436.786135 | 0.024 |
| $KKHKCO_2[KH KHC O_3]_2$ | 442 | 441.74 | 441.744375 | 0.004 |
| $K[KH KHC O_3]_3$ | 459 | 458.72 | 458.74711 | 0.027 |
| $H[KH KOH]_2[K_2CO_3]_2$ or $K_4O_2H[KH KHC O_3]_2$ | 469 | 468.70 | 468.708085 | 0.008 |
| $K[K_2CO_3][KHC O_3]_3$ | 477 | 476.72 | 476.744655 | 0.025 |
| $K_2OH[KH KHC O_3]_3$ | 515 | 514.72 | 514.713555 | 0.006 |
| $K_3O[KH KHC O_3]_3$ | 553 | 552.67 | 552.66944 | 0.001 |
| $K[KH KHC O_3]_4$ | 599 | 598.65 | 598.67491 | 0.025 |
| $K_2OH[KH KHC O_3]_4$ | 655 | 654.65 | 654.641355 | 0.009 |
| $K_3O[KH KHC O_3]_4$ | 693 | 692.60 | 692.59724 | 0.003 |
| $K[KH KHC O_3]_5$ | 739 | 738.65 | 738.60271 | 0.047 |
| $K_3O[KH KHC O_3]_5$ | 833 | 832.50 | 832.52504 | 0.025 |
| $K[KH KHC O_3]_6$ | 879 | 878.50 | 878.53051 | 0.031 |
| $K_3O[KH KHC O_3]_6$ | 973 | 972.50 | 972.45284 | 0.047 |

Table II. The binding energies of XPS peaks of K_2CO_3 and the $KHKHCO_3$ electrolytic cell sample.

| XPS # | C 1s (eV) | O 1s (eV) | K 3p (eV) | K 3s (eV) | K 2p ₃ (eV) | K 2p ₁ (eV) | K 2s (eV) |
|--------------|--------------|--------------|--------------|--------------|---------------------------|---------------------------|--------------|
| K_2CO_3 | 288.4 | 532.0 | 18 | 34 | 292.4 | 295.2 | 376.7 |
| $KHKHCO_3$ | 288.5 | 530.4 | 16.2 | 32.1 | 291.5 | 293.7 | 376.6 |
| Electrolytic | | 537.5 | 22.8 | 38.8 | 298.5 | 300.4 | 382.8 |
| Cell | | 547.8 | | | | | |
| Sample | | | | | | | |
| Min | 280.5 | 529 | | | 292 | | |
| Max | 293 | 535 | | | 293.2 | | |

Table III. The NMR peaks of the $KH KHCO_3$ electrolytic cell sample with their assignments.

| Peak at Shift (ppm) | Assignment |
|------------------------|------------------------------|
| +34.54 | side band of +17.163 peak |
| +22.27 | side band of +5.066 peak |
| +17.163 | $KH KHCO_3$ |
| +10.91 | $KH KHCO_3$ |
| +8.456 | $KH KHCO_3$ |
| +7.50 | $KH KHCO_3$ |
| +5.066 | H_2O |
| +1.830 | $KH KHCO_3$ |
| -0.59 | side band of +17.163 peak |
| -12.05 | $KH KHCO_3$ ^a |
| -15.45 | $KH KHCO_3$ |

^a small shoulder is observed on the -12.05 peak
which is the side band of the +5.066 peak

Table IV. Alkali emission lines recorded on plasma electrolysis cells.

| Plasma Electrolysis | Alkali Metal (M) | M ⁺ | M ²⁺ |
|---------------------|---|----------------|-----------------|
| Electrolyte | Emission (nm) | Emission (nm) | Emission (nm) |
| Na_2CO_3 | 497.9 498.3 589 589.6 819.5 | None | None |
| K_2CO_3 | 766.5 769.9 | 404.3 | None |
| Rb_2CO_3 | 794.7 780 761.9 | 408.4 | None |
| Cs_2CO_3 | 852.1 894.3 | None | 404.5 |

THIS PAGE BLANK (USPTO)

EO

Comparison of Excessive Balmer α Line Broadening of Glow Discharge and Microwave Hydrogen Plasmas with Certain Catalysts

R. L. Mills, P. Ray, B. Dhandapani, J. He

BlackLight Power, Inc.

493 Old Trenton Road

Cranbury, NJ 08512

ABSTRACT

From the width of the 656.2 nm Balmer α line emitted from microwave and glow discharge plasmas, it was found that a strontium-hydrogen microwave plasma showed a broadening similar to that observed in the glow discharge cell of 27-33 eV; whereas, in both sources, no broadening was observed for magnesium-hydrogen. Microwave helium-hydrogen and argon-hydrogen plasmas showed extraordinary broadening corresponding to an average hydrogen atom temperature of 110-130 eV and 180-210 eV, respectively. The corresponding results from the glow discharge plasmas were 30-35 eV and 33-38 eV, respectively, compared to ≈ 4 eV for plasmas of pure hydrogen, neon-hydrogen, krypton-hydrogen, and xenon-hydrogen maintained in either source. Similarly, the average electron temperature T_e for helium-hydrogen and argon-hydrogen microwave plasmas were high, $28,000 \pm 5\% K$ and $11,600 \pm 5\% K$, respectively; compared to $6800 \pm 5\% K$ and $4800 \pm 5\% K$ for helium and argon alone, respectively. Stark broadening or acceleration of charged species due to high fields can not explain the microwave results since no high field was present. Rather, a resonant energy transfer mechanism is proposed.

Key Words: microwave plasma, glow discharge plasma, significant line broadening, electron temperature, resonant energy transfer mechanism

I. INTRODUCTION

Glow discharge devices have been developed over decades as light sources, ionization sources for mass spectroscopy, excitation sources for optical spectroscopy, and sources of ions for surface etching and chemistry [1-3]. A Grimm-type glow discharge is a well established excitation source for the analysis of conducting solid samples by optical emission spectroscopy [4-6]. Despite extensive performance characterizations, data was lacking on the plasma parameters of these devices. M. Kuraica and N. Konjevic [7] and Videnocic et al. [8] have characterized these plasmas by determining the excited hydrogen atom concentrations and energies from measurements of the line broadening of the 656.2 nm Balmer α line. The data was analyzed in terms of Stark and Doppler effects wherein acceleration of charges such as H^+ , H_2^+ , and H_3^+ in the high fields (e. g. over 10 kV/cm) which were present in the cathode fall region was used to explain the Doppler component.

More recently, microhollow glow discharges have been spectroscopically studied as candidates for the development of an intense monochromatic EUV light source (e.g. Lyman α) for short wavelength lithograph for production of the next generation of integrated circuits. A neon-hydrogen microhollow cathode glow discharge has been proposed as a source of predominantly Lyman α radiation. Kurunczi, Shah, and Becker [9] observed intense emission of Lyman α and Lyman β radiation at 121.6 nm and 102.5 nm, respectively, from microhollow cathode discharges in high-pressure Ne (740 Torr) with the addition of a small amount of hydrogen (up to 3 Torr). With essentially no molecular emission observed, Kurunczi et al. attributed the anomalous Lyman α emission to the near-resonant energy transfer between the Ne_2^* excimer and H_2 which leads to formation of $H(n=2)$ atoms, and attributed the Lyman β emission to the near-resonant energy transfer between excited Ne^* atoms (or vibrationally excited neon excimer molecules) and H_2 which leads to formation of $H(n=3)$ atoms. Despite the emission characterization of this source, data is lacking about plasma parameters.

For analyses of solids, direct current (dc) glow discharge sources have been successfully complemented by radio-frequency (rf) discharges [10]. The use of dc discharges is limited to metals; whereas, rf discharges

are applicable to non-conducting materials. Other developed sources that provide a usefully intense plasma are synchrotron devices, inductively coupled plasma generators [11], and magnetically confined plasmas. Plasma characterization data on these sources is also limited.

A new plasma source has been developed that operates by incandescently heating a hydrogen dissociator and a catalyst to provide atomic hydrogen and gaseous catalyst, respectively, such that the catalyst reacts with the atomic hydrogen to produce a plasma. It was extraordinary, that intense EUV emission was observed by Mills et al. [12-19] at low temperatures (e.g. $\approx 10^3$ K) from atomic hydrogen and certain atomized elements or certain gaseous ions which singly or multiply ionize at integer multiples of the potential energy of atomic hydrogen, 27.2 eV that comprise catalysts. The only pure elements that were observed to emit EUV were those wherein the ionization of i electrons from an atom to a continuum energy level is such that the sum of the ionization energies of the i electrons is approximately $m \cdot 27.2$ eV where i and m are each an integer.

Since Ar^+ , He^+ , and strontium each ionize at an integer multiple of the potential energy of atomic hydrogen, a discharge with one or more of these species present with hydrogen is anticipated to form a plasma called a resonance transfer (rt) plasma. The plasma forms by a resonance transfer mechanism involving the species providing a net enthalpy of a multiple of 27.2 eV and atomic hydrogen.

Mills and Nansteel [14, 19] have reported that strontium atoms each ionize at an integer multiple of the potential energy of atomic hydrogen and caused emission. (The enthalpy of ionization of Sr to Sr^{5+} has a net enthalpy of reaction of 188.2 eV, which is equivalent to $m=7$.) The emission intensity of the plasma generated by atomic strontium increased significantly with the introduction of argon gas only when Ar^+ emission was observed. Whereas, no emission was observed when chemically similar atoms that do not ionize at integer multiples of the potential energy of atomic hydrogen (sodium, magnesium, or barium) replaced strontium with hydrogen, hydrogen-argon mixtures, or strontium alone.

Mills and Nanstell [14, 19] measured the power balance of a gas cell having vaporized strontium and atomized hydrogen from pure hydrogen

or argon-hydrogen mixture (77/23%) by integrating the total light output corrected for spectrometer system response and energy over the visible range. Hydrogen control cell experiments were identical except that sodium, magnesium, or barium replaced strontium. In the case of hydrogen-sodium, hydrogen-magnesium, and hydrogen-barium mixtures, 4000, 7000, and 6500 times the power of the hydrogen-strontium mixture was required, respectively, in order to achieve that same optically measured light output power. With the addition of argon to the hydrogen-strontium plasma, the power required to achieve that same optically measured light output power was reduced by a factor of about two. The power required to maintain a plasma of equivalent optical brightness with strontium atoms present was 8600 and 6300 times less than that required for argon-hydrogen and argon control, respectively. A plasma formed at a cell voltage of about 250 V for hydrogen alone and sodium-hydrogen mixtures, 140-150 V for hydrogen-magnesium and hydrogen-barium mixtures, 224 V for an argon-hydrogen mixture, and 190 V for argon alone; whereas, a plasma formed for hydrogen-strontium mixtures and argon-hydrogen-strontium mixtures at extremely low voltages of about 2 V and 6.6 V, respectively.

It was reported [13] that characteristic emission was observed from a continuum state of Ar^{2+} which confirmed the resonant nonradiative energy transfer of 27.2 eV from atomic hydrogen Ar^+ . The transfer of 27.2 eV from atomic hydrogen to Ar^+ in the presence of a electric weak field resulted in its excitation to a continuum state. Then, the energy for the transition from essentially the Ar^{2+} state to the lowest state of Ar^+ was predicted to give a broad continuum radiation in the region of 45.6 nm. This broad continuum emission was observed. This emission was dramatically different from that given by an argon microwave plasma wherein the entire Rydberg series of lines of Ar^+ was observed with a discontinuity of the series at the limit of the ionization energy of Ar^+ to Ar^{2+} . The observed Ar^+ continuum in the region of 45.6 nm confirmed the rt-plasma mechanism of the excessively bright, extraordinarily low voltage discharge. With Ar^+ as the catalyst, the product hydride ion was predicted to have a binding energy of 3.05 eV, and it was observed spectroscopically at 407 nm [13].

He^+ ionizes at 54.417 eV which is 2·27.2 eV, and novel EUV emission

lines were observed from microwave and glow discharges of helium with 2% hydrogen [20]. The observed energies were $q \cdot 13.6 \text{ eV}$ ($q = 1, 2, 3, 4, 6, 7, 8, 9, \text{ or } 11$) or these energies less 21.2 eV due to inelastic scattering of the lines by helium atoms in the excitation of $\text{He}(1s^2)$ to $\text{He}(1s'2p')$. These lines can be explained by the resonance transfer of $m \cdot 27.2 \text{ eV}$ [20].

It was anticipated that microwave and glow discharges would also provide atomic hydrogen and vaporized catalyst to form a rt-plasma. To further characterize the plasma parameters observed in rt-plasmas and to study the difference between microwave and discharge sources, 1.) a comparison between the width of the Lyman α line of an argon-hydrogen plasma emitted from a glow discharge cell and a microwave cell was compared, 2.) by measuring the line broadening of the 656.2 nm Balmer α line, the excited hydrogen atom energy and concentration were determined on plasmas of hydrogen and a catalyst or plasmas comprising hydrogen with chemically similar controls that did not provide gaseous ions having electron ionization energies which are a multiple of 27.2 eV , and 3.) the electron temperature T_e was measured on microwave plasmas using the ratio of the intensity I of two noble gas or metal lines in two quantum states such as the ratio $I(\text{He } 501.6 \text{ nm line}) / I(\text{He } 492.2 \text{ nm line})$ and the ratio $I(\text{Ar } 104.8 \text{ nm line}) / I(\text{Ar } 420.06 \text{ nm line})$ for plasmas having helium and argon, respectively, alone or as a mixture with hydrogen.

II. EXPERIMENTAL

A. Measurement of Lyman α emission by EUV spectroscopy

Extreme ultraviolet (EUV) spectroscopy was recorded on microwave and discharge cell light sources. Due to the extremely short wavelength of this radiation, "transparent" optics do not exist. Therefore, a windowless arrangement was used wherein the microwave or discharge cell was connected to the same vacuum vessel as the grating and detectors of the extreme ultraviolet (EUV) spectrometer. Differential pumping permitted a high pressure in the cell as compared to that in the spectrometer. This was achieved by pumping on the cell outlet and pumping on the grating side of the collimator that served as a pin-hole

inlet to the optics. The spectrometer was continuously evacuated to 10^{-4} – 10^{-6} torr by a turbomolecular pump with the pressure read by a cold cathode pressure gauge. The EUV spectrometer was connected to the cell light source with a 1.5 mm X 5 mm collimator which provided a light path to the slits of the EUV spectrometer. The collimator also served as a flow constrictor of gas from the cell. The cell was operated under gas flow conditions while maintaining a constant gas pressure in the cell.

Spectra were obtained on glow discharge and microwave plasmas of an argon-hydrogen mixture (97/3%). Each gas was ultrahigh pure. The gas pressure inside the cell was maintained at about 300 mtorr with an argon flow rate of 5.2 sccm and a hydrogen flow rate of 0.3 sccm. Each gas flow was controlled by a 0-20 sccm range mass flow controller (MKS 1179A21CS1BB) with a readout (MKS type 246).

For spectral measurement, the light emission from discharge and microwave plasmas of argon-hydrogen (97/3%) was introduced to a normal incidence McPherson 0.2 meter monochromator (Model 302, Seya-Namioka type) equipped with a 1200 lines/mm holographic grating with a platinum coating. The wavelength region covered by the monochromator was 5–560 nm. The UV spectrum (100–170 nm) of the cell emission was recorded with a photomultiplier tube (PMT) and a sodium salicylate scintillator. The PMT (Model R1527P, Hamamatsu) used has a spectral response in the range of 185–680 nm with a peak efficiency at about 400 nm. The wavelength resolution was about 1 nm (FWHM) with an entrance and exit slit width of 300 μ m. The increment was 0.1 nm and the dwell time was 500 ms.

B. Glow discharge emission spectra

The extreme ultraviolet emission spectrum was obtained on an argon-hydrogen mixture (97/3%) glow discharge plasma. A diagram of the discharge plasma source is given in Figure 1. The experimental setup for the discharge measurements is illustrated in Figure 2. The cell comprised a five-way stainless steel cross that served as the anode with a hollow stainless steel cathode. The hollow cathode was constructed of a stainless steel rod inserted into a steel tube, and this assembly was inserted into an Alumina tube. The gas mixture was flowed through the

five-way cross. An AC power supply ($U = 0 - 1$ kV, $I = 0 - 100$ mA) was connected to the hollow cathode to generate a discharge at the hollow cathode inside the discharge cell. The AC voltage and current at the time the EUV spectrum was recorded were 200 V and 40 mA, respectively. A Swagelok adapter at the very end of the steel cross provided a gas inlet and a connection with the pumping system, and the cell was pumped with a mechanical pump. Valves were between the cell and the mechanical pump, the cell and the monochromator, and the monochromator and its turbo pump. A flange opposite the end of the hollow cathode connected the spectrometer with the cell. It had a small hole that permitted radiation to pass to the spectrometer. The hollow cathode and EUV spectrograph were aligned on a common optical axis using a laser. The light emission was introduced into a normal incidence EUV spectrometer. (See EUV-Spectroscopy section).

C. Microwave discharge emission spectra

The extreme ultraviolet emission spectrum was obtained on an argon-hydrogen mixture (97/3%) microwave discharge plasma. The experimental set up comprising a microwave discharge gas cell light source and an EUV spectrometer which was differentially pumped is shown in Figure 3. The gas mixture was flowed through a half inch diameter quartz tube fitted with an Opthos coaxial microwave cavity (Evenson cavity). The microwave generator was an Opthos model MPG-4M generator (Frequency: 2450 MHz). The input power to the plasma was set at 40 watts. The light emission was introduced into a normal incidence EUV spectrometer. (See EUV-Spectroscopy section).

D. Measurement of hydrogen ion temperature and number density from Balmer line broadening

The Doppler-broadened line shape for atomic hydrogen has been studied on many sources such as hollow cathode [8, 21] and rf [22-23] discharges. The method of Videnocic et al. [8, 25] was used to calculate the energetic hydrogen atom densities and energies from the width of the 656.2 nm Balmer α line emitted from glow discharge and microwave

plasmas. Gigosos et al. [24] have reviewed the literature and have discussed the limitations of this method. The full half-width $\Delta\lambda_G$ of each Gaussian results from the Doppler ($\Delta\lambda_D$) and instrumental ($\Delta\lambda_I$) half-widths:

$$\Delta\lambda_G = \sqrt{\Delta\lambda_D^2 + \Delta\lambda_I^2} \quad (1)$$

$\Delta\lambda_I$ in our experiments was 0.006 nm. The temperature was calculated from the Doppler half-width using the formula:

$$\Delta\lambda_D = 7.16 \times 10^{-7} \lambda_0 \left(\frac{T}{\mu} \right)^{1/2} \quad (\text{nm}) \quad (2)$$

where λ_0 is the line wavelength in nm, T is the temperature in K ($1 \text{ eV} = 11,605 \text{ K}$), and μ is the molecular weight (=1 for hydrogen). In each case, the average Doppler half-width that was not appreciably changed with pressure varied by $\pm 5\%$ corresponding to an error in the energy of $\pm 5\%$. The corresponding number densities for noble gas-hydrogen mixtures varied by $\pm 20\%$ depending on the pressure.

a. Balmer line broadening recorded on glow discharge plasmas

The width of the 656.5 nm Balmer α line emitted from gas discharge plasmas having atomized hydrogen from pure hydrogen alone, strontium or magnesium with hydrogen, and a mixture of 10% hydrogen and helium, argon, neon, krypton, or xenon was measured with a high resolution visible spectrometer with a resolution of $\pm 0.025 \text{ nm}$ over the spectral range 190-860 nm. The plasmas were maintained in the cylindrical stainless steel gas cell shown in Figure 4.

The 304-stainless steel cell cylindrical cell was 9.21 cm in diameter and 14.5 cm in height. The base of the cell contained a welded-in stainless steel thermocouple well (1 cm OD) which housed a thermocouple probe in the cell interior approximately 2 cm from the discharge and 2 cm from the cell axis. The top end of the cell was welded to a high vacuum 11.75 cm diameter conflat flange. A silver plated copper gasket was placed between a mating flange and the cell flange. The two flanges were clamped together with 10 circumferential bolts. The mating flange contained three penetrations comprising 1.) a stainless steel thermocouple well (1 cm OD) also housing a thermocouple probe in the cell interior approximately 2 cm from the discharge and 2 cm from the

cell axis, 2.) a centered high voltage feedthrough which transmitted the power, supplied through a power connector, to a hollow cathode inside the cell, and 3.) a stainless steel tube (0.95 cm diameter and 100 cm in length) welded flush with the bottom surface of the top flange that served as a vacuum line from the cell and the line to supply the test gas.

The axial hollow cathode glow discharge electrode assembly comprised a stainless steel plate (42 mm diameter, 0.9 mm thick) anode and a circumferential stainless steel cylindrical frame (5.08 cm OD, 7.2 cm long) perforated with evenly spaced 1 cm diameter holes. The cathode was attached to the cell body by a stainless steel wire, and the cell body was grounded.

A 1.6 mm thick UV-grade sapphire window with 1.5 cm view diameter provided a visible light path from inside the cell. The viewing direction was normal to the cell axis.

The cell was sealed in the glove box, removed, and then evacuated with a turbo vacuum pump to a pressure of 4 mTorr. The gas was ultrahigh purity hydrogen or noble gas-hydrogen mixture (90/10%) at 2 Torr total pressure. The pressure of each test gas comprising a mixture with 10% hydrogen was determined by adding the pure noble gas to a given pressure and increasing the pressure with hydrogen gas to a final pressure. The partial pressure of the hydrogen gas was given by the incremental increase in total gas pressure monitored by a 0-10 Torr absolute pressure gauge. The discharge was carried out under static gas conditions. The discharge was started and maintained by a DC electric field supplied by a constant voltage DC power supply at 275 V which produced a current of about 0.2 A. In the case of strontium-hydrogen, helium-hydrogen, and argon-hydrogen plasmas, the voltage was increased at 50 V increments from 275 V to 475 V, and the high resolution visible spectra were recorded to observe the effect of voltage on the Balmer α line broadening.

The plasma emission from the glow discharges of pure hydrogen, strontium or magnesium with hydrogen, and noble gas-hydrogen mixtures was fiber-optically coupled to the spectrometer through a 220F matching fiber adapter. The entrance and exit slits were set to 20 μm . The spectrometer was scanned between 656-657 nm using a 0.01 nm step size. The signal was recorded by a PMT with a stand alone high voltage

power supply (950 V) and an acquisition controller. The data was obtained in a single accumulation with a 1 second integration time.

b. Balmer line broadening recorded on microwave discharge plasmas

The width of the 656.2 nm Balmer α line emitted from microwave discharges of pure hydrogen alone, strontium or magnesium with hydrogen, and a mixture of 10% hydrogen and helium, argon, neon, krypton, or xenon was measured with a high resolution visible spectrometer. Each pure test gas or mixture was flowed through a half inch diameter quartz tube at 0.3 Torr maintained with a noble gas flow rate of 9.3 sccm or an noble gas flow rate of 8.3 sccm and a hydrogen flow rate of 1 sccm. Each gas flow was controlled by a 0-20 sccm range mass flow controller (MKS 1179A21CS1BB) with a readout (MKS type 246). The cell pressure was monitored by a 0-10 Torr MKS Baratron absolute pressure gauge. Magnesium or strontium was added to the plasma by transferring 50 mg of solid metal into the quartz tube with flowing argon. The plasma discharge partially vaporized the metal during the experiment. The tube was fitted with an Ophos coaxial microwave cavity (Evenson cavity). The microwave generator shown in Figure 3 was an Ophos model MPG-4M generator (Frequency: 2450 MHz). The input power to the plasma was set at 40 watts with forced air cooling of the cell.

The plasma emission was fiber-optically coupled through a 220F matching fiber adapter positioned 2 cm from the cell wall to a high resolution visible spectrometer with a resolution of $\pm 0.006 \text{ nm}$ over the spectral range 190-860 nm. The spectrometer was a Jobin Yvon Horiba 1250 M with 2400 groves/mm ion-etched holographic diffraction grating. The entrance and exit slits were set to 20 μm . The spectrometer was scanned between 655.5-657 nm using a 0.005 nm step size. The signal was recorded by a PMT with a stand alone high voltage power supply (950 V) and an acquisition controller. The data was obtained in a single accumulation with a 1 second integration time.

F. Electron temperature T_e measurements of microwave discharge plasmas

The most commonly used spectroscopic diagnostic method to determine the electron temperature T_e of laboratory plasmas is based on determining the relative intensities of two spectral lines as described by Griem [25]. It may be shown that for two emission lines at wavelengths λ_A and λ_B

$$\frac{I_A}{I_B} = \frac{(\sigma g_2 A_{21})_A}{(\sigma g_2 A_{21})_B} e^{-\frac{(E_{2A} - E_{2B})}{kT_e}} \quad (3)$$

where I_A and I_B are the intensities measured at λ_A and λ_B , and $\sigma \propto n^4$ for excited state atomic hydrogen. The frequency ν , the transition probability A , the degeneracy g , and the upper level E are known constants from which T_e was determined. T_e was measured on microwave plasmas of helium alone and helium-hydrogen mixture (90/10%) from the ratio of the intensity of the He 501.6 nm (upper quantum level $n=3$) line to that of the He 492.2 nm ($n=4$) line. T_e was measured on microwave plasmas of argon alone and argon-hydrogen mixture (90/10%) from the ratio of the intensity of the Ar 104.8 nm (upper quantum level $n=3$) line to that of the Ar 420.06 nm ($n=4$) line. T_e was also measured by the same method on microwave plasmas of pure hydrogen alone, strontium or magnesium with hydrogen, and a mixture of 10% hydrogen and neon, krypton, or xenon using the ratio of the intensities of two noble gas or alkaline earth metal lines in two quantum states.

The experimental set up comprising a microwave discharge gas cell light source and an UV-VIS spectrometer which was differentially pumped is shown in Figure 3. In each case, the microwave plasma cell was run under the conditions given in section B. The spectrometer was a normal incidence McPherson 0.2 meter monochromator (Model 302, Seya-Namioka type) equipped with a 1200 lines/mm holographic grating with a platinum coating. The wavelength region covered by the monochromator was 2–560 nm. The visible spectra (400–560 nm) of the cell emission was recorded with a photomultiplier tube (PMT) and a sodium salicylate scintillator. The PMT (Model R1527P, Hamamatsu)

used has a spectral response in the range of 185–680 nm with a peak efficiency at about 400 nm. The scan interval was 0.4 nm. The inlet and outlet slit were 300 μm with a corresponding wavelength resolution of 2 nm. The spectra were repeated five times per experiment and were found to be reproducible within less than $\pm 5\%$.

III. RESULTS AND DISCUSSION

A. EUV Spectroscopy

Extreme ultraviolet (EUV) spectroscopy was recorded on microwave and discharge cell light sources to compare Lyman α line widths from the two sources. The EUV spectra (100–170 nm) of emission from the discharge and microwave plasmas of argon-hydrogen mixture (97/3%) are shown in Figure 5. The microwave plasma showed significant broadening relative to the discharge plasma. The width of the microwave plasma Lyman α line was 10 nm; whereas, the width of the glow discharge plasma Lyman α line was 2.6 nm. In addition, the intensity of the Lyman α emission compared to the molecular hydrogen emission was significantly higher in the case of the microwave plasma. The Lyman α line broadening and increased intensity indicate a much higher ion temperature in the microwave plasma which was confirmed by high resolution measurements of the Balmer α line width which gave quantitative ion temperature measurements reported sections B and C. No electric field was present in the microwave plasmas. Thus, the results can not be explained by Stark broadening or acceleration of charged species due to high fields of over 10 kV/cm as proposed by Videnocic et al. [8] to explain excessive broadening observed in glow discharges.

B. Balmer line broadening recorded on glow discharge plasmas

The 656 nm Balmer α line width recorded with a high resolution (± 0.025 nm) visible spectrometer on glow discharge plasmas of hydrogen compared with each of xenon-hydrogen (90/10%), strontium-hydrogen and argon-hydrogen (90/10%) are shown in Figures 6–8, respectively. The energetic hydrogen atom densities and energies of the plasmas of

hydrogen alone, strontium or magnesium with hydrogen, and hydrogen-noble gas mixtures were calculated using the method of Videnocic et al. [8] and are given in Table 1. It was found that strontium-hydrogen, helium-hydrogen, and argon-hydrogen showed significant broadening corresponding to an average hydrogen atom temperature of 23-38 eV; whereas, pure hydrogen, neon-hydrogen, krypton-hydrogen, and xenon-hydrogen showed no excessive broadening corresponding to an average hydrogen atom temperature of ≈ 4 eV. No voltage effect was observed with the strontium-hydrogen, helium-hydrogen, or argon-hydrogen plasmas.

C. Balmer line broadening recorded on microwave discharge plasmas

The 656 nm Balmer α line width recorded with a high resolution (± 0.025 nm) visible spectrometer on microwave discharge plasmas of hydrogen compared with each of xenon-hydrogen (90/10%), magnesium-hydrogen, and helium-hydrogen (90/10%) are shown in Figures 9-11, respectively. The energetic hydrogen atom densities and energies of plasmas of hydrogen alone, strontium or magnesium with hydrogen, and noble gas-hydrogen mixtures were calculated using the method of Videnocic et al. [8] and are given in Table 2. It was found that the strontium-hydrogen microwave plasma showed a broadening similar to that observed in the glow discharge cell of 27-33 eV; whereas, in both sources, no broadening was observed for magnesium-hydrogen. Furthermore, the microwave helium-hydrogen, and argon-hydrogen plasmas showed extraordinary broadening corresponding to an average hydrogen atom temperature of 110-130 eV and 180-210 eV, respectively, and an atom density of $3.5 \times 10^{14} \pm 20\%$ atoms/cm³ and $4.8 \times 10^{14} \pm 20\%$ atoms/cm³, respectively. Whereas, pure hydrogen, neon-hydrogen, krypton-hydrogen, and xenon-hydrogen showed no excessive broadening corresponding to an average hydrogen atom temperature of ≈ 4 eV and an atom density of only $7 \times 10^{13} \pm 20\%$ atoms/cm³ even though 10 times more hydrogen was present. These studies demonstrate excessive line broadening in the absence of an observable effect attributable to an electric field since the hydrogen emission shows no broadening.

Excessive line broadening was only observed in the cases where an ion was present which could provide a net enthalpy of reaction of an integer multiple of the potential energy of atomic hydrogen (Sr , Ar^+ , or He^+). Whereas plasmas of chemically similar controls that do not provide gaseous atoms or ions that have electron ionization energies which are a multiple of 27.2 eV. These support the rt-plasma mechanism.

Rt-plasmas formed with hydrogen-potassium mixtures have been reported previously [17-18] wherein the plasma decayed with a two second half-life when the electric field was set to zero. This was the thermal decay time of the filament which dissociated molecular hydrogen to atomic hydrogen. This experiment showed that hydrogen line emission was occurring even though the voltage between the heater wires was set to and measured to be zero and indicated that the emission was due to a reaction of potassium atoms with atomic hydrogen. Potassium atoms ionize at an integer multiple of the potential energy of atomic hydrogen, $m \cdot 27.2 \text{ eV}$. The enthalpy of ionization of K to K^{3+} has a net enthalpy of reaction of 81.7426 eV, which is equivalent to $m=3$.

A rt-plasma of hydrogen and certain alkali ions formed at low temperatures (e.g. $\approx 10^3 \text{ K}$) as recorded via EUV spectroscopy, and an excessive afterglow duration was observed by hydrogen Balmer and alkali line emissions in the visible range [18]. The observed plasma formed from atomic hydrogen generated at a tungsten filament that heated a titanium dissociator and one of potassium, rubidium, cesium, and their carbonates and nitrates. These atoms and ions ionize to provide a net enthalpy of reaction of an integer multiple of the potential energy of atomic hydrogen ($m \cdot 27.2 \text{ eV}$, $m = \text{integer}$) to within 0.17 eV and comprise only a single ionization in the case of a potassium or rubidium ion. Whereas, the chemically similar atoms of sodium and sodium and lithium carbonates and nitrates which do not ionize with these constraints caused no emission. To test the electric dependence of the emission, the weak electric field of about 1 V/cm was set and measured to be zero in $< 0.5 \times 10^{-6} \text{ sec}$. An afterglow duration of about one to two seconds was recorded in the case of potassium, rubidium, cesium, K_2CO_3 , RbNO_3 , and CsNO_3 . Hydrogen line or alkali line emission was occurring even though the voltage between the heater wires was set to and measured to be zero. These atoms and ions ionize to provide a net

enthalpy of reaction of an integer multiple of the potential energy of atomic hydrogen to within less than the thermal energies at $\approx 10^3$ K and comprise only a single ionization in the case of a potassium or rubidium ion. Since the thermal decay time of the filament for dissociation of molecular hydrogen to atomic hydrogen was similar to the rf-plasma afterglow duration, the emission was determined to be due to a reaction of atomic hydrogen with each of the atoms or ions that did not require the presence of an electric field to be functional.

D. T_e measurements of microwave discharge plasmas

The results of the T_e measurements on microwave plasmas of pure hydrogen alone, strontium or magnesium with hydrogen, and a mixture of 10% hydrogen and helium, neon, argon, krypton, or xenon are given in Table 2. Similarly to the ion measurement, the average electron temperature for helium-hydrogen plasma was $28,000 \pm 5\%$ K; whereas, the corresponding temperature of helium alone was only $6800 \pm 5\%$ K. The average electron temperature for argon-hydrogen plasma was $11,600 \pm 5\%$ K; whereas, the corresponding temperature of argon alone was only $4800 \pm 5\%$ K.

IV. SUMMARY AND CONCLUSIONS

The argon-hydrogen microwave plasma showed significant broadening of the width of the Lyman α line of 10 nm; whereas, the width of the Lyman α line emitted from the glow discharge plasma was 2.6 nm. In addition, the intensity of the Lyman α emission compared to the molecular hydrogen emission was significantly higher in the case of the microwave plasma. The results indicate a much greater ion temperature in the microwave plasma.

Line broadening of the hydrogen Balmer lines provides a sensitive measure of the number and energy of excited hydrogen atoms in a glow discharge plasma. The width of the 656.5 nm Balmer α line emitted from glow discharge plasmas having atomized hydrogen from pure hydrogen alone, strontium or magnesium with hydrogen, and a mixture of 10% hydrogen and helium, argon, neon, krypton, or xenon was

measured with a high resolution ($\pm 0.025 \text{ nm}$) visible spectrometer. The energetic hydrogen atom density and energies were determined from the broadening, and it was found that strontium-hydrogen, helium-hydrogen, and argon-hydrogen showed significant broadening corresponding to an average hydrogen atom temperature of 23-38 eV; whereas, pure hydrogen, neon-hydrogen, krypton-hydrogen, and xenon-hydrogen showed no excessive broadening corresponding to an average hydrogen atom temperature of $\approx 4 \text{ eV}$. Thus, line broadening was only observed for the ions which provided a net enthalpy of reaction of a multiple of the potential energy of the hydrogen atom.

Kuraica and Konjevic [7] and Videnocic et al. [8] studied 97% argon and 3% hydrogen mixtures in Grimm-type discharges with a hollow anode. In our studies with argon-hydrogen plasmas, the voltage was increased at 50 V increments from 275 V to 475 V, and the high resolution visible spectra were recorded to observe the effect of voltage on the Balmer α line broadening. In contrast to an increase in broadening with voltage predicted by Kuraica and Konjevic [7], no voltage effect was observed. Also, no voltage effect was also observed with the strontium-hydrogen plasma which supports the rt-plasma mechanism of the low voltage strontium-hydrogen and strontium-argon-hydrogen plasmas reported by Mills and Nansteel [14-15, 19]. Similarly, no voltage effect was observed in the case of the helium-hydrogen plasma which supports the rt-plasma mechanism as the source of the excessive broadening.

The 656.5 nm Balmer α line width measurements were repeated with microwave discharge plasmas rather than the glow discharge plasmas, and significant differences were observed between the plasma source while the same trend was observed for the particular plasma gas. It was found that the strontium-hydrogen microwave plasma showed a broadening similar to that observed in the glow discharge cell of 27-33 eV; whereas, in both sources, no broadening was observed for magnesium-hydrogen. Furthermore, the microwave helium-hydrogen, and argon-hydrogen plasmas showed extraordinarily higher broadening corresponding to an average hydrogen atom temperature of 110-130 eV and 180-210 eV, respectively, and an atom density of $3.5 \times 10^{14} \pm 20\% \text{ atoms/cm}^3$ and $4.8 \times 10^{14} \pm 20\% \text{ atoms/cm}^3$, respectively.

Whereas, similarly to the glow discharge case, pure hydrogen, neon-hydrogen, krypton-hydrogen, and xenon-hydrogen showed no excessive broadening corresponding to an average hydrogen atom temperature of ≈ 4 eV and an atom density of only $7 \times 10^{13} \pm 20\%$ atoms/cm³ even though 10 times more hydrogen was present. Similarly, the average electron temperature for helium-hydrogen plasma was $28,000 \pm 5\%$ K; whereas, the corresponding temperature of helium alone was only $6800 \pm 5\%$ K. And, the average electron temperature for argon-hydrogen plasma was $11,600 \pm 5\%$ K; whereas, the corresponding temperature of helium alone was only $4800 \pm 5\%$ K.

Thus, excessive line broadening and an elevated electron temperature were only observed for the ions which provided a net enthalpy of reaction of a multiple of the potential energy of the hydrogen atom. No electric field was present in the microwave plasmas. Thus, the results can not be explained by Stark broadening or acceleration of charged species due to high fields of over 10 kV/cm as proposed by Videnovic et al. [8] to explain excessive broadening observed in glow discharges. The results are consistent with an energetic reaction caused by a resonance energy transfer between hydrogen atoms and strontium atoms, Ar^+ , or He^+ as the source of the excessive line broadening. The reaction rate is higher under the conditions of a microwave compared to a glow discharge plasma even at a lower input power.

ACKNOWLEDGMENT

Special thanks to O. Klueva of Jobin Yvon Horiba, Inc, Edison, NJ for assistance and use of the high resolution (± 0.025 nm) visible spectrometer, and to Alex Echezuria for preparing plasma experiments.

REFERENCES

1. P. W. J. M. Boumans, Spectrochim. Acta Part B, 46 (1991) 711.
2. J. A. C. Broekaert, Appl. Spectrosc., 49, (1995) 12A.
3. P. W. J. M. Boumans, J. A. C. Broekaert, and R. K. Marcus, Eds., Spectrochim. Acta Part B, 46 (1991) 457.
4. M. Dogan, K. Laqua, and H. Massmann, "Spektrochemische Analysen mit

- einer Glimmentladungslampe als Lichtquelle—I," *Spectrochim. Acta*, Volume 26B, (1971) 631-649.
5. M. Dogan, K. Laqua, and H. Massmann, "Spektrochemische Analysen mit einer Glimmentladungslampe als Lichtquelle—II," *Spectrochim. Acta*, Volume 27B, (1972) 65-88.
 6. J. A. C. Broekaert, *J. Anal. At. Spectrom.*, 2 (1987) 537.
 7. M. Kuraica, N. Konjevic, "Line shapes of atomic hydrogen in a plane-cathode abnormal glow discharge", *Physical Review A*, Volume 46, No. 7, October (1992), pp. 4429-4432.
 8. I. R. Videnovic, N. Konjevic, M. M. Kuraica, "Spectroscopic investigations of a cathode fall region of the Grimm-type glow discharge", *Spectrochimica Acta*, Part B, Vol. 51, (1996), pp. 1707-1731.
 9. P. Kurunczi, H. Shah, and K. Becker, "Hydrogen Lyman- α and Lyman- β emissions from high-pressure microhollow cathode discharges in Ne- H_2 mixtures", *J. Phys. B: At. Mol. Opt. Phys.*, Vol. 32, (1999), L651-L658.
 10. M. Parker and R. K. Marcus, *Appl. Spectrosc.*, 48, (1994) 623.
 11. J. A. R. Sampson, *Techniques of Vacuum Ultraviolet Spectroscopy*, Pied Publications, (1980), pp. 94-179.
 12. R. Mills, P. Ray, "Spectroscopic Identification of a Novel Catalytic Reaction of Potassium and Atomic Hydrogen and the Hydride Ion Product", *Int. J. Hydrogen Energy*, Vol. 27, No. 2, February, (2002), pp. 183-192.
 13. R. Mills, "Spectroscopic Identification of a Novel Catalytic Reaction of Atomic Hydrogen and the Hydride Ion Product", *Int. J. Hydrogen Energy*, Vol. 26, No. 10, (2001), pp. 1041-1058.
 14. R. Mills and M. Nansteel, "Argon-Hydrogen-Strontium Plasma Light Source", *IEEE Transactions on Plasma Science*, submitted.
 15. R. Mills, M. Nansteel, and Y. Lu, "Excessively Bright Hydrogen-Strontium Plasma Light Source Due to Energy Resonance of Strontium with Hydrogen", *European Journal of Physics D*, submitted.
 16. R. Mills, J. Dong, Y. Lu, "Observation of Extreme Ultraviolet Hydrogen Emission from Incandescently Heated Hydrogen Gas with Certain Catalysts", *Int. J. Hydrogen Energy*, Vol. 25, (2000), pp. 919-943.
 17. R. Mills, "Temporal Behavior of Light-Emission in the Visible Spectral Range from a Ti-K₂CO₃-H-Cell", *Int. J. Hydrogen Energy*, Vol. 26, No. 4,

- (2001), pp. 327-332.
18. R. Mills, T. Onuma, and Y. Lu, "Formation of a Hydrogen Plasma from an Incandescently Heated Hydrogen-Catalyst Gas Mixture with an Anomalous Afterglow Duration", *Int. J. Hydrogen Energy*, Vol. 26, No. 7, July, (2001), pp. 749-762.
 19. R. Mills, M. Nansteel, and Y. Lu, "Observation of Extreme Ultraviolet Hydrogen Emission from Incandescently Heated Hydrogen Gas with Strontium that Produced an Anomalous Optically Measured Power Balance", *Int. J. Hydrogen Energy*, Vol. 26, No. 4, (2001), pp. 309-326.
 20. R. Mills, P. Ray, "Spectral Emission of Fractional Quantum Energy Levels of Atomic Hydrogen from a Helium-Hydrogen Plasma and the Implications for Dark Matter", *Int. J. Hydrogen Energy*, in press.
 21. S. Alexiou, E. Leboucher-Dalimier, "Hydrogen Balmer- α in dense plasmas", *Phys. Rev. E*, Vol. 60, No. 3, (1999), pp. 3436-3438.
 22. S. Djurovic, J. R. Roberts, "Hydrogen Balmer alpha line shapes for hydrogen -argon mixtures in a low-pressure rf discharge", *J. Appl. Phys.*, Vol. 74, No. 11, (1993), pp. 6558-6565.
 23. S. B. Radovanov, K. Dzierzega, J. R. Roberts, J. K. Olthoff, "Time-resolved Balmer-alpha emission from fast hydrogen atoms in low pressure, radio-frequency discharges in hydrogen", *Appl. Phys. Lett.*, Vol. 66, No. 20, (1995), pp. 2637-2639.
 24. M. A. Gigosos, V. Cardenoso, "New plasma diagnosis tables of hydrogen Stark broadening including ion dynamics", *J. Phys. B: At. Mol. Opt. Phys.*, Vol. 29, (1996), pp. 4795-4838.
 25. H. R. Griem, *Principle of Plasma Spectroscopy*, Cambridge University Press, (1987).

Table 1. The energetic hydrogen atom densities and energies for catalyst and noncatalyst glow discharge plasmas.

| Plasma Gas | Hydrogen Atom Density ^a (10^{13} atoms/cm ³) ($\pm 20\%$) | Hydrogen Atom Energy ^b (eV) ($\pm 5\%$) |
|-------------------------|---|--|
| <i>H₂</i> | 5 | 3-4 |
| <i>Mg/H₂</i> | 6 | 4-5 |
| <i>Sr/H₂</i> | 10 | 23-25 |
| <i>Ne/H₂</i> | 2.1 | 5-6 |
| <i>Kr/H₂</i> | 1 | 3-4 |
| <i>Xe/H₂</i> | 1 | 3-4 |
| <i>Ar/H₂</i> | 3 | 30-35 |
| <i>He/H₂</i> | 3 | 33-38 |

^a Approximate Calculated [8]

^b Calculated [8]

Table 2. The energetic hydrogen atom densities and energies and the electron temperature for catalyst and noncatalyst microwave discharge plasmas.

| Plasma Gas | Hydrogen Atom Density ^a (10^{13} atoms/cm ³) ($\pm 20\%$) | Hydrogen Atom Energy ^b (eV) ($\pm 5\%$) | Electron Temperature T_e ^c (K) ($\pm 5\%$) |
|------------|---|--|---|
| H_2 | 7 | 3-4 | 5500 |
| Mg/H_2 | 11.1 | 4-5 | 5800 |
| Sr/H_2 | 18.5 | 27-33 | 10,280 |
| Ne/H_2 | 9 | 5-6 | 7800 |
| Kr/H_2 | 4 | 3-4 | 6700 |
| Xe/H_2 | 3 | 3-4 | 6500 |
| Ar/H_2 | 35 | 110-130 | 11,600 |
| He/H_2 | 48 | 180-210 | 28,000 |

^a Approximate Calculated [8]

^b Calculated [8]

^c Calculated [25]

Figure Captions

Figure 1. Cross sectional view of the discharge cell.

Figure 2. The experimental set up comprising a discharge gas cell light source and an EUV spectrometer which was differentially pumped.

Figure 3. The experimental set up comprising a microwave discharge gas cell light source and an EUV-UV-VIS spectrometer which was differentially pumped.

Figure 4. Cylindrical stainless steel cell for studies of the broadening of the Balmer α line emitted from glow discharge plasmas of 1.) pure hydrogen alone, 2.) hydrogen with strontium or magnesium, and 3.) a mixture of 10% hydrogen and helium, argon, krypton, or xenon.

Figure 5. The EUV spectra (100-170 nm) of emission from the discharge and microwave plasmas of argon-hydrogen mixture (97/3%). The microwave plasma showed significant broadening of the width of the Lyman α line of 10 nm; whereas, the width of the Lyman α line emitted from the glow discharge plasma was 2.6 nm. In addition, the intensity of the Lyman α emission compared to the molecular hydrogen emission was significantly higher in the case of the microwave plasma. The results indicate a much greater ion temperature in the microwave plasma.

Figure 6. The 656 nm Balmer α line width recorded with a high resolution (± 0.025 nm) visible spectrometer on a xenon-hydrogen (90/10%) and a hydrogen glow discharge plasma. No line excessive broadening was observed corresponding to an average hydrogen atom temperature of 3-4 eV.

Figure 7. The 656 nm Balmer α line width recorded with a high resolution (± 0.025 nm) visible spectrometer on a strontium-hydrogen and a hydrogen glow discharge plasma. Significant broadening was observed corresponding to an average hydrogen atom temperature of 23-25 eV.

Figure 8. The 656 nm Balmer α line width recorded with a high resolution (± 0.025 nm) visible spectrometer on an argon-hydrogen (90/10%) and a hydrogen glow discharge plasma. Significant broadening was observed corresponding to an average hydrogen atom temperature of 30-35 eV.

Figure 9. The 656 nm Balmer α line width recorded with a high resolution (± 0.006 nm) visible spectrometer on a xenon-hydrogen

(90/10%) and a hydrogen microwave discharge plasma. No line excessive broadening was observed corresponding to an average hydrogen atom temperature of 3-4 eV.

Figure 10. The 656 nm Balmer α line width recorded with a high resolution (± 0.006 nm) visible spectrometer on an magnesium-hydrogen and a hydrogen microwave discharge plasma. No line excessive broadening was observed corresponding to an average hydrogen atom temperature of 4-5 eV.

Figure 11. The 656 nm Balmer α line width recorded with a high resolution (± 0.006 nm) visible spectrometer on a helium-hydrogen (90/10%) and a hydrogen microwave discharge plasma. Significant broadening was observed corresponding to an average hydrogen atom temperature of 180-210 eV.

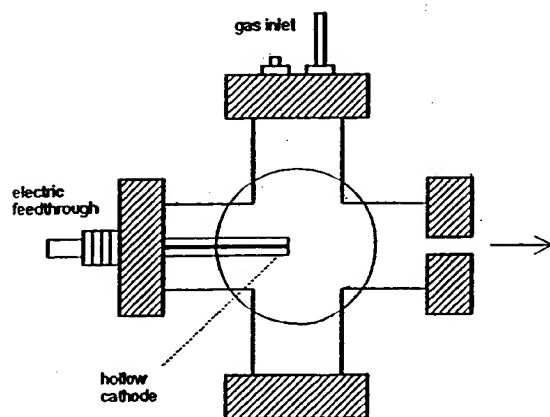


Fig. 1

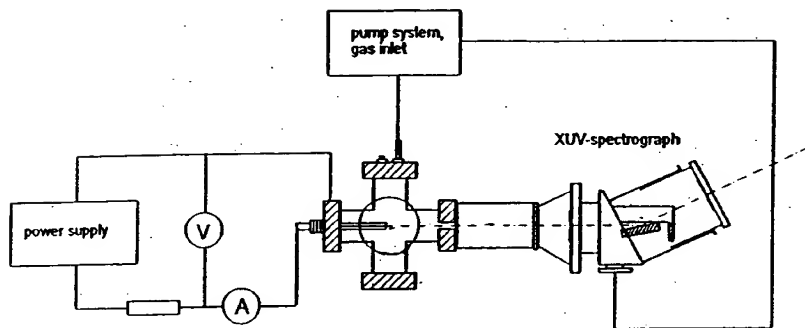


Fig. 2

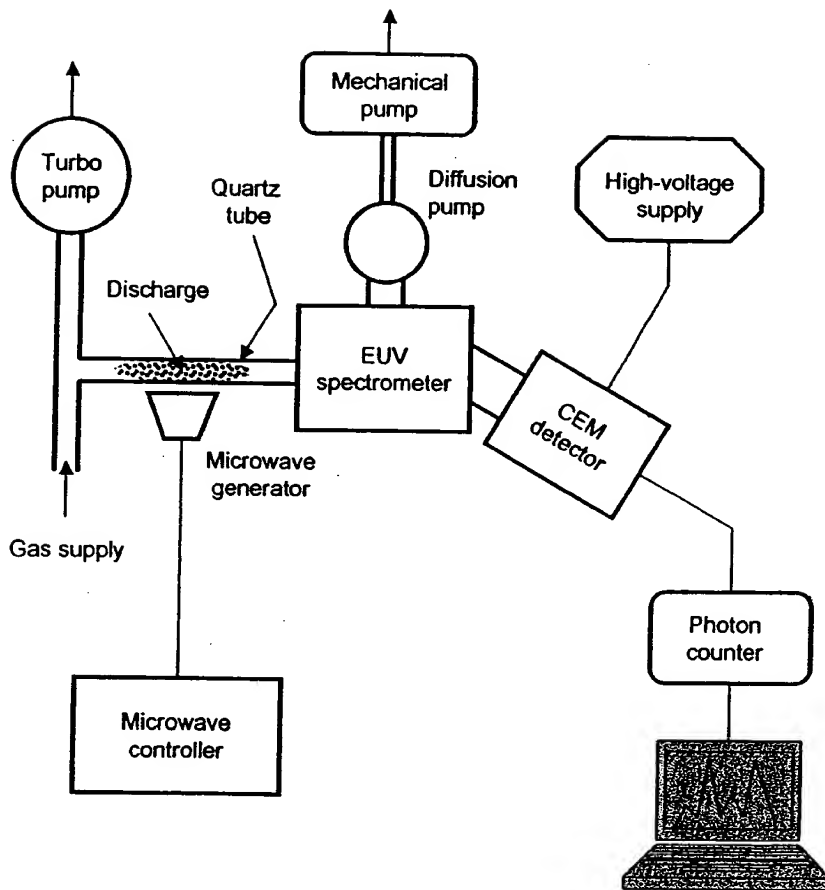


Fig. 3

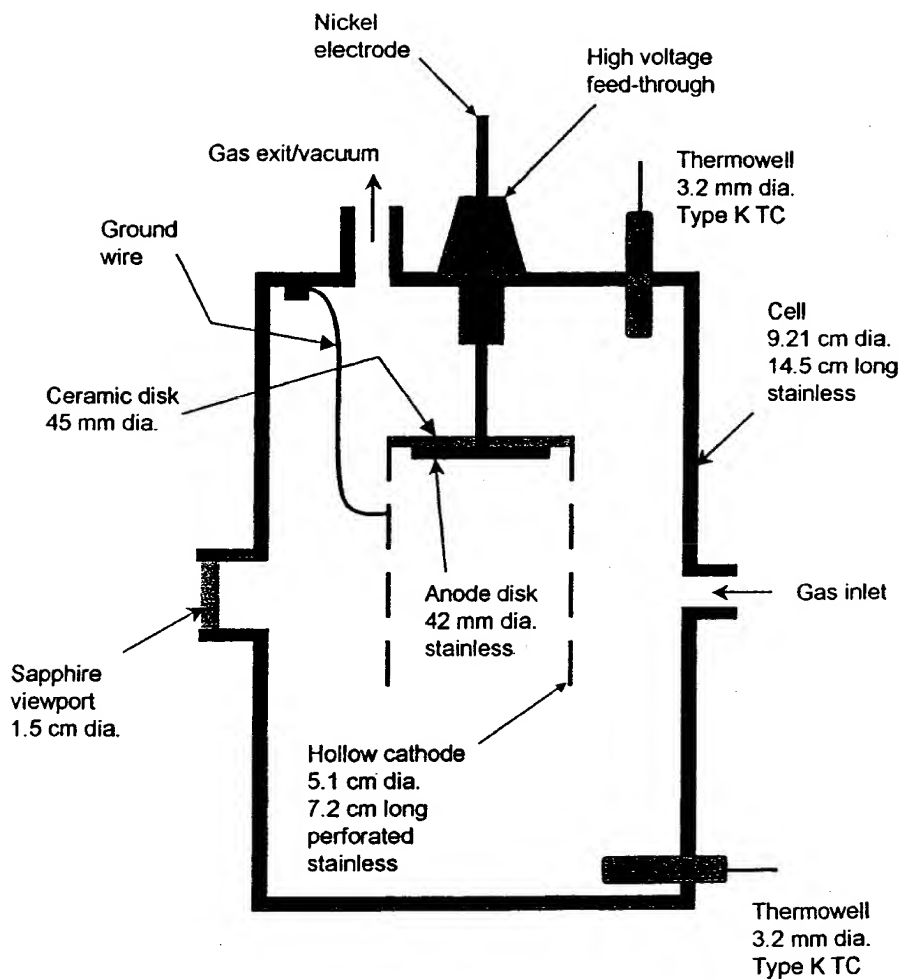


Fig. 4

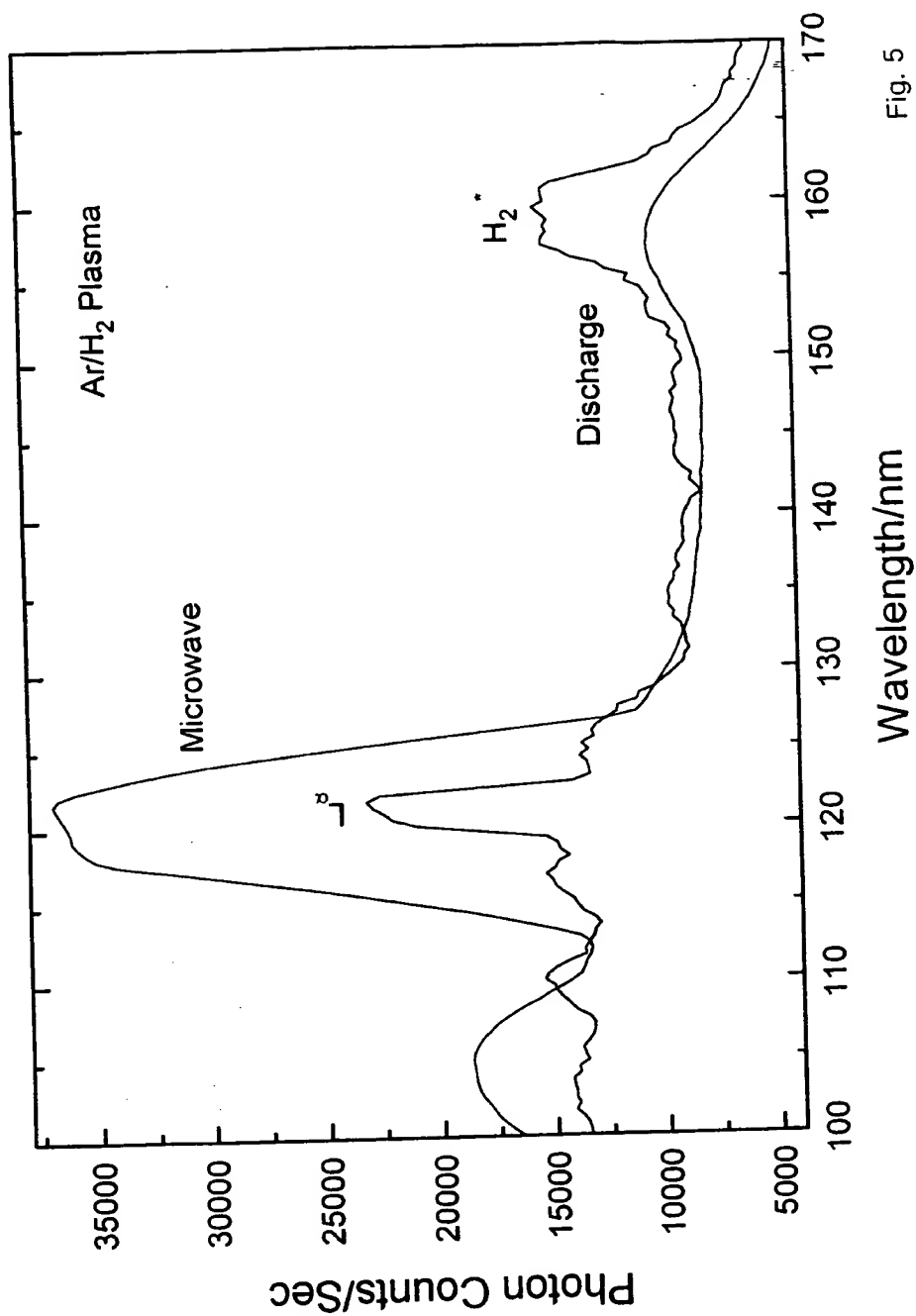


Fig. 5

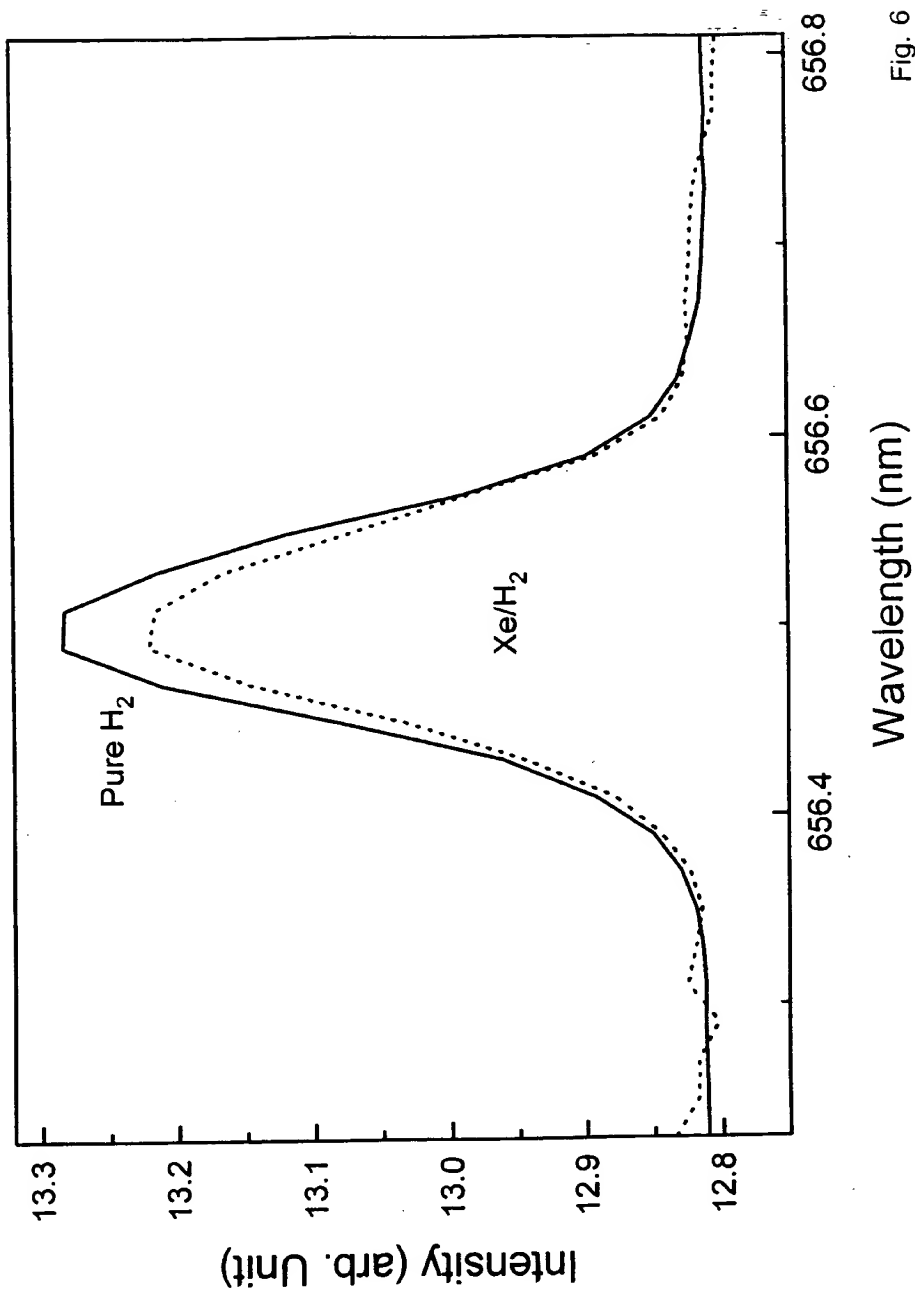


Fig. 6

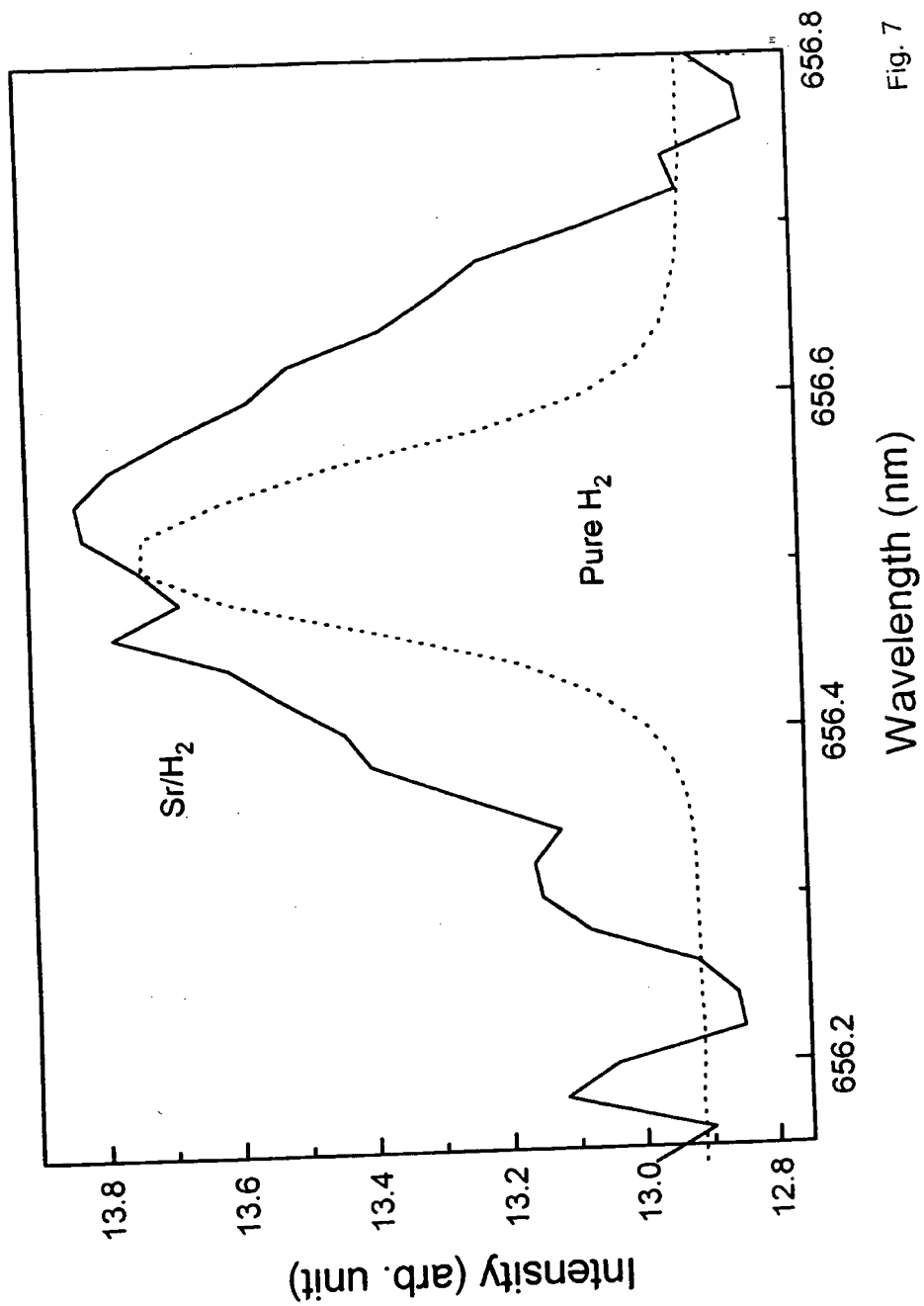


Fig. 7

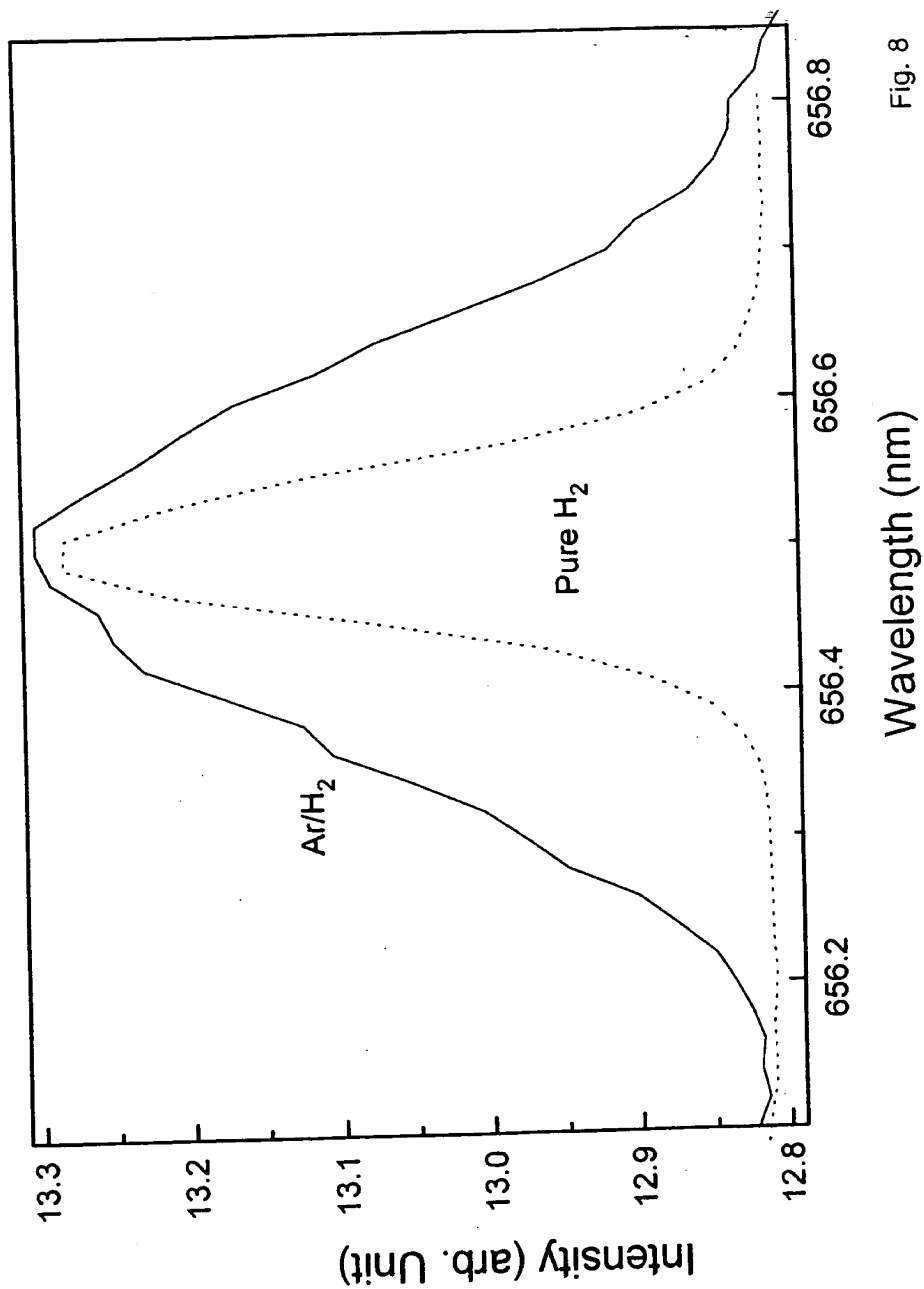


Fig. 8

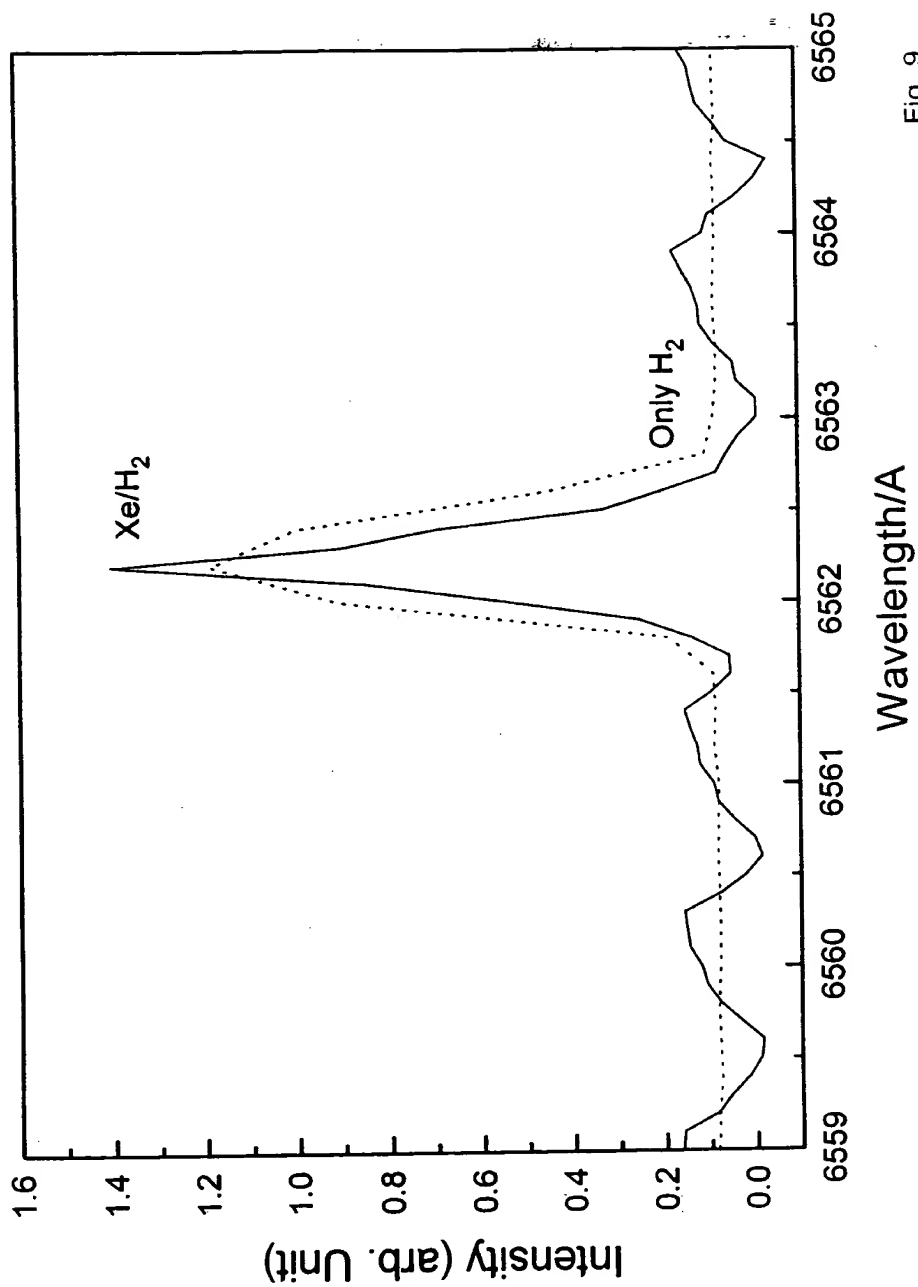


Fig. 9

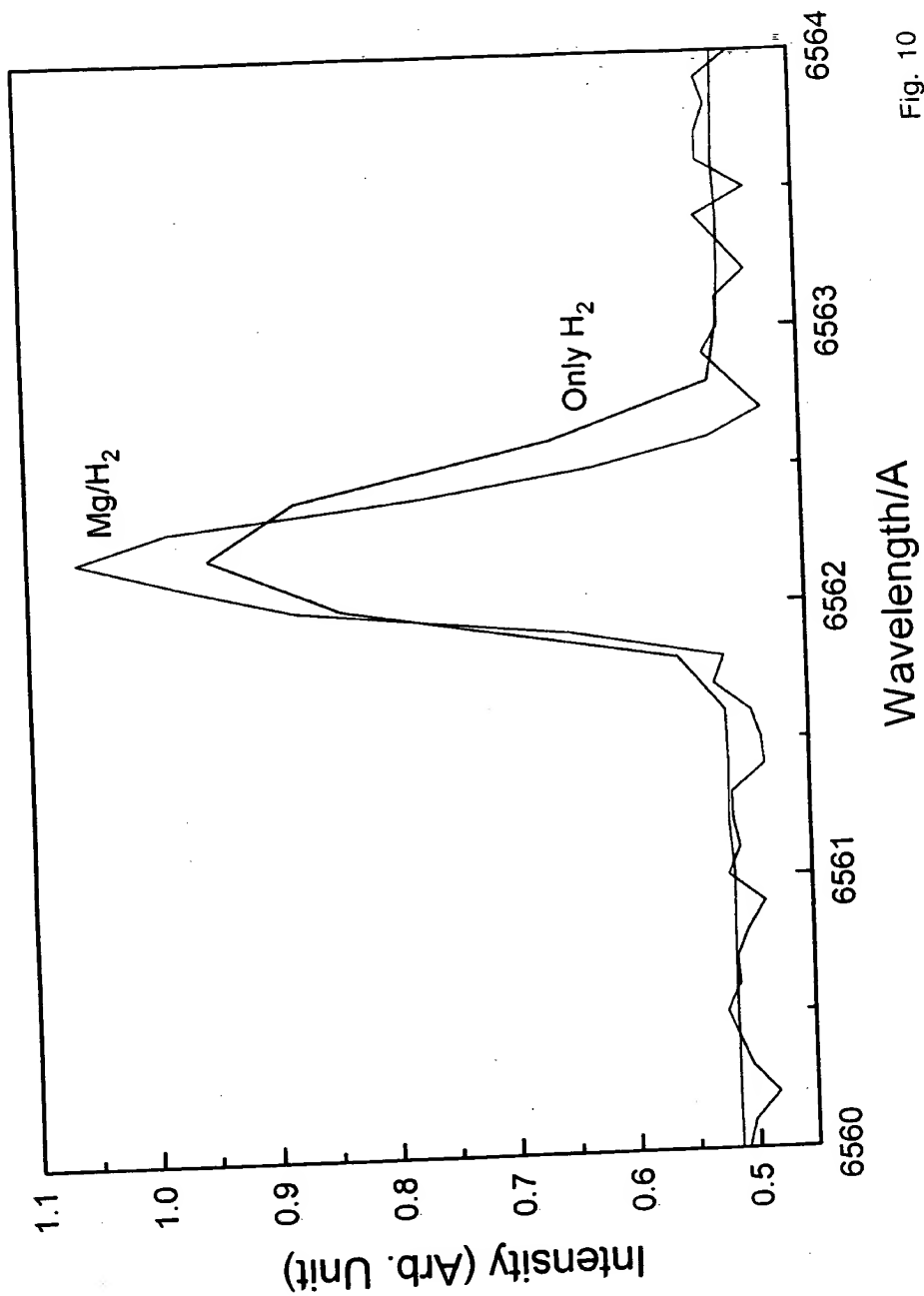


Fig. 10

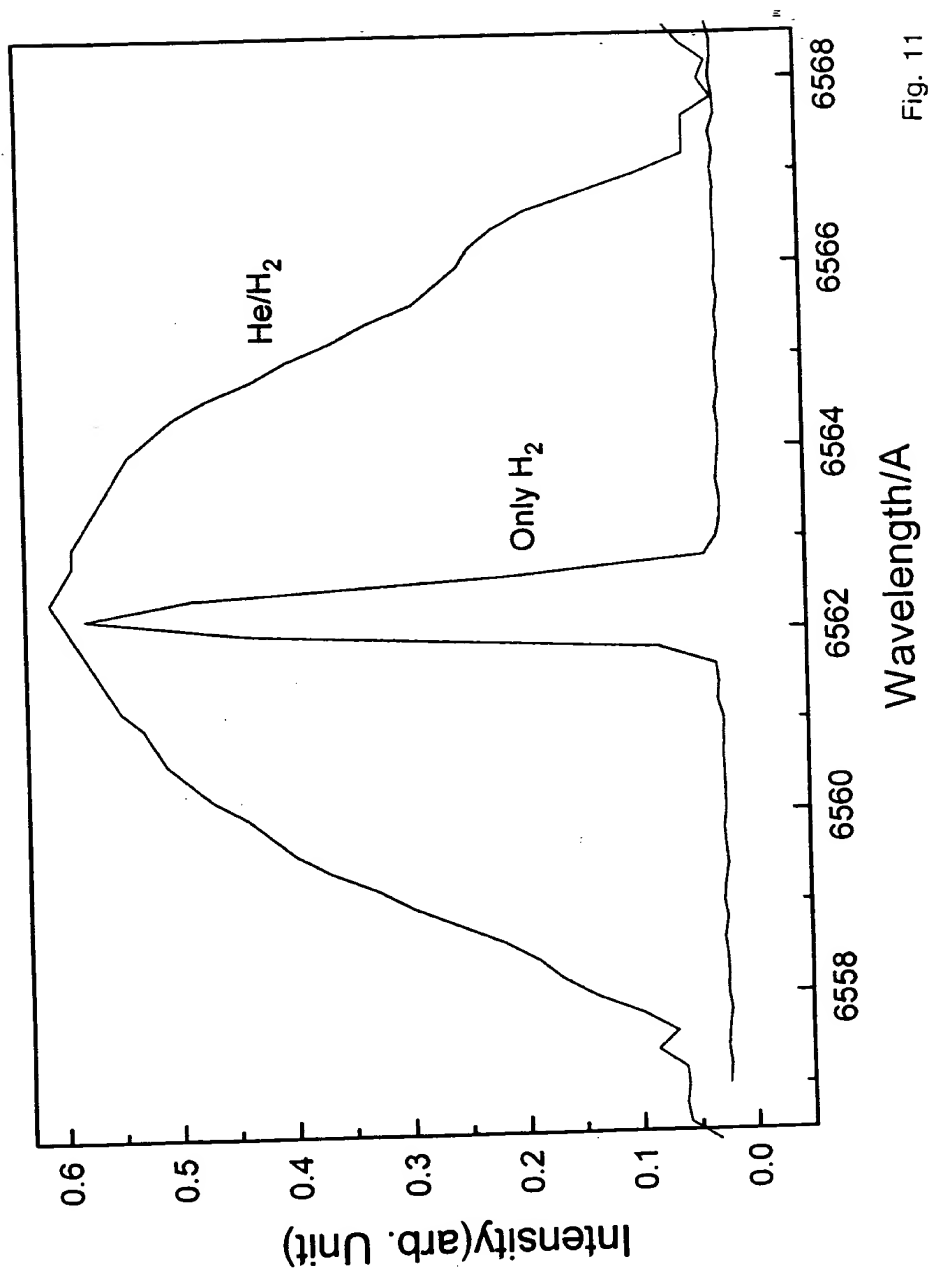


Fig. 11